

Fixing the Conformation in Helicenes: Enantioselective
Synthesis of [5]Helicenes and Synthesis of In-Fjord
Substituted Expanded Helicenes

Dissertation

zur Erlangung des mathematisch-naturwissenschaftlichen Doktorgrades

„Doctor rerum naturalium“

der Georg-August-Universität Göttingen

im Promotionsprogramm: Chemie

der Georg-August University School of Science (GAUSS)

vorgelegt von

Pablo Redero

aus Salamanca, Spanien

Göttingen, 2022

Betreuungsausschuss:

Prof. Dr. Manuel Alcarazo, Institut für Organische und Biomolekulare Chemie, Tammannstraße 2, 37077 Göttingen

Jun.-Prof. Dr. Johannes Walker, Institut für Organische und Biomolekulare Chemie, Tammannstraße 2, 37077 Göttingen

Prof. Dr. Inke Siewert, Institut für Anorganische Chemie, Tammannstraße 4, 37077 Göttingen

Mitglieder der Prüfungskommission:

Referent: Prof. Dr. Manuel Alcarazo, Institut für Organische und Biomolekulare Chemie, Tammannstraße 2, 37077 Göttingen

Korreferent: Jun.-Prof. Dr. Johannes Walker, Institut für Organische und Biomolekulare Chemie, Tammannstraße 2, 37077 Göttingen

ggf. 2. Korreferent/in: Prof. Dr. Inke Siewert, Institut für Anorganische Chemie, Tammannstraße 4, 37077 Göttingen

Weitere Mitglieder der Prüfungskommission:

Prof. Dr. Ricardo Mata, Institut für physikalische Chemie, Tammannstraße 6, 37077 Göttingen

Dr. Daniel Janßen-Müller, Institut für Organische und Biomolekulare Chemie, Tammannstraße 2, 37077 Göttingen

Dr. Alessandro Bismuto, Institut für Organische und Biomolekulare Chemie, Tammannstraße 2, 37077 Göttingen

Tag der mündlichen Prüfung: 25.11.2022

Die vorliegende Arbeit entstand unter Anleitung von Prof. Dr. Manuel Alcarazo in der Zeit von November 2018 bis Dezember 2021 an der Georg-August-Universität zu Göttingen.

Teile dieser Arbeit wurde bereits veröffentlicht:

P. Redero, T. Hartung, J. Zhang, L. D. M. Nicholls, G. Zichen, M. Simon, C. Golz, M. Alcarazo, *Angew. Chem. Int. Ed.* **2020**, *59*, 23527-23531.

S. Suárez-Pantiga, P. Redero, X. Aniban, M. Simon, C. Golz, R.A. Mata, M. Alcarazo, *Chem. – Eur. J.* **2021**, *27*, 13358-13366.

Ich versichere, dass ich die eingereichte Dissertation selbstständig verfasst und keine anderen als die angegebenen Quellen und Hilfsmittel benutzt, sowie Zitate kenntlich gemacht habe.

.....
Pablo Redero

Acknowledgements

Firstly, I would like to thank Prof. Dr. Manuel Alcarazo for the opportunity to continue my research career in his group, the interesting topic topics I was assigned during the last three years and for his support and kind attention and guidance provided when difficulties were encountered. I would like to thank him as well for his efforts in creating an enjoyable work atmosphere inside and outside the laboratory by organizing numerous group activities and by always exhibiting a warm and close attitude toward all co-workers of the group.

In addition, I would like to thank Jun.-Prof. Dr. Max Hansmann for accepting the role of second supervisor during the first stages of my thesis and Jun.-Prof. Dr. Johannes Walker for taking up his role once he moved to Dortmund. I would like to thank as well Prof. Dr. Inke Siewert for her interest shown in my topic during our TAC meetings and for her recommendations. I also thank Prof. Dr. Ricardo Mata, Dr. Daniel Janßen-Müller and Dr. Alessandro Bismuto for their participation in my thesis committee.

I wish to extend my special thanks to the technical staff for their kind and generous help to all members of our group during my time in this laboratory: Martina Pretor, Martin Simon and Marvin Blau. Likewise, I would like to thank Sabine Schacht and Angela Heinemann for their assistance with bureaucratic issues and Dr. Christopher Golz for his advice and for the preparation of all X-Ray samples and studies herein exposed.

I wish to show my appreciation to the NMR and mass spectrometry departments for the measurement and assignment of my samples.

I wish to express my gratitude to Dr. Sergei I. Kozhushkov and Dr. Valentina Pelliccioli for their proofreading of my thesis.

I would like to sincerely thank all current and former members of the Alcarazo group for the enjoyable atmosphere I enjoyed during these last years. A very special thanks to Martí Recort (what a journey it has been!), Zeyu Feng, Morwenna Mögel, Steve Karreman, Dr. Carmen García, Dr. Juan Miguel López, Dr. Xavier Marset, Jaime Tostado and Dr. Valentina Pelliccioli, which always had time for me and with whom I have shared great memories. Moreover, I would like to express my gratitude to Dr. Thierry Hartung, Dr. Beate Rissom and Dr. Samuel Suárez Pantiga for their unselfish scientific guidance during the earliest and most difficult stages of my PhD. I would like to thank likewise the students I supervised during my PhD for their work: Guo Zichen, Michael Fitzner and Tobias Ketzler.

I would like to thank all my friends in Salamanca for their support and all the friends I have made in Göttingen since I arrived. Their company in my daily life has made these years one of the best periods of my life.

I would like to thank Ane Anduaga for her unconditional support, faith and help in every aspect since we met. Eskerrik asko, Ane. Arrakasta honen zati garrantzitsu bat beti izango da zurea.

My biggest thanks go to my parents, my daily source of inspiration, for their dedication and trust in me throughout my entire life.

Abbreviations

[Au]	Generic gold species	d	doublet (NMR)
[Ru]	Generic ruthenium species	dd	doublet of doublets (NMR)
°C	degrees Celsius	ddd	doublet of doublet of doublets (NMR)
Å	ångström (10^{-10} m)	<i>d</i>	helical diameter
A_N	Normalized absorption	dba	dibenzylideneacetone
Ac	Acetyl	DCD	Dewar–Chatt–Duncanson
aq.	aqueous	DCE	1,2-dichloroethane
Ar	Aryl	DCM	Dichloromethane
BINAP	2,2'-bis(diphenylphosphino)-1,1'-binaphthalene	DDQ	2,3-Dichloro-5,6-dicyano-1,4-benzoquinone
BINOL	1,1'-bi-2-naphthol	ddt	doublet of doublet of triplets (NMR)
BIPHEP	2,2'-Bis(diphenylphosphino)-biphenyl	DFT	Density Functional Theory
Bn	Benzyl	DID	Dispersion Interaction Density
br	broad (NMR)	DMA	Dimethylacetamide
Bu	Buthyl	DME	Dimethoxyethane
calcd	calculated	DMF	Dimethylformamide
cat.	catalytic	dppf	1,1'-Bis(diphenylphosphino)-ferrocene
CD	Circular Dichroism	dq	doublet of quartets
Cp	Cyclopentadienyl	<i>dr</i>	diastereomeric ratio
Cy	Cyclohexyl	dtbm	di- <i>tert</i> -buthylmethoxy
Cod	1,5-cyclooctadiene	DUPHOS	1-{2-[(2 <i>R</i> ,5 <i>R</i>)-2,5-dimethylphospholan-1-yl]phenyl}-2,5-dimethylphospholane
d	days		

E	Electrophile	<i>i</i> -Pr	isopropyl
ECD	Electronic Circular Dichroism	IR	Infrared spectroscopy
E _{gap}	HOMO-LUMO energy gap	<i>J</i>	Coupling constant (NMR)
EI	Electron Impact	J	Joule
equiv.	equivalents	K	Kelvin
ESI	Electrospray Ionization	kcal	kilocalorie
Et	Ethyl	L	Ligand
<i>ee</i>	enantiomeric excess	L	Liter
E _P (Ox.)	Electrochemical oxidation potential	LUMO	Lowest Unoccupied Molecular Orbital
<i>er</i>	enantiomeric ratio	M	multiplet (NMR)
eV	Electronvolt	<i>m</i>	<i>meta</i>
<i>et al.</i>	<i>et alii</i> /and others	mL	microliters
g	grams	M	Metal
h	hours	M	Molar (mol dm ⁻³)
<i>hν</i>	Light irradiation	Me	Methyl
HOMO	Highest Occupied Molecular Orbital	min	minutes
HPLC	High Performance Liquid Chromatography	Mes	Mesityl
HR-MS	High Resolution Mass Spectrometry	MHz	Megahertz
<i>i.e.</i>	id est/that it	MOM	Methoxymethyl
IMes	1,3-bis(2,4,6-trimethylphenyl)-1,3-dihydro-2 <i>H</i> -imidazol-2-ylidene	MS	Molecular sieve
IMes ^{Me}	1,3-bis(2,4,6-trimethylphenyl)4,5-dimethyl-1,3-dihydro-2 <i>H</i> -imidazol-2-ylidene	MW	Megawatt
INT	Intermediate	<i>n</i>	generic number
IPA	isopropyl alcohol	N	(equiv. L ⁻¹)
		NBS	N-bromosuccinamide

NHC	N-heterocyclic	rt	room temperature
n.d.	not determined	s	singlet (NMR)
nm	nanometres	sat.	saturated
NMR	Nuclear Magnetic Resonance	SEGPPOS	5,5'-Bis-(diphenylphosphino)-4,4'-bi-1,3-benzodioxol, [4(<i>R</i>)-(4,4'-bi-1,3-benzodioxol)-5,5'-diyl]-bis-[diphenylphosphin]
Nu	Nucleophile	sext	sextet (NMR)
<i>o</i>	<i>ortho</i>	SFC	Supercritical Fluid Chromatography
<i>o</i>	octet (NMR)	SPhos	2-Dicyclohexylphosphino-2',6'-dimethoxybiphenyl
OFET	Organic field-effect transistor	sTD-DFT	Simplified Time Dependent Density Functional Theory formalism
OLED	Organic light-emitting diode	<i>t</i> -Bu	<i>tert</i> -butyl
OPV	Organic photovoltaic solar cell	t	triplet (NMR)
ORD	Optical rotatory dispersion	td	triplet of doublets (NMR)
ovn.	overnight	TADDOL	$\alpha,\alpha,\alpha',\alpha'$ -tetraaryl-2,2-disubstituted 1,3-dioxolane-4,5-dimethanol
<i>p</i>	<i>para</i>	TBF	Tetrabenzofluorene
<i>p</i> -TsOH	<i>p</i> -Toluenesulphonic acid	TBS	Tributhylsilyl
PAH	Polyaromatic hydrocarbons	TCE	1,1,2,2-tetrachloroethane
Ph	Phenyl	td	triplet of doublets
pin	pinacol	TEP	Tolman Electronic Parameter
ppm	parts per million	Tf	Trifluoromethanesulfonyl
Pr	Propyl	THF	Tetrahydrofuran
psi	pound per square inch	TIPS	Triisopropylsilyl
q	quartet (NMR)	TLC	Thin-layer chromatography
quant.	quantitative		
R	General residue		
<i>rac</i>	racemic		
RMS	Root Mean Square deviation		

TMEDA	N,N,N',N'-Tetramethylethylene-diamine	Δ	Heat
		ΔE^\ddagger	Enantiomerization barrier
TMS	Trimethylsilyl	$\Delta\varepsilon$	Molar circular dichroism
Tol	Toluene	ε	extinction coefficient
tt	triplet of triplets	λ	Wavelength
Ts	Tosyl	λ_{\max}	Wavelength at maxima
TS	Transition State	ν_{CO}	CO stretching frequency
UV	Ultraviolet light	Φ	Angle (solid-state studies)
UV-Vis	Ultraviolet and visible light	Φ_{F}	Fluorescence quantum yield
$\tilde{\nu}$	wavenumbers	μ_{e}	Electric dipole moment
W	Watt	μ_{m}	Magnetic dipole moment
w/w	weight for weight	Θ	Interplanar angle
$[\alpha]$	Specific rotation		

Table of contents

1. Abstract	1
2. Introduction	2
2.1. Helicenes.....	2
2.1.1. General properties	2
2.1.2. Applications of helicenes.....	12
2.1.3. Racemic synthesis of helicenes	17
2.1.4. Asymmetric synthesis of helicenes	26
2.2. Gold catalysis	30
2.2.1. Gold as a carbophilic Lewis acid	31
2.2.2. Applications of Au(I)-mediated π -acid catalysis	34
2.2.3. Cationic phosphines	39
3. Previous research in our group	48
3.1. Enantioselective synthesis of [4]- and carbo[6]helicenes	48
3.2. Enantioselective synthesis of dithia[5]helicenes.....	52
4. Objectives of the project.....	54
5. Results	57
5.1. Enantioselective synthesis of benzo[5]helicenes.....	57
5.1.1. Synthesis of novel BINOL-derived cationic phosphonites and gold complexes.....	57
5.1.2. Preparation of benzo[5]helicenes.....	60
5.1.3. Synthesis of key intermediates	61
5.1.4. Optimization of Au(I)-catalysed hydroarylation step.....	62
5.1.5. Substrate scope.....	65
5.1.6. Absolute configuration and chiroptical properties	69
5.1.7. Conclusion	71
5.2. Enantioselective synthesis of thia[5]helicenes	73
5.2.1. Preparation of thia[5]helicenes.....	73
5.2.2. Preliminary screening of model reaction	73
5.2.3. Substrate scope.....	76
5.2.4. Conclusion	77
5.3. In-fjord substitution in expanded helicenes and its consequences	79
5.3.1. Synthesis of in-fjord substituted expanded helicenes	79
5.3.2. Solid-state structures	86
5.3.3. Electronic structure calculations and helical inversion mechanism	91

5.3.4. Photophysical properties of synthesized helicenes	94
5.3.5. Conclusion	99
6. Experimental	101
6.1. General remarks.....	101
6.1.1. General working methods.....	101
6.1.2. Starting materials	101
6.1.3. General analytical methods.....	102
6.2. Enantioselective synthesis of 1-Aryl Benzo[5]helicenes.....	104
6.2.1. Synthesis of α -cationic Phosphonites.....	104
6.2.2. Synthesis of precursors 161a-n	112
6.2.3. Au(I) Catalyzed Hydroarylation towards [5]Helicenes	123
6.3. Enantioselective synthesis of thia[5]helicenes	133
6.3.1. Synthesis of precursors	133
6.3.2. Au(I)-Catalyzed Hydroarylation towards Thia[5]helicenes.....	140
6.4. Synthesis of in-Fjord substituted expanded helicenes	147
6.4.1. Synthesis of the starting materials.....	147
6.4.2. Synthesis of Helicenes	160
6.4.3. Fluorescence quantum yield (Φ_F).....	165
6.5. Theoretical calculations	166
6.5.1. DID Visualization.....	166
6.5.2. Nudged elastic band calculations.....	167
6.5.3. Computed absorption spectra.....	168
7. Literature.....	215
8. Appendix	227
8.1. NMR Spectra	227
8.2. HPLC Chromatograms	328
8.3. X-ray structures.....	360
8.4. Photophysical properties of helicenes.....	394

1. Abstract

By combining the 3,3'-disubstituted BINOL-derived backbone and different cationic rests, a new family of α -cationic chiral phosphonites has been synthesized. Coordination to Au(I) afforded the corresponding precatalysts. These novel compounds were applied as ancillary ligands in Au(I)-catalyzed synthesis of 1-arylbenzo[5]helicenes. High regio- and enantioselectivities were accomplished through the intramolecular hydroarylation of alkynyl-functionalized [4]helicenes. Hence, a family of 1-arylbenzo[5]helicenes containing a series of substituents at a diverse external positions of the helicene rim as well as by the modification of the hanging phenyl moiety has been prepared. The connectivities in these structures and their absolute configurations were confirmed by X-ray diffraction analysis. Also, the chiroptical properties of the materials prepared were studied by UV-Vis absorption, fluorescence emission and circular dichroism.

In accordance with previous results, a number of thia[5]helicenes containing an embedded thiophene ring were obtained by the same methodology with BINOL- and TADDOL-based Au(I) precatalysts. The high versatility of these compounds enabled the obtention of a widely tuned series of thia[5]helicenes exhibiting exceptional regio- and enantioselectivities. This task was achieved in collaboration with Dr. Valentina Pelliccioli.

In collaboration with Dr. Samuel Suárez Pantiga, a group of expanded helicenes of different sizes and shapes with phenyl- and biphenyl-substituents at inner fjord region have finally been synthesized *via* sequential Au(I)-catalyzed hydroarylation of appropriately designed substrates. Along with Dr. Christopher Golz, single crystals of these compounds suitable for X-ray analyses were grown in order to measure and quantify several structural features. Additionally and in cooperation with Prof. Dr. Ricardo Mata and M. Sc. Xaiza Aniban, the conformational dynamics and racemization barriers of the obtained compounds were calculated *via* electronic structure methods. The estimated energetic profiles were compared to those of unsubstituted core architectures, observing noticeable differences in the relative energy values as well as in the shape of the profile, i. e. number of transition states and intermediates. Also photophysical studies of these expanded helicenes were performed in order to study the effect of the substitution pattern and the extension of the π -system on their chiroptical properties.

2. Introduction

2.1. Helicenes

2.1.1. General properties

Helical structures are widespread in nature and have intrigued mankind for centuries. In chemistry, such as geometry can be observed in helicenes among other helicoidal molecules.

Helicenes are a family of compounds containing *ortho*-fused aromatic rings in a helicoidal structure possessing a chiral axis. Such structure can be explained through the conformational distortion of the π -system imposed by a strong steric strain and, in a minor influence, by an electronic contribution. In comparison to their *meta*-fused homologues, acenes, helicenes show not only higher stability, but also their own notable chiroptical properties like optical rotation, high UV-Vis absorption and characteristic circular dichroism values.^[1-3]

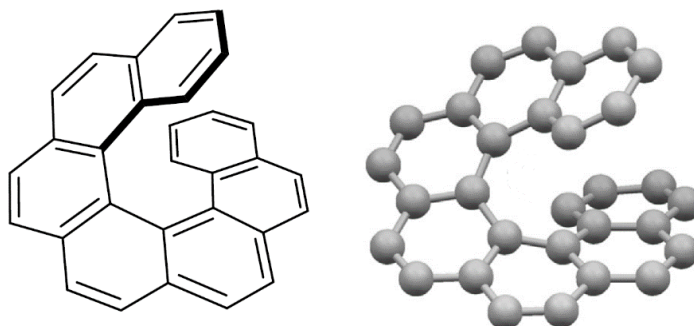


Figure 1. Representation of a helicene structure. Image modified from: N. Hoffmann, *J. Photochem. Photobiol. C Photochem. Rev.* **2014**, *19*, 1–19.^[4]

Although the first helicene reports date from the early 20th century,^[5-7] the first nomenclature was adopted by Newman and Lednicer in 1956. It was then stated that the helicene structure would be classified by the number of aromatic rings [*n*] in brackets and the prefixes penta, hexa, hepta, etc. would define those compounds containing five, six, seven, etc. aromatic rings.^[8]

Depending on their composition, helicenes can be described as carbohelicenes, when their skeleton is merely formed by carbon atoms, or heterohelicenes, when containing at least one heteroatom in their rim such as N, O, S, P or Si. In this latter case, new denotations appear, and one can speak of aza-, oxa-, thia-, phospho- or sila[*n*]helicenes in order to differentiate them from the previously mentioned carbohelicenes (Figure 2).^[9,10] Within this class of compounds, thiahelicenes have recently acquired great importance. Their chiroptical properties associated

to their chiral structure, along with their extraordinary electronic properties due to their extensive π -conjugated system, have made them the research subject of numerous projects in the past decade.^[10–16]

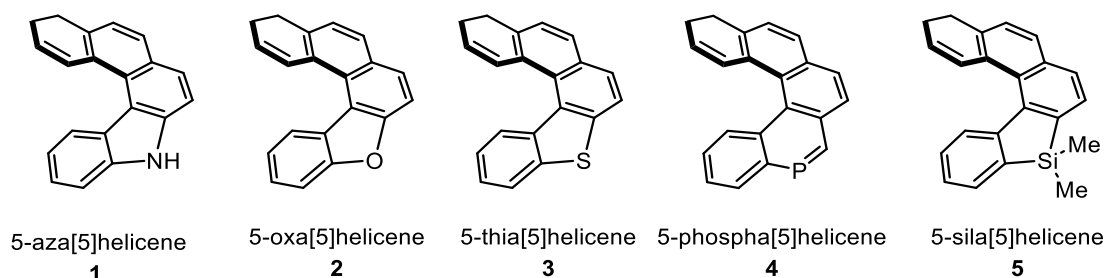


Figure 2. Examples of different hetero[5]helicenes.

As a consequence of their geometry, helicenes can wind in opposite directions and have a C_2 -symmetric axis, which is perpendicular to the helical axis. This feature confers them chirality, even though they have no asymmetric carbons or other chiral centers (Figure 3a),^[2,17] for this reason, helicenes undergo the Cahn-Ingold-Prelog rules. As chiral molecules, helicenes have as well the capacity to rotate linearly polarized light and exhibit large optical rotation values that are proportional to the number of rings present in the molecule.^[18,19]

As for the enantiomers, helicenes containing a left-handed helix are designated “minus” and denoted by *M*, whereas right-handed ones are designated “plus” and denoted by *P* (Figure 3b).^[20,21] Moreover, as has been disclosed by optical rotatory dispersion (ORD) and electronic circular dichroism (ECD) studies, the (*P*)-helicenes are dextrorotatory, whereas (*M*)-helicenes are levorotatory, demonstrating a direct relation between the absolute configuration and the chirality.^[22–24]

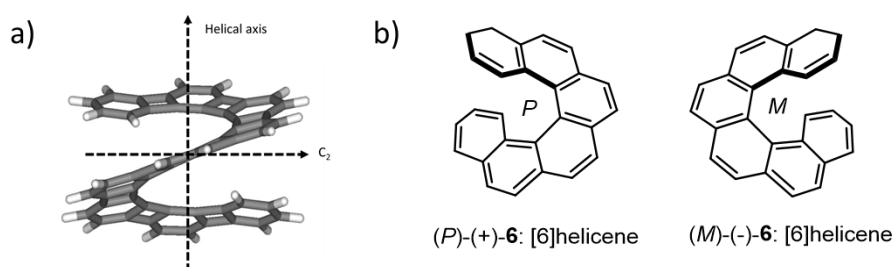


Figure 3. a) Image of helical axis and of C_2 axis as well as b) both enantiomers of [6]helicene (**6**) (b). Figure adopted from: P. Sehnal, I. G. Stará, D. Šaman, M. Tichý, J. Míšek, J. Cvačka, L. Rulíšek, J. Chocholoušová, J. Vacek, G. Goryl, M. Szymonski, I. Císařová, I. Starý, *Proc. Natl. Acad. Sci. U. S. A.* **2009**, *106*, 13169–13174.^[17]

As the number of fused rings in a helicene increases, its structure tends to be cylindrical with a constant pitch in both the inner and outer surfaces of the helix. For helicenes formed by six-membered aromatic rings, it takes six rings to cover a nearly complete 360° turn of a screw. On the other hand, when helicenes contain five-membered rings embedded in their structure,

more building blocks are required since their smaller in-plane turn (Θ_2) has a smaller contribution to the helical structure (Figure 4).

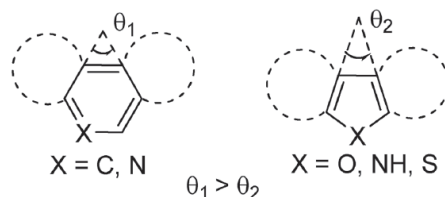


Figure 4. Comparison of the in-plane turns Θ_1 and Θ_2 present in 6- and 5-membered rings, respectively.

When discussing the helicity of these compounds, a new concept of helix pitch arises, which is the distance between two terminal rings.^[25] In terms of atomic arrangement, helicenes have two apparent helices: one formed by atoms in the inner rim, like a, b, c, d, and the other formed by outer atoms, like A, B, C, D. Even if both of them have constant helical pitch, the latter is slightly larger than the former (Figure 5).^[18,25]

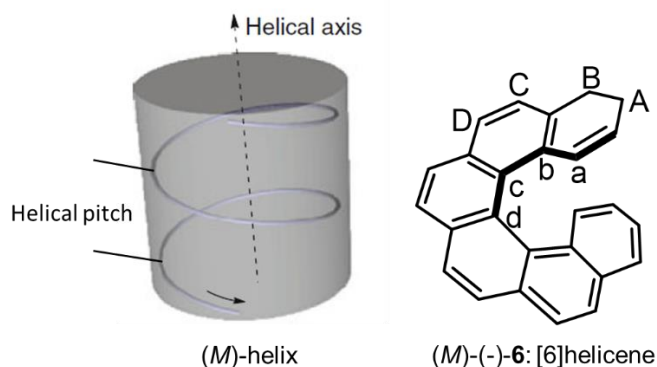


Figure 5. Examples of helical axis (left) as well as inner and outer pitch of [6] helicene [(M)-(-)-6] (right). Figure adopted from: C. Chen, Y. Shen, *Helicene Chemistry: From Synthesis to Applications*, Springer, Berlin, Heidelberg, 2016.^[18]

The length of the helical pitch can be explained by the differences in angles of the helicene-forming aromatic rings: whereas six-membered rings like benzene or pyridine possess angles of 60° , five-membered ones', like thiophene or furan, are considerably smaller (45° and 32° respectively). Ergo, in this latter case, more rings would be necessary to complete an entire rotation.^[26]

The distortion of a helicene can be described by both the interplanar angle as well as the torsional one. The former is the angle between the two terminal benzene rings, whereas the latter is the dihedral angle between the four adjacent inner carbon atoms (Figure 6a). It is significantly influenced by the presence of functional groups in the inner part of the helicene rim. In Figure 6b this aspect is represented in different structures of 1-substituted [5]helicene: the bulkier the substituent becomes, the wider the torsional angle between all four adjacent inner carbon atoms.^[18,27,28]

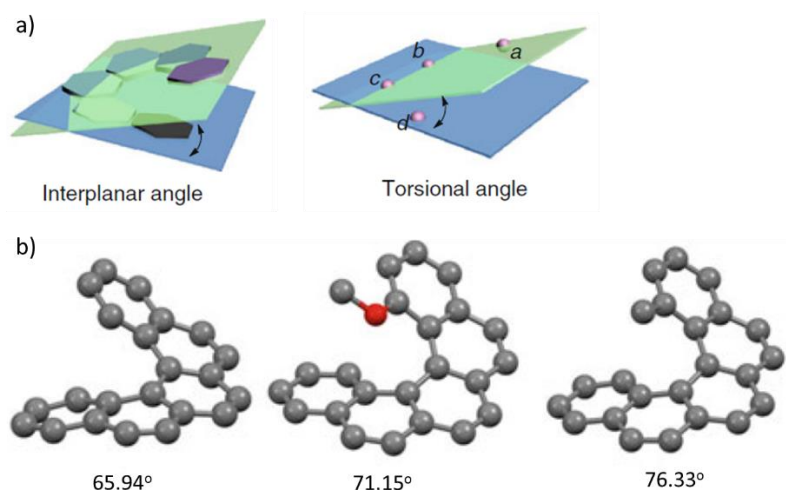


Figure 6. a) Depiction of interplanar and torsional angles and. b) torsional angles and crystal structures of several [5]helicenes (grey carbon atoms and red oxygen atoms; hydrogen atoms were omitted for clarity). Figure taken from: C. Chen, Y. Shen, *Helicene Chemistry: From Synthesis to Applications*, Springer, Berlin, Heidelberg, **2016**.^[18]

Another remarkable characteristic of helicenes is their racemization. Since most of helicenes possess chirality, their enantiomers can be interconverted into each other through a racemization process.

The crucial point in this context is the configurational stability: whereas the racemization barrier is considerably low for small helicenes, it increases as more aromatic rings are incorporated into the helical structure. This phenomenon becomes apparent when comparing the racemization barriers of different carbohelicenes (Figure 7). The first member of the carbohelicene family with a helicoidal structure, [4]helicene (**7**), is configurationally unstable under ambient conditions.^[29] By introducing a methyl group in its position 1, the situation is completely reversed, and the racemization barrier in **8** increases significantly up to 21.2 kcal·mol⁻¹.^[30] The next representative, [5]helicene (**9**), possesses a higher barrier than its parent analogue; nonetheless, it is not high enough to prevent racemization, which occurs after 36 hours. Again, this issue can be overturned by introducing a methyl moiety in the same position as before, increasing the racemization barrier up to 39.1 kcal·mol⁻¹ and facilitating the chiral resolution of this [5]helicene (**10**).^[31]

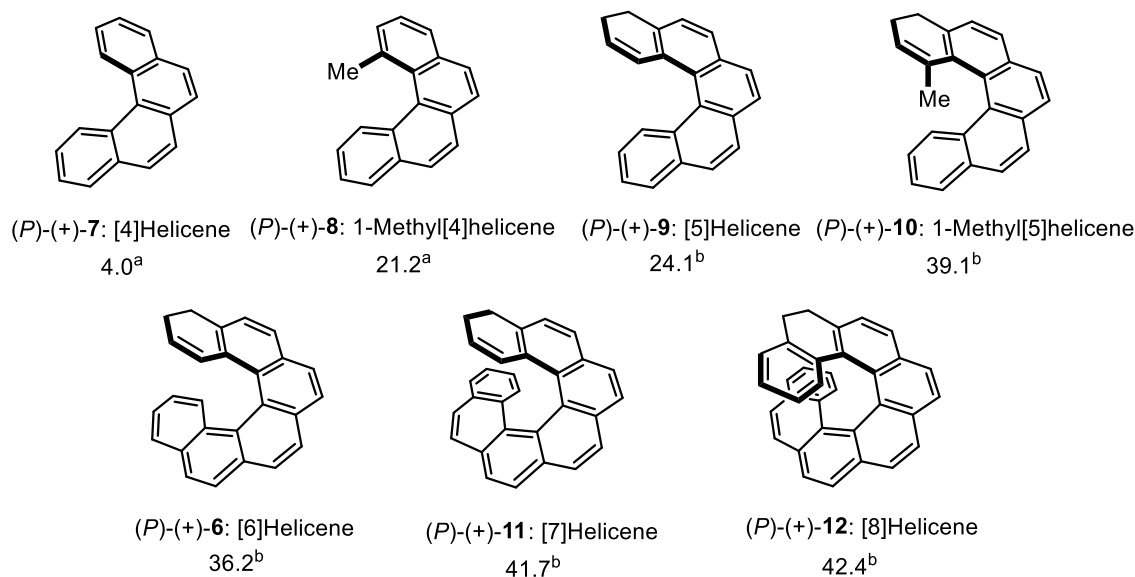


Figure 7. [4]-, [5]-, [6]-, [7]-, [8]-Helicenes, some of their methyl-substituted derivatives and their respective racemization barriers (in kcal·mol⁻¹).^[32,33] [a] Calculated values at the B3LYP/6-31G(d) level of theory; [b] experimental values ΔG^\ddagger .^[32-34]

As have been determined in several studies, the mechanism of the racemization process involves participation of different transition states (TS[‡]) between both enantiomeric forms. In the case of [4]helicene, the TS[‡] adopts a planar C_{2v} configuration, which is higher in energy than the corresponding “helix”, while the TS[‡] for [5]-, [6]-, and [7]helicenes have the C_s symmetry, respectively. Even though Lindner suggested in 1975 a planar TS[‡] for the [5]helicene, more recent reports agree that a C_{2s} TS[‡] is more likely (Figure 8).^[32,35-38]

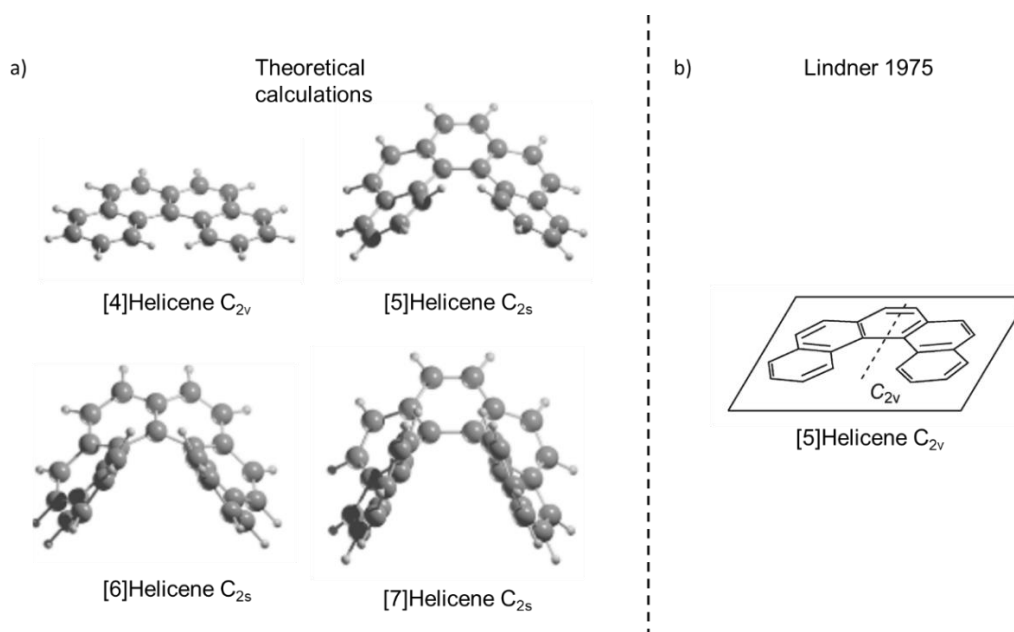


Figure 8. a) Recomputed structures of TS of different carbohelicenes at the TPSS-D3BJ/6-331G(d,p) level; b) Planar TS of [5]helicene suggested by Lindner in 1975. Figure modified from: J. Barroso, J. L. Cabellos, S. Pan, F. Murillo, X. Zarate, M. A. Fernandez-Herrera, G. Merino, *Chem. Commun.* **2018**, 54, 188–191.

The cases of helicenes containing eight or more rings in their helixes are completely different: due to their tangled topology, more than one TS[‡] takes place in the racemization process of both enantiomers.^[32] This aspect becomes even more intricate when the helicene shows more complexities within its structure, such as multiple helixes, extensions of their π -system or multiple and bulky substituents in their inner pitch.^[39–42]

Although one of the most recognizable features of helicenes is their *ortho*-fused aromatic rings, they can also experience other kind of structural expansions like lateral extensions of their π -system or successions of linear and angular ring fusions (“expanded helicenes”). The combination of these two can also generate laterally extended expanded helicenes, as the Tilley group mentioned for the first time in 2017 (Figure 9).^[43]

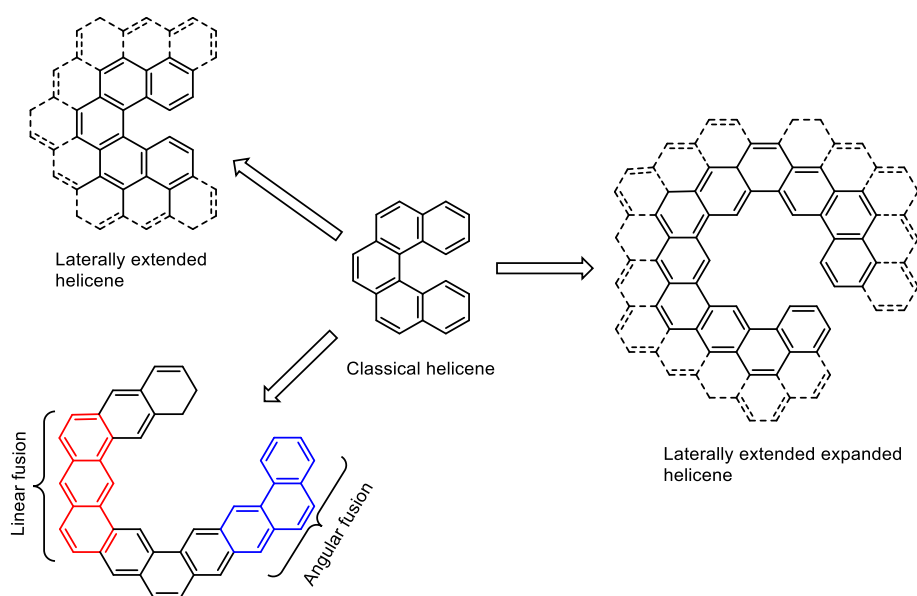


Figure 9. Classification of larger helicenes according to Tilley.^[43]

This family of helicenes has attracted a lot of interest in the past years because of their enhanced photophysical, electronic and supramolecular properties, especially by virtue of their expanded π -system. This might be also beneficial regarding semiconducting properties and the aggregation capacity of large conjugated systems. Moreover, their flexible structures could make them more soluble than analogous linear polyaromatic hydrocarbons (PAHs) and their larger cavities are suitable for applications that depend on porosity (e.g., sensing or catalysis).^[43–46]

Another interesting feature of helicenes is the π -interactions within their polyaromatic systems and the resulting absorbance and emission spectra. Although their entire structure is composed by aromatic rings, some local aromaticity is lost in comparison to their linear analogues due to their coiled geometry. For this reason, terminal rings remain the most

aromatic ones, whereas the main loss of aromaticity happens in the inner part of the helicene.^[47–50]

Speaking of HOMO-LUMO transitions, it has been indicated in many computational studies that the transannular interaction between two superimposed terminal rings can reduce the HOMO-LUMO gap (E_{gap}) via through-space delocalization.^[51] Nonetheless, the observed wavelength of maximum absorption from [4]- to [16]helicenes does not vary excessively, which proves that increasing the number of benzene rings in the structure is not the most suitable strategy in order to reduce the HOMO-LUMO gap.^[18]

One well-known strategy to reduce this gap is the introduction of thiophene and furan subunits into the helicene structure, as long as these five-membered rings are intercalated with benzene ones in order to preserve the effective π -conjugation of the whole system. A remarkable support of this idea was reported by Kertesz *et al.*, who calculated and compared the HOMO-LUMO band gaps of carbohelicenes, thiahelicenes and carbo-sulphur helicenes (Figure 10).^[15] As a result, thiahelicenes appeared to exhibit a lower gap (2.5 eV) than carbo- (2.9 eV) and carbo-sulphur helicenes (4.1 eV). The main rationale behind this observation could be a slight destabilization and increase in electron density due to the inclusion of a sulphur atom in the structure, leading to a diminution of the HOMO-LUMO gap. On the other hand, if the amount of thiophene units increases, the main consequence is a notable loss of aromaticity and therefore, an augmentation of this gap.

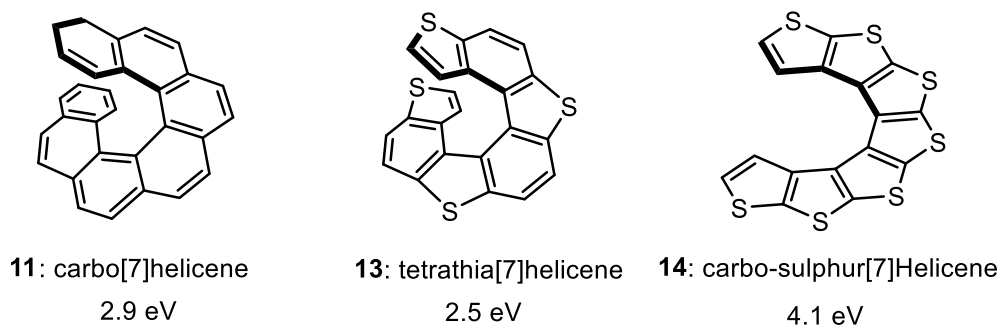


Figure 10. Values of E_{gap} in carbo- and heterohelicenes **11**, **13** and **14**, as calculated via DFT studies in gas phase.^[15]

This hypothesis was corroborated by Górski *et al.* in their study of truxenes: the substitution of a carbon with a sulphur atom entailed a destabilization of the HOMO and an increment of its energy, whereas the LUMO remained unaltered.^[52]

Other suitable methods for decreasing the E_{gap} are the extension of the π -system, thus increasing the area of electron delocalization, and the formation of pull-push structures through the introduction of donor and acceptor substituents at opposite sides of the molecule. Thereby, absorption and emission spectra of these helicenes are shifted to longer wavelengths.

Both strategies were applied and tested by Itami and co-workers: Primarily, through the extension of the π -system of carbo[6]helicene (**6**) by adding more aromatic rings and an extra helix to produce the double [6]helicene **15** (Figure 11a), and secondly, through the chlorination of π -extended dithia[6]helicenes **16** to obtain the homologue **17** (Figure 11b). In both cases, these modifications meant remarkable increases in their λ_{\max} and, consequently, a decrease of their E_{gap} .^[53,54]

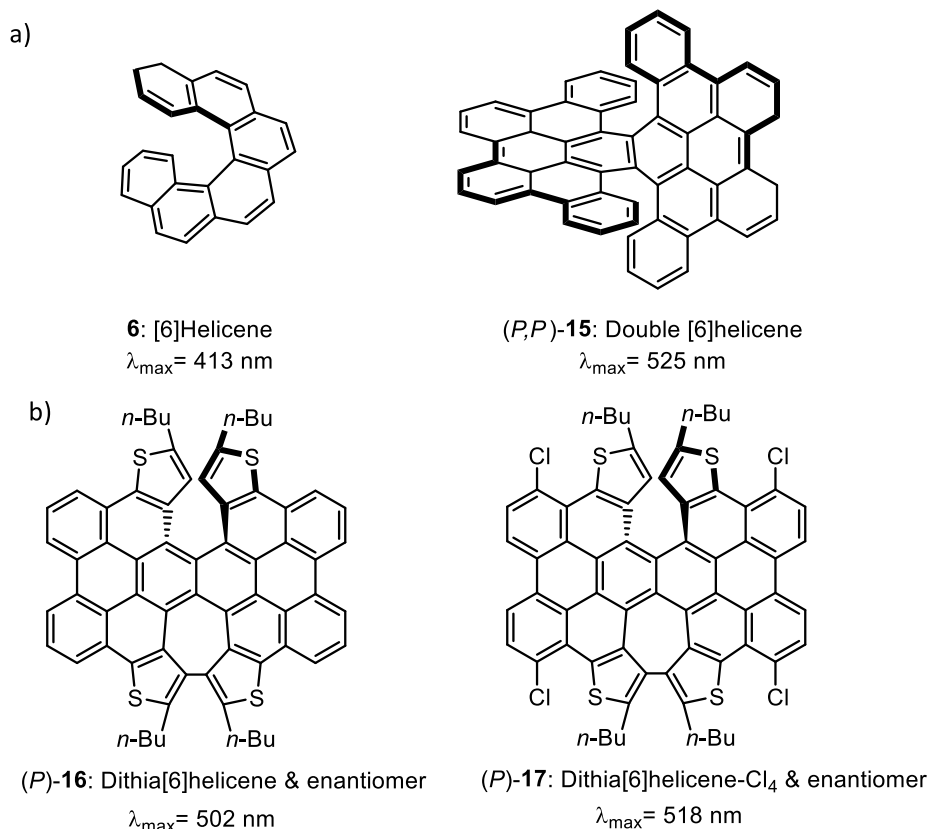
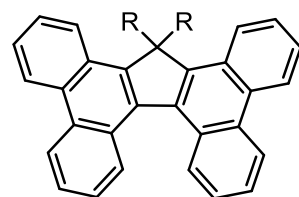


Figure 11. a) λ_{\max} for [6]helicene (**6**) and (P,P)-double [6]helicene **15**. b) λ_{\max} for (P)-dithia[6]helicene **16** and (P)-tetrachlorodithia[6]helicene **17**.

Helicenes are also very fluorescent compounds. Nonetheless, their quantum yield (Φ_f) is relatively low as a consequence of the non-emissive quenching events that decrease the efficiency of fluorescence, and it drops as more aromatic rings are added to the helical structure.^[55] However, in many cases this can be reverted by several strategies, such as the introduction of alkyl chains, the embedment of high light-emitting functional groups or the formation of heterocycles among other methods. Kitamura, Kawase and colleagues demonstrated their efficacy first in the synthesis of 17,17-dialkyltetrabenzo[*a,c,g,i*]fluorenes (dialkylTBFs) **18a-g**. They observed a solid-state fluorescence trend for those helicenes containing alkyl groups at the position 17: the longer the alkyl chain, the higher the fluorescence quantum yield. Thus, the longer alkyl substituents acted as a spacer to prevent

molecules from aggregation. The π - π interactions inside the helicenes proved to play an important role in the fluorescence as well (Figure 12).^[56]



18a	R = H	$\Phi_F = 0.009$
18b	R = Me	$\Phi_F = 0.55$
18c	R = Et	$\Phi_F = 0.27$
18d	R = <i>n</i> -Pr	$\Phi_F = 0.95$
18e	R = <i>n</i> -Bu	$\Phi_F = 0.95$
18f	R = <i>n</i> -Pen	$\Phi_F = \sim 1.00$
18g	R = <i>n</i> -Hex	$\Phi_F = 0.87$

Figure 12. Quantum yield (Φ_F) of different 17,17-substituted dialkylTBFs **18**.

Similarly, Matsuda and Nozaki's groups applied two other strategies, respectively: Matsuda enhanced the fluorescence quantum yield of carbo[5]helicene by introducing cyano- and 2,2-dicyanovinyl groups (Figure 13a), while Nozaki achieved a remarkable quantum yield increase of carbo[7]helicene by replacing a benzene ring with a dimethylsilole one (Figure 13b).^[57,58]

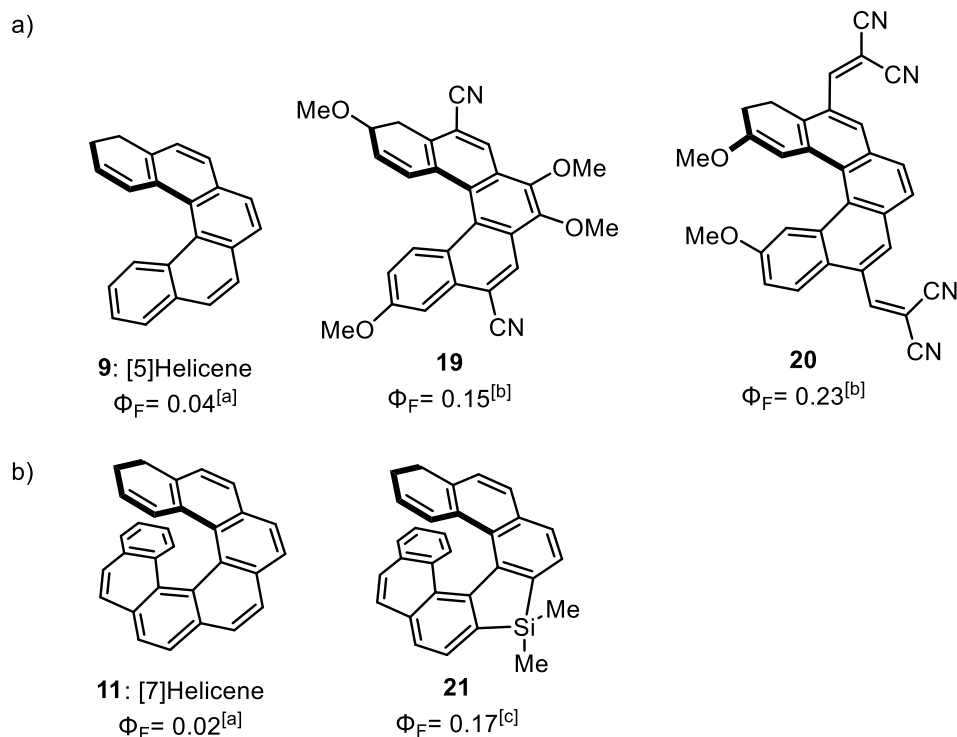


Figure 13. a) Enhancement of the quantum yields of [5]helicene (**9**) and [7]helicene (**11**) by introducing cyano-based functional groups and silole rings, respectively. Data taken from: [a] J. B. Birks, D. J. S. Birch, E. Cordemans, E. Vander Donckt, *Chem. Phys. Lett.* **1976**, *43*, 33–36^[55]; [b] H. Kubo, T. Hirose, K. Matsuda, *Org. Lett.* **2017**, *19*, 1776–1779^[57] and [c] H. Oyama, K. Nakano, T. Harada, R. Kuroda, M. Naito, K. Nobusawa, K. Nozaki, *Org. Lett.* **2013**, *15*, 2104–2107.^[58]

Finally, one of the most significant features of helicenes are their chiroptical properties. Chiral molecules are generally characterized by their ability to rotate linearly polarized light, and helicenes exhibit large optical rotation values in virtue of their helical chirality. The optical rotation value of $[n]$ helicenes is directly related to the number n of aromatic rings present in the molecule: It increases with growing number of benzene rings, but the increments become continuously smaller as the structure continues to expand (Figure 14).

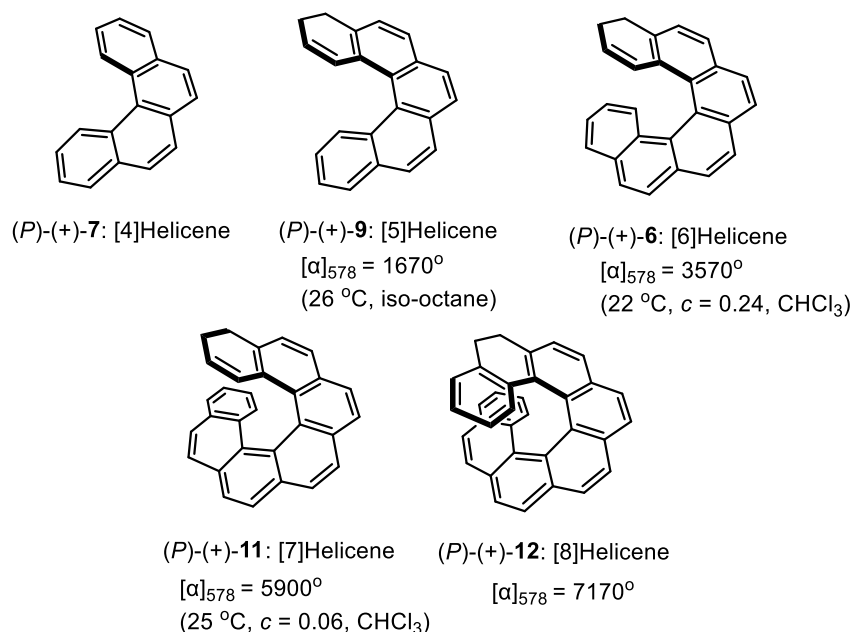


Figure 14. Carbohelicenes: absolute configuration along with their corresponding optical rotation values. Data taken from: M. Gingras, G. Félix, R. Peresutti, *Chem. Soc. Rev.* **2013**, *42*, 1007–1050.^[19]

Another important characteristic of helicenes is their circular dichroism (CD). It is the ability of enantioenriched chiral molecules to differently absorb left- or right-handed circularly polarized light. In particular, electronic circular dichroism (ECD) occurs in accordance with electronic transitions and represents the chiroptical counterpart of the more common UV-Vis absorption spectroscopy. The spectra obtained, one for each enantiomer and each a mirror image of the other (Figure 15), are characteristic properties of chiral helicenes. Materials presenting circular dichroism activity are believed to be very valuable in multiple applications like advanced optical information storage, security ink, circularly polarized luminescence lasers or chiroptical probes in biological processes.^[59–61]

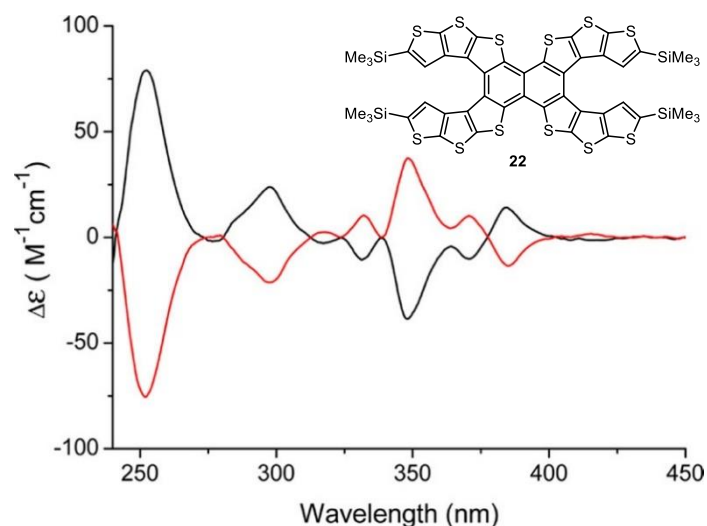


Figure 15. CD spectra of *(P,P)*-(+)- (black) and *(M,M)*-(-)-**22** (red) in hexane. Taken from: X. Liu, P. Yu, L. Xu, J. Yang, J. Shi, Z. Wang, Y. Cheng, H. Wang, *J. Org. Chem.* **2013**, *78*, 6316–6321.^[62]

2.1.2. Applications of helicenes

Almost since the first helicene structure was reported, this family of compounds has been investigated in order to develop new and diverse applications. Since helicenes exhibit unique chiroptical and electronic properties, they have been involved in such varied fields like nanoscience, material science, macromolecular chemistry or asymmetric catalysis. Some of their most important applications will be highlighted in this Section.

2.1.2.1. Molecular machines

One noteworthy application of helicenes are molecular machines. Kelly and co-workers were pioneers in the use of helicenes as part of this kind of molecules when they synthesized one of the first molecular ratchets from a carbo[4]helicene in 1997. Here, a triptycene substituent acted as a gear, and the [4]helicene moiety as the pawl and the spring (Figure 16). The slow rotation of the triptycene was detected *via* high temperature ¹H NMR studies, as well as a bidirectional rotation *via* spin polarization transfer NMR.^[63]

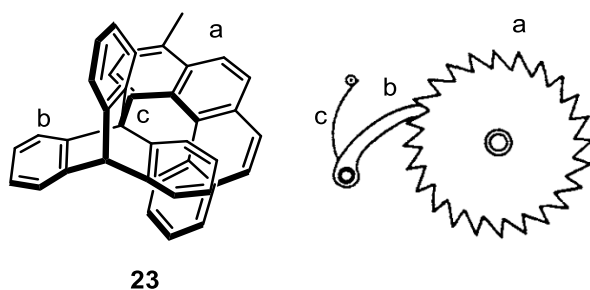


Figure 16. Kelly's molecular ratchet **23** and its different components. a) gear, b) pawl, c) spring. Image modified from: T. R. Kelly, I. Tellitu, J. P. Sestelo, *Angew. Chem. Int. Ed. Engl.* **1997**, *36*, 1866–1868.^[63]

2.1.2.2. Optoelectronics

In the last decades, numerous organic π -conjugated semiconductors have been employed in the growing field of organic electronic devices, particularly in organic field-effect transistors (OFETs), organic light-emitting diodes (OLEDs) and organic photovoltaic solar cells (OPVs).^[64–67] Helicenes are not an exception and have taken part in multiple studies by virtue of their optimal packing motif compared to that of their planar analogues, since their helical structure enables a wide range of possible intermolecular contacts. Miao and co-workers have been outstanding contributors to this field. Among their most important discoveries, it is worth to highlight their report about the use of double helicenes as p-type semiconductors in OFETs. Through X-ray crystallography, they revealed an unusual arrangement of double carbo[6]helicene **24** (Figure 17a), in which the *P* enantiomer stacks with the *M* enantiomer in a 1:4 proportion, as represented in Figure 17b, forming a bidirectional π - π stacking. OFETs produced from monolayers containing this helicene exhibited hole mobilities as high as $0.076 \text{ cm}^2 \text{ V}^{-1} \text{ S}^{-1}$. Moreover, they also carried out the synthesis of the double thia[6]helicene **25** (Figure 17c), in which a similar brickwork arrangement of twisted π faces was observed (Figure 17d). As a result of this packing motif, these layers were arranged into processed films working as a p-type semiconductor with a hole mobility of $0.033 \text{ cm}^2 \text{ V}^{-1} \text{ S}^{-1}$.^[68–71]

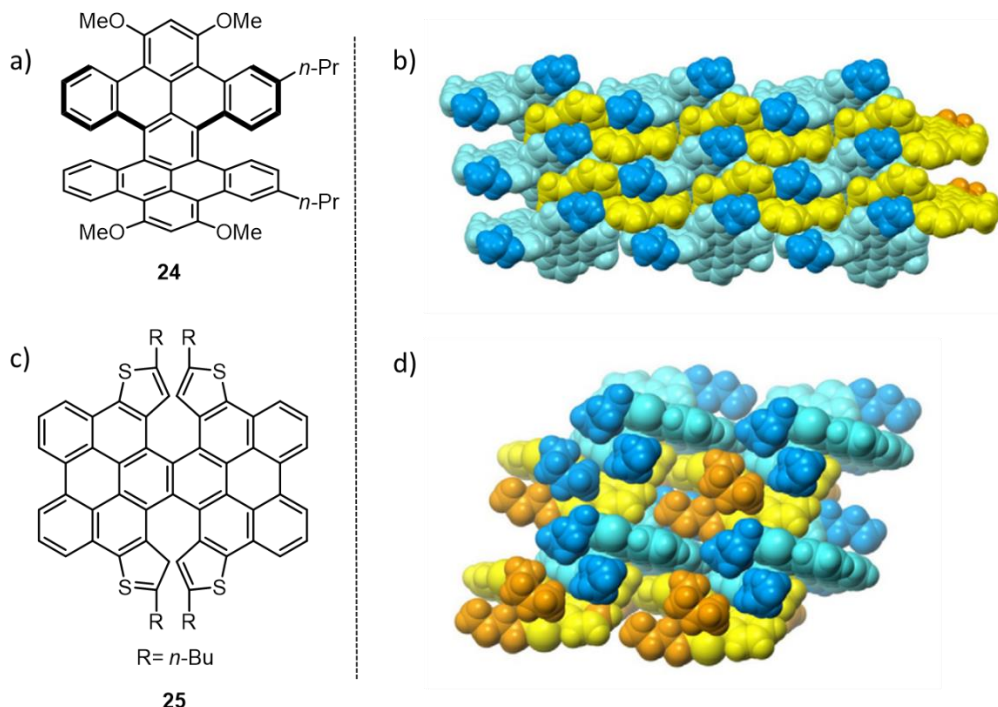


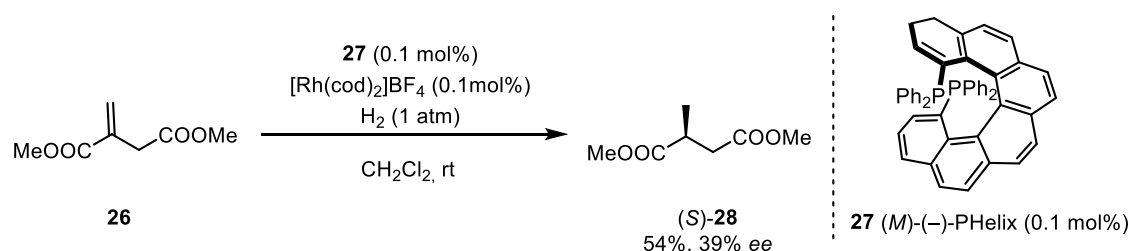
Figure 17. a) Structure of double carbo[6]helicene **24** and double thia[6]helicene **25**. b) Corresponding molecular packing. (The *M* enantiomers are shown in light blue and the *P* enantiomers are shown in yellow; the alkyl substituents in the *M* and *P* enantiomers are shown in blue and orange, respectively). Figure adapted from: C. Li, Y. Yang, Q. Miao, *Chem. Asian J.* **2018**, *13*, 884–894.^[71]

2.1.2.3. Asymmetric catalysis

Although helicenes are widely employed in multiple and various practical fields, such as dye materials, polymers, molecular recognition or even biologically active objects, their most intriguing application remains asymmetric catalysis.^[72–77]

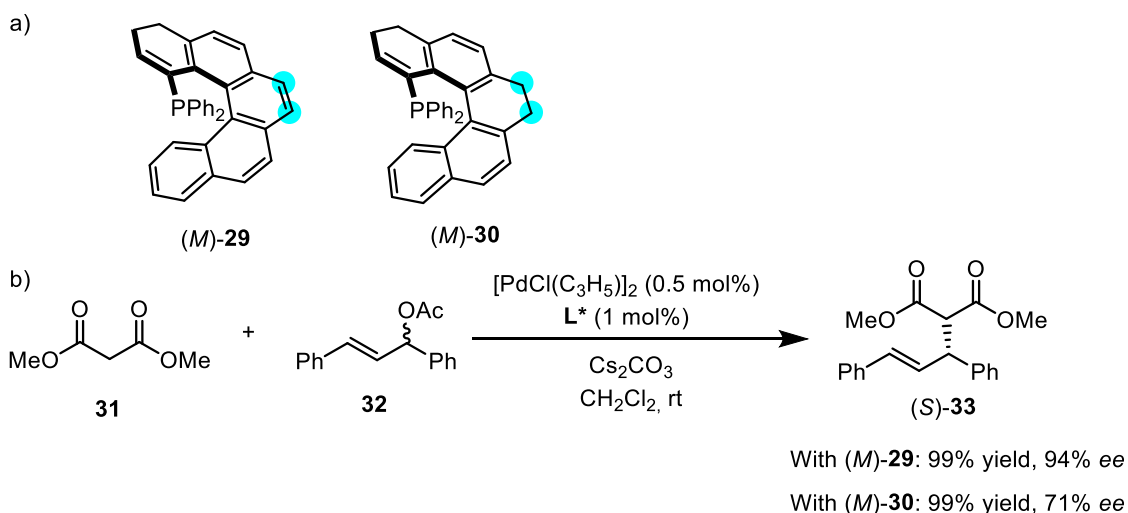
Since Bredig managed to prepare mandelonitrile in 1912 by utilizing quinine as a catalyst, the field of asymmetric catalysis has not ceased growing.^[78] Many groups developed ligands with central, planar or axial chirality, but it was not until the mid-1980s when Martin and co-workers first used substituted carbo[7]helicenes as chiral auxiliaries or chiral ligands in a variety of diastereoselective reactions such reduction of α -keto esters, hydroxyamination and epoxidation of olefins, synthesis of atrolatic ester and the ene reaction.^[79–83]

Later, in 1997, Reetz and co-workers first demonstrated the utility of optically active helical diphosphanes in enantioselective transition metal catalysis. They reproduced the synthesis of 2,15-bis(diphenylphosphino)hexahelicene (PHelix) (**27**) in enantioselective form with the help of chiral HPLC and used this compound in the hydrogenation of itaconic acid ester **26**, obtaining the (*S*)-diester **28** with 39% *ee* (Scheme 1).^[84]



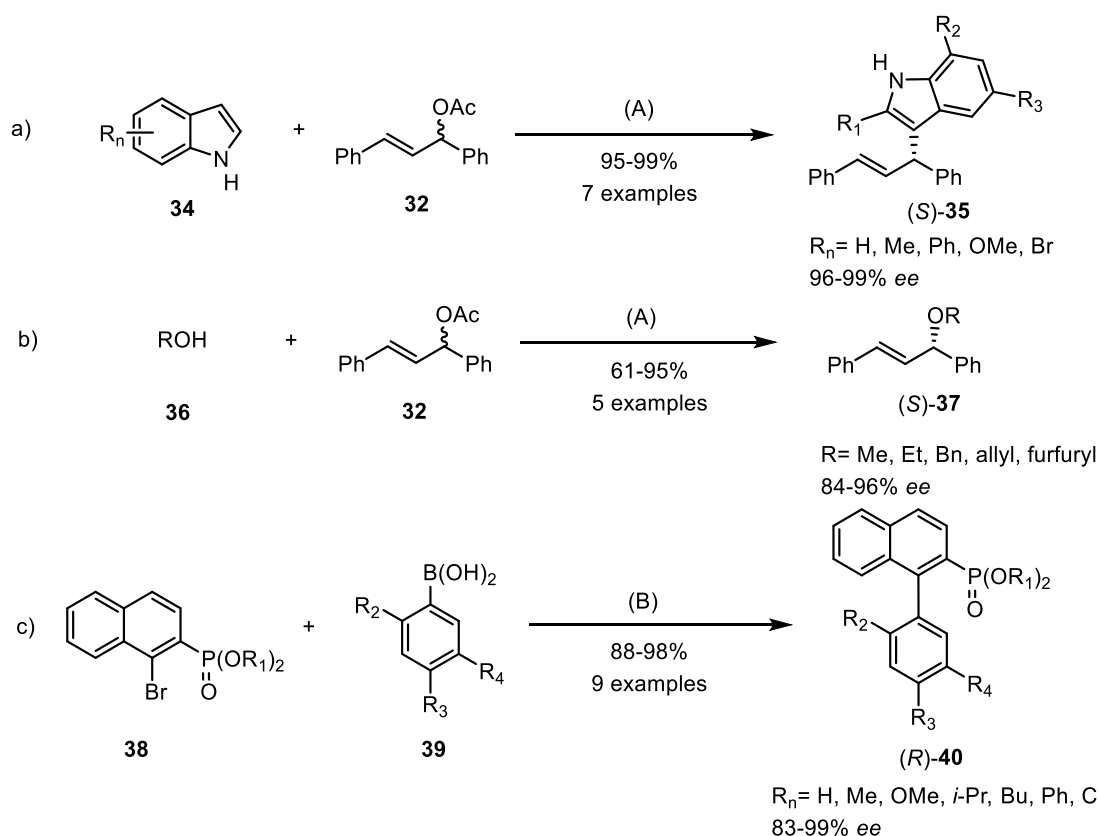
Scheme 1. Use of 2,15-bis(diphenylphosphino)hexahelicene (**27**) as a chiral ligand in the enantioselective hydrogenation of itaconic acid ester.

A more recent example was reported by Yamamoto and co-workers in 2016. They synthesized a series of optically active [5]helicene-derived phosphine ligands **29** and **30** with a 7,8-dihydro[5]helicene or a fully aromatic [5]helicene core structure, respectively (Scheme 2a). After satisfactory results were obtained in the study of the catalytic ability of both ligands in a model asymmetric allylation reaction (94 and 71% *ee*, respectively; Scheme 2b), a number of different Pd-catalyzed asymmetric transformations were carried out.^[85]



Scheme 2. a) Structures of ligands (*M*)-**29** and (*M*)-**30**. b) Allylation of racemic 1,3-diphenylallyl acetate (**32**) as a model reaction.^[85]

Structural differences between both ligands proved to be crucial in the mechanism of the different reactions that were tested: Whereas **29** showed high effectiveness in the asymmetric allylation of indoles **34** with 1,3-diphenylallyl acetate (**32**) (up to 99% *ee*) and in the etherification of alcohols **36** (up to 96% *ee*) (Scheme 3a,b), **30** was more efficient in controlling the enantioselectivity of several Suzuki–Miyaura coupling reactions (up to 99% *ee*) (Scheme 3c). Thus, the excellent yields and high *ee*'s observed in the transformation of these substrates supported the utility of carbohelices as chiral ligands in asymmetric reactions.

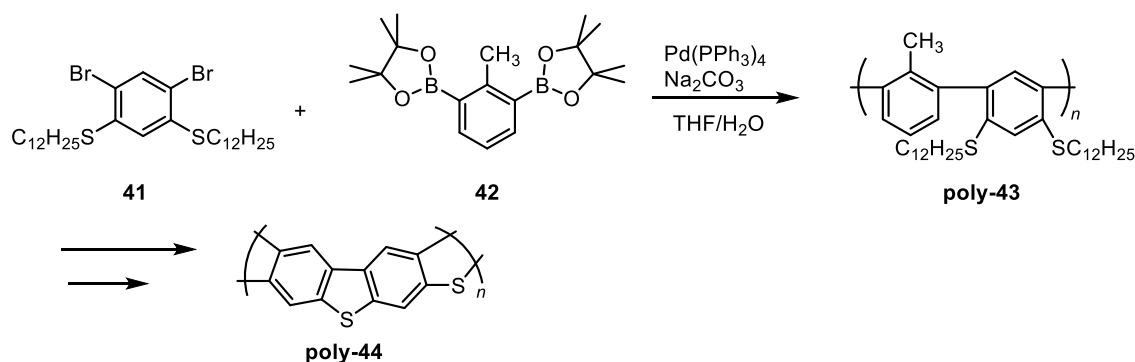


Scheme 3. a) Alkylation of indoles **34**. b) Etherification of alcohols **36**. c) Suzuki-Miyaura couplings. Reactants and conditions: (A) $[\text{PdCl}(\text{C}_3\text{H}_5)_2]$ (0.5 mol%), (*M*)-**29** (1 mol%), Cs_2CO_3 , CH_2Cl_2 , rt. (B) $\text{Pd}(\text{OAc})_2$, (*M*)-**30**, K_3PO_4 , toluene, 50 °C.

2.1.2.4. Applications of thiahelicenes

Finally, based on the unequal distribution of their electron density, heterohelicenes also show numerous applications, especially in the fields of optoelectronics, material science, catalysis, polymers or biology. In particular, thiahelicenes are among the most versatile forms of helicenes for which a huge number of applications have been envisaged and investigated.^[86]

In 2008, Nishide *et al.* reported the synthesis of thiahelicene-based polymer **44** and measured its electrical properties. It was observed that the polymerization process had enhanced the intrinsic electric conductivity of this compound (Scheme 4). Further experiments proved that this conductivity could be improved up to 30 times by doping with iodine.^[87]



Scheme 4. Synthesis of Nishide's thiahelicene-based polymer **44**.^[87]

Since thiahelicenes have exceptional chiroptical properties,^[81a] many studies have been performed in order to find new applications for them in nanoscience. A noteworthy case was reported by Katz *et al.* in 2001 when they discovered a self-aggregation phenomenon in their enantiopure thiahelicene sample into columnar arrays. Not only these aggregated species showed distinctive chiroptical properties (circular dichroism, specific rotations and fluorescent emission), but also a much higher circular polarization of their fluorescent emission after excitation by unpolarized light (Figure 18).^[88,89]

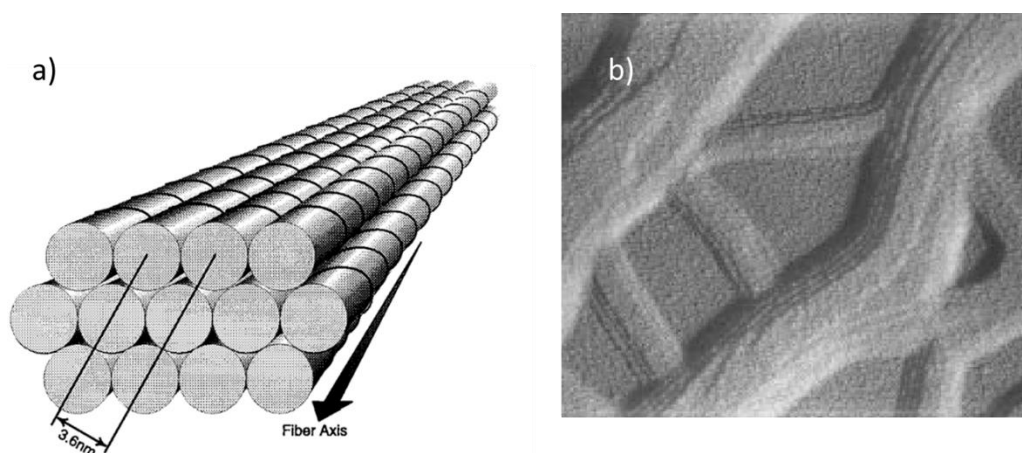


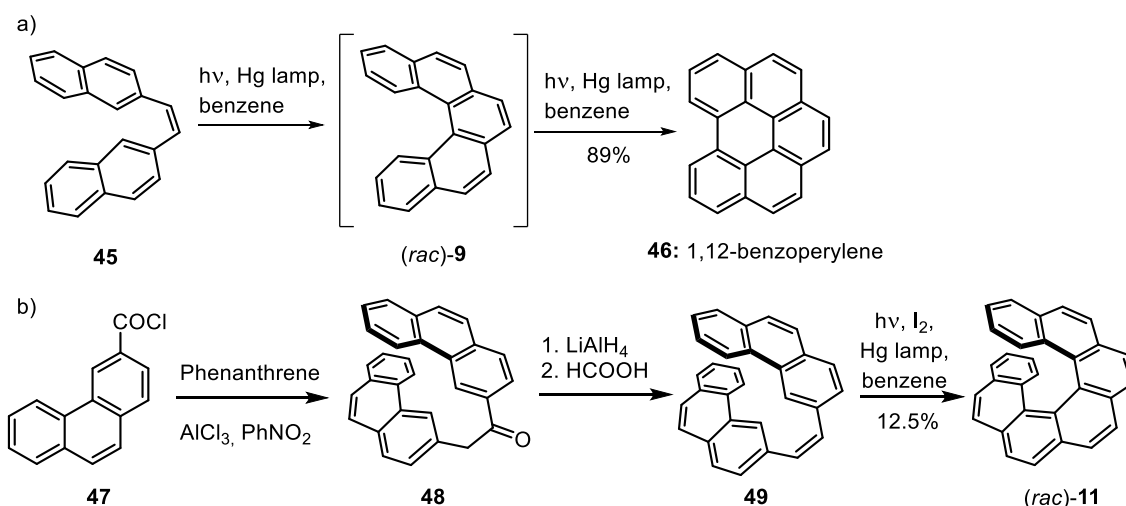
Figure 18. a) Schematic representation of the arrangement of thiahelicene fibers. b) Transmission electron micrograph of fibers of thiahelicene. Taken from: K. E. S. Phillips, T. J. Katz, S. Jockusch, A. J. Lovinger, N. J. Turro, *J. Am. Chem. Soc.* **2001**, *123*, 11900–11907.^[88]

2.1.3. Racemic synthesis of helicenes

The first reported helicene dates back to 1912, when Weitzenböck achieved the synthesis of a racemic carbo[4]helicene employing a Pschorr reaction followed by a twofold decarboxylation. This was a rudimentary process, but nonetheless the first milestone in such a broad research field like the synthesis of helicenes.^[6]

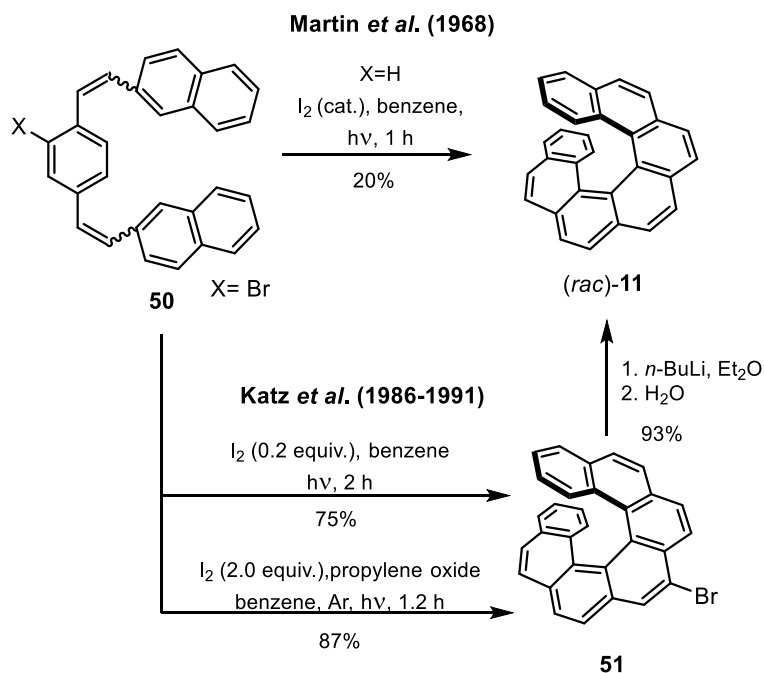
2.1.3.1. Oxidative photocyclization

Some decades later, in 1955, Newman *et al.* carried out the synthesis and resolution of [6]helicene with a charge-transfer complex,^[8] but it was not until 1967 when the first photochemical synthesis of a helicene took place: Schölz and co-workers obtained 1,12-benzoperylene **46** from the photocyclization of (*Z*)-1,2-di(naphthalen-2-yl)ethene (**45**).^[90] It is strongly believed that this product came from an internal rearrangement of [5]helicene **9** (Scheme 5a). Furthermore, Martin and his group reported some weeks later the first synthesis of [7]helicene **11** in a racemic manner from stilbene-type derivatives (Scheme 5b).^[91] These two discoveries were extremely significant in the history of helicene chemistry, because they set the stage for new methods for the preparation of polyaromatic hydrocarbons, among others, by photocyclization reactions.^[92–94]



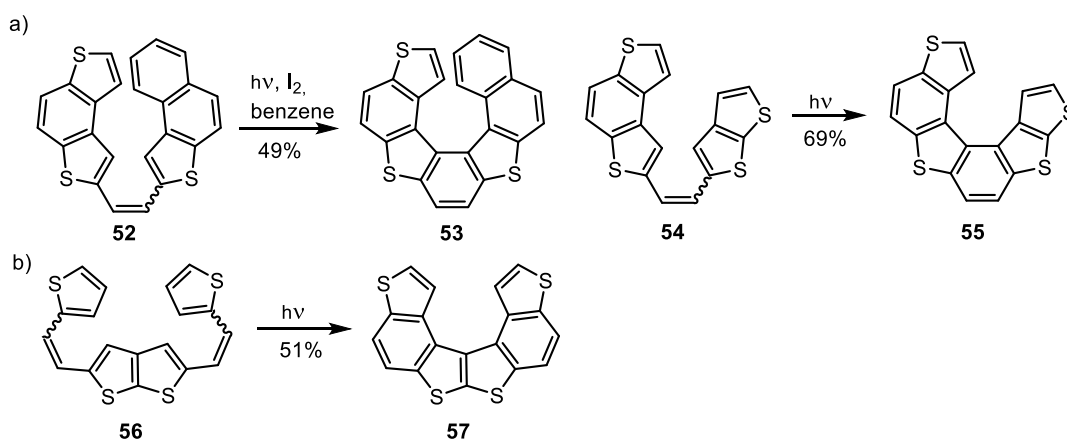
Scheme 5. a) Schölz's photosynthesis of carbo[5]helicene intermediate by an oxidative photocyclodehydrogenation and conversion into 1,12-benzoperylene **46**.^[91] b) Martin's synthesis of [7]helicene (*rac*)-**11** by oxidative photocyclization.^[91]

Further studies in this methodology focused on the improvement of regioselectivity since the yield of this last step in the synthesis of helicenes remained still very low. In an attempt to overcome this issue, Katz and co-workers became the main contributors in the late 1980's and early 1990's (Scheme 6). First, they developed a bromine-directed method in which [7]helicene **11** could be produced in a 70% total yield, improving the 20% reported to that date.^[95] They also introduced new reaction conditions, such as the use of propylene oxide as a scavenger and a stoichiometric amount of iodine in inert conditions, which not only improved the yield, but also prevented photoreduction or photooxidative side reactions of double bonds. Moreover, the remaining bromine atom could allow further functionalization through Br/Li exchange.^[96,97]



Scheme 6. Summary of Katz *et al.* contributions to the photocyclization of carbohelicenes.^[95-97]

Oxidative photocyclizations have also been applied to synthesize a broad variety of thiahelicenes containing multiple thiophene rings. Despite the obvious structural references with carbohelicenes, this technique was a key step in the synthesis of this family of helicenes. Wynberg and co-workers carried out pioneering work on mono- and double photocyclization reactions towards various thiahelicenes in the early 1970's. Precursors were obtained mainly through well-known Wittig reactions before undergoing photocyclization processes. Thiahelicenes were generally obtained after short synthesis routes in moderate and good yields, sometimes even in the absence of an oxidant. Some of the most relevant examples are depicted in Scheme 7.^[98,99]

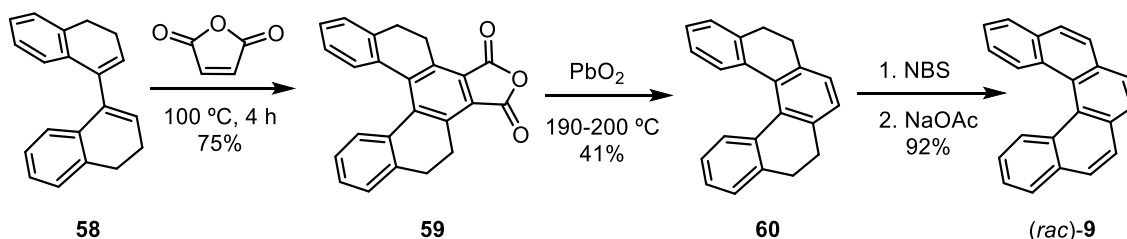


Scheme 7. a) Monophotocyclization of stilbenes **52** and **54** to afford thiahelicenes **53** and **55**, respectively. b) Twofold photocyclization of diene **56** to achieve tetrathia[6]helicene **57**.^[98,99]

Although these synthetic routes are relatively simple and excellent results can be achieved by oxidative photocyclization, this method involves certain difficulties: it requires photochemical equipment as well as very specific conditions such as extremely pure and carcinogenic solvents and high dilution. Moreover, it turned out that it lacks tolerance to certain functional groups, like NH_2 and NO_2 . For this reason, other important alternatives to this method of helicene synthesis are worth mentioning.

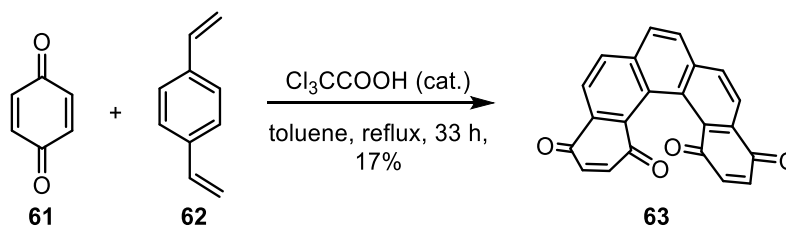
2.1.3.2. Diels-Alder reactions

Diels-Alder reactions have been widely used in organic chemistry since their discovery in 1928 and have demonstrated to be a prominent strategy to form six-membered rings in the synthesis of polyaromatic compounds.^[2,100] One of the first reports on the synthesis of carbohelicenes by using Diels-Alder conditions belongs to Weidlich, when he carried out the formation of defunctionalized carbo[5]helicene (*rac*)-**9** by applying this strategy on the first step (Scheme 8, as modified by Altman and Ginsburg).^[101] Weidlich's work inspired many further researchers, and many various examples of employing this methodology have since been reported.^[102–105]



Scheme 8. First reported use of a Diels-Alder reaction in the synthesis of helicenes^[101] modified by Altman and Ginsburg.^[104]

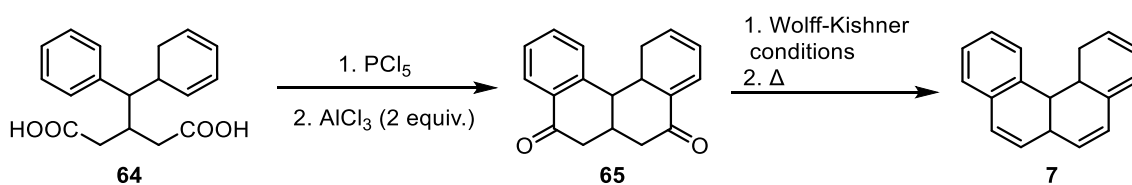
It was not until 1990 when the first multi-gram preparation of helicenes *via* Diels-Alder reaction took place. Katz and Liu utilized a double cycloaddition of an excess of commercially available 1,4-benzoquinone (**61**) and 1,4-divinylbenzene (**62**) in refluxing toluene to produce 2.93 g of [5]helicenebisquinone **63** in 17% yield (Scheme 9).^[106] This low yield might be explained by participation of the energetically unfavorable transition state due to the use of vinylic aromatic compounds as dienes. Nonetheless, the simplicity of this method incentivized the production of large helicenes on a gram-scale. Nowadays, the Diels-Alder strategy in helicene chemistry is by far the main synthetic choice among the non-photochemical methods.



Scheme 9. Multi-gram Diels-Alder reaction to generate [5]helicenebisquinone **63**, as reported by Katz and Liu.^[106]

2.1.3.3. Friedel-Crafts-type reactions

The first synthesis of helicenes involving Friedel-Crafts-like intramolecular cyclizations dates back to 1938, when Newman *et al.* obtained carbo[4]helicene **7** after carrying out a double ring closure of acid chlorides, subsequent Wolff-Kishner deoxygenation of **65** and final catalytic dehydrogenation (Scheme 10).^[107] This work inspired further synthesis of carbohelicenes, as Friedel-Crafts reactions proved to be very useful, reliable and straightforward tools when performing internal cyclizations.^[108–110]

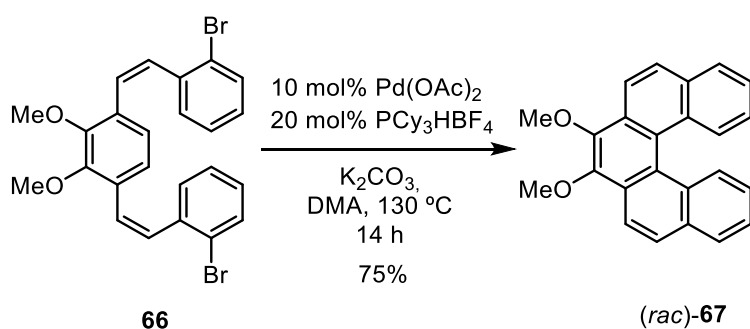


Scheme 10. First employment of intramolecular Friedel-Crafts reaction in helicene chemistry.^[107]

2.1.3.4. Metal-catalyzed syntheses

Transition metal catalysis has been of great importance in the synthesis of helicenes in the last century. Because of its versatility and capacity to form new C–C bonds, this kind of reactions became a great resource and, in many cases, a key step in the formation of helicenes.

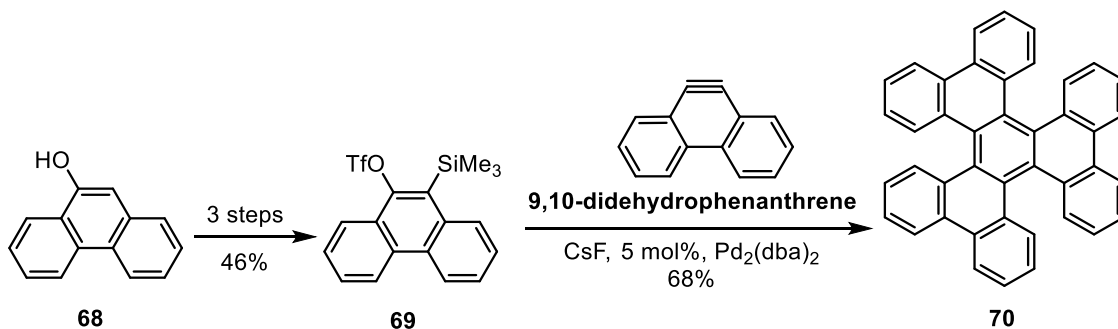
Some of the most significant examples rely on the use of palladium as a catalyst. Since this is an extremely versatile metal in cross-coupling reactions, multiple studies describing syntheses of helicenes *via* these methods have been reported.^[111–114] On the other hand, Pd catalysts can also promote C–H bond activations: thus, Kamikawa and co-workers exploited this tool in their synthesis of [5]helicene **67** by double intramolecular C–H arylation reaction (Scheme 11).^[115]



Scheme 11. Twofold intramolecular arylation via C–H activation for making functionalized helicene (*rac*)-**67**.^[115]

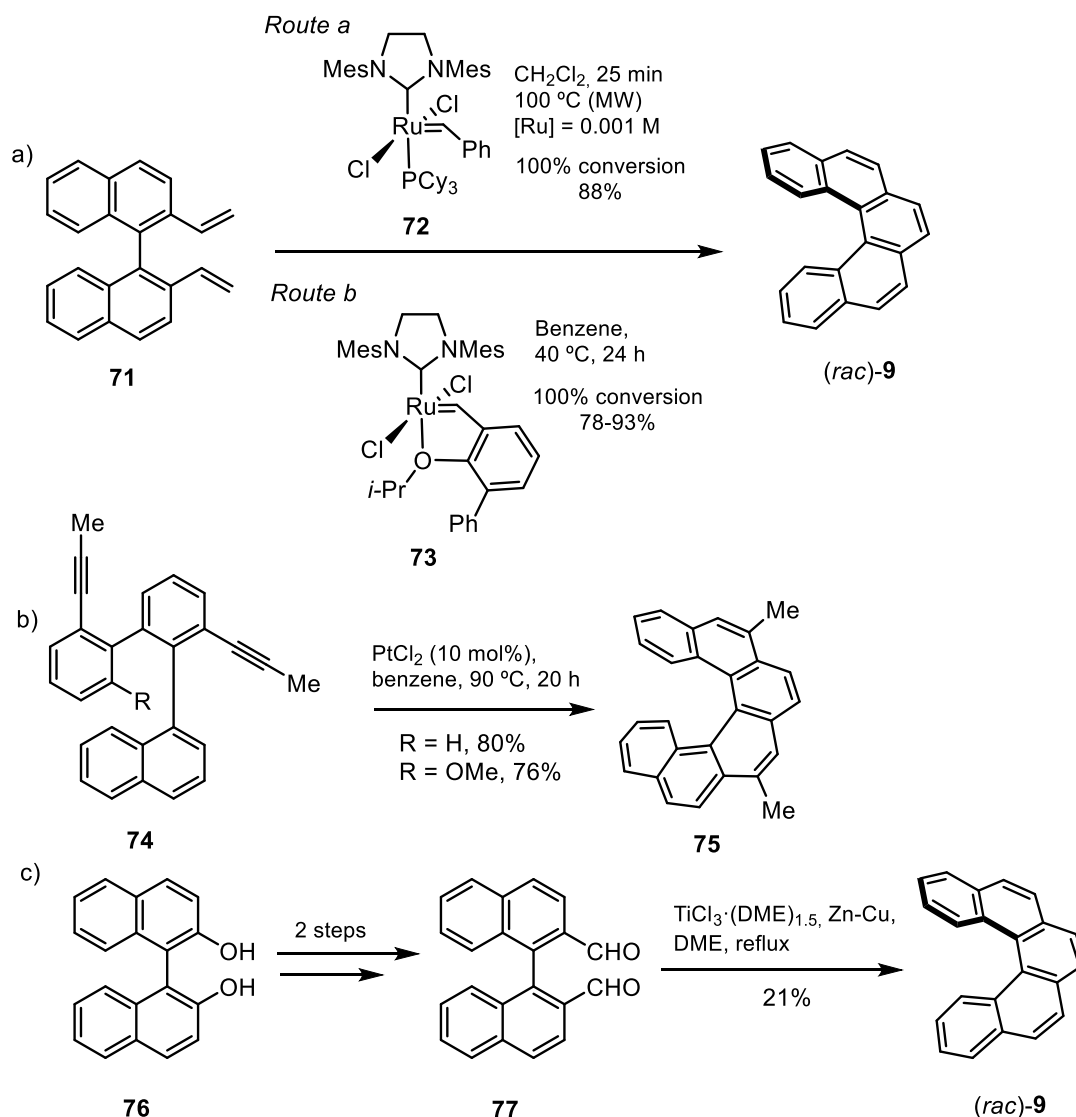
Palladium has been used as well in ingenious $[2\pi + 2\pi + 2\pi]$ cyclotrimerizations for the synthesis of polyaromatic compounds. These are frequently very favorable processes, since the driving force towards the final products originates from the strong conjugation and resonance, which overcomes an unfavorable distortion of the π -system over many carbon atoms. A very original synthesis of a D_{3h} -symmetric triple [5]helicene **70** via cyclotrimerization

of intermediate 9,10-didehydrophenanthrene was reported by Guitán, Pérez and co-workers in 2000 (Scheme 12).^[116]



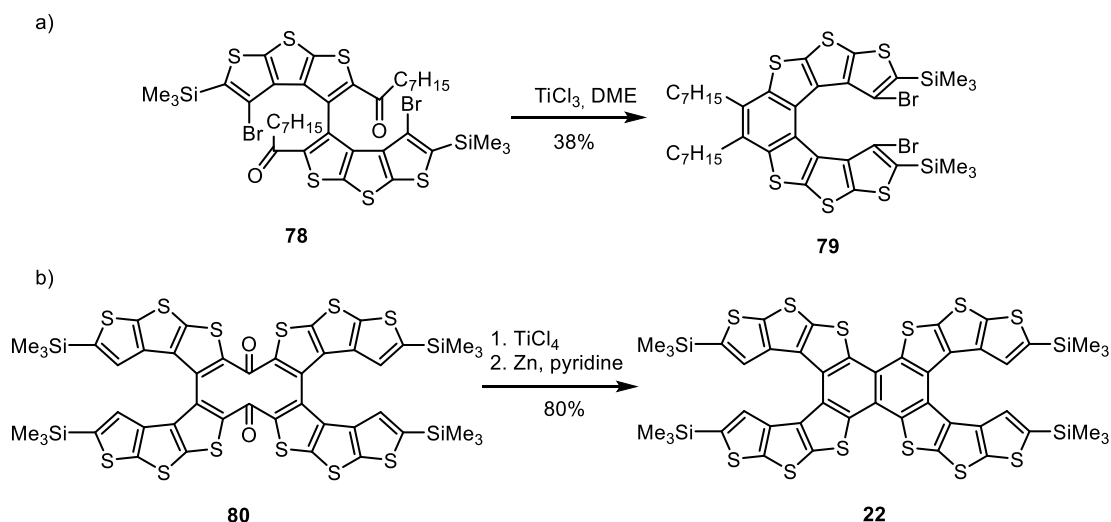
Scheme 12. Cyclotrimerization of 9,10-didehydrophenanthrene to obtain triple [5]helicene **70** reported by Guitán and Perez.^[116]

Besides palladium, many other transition metals have been utilized in the racemic syntheses of helicenes. For example, Collins *et al.* reported in 2006 the first synthesis of [5]carbohelicene (*rac*)-**9** by ring-closing metathesis in **71** with a modified ruthenium Hoveyda-Grubbs catalysts **72**, **73** (Scheme 13a)^[117] Storch *et al.* and other researchers studied the synthesis of polysubstituted carbo[6]helicene **75** through platinum-catalyzed twofold intramolecular hydroarylation (Scheme 13b).^[118] Moreover, other metals like titanium have been employed in some cases, for example, in the synthesis of carbo[5]helicene (*rac*)-**9** via McMurry reductive coupling of dicarbonyl compound **77**, as reported by Gingras and Dubois (Scheme 13c).^[119]



Scheme 13. Alternative metal-catalyzed synthesis of carbohelicenes. a) Synthesis of [5]helicene (*rac*)-**9** via ring-closing metathesis with a modified ruthenium Hoveyda-Grubbs catalyst.^[117] b) Synthesis of 7,11-dimethyl[6]helicene (**75**) via double hydroarylation.^[118] c) Synthesis of [5]helicene (*rac*)-**9** via McMurry reaction.^[119]

Due to the wide versatility of this last olefination, other types of helicenes have been synthesized, such as the various aforementioned thiahelicenes. Rajca and co-workers reported a representative example in 2004 with the obtention of hexathia[7]helicene **79** from diketone **78** in a modest yield of 38% (Scheme 14a).^[120] Six years later, in 2010, inspired by this work, Cheng, Wang and colleagues accomplished the synthesis of double helicene **22** under different reaction conditions. This simultaneous formation of two *ortho*-fused arene rings was realized in 80% yield (Scheme 14b).^[121] Thereafter, in 2013, this research team carried out the chiral resolution of both enantiomers of **22** and reported their CD spectra, which were previously depicted in Figure 15.^[62]

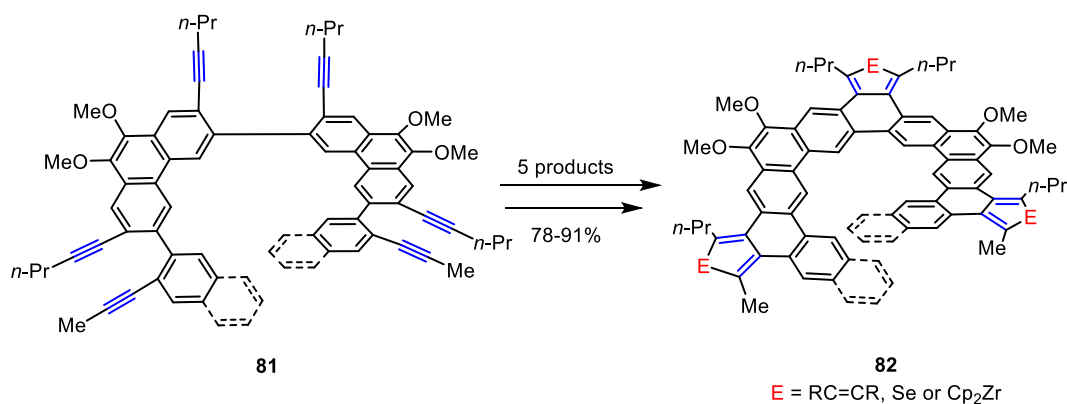


Scheme 14. a) Synthesis of thiahelicene **79**.^[120] b) Synthesis of double thiahelicene **22**.^[121]

2.1.3.5. Synthesis of chiral expanded helicenes

Although the enantioselective synthesis of expanded helicenes has not yet been reported, multiple examples of chiral structures can be found in the literature.

In 2017, Tilley and co-workers carried out the synthesis of the first expanded helicenes **82** combining angular and linear ring fusion by means of $[2 + 2 + n]$ ($n = 1$ or 2) cycloaddition (Scheme 15).^[43]



Scheme 15. Synthesis of Tilley's expanded helicene via $[2 + 2 + n]$ cycloaddition.^[43]

However, although the terminal rings of these compounds overlapped each other's, their racemization barriers were extremely low compared to those of similar structures like [7]helicene or [7]heliophene, and no separation of both enantiomers was possible. This might be attributed to the enormous flexibility of the whole structure and the fact that the distortion required for a clear racemization was spread over a large number of bonds and angles.

In order to overcome this difficulty, they introduced two modifications in their expanded helicene's structure: an arylene-bridge meant to increase configurational stability in **83** and the transformation into figure-eight dimer **84** again *via* $[2+2+2]$ cycloaddition (Figure 19).

Unfortunately, these modifications did not have a significant effect on the enantiomerization barrier, and no chiral resolution of their enantiomers at room temperature was possible by any means.

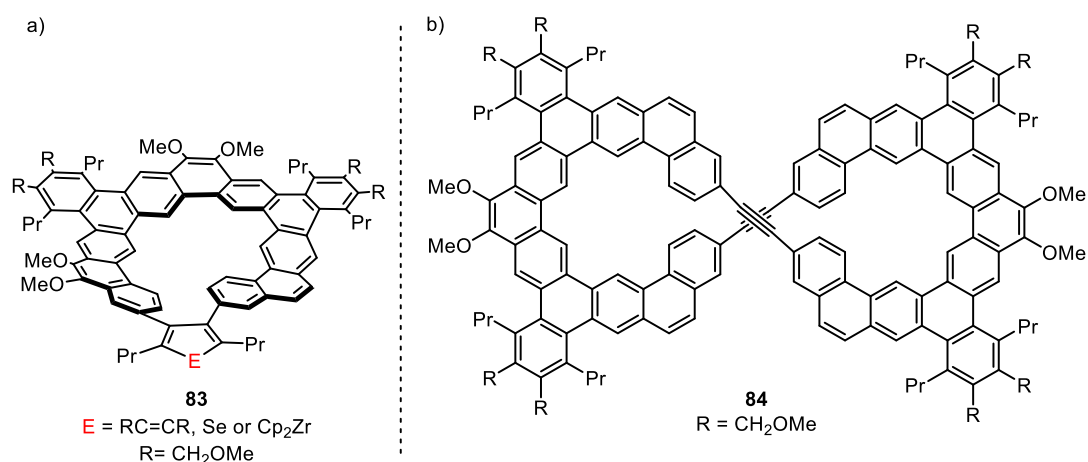


Figure 19. a) Arylene-bridged expanded helicene. b) Figure-eight expanded helicene.

Among other researchers, Matsuda and co-workers contributed to the expansion of this field. They achieved the synthesis of potentially chiral helical analogue of kekulene **86** *via* ring-closing metathesis as a key step and looked into the study of its structure, luminescent properties and racemization process. However, the excessive flexibility of the structure could not provide a high enough racemization barrier, and no separation method to isolate both enantiomers could be found (Figure 20).^[45]

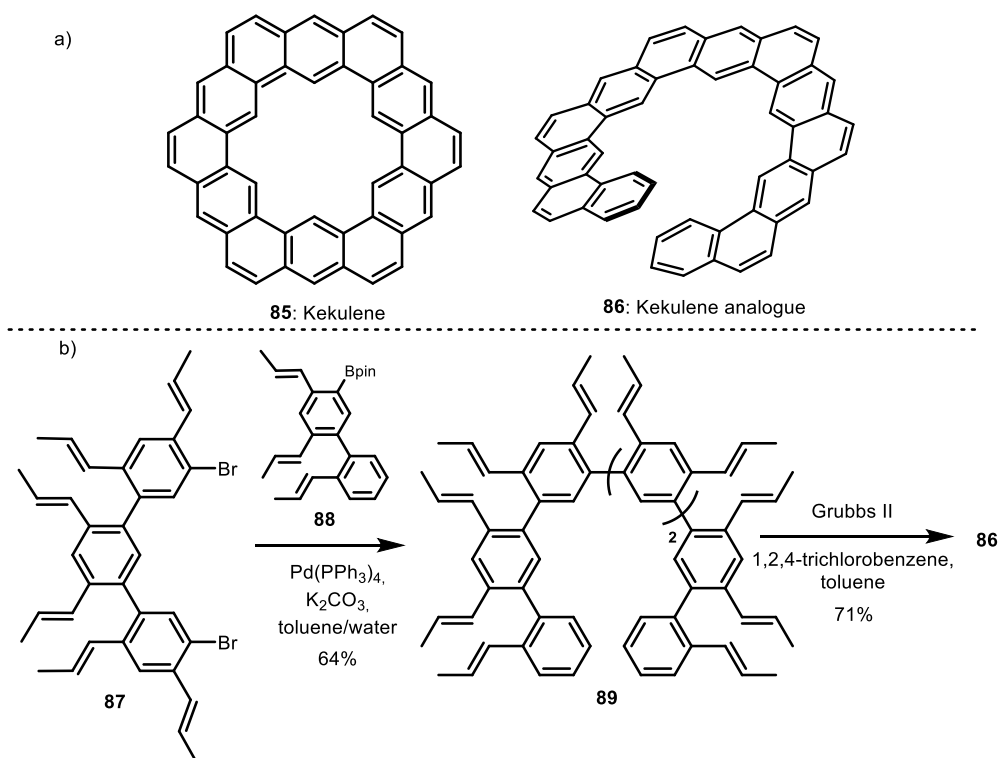


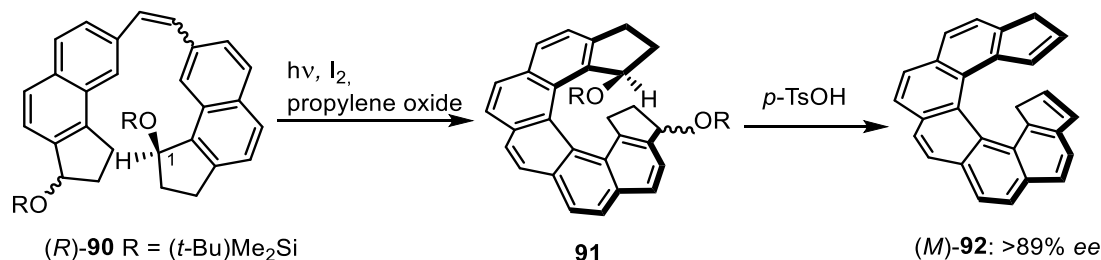
Figure 20. a) Kekulene (**85**) and Matsuda's kekulene analogue **86**. b) Key steps in the synthesis of the helically twisted analogue of kekulene **86**.

2.1.4. Asymmetric synthesis of helicenes

Although numerous reports were published since the first helicene was produced in 1912, it was not until many decades later in the 1970s, when the first asymmetrical syntheses of helicenes came to light. A pioneer in this topic was Weissman, who carried out the enantioselective reduction of racemic [6]helicene with potassium metal in (+)-2,3-dimethoxybutane. The resulting radical anion also demonstrated enough configurational stability to show optical activity by circular dichroism spectroscopy.^[122] However, the challenge of producing helicenes in a stereoselective manner was carried out through different methodologies.

2.1.4.1. Chemically induced asymmetric photocyclization

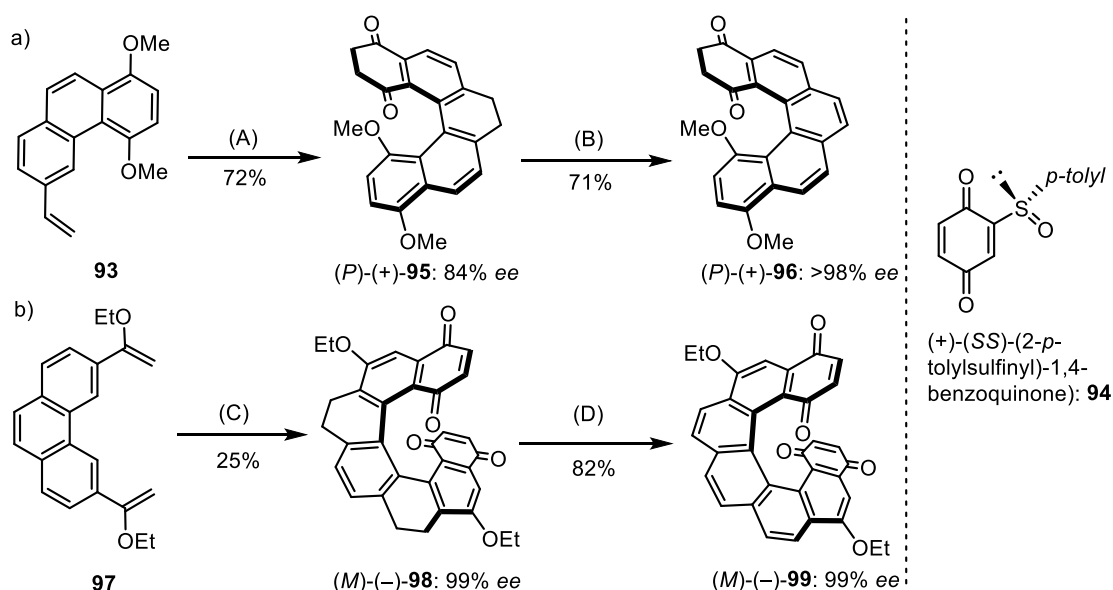
A very efficient method for generating enantioenriched helicenes is the introduction of bulky substituents at an already existing chiral center. This strategy was developed by Katz and Sudhakar in 1986 when they introduced a bulky *tert*-butyl-dimethylsilyloxy group in a chiral center at the position 1. This influenced strongly the further photocyclization by keeping the bulky substituent outside to lower the activation energy and, as a result, a big excess of carbo[7]helicene **92** in its *M* form was obtained (Scheme 16).^[95]



Scheme 16. Enantioselective photosynthesis of a carbo[7]helicene developed by Katz and Sudhakar.^[95]

2.1.4.2. Asymmetric Diels-Alder reactions

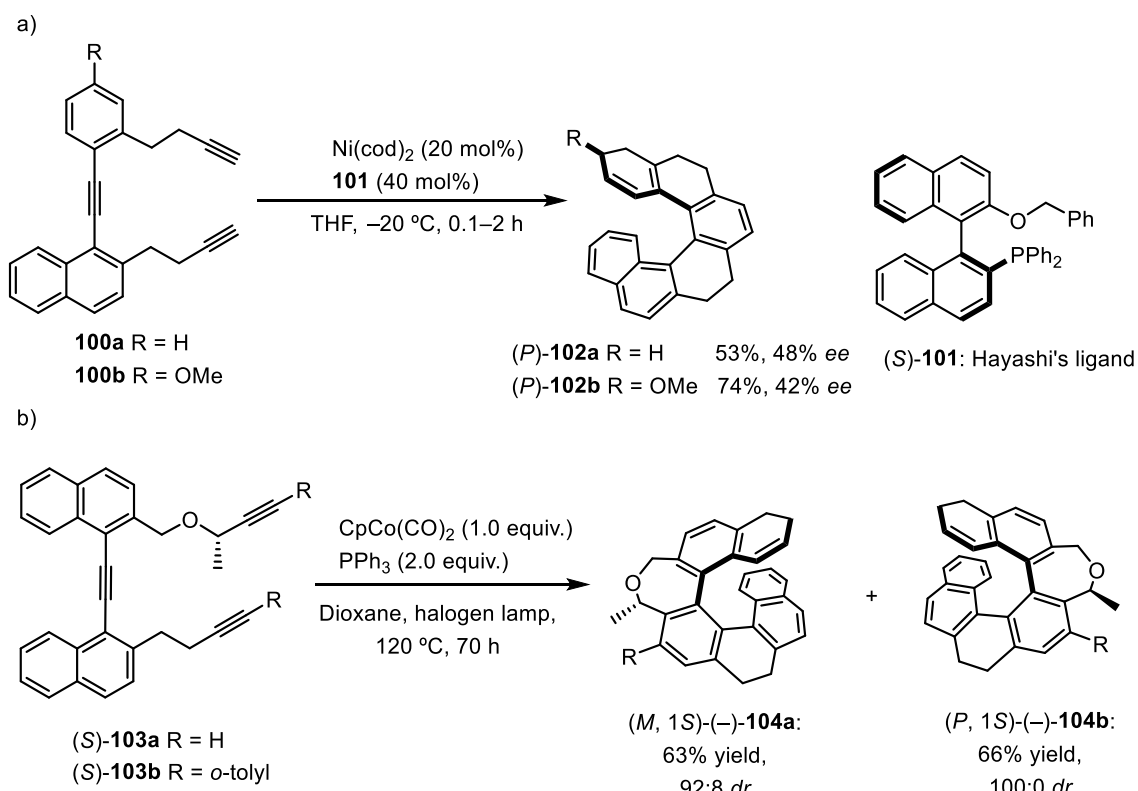
In 2001, Carreño and Urbano, who were experienced in the stereoselective synthesis of carbohelicenes,^[123] reported on the first enantioselective synthesis of a (*P*)-[5]helicene (*P*)-(+)-**96** *via* Diels-Alder reactions with *ee* superior to 98%. To achieve this, they clarified four key conditions: low temperatures to enhance enantioselectivity, the presence of electron-donating substituents in the dienes to lower the activation energy, the use of (+)-(SS)-(2-*p*-tolylsulfanyl)-1,4-benzoquinone **94** as the dienophile and, finally, employment of electron-rich dienes to facilitate the aromatization procedure (Scheme 17a).^[124] Their success in this project encouraged them to apply the same strategy in order to obtain [7]helicene **99** with excellent *ee* as well (Scheme 17b).^[125]



Scheme 17. Enantioselective Diels-Alder reactions for the synthesis of [5]- and [7]helicenes. Reactants and conditions: (A) (SS)-**94** (2 equiv.), CH_2Cl_2 , -20°C , 7 d. (B) DDQ, benzene, reflux, 4 d. (C) (SS)-**94** (4 equiv.), CH_2Cl_2 , -20°C . (D) DDQ, toluene, Δ .

2.1.4.3. Metal-catalyzed asymmetric synthesis

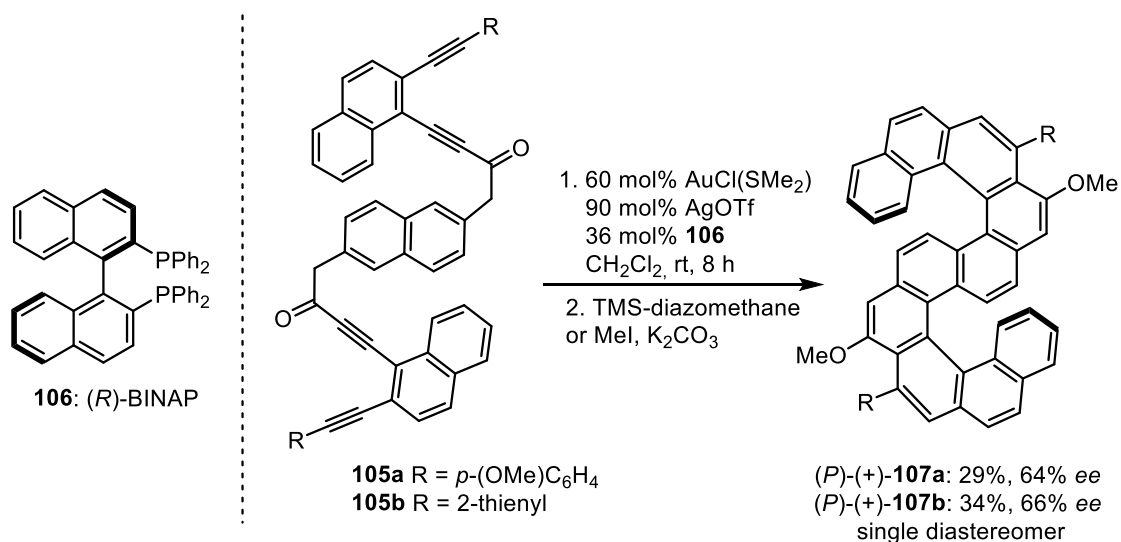
Starý and Stará reported one of their first experiences in the enantioselective synthesis of helicenes in 2003 when they performed a stereoselective [2+2+2] cycloisomerization of triynes **100a** and **100b** in the presence of a Ni(0) catalyst and Hayashi's ligand to obtain tetrahydro[6]helicenes **102a-b** with moderate *ee* (Scheme 18a).^[126,127] Two years later, they updated their methodology through a new approach: the transference of central to helical chirality. This time the key of the [2+2+2] cycloisomerization of aromatic triynes was the presence of a chiral center and its influence on the Co(I)-mediated cyclization. A scope of different substrates **103** containing such pre-defined center alongside a *p*-tolyl group in the alkyne moieties underwent photocyclization under a wide range of temperature and time conditions, affording [7]helicene-like frameworks **104a-b** in diastereomeric ratios up to 100:0 (Scheme 18b).^[128]



Scheme 18. Cycloisomerization of triynes to provide tetrahydro[6]helicenes **102** ^[126] and [7]helicene-like scaffolds **104**. ^[128]

Although π -acid-catalyzed cycloisomerization is widely used in the synthesis of helicenes, its application in their enantioselective synthesis is relatively recent.

One of the most remarkable achievements in this area dated back to 2013, when Stará, Starý and co-workers reported the first enantioselective synthesis of a carbo[6]helicene by Ni-catalyzed [2+2+2] cycloaddition of aryl alkynes.^[129] Later, in 2018, Tanaka's group investigated the enantioselective synthesis of helicenes bearing varied structures *via* either Rh(I)-catalyzed intramolecular cycloadditions^[130] or Au(I)-catalyzed intramolecular hydroarylation (Scheme 19).^[131]

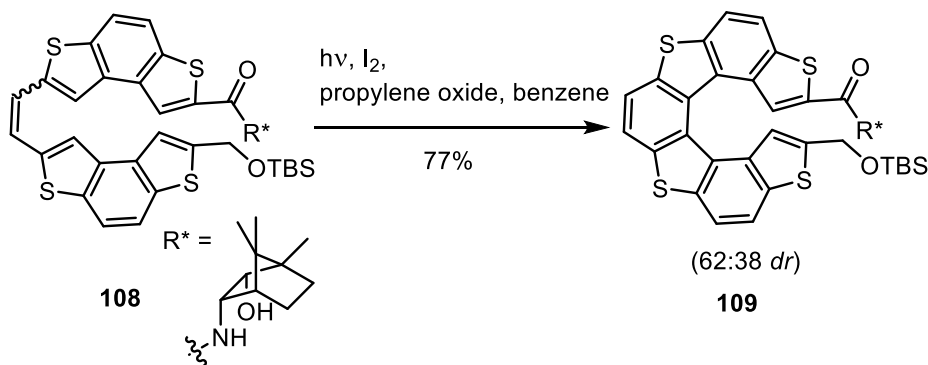


Scheme 19. Enantioselective synthesis of double [6]helicenes **107a-b** by Tanaka and co-workers.^[131]

In this latter case, the formation of single and double carbo[6]helicenes in moderate *ee* was achieved by using Au(I)-based catalyst AuCl(SMe₂) alongside the chiral ligand (*R*)-BINAP **106**. This was the first ever reported enantioselective synthesis of completely benzenoid multihelicenes.

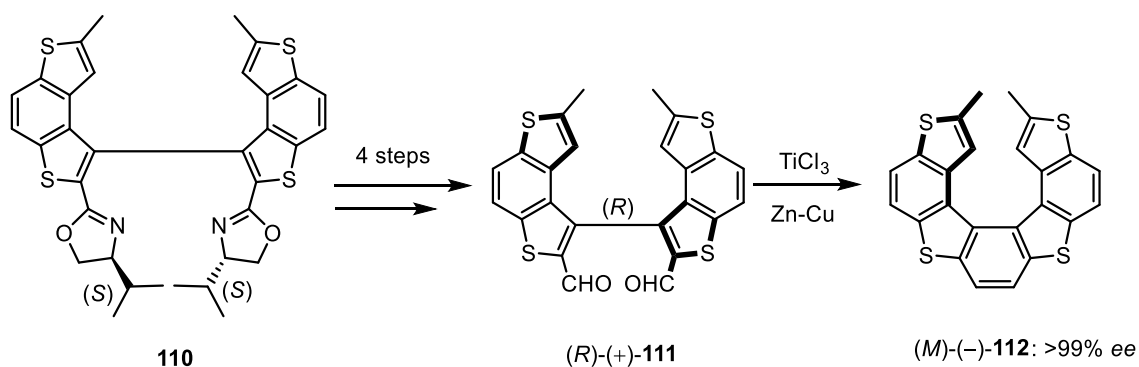
2.1.4.4. Asymmetric synthesis of thiahelicenes

As with the carbohelicenes, the preparation of the first enantio-enriched samples of thiahelicenes was a major synthetic challenge that had been worked on for more than four decades. The first preparations consisted of the application of photochemical techniques to olefin-based substrates embedding multiple sulfur atoms and subsequent enantiomers resolution.^[99,132] However, the poor chiral separations achieved prompted further researchers to seek for more effective methods like the introduction of chiral auxiliaries or chiral elements (Scheme 20). Such changes should enhance the stereoselectivity of the reaction and, therefore, facilitate further separation of the resulting diastereomers.



Scheme 20. Photocyclization of **108** to furnish tetrathia[7]helicene **109**.

It was not until 1997 that successful asymmetric syntheses of thiahelicenes came to light. The most remarkable case was reported by Tanaka and co-workers, who accomplished a novel and efficient synthesis of thiahelicenes based on biaryl- and carbonyl-coupling reactions.^[133] Soon after, they applied this methodology in the synthesis of similar adducts containing chiral centers. Because these had the capacity to influence the helical chirality, highly enantioenriched samples of thiahelicenes **112** were obtained, giving rise to the first reported stereoselective synthesis of this kind of polyaromatic compounds (Scheme 21).^[134]



Scheme 21. Tanaka's stereoselective synthesis of thia[7]helicenes.^[134]

In summary, despite all these advancements in the last century, the asymmetric synthesis of helicenes is yet to be developed and investigated, especially in the field of heterohelicenes. Moreover, the synthesis of expanded helicenes remains enormously intriguing and most recent studies have demonstrated the existence of suitable tools to achieve the generation of configurationally stable examples of these molecules. As it will be discussed in the following Section, one elegant way to achieve this goal is the use of such transition metals like platinum, palladium or gold.

2.2. Gold catalysis

Gold has had for millennia an unquestionable presence in popular culture. Due to its rareness, it has been widely used in the production of valuable items like coins or jewelry. Nevertheless, gold possesses as well great mechanical properties: it is a highly ductile and durable metal, and it shows great resistance towards oxidation or light. For this reason, its usage has been extended to the production of materials suitable for such varied fields like medicine or electronics. When speaking of its role in chemistry, gold had been ignored for decades as a potential catalyst despite owning a rich coordination and organometallic chemistry.

It was not until 1973, when it was first used as such in the heterogeneous catalysis of olefins by Bond and co-authors.^[135] This report became a landmark for further research, in which this metal was used in the hydrochlorination of acetylene^[136] and the oxidation of carbon

monoxide.^[137] Since then, gold has gained increasing importance amongst other transition metals in catalytic research.

2.2.1. Gold as a carbophilic Lewis acid

Gold is a Group 11 element and its oxidation states ranges from -1 to $+5$, but it is most seen as either Au(I) or Au(III). In coordination chemistry, the former is mostly observed forming linear complexes, whereas the latter tends to form square planar ones. When speaking about Au(I) complexes, geometrical constraint generally places the ligand (L) and the substrate on opposite sides of the metal center. On the other hand, mono-coordination enables a wide a free rotation of all components around the existing single bonds (Figure 21).^[138]

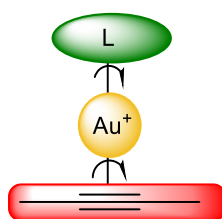


Figure 21. Coordination mode for Au(I) complexes. ^[138]

Due to its low lying, large and polarizable empty orbitals, gold is considered a reliable, carbophilic and chemically soft Lewis acid, with π -acid catalysis being its most important application.^[139–141]

π -Acid catalysis is the electrophilic activation of C-C π bonds with a Lewis acid. It is a useful and elegant way to convert alkyne, alkene or allene derivatives into useful building blocks. Although other elements such as platinum, indium or even gallium have been extensively used in this area, gold is still one of the most demanded Lewis acids because of its unique properties.^[142]

The basic mechanism of this reaction performed by a Au(I) complex is depicted in Figure 22.^[143–145] Such species is initially present as L·AuX, where L represents an auxiliary ligand and X is a counterion, usually Cl⁻.

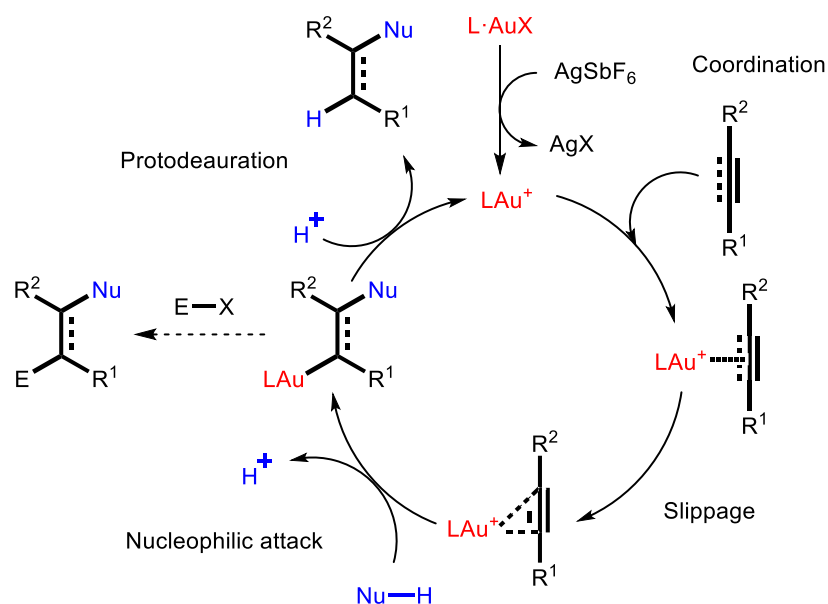
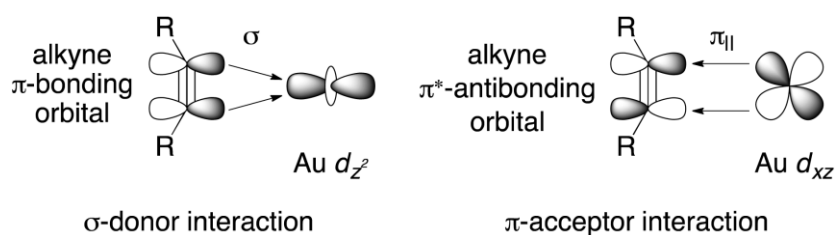


Figure 22. General mechanism of gold-mediated π -acid catalysis reaction.

In general, the π -acid catalytic cycle of Au(I) begins with the activation of the gold species through silver-mediated abstraction. The Ag^+ cation, in this case coming from AgSbF_6 , reacts with the gold's counterion, forming an insoluble salt, and releases the Au(I) activated species. This latter one possesses a coordination vacancy, which is then filled by the formation of a π -complex with a suitable donor, such as an alkyne, allene or alkene. The following step takes place *via* π -slippage, this step involves the movement of the metal fragment along the axis of the ligand which, in turn, results in enhanced electrophilicity. This slippage depends on the substituents of the alkyne as well: their electronic or steric distribution among other factors can determine the different regioisomers that can be originated.^[140] Then, an external nucleophile attacks the gold- π -system in an outer sphere mechanism and forms an *anti*-oriented gold carbenoid intermediate. Once this step has taken place, the created species can undergo either a protodeauration process to form the desired product and to re-originate the active gold catalyst, or alternatively, several further cascades, polymerizations or rearrangements.^[146–148]

The bonding situation in transition metal complexes with alkenes or alkynes as π -ligands is usually explained through the Dewar-Chatt-Duncanson (DCD) model, which interprets the bond as a donor–acceptor interaction between two closed-shell fragments.^[149,150]



Scheme 22. Schematic representation of the Dewar-Chatt-Duncanson model. Image taken from: C. J. V. Halliday, J. M. Lynam, *Dalton Trans.* **2016**, 45, 12611–12626.^[151]

It is generally accepted that a σ -bond is formed by electron donation of the ligand to an empty metal orbital of suitable symmetry, on the contrary, a π interaction takes place through the back donation of electron density from an occupied metal d orbital into an antibonding π^* orbital of a ligand.

In Figure 23, four possible interactions contributing to the bonding of alkynes as ligands have been represented. In the first place, the alkyne can form a $M \leftarrow L$ σ -complex by donating electron density of its in-plane $\pi_{||}$ orbital into the empty d_{z^2} metal orbital. In the same way, π -symmetric $M \rightarrow L$ back-donation can take place between the d_{xz} metal orbital and the $\pi_{||}^*$ orbital of the alkyne. Besides, other remarkable metal-alkyne interactions are the $M \leftarrow L$ π -donation from the orthogonal, out-of-plane alkyne π_{\perp} orbitals to the empty d_{yz} metal orbital, in which the ligand acts as a four-electron donor. Lastly, $M \rightarrow L$ δ symmetry interactions between the filled metal d_{xy} orbital and the empty π_{\perp}^* orbital of the alkyne are also possible. The δ symmetry of this latter interaction results in only a weak overlap, and therefore leads to a minor contribution to the bonding.^[140]

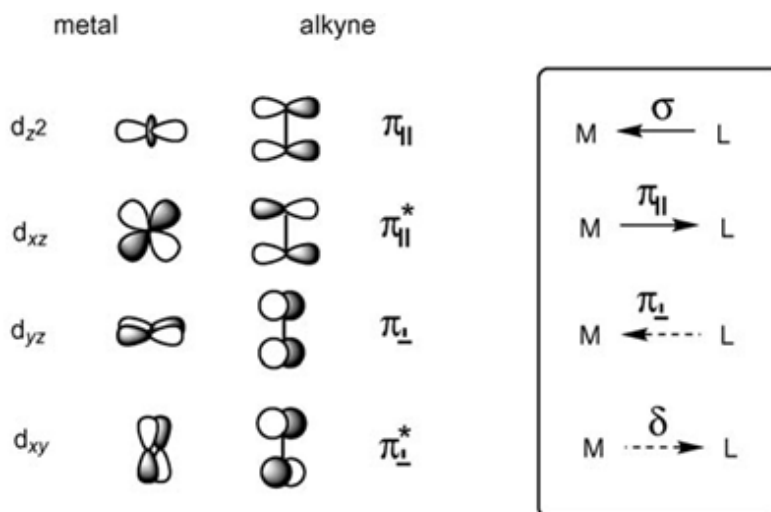


Figure 23. Qualitative orbital diagram displaying the interaction between a transition metal and an alkyne in the framework of π -acid catalysis. Modified image from: A. Fürstner, P. W. Davies, *Angew. Chem. Int. Ed.* **2007**, 46, 3410–3449.^[140]

Furthermore, the contributions of these four interactions to the Au-alkyne bond were calculated by high level computational methods. For the Au⁺-acetylene complex [Au⁺(C₂H₂)], the δ-interaction proved to provide the largest contribution (ca. 65%), followed by the in-plane π_{||} back-donation (ca. 27%), the effect of the orthogonal π_⊥ term, and lastly, that of M→L δ term (ca. 1%). As a conclusion, alkynes (as well as alkenes) are strong two-electron δ-donors and provide the biggest contribution to the bond energy, but at the same time, they are weak π-acceptors towards Au(I). Nonetheless, the back-donation from the gold center has as well an important involvement in the bond that should be considered.^[152–154]

As expected, the formation of the complex entails a change in the bond length and in its geometry: According to the DCD model, an elongation of the double or triple bond takes place due to the net shift of electron density from the bonding π orbital into the antibonding π* orbital. Additionally, as a consequence of rehybridization, a deformation in the ligand takes place: alkynes experience bending in their geometry, whereas alkenes undergo partial pyramidalization.

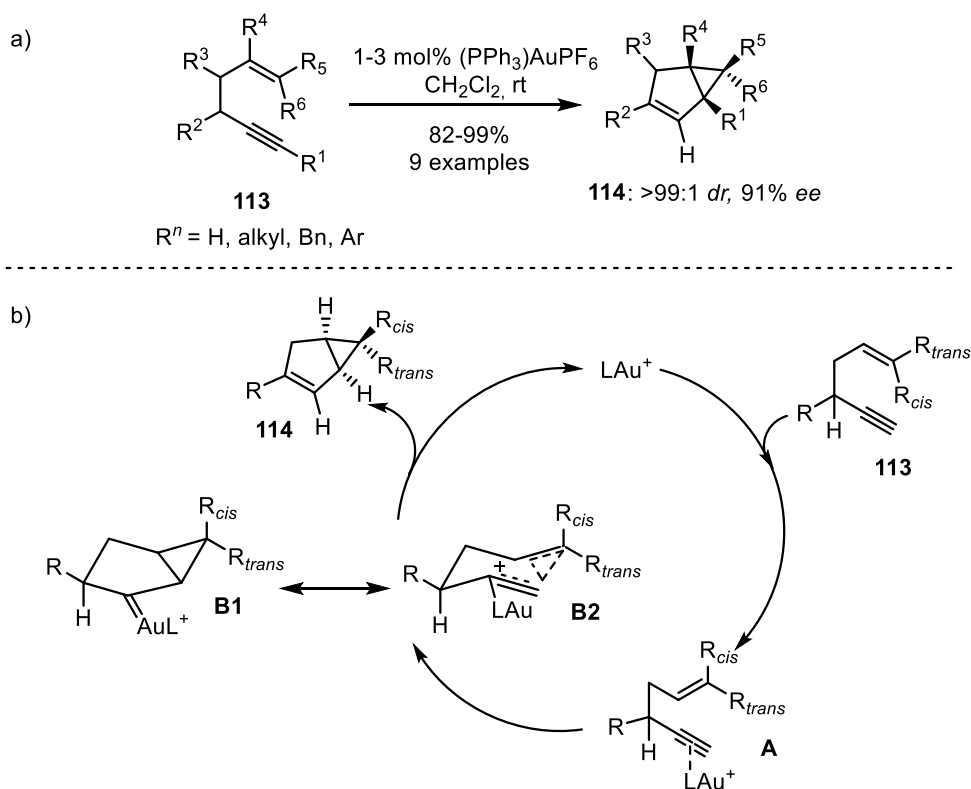
2.2.2. Applications of Au(I)-mediated π-acid catalysis

Since the early report from Bond *et al.* in 1973,^[135] the use of gold has experienced an exponential growth in the field of homogeneous catalysis and has showed multiple and important virtues: operationally safe, simple and practical reaction conditions, elegant and notably atom-economical catalyses or an exceptional chemoselectivity towards C-C π-systems, leaving most of other existing functional groups intact. Hundreds of reports concerning such varied topics like carbonyl activation, oxidations, reductive and dehydrogenative processes or group transfer reactions have been published in the last decades,^[155–162] nevertheless, this Section will be focused on the addition of carbon nucleophiles to electrophilic π-systems.

2.2.2.1. Cascade reactions

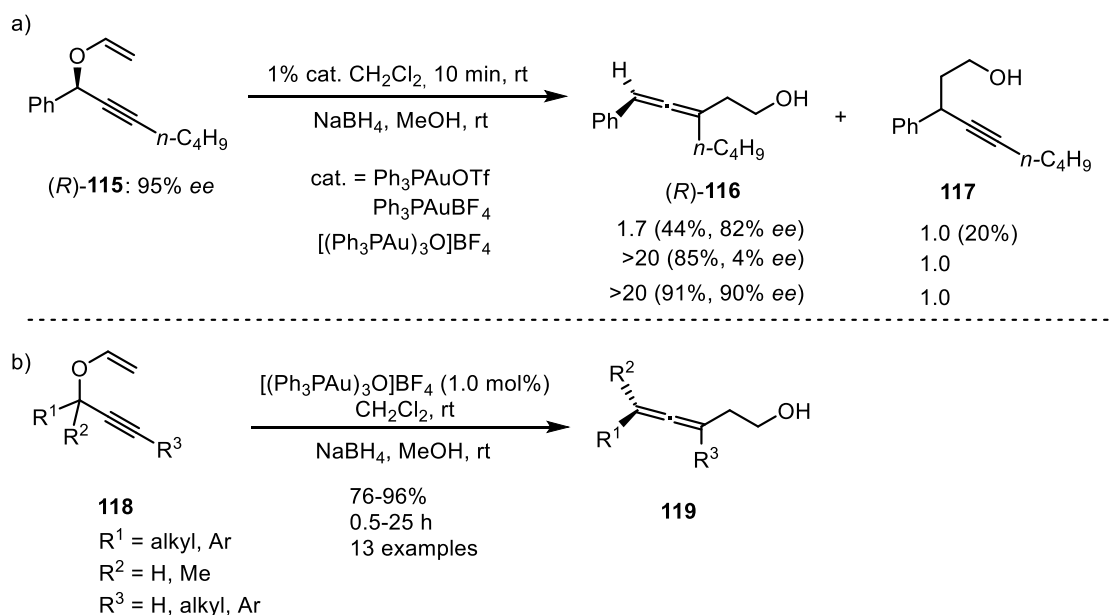
One example of this latter case is the cascade reaction. In 2004, Toste and co-workers reported the catalytic isomerization of 1,5-enynes to form bicyclo[3.1.0]hexenes.^[163,164] After optimization of catalysis conditions, they found out that (PPh₃)AuPF₆ was the most suitable catalyst for such rearrangement. A wide range of 1,5-enyne substrates **113** underwent this Au(I)-catalyzed transformation. Despite the presence of different and numerous substituents along the enyne structure, yields up to 99% and excellent *dr* as well as *ee* were obtained, proving the aforementioned selectivity of this kind of reactions (Scheme 23a). Based on the obtained results, they proposed the following mechanistic rationalization depicted in Scheme 23b: Coordination of the active species of Au(I) to the alkyne moiety in **113** followed by 5-*exo*-

dig-cyclization via nucleophilic addition of the pendant olefin in the intermediate **A** produces positively charged cyclopropyl gold carbene **B1**, which may be considered in resonance form of bicyclobutonium-type intermediate **B2**. Finally, the bicyclo[3.1.0]hexene product is generated by a 1,2-hydrogen shift onto a cationic or carbenoid center. The final bicyclic product **114** is formed upon release of Au(I) catalytic active species. Regarding stereoselectivity and stereospecificity, the reaction can be accounted for by considering half-chair transition states, with the large groups occupying pseudoequatorial positions, similar to those proposed for the acetylenic Cope rearrangement.^[165]



Scheme 23. a) Scope of Au(I)-Catalyzed synthesis of bicyclo[3.1.0]hexenes **114**. b) Proposed mechanism for the Au(I)-catalyzed cycloisomerization.^[163]

Another interesting example was reported by Toste in the same year as well. In full swing of Au(I)-mediated catalysis, Toste developed a suitable methodology for propargyl Claisen rearrangements replacing common transition metal cations like Hg(II) and Pd(II) with Au(I).^[166] An optimization of the catalytic conditions was carried out in the first place (Scheme 24a). Out of the three tested Au(I) catalysts, [(Ph₃PAu)₃O]BF₄ demonstrated to be the most suitable one showing the best yield and regioselectivity without barely modifying the existing chiral center in the allene **116**. Once the optimal catalyst was identified, a complete scope with 13 examples containing different substituents was accomplished in very good yields and short reaction times (Scheme 24b). Not only this catalyst was compatible with mild conditions and low moisture, but it proved to be suitable for enantioenriched samples as well.



Scheme 24. a) Comparison between different Au(I) catalysts. b) Scope of Au(I)-catalyzed propargyl Claisen rearrangement.^[166]

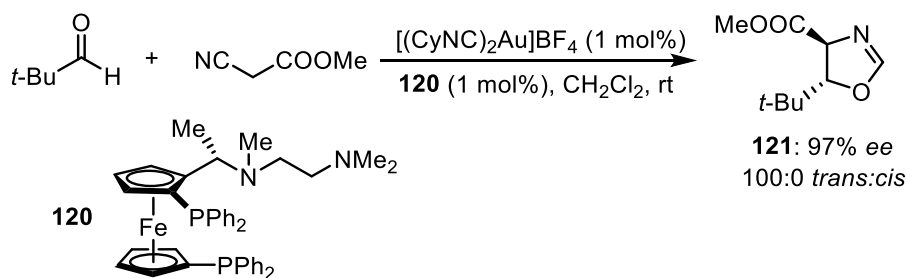
2.2.2.2. Asymmetric Au(I)-catalysis

Asymmetric catalysis is typically a strategy where a transition metal complex containing a chiral ligand catalyses the transformation of a prochiral substrate into one enantiomer as a major product.^[167] The selective synthesis of a single stereoisomer over others has been a challenge of great importance in industry over the past century, not only in the pharmaceutical area, but also in others like material science or agrochemicals. With this in mind, the direct enantioselective functionalization of C-H bonds has become a prominent tool towards the production of enantioenriched samples of chiral compounds, very occasionally based on transition metal catalysis.

Regarding gold catalysis, the development of effective asymmetric catalytic transformations is still a laborious task. The main difficulty is related to the linear geometry of Au(I) complexes: since the gold reactive center is placed at the opposite side of the chiral complex, the induction of stereoselectivity can be extremely hard.^[168] In this context, Au (III) complexes might be more appealing due to their square planar structures capable of bringing the substrate closer to the chiral ligand, but the synthesis of stable and catalytically active species containing this cation remains very difficult.^[169,170]

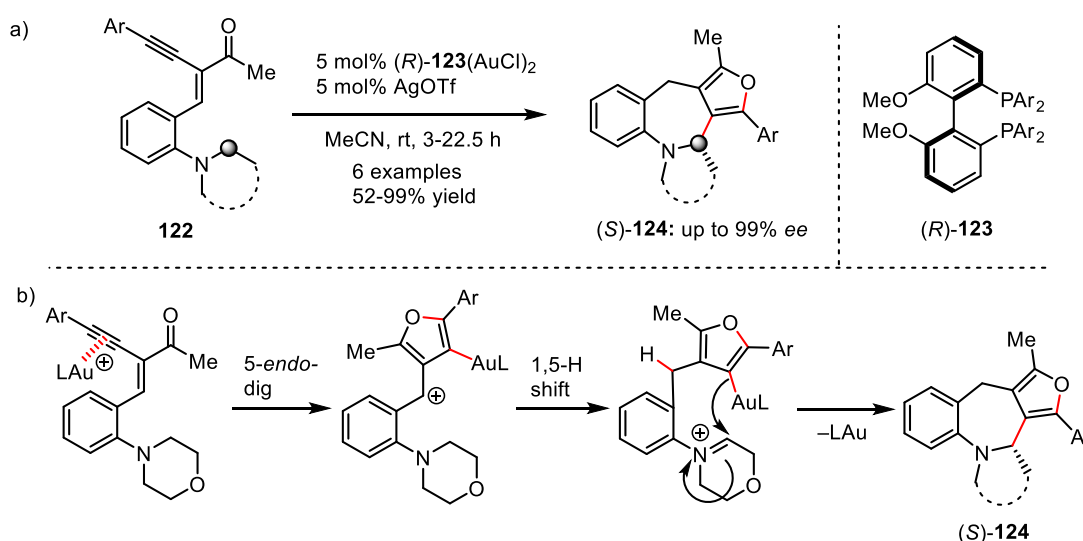
The first report on asymmetric gold catalysis dates back to 1986, when Ito, Hayashi and colleagues performed an asymmetric aldol reaction between pivalaldehyde and isocyanidoacetate catalysed by a Au(I)-ferrocenylphosphine complex **120**, which has a planar

chirality (Scheme 25). The presence of the bulky amino group was one of the keys to achieve high diastereo- and enantioselectivities.^[162]



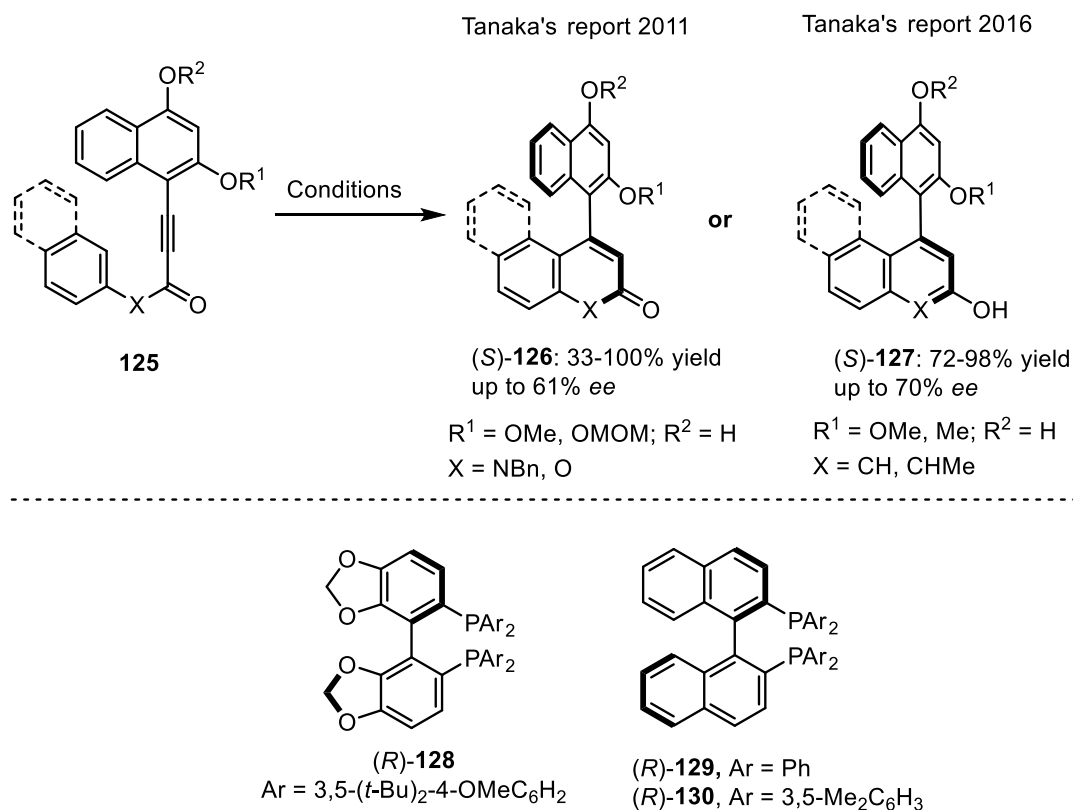
Scheme 25. Asymmetric aldol reaction performed by Ito, Sawamura and Hayashi.^[162]

Since this early discovery, asymmetric Au(I) catalysis has been broadly used in the C-H functionalization chemistry. Starting with C(sp³)-H functionalization, this application of Au(I) catalysis has experienced a considerable growth, despite the difficulties associated with it (e.g., low acidity of Csp³-H bonds or high bond dissociation energy). In 2011 Zhang *et al.* reported the Au(I)-catalyzed asymmetric synthesis of furan-fused azepines **124** from yne-enones **122**.^[171] They presented the first example of enantioselective redox-neutral domino reaction catalyzed by Au(I) resulting in the direct functionalization of unreactive sp³ C-H bonds. After screening different phosphine ligands, six examples of this family of compounds were obtained in good yields and excellent *ee* by using different bulky (*R*)-MeO-dtbm-BIPHEP **123** as chiral ligands alongside AgOTf (Scheme 26a). The proposed mechanism suggests that the reaction proceeds *via* 5-*endo*-dig cyclization to generate cationic intermediate which would undergo 1,5-hydride shift and further cyclization to form the desired furan-fused azepines **124** (Scheme 26b).



Scheme 26. a) Scope of the asymmetric gold(I)-catalyzed redox-neutral domino reactions. b) Proposed mechanism.^[171]

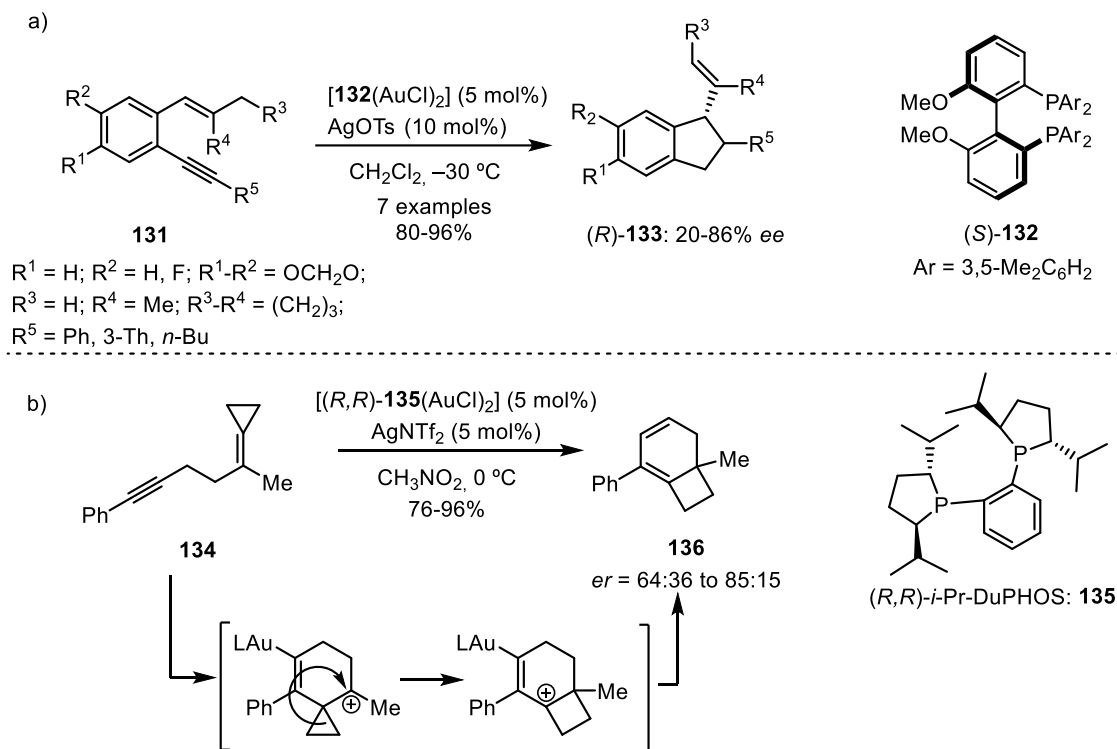
However, the hydroarylation reactions through enantioselective gold-catalyzed C(sp²)-H functionalization has been the most fruitful method in comparison to that involving C(sp³) or C(sp). These transformations turned out to be a convenient key step in the formation of new C(sp²)-C(sp²) bonds, which determine the chirality of a molecule. The most notorious applications of this strategy are among others the enantioselective intramolecular hydroarylation of allenes and alkynes. In the framework of the latter, Tanaka and co-workers became pioneers in 2011 when they reported the atroposelective synthesis of axially chiral 4-aryl-2-quinolinones and 4-arylcoumarins **126** *via* hydroarylation of alkynes **125**. The species chosen for this task were (*R*)-dtbm-SEGPHOS- and (*R*)-BINAP-based gold catalysts **128** and **129**, two dinuclear complexes which afforded the desired products in moderate *ee*'s up to 61%.^[172] Later, in 2016, they extended this strategy to all-benzenoid derivatives by using (*R*)-xylyl-BINAP **130** as a chiral ligand, obtaining seven different products in up to 70% *ee* (Scheme 27).^[173]



Scheme 27. Gold(I)-catalyzed asymmetric synthesis of axially chiral biaryls via intramolecular hydroarylation of alkynes. Reactants and conditions: (A) 20 mol% AuCl·SMe₂, 10 mol% (*R*)-**128** or (*R*)-**129**, 20 mol% AgBF₄, CH₂Cl₂, rt, 40-72 h; (B) 20 mol% AuCl·SMe₂, 12 mol% (*R*)-**130**, 20 mol% AgOTf, CH₂Cl₂, 40 °C, 24 h.^[172,173]

Other researchers have exploited the usage of binuclear complexes in the activation of alkynes with Au(I) as well. Sanz and co-workers investigated the catalytic applications of (*S*)-MeO-BIPHEP-based ancillary ligands like **132** containing Au(I) centers. When bearing xylyl groups, these ligands proved to afford the desired products in high enantioselectivities, again due to these bulky substituents (Scheme 28a).^[174] In another example, Gagné's group reported the

enantioselective ring-expanding cycloisomerization of 1,5-enynes **134** to provide bicyclo[4.2.0]octadienes **136** in excellent yields and good *er*'s (Scheme 28b).^[175]



Scheme 28. a) Sanz's enantioselective cycloisomerization of 2-Alkynylstyrenes **110**.^[174] b) Gagné's enantioselective ring-expanding cycloisomerization of cyclopropylidene 1,5-Enynes **113**.^[175]

Lastly, regarding the Au(I)-catalyzed enantioselective functionalization of C(sp)-H bond, only one report from the group of Toste was published in 2011.^[176] Additionally, the utilization of Au(I)-based phosphine ligands was found applications in the synthesis of natural products, showing in many cases excellent diastereo- and enantioselectivity.^[177,178]

2.2.3. Cationic phosphines

As noted in the previous Section, phosphorus-based ligands are a powerful tool of great relevance in organometallic chemistry and catalysis. In particular, phosphines have proven to serve as ancillary ligands for an impressive variety of homogenous transition metal catalyzed transformations.^[179] Their peculiarity lies in the easy modification of their electronic and steric parameters by simply varying the substitution pattern in the phosphorus center, facilitating the construction of large ligand libraries to be screened for specific catalytic processes.^[180-182]

2.2.3.1. Properties of cationic phosphines

Phosphines have proven to be extremely reactive and selective in transition metal-mediated catalysis, for this reason, in addition to those mentioned above, their use as ancillary ligands has spread to asymmetric homogeneous catalysis.^[183,184] In general, electron-poor metals

readily undergo reductive elimination reactions, whereas oxidative addition is favored on electron-rich metal centers, which can be in part obtained by the application of strongly electron-donating ligands. Both opposite cases, potent donor and strong acceptor ligands, can be achieved in phosphines by proper selection of substituents on the phosphorus core.^[185,186]

Phosphines are considered as σ -donor π -acceptor ligands: they interact with the vacant metal orbital of adequate symmetry through their lone pair of electrons, but at the same time experience π -backbonding due to the interaction between their σ^* antibonding orbitals and the occupied metal orbitals (Figure 24).^[187,188]

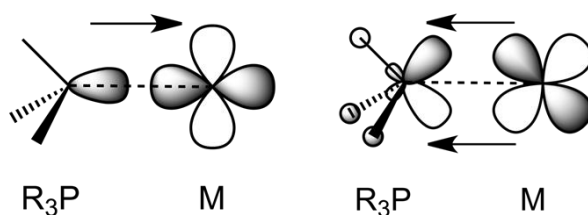


Figure 24. σ -Bonding and π -backbonding in phosphines-metal interactions. Image adapted from: A. G. Orpen, N. G. Connelly, *Organometallics* **1990**, *9*, 1206–1210.^[187]

While neutral phosphines are commonly regarded as weak π -acidic ligands, an increase of the electronegativity within the molecule results in a lowering of the LUMO-energy, rendering them mild π -acceptor ligand properties.^[181,185,187] One such strategy to increase the electronegativity is the introduction of cationic moieties in the α -position to the phosphorus atom, transforming neutral phosphines in α -cationic ones. This phenomenon can be explained through frontier orbitals, since the HOMO is primarily located at the phosphorus lone pair, and therefore providing the σ -donation, and the LUMO is composed by the σ^* -orbitals related to the three phosphorus substituents, providing the ligand with π -accepting properties. This formal increment of electronegativity is expected to lower the energy of all molecular orbitals of the phosphine at the same time, especially those with a significative component of the atomic orbitals of this particular R group (Figure 25, orbitals 1-5a'). As a consequence, the phosphine ligand behaves as an even poorer σ -donor and as a better π -acceptor.^[185]

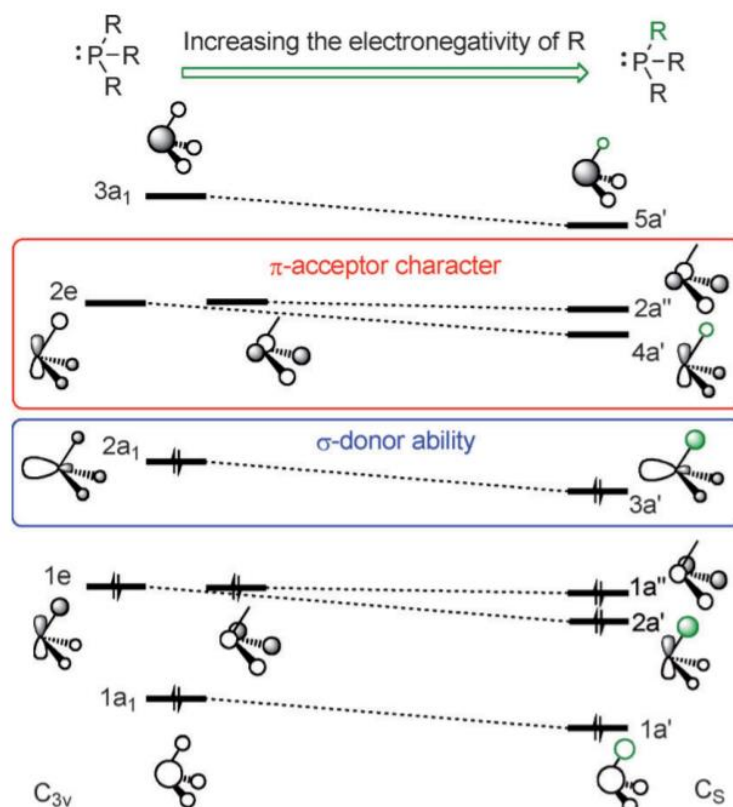


Figure 25. Depiction of the simplified molecular orbital diagram of a phosphine PR_3 and the resulting perturbation of replacing one R group with an electron-withdrawing substituent (green). Adapted from: Y. Jean, *Molecular Orbitals of Transition Metal Complexes*, Oxford University Press, Oxford, **2005**.^[189]

In addition to this basis, it is important to remark that most positively charged substituents that are introduced in a phosphine ligand are aromatic rings that may also contain empty low-lying π^* -orbitals capable of overlapping with those of the phosphine that possess adequate symmetry. Concerning these secondary interactions, two are especially important: the overlap between the phosphorus lone pair and the vacant π^* -orbitals of the cationic rest (Figure 26a) and the interaction between the π^* -orbitals of the R group and the one of the σ^* (P-C) orbitals (Figure 26b).^[181,185] The influence of this interaction has a noteworthy dependence on the LUMO energy of the positively charged rest and its spatial orientation. For this reason, those fragments conferred with the lowest LUMO energy will be able to maximize these secondary interactions and will present a higher tendency to behave as poor electron-releasing ligands.

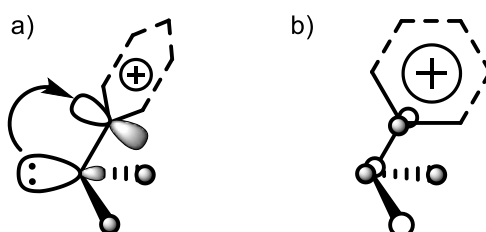


Figure 26. Secondary interactions between phosphines and positively charged aromatic substituents. a) interaction of the P lone pair with a π^* -orbital. b) overlap of a σ^* (P-C) orbital with a π^* -orbital of the cationic substituent. Adapted from: M. Alcarazo, *Chem. – Eur. J.* **2014**, *20*, 7868–7877.^[185]

One way to evaluate the donor and acceptor properties of cationic phosphines in a semi-quantitative manner is the Tolman analysis. It consists of the study of A_1 -symmetrical CO stretching frequency in compounds of general formula $Ni(CO)_3(L)$ in which L represents the phosphine concerned by comparing it with the stretching frequency of free CO (2143 cm^{-1}).^[190]

Thus, the so called Tolman electronic parameter (TEP) can be used to compare the net σ -donor and π -acceptor properties, not only for phosphorus-based ligands, but also for arsines and carbenes.^[191]

Strong σ -donors increase the electron density at the metal core, simultaneously weakening the C–O bond of the probe ligand and therefore, decreasing the energy of its stretching vibration. On the other hand, π -acceptor ligands compete with CO molecules for electron density of the metal and as a consequence, the difference in energy of the stretching vibration is less pronounced compared to that of free CO. This method implies nonetheless the important disadvantage of handling the highly volatile and extremely toxic $Ni(CO)_4$ to prepare the carbonyl ligands. Moreover, the substitution of a carbonyl group by another weakly releasing ligand is not an especially favored process and may take long reaction times. For this reason, other suitable alternatives like the use of $[MX(CO)_2L]$ ($M = Rh, Ir; X = Cl, I$) and $[RhCl(CO)L_2](X)_2$ have been used to analyze the overall σ -donor and π -acceptor properties.^[190,192] However, steric bulkiness of the ligands might distort the square planar geometry of the resulting complexes and, as a consequence, to alteration of the overlap between the orbitals of the metal and CO moieties. Because of this slight miscalculation, comparison of the resulting stretching frequencies is not always possible.^[180,193]

An important tool in the formation of coordination complexes is the Tolman stereoelectronic map, which facilitates the choice of an appropriate ancillary ligand regarding steric and electronic properties. It contains a great variety of ligands sorted by their cone angle (Θ) and their CO stretching frequency (ν_{CO}) (Figure 27).^[194]

properties of phosphines.^[194,198] This method is directly carried out on the free phosphine and reflects its TEP, since electron-rich phosphines can be oxidized more easily than electron-deficient ones and, therefore, the former exhibit lower oxidation potentials than the latter. Even though this method is used to a lesser extent than the Tolman analysis, it implies considerable advantages: it does not require the preparation of any toxic metal–carbonyl complex to perform the measurements, and it is also formally independent of steric factors, as it is directly carried out on the free ligand.

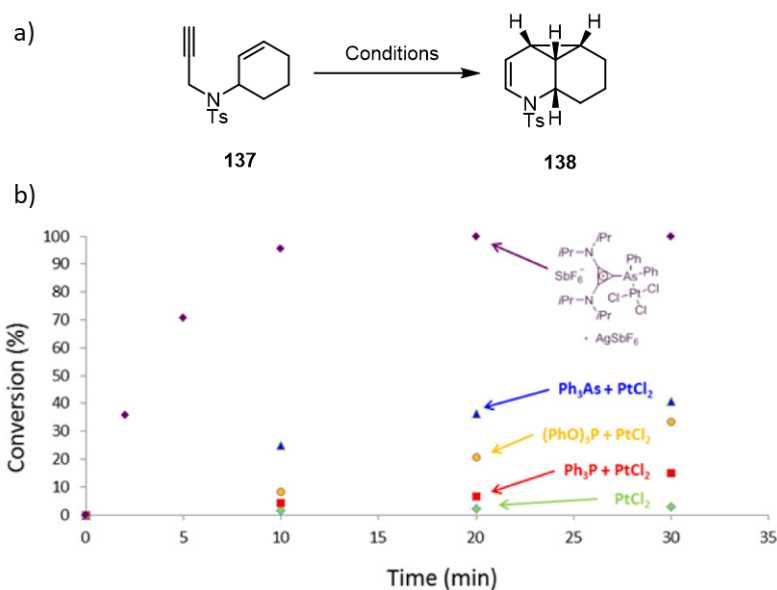
2.2.3.2. Applications in catalysis

Based on their saline nature, their high stability and their polarity, α -cationic phosphines were initially utilized in recyclable phase-transfer catalysts in polar or biphasic media. Many studies concerning the use of these compounds in greener media such as ionic liquids have proven to be a greener alternative to other more volatile and toxic solvents.^[182,199–202]

As mentioned above, the σ -donor properties of α -cationic phosphines have a significant influence on the electronic properties of the metals they coordinate. Furthermore, cationic ligands, as strong π -accepting substituents, can play a key role in catalysis: Either the unique electronic nature of the catalyst can influence the outcome of the reaction or their enhanced electrophilicity can alter the rate determining step.

Much of the pioneering works in this area were focused on different processes including hydrogenations^[203], hydrosilylations^[204] or hydroformylation of olefins^[205] as well as transition metal-mediated reactions such as Suzuki, Negishi, Sonogashira or Heck cross-couplings.^[199,206] However, the most interesting application of these ligands is the aforementioned π -acid catalysis involving Rh(I), Pt(II) and Au(I), which outperformed in many cases other commercially available catalysts.^[181,193,207–212] The point is that in these transformations, the nucleophilic attack proceeding from an external nucleophile is generally rate determining. Consequently, the additional electrophilicity induced at the metal is translated into faster reaction rates.^[182]

In the last decade, the Alcarazo group has taken an active interest in this field, applying a variety of structurally different α -cationic ligands to diverse catalytical processes. A reported example described the cycloisomerization of 1,6-enyne **137** to afford cyclopropa[de]hexahydroquinoline **138** using Pt(II) with different sorts of neutral and cationic ligands (Scheme 29).^[213]

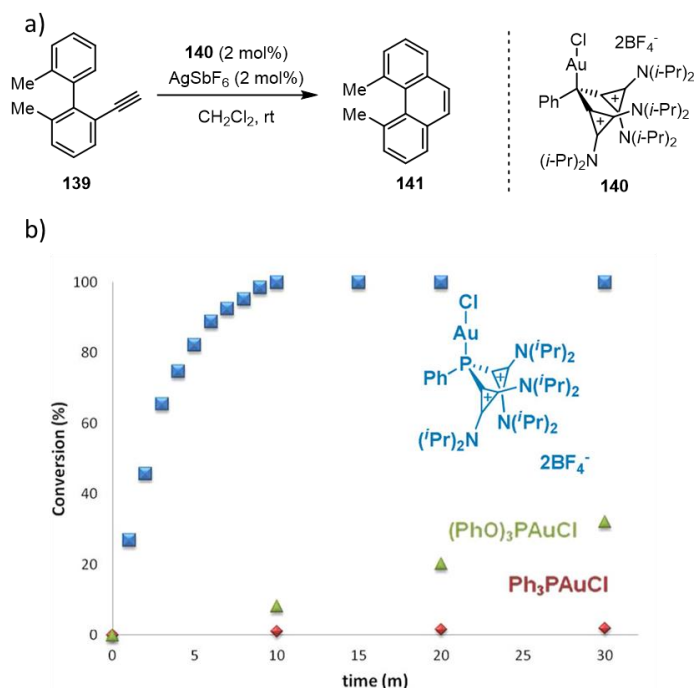


Scheme 29. a) π -Acid catalyzed synthesis of **138** from enyne **137**. b) Ligand effect on the Pt-catalyzed cycloisomerization. Reactants and conditions: **137** (0.05 M), Pt precatalyst, 2 mol%, AgSbF₆ 2 mol%, DCE, 80 °C. Image adopted from: J. W. Dube, Y. Zheng, W. Thiel, M. Alcarazo, *J. Am. Chem. Soc.* **2016**, *138*, 6869–6877.^[213]

In a preliminary study, the Au(I) complexes proved to be unsuitable catalysts and afforded very low yields with the concomitant formation of polymerization side products. Besides, those reactions catalyzed by platinum neutral species proceeded extremely slowly even when heated. Despite these suboptimal results, Pt(II)-based complexes with cationic phosphines demonstrated a catalytic activity far superior to that of any other catalyst tested. These results displayed how the modulation of the electrophilicity at the Pt atom can be translated into higher reactivities.

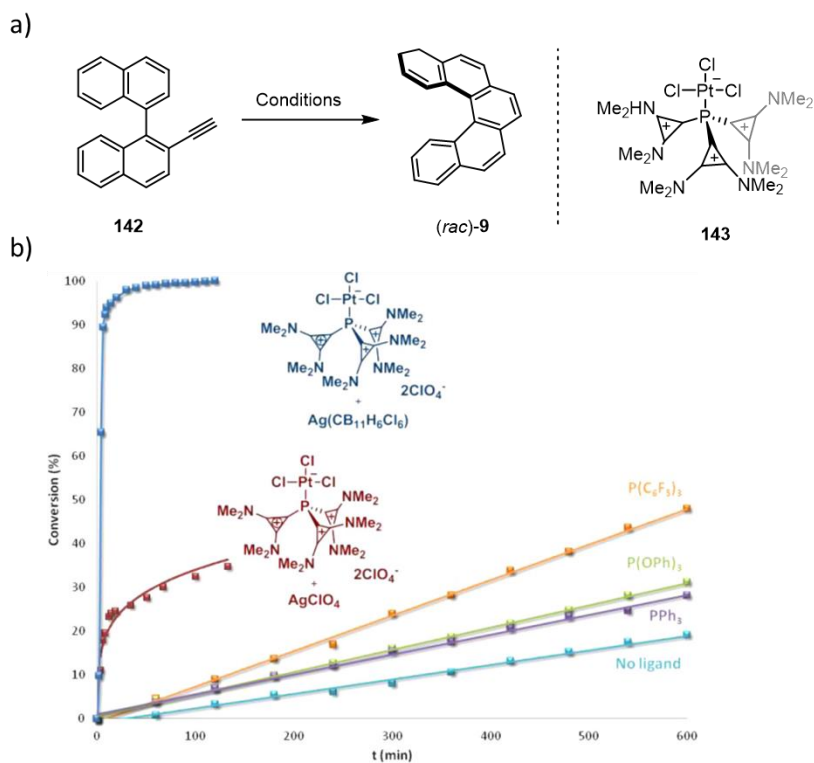
As stated in previous Sections, hydroarylation of alkynes are a reaction of great importance in the functionalization of C(sp²)-H bonds. One elegant and efficient manner to achieve this is through π -acid catalysis with the use of strong π -acceptor ligands. Hence, our group explored this issue through the catalyzed cyclization of 2-ethynylbiphenyls **139** into sterically hindered 4,5-disubstituted phenanthrenes **141**.^[181] In these substrates, the difficulties in forming the desired six-membered ring from the alkyne is due to the noteworthy torsion imposed by the internal substituents at positions 6 and 6', which undoubtedly hindered the approach of the aromatic ring to the gold-activated alkyne. In an initial screening, it was observed that cyclizations using Au(I) complexes containing polycationic moieties like **140** proceeded with an exceptionally high rate in comparison to other commercially available ligands (Scheme 30). It was assumed that a stronger activation of the alkyne moiety was due to higher Lewis acidity of the metal center. This change might have provided an earlier transition state for this step in which steric factors were less determining. This observation proved that simply replacing the ancillary ligand with a more π -acceptor one could turn the low-yielding reaction into a useful

tool for the synthesis of 4,5-disubstituted phenanthrenes and probably other polyaromatic structures as well.



Scheme 30. a) Gold-catalyzed intramolecular hydroarylation of *o*-alkynylbiphenyl **139** to afford 4,5-disubstituted phenanthrene **141**. b) Plot of conversion versus time comparing the catalytic activity of different Au(I)-phosphorus-based complexes. Image adapted from: J. Carreras, G. Gopakumar, L. Gu, A. Gimeno, P. Linowski, J. Petušková, W. Thiel, M. Alcarazo, *J. Am. Chem. Soc.* **2013**, *135*, 18815–18823. ^[181]

The synthetic potential of cationic phosphines as ancillary ligands was once again confirmed by the Alcarazo group in the Pt(II)-catalyzed intramolecular hydroarylation of binaphthalene **142** to form racemic [5]helicene **9**.^[214] This reaction was chosen as a model due to the low nucleophilicity of the naphthalene moiety. Thus, the nucleophilic attack on the activated alkyne, facilitated by the π -acidity of the metal center, became rate-determining (Scheme 31a). Commercially available phosphanes like (PhO)₃P, (C₆F₅)₃P or PPh₃ were employed as auxiliary ligands showing moderate accelerations. Unlike these neutral species, cationic phosphine **143** demonstrated a higher and more rapid conversion rate, especially when combined with the less coordinating and more soluble carborane-based silver salt Ag[CB₁₁H₆Cl₆] (Scheme 31b). With this late experiment, it was demonstrated that cationic phosphines were promising ancillary ligands in the π -acid catalyzed synthesis of helicenes and other PAH. With the optimized catalyst in hand, a library consisting of 22 biaryl-substituted alkynes was prepared and submitted to this procedure. The results demonstrated not only great conversions and regioselectivities, but also high functional group compatibility. The promising results of this report encouraged the group to continue their research on this topic and on more applications to this family of ligands.



Scheme 31. a) Cyclization of 2-ethynyl-1,1'-binaphthalene **121** into [5]helicene **9**. b) Ligand effect on the Pt(II)-mediated catalysis. Reactants and conditions: (A) Conditions for ligand = PPh₃, P(OPh)₃, P(C₆F₅)₃: **121** (0.05 M), PtCl₂ (5 mol %), and ligand (5 mol %), Cl(CH₂)₂Cl, 80 °C. (B) Conditions for precatalyst **122**: **121** (0.05 M), **122** (5 mol %), AgClO₄ or Ag[CB₁₁H₆Cl₆] (5 mol %), Cl(CH₂)₂Cl, 80 °C. Image adapted from: J. Carreras, M. Patil, W. Thiel, M. Alcarazo, *J. Am. Chem. Soc.* **2012**, *134*, 16753–16758.^[214]

In conclusion, gold-mediated π -acid catalysis has demonstrated to be an easy and elegant way to modify and functionalize C-C conjugated π -systems. One effective way to carry out this reaction is the use of cationic phosphines as ancillary ligands due to their excellent electronic properties as π -acceptor ligands withdrawing electron density from the metal center. Even though the use of these species extended to asymmetric catalysis in the synthesis of multiple π -systems, the employment of ligands containing novel tunable chiral backbones in the synthesis of helicenes remains a challenge.

3. Previous research in our group

Besides the study of Au(I)-mediated catalysis and the use of cationic phosphines as ancillary ligands, the Alcarazo group has additionally focused their research on the development of a series of chiral cationic phosphonites. These ligands were the next step in the development of chiral versions of cationic phosphines, specifically, cationic phosphonites of general formula **144** were chosen as target structures because of the chiral information provided by well-precedented TADDOL-derived moieties, their low price, their ease to be tuned and their suitability in asymmetric Au(I) catalysis.^[202,215,216]

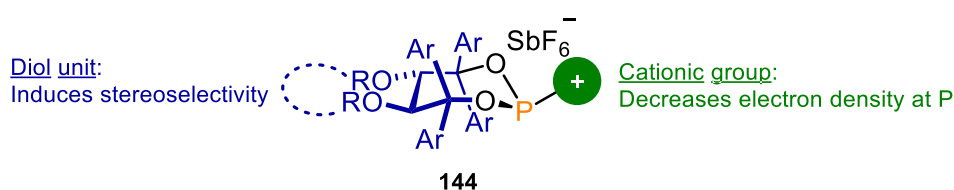
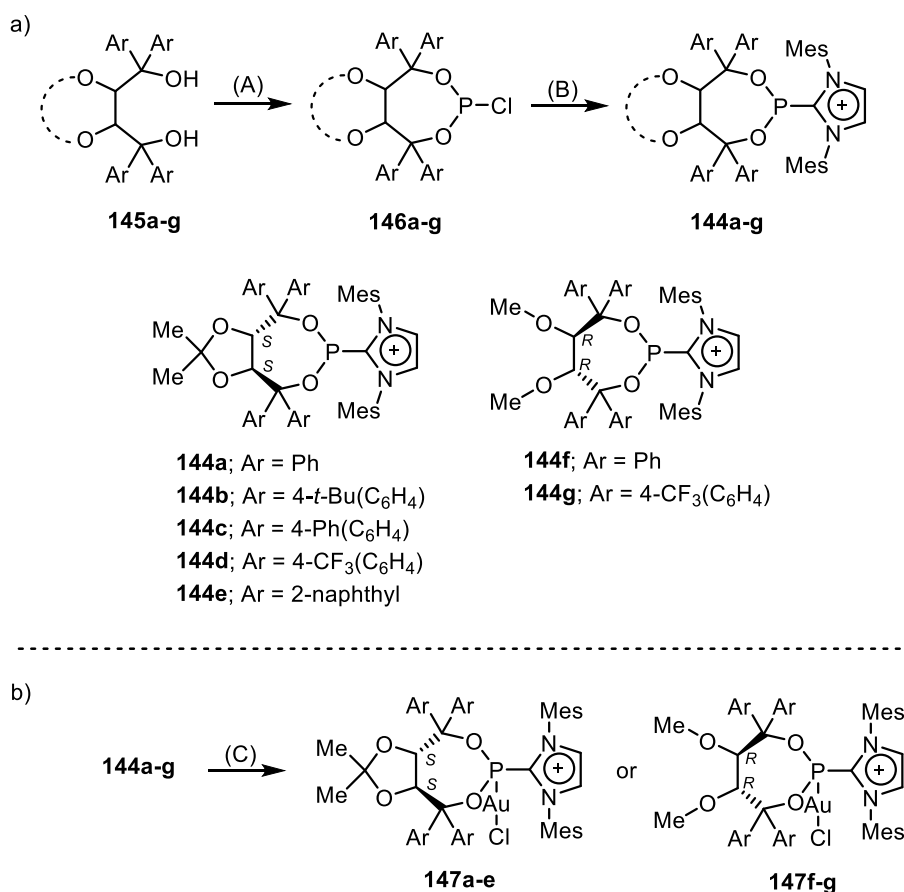


Figure 29. General design of cationic phosphonites.

These ligands demonstrated exceptional characteristics in the Au(I)-catalyzed enantioselective synthesis of carbohelicenes, exhibiting not only a great enhancement of the reaction rate, but also a remarkable control of stereoselectivity by virtue of their tunable chiral skeleton.^[217–219]

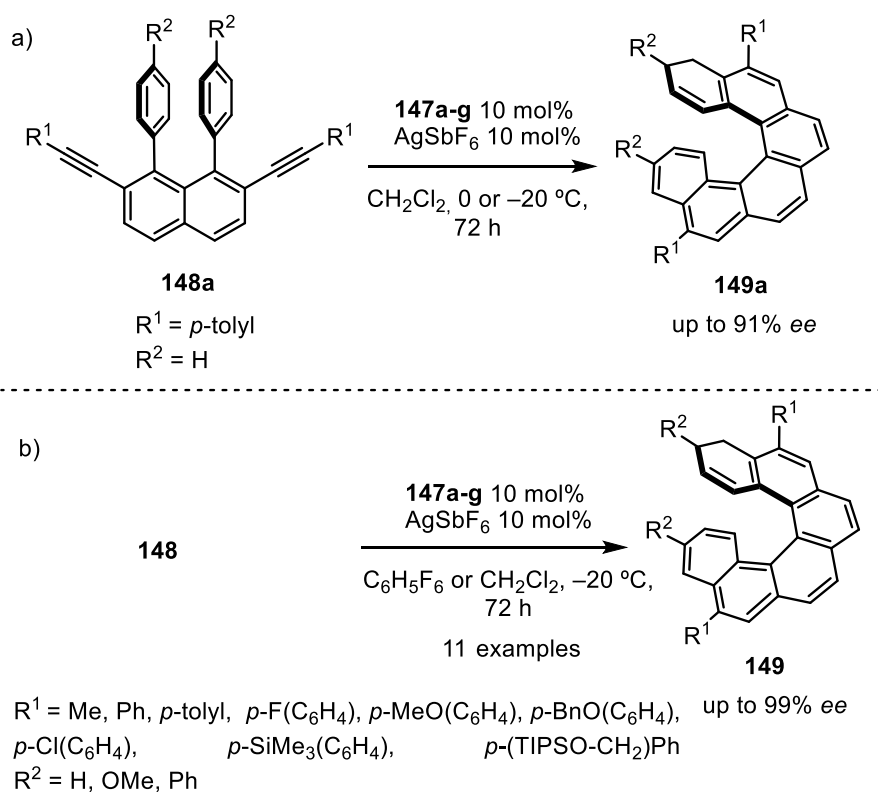
3.1. Enantioselective synthesis of [4]- and carbo[6]helicenes

The first studies carried out in our group targeted the enantioselective synthesis of carbo[6]helicenes by well-known sequential Au-catalyzed intramolecular hydroarylation of diynes. To achieve this task, the chosen cationic phosphonites **144a-g** were firstly synthesized from their corresponding diols **145** and the N-heterocyclic carbene moieties (Scheme 32a) and then coordinated to the Au(I) center to afford the desired gold complexes **147** (Scheme 32b).^[217]



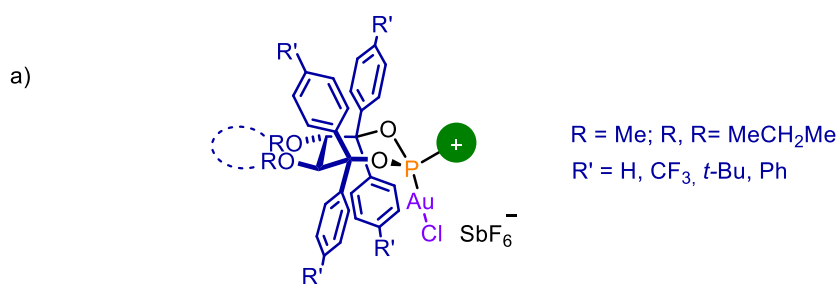
Scheme 32. a) Synthesis and structures of chiral cationic phosphonites **144a-g**. b) Synthesis of Au(I) complexes **147a-g**. Reactants and conditions: (A) PCl₃, Pyridine, Tol, 0 \rightarrow 60 $^{\circ}$ C. (B) IMes carbene, Et₂O, -78 \rightarrow 0 $^{\circ}$ C and then NaSbF₆. (C) (Me₂S)AuCl, CH₂Cl₂, -20 $^{\circ}$ C \rightarrow rt.^[217]

An initial screening was performed on diyne **148a** in order to choose the most effective catalyst in terms of both regio- and enantioselectivity as well as conversion rate (Scheme 33a). With all the results in hand, **147g** was designated as the model catalyst for the following screening on substrates **148a-k**. Yields between 76 and 94% and *ee*'s up to 99% confirmed the efficiency of this novel series of cationic phosphonites as ancillary ligands in the Au(I)-catalyzed enantioselective synthesis of PAH (Scheme 33b).^[217]

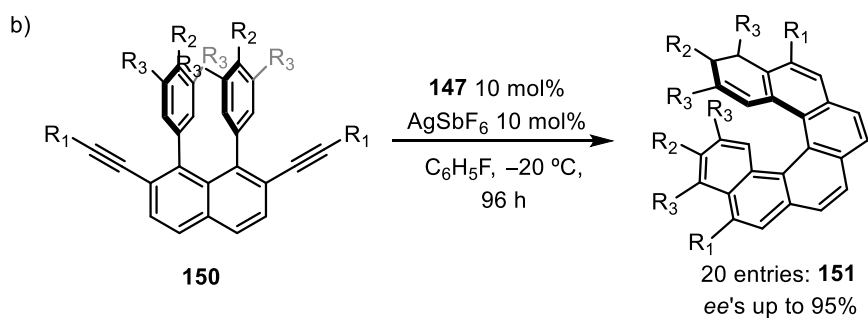
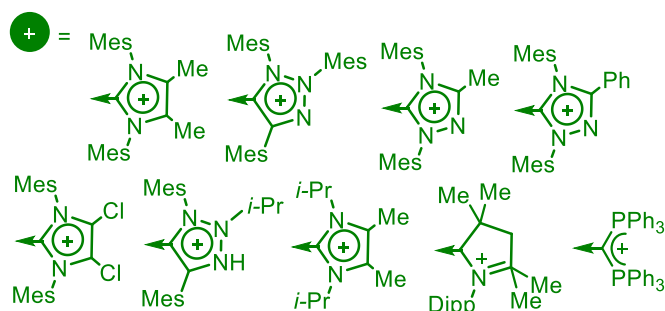


Scheme 33. a) Screening of chiral Au(I)-phosphonite complexes **147a-g**. b) Scope of diynes **148a-k** to afford enantioenriched samples of [6]helicenes **149a-k**.^[217]

Hereinafter and in a similar manner, a new series of TADDOL-based cationic phosphonites were synthesized and tested as chiral ancillary ligands on the Au-catalyzed intramolecular hydroarylation of diynes to synthesize a new set of carbo[6]helicenes containing different substitution patterns. The second generation of ligands synthesized in this report exhibited not only novel tuning motifs in their chiral backbone, but also a new series of N-heterocyclic cationic rests attached to the phosphorus atom (Scheme 34a). The corresponding Au(I)-complexes **147** were obtained and tested in an initial screening and, once the most appropriate catalyst was identified, the synthesis of the desired trisubstituted carbo[6]helicenes **148** with *ee* up to 95% was performed. (Scheme 34b). Again, new bulky cationic moieties and substitution patterns proved to be reliable factors when inducing chirality to the resulting carbo[6]helicenes **151**.^[218]

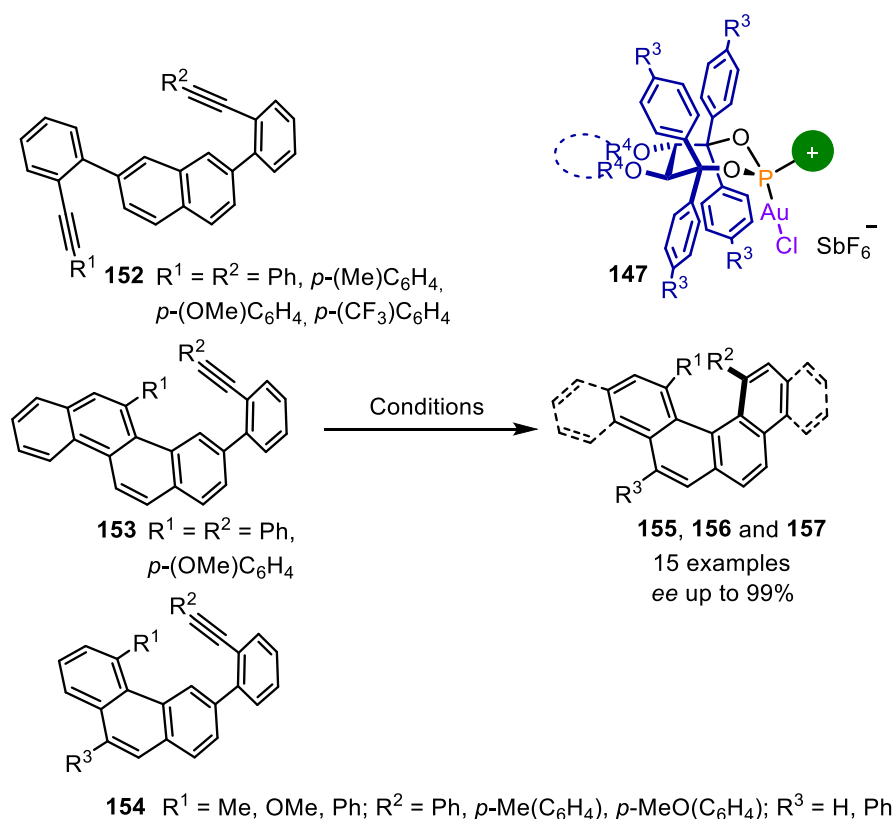


13 new examples: **147h-t**



Scheme 34. a) Second generation of cationic phosphonites and structural design. b) Substrate scope on a new set of diynes **127**.^[217]

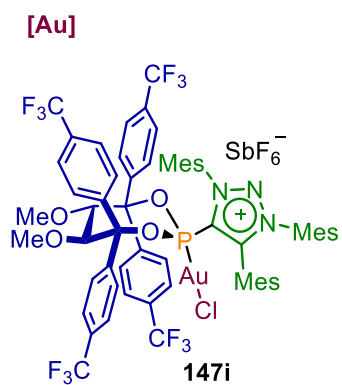
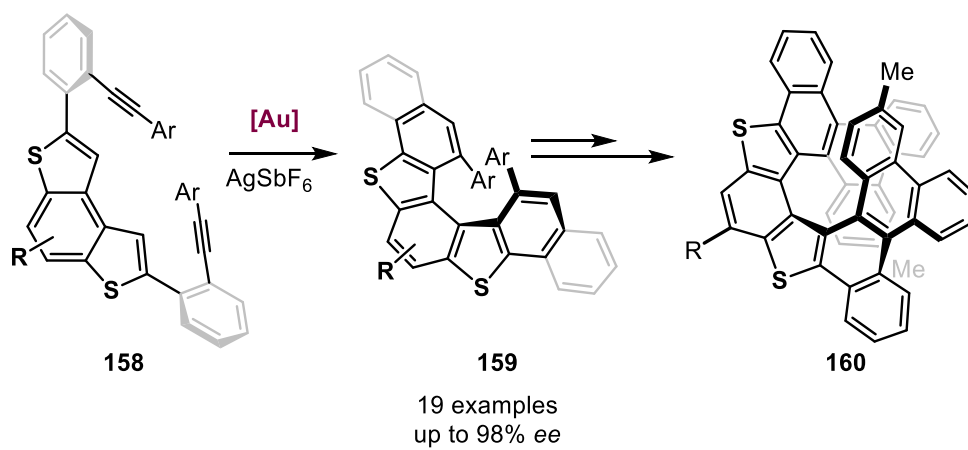
Along the same lines, TADDOL-based chiral cationic phosphines were once again a key component in the enantioselective synthesis of 1,12-disubstituted carbo[4]helicenes. Intramolecular hydroarylation of alkynes **152-154** catalyzed with different Au(I) complexes of general formula **147** afforded configurationally stable [4]helicenes **155-157** with excellent ee 's up to 99%. (Scheme 35).^[219]



Scheme 35. Enantioselective synthesis of carbo[4]helicenes **155-157**. Reactants and conditions: **147** (10 mol% for **152** and 5 mol% for **153** and **154**), AgSbF₆ (10 mol% for **152** and 5 mol% for **153** and **154**), C₆H₅F for **152** and **153**, CH₂Cl₂ for **154**; -20 °C, 96 h.^[219]

3.2. Enantioselective synthesis of dithia[5]helicenes

Aware of the validity of this family of ligands **147** as a key tool in the assembly of chiral polyarenes, our group later investigated and reported the first highly enantioselective synthesis of dithiahelicenes.^[220] Herein, 19 enantioenriched samples of dithia[5]helicenes **159** containing varied substitution motifs were obtained from diyne precursors **158** by Au(I)-catalyzed alkyne hydroarylation with Au(I) complex **147i**. The functional group at the other side of the alkyne highly influenced the enantioselectivity of the reaction, since those substrates containing *p*-substituted hanging phenyls afforded products with *ee*'s around 90%. On the other hand, those products bearing weaker activating groups, like *o*- and *m*-substituted phenyls or alkyl chains, showed from poor to mediocre *ee*'s. Furthermore, the presence of an embedded sulphur atom in the helicene rim enabled the possibility of postsynthetic functionalization *via* S-oxidation and bromination among other processes to afford dithia[9]helicenes **160** without hardly damaging the enantiopurity of the original adduct (Scheme 36).



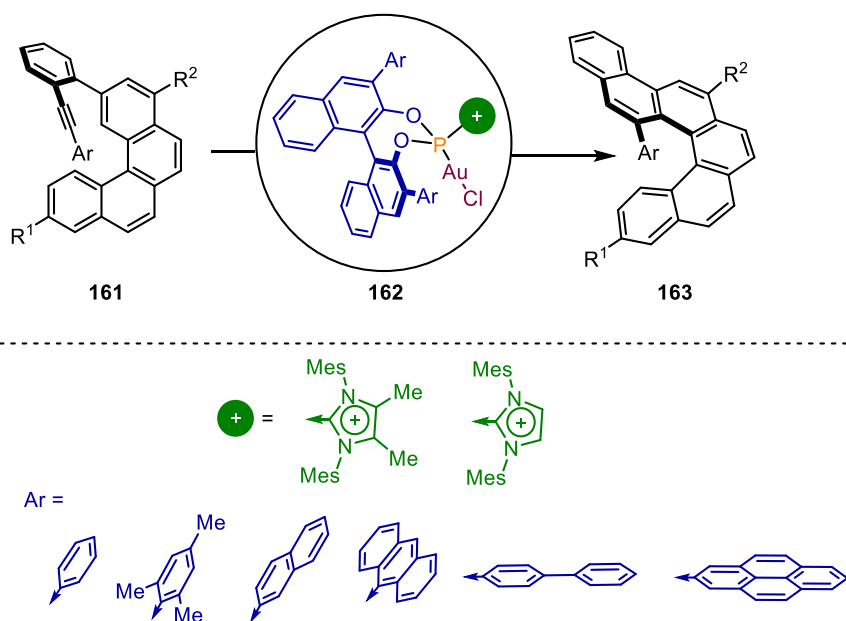
Scheme 36. Enantioselective synthesis of dithia[5]helicenes **159** and their further transformation into dithia[9]helicenes **160**.^[220]

4. Objectives of the project

In the light of the group's previous research in α -cationic phosphonites and their application in the enantioselective synthesis of helicenes, three main objectives were proposed:

a) The enantioselective synthesis of benzo[5]helicenes

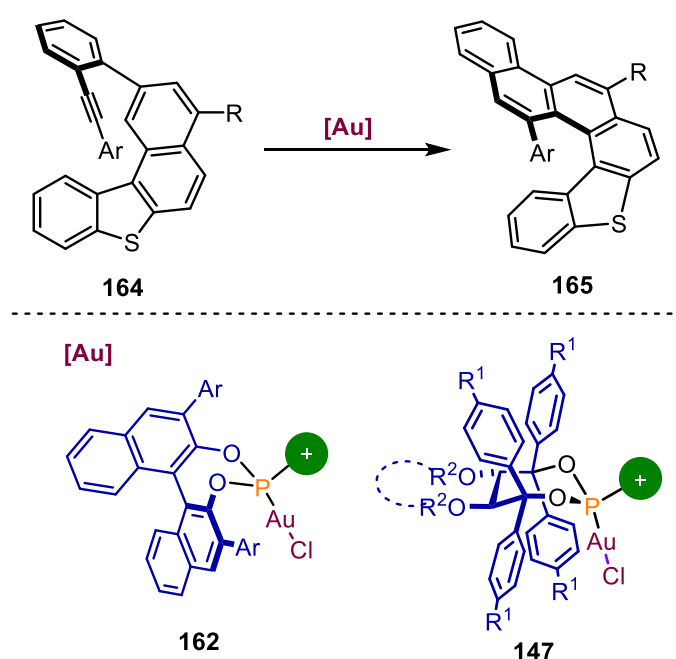
A novel series of BINOL-based cationic phosphonites of general formula **162** should be synthesized and tested as ancillary ligands in the Au(I)-catalyzed enantioselective synthesis of benzo[5]helicenes **163** in collaboration with Dr. Jianwei Zhang and Dr. Thierry Hartung. Based on the methodology of our group, an initial screening will be performed in a model reaction in order to find the most suitable gold catalyst. After this, a set of substrates of general formula **161** bearing different substituents should be prepared in order to evaluate the scope of the reaction and its enantioselectivity (Scheme 37).



Scheme 37. Au(I)-catalyzed intramolecular hydroarylation reaction for the assembly of enantioenriched benzo[5]helicenes **163**.

b) The enantioselective synthesis of thia[5]helicenes

Given our group's experience in enantioselective syntheses of dithia[5]helicenes^[220] and the use of varied chiral cationic phosphonites as ancillary ligands^[217-221], a highly enantioselective synthesis of thia[5]helicenes should be worked out in collaboration with Dr. Valentina Pelliccioli and Wei Fu, M.Sc. To achieve this objective, both TADDOL- and BINOL-based Au(I) complexes of general formula **162** and **147** will be evaluated in the transformation of adducts **164** into chiral thia[5]helicenes **165** (Scheme 38). This project should be included in the same framework as parallel enantioselective syntheses of oxa[5]-, [6]- and [7]helicenes with the same Au(I) catalysts.



Scheme 38. Enantioselective synthesis of thia[5]helicenes **165** and Au(I)-complexes employed in the key step of alkyne hydroarylation.

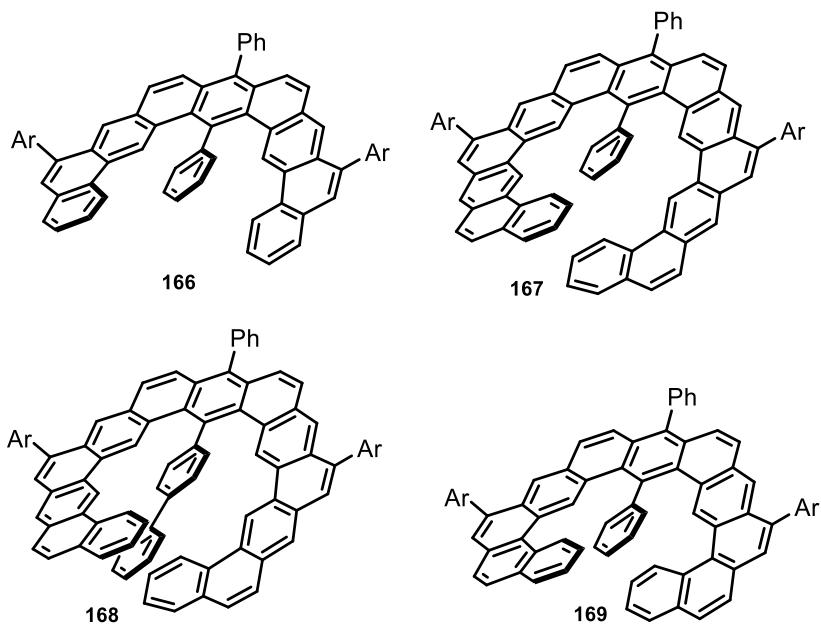
c) In-fjord substitution in expanded helicenes and its consequences

Aware of the latest progress reported in the field of expanded helicenes^[45], the synthesis of in-fjord-substituted expanded helicenes (Figure 30) was envisioned in collaboration with Dr. Samuel Suárez Pantiga. To achieve configurational stability in all molecules, phenyl and biphenyl groups will be utilized as internal substituents. Given the already proven versatility of Au(I) catalysis to assemble complex polyaromatic architectures via alkyne hydroarylation, this strategy can be employed as the key tool for the final assembly of the desired structures.

In collaboration with Dr. Christopher Golz, helicenes **166-169** should further be subjected to X-ray crystallography studies as well as electronic structure calculations in order to deeply study

their structural complexity and the racemization processes that this series of compounds may experience.

Additionally, and in collaboration with Prof. Dr. Ricardo Mata and co-workers, it was planned to conduct photophysical studies of compounds **166-169** aiming to analyze the consequences of the extension of the π -system on the chiroptical properties of these compounds.



Ar = $p\text{-MeO}(\text{C}_6\text{H}_4)$

Figure 30. Target in-fjord substituted expanded helicenes synthesized in this study.

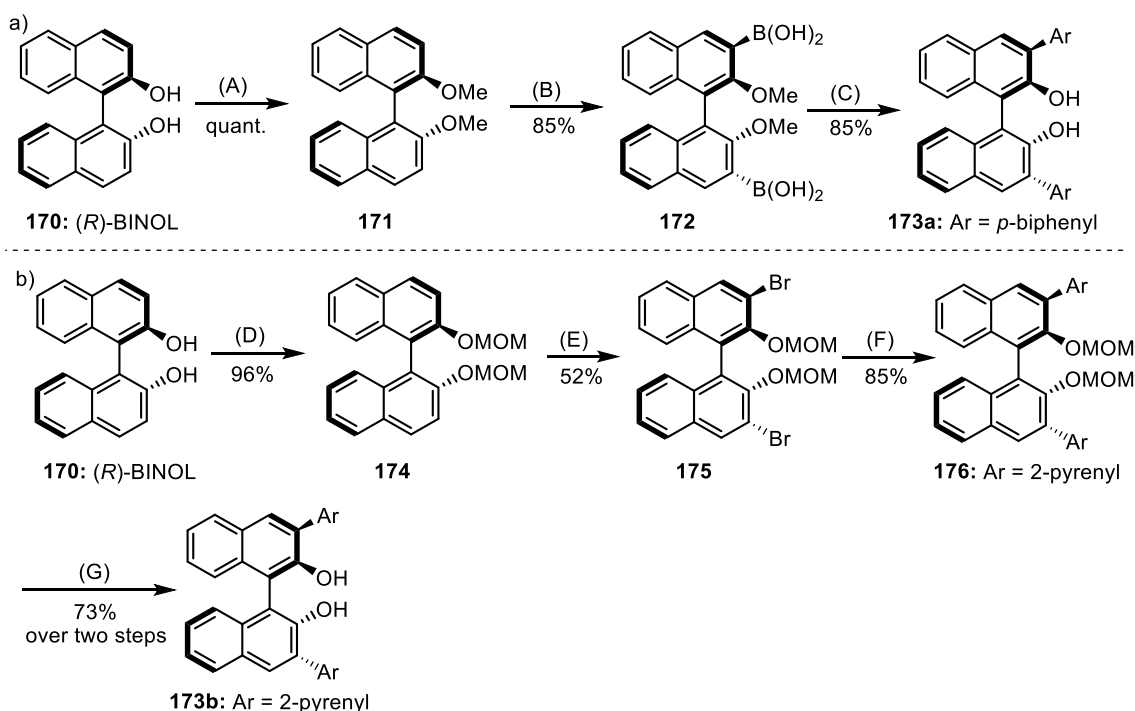
5. Results

5.1. Enantioselective synthesis of benzo[5]helicenes

5.1.1. Synthesis of novel BINOL-derived cationic phosphonites and gold complexes

As discussed above, a novel family of BINOL-derived α -cationic phosphines was envisaged as potential precursors of Au(I) complexes in collaboration with Dr. Jianwei Zhang with a purpose to promote the formation of chiral PAH *via* alkyne hydroarylation. Since 1979 BINOL has been used as a profitable chiral backbone in multiple ligands due to its versatile architecture and ease to tune.^[222] It has been demonstrated that further modifications in their structure affect not only the reaction environment, but also the electronic properties of phosphorus and metal cores. Furthermore, its C_2 -symmetry ensures an efficient asymmetric induction. For these reasons, BINOL emerges as a promising candidate for the formation of new cationic phosphonites.^[223]

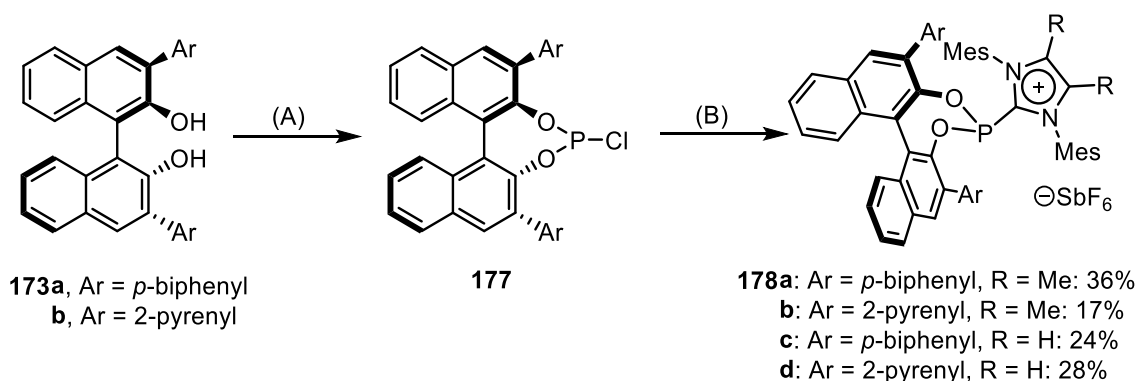
The initial steps for the synthesis of the precursors of BINOL-based ligands are depicted in Scheme 39. Two pathways were envisioned to produce 3,3'-disubstituted diols **173a-b** from commercially available (*R*)-BINOL **170** employing procedures reported in the literature (Scheme 39).^[224–228] Thus, after initial protection of the hydroxyl groups in **170** with methyl or methoxymethyl groups and lithiation, compounds **171** and **174** were either borylated or brominated furnishing intermediates **172** or **175**, respectively.



Scheme 39. Synthesis of (R)-diols **173a,b**. Reactants and conditions: (A) K_2CO_3 (3.3 equiv.), MeI (5.5 equiv.), acetone, reflux, 24 h. (B) 1. TMEDA, Et_2O , rt; 2. *n*-BuLi (3 equiv.), rt, 30 min \rightarrow 3 h; 3. $\text{B}(\text{OEt})_3$ (7 equiv.) $-78^\circ\text{C} \rightarrow$ rt, overnight; 4. 0°C , HCl (aq.), rt, 2 h. (C) 1. Ar-I (3 equiv.), $\text{Pd}(\text{PPh}_3)_4$ (4 mol%), $\text{Ba}(\text{OH})_2 \cdot 8\text{H}_2\text{O}$ (3 equiv.), dioxane: H_2O 3:1, overnight. 2. BBr_3 (6 equiv.), CH_2Cl_2 , $0^\circ\text{C} \rightarrow$ rt, 24 h. (D) NaH (2.5 equiv.), MOMCl (2.5 equiv.). (E) 1. *n*-BuLi (2.4 equiv.), hexane, $-78^\circ\text{C} \rightarrow$ rt, 1 h; 2. Br_2 , pentane, $-78^\circ\text{C} \rightarrow$ rt, 15 min; 3. Na_2SO_3 (aq.). (F) Ar-B(pin) (2.8 equiv.), K_2CO_3 (12 equiv.), $\text{Pd}(\text{OAc})_2$ (5 mol%), $\text{P}(\text{t-Bu})_3$ (10 mol%), DME: H_2O , 90°C , 3 h. (G) HCl (6 N), dioxane, 90°C .

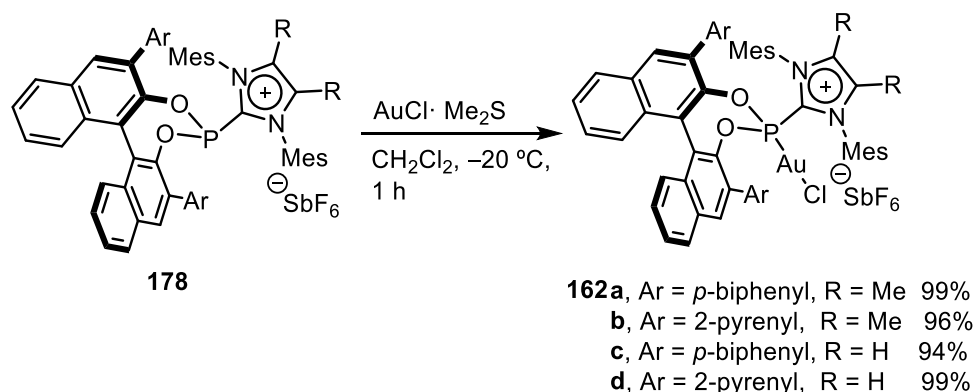
Compound **172** after Suzuki coupling with 4-iodo-1,1'-biphenyl and deprotection with BBr_3 afforded *p*-biphenyl-disubstituted BINOL **173a** (Scheme 39a; 72% yield over 3 steps). In the second pathway, a Suzuki reaction of **175** with pyrene-2-boronic acid pinacol ester followed by deprotection of adduct **176** with diluted HCl gave pyrenyl-disubstituted BINOL **173b** in 31% overall yield (Scheme 39b).

BINOL-derived cationic phosphonites **178** were prepared through a two-step process starting from 3,3'-disubstituted diols **173a-b**. The first step consisted in the formation of the crude chlorophosphites **177** by heating solutions of the BINOL derivative, phosphorus trichloride, pyridine and molecular sieves 4 \AA in toluene, followed by filtration to remove the pyridinium chloride along with other by-products and concentration *in vacuo*. Carbenes IMes and IMes^{Me} were synthesized according to the published protocols^[226,229] and added to a solution of chlorophosphite **177** in the presence of NaSbF_6 (Scheme 40). The formation of cationic phosphonites **178** was confirmed by ^{31}P NMR, where clear signals were estimated at about 142 ppm, in a range close to previously reported for cationic phosphonites.^[217,218] Finally, purification by column chromatography at -10°C afforded pure cationic phosphonite ligands **178a-d**.



Scheme 40. Synthesis and structure of BINOL-derived α -cationic phosphonites **178a-d**. Reactants and conditions: (A) PCl_3 (1.1 equiv.), pyridine (3 equiv.), toluene, 60 °C, 1 h; (B) IMes^{Me} or IMes carbene (0.95 equiv.), NaSbF_6 (3 equiv.), Et_2O , $-78\text{ }^\circ\text{C} \rightarrow \text{rt}$, overnight.

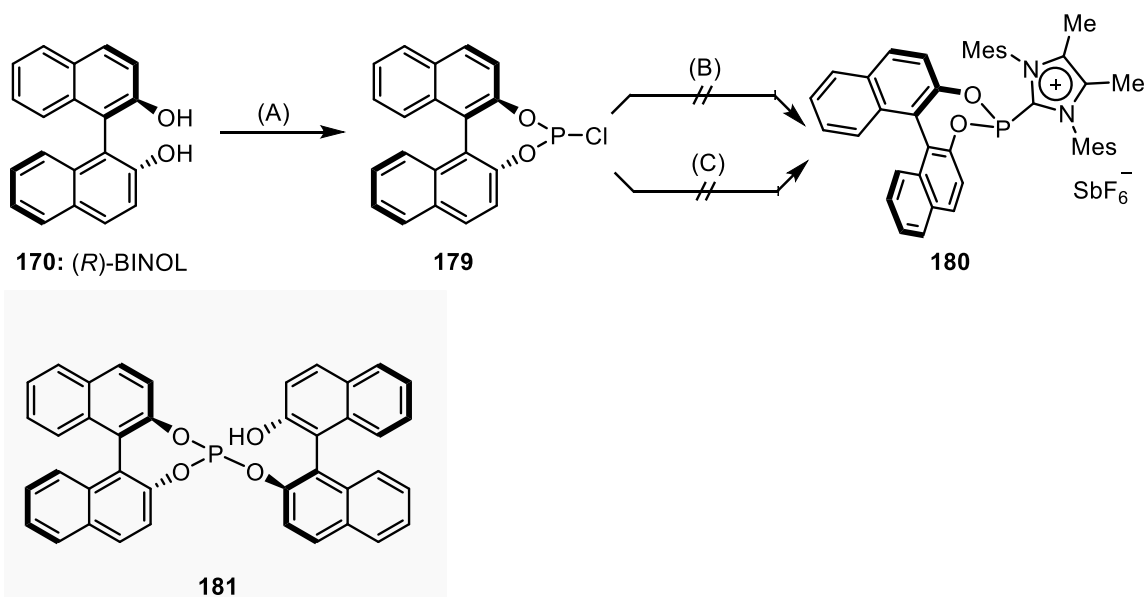
Ligands **178** reacted with $\text{AuCl}\cdot\text{Me}_2\text{S}$ in CH_2Cl_2 to form the corresponding Au(I) complexes **162**, which were obtained as white or light-yellow solids in excellent isolated yields (Scheme 41). The coordination of the Au(I) center to the phosphonites caused a pronounced upfield shift of their ^{31}P NMR signals at about 112 ppm.



Scheme 41. Formation and structure of Au(I) complexes **162**.

Furthermore, the synthesis of an extra BINOL-based ligand was envisioned and attempted. Compound **180** bearing a bare BINOL backbone and an imidazolium cationic rest was envisaged as the least bulky alternative to ligands **178a-d** within the whole ligand series. Its substituent-free rim would allow us to witness the direct influence of the steric hindrance of the catalyst on the enantiopurity of the helicene sample. Such study would be carried out through the comparison of the enantioinduction of catalysts carrying varied substituents like *p*-biphenyl, phenyl groups and the aforementioned **180**. Hence, a direct relation between the bulkiness of the substituent and the *ee*'s of the helicene samples would be expected.

The first step to obtain chlorophosphite **179** was successfully achieved following procedures reported in the literature;^[230] however, the addition of the IMes^{Me} carbene moiety could not be accomplished in several attempts despite having utilized different reaction conditions. Only side-product **181** was detected by HR-MS, but could not be properly isolated.

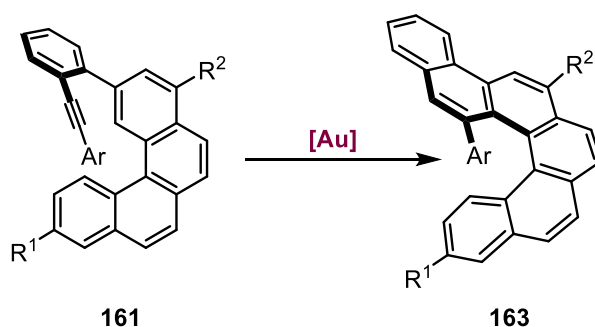


Scheme 42. Structure and attempted synthesis of BINOL-derived α -cationic phosphonite **180**. Reactants and conditions: (A) PCl_3 (20.0 equiv.), toluene, 60 °C, 5 h; (B) IMes^{Me} carbene (0.95 equiv.), NaSbF_6 (3 equiv.), Et_2O , -78 °C \rightarrow rt, overnight; (C) IMes^{Me} carbene (0.95 equiv.), NaSbF_6 (3 equiv.), THF, -78 °C \rightarrow rt.

It was suggested that the absence of substituents at positions 3 and 3' in the BINOL backbone was the main obstacle to the formation of ligand **180**. Not only do they impart increased electrophilicity to the phosphorus atom by reducing its electron density, but they can also form a pocket around this atom, preventing possible hydrolysis during the ongoing reaction.

5.1.2. Preparation of benzo[5]helicenes

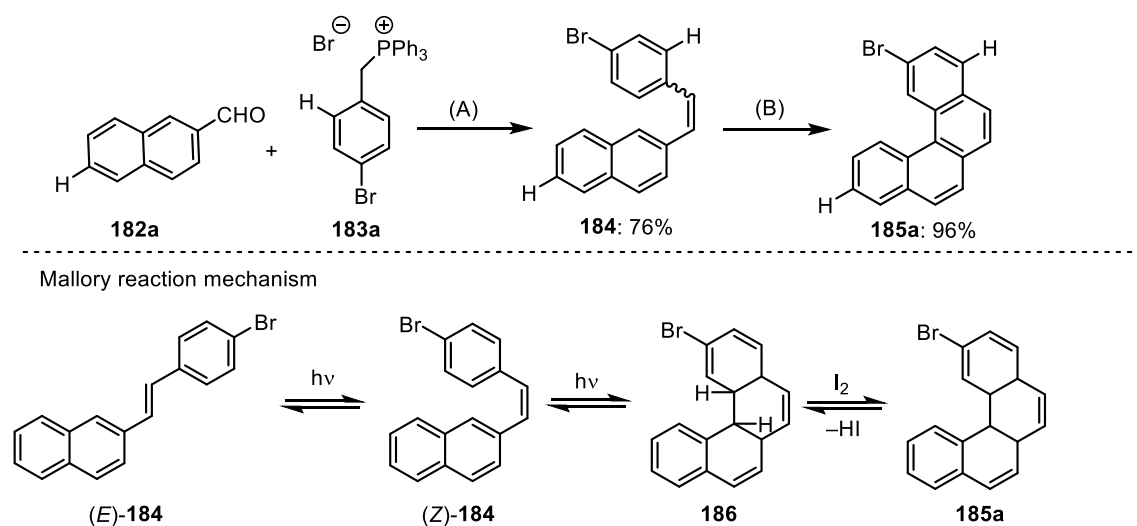
Since regular carbo[5]helicenes possess a relatively low configurational stability that enables easy racemization at room temperature, a new molecular design for these molecules was envisaged. The key to prevent a loss of enantiopurity was the introduction of a structural element bulky enough to hamper the interconversion between both enantiomeric forms of the helicene. Such building block chosen was a substituted phenyl group pending from an alkyne moiety that later cyclized with a [4]helicene core to afford the desired helicene product *via* π -acid catalyzed hydroarylation (Scheme 43).



Scheme 43. Formation of benzo[5]helicenes **163** from alkyne precursors **161**.

5.1.3. Synthesis of key intermediates

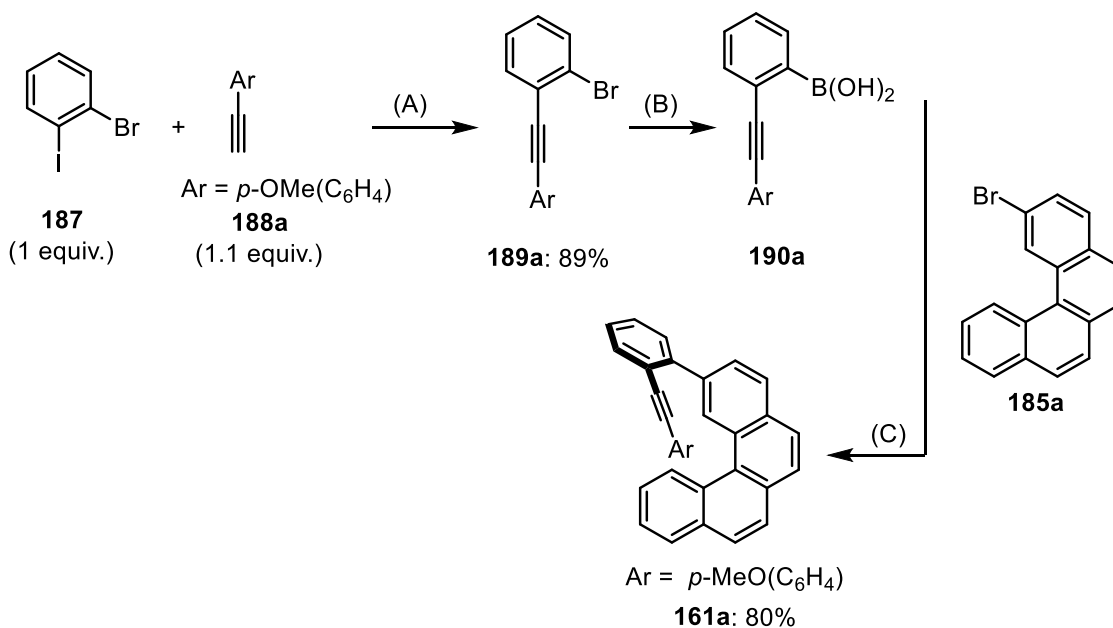
With the new BINOL-derived Au(I) complexes in hand, tests on their efficacy in the Au(I)-catalyzed hydroarylation of alkyne-based substrates **161** were performed. The synthesis of this model substrate **161a** began with the preparation of 2-bromobenzo[*c*]phenanthrene **185a** according to procedures reported in the literature:^[231] a Wittig reaction between commercially available 2-naphthaldehyde (**182**) and an ylide prepared in situ from (4-bromobenzyl)triphenylphosphonium bromide (**183**) gave stilbene **184** as a mixture of *cis*- and *trans*-isomers. Mallory's subsequent reaction with this mixture gave **184** as the main product. Although only *Z*-forms undergo this photocyclization, reaction conditions under UV light facilitate an *in situ* interconversion between both diastereomers and, therefore, the complete conversion of the starting material. The presence of an oxidizing agent like I₂ ensures the transformation of dihydro[4]helicene intermediate **186** into the desired 2-bromo[4]helicene **185a** (Scheme 44). It has been proposed that I₂ is photochemically cleaved into radicals that react in a chain reaction affording HI. Finally, this acid is reoxidized into I₂ by the oxygen present in the solution.^[232] Fortunately, unlike in other reported photocyclizations of the same kind,^[97,231,233] no scavenger agents were necessary in order to prevent parasitic reductions of **185a** by HI. Although the reaction took place in toluene, I₂ needed to be dissolved in THF due to better solubility, and the entire solution was added dropwise.



Scheme 44. Synthesis of [4]helicene framework **185a** and Mallory reaction mechanism. Reactants and conditions: (A) MeONa/MeOH, 0 °C →rt, overnight. (B) hv, I₂ (1.1 equiv.), THF, toluene, 125 W, rt, overnight.

In a parallel fashion, Sonogashira cross-coupling reaction between readily accessible reactants **187** and **188** gave bromoalkyne **189** in up to 89% yield. Further borylation furnished **190a**, which was used as a crude material in the next step, following the methodology of our group.^[219] Finally, Suzuki cross-coupling reaction in THF:H₂O 5:1 between both moieties **185a**

and **190a** afforded the benzo[5]helicene precursor **161a** in good yield (Scheme 45). The choice of this biphasic system as solvent was made thoroughly, as it should facilitate the solubility of both the base (in the aqueous phase) and the catalyst and substrates (in the organic one).^[234]



Scheme 45. Synthesis of model substrate **161a** decorated with an alkyne moiety. Reactants and conditions: (A) PdCl₂(PPh₃)₂ (2 mol%), CuI (3 mol%), NEt₃, rt, overnight. (B) 1. *n*-BuLi (1.3 equiv.), Et₂O, -78 °C, 1 h. 2. B(*Oi*-Pr)₃ (1.5 equiv.), -78 °C → rt, overnight. 3. HCl/H₂O, rt, 1h. (C) **185a** (1 equiv., 0.02 M), **190a** (1.5 equiv., 0.03 M), Pd₂(dba)₃ (4 mol%), SPhos (8 mol%), Cs₂CO₃ (3 equiv.), THF:H₂O 5:1, 80 °C, overnight.

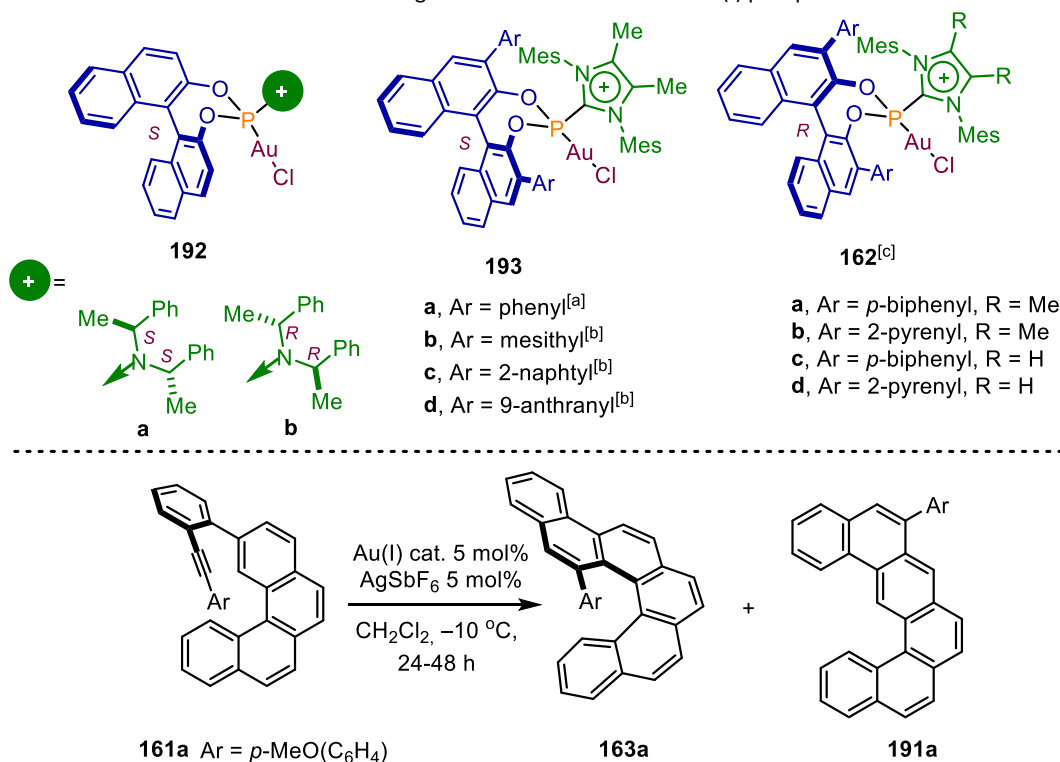
5.1.4 Optimization of Au(I)-catalysed hydroarylation step

Once the precursor **161a** was synthesized, attention was turned towards its transformation into [5]helicene **163a**. An initial screening with TADDOL-derived Au(I) catalyst **147h**, which was previously described and utilized by the Alcarazo group^[218], was performed under different experimental conditions (Table 1).

Based on our previously gained experiences with carbo[4]- and [6]helicenes,^[217–219] the initially chosen for screening reaction conditions consisted in employing fluorobenzene as a solvent, a precatalyst **147h** and AgSbF₆ (loading 5 mol% of each) at -20 °C (Table 1, entry 1). Despite good conversion was achieved, poor **163a:191a** ratio and low *ee* values were obtained. This justified the search for more optimal conditions. Poor solubility of **147h** in fluorobenzene suggested that lower concentrations and a slightly longer reaction time would lead to a better development of the reaction and therefore, enhanced values of both **163a:191a** ratio and *ee*. As a consequence, a small improvement was observed but at the cost of a remarkable decrease in the conversion (entry 2). On the other hand, despite increasing the temperature to -10 °C, employing CH₂Cl₂ as a solvent resulted in a counterproductive effect on the reaction blocking conversion of the substrate **161a**, which was quantitatively recovered (entry 3).

performed the cyclization in excellent conversion rate plus excellent regio- and enantioselectivities (Table 2, entries 3 and 5, respectively). On the other hand, Au(I) catalysts **193b** and **193d** containing bulkier substituents, such as mesityl and 9-anthranly groups, exhibited a noticeable detriment of both conversion and enantioselectivity (Table 2, entries 4 and 6), particularly in this latter case with lower than 5% conversion and 8% *ee*. Finally, the new family of (*R*)-BINOL-based Au(I) catalysts was evaluated under the same conditions. These four last complexes are characterized by the presence of 2-pyrenyl and *p*-biphenyl groups at their backbone and IMes and IMes^{Me} substituents as cationic rests. Excellent results in terms of conversion, regio- and enantioselectivity were obtained, with conversion ratios >99:1 and *ee*'s in the range of 93-95% (Table 2, entries 7-10). To our surprise, the absence of methyl groups at the imidazolium moiety in **162c** and **162d** did not result in any remarkable difference in enantioselectivity, as it was previously observed in earlier research in our group.^[221]

Table 2. Screening of different BINOL-derived Au(I) phosphonites.



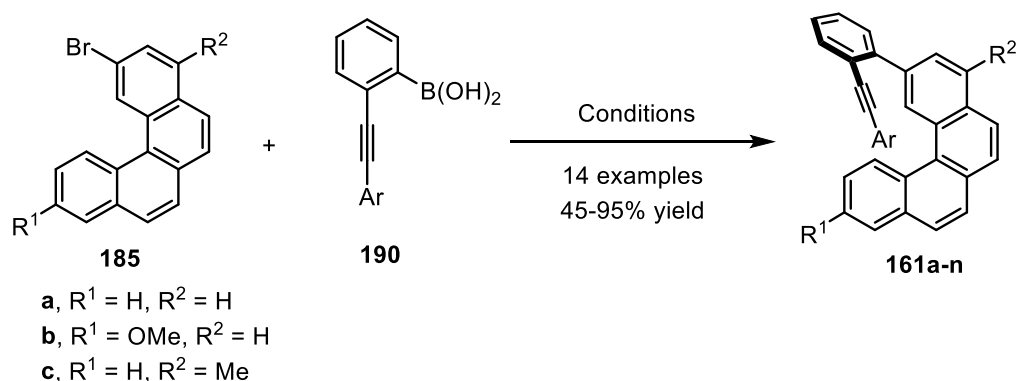
Entry	Catalyst	Conversion [%] ^[d]	163a:192a ^[b]	ee [%] ^[e]
1	192a	11	>99:1	(-)-61
2	192b	35	85:15	(-)-40
3	193a	>98	98:2	(-)-93
4	193b	55	97:3	(-)-86
5	193c	>98	95:5	(-)-97
6	193d	<5	n.d.	(-)-8
7	162a	>98	>99:1	(+)-94
8	162b	>98	>99:1	(+)-95
9	162c	>98	>99:1	(+)-94
10	162d	>98	>99:1	(+)-93

[a] Synthesized by Dr. Leo Nicholls. [b] Synthesized by Dr. Thierry Hartung. [c] Synthesized by Dr. Jianwei Zhang. [d] Conversion determined by chiral-phase HPLC. [e] determined by ¹H NMR of the crude reaction mixtures.

As a conclusion of this screening, **162b** was selected as the catalyst with the most consistent results among the ten different species tested since it provided superb conversion rate and ratio as well as an excellent enantioselectivity.

5.1.5. Substrate scope

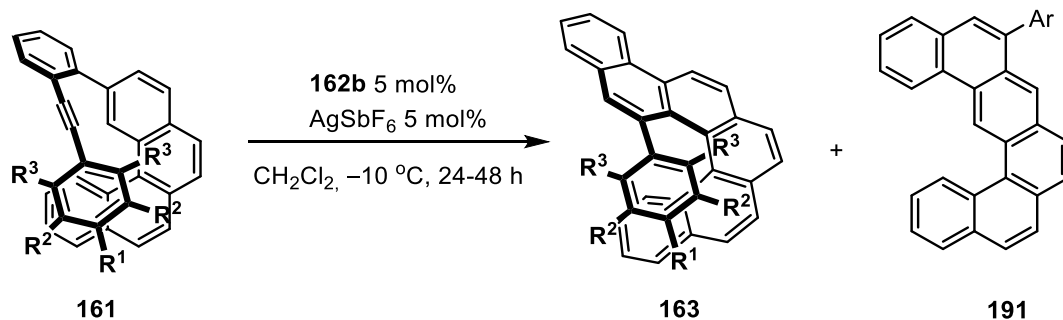
Once **162b** was chosen as the model catalyst, the scope of the Au(I)-catalyzed hydroarylation for the synthesis of [5]helicenes **163** was evaluated. A series of alkyne-containing substrates **161** bearing different substitution patterns at the hanging phenyl were synthesized following the same strategy as for **161a**, utilizing different boronic acid moieties in the Suzuki cross-coupling reaction (Scheme 46).



Scheme 46. Suzuki cross-coupling reaction for the synthesis of helicene precursors **161a-n**. Conditions: **185** (1 equiv., 0.02 M), **190** (1.5 equiv., 0.03 M), Pd₂(dba)₃ (4 mol%), SPhos (8 mol%), THF:H₂O 5:1, 80 °C, overnight.

Thus, the optimized conditions from the last step, as well as the viability of the model reaction, were broadly tested. The presence of certain functional groups at this part of the substrate's structure had a great influence on the outcome of the cyclization as it is depicted in Table 3.

Table 3. Substrate scope of compounds **161** with different substitution patterns at the aryl substituent.



Entry	161	R ¹	R ²	R ³	163	163:191 ^[a]	Yield (%) ^[b]	<i>ee</i> (%) ^[c]
1	161a	OMe	H	H	163a	>99:1	88	(+)-95
2	161b	Me	H	H	163b	>99:1	90	(+)-95
3	161c	OBn	H	H	163c	>99:1	71	(+)-95
4	161d	SiMe ₃	H	H	163d	>99:1	90	(+)-95
5	161e	OPh	H	H	163e	>99:1	90	(+)-97
6	161f	H	OMe	H	163f	>99:1	77	(+)-68
7	161g	H	Me	H	163g	99:1	80	(+)-68
8	161h	H	H	OMe	163h	3:1	35	0
9	161i	H	H	Me	163i	<1:99	31	(+)-20
10	161j	H	H	H	163j	>99:1	15	(+)-94

[a] Ratios determined by ¹H NMR. [b] Yields of isolated products. [c] *ee* values determined by chiral-phase HPLC.

Those substrates bearing *p*-substituents at the hanging phenyl group gave unquestionably the best results (Table 3, entries 1-5) and afforded benzo[5]helicenes **163a-e** in excellent regio- and enantioselectivities as well as in very good yields. Surprisingly, the effectiveness of the process did not experience any erosion regardless of carrying electron-rich (Table 3, entries 1-3 and 5) or electron-poor substituents (Table 3, entry 4): in every case the conversion ratio was superior to 99% and the *ee* ranged from 95 to 97%. Moreover, *m*-substituted with OMe and Me starting materials **161f** and **161g** were tolerated and showed good conversions, ratios and yields (99 and 77-80%, respectively), albeit with an obvious erosion in the enantioselectivity (68 and 69% *ee* correspondingly; Table 3, entries 6-7) in comparison to the previous substrates **161a-e**. However, it was observed that the most unfavored substitution patterns corresponded to the cases of *o*-substituents compounds **163h-i**: Indeed, the introduction of OMe and Me groups at the *o*-positions clearly worsened yield and conversion ratio (15-35% and down to <1%, respectively), along with a very low enantioselection such as 20% *ee* in the case of Me (Table 3, entry 9) or isolation of the desired helicene **163h** with OMe group as a racemate (Table 3, entry 8). These obtained results revealed the obvious influence of the substitution

pattern in the progression of the hydroarylation reaction. Finally, when the substrate simply contained a bare phenyl group (**163j**), regio- and enantioselectivities are better again despite the low yield.

Interesting structural features were observed in the ^1H NMR spectra at 25 °C: Those [5]helicenes possessing *p*-substituted phenyl groups, like **163a**, showed coalescence phenomena at their protons H_a and H_b due to the partially blocked rotation of the pending aromatic ring. This is clearly noticeable in the integration of all four protons as a broad singlet at 5.5-6.5 ppm (Figure 31a). On the other hand, the products **163f** and **163h** bearing *m*- and *o*-substituted phenyl groups exhibited sharper aromatic signals associated with this fragment of the molecule. This phenomenon presumably corresponds to a rigidification of the structure due to steric hindrance obstructing any possible rotation of the phenyl ring, as depicted in Figures 31b and 31c.

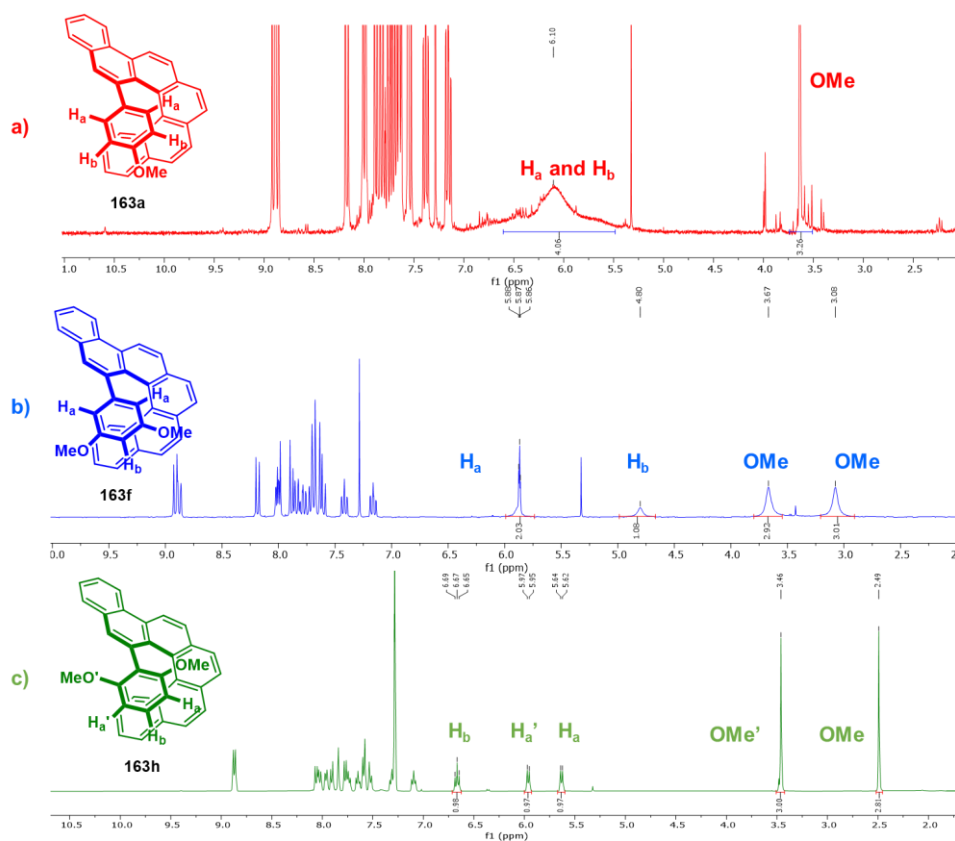


Figure 31. Rigidification of the hanging phenyl group manifested in the ^1H NMR at rt.

X-ray analysis would make it possible to assess more clearly the influence of substitution patterns in **161i** and **163f** (Figure 32). Methyl groups present in the former clearly hinder the approximation of the activated alkyne fragment to the [4]helicene moiety, whereas methoxy groups in the latter appears to act as a paddle wheel with very restricted rotation at rt.

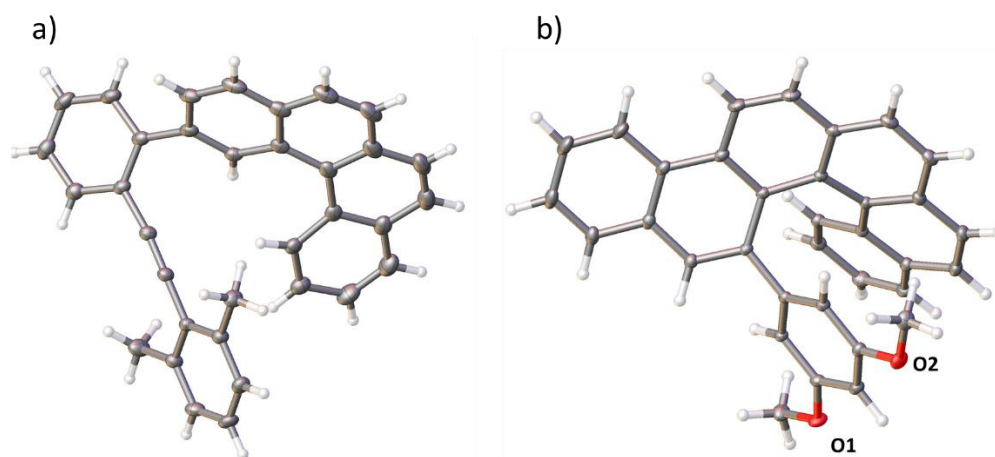
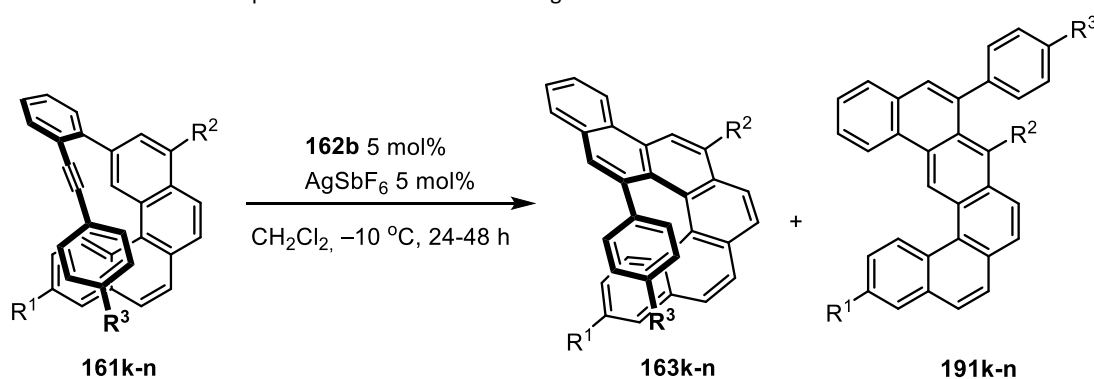


Figure 32. Structures of **161i** (a) and **163f** (b) grown from hexane in the crystals. Solvent molecules were removed for clarity.

Besides this first scope, the Au(I)-catalyzed hydroarylation with precatalyst **162b** was also evaluated in substrates containing different substituents at the external rim of the structure, specifically at positions 8 and 13. As it is depicted in Table 4, the incorporation of these elements was surprisingly well tolerated and did not harm either regio- or enantioselectivity, producing helicenes **163k-n** in up to 77% yields with *ee*'s up to 98%.

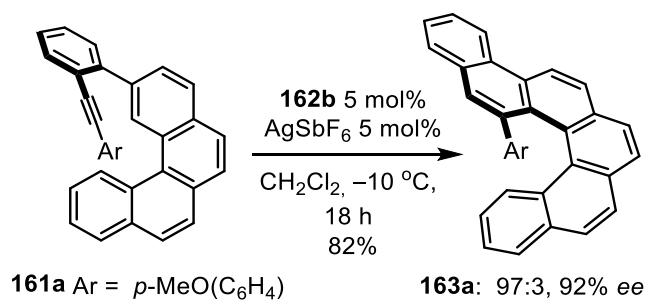
Table 4. Scope of substrates **140k-n** bearing different substituents at the external rim.



Entry	161	R ¹	R ²	R ³	163	163:191 ^[a]	Yield (%) ^[b]	<i>ee</i> (%) ^[c]
1	161k	OMe	H	OMe	163k	93:7	54	(+)-93
2	161l	OMe	H	Me	163l	>99:1	70	(+)-88
3	161m	OMe	H	OBn	163m	94:6	77	(+)-88
4	161n	H	Me	OMe	163n	97:3	65	(+)-98

[a] Ratios determined by ¹H NMR. [b] Yields of isolated products. [c] *ee* values determined by chiral-phase HPLC. Entry 1 was carried out by Guo Zichen, B.Sc., as part of his bachelor thesis.^[233]

To conclude this Section, hydroarylation of **161a** catalyzed with Au(I) complex **162b** was repeated utilizing 250 μmol of substrate, ten times more than that of previous experiments, to confirm the viability of a scale-up of this process. We were pleased to observe that this increase of the reaction scale did not entail any significant loss of regio- or enantioselectivity (Scheme 47), as it could be expected from previous experience with such processes.



Scheme 47. Enantioselective hydroarylation of **161a** scaled up to 250 μmol .

5.1.6. Absolute configuration and chiroptical properties

Additionally, crystals of enantioenriched helicene sample **163a** were grown by vapor diffusion of hexane into dichloromethane in order to determine its connectivity and its absolute configuration (Figure 33a). According to X-ray diffraction analysis and supported by both Flack and Hooft parameters [0.05(5) and 0.05(3), respectively], absolute configuration was revealed to be *P*. In a similar manner, a pure sample of **191k** was isolated *via* preparative HPLC and crystallized from hexane (Figure 33b). This last analysis confirmed the correctness of the structure determination of the main by-product obtained from the hydroarylation reaction of substrate **161k**.

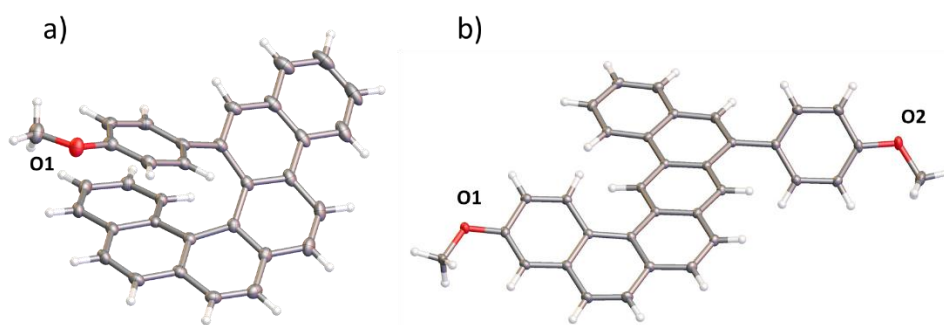


Figure 33. X-ray structures of **163a** (a) and **191k** (b).

In order to ensure a correct determination of the absolute configuration of **163a**, ECD measurements of an enantioenriched sample of this compound were carried out at rt. Further comparison of these spectra with previously reported literature data validated (*P*)-assignment as its absolute configuration (Figure 34).^[31,235,236]

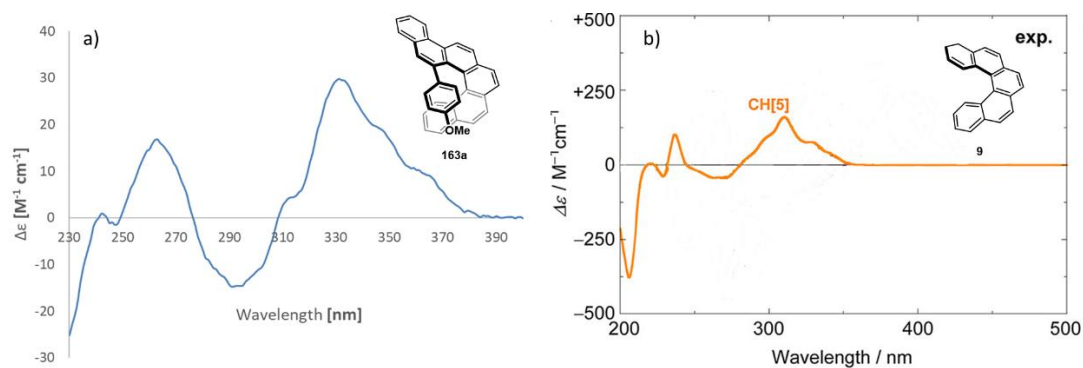


Figure 34. a) ECD spectrum (10 μM in CH_2Cl_2 at rt) of **163a**. b) Experimental ECD spectrum (10 μM in n-hexane/2-propanol 98:2 at 0 $^\circ\text{C}$) of (*P*)-[5]helicene reported by Mori's group. Image adapted from: Y. Nakai, T. Mori, Y. Inoue, *J. Phys. Chem. A* **2012**, 116, 7372–7385.^[235]

As expected for highly conjugated aromatic system, model [5]helicene **163a** exhibited optical properties reflected by their UV-Vis absorption and fluorescence spectra, which were measured and displayed in normalized view in Figure 35. Absorption showed a very pronounced shoulder between 280 and 380 nm with a maximum of roughly $46000 \text{ M}^{-1}\cdot\text{cm}^{-1}$ at 303 nm (see Appendix). Conversely, fluorescence seemed to be blue-shifted exhibiting a remarkable two-shoulder band between 350 and 600 nm and an emission maximum of 426 nm, leading to a Stokes shift of approximately 9500 cm^{-1} .

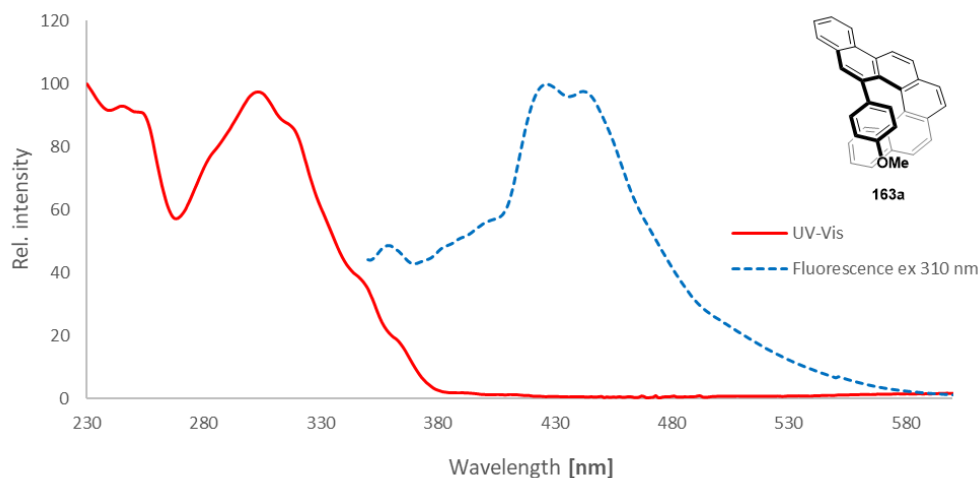


Figure 35. UV-Vis and fluorescence spectra of helicene **163a**. Spectra normalized to the relative maxima of each spectrum. Both samples measured in CH_2Cl_2 (10 μM).

When comparing the obtained spectra with those reported for other carbo[5]helicenes, similarities regarding the morphology of the curves and the recorded maxima were observed (Figure 36). Carbo[5]helicene spectra published by Matsuda *et al.* displayed a very similar absorption band to that of **163a** between 280 and 350 nm and a noticeable maximum at approximately 300 nm. In addition, two small shoulders in the blue region and an emission maximum at 424 nm were also found in the emission spectrum, very close to that detected for **163a** (Figure 36a).^[57] Similarly, Juríček *et al.* recorded the absorption spectra of three different

1,14-difunctionalized [5]helicenes **194** and compared them to each other (Figure 36b).^[31] In this latter study, it was observed that all three compounds exhibited coincident bands at the same region regardless of the functional group and bearing a great resemblance to that of **163a** despite the structural differences.^[31]

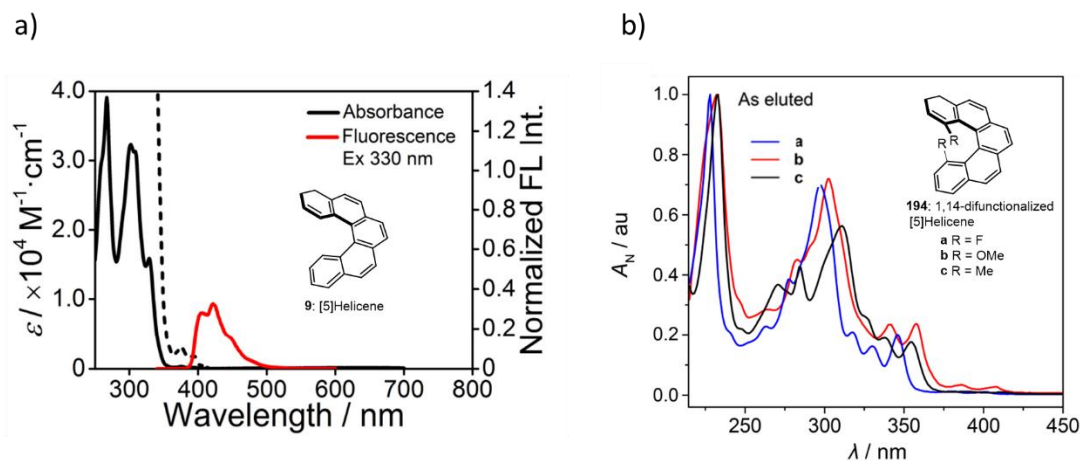


Figure 36. a) Absorption and emission spectra of carbo[5]helicene **9**. b) Normalized absorption spectra of 1,14-difunctionalized [5]helicenes **194**. Images adapted from: H. Kubo, T. Hirose, K. Matsuda, *Org. Lett.* **2017**, *19*, 1776–1779^[57] and P. Ravat, R. Hinkelmann, D. Steinebrunner, A. Prescimone, I. Bodoky, M. Juriček, *Org. Lett.* **2017**, *19*, 3707–3710.^[31]

5.1.7. Conclusion

In summary, four novel BINOL-based α -cationic phosphonites **162a-d** were synthesized and fully characterized. A screening along with other chiral ligands tested their regio- and enantioselectivity in the Au(I)-catalyzed intramolecular hydroarylation reaction to synthesize chiral 1-aryl benzo[5]helicenes **163**.

Experiments with TADDOL-derived precatalyst **162a** were immediately terminated due to their poor results in terms of conversion, regio- and enantioselectivity, despite the various reaction conditions were tried. BINOL-based phosphoramidites **192** provided poor enantioselectivities and reaction conversion, presumably because of a lower π -acidity from the Au(I) core. BINOL-derived ligands **193a**, **193c** and **162a-d** displayed magnificent outcomes concerning conversion ratio and enantiomeric excess of the resultant 1-aryl benzo[5]helicene. 2-Pyrenyl, *p*-biphenyl and 2-naphthyl building blocks attached to the BINOL backbone induced excellent enantioselectivities, and cationic imidazolium rests provided enhanced π -acidity when activating the alkyne for further hydroarylation as well. On the other hand, the presence of an excessively bulky group at the ligand's rim like 9-anthranlyl implied a complete hamper of this reaction.

Complex **162b** was identified as the most efficient Au(I) catalyst across the entire library in terms of regio- and enantioselectivity. Subsequently, the scope of this reaction catalyzed by **162b** was evaluated by preparing and submitting a series of ten alkyne substrates bearing diverse substitution patterns in the hanging phenyl. The presence of electron-rich groups in its *p*-position became pivotal not only when enhancing the conversion by activation of the alkyne, but also by not damaging the enantioselectivity of the reaction. Conversely, the presence of *m*- and *o*-substituents, like in compounds **161f-i**, proved to be detrimental for both regio- and enantioselectivity. Addition of further substituents at the outer part of the rim in substrates **161k-n** did not mean any impediment to the obtention of additional carbo[5]helicenes in notably high purity and enantiomeric excess by Au(I) catalyst **162b**. Using X-ray diffraction analysis, the connectivities in the new structures of carbo[5]helicene and their absolute configurations were established. The latter was additionally corroborated upon circular dichroism studies and comparison with previously reported data. Therefore, the use of catalyst **162b** afforded benzo[5]helicenes **163** with an excess of the (*P*)-form.

UV-Vis absorption and emission studies were performed on model [5]helicene **163a**, and the obtained spectra were compared with two examples reported in the literature. The observed remarkable resemblance with these two sources demonstrated the consistency of the data recorded for this study.

5.2. Enantioselective synthesis of thia[5]helicenes

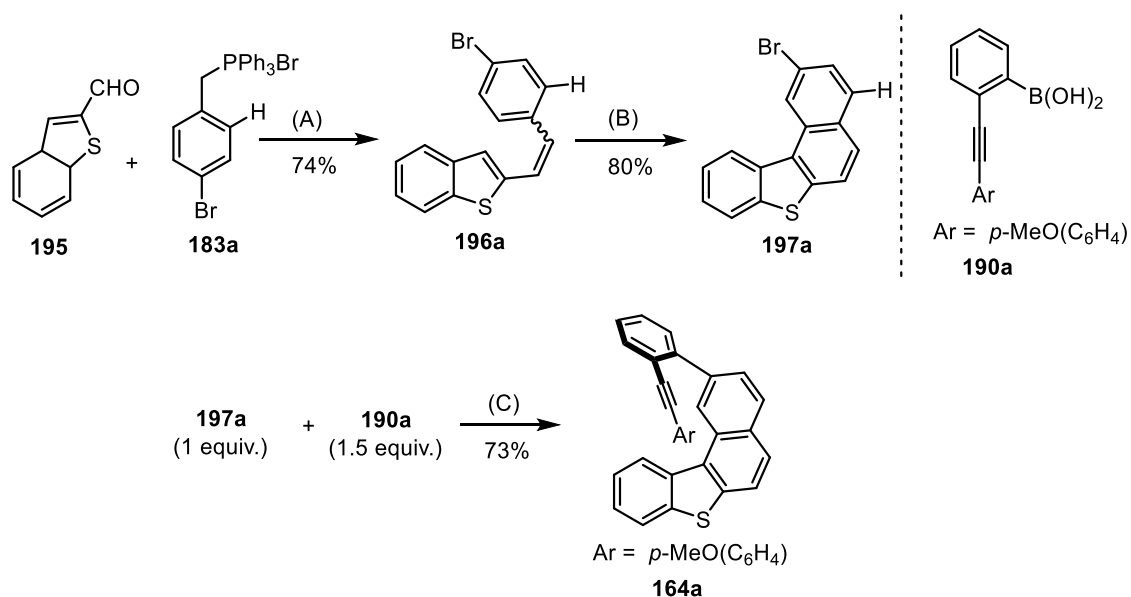
5.2.1. Preparation of thia[5]helicenes

To further investigate the application of these novel BINOL-based Au(I) complexes described in Section 5.1, and encouraged by our group's prior satisfactory experience with dithia[5]helicenes **159**,^[220] a similar approach for the highly enantioselective synthesis of thia[5]helicenes was put forward. As it was previously depicted in Figure 2, a thiahelicene can be formed by replacing one of the fused benzene rings with a five-membered thiophene one. The simplest path to achieve the introduction of this element was the utilization of commercially available benzo[*b*]thiophene-2-carbaldehyde at the first stages of the synthesis of the helicene.

As for the case of carbo[5]helicenes **163**, the introduction of a hanging phenyl at position 1 of the thiahelicene was crucial to preserve the configurational stability of these molecules.

5.2.2. Preliminary screening of model reaction

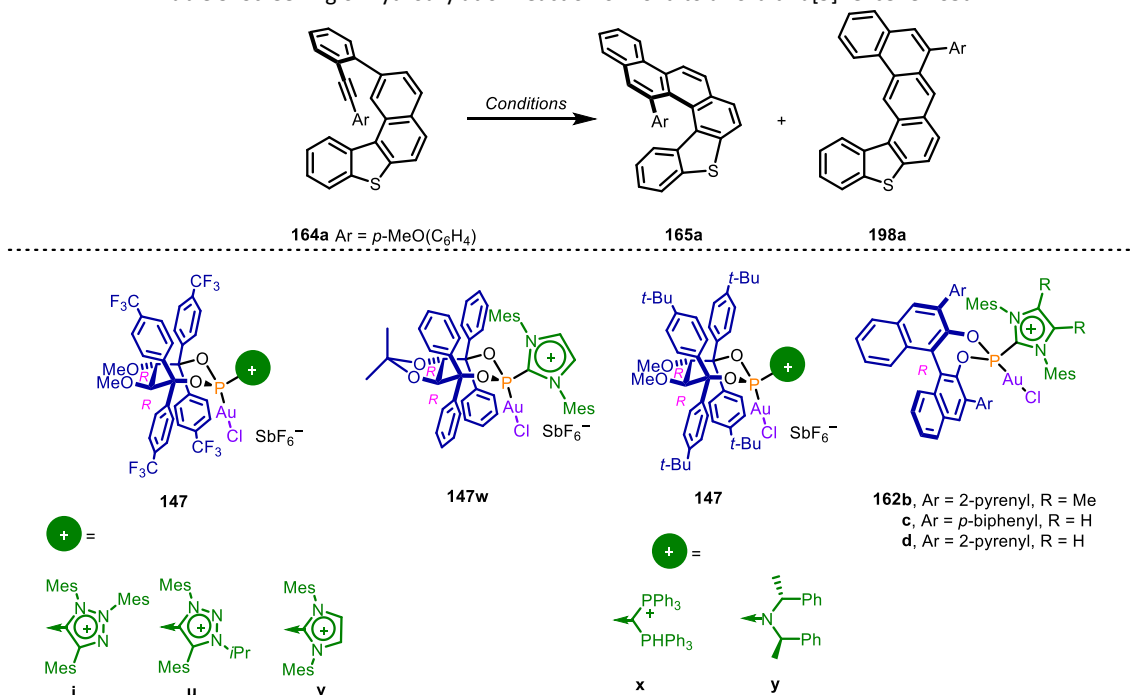
The synthesis of alkyne substrate **164a** was performed following the same strategy as for aforementioned **161a**. As depicted in Scheme 48, stilbene **196a** was obtained as a mixture of both *E*- and *Z*- diastereomers *via* Wittig reaction from commercially available benzo[*b*]thiophene-2-carbaldehyde (**195**) and ylide *in situ* generated from (4-bromobenzyl)triphenylphosphonium bromide (**183**) in a remarkable 74% yield. Subsequent Mallory reaction yielded **197a** as main product in 80% yield. These two first steps were carried out according to the procedures reported in the literature.^[12] In the case of this last transformation, no traces of a dibrominated side product were detected in the crude NMR. This fact, along with the high yield and formation of a single clear product, demonstrated the robustness and versatility of the Mallory reaction, also when forming heterocycles. Finally, Suzuki cross-coupling reaction between **197a** and boronic acid **190a**, obtained as mentioned above in Scheme 45, gave alkyne-substituted substrate **164a**.



Scheme 48. Synthesis of model alkyne-substituted substrate **164a**. Reactants and conditions: (A) MeONa/MeOH, 0 °C → rt, overnight. (B) hv, I₂ (1.1 equiv.), THF, toluene, 125 W, rt, overnight. (C) **197a** (1 equiv., 0.02 M), **190a** (1.5 equiv., 0.03 M), Pd₂(dba)₃ (4 mol%), SPhos (8 mol%), THF:H₂O 5:1, 80 °C, overnight. This synthesis was optimized with the help of MeMo students Tobias Ketzler, B.Sc., and Michael Fitzner, B.Sc.

Once substrate **164a** was obtained and purified, it was then subjected to model hydroarylation reaction catalyzed by Au(I) complex **147i**. This TADDOL-based complex was chosen as a suitable candidate for the first preliminary catalyst due to the high enantioselectivity induced in synthesis of dithia[5]helicenes.^[220] Although very high regio- and enantioselectivities (90% yield and 87% *ee*, Table 5, entry 1) were observed in this first attempted preparation of thia[5]helicene **165a**, substrate **164a** was subsequently screened with eight additional Au(I) precatalysts. Ligands **147u** and **147v** containing an identical TADDOL backbone but different cationic rests were also tested as potential catalysts. Both induced excellent regioselectivities and good enantioselectivities (>99:1 conversion ratio in both cases, 83% and 76% *ee*, respectively, Table 5, entries 2 and 3). Nonetheless, elimination of electrondeficient *p*-trifluoromethyl groups at the backbone in **147w** proved to have a detrimental effect on the enantioselectivity, which dropped to 27% *ee* (Table 5, entry 4). This result curiously resembles to the 28% *ee* this catalyst induced to 1,12-disubstituted [4]helicenes in previous research of our group.^[219] Reactions catalyzed by complexes **147x-y** bearing *p*-*tert*-Bu-phenyl groups at the ligand's backbone did not take place, as shown by zero conversion when they were catalysts. This fact can be presumably attributed to a diminution of the π -acidity of the Au(I) core. The replacement of N-heterocyclic (NHCs) cationic rests attached to the phosphorus atom with biphosphonium and neutral phosphoramidite groups entailed a detriment of the π -acceptor properties of the phosphonite and therefore, an augmentation of the electronic density around the Au(I) atom.

Table 5. Screening of hydroarylation reaction of **164a** to afford thia[5]helicene **165a**.



Entry	Catalyst	Temperature [°C]	Conversion [%] ^[a]	165a:198a ^[b]	Isolated yield [%]	<i>ee</i> [%] ^[a]
1 ^[c]	147i	-20	>99	>99:1	90	(+)-87
2 ^[c]	147u	-20	>99	>99:1	95	(+)-83
3 ^[c]	147v	-20	>99	>99:1	96	(+)-76
4 ^[c]	147w	-20	>99	>99:1	95	(+)-27
5 ^[c]	147x	-20	0	-	-	-
6 ^[c]	147y	-20	0	-	-	-
7	162b	-10	>99	>99:1	73	(+)-90
8 ^[c]	162c	-10	>99	>99:1	96	(+)-91
9 ^[c]	162d	-10	>99	>99:1	96	(+)-89

Reaction conditions: **164a** (0.05 M), Au(I)-cat. (5 mol%), AgSbF₆ (5 mol%), CH₂Cl₂, 48 h. [a] Conversion determined by chiral-phase HPLC. [b] determined by ¹H NMR of the crude reaction mixtures. [c] Reactions carried out by Dr. Valentina Pelliccioli.

Finally, BINOL-based Au(I) complexes **162b-d** were also subjected to screening in this reaction. Gratifyingly, helicene **165a** was obtained in these last three cases with excellent regio- and enantioselectivities (Table 5, entries 7-9), as it was previously observed for carbo[5]helicenes in Section 5.1.4. The best compromise was obtained by reinforcement of structural rigidity in the BINOL-based catalyst **162c** with *p*-biphenyl groups and applying a 2-imidazolium cationic rest. All catalysts utilized in this preliminary study were kindly provided by Dr. Jianwei Zhang, Dr. Thierry Hartung and Wei Fu, M.Sc.

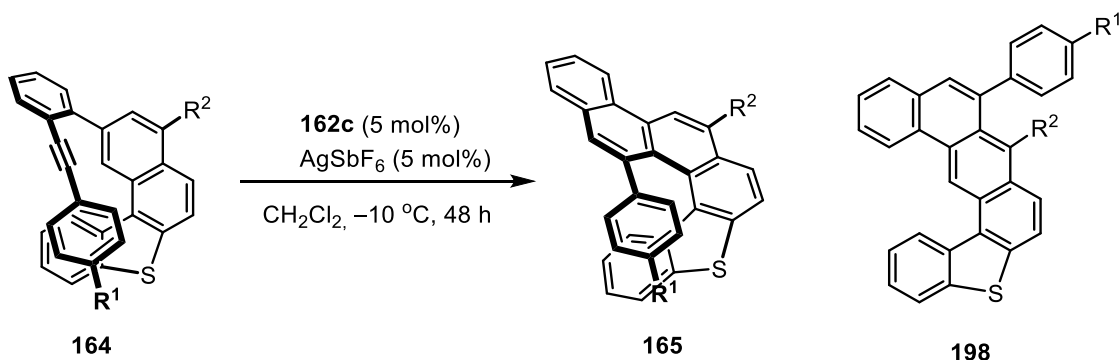
5.2.3. Substrate scope

As soon as the versatility of the approach was demonstrated by the synthesis of this new class of thia[5]helicenes and the most efficient catalyst was identified, a library of key intermediates **164** was prepared according to the established procedure shown in Scheme 48 (see also Scheme 58 in the Experimental Section). In particular, eight alkyne substrates containing a broad variety of substitution patterns at the hanging phenyl were obtained *via* Suzuki cross-coupling from moderate to good yields. Since *o*- and *m*-substitution in the terminal ring of a tolane moiety implied an erosive effect on obtaining enantiopure samples of carbo[5]helicenes, as indicated in Section 5.1.5 (Table 3), this group focused on the introduction of *p*-substituents in this position of a helicene.

With these precursors in hand, a wide substrate scope of precursors **164** was transformed into thia[5]helicenes **165** by Au(I)-catalyzed enantioselective hydroarylation (Table 6). Substrates containing electron-rich substituents, such as **164a-f** used in entries 1-6 of the Table 6, cyclized into their corresponding thia[5]helicenes **165a-f** in extremely good yields and conversion ratios, as well as in with excellent enantioselectivities in the range of 91-99% *ee*. Obviously, the presence of these well-known and contrasting substituents was a key factor in obtaining these results. It is noteworthy that even the availability of electronegative groups, such as fluorine or trifluoromethyl, does not prevent the almost complete transformation of **164g** and **164h** into the corresponding helicenes. On the other hand, helicene **164g** was obtained with excellent enantioselectivity (entry 7), whereas **164h** containing a *p*-CF₃ group barely reached a moderate 68% *ee*. It is still an open question whether the steric volume of this substituent had a huge impact on the stereoselectivity of this reaction. Electronic effects might have also played an important role in the erosion of the enantioselectivity, as the polarity of the trifluoromethyl group extremely differs from that of the rest of substituents.

Additionally, two extra substrates **164i** and **164j** bearing a methyl group at the outer part of the rim, i. e. methylated **164a** and **164j**, were successfully synthesized and submitted to this reaction as well. This further feature was completely harmless to the enantioselectivity of the process (Table 6, entries 9, 10), as almost identical *ee*'s were observed in comparison to their 'bare' helicene homologous **165a** and **165b**.

Table 6. Substrate scope of compounds **164** with different substitution patterns at the aryl substituent and at the helicene rim.



Entry	164	R ¹	R ²	165	165:198 ^[a]	Yield (%)	<i>ee</i> (%) ^[b]
1	164a	OMe	H	165a	>99:1	96	91
2	164b	Me	H	165b	>99:1	98	96
3	164c	OBn	H	165c	>99:1	91	96
4	164d	SiMe ₃	H	165d	>99:1	80	99
5	164e	OPh	H	165e	>99:1	97	97
6	164f	OBu	H	165f	>99:1	99	97
7	164g	F	H	165g	>99:1	95	93
8	164h	CF ₃	H	165h	>99:1	95	68
9	164i	OMe	Me	165i	>99:1	97	91
10	164j	Me	Me	165j	>99:1	96	95

[a] Determined by ¹H NMR of the crude reaction mixtures. [b] Determined by chiral-phase HPLC. Entries 2-10 were performed by Dr. Valentina Pelliccioli.

5.2.4. Conclusion

In order to continue expanding the applicability of Au(I)-catalyzed hydroarylation for the enantioselective synthesis of helicenes, 9 different BINOL- and TADDOL-based Au(I) catalysts were initially employed in a preliminary screening in a model reaction to produce thia[5]helicene **165a** from **164a**.

TADDOL-based Au(I)-catalysts **147i** and **147u** bearing a triazolium cationic moiety performed this reaction in excellent conversion ratios with very good *ee*'s, whereas **147v** containing a less bulky imidazolium moiety exhibited a slightly inferior enantioselectivity, but no conversion decrease. On the other hand, the suppression of the *p*-CF₃ groups present at the chiral backbone implied a tremendous erosion in the enantioselectivity, as it was observed in the case of **147w**. TADDOL-based Au(I) complexes **147x-y** with *p*-*tert*-Bu-phenyl groups at the ligand's backbone had nonexistent catalytic activity, since zero conversion to thia[5]helicene

165a was observed. These results could be attributed to a diminution of the π -acidity of the Au(I) core. Fortunately, screening of BINOL-based Au(I) complexes **162b-d** in this hydroarylation process was more successful, as excellent *ee*'s values and conversion ratios were observed.

Once **162c** was distinguished as the most suitable catalyst in terms of regio- and enantioselectivity, the scope of the hydroarylation towards thia[5]helicenes **165** was evaluated through the preparation of ten alkyne-decorated substrates **164** with diversely substituted hanging phenyl groups or a tuned outer rim. Since the presence of *m*- and *o*-substituents proved to be detrimental in the case of prior carbohelicenes **163**, only *p*-substituents were tested in this Section. Gratifyingly, nine out of ten helicenes (**165a-g, i, j**) were obtained with excellent *ee*'s, conversions and yields regardless of the activating or deactivating character of the substituent. Only **165h** containing a *p*-CF₃ substituent experienced an erosion in its enantioselectivity, presumably attributed to intense electronic and steric effects. The presence of a methyl group at the outer part of the helicene skeleton did not imply any loss of regio- or enantioselectivity in the case of compounds **165i,j**.

5.3. In-fjord substitution in expanded helicenes and its consequences

Inspired by Matsuda's attempt of synthesis of a chiral expanded helicene,^[45] the preparation of compounds **166-169** was envisaged (Figure 37). As previously mentioned, the excessive flexibility of **86** facilitated the interconversion between its two possible enantiomeric forms, manifested as a low energetic barrier. In order to circumvent this difficulty, our strategy focused on the introduction of aryl substituents at the inner fjord of the helicene's structure and the study of its effect on the enantiomerization process.

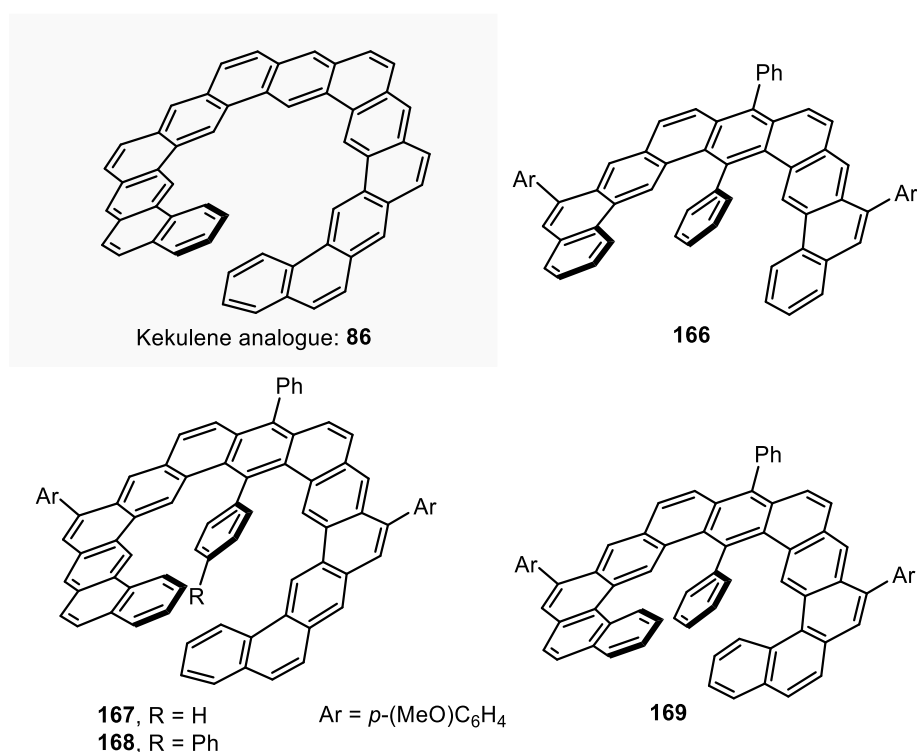


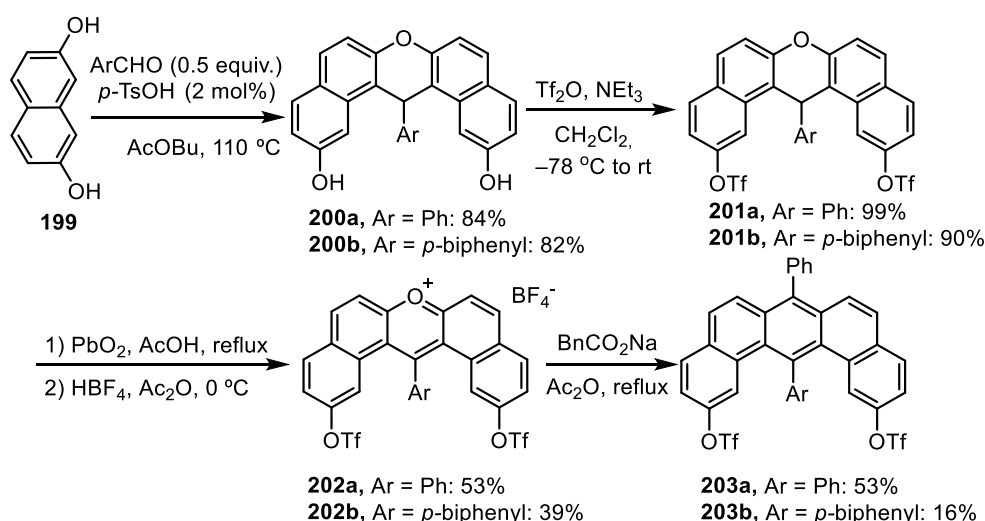
Figure 37. Matsuda's kekulene analogue and target molecules **166-169**.

Due to the inherent difficulty of this task, the inner substituents were introduced at the first stage of the synthesis as depicted in the following Section. C_2 symmetry present in these structures allowed these architectures to be created simultaneously and gracefully reduced the number of synthesis steps.

5.3.1. Synthesis of in-fjord substituted expanded helicenes

Since the functionalization of the inner part of a complex π -expanded system like these compounds is extremely complicated, the syntheses reported here began with the introduction of such substituent from the first step.

Commercially available 2,7-naphthalenediol **199** was efficiently transformed into xanthenes **200**. The condensation reaction was performed with 0.5 equiv. of the appropriate aromatic aldehyde under acidic catalysis (Scheme 49) in up to 84% yield. Due to the enhanced temperature and polarity required for this process, butyl acetate with a boiling point of 126 °C was the most suitable candidate as a reaction solvent. Subsequent triflation of both **200** alcohols gave triflates **201** in excellent yields. This transformation was followed by oxidation of the polycyclic core with PbO₂, and the resulting crude product was utilized without further purification for acid-promoted elimination with aq. HBF₄ to afford key pyrylium salts **202**. The condensation reaction between the latter and sodium phenylacetate, based on published reports concerning pyrylium salts chemistry,^[237–239] afforded the desired benzo[*m*]tetraphene core in a gram scale *via* in situ decarboxylation. It can be noted that, due to steric hindrance and solubility reasons, compound **203b** was obtained in a noticeable lower yield (16%) in comparison to **203a** (53%). The overall yield of **203a** and **203b** was 23 and 5%, respectively.

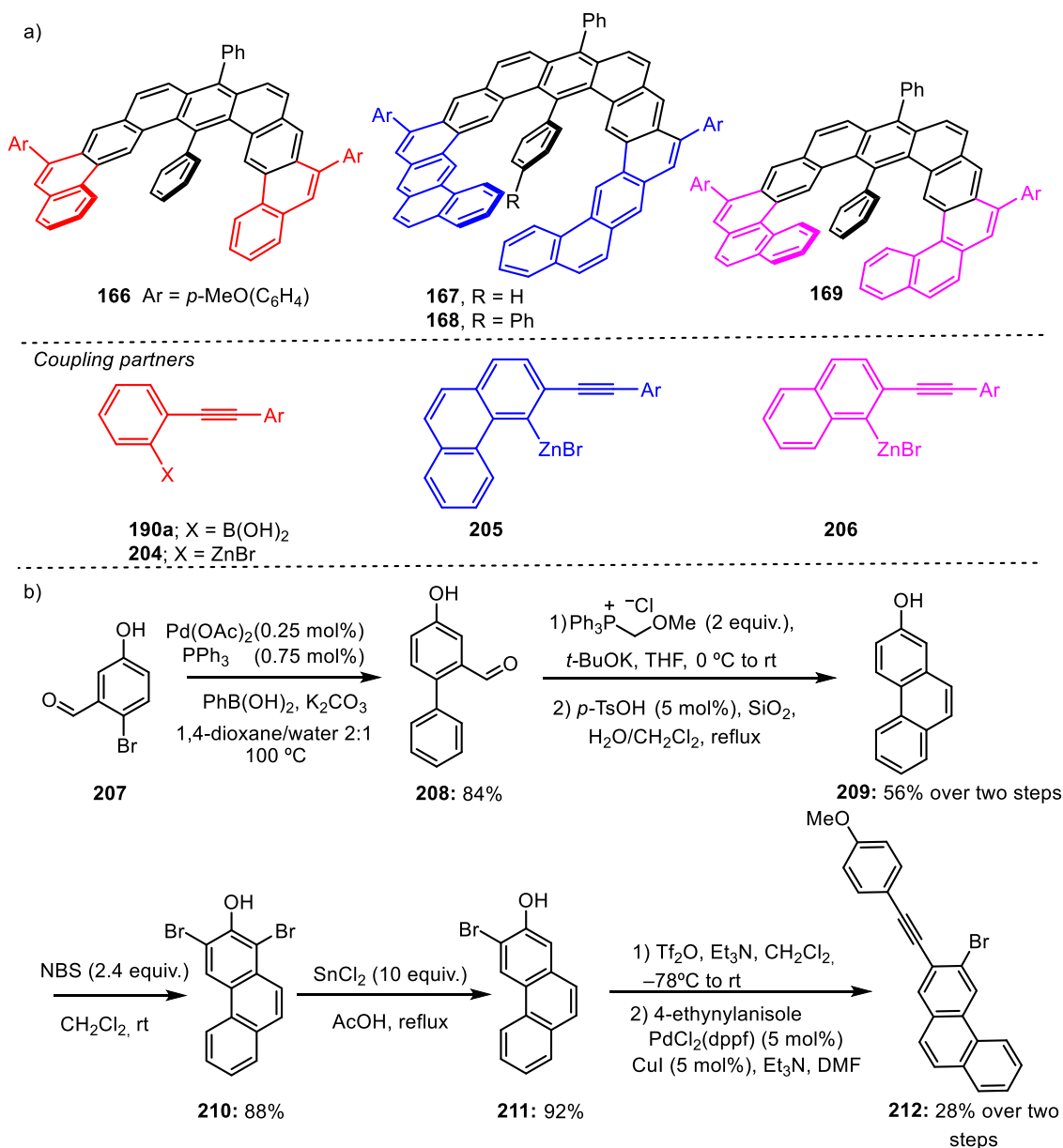


Scheme 49. Synthesis of benzo[*m*]tetraphene core.

In tandem with this approach, the various coupling partners for this helicene core were designed and synthesized, as depicted in Scheme 50a. Compounds **190a**, **204** and **206** were prepared following procedures reported in the literature,^[131,219] whereas a particular synthesis for the alkyne-containing phenanthrene moiety **205** was elaborated (Scheme 50b).

Commercially available 2-bromo-5-hydroxybenzaldehyde (**207**) was reacted with benzeneboronic acid via Suzuki cross-coupling procedure to produce 4-hydroxy-[1,1'-biphenyl]-2-carbaldehyde **208** in good yield; fortunately, the presence of a hydroxyl group in the molecule did not interfere with the reaction, and the desired compound was obtained in 84% yield. Further Wittig reaction with ylide prepared in situ from (methoxymethyl)triphenylphosphonium chloride followed by immediate cyclization catalyzed

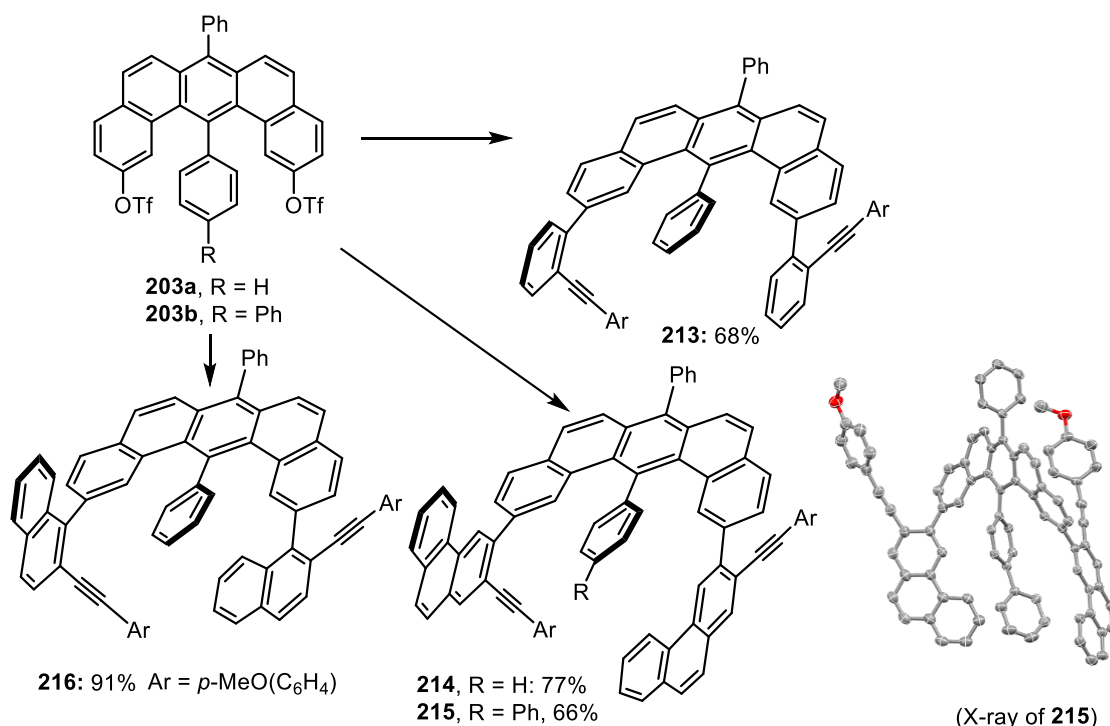
with *p*-TsOH in the presence of silica yielded phenanthren-2-ol (**209**) in moderate yield over two steps. Subsequent dibromination and partial debromination successively afforded products **210** and **211** in very good yields, thus introducing the halide in the desired position.



Scheme 50. a) Coupling partners for the synthesis of compounds **166-169**. b) Synthesis of the phenanthrene **205** containing an alkyne moiety.

Finally, a challenging one-pot triflation and Sonogashira cross-coupling gave the target 3-bromo-2-[(4-methoxyphenyl)ethynyl]phenanthrene (**212**) in poor yield (28%). It is important to note that *p*-MeO(C₆H₄) substituents were strategically located at the alkyne termini of **190a**, **204-206** with the aim of suppressing parasitic 5-*exo*-dig cyclizations and the subsequent formation of non-benzenoid rings during the final Au(I)-catalyzed hydroarylation reaction, as based on previous experience of our group with [*n*]helicenes.^[217,218]

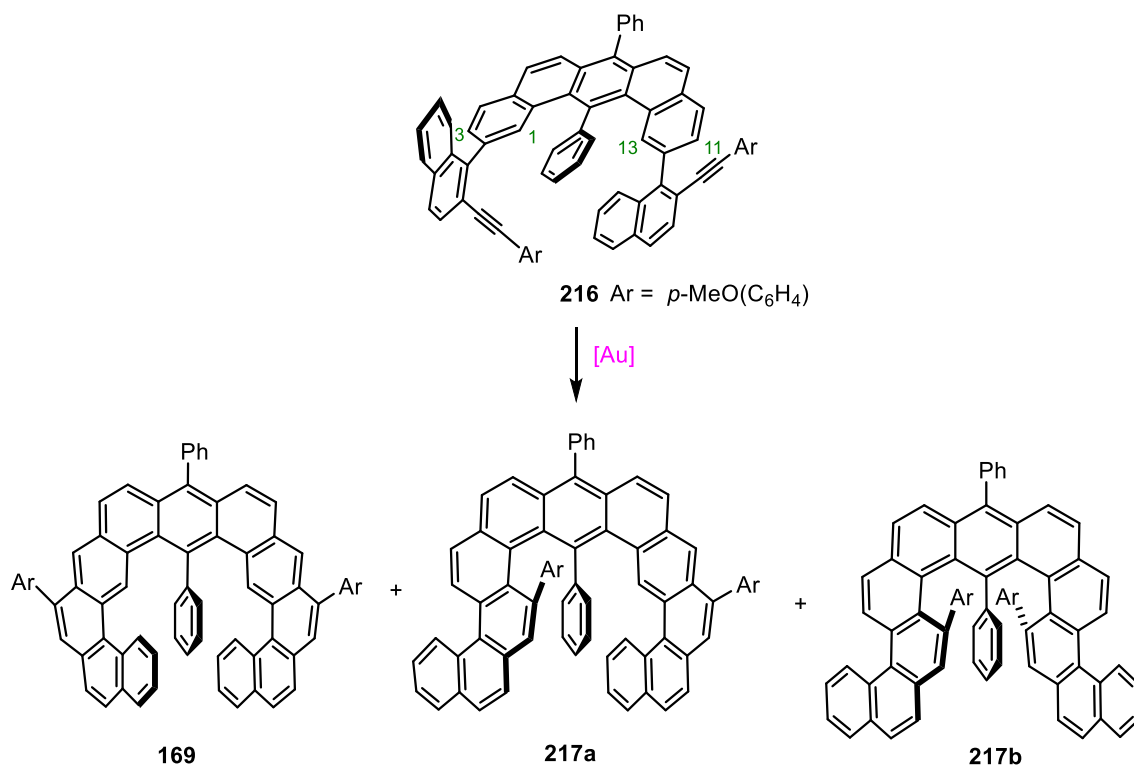
Initial attempts to couple **203a** with an excess of boronic acid **190a** (5.0 equiv.) *via* Suzuki reaction afforded **213** in a quite modest yield, mainly due to the protodeborylation of **190a**. Interestingly, Müllen *et al.*^[238] described the synthesis of similar to **203** substrates, but containing bromide groups instead of triflates; however, handling with **203-Br** was more problematic in terms of solubility and purification compared to bistriflates. Once the coupling partners **204-206** were synthesized, expanded helicenes substrates were obtained *via* Negishi coupling after thorough optimization of the reaction conditions. Taking into account the efficacy of microwave irradiation in contrast to conventional heating,^[240,241] this set of reactions seems to be carried out most efficiently by this method after the preparation of the corresponding organozinc compounds **204-206**. Most optimal conditions proved to be heating at 100 °C with medium power for 30 min under Ar atmosphere, as depicted in Scheme 51. Remarkably, the steric hindrance of the in-fjord substituent had an obvious effect on the yield of this reaction, as can be observed when comparing the reaction yields of **214** and **215**. Additionally, the connection in coupling product **215** was confirmed by X-ray crystallography of single crystal by (Scheme 51, bottom, right). The appropriate single crystals were grown by hexane diffusion into an ethyl acetate solution.



Scheme 51. Syntheses of expanded helicene substrates **213-216**. Reactants and conditions: **204-206** (5.0 equiv.), Pd₂(dba)₃ (2.5 mol%), SPhos (15 mol %), μ w 100 °C, 30 min.

In order to obtain the target expanded helicenes, a final step based on the Au(I)-mediated π -acid catalysis methodology of our group was envisioned. Since a potential hydroarylation reaction could take place at two different sites of benzo[*m*]tetraphene core **216** – the

electronically more activated but sterically hindered positions 1 and 13 or the more accessible external ones 3 and 11 – a preliminary study of the reaction conditions was necessary. Three products of 6-*endo*-dig cyclization were obtained from the Au(I)-catalyzed hydroarylation of precursor **216** – compounds **169**, **217a** and **217b**. Product **169** corresponds to the desired expanded helicene and originates from cyclization at both external positions of the benzo[*m*]tetraphene core. Structure **217a** is a stereochemically fixed polyarene derived from internal and external cyclizations at positions 1 and 11, respectively. Finally, **217b** is a C₂-symmetric double S-shape ribbon (Scheme 52). Once this strategy based on Au(I) catalysis was confirmed as suitable, a screening to choose the most efficient catalyst was executed (Table 7).



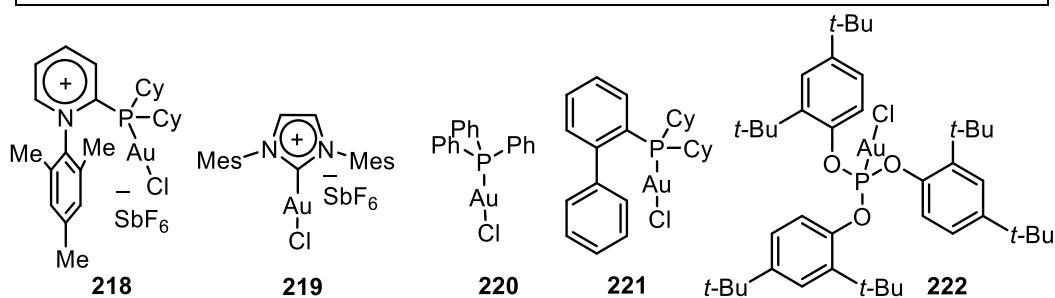
Scheme 52. Products of Au(I)-catalyzed hydroarylation of precursor **216**. Reactant and conditions: **216** (0.03 M), Au-catalyst (10 mol%), AgSbF₆ (10 mol%), CH₂Cl₂, rt.

Precatalyst **219**, based on a strong σ -donating NHC ligand, exhibited the lowest reactivity in the entire scope along with very low discrimination between the different possible products (Table 7, entry 1). In fact, intermediates of only monohydroarylation were the main compounds observed by NMR analyses of these reaction crudes, which demonstrated the suboptimal catalytic performance of this complex. Catalyst **220**, consisting of PPh₃ as ancillary ligand, furnished a much faster reaction and yields were substantially increased; however, the reaction outcome remained poor in terms of product selectivity (Table 7, entry 2). When evaluating the possible influence of bulkiness on the reaction outcome, catalyst **221** was employed and directed more preferentially the hydroarylation at the external and less

hindered position of the benzo[m]tetraphene core (Table 7, entry 3). Since the utilization of a strong π -acceptor phosphite ancillary ligand could accelerate the reaction rate and increase conversion, phosphite-Au(I) complex **222** was tested as a potential candidate. Nonetheless, it proved to favor the formation of the undesired product of double internal cyclisation **217b** as well (Table 7, entry 4). The summary of results demonstrated that the employment of a ligand combining both bulkiness and a strong π -acceptor character could be ideal to promote the selective formation of **169** with better yields. For this reason, Au(I) complex **218** with a *N*-arylpyridinium phosphine as ancillary ligand was chosen as the most suitable catalyst for this task. Despite the long reaction time, enhanced conversion, regioselectivity and yield made **218** the best candidate from all Au(I) complexes tested in this screening. Optimization of the solvent and temperature, as described in the Experimental part, allowed the isolation of **169** in a remarkable yield of 60%.

Table 7. Ligand effect in the Au-catalyzed intramolecular hydroarylation of **216**.

Entry	Catalyst	Time	Conversion/Ratio 169:217a:217b	Yields (%) ^[a] 169:217a:217b
1	219	36 h	60/35:30:35	11:9:11
2	220	5 h	95/30:30:40	19:19:26
3	221	12 h	95/30:52:18	16:28:10
4	222	3 h	>98/14:32:54	10:24:40
5	218	2 h	98/49:29:22	32:19:15
6 ^[b]	218	3 h	98/67:27:6	46:18:4
7 ^[b,c]	218	4 d	95/78:22:0	60:17:0



[a] Isolated yields of each product; [b] A 3:1 mixture of $C_6H_5F:CH_2Cl_2$ was used as solvent; [c] Reaction carried out at 4 °C.

Confirming the discoveries of prior studies relevant to cationic phosphines,^[185] those ligands based on *N*-substituted pyridiniophosphine moieties are the best π -acceptor phosphines among monocationic ones. In virtue of their unmatched structural features, they can depict outstanding performances in transition metal-catalyzed hydroarylation reactions (Figure 38).

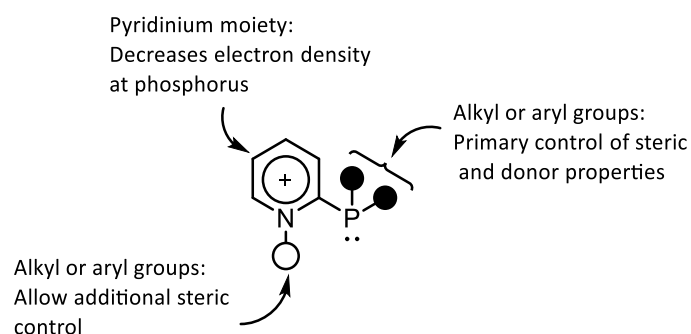
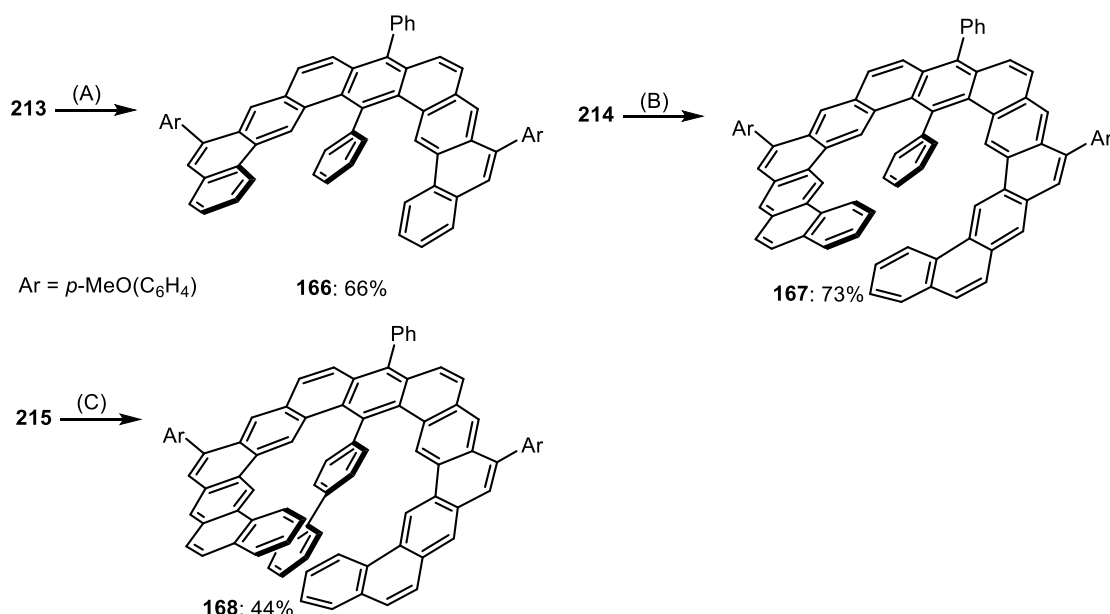


Figure 38. Structural features of a typical pyridinium-substituted ligand. Adapted from: M. Alcarazo, *Chem. – Eur. J.* **2014**, *20*, 7868–7877.^[185]

After finding the optimal catalyst and conditions to favor the cyclisation towards expanded helicene **169** over other regioisomers, identical procedures on substrates **213-216** were performed (Scheme 53). The cyclisation of **213** afforded a 5:1 mixture of products from which expanded helicene **166** was isolated in 66% yield. An identical cycloisomerization of **214** gave a 8:1 mixture of products, from which expanded helicene **167** was isolated in a remarkable 73% yield. Finally, biphenyl-substituted expanded helicene **168** was obtained in a modest 44% yield from a relatively complex reaction mixture (Scheme 53). In this latter case, difficulties concerning the solubility of such an expanded π -system hampered not only realization of the reaction, but also the subsequent purification process. Because of the difficulties encountered at this point and with the help of NMR studies, it is strongly believed that its complex structure acted as a cage for small aliphatic solvent molecules. These new expanded helicenes showed poor solubility in alkanes and chlorinated solvents, but, like buckminsterfullerene C_{60} , high in CS_2 and warm toluene, especially in the case of compound **168**. This observation suggested that π -stacking aggregation between molecules was superior in these media than in the first mentioned solvents.



Scheme 53. Final Au(I)-catalyzed hydroarylation of alkynes **213-215** to afford in-fjord substituted expanded helicenes **166-168**. Reagents and conditions: (A) **213** (0.030 M), **218** (10 mol%), AgSbF₆ 10 mol%, PhF, 0 °C to rt, 14 h; (B) **214** (0.013 M), **218** (10 mol%), AgSbF₆ (10 mol%), PhF:CH₂Cl₂ 2:1, rt, 24 h; (C) **215** (0.016 M), **218** (10 mol%), AgSbF₆ (10 mol%), C₂H₂Cl₄, rt, 1 h.

5.3.2. Solid state structures

Once the entire set of in-fjord substituted expanded helicenes was synthesized, suitable for X-ray analyses single crystals of these species were grown applying different methods, and their solid state structures were determined.

In the case of expanded helicene **166**, its crystals were obtained by vapor diffusion of hexane into a chloroform solution. Not only its connectivity was verified via X-ray analysis, but also the local aromaticity of each aromatic ring of the molecule was calculated (Figure 39a). Compound **166** also exhibited a loss of planarity due to the presence of the phenyl group Z, as depicted in Figures 39b-c, with a helical pitch d_{A-I} of 9.8 Å and an interplanar angle Θ_{A-I} of 45.8°.

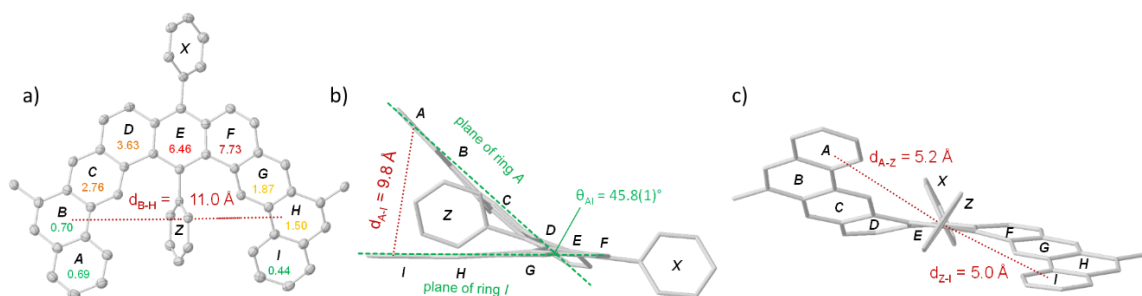


Figure 39. a) X-ray structure of **166**, deviation of each benzene ring from the mean plane represented in % and distance between rings B and H (helical diameter). b) Representation of the deviation of planarity in **166** and calculation of the helical pitch d_{A-I} . c) Calculation of interplanar distances d_{A-Z} and d_{Z-I} from each of the terminal rings to the inner phenyl substituent Z. Only the ipso-carbon from the external *p*-(OMe)C₆H₄ substituents is shown. Hydrogen atoms were removed for clarity; ellipsoids are represented at 50%. Root mean square deviation (RMS) from mean plane on each aromatic ring is given in %.

Despite this result, the short arms of **166** precluded an exhaustive study of the influence of an inner substituent in the structure. For this reason, the comparison between the structures of **168** and **86**^[45] was more suitable when analyzing the influence of in-fjord substitution on the structural deformation, electronic structure, local aromaticity and, indirectly, on the helical inversion barrier of π -expanded helicenes as well (Figure 40a). Compound **168** crystallized as a racemate from a mixture of warm toluene and cyclohexane after approximately 3 months. The two enantiomers separately stacked along the *b*-axis, in the way that parallel columns of only *P*- and *M*-enantiomers are formed in a similar fashion as other extended aforementioned π -systems.^[71] Rings D, E and I, J of consecutively piled molecules overlap, with the shortest π -stacking distance of 3.5 Å; disordered hexane molecules occupied the channel between these columns (see Appendix, Section 8.3). As depicted in Figure 40b, belonging to the fjord cavity rings F, G and H seemed to be clearly twisted, whereas both helical arms were virtually planar. This was also evident from the comparison of the root mean square deviation (RMS) of the carbon atom positions from the mean plane of the benzene ring to which they belong. These values in % are represented inside of each aromatic ring in Figure 40b. Another remarkable feature of this discovery was that the Y-ring of the biphenyl inner substituent also produced repulsive interactions with the internal protons of rings E and I. As a consequence, the helicene arms open in a plane perpendicular to the helicoidal axis, increasing the helical diameter of **168** ($d_{D-J} = 10.9$ Å) in comparison to that of the unsubstituted core structure **86** ($d_{D-J} = 10.2$ Å). As it was expected, **168** showed a helical pitch larger than that of **86** ($d_{A-M} = 7.7$ Å in the case of **168** and $d_{A-M} = 3.7$ Å in the case of **86**) (Figure 40c). Surprisingly, it was observed that the innermost anthracene unit of the fjord cavity accumulated most of the necessary distortion to accommodate the biphenyl insert, as reflected by the torsion angles along the helical inner rim ($\Phi = 4.1^\circ, 4.0^\circ, 14.6^\circ, 21.3^\circ, 1.6^\circ, 4.5^\circ$ for **168**). Curiously, the terminal edges of the helicene arms in **168** (rings A and M, respectively) were conveniently stacked on the top and bottom of ring Z of the biphenyl substituent, respectively; representing the interplanar distances, measured from the centroids of the rings, $d_{A-Z} = 4.0$ Å and $d_{M-Z} = 3.8$ Å and $d_{A-M} = 7.7$ Å (Figure 40d). Interestingly, these values are very similar to the pitches found in high order helicenes like [16]helicene reported by Fujita *et al.*^[242]

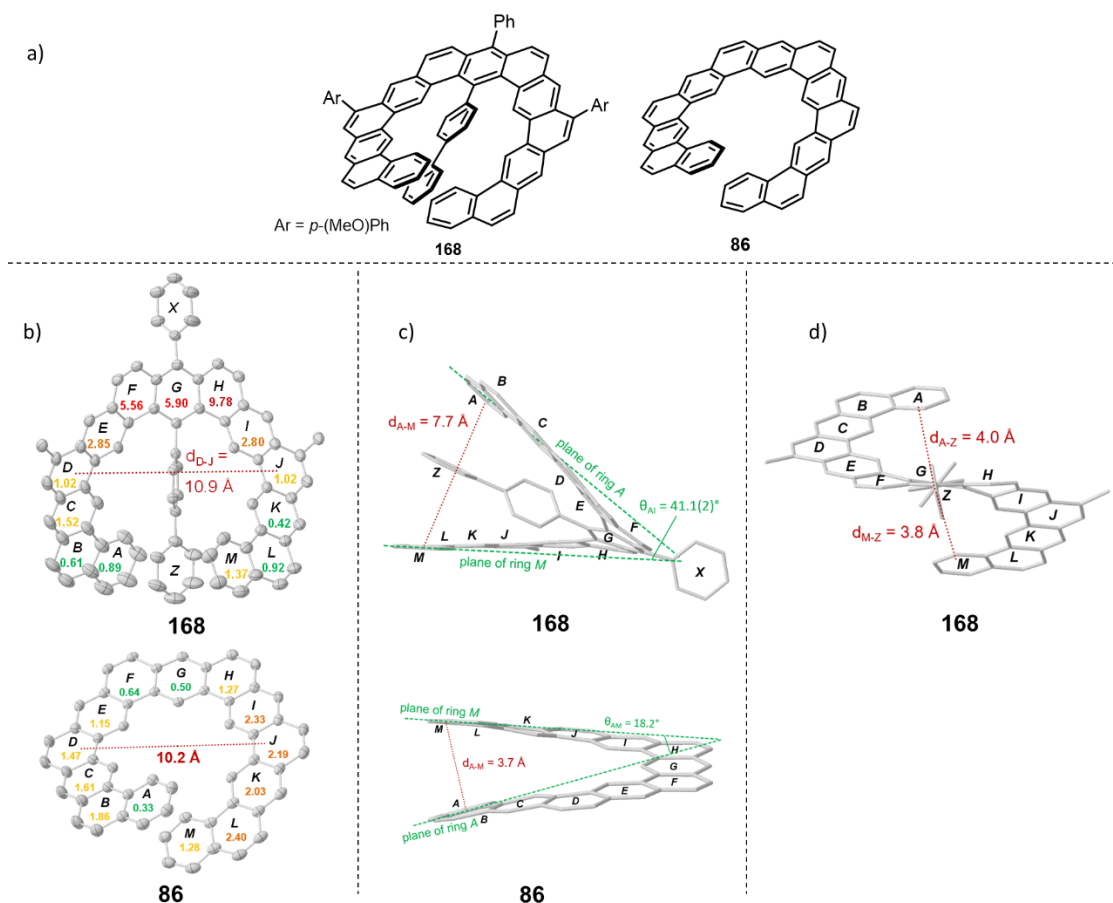


Figure 40. a) Target expanded helicene **168** and Matsuda's kekulene analogue **86**. b) Depiction of their X-rays structures, including the calculation of their helical diameters and deviations of each ring from the mean plane. c) Comparison of helical pitches and interplanar angles of **168** and **86**. d) Calculation of interplanar distances d_{A-Z} and d_{M-Z} , whose sum nearly coincides with the helical pitch. Only the ipso-carbon from the external p -OMe- C_6H_4 substituents is shown in d). Hydrogen atoms were removed for clarity; ellipsoids are represented at 15% probability for **168**. Root mean square deviation (RMS) from mean plane on each aromatic ring is given in %.

Even though it was not possible to obtain a crystal of **167** suitable for X-ray analysis, calculations at the PBEh3c level of theory closely reproduced its solid state structure. The same phenomenon as in previous helicenes was observed in the anthracene moiety formed by rings F, G and H with relatively high RMS values. Additionally, the helical diameter of **167** ($d_{D-J} = 10.9$ Å) (Figure 41a) was predicted and proved to be identical to that of **168** and extremely similar to that of **166** (11.0 Å) (Figure 39a). These calculations, which closely reproduced the pitches of **166**, **168** and **169**, predicted $d_{A-M} = 8.2$ Å in the architecture of **169** as well. This meant that this compound exhibited a longer helical pitch than that of **168** (*cf.* Figures 40c and 41b), which could only be explained by the assumption of the presence of attractive π - π interactions between the helicene arms and ring Z of the insert in **168** (See Appendix, Section 8.3).

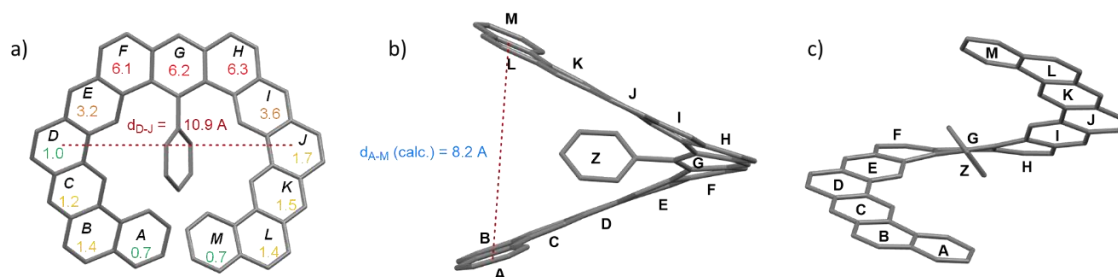


Figure 41. a) X-ray structure of **167** and representation of the RMS deviation from mean plane of each benzene ring given in %; b) Prediction of the helical pitch d_{A-M} of **167**; c) Display of the helical structure of **167** from a frontal plane. Hydrogen atoms were removed for clarity; ellipsoids are represented at 50% probability. Root mean square deviation (RMS) from mean plane on each aromatic ring is given in %.

Finally, the solid state structure of **169** was quite informative as well. The molecule adopted an approximately C_2 -symmetric conformation, and its helical pitch measured from the centroids of the rings A, and K (8.5 Å) was the biggest one in the series due to the angular-angular junction of terminal rings A-B and J-K, which increased the unfavorable steric interaction of these moieties with ring Z and forces ring tilting also at the arms. Subsequently, the torsion angles along the helical inner rim ($\Phi = 20.4^\circ, 20.0^\circ, 20.4^\circ, 25.7^\circ, 21.5^\circ, 17.5^\circ$) and the RMS deviation of the carbon atoms from the ideal benzene plane (Figure 42a) revealed high evenly distributed deformations along the complete structure unlike previous expanded helicenes, which manifests a clear loss of planarity in this molecule. This was the main difference between **169**, **166** ($\Phi = 1.1^\circ, 14.9^\circ, 25.7^\circ, 6.2^\circ$) and **168** (Figures 40-42). Due to the wide helical pitch observed, **168** presented a narrower interplanar angle ($\theta_{AK} = 38.3^\circ$) in comparison to **166** and **168**.

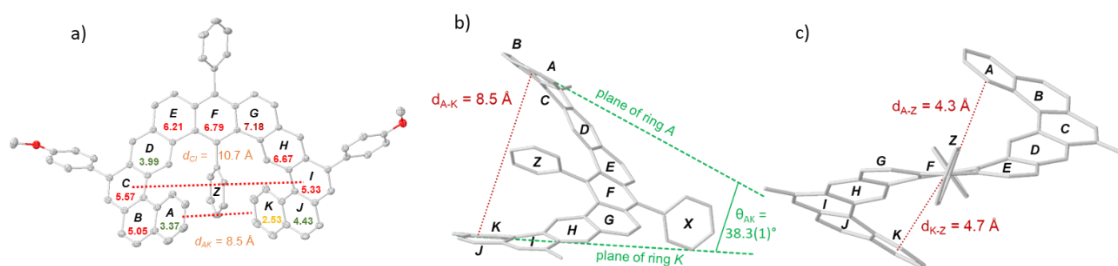


Figure 42. a) X-ray structure of **168**, prediction of d_{C-I} and helical pitch d_{A-K} and representation of the RMS deviation from mean plane of each benzene ring given in %. b) Helical pitch and interplanar angle of **168**. c) Calculation of interplanar distances d_{A-Z} and d_{K-Z} . Only the ipso-carbon from the external p -(OMe) C_6H_4 substituents is shown in b) and c). Hydrogen atoms were removed for clarity; ellipsoids are represented at 50% probability.

Finally, the connectivity in **217a-b** was confirmed *via* X-ray analysis as well (Figure 43). Single crystals were grown by slow diffusion of hexane to their solutions in a mixture of $CHCl_3$ and CH_2Cl_2 in the case of **217a** or tetrahydrofuran and pentane in the case of **217b**.

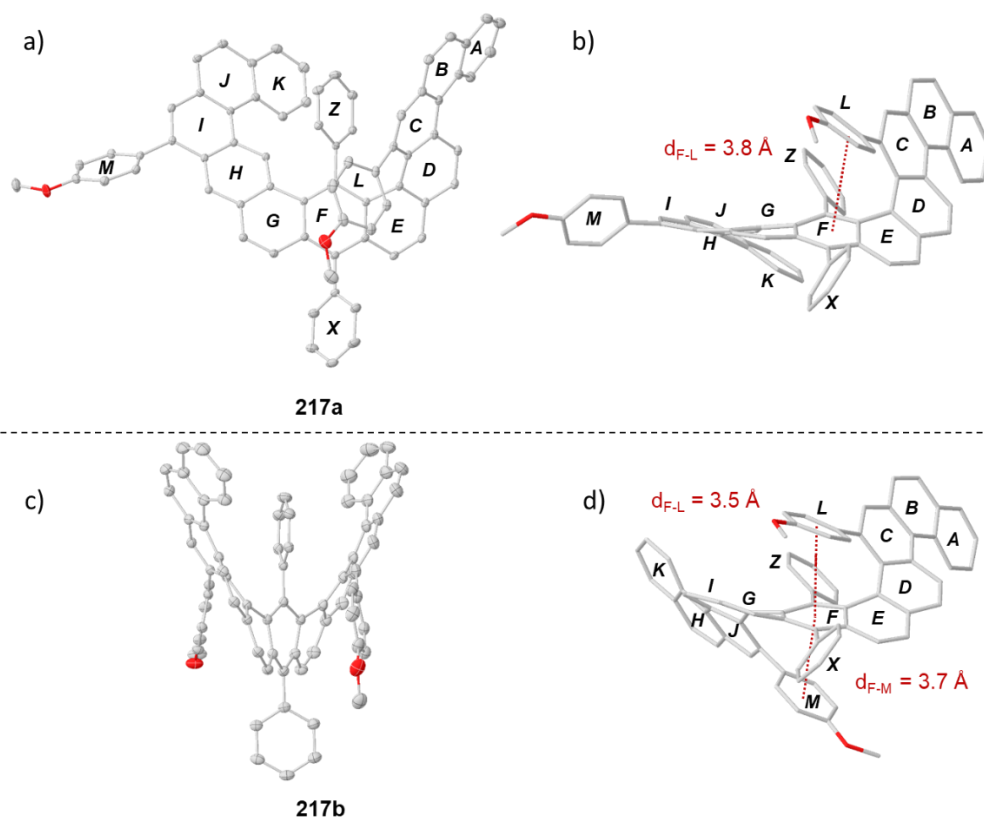


Figure 43. X-ray structures of **217a** [a) and b)] and **217b** [c) and d)]. Solvent molecules and hydrogen atoms were omitted for clarity. Ellipsoids are represented at 50% probability for **217a** and at 25% probability for **217b**.

Gratifyingly, **217a** and **217b** were configurationally stable at room temperature. This was due to the presence of embedded stereochemically fixed 1,12-disubstituted [4]helicene units in their architecture, one in the case of **217a** and two in the case of **217b**. In **217a** the torsion angles along the helical inner rim of the [4]helicene moiety were quite pronounced ($\Phi = 4.8^\circ, 36.1^\circ, 34.3^\circ, 15.0^\circ$), in agreement with the data available for this structural subunit.^[219] Rings L and F did not completely overlap but depicted an interplanar distance of 3.8 \AA (Figure 43b). Similar geometric parameters were found at each arm of the C_2 -symmetric double S-shape ribbon **217b** ($\Phi_1 = 17.1^\circ, 32.2^\circ, 32.0^\circ, 11.0^\circ$ and $\Phi_2 = 5.0^\circ, 35.7^\circ, 32.7^\circ, 12.2^\circ$ for each of the [4]helicene moieties). Note that in order to accommodate the [4]helicene moieties, the anthracene EFG unit of **217b**, distorted 45.4° from planarity, which was the highest value observed along this entire series of expanded helicenes. Clear π - π interactions were also observed between the rings L-F and F-M, being the interplanar distances measured from the centroids of these rings, $d_{F-L} = 3.5 \text{ \AA}$ and $d_{F-M} = 3.7 \text{ \AA}$ (Figure 43d) and, therefore, a helical pitch of approximately 7.2 \AA .

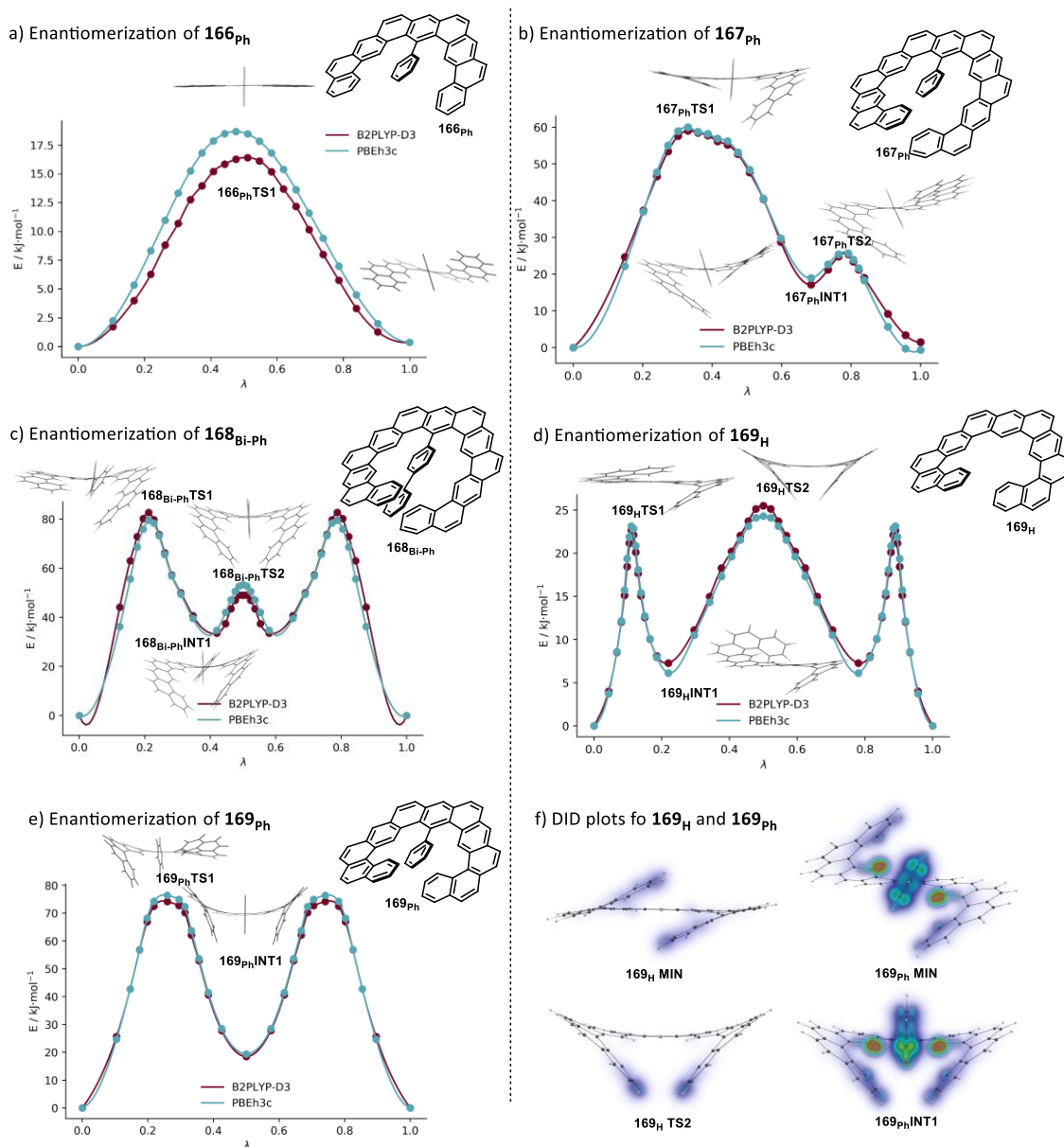
5.3.3. Electronic structure calculations and helical inversion mechanism

After the synthesis of expanded helicenes **166-169**, their conformational dynamics were examined *via* Density Functional Theory (DFT) calculations. In order to understand more clearly the influence of inner substituents in the inversion barrier heights, the pathways of unsubstituted equivalents of **166-169** were also calculated. All structures depicted here were optimized at the PBEh3c level of theory,^[243] with energies recomputed with the double hybrid functional B2PLYP,^[244] including D3 dispersion corrections with Becke-Johnson damping^[245,246], the def2-TZVP basis set^[247] and default fitting basis.^[248,249] The aforementioned calculations were carried out with the Orca 4.2.1 program package.^[250] All substitutions in the outer rim were removed to facilitate computation processes and the internal substituent is indicated as subindex. The energies reported were electronic energies unless otherwise noted. The difference between the latter values and Gibbs free energies barriers were small. In order to better understand some of the trends observed, dispersion interaction density (DID) analyses of the structures were carried out.^[251] The energies were computed at the SCS-LMP2 level of theory with the Molpro2020.1 program package.^[252,253] Details for the calculation setup, in particular how the intramolecular analysis was defined, are provided in Section 6.5.

In the first place, unsubstituted **166** (**166_H**) did not present any helix and the most stable structure adopted a planar conformation, as expected. After introducing the inner phenyl substituent (**166_{Ph}**), two enantiomeric conformations of **166_{Ph}** came onto the scene separated by a single and rather small barrier **166_{Ph}TS1** of only 15.9 kJ·mol⁻¹ in the NBE computed energy profile (free barrier for activation of 19.1 kJ·mol⁻¹, Scheme 54a). Interestingly, compounds **167-169** possessed more complex potential energy hypersurfaces and in all cases, the corresponding interconversions took place via stepwise mechanisms (Scheme 54b-e).

The energetic profile for the enantiomerization of **167_{Ph}** is represented in Scheme 54b. The barrier was calculated to be $\Delta E^\ddagger = 59.0$ kJ·mol⁻¹, which was very similar to the one reported for the unsubstituted kekulene analogue **86** ($\Delta G^\ddagger = 54.3$ kJ·mol⁻¹).^[45] This indicated that the presence of the phenyl insert in **167** did not have a significant impact on its inversion barrier, probably due to the length of the arms. Against all odds, the potential energy diagram of **167_{Ph}** was not C_s symmetric, this implied that both arms move coordinated at different pace through the minimum energy pathway. Therefore, while the left arm in Scheme 54b nearly reaches the central anthracene plane, the right one squirms itself to facilitate this step **167_{Ph}TS1**. Once the left arm achieves its final position **167_{Ph}INT1**, the right one completes the enantiomerization, now through a quite low barrier **167_{Ph}TS2**, as it is already appropriately positioned. In this

manner, a possible C_s structure was avoided, which could have meant an increase in energy due to the steric clash between the phenyl substituent and the arms.



Scheme 54. Enantiomerization mechanism of a) **166_{ph}**, b) **167_{ph}**, c) **168_{Bi-ph}**, d) **169_H**, e) **169_{ph}** calculated at the PBEh3c level of theory (single point calculations at the B2LYP-D3/def2-TZVP level). Only selected transition states and energy-minimum structures are represented together to the energy profiles. f) DID plots for the interactions between the arms and the central substituent in **169_{ph}** calculated at the SCS-LMP2 level. λ = normalized abelian distance between the structures from reactant to product.

The substitution of the phenyl insert by a *p*-biphenyl one originated **168_{Bi-ph}**. Primary approaches indicated that the enantiomerization barrier increased by around 20 $\text{kJ}\cdot\text{mol}^{-1}$ in comparison to **167_{ph}**. This phenomenon could be attributed to two factors: the loss of the stabilizing π -stacking interaction between the Z-ring of the biphenyl and the arm that started the inversion, and the need to bend away the internal substituent more abruptly than in **167_{ph}** to reduce steric hindrance. It was also very remarkable that the potential energy diagram was again C_s symmetric, which suggested that both arms operated independently, one after the

other. Additionally, the C_s -symmetric conformer corresponded to a local energetic maximum, **168_{Bi-Ph}TS2**; subsequently, minimal rotation of the biphenyl Z ring either to the right or the left reestablished a stabilizing π -stating interaction with one or the other arm **168_{Bi-Ph}INT1** (Scheme 54c).

Schemes 54d and e depict the inversion processes in both **169_H** and **169_{Ph}**. As can be observed in Scheme 54d, one of the [4]helicene moieties of **169_H** located at the end of the arms initially inverted via **169_HTS1** to originate an intermediate **169_HINT1**, by which the inverting arm edge ring pointed towards the opposing arm. From this point, the C_s symmetric **169_HTS2** transition state was found, exhibiting a rather similar barrier. In this structure, both arms were pointing at the same direction. A completely symmetric process involving the other arm furnishes the other enantiomeric form of **169_H**. Finally, the calculated barrier to helical inversion for **202_H** was $\Delta E^\ddagger = 25.5 \text{ kJ}\cdot\text{mol}^{-1}$ corresponding to the barrier in **169_HTS2**. Surprisingly, the isomerization profile and the inversion mechanism of **169_H** were very similar to that described for [8]helicene by Merino *et al.*, neglecting terms of absolute energy values (Figure 44).^[32]

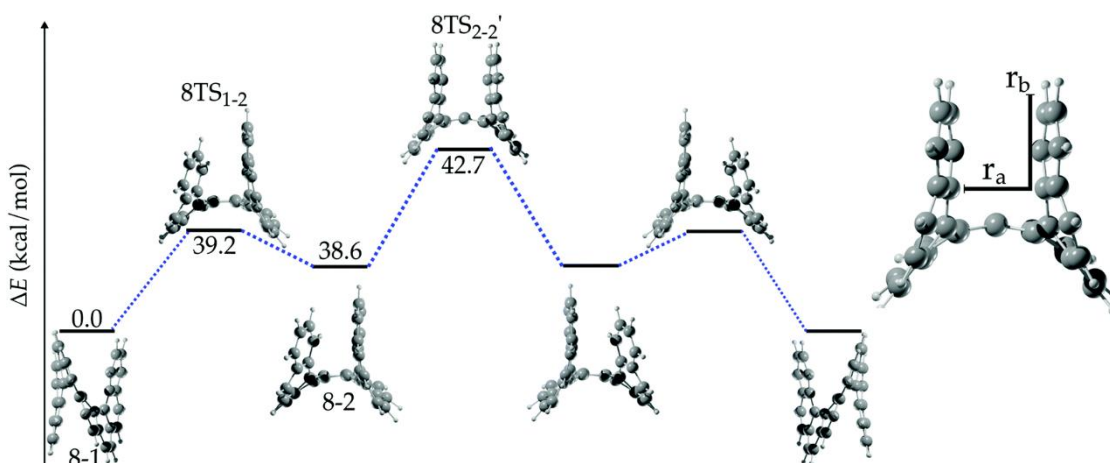


Figure 44. Energy profile for the enantiomerization of [8]helicene. Image adopted from J. Barroso, J. L. Cabellos, S. Pan, F. Murillo, X. Zarate, M. A. Fernandez-Herrera, G. Merino, *Chem. Commun.* **2017**, 54, 188–191.^[32]

As can be appreciated on Scheme 54e, the introduction of the internal phenyl substituent in **169_{Ph}** dramatically changed the shape of the isomerization profile. This time, only two transition states with relatively high barriers ($\Delta E^\ddagger = 74.2 \text{ kJ}\cdot\text{mol}^{-1}$) were observed instead of three, as in the previous case. Such transition states beared resemblance to **169_HTS1** due to the inversion of a terminal [4]helicene moiety, nonetheless, the C_s -symmetric structure, with the two arms facing each other, was no longer the highest transition state as it was in **169_H**, instead, it was a minimum, **169_{INT1}**. Even though the phenyl substituent was expected to hinder the enantiomerization process and to increase the deformation in the helical framework, it was noted that this change in the architecture implied an energetic penalty when one arm pointed towards the center of the helix: A $22.7 \text{ kJ}\cdot\text{mol}^{-1}$ barrier for **169_HTS1** and

74.2 for **169_{Ph}TS1**. However, in the C_s -symmetric intermediate **169_{Ph}INT1**, the Ph-substituent actually acted as a slightly stabilizing factor. Its structure was energetically $18.5 \text{ kJ}\cdot\text{mol}^{-1}$ above the global minimum, whereas the same structural motif in **169_H**, which is actually a transition state, was clearly $25.5 \text{ kJ}\cdot\text{mol}^{-1}$ above the starting configuration. Finally, DIDs (Dispersion Interaction Density) were plotted for the interactions between the arms and the central substituent in **169_{Ph}** and compared them at the same scale with the interactions between the arms of **169_H** (Scheme 54f). There was a clear difference between the dispersion interactions (quantified at the SCS-LMP2 level) of **169_{Ph}INT1** ($29 \text{ kJ}\cdot\text{mol}^{-1}$) and those of **169_HTS2** ($3 \text{ kJ}\cdot\text{mol}^{-1}$). To conclude, London forces derived from the presence of the Ph-insert effectively compensated the energetic penalty to be paid in **169_{Ph}INT1** as a consequence of a more pronounced deformation of the polyaromatic skeleton. Furthermore, the inversion barrier in **169_{Ph}** might have been lowered by dispersion as well because this interaction was also partially present in **169_{Ph}INT1** between the Ph-insert and one of the helicene arms.

Although none of the barriers calculated was sufficiently high to allow the conformational resolution of the enantiomers of **166-169** at room temperature, these examples show how through substitution, the inversion process of the original helicene structure can be modified, even by eliminating or creating new barriers to overcome.

5.3.4. Photophysical properties of synthesized helicenes

5.3.4.1. Absorption and emission spectra

In order to study the influence of the extension of the π -system on chiroptical properties, UV-Vis absorption and fluorescence spectra of **166-169** and **217a-b** have been recorded in CHCl_3 at room temperature (absorption) and 10°C (emission). Figure 45 contains the plotted absorption spectra of in-fjord substituted expanded helicenes **166-169**, and Table 8 highlights all relevant data.

As can be seen in this graph, these four species describe similar absorption bands in specific wavelength ranges (*i.e.*, 260-340, 360-400 and 400-420 nm) presumably belonging to their first three HOMO-LUMO transitions. Helicene **166** exhibited the least intense and most left-shifted bands of all four helicenes, which means that it is not as capable of absorbing light as the other species and its HOMO-LUMO transitions are the most energetic ones. Likewise, **168** and **169** present analogous and bathochromically shifted spectra as a consequence of the extension of the π -system and, therefore, the reduction of the HOMO-LUMO gap. Lastly, **167** displayed the most intense absorption bands and maxima location similar to **169**. When comparing the detected maxima of **167** and **168** with their equivalent in Matsuda's kekulene analogue **86**^[45]

(320 nm, $\epsilon = 1.4 \cdot 10^5 \text{ M}^{-1}\text{cm}^{-1}$; 375 nm, $\epsilon = 3.5 \cdot 10^4 \text{ M}^{-1}\text{cm}^{-1}$ and 395 nm, $\epsilon = 3.8 \cdot 10^4 \text{ M}^{-1}\text{cm}^{-1}$), a red shift of the transitions can be observed as the inner substituent enlarges.

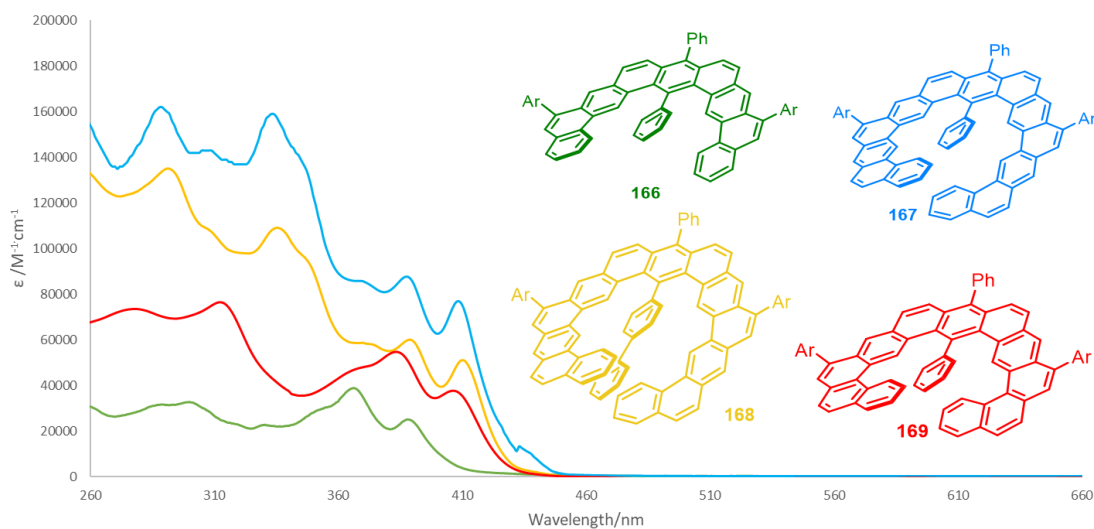


Figure 45. Absorption spectra of expanded helicenes **166-169** in CHCl_3 at room temperature.

Table 8. Absorption maxima of compounds **166-169** and molar absorption coefficients ϵ .

Compound	Absorption λ_{max} (nm)	ϵ_{max} ($\text{M}^{-1}\cdot\text{cm}^{-1}$)
166	300	3.26×10^4
	366	3.88×10^4
	388	2.51×10^4
167	290	1.62×10^5
	333	1.59×10^5
	388	8.78×10^4
	409	7.69×10^4
168	293	1.31×10^5
	336	1.09×10^5
	390	6.15×10^4
	411	5.27×10^4
169	312	7.66×10^4
	383	5.49×10^4
	406	3.79×10^4

Regarding emission phenomena, the fluorescence spectra appear to follow a tendency consistent with the normalized absorption spectra since **166** maxima are blue-shifted when compared to those of **167-169** (Figure 46). Fluorescence quantum yields for these helicenes were measured as well. As expected, those compounds possessing a more extended and more flexible structure presented a lower quantum yield under identical conditions (Table 9). This

decrease of the fluorescence quantum yield through the expansion of the π -system is a common tendency in carbohelicenes that has been observed multiple times.^[55]

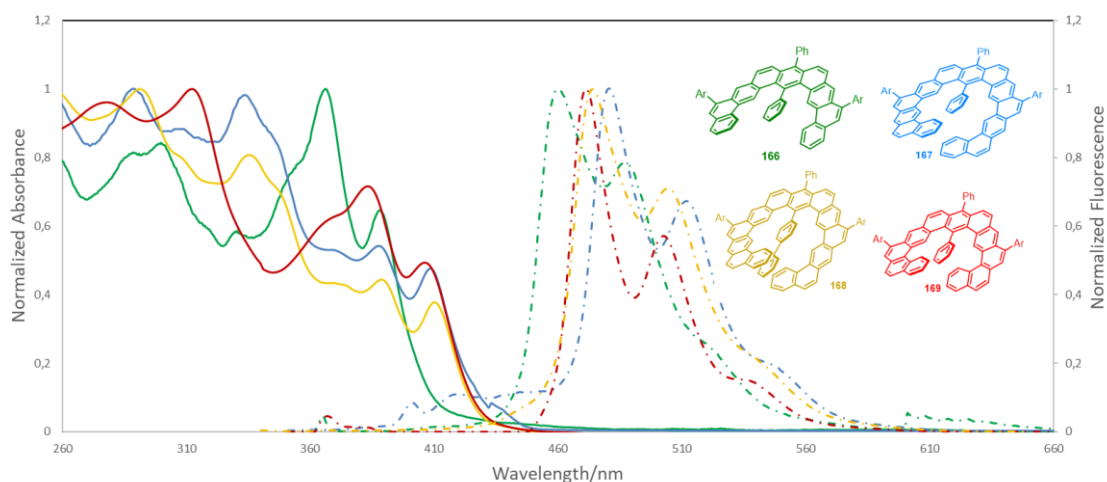


Figure 46. Normalized absorption (continuous line) and fluorescence spectra (dashed line) of expanded helicenes **166-169**.

Table 9. Emission maxima of compounds **166-169**, fluorescence quantum yield Φ_F .

Compound	λ_{em} maxima (nm) ^[a]	Φ_F (nm) ^[b]
166	457 486	0.29 (366)
167	481 512	0.07 (333)
168	474 504	0.02 (330)
169	471 503	0.09 (312)

[a] Measured in CHCl_3 at 10 °C. [b] Excitation wavelength.

DFT calculations were performed to obtain the spectra of compounds **166-169**. The simplified time dependent density functional theory formalism (sTD-DFT)^[254] with the ω B97X functional^[255] and the def2-TZVP basis set was the chosen tool to accomplish this task.

The functional was chosen for its correct long-range asymptotic exchange, which is important in such extended π -systems. As in previously reported absorption studies for helicenes, the computed absorption energies were shifted by 1 eV.^[256] The trends observed in the measured spectra are well replicated in the DFT spectra (based on PBEh3c structures). The red shifts of the transitions of **167** and **168** if compared to **86** could be justified by their increased helical pitches (see Section 6.5.3).

Lastly, identical photophysical studies were carried out in twisted helicenes **217a-b**. Despite their structural differences, both compounds illustrated similar absorption and emission spectra as depicted in Figure 47; moreover, they present similar Stoke shifts: 6400 cm^{-1} in the case of **217a** and 6600 cm^{-1} in the case of **217b**. Concerning fluorescence, it was observed that **217b** presented a considerably lower fluorescence quantum yield than its analogue **217a** (Table 10).

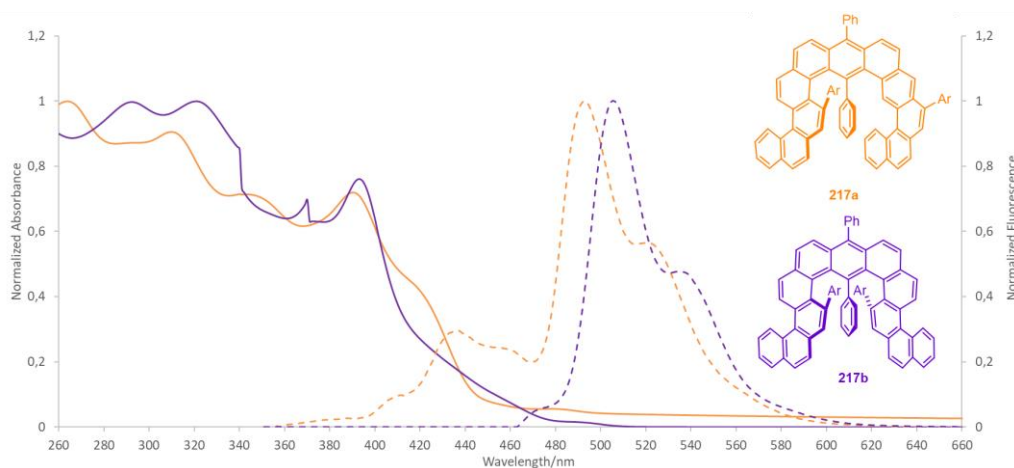


Figure 47. Normalized absorption (continuous line) and fluorescence spectra (dashed line) of helicenes **217a-b**.

Table 10. Absorption and emission relevant data of twisted helicenes **217a-b**.

Compound	Absorption λ_{max} (nm)	ϵ_{max} ($\text{M}^{-1}\cdot\text{cm}^{-1}$)	λ_{em} maxima (nm)	Φ_{F} (nm) ^[a]
217a	310	3.40×10^5	494	0.33 (310)
	339	2.60×10^5	521	
	390	2.70×10^5		
217b	292	1.66×10^5	506	0.12 (321)
	321	1.68×10^5	533	
	370	1.17×10^5		
	394	1.27×10^5		

[a] Excitation wavelength.

Red shift and poorer fluorescence quantum efficiency in **217b** in comparison to **217a** are both phenomena attributed to the high distortion and strain of the helical structure. Similar observations were recently reported for twisted anthracenes: Twisting and bending in anthracenes in various ways implied a torsion of the π -bonds present in the molecule, breaking the symmetry and sometimes a mixing of π and σ symmetries as well. Hence, the HOMO-LUMO energy levels are strongly affected, generally through a decrease of their gap as the distortion degree increases and therefore, a shift towards red in absorption and emission spectra.^[257,258]

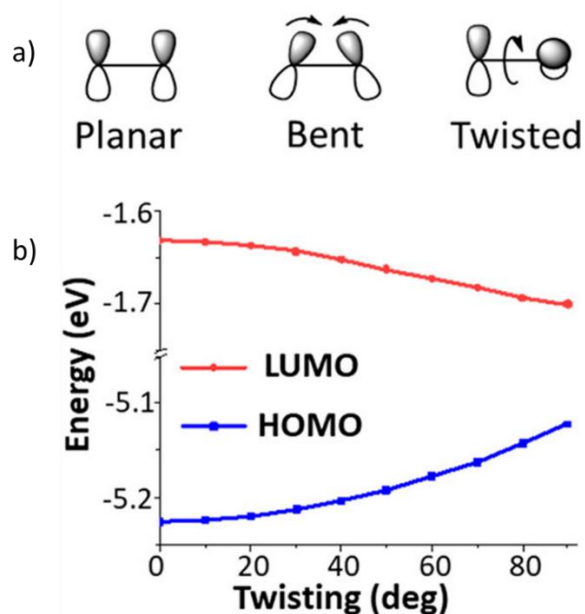


Figure 48. a) Representation of two adjacent π -orbitals in planar, bent, and twisted conformations. b) Calculated (UB3LYP/6-31G(d)) HOMO and LUMO energy levels of anthracene with different end-to-end dihedral twists. Image adapted from: A. Bedi, O. Gidron, *Acc. Chem. Res.* **2019**, *52*, 2482–2490.^[257]

Concerning the effect of distortion on fluorescence quantum yields, a link has been observed between the twisting angle of substituted anthracenes and the diminution of such optical property. Although multiple factors come into play, the main cause is again attributed to the distortion of the anthracene moiety. As it was previously discussed in the solid state structures Section, **217b** presented a remarkable distortion in its anthracene unit in comparison to **217a**, thus it was assumed that this phenomenon was the main cause behind the differences in the optical properties of both compounds.

5.3.4.2. Circular dichroism

As discussed in the previous Section, isolated enantiomers of chiral helicenes present mirror images of their circular dichroism spectra in virtue of their differently polarized light absorption. Resolution of the enantiomers of **217a-b** was accomplished via chiral HPLC, and the ECD of each isomer were measured in CHCl_3 and plotted. As can be seen from Figure 49, not only is the mirror image feature noted above clearly expressed, but the graphs of **217a** and **217b** are also identical. This means that both compounds experience similar, if not identical, electronic transitions despite their obvious structural differences. When comparing both graphs, a relatively strong Cotton effect, namely intensification of the CD bands, can be observed in **217b** manifested as a growth of the overall $\Delta\epsilon$. This was again described by Gidron et al. as a consequence of the elevated distortion degree of anthracene units, like those present in this compound: When the π - π^* (1L_a) transition takes place in twisted anthracenes,

μ_e decreases by approximately 5% while μ_m increases by 500%, resulting in a significant growth of the complete Cotton effect.^[257] As conclusion, the resolution of the racemic mixtures of **217a** and **217b**, in addition to their CD spectra, were the most solid evidences of the chirality and configurational stability of these two helicenes at room temperature.

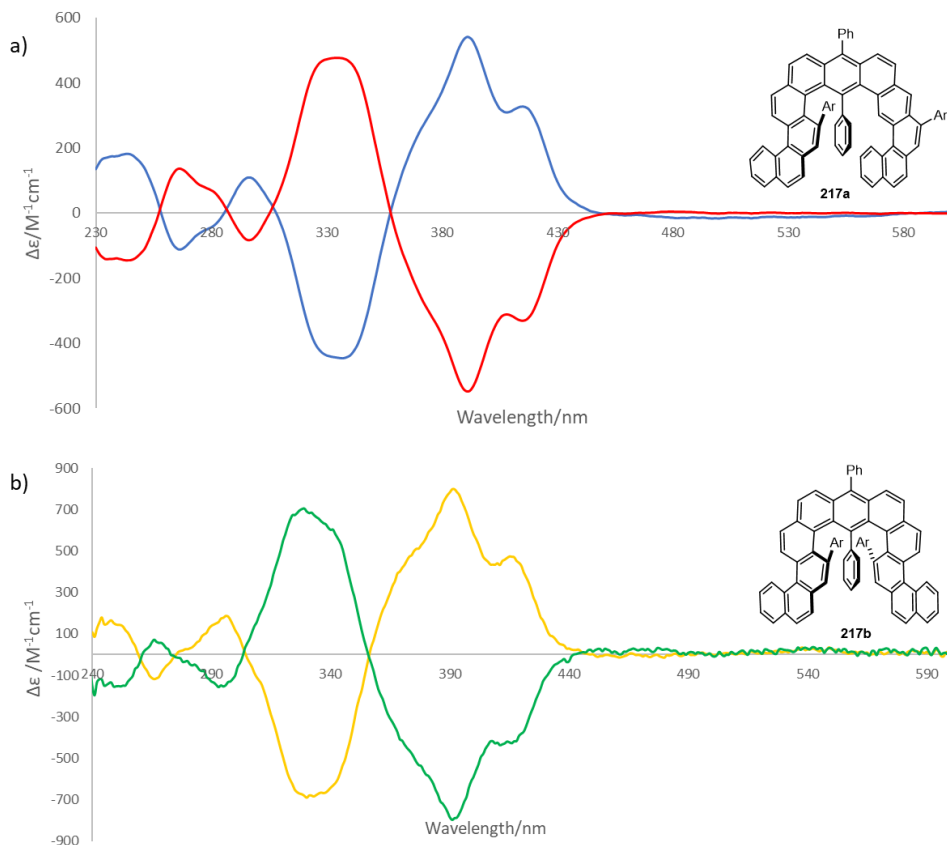


Figure 49. ECD spectra of separated enantiomers **217a** (a) and **217b** (b) in CHCl_3 at rt.

5.3.5. Conclusion

The design and synthesis of in-fjord-substituted expanded helicenes **166-169** was achieved through varied multi-step routes, including a final Au(I)-catalyzed hydroarylation with cationic phosphine-based Au(I) complex **218**. This catalyst was identified as the most effective one of an entire screening in terms of yield and regioselectivity. In the meantime, two additional twisted expanded helicenes, **217a** and **217b**, were additionally synthesized, isolated and characterized.

Crystals of these six compounds suitable for X-ray analysis were grown and underwent solid state structure studies in order to elucidate the influence of the inner substituent. The presence of this component at the fjord region of these helicenes proved to play a pivotal role

in the alteration of certain structural aspects, such as interplanar angle, helical diameter, helical pitch or aromaticity distribution.

DFT calculations were carried out in order to examine the conformational dynamics of helicenes **166-169**. For this purpose, the energy profile of the targeted helicenes was compared to that of their unsubstituted parent structures, showing significant differences regarding energy values, the shape of the transition profile and number of TS and intermediates.

The influence of in-fjord substituents was also examined *via* photophysical studies. Absorption and emission spectra of these six novel expanded helicenes were recorded and compared in order to understand the impact of this substitution pattern on their optical properties. Finally, chiral resolution of twisted helicenes **217a** and **217b** *via* HPLC afforded their isolated enantiomers. Electronic circular dichroism studies demonstrated, not only the chirality of these species, but also the impact of their structural differences on their chiroptical properties.

6. Experimental

6.1. General remarks

6.1.1. General working methods

Unless otherwise stated, all reactions were carried out in dried glassware under an inert atmosphere (nitrogen or argon if specifically noted) using standard Schlenk techniques, or under an atmosphere of nitrogen in a MBraun UNIlab plus glovebox. Dry and degassed solvents were obtained by distillation over the appropriate drying agents and stored under nitrogen. Alternatively, dry solvents were obtained using an MBraun MB-SPS-800 solvent purification system (tetrahydrofuran, diethyl ether, toluene, pentane, dichloromethane, acetonitrile).

Flash chromatography was performed on Macherey Nagel 60 (40-63 μm) silica gel. Semipreparative TLC was performed using glass Merck 500-1000 μm TLC-plates. Reactions were controlled by thin-layer chromatography (TLC) analysis, performed using polygram SIL G/UV254 TLC-plates from Macherey Nagel, and visualized by UV irradiation ($\lambda = 254 \text{ nm}$).

Photoreactions were carried out with a Peschl Ultraviolet MPDS Photoreactor, composed of a photoLAB Batch-M reaction vessel outfitted with a novalIGHT TQ150 medium pressure 125 W mercury UV lamp in a photonCABINET safety cabinet.

6.1.2. Starting materials

Unless otherwise specified, all reagents were used as received from commercial suppliers (ABCR, Acros Organics, Alfa Aesar, Chempur GmbH, Fluorochem, J and K Scientific, Sigma Aldrich, Thermo Fisher Scientific, Tokyo Chemical Industry). Compounds synthesized according to previously described in the literature procedures are the following: (*R*)-3,3'-di([1,1'-biphenyl]-4-yl)-[1,1'-binaphthalene]-2,2'-diol (**173a**),^[224,225,227] 1,3-bis(2,4,6-trimethylphenyl)-4,5-dimethyl-1,3-dihydro-2*H*-imidazol-2-ylidene (**IMes**^{Me}^[229] 1,3-bis(2,4,6-trimethylphenyl)-1,3-dihydro-2*H*-imidazol-2-ylidene (**IMes**),^[226] 2-bromobenzo[*c*]phenanthrene (**185a**) and precursors,^[231] 2-bromo-10-methoxybenzo[*c*]phenanthrene (**185b**) and precursors,^[259] 2-bromo-6-methylbenzo[*c*]phenanthrene (**185c**) and precursors,^[260] terminal alkynes **188c-i**,^[261-266] bromoalkynes **189a-b**, **d-f** and **j-l**,^[267-272] racemic catalyst **223**,^[273] 2-(4-bromostyryl)benzo[*b*]thiophene (**196a**) and 2-bromobenzo[*b*]naphtho[1,2-*d*]thiophene

(**197a**),^[12] complex of gold(I) chloride with [2-(dicyclohexylphosphanyl)-1-mesitylpyridin-1-ium] hexafluoroantimonate (**218**)^[273] and precursor of **205** 1-bromo-2-[(4-methoxyphenyl)ethynyl]naphthalene.^[274] Analytical data of these compounds correspond to those reported in the aforementioned references.

6.1.3. General analytical methods

NMR: spectra were recorded on Bruker AV600, AV500, AV400, AV300 or Varian Inova 500 spectrometers; ¹H, and ¹³C chemical shifts (δ) are given in ppm relative to TMS, using the residual solvent signals as references and converting the chemical shifts to the TMS scale. ³¹P and ¹⁹F chemical shifts (δ) are given in ppm relative to H₃PO₄ and CFCl₃, respectively (external standard). Coupling constants (*J*) are given in Hz. Solvents for NMR spectroscopy were used as received from Eurisotop.

HR-MS: Finnigan MAT 95 (70 eV, EI), Finnigan LCQ (ESI) and APEX IV 7T FTICR, Bruker Daltonic (HR-MS).

IR: FT/IR-4600 (Jasco), wavenumbers ($\tilde{\nu}$) in cm⁻¹.

HPLC: the relative ratios of products in reaction mixtures were determined by analytical HPLC using either Shimadzu Nexera-i LC 2040 3D with integrated downstream UV/Vis PDA detector (detection at 254 nm, reverse phase) or a Shimadzu Prominence-i LC-2030C 3D Plus with integrated downstream UV/Vis PDA detector (detection at 254 nm, normal phase). Separation was carried out on Agilent ZORBAX SB-C18, 4.6×250 mm, 3.5 μ m column or YMC PVA-Sil NP, 4.6×250mm, 5 μ m column. Specific conditions such as eluent mixtures, flow rates and temperatures are stated for each case. System control and chromatogram analysis were carried out with LabSolutions (Shimadzu) software.

Chiral HPLC: the enantiomeric excesses of the products were determined using either a Shimadzu Nexera-i LC 2040 3D with integrated downstream UV/Vis PDA detector (detection at 254 nm, reverse phase) or a Shimadzu Prominence-i LC-2030C 3D Plus with integrated downstream UV/Vis PDA detector (detection at 254 nm, normal phase). Separation was carried out on Daicel Chiral Technologies 4.6×150 mm, 3 μ m columns. Specific conditions such as column type used, eluent mixtures, flow rates and temperatures are stated for each compound. System control and chromatogram analysis were carried out with LabSolutions (Shimadzu) software. Further analysis was carried out using a Waters Acquity multidimensional high-performance liquid chromatograph (MD-UPLC), custom configuration with column switching in both separation dimensions. Detection via PDA-UV, trap-and-elute transfer to

second dimension with separate PDA-UV coupled with fluorescence or single-quad MS detection.

Chiral SFC: the enantiomeric excesses of the products were determined using a Waters UPC² with integrated downstream UV/Vis PDA detector (detection at 254 nm). Separation was carried out on Daicel Chiral Technologies, 3.0×100°mm, 3µm columns. Specific conditions such as column type used, CO₂ cosolvent type and amounts, flow rates, temperatures and set system backpressure are stated for each compound. System control and chromatogram analysis were carried out with Empower 3 (Waters) software.

Preparative HPLC: preparative separations were carried out on an Interchim PuriFlash 4250 (RP separations) using either an Agilent ZORBAX SB-C18, 21.2×250 mm, 7 µm column (up to 50 mg) or an 4 Agilent ZORBAX 7 SB-C18, 50.0×250 mm, 7µm column (>50 mg), or on a Jasco semipreparative modular HPLC using a YMC PVA-Sil NP, 20.0×250mm, 5µm column.

Specific rotations: were measured using a Jasco P-2000 polarimeter at the stated temperature using a Na/Hg lamp, $\lambda = 589 \text{ nm}$ (*c* in g/100 mL).

Electro-optical Properties: Circular dichroism (CD) spectra were measured on a Jasco J-1500 spectrometer using a 5 mm quartz sample cell. UV/Vis spectra were conducted using a Jasco J-1500 or a Jasco V-630 spectrometer using a 5 mm and a 10 mm quartz sample cell respectively. Fluorescence spectra were conducted using a Jasco FP-8500 spectrofluorometer using a 10×2 mm quartz sample cell. Fluorescence and CD spectra were measured at 10 °C, unless otherwise is stated. Data were processed with SpectraManager™ and Spectragryph 1.2 software. Concentrations are stated in each case.

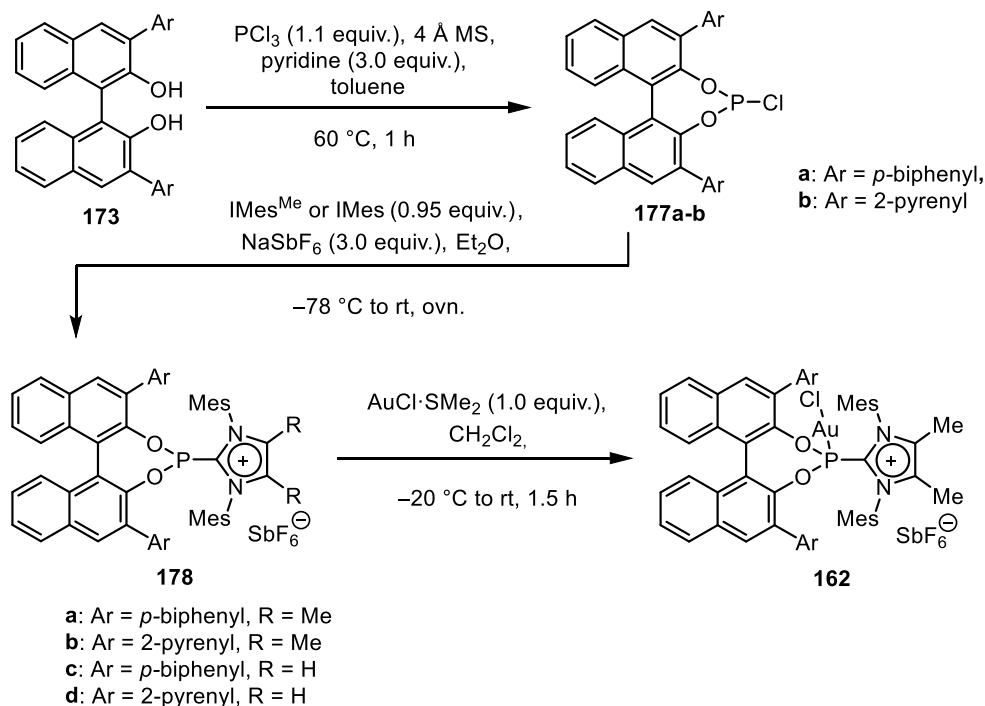
X-ray diffraction: Structures were solved by Dr. Christopher Golz. Data collection was done on two dual source equipped *Bruker D8 Venture* four-circle-diffractometer from *Bruker AXS GmbH*; used X-ray sources: microfocus *IµS 2.0* Cu/Mo and microfocus *IµS 3.0* Ag/Mo from *Incoatec GmbH* with mirror optics *HELIOS* and single-hole collimator from *Bruker AXS GmbH*; used detector: *Photon III CE14* (Cu/Mo) and *Photon III HE* (Ag/Mo) from *Bruker AXS GmbH*.

Used programs: *APEX3 Suite* (v2018.7-2) for data collection and therein integrated programs *SAINT V8.38A* (Integration) und *SADABS 2016/2* (Absorption correction) from *Bruker AXS GmbH*; structure solution was done with *SHELXT*, refinement with *SHELXL-2018/3*.

Special Utilities: *SMZ1270* stereomicroscope from *Nikon Metrology GmbH* was used for sample preparation; crystals were mounted on *MicroMounts* or *MicroLoops* from *MiTeGen* in NVH oil.

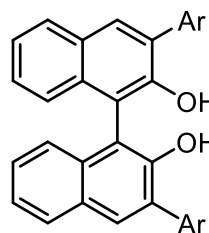
6.2. Enantioselective synthesis of 1-Aryl Benzo[5]helicenes

6.2.1. Synthesis of α -cationic Phosphonites



Scheme 55. Synthesis of α -cationic BINOL-phosphonites and their Au(I) complexes via their respective chlorophosphites.

(*R*)-3,3'-Di(pyren-2-yl)-[1,1'-binaphthalene]-2,2'-diol (173b):



Ar = 2-pyrenyl

The compound was prepared adopting a previously published procedure.^[228] A Schlenk flask equipped with a magnetic stirring bar was charged with a mixture of (*R*)-3,3'-dibromo-2,2'-bis(methoxymethoxy)-1,1'-binaphthalene (**175**) (0.53 g, 1.0 mmol, 1.0 equiv.), pyrene-2-boronic acid pinacol ester (1.0 g, 3.0 mmol, 3.0 equiv.), K₂CO₃ (1.6 g, 12.0 mmol, 5.0 equiv.) in DME (8.5 mL, 0.12 M) and H₂O (6.0 mL, 2.0 M) and degassed with Ar for 10 minutes. Then P(*t*-Bu)₃ (24 μ L, 20 mg, 99 μ mol, 0.1 equiv.) followed by Pd(OAc)₂ (11.2 mg, 50 μ mol, 5 mol%) were added, and the resulting mixture was stirred at 90 °C for 3 h. The reaction mixture was exposed to air, cooled to rt, diluted with CH₂Cl₂ (10 mL). The layers were separated, and the aqueous layer was extracted with CH₂Cl₂ (2 \times 5 mL). The combined organic layers were washed with NH₄Cl (saturated) and brine (10 mL each), dried (Na₂SO₄), filtered and concentrated under reduced pressure. Purification by column chromatography (SiO₂, EtOAc/hexanes 3:97 to 1:24) and filtration yielded (*R*)-2,2'-[2,2'-bis(methoxymethoxy)-

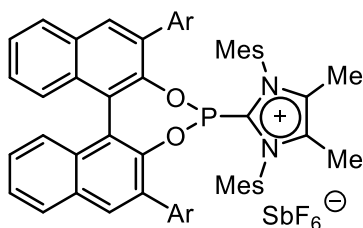
[1,1'-binaphthalene]-3,3'-diyl)dipyrene (**176**) as a colorless solid (0.66 g, 0.85 mmol, 85%). Further deprotection of this compound was carried out by dissolving it in dioxane (7 mL) and aq. HCl (6 N, 9 mL) at rt. The reaction mixture was warmed up to 90 °C and stirred for 3 h. Once no further conversion of **175** was observed by TLC, the mixture was cooled down to rt, and the volatiles were evaporated under reduced pressure. Residual material was diluted with DCM and washed with NaHCO₃, water and brine. The organic layer was dried over MgSO₄, and the volatiles were removed under reduced pressure. The crude compound was purified by column chromatography (SiO₂, EtOAc/hexanes 1:9) to afford pure **173b** as a white solid (0.50 g, 0.73 mmol, 73% over two steps).

$[\alpha]_{20}^D$: -250.4 (*c* = 0.25, CH₂Cl₂); ¹H NMR: (300 MHz, CDCl₃) δ = 8.57 (s, 4H), 8.27 (s, 2H), 8.22 (d, *J* = 7.6 Hz, 4H), 8.13 (m, 6H), 8.03 (dd, *J* = 8.3, 7.1 Hz, 4H), 7.52 – 7.35 (m, 6H), 5.63 (d, *J* = 0.5 Hz, 2H), 5.30 (s, 2H) ppm; ¹³C{¹H} NMR: (101 MHz, CDCl₃) δ = 150.5, 135.2, 133.4, 132.5, 131.5, 131.4, 131.1, 129.8, 128.8, 128.0, 127.7, 127.6, 126.2, 125.4, 125.3, 124.7, 124.6, 124.6, 124.2, 113.0 ppm; IR: (neat, cm⁻¹) $\tilde{\nu}$ = 419, 434, 458, 476, 497, 610, 669, 684, 708, 725, 753, 791, 818, 840, 870, 881, 1126, 1144, 1175, 1197, 1213; HR-MS: calcd *m/z* for C₅₂H₃₁O₂ [M+H]⁺: 687.2319; found (ESI) 687.2310.

General Procedure A for the synthesis of α-cationic phosphonite ligands

The synthesis was carried out following a literature procedure.^[218] Schlenk flask was charged with the respective BINOL derivative (1.0 equiv.), powdered 4 Å molecular sieves (2-3 spatula tips) and toluene (0.02 M). Anhydrous pyridine (3.0 equiv.) and PCl₃ (1.05 equiv.) were added successively. The reaction mixture was then heated to 60 °C for 1.5 h. After cooling to room temperature, the mixture was filtered utilizing a canula equipped with a glass-fiber filter. The filtrate was evaporated and then dried *in vacuo*. After checking conversion *via* NMR, to the residue was added NaSbF₆ (3 equiv.), the mixture was suspended in diethyl ether (0.1 M) and cooled to -78 °C. A solution of the respective carbene (0.9 equiv.) in diethyl ether (0.2 M) was slowly added, and the mixture was allowed to warm up to room temperature overnight. The solvent was removed *in vacuo*, the residual solid was taken up with dichloromethane and filtered using a cannula equipped with a glass-fiber filter. The volatiles were removed *in vacuo*, and the resulting crude product was further purified by column chromatography (SiO₂) at -10 °C as specified for the individual cases.

(R)-2-{2,6-Di([1,1'-biphenyl]-4-yl)dinaphtho[2,1-d:1',2'-f][1,3,2]dioxaphosphepin-4-yl}-1,3-dimesityl-4,5-dimethyl-1H-imidazol-3-ium hexafluoroantimonate (178a):



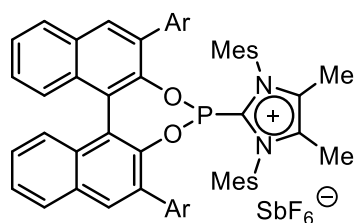
Ar = *p*-biphenyl

The compound **178a** was prepared according to General Procedure **A** using (*R*)-3,3'-di([1,1'-biphenyl]-4-yl)-[1,1'-binaphthalene]-2,2'-diol (**173a**) (280 mg, 0.474 mmol, 1 equiv.), pyridine (114 mg, 116 μ L, 1.44 mmol, 3.0 equiv.) and PCl_3 (72 mg, 46 μ L, 0.524 mmol, 1.1 equiv.) for the formation of the chlorophosphite. The chlorophosphite was then reacted with NaSbF_6 (372 mg, 1.44 mmol, 3.0 equiv.) and 1,3-

bis(2,4,6-trimethylphenyl)-4,5-dimethyl-1,3-dihydro-2*H*-imidazol-2-ylidene (IMes^{Me}) (152 mg, 0.457 mmol, 0.95 equiv.) to give the crude ligand. Column chromatography (DCM/EtOAc 100:1) yielded the ligand **178a** as a white solid (195 mg, 0.164 mmol, 36% yield).

$[\alpha]_{20}^D$: -123.3 ($c = 0.30$, CH_2Cl_2); $^1\text{H NMR}$: (300 MHz, CD_3CN) $\delta = 8.17$ (d, $J = 11.7$ Hz, 2H), 8.05 (s, 1H), 7.98 (d, $J = 8.2$ Hz, 1H), 7.87 – 7.65 (m, 11H), 7.65 – 7.38 (m, 10H), 7.32 (ddd, $J = 8.3$, 6.8, 1.3 Hz, 1H), 7.20 – 7.08 (m, 2H), 6.87 (s, 1H), 6.74 (dd, $J = 13.1$, 8.6 Hz, 2H), 6.62 (d, $J = 1.8$ Hz, 1H), 2.37 (s, 3H), 1.81 (s, 3H), 1.78 (s, 3H), 1.74 (s, 3H), 1.71 (s, 3H), 1.42 (s, 3H), 1.38 (s, 3H), 0.98 (s, 3H) ppm; $^{13}\text{C}\{^1\text{H}\}$ NMR: (101 MHz, CD_3CN) $\delta = 146.3$ (d, $J_{\text{C-P}} = 11.1$ Hz), 146.0, 143.6, 143.4, 142.4, 141.9, 141.8, 141.3, 141.0 (d, $J_{\text{C-P}} = 7.1$ Hz), 137.1 (d, $J_{\text{C-P}} = 2.0$ Hz), 137.0 (d, $J_{\text{C-P}} = 1.0$ Hz), 135.5 (d, $J_{\text{C-P}} = 4.0$ Hz), 135.4, 135.1 (d, $J_{\text{C-P}} = 2.0$ Hz), 134.1 (d, $J_{\text{C-P}} = 3.0$ Hz), 133.8, 133.7, 133.5, 133.2, 132.9, 132.8, 132.5, 132.3, 131.4, 131.3, 131.3, 130.7, 130.6, 130.3, 130.2, 130.1, 129.5, 129.3, 129.3, 129.0, 129.0, 128.9, 128.9, 128.9, 128.4, 128.0, 127.9, 127.8, 127.7, 127.4, 127.3, 127.1, 125.3 (d, $J_{\text{C-P}} = 6.1$ Hz), 124.2 (d, $J_{\text{C-P}} = 4.0$ Hz), 21.3, 19.0, 18.0 (d, $J_{\text{C-P}} = 9.1$ Hz), 17.6, 15.9, 9.1 ppm; $^{31}\text{P}\{^1\text{H}\}$ NMR: (121 MHz, CD_3CN) $\delta = 142.3$ ppm; $^{19}\text{F}\{^1\text{H}\}$ NMR: (376 MHz, CD_3CN) $\delta = -124.0$ (oct, $J_{\text{F-}^{123}\text{Sb}} = 1045.3$ Hz), -124.0 (sext, $J_{\text{F-}^{121}\text{Sb}} = 1932.6$ Hz) ppm; IR: (neat, cm^{-1}) $\tilde{\nu} = 485, 504, 545, 553, 567, 604, 612, 697, 734, 752, 771, 785, 818, 842, 856, 885, 961, 1193, 1397, 1416, 1487$; HR-MS: calcd m/z for $\text{C}_{67}\text{H}_{56}\text{N}_2\text{O}_2\text{P}^+ [\text{M}-\text{SbF}_6]^-$: 951.4074; found (ESI) 951.4067.

(R)-2-{2,6-Di(pyren-2-yl)dinaphtho[2,1-d:1',2'-f][1,3,2]dioxaphosphepin-4-yl}-1,3-dimesityl-4,5-dimethyl-1H-imidazol-3-ium hexafluoroantimonate (178b):



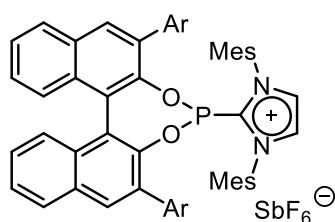
Ar = 2-pyrenyl

The compound **178b** was prepared according to General Procedure **A** using (*R*)-3,3'-di(pyren-2-yl)-[1,1'-binaphthalene]-2,2'-diol **173b** (336 mg, 0.490 mmol, 1.0 equiv.), pyridine (116 mg, 118.1 μ L, 1.47 mmol) and PCl_3 (71 mg, 45.2 μ L, 0.52

mmol, 1.1 equiv.) for the formation of the chlorophosphite. The chlorophosphite was then reacted with NaSbF₆ (380 mg, 1.47 mmol, 3.0 equiv.) and 1,3-bis(2,4,6-trimethylphenyl)-4,5-dimethyl-1,3-dihydro-2*H*-imidazol-2-ylidene (IMes^{Me}) (155 mg, 0.466 mmol, 0.95 equiv.) to give the crude ligand. Column chromatography (DCM/EtOAc 100:1) yielded the ligand **178b** as a white solid (102 mg, 79.4 μmol, 17% yield).

[α]₂₀^D: -245.8 (*c* = 0.30, CH₂Cl₂); ¹H NMR: (300 MHz, CD₃CN) δ = 8.54 (d, *J* = 2.0 Hz, 2H), 8.47 (s, 1H), 8.34 (dd, *J* = 7.7, 4.8 Hz, 4H), 8.30 – 8.17 (m, 9H), 8.17 – 8.09 (m, 3H), 8.09 – 8.02 (m, 2H), 8.00 (d, *J* = 8.5 Hz, 1H), 7.69 (t, *J* = 7.5 Hz, 1H), 7.51 (t, *J* = 7.5 Hz, 1H), 7.47 – 7.37 (m, 1H), 7.21 (t, *J* = 8.0 Hz, 1H), 6.88 (dd, *J* = 14.3, 7.2 Hz, 3H), 6.74 (s, 1H), 5.81 (s, 1H), 5.52 (s, 1H), 2.23 (s, 3H), 1.84 (s, 3H), 1.50 (s, 3H), 1.41 (s, 3H), 1.36 (s, 3H), 1.10 (s, 3H), 0.81 (s, 3H), -0.28 (s, 3H) ppm; ¹³C{¹H} NMR: (101 MHz, CD₃CN) δ = 146.6 (d, *J*_{C-P} = 11.1 Hz), 146.3, 143.1, 142.9, 141.9, 141.4, 136.2, 135.7, 135.3, 135.2, 135.0, 135.0, 134.9, 134.7, 133.9, 133.9, 133.8, 133.6, 133.3, 133.1, 132.9, 132.6, 132.4, 132.4, 132.3, 132.1, 132.0, 130.6, 130.3, 130.2, 130.1, 129.6, 129.4, 129.3, 129.1, 129.0, 128.5, 128.4, 128.2, 128.1, 127.9, 127.8, 127.7, 127.6, 127.4, 127.3, 127.1, 126.8, 126.6, 126.5, 125.4 (d, *J*_{C-P} = 6.1 Hz), 125.0, 125.02, 124.9 (d, *J*_{C-P} = 3.0 Hz), 124.7, 124.3 (d, *J*_{C-P} = 4.0 Hz), 21.3, 21.2, 19.0, 17.6, 17.0 (d, *J*_{C-P} = 1.0 Hz), 15.0, 8.9, 8.6 ppm; ³¹P{¹H} NMR: (121 MHz, CD₃CN) δ = 142.2 ppm; ¹⁹F{¹H} NMR: (376 MHz, CD₃CN) δ = -124.0 (oct, *J*_{F-¹²³Sb} = 1047.2 Hz), -124.0 (sext, *J*_{F-¹²¹Sb} = 1933.4 Hz) ppm; IR: (neat, cm⁻¹) $\tilde{\nu}$ = 497, 564, 580, 589, 605, 713, 751, 773, 802, 825, 843, 853, 869, 882, 917, 1226, 1406; HR-MS: calcd *m/z* for C₇₅H₅₆N₂O₂P⁺ [M-SbF₆]⁺: 1047.4074; found (ESI) 1047.4074.

(*R*)-2-{2,6-Di([1,1'-biphenyl]-4-yl)dinaphtho[2,1-*d*:1',2'-*f*][1,3,2]dioxaphosphepin-4-yl}-1,3-dimesityl-1*H*-imidazol-3-ium hexafluoroantimonate (178c**):**

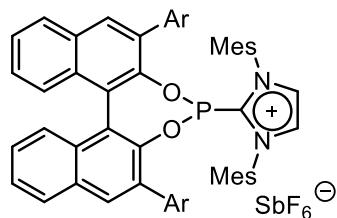


Ar = *p*-biphenyl

The compound **178c** was prepared according to General Procedure **A** using (*R*)-3,3'-di([1,1'-biphenyl]-4-yl)-[1,1'-binaphthalene]-2,2'-diol **173a** (280 mg, 474 μmol, 1.0 equiv.), pyridine (114 mg, 116 μL, 1.44 mmol, 3.0 equiv.) and PCl₃ (72 mg, 45.9 μL, 524 μmol, 1.1 equiv.) for the formation of the chlorophosphite. The chlorophosphite was then reacted with NaSbF₆ (372 mg, 1.44 mmol, 3.0 equiv.) and 1,3-bis(2,4,6-trimethylphenyl)-1,3-dihydro-2*H*-imidazol-2-ylidene (IMes) (139 mg, 457 μmol, 0.96 equiv.) to give the crude ligand. Column chromatography (DCM/EtOAc 100:1) yielded the ligand **178c** as a white solid (132 mg, 113.8 μmol, 24% yield).

$[\alpha]_{20}^D$: -110.2 ($c = 0.09$, CH_2Cl_2); $^1\text{H NMR}$ (300 MHz, CD_3CN): δ 8.21 (s, 1H), 8.18 (d, $J = 8.4$ Hz, 1H), 8.08 (s, 1H), 8.00 (d, $J = 8.3$ Hz, 1H), 7.80 (d, $J = 8.3$ Hz, 4H), 7.74 (d, $J = 11.7$ Hz, 6H), 7.66-7.41 (m, 13H), 7.34 (t, $J = 7.7$ Hz, 1H), 7.23-7.16 (m, 1H), 7.12 (s, 1H), 6.87 (s, 1H), 6.79 (d, $J = 8.6$ Hz, 1H), 6.73 (d, $J = 8.6$ Hz, 1H), 6.62 (s, 1H), 2.36 (s, 3H), 1.82 (s, 3H), 1.77 (s, 3H), 1.49 (s, 3H), 1.45 (s, 3H), 1.07 (s, 3H) ppm; $^{13}\text{C}\{1\text{H}\}$ NMR (126 MHz, CD_3CN): δ 146.6, 146.3 (d, $J_{\text{C-P}} = 10.9$ Hz), 145.7, 145.6, 143.4, 142.1, 141.9, 141.4, 141.1 (d, $J_{\text{C-P}} = 10.5$ Hz), 136.8, 136.8, 136.6, 135.6, 135.3 (d, $J_{\text{C-P}} = 3.8$ Hz), 135.2, 134.1 (d, $J_{\text{C-P}} = 2.4$ Hz), 133.7, 133.5, 133.2, 133.1, 133.0, 132.6, 132.4, 132.3, 132.2, 131.3 (d, $J_{\text{C-P}} = 3.4$ Hz), 131.2, 130.8 (d, $J_{\text{C-P}} = 3.4$ Hz), 130.6, 130.5 (d, $J_{\text{C-P}} = 4.1$ Hz), 130.3, 130.2, 130.1, 129.6, 129.4, 129.1, 128.9, 128.9, 128.8, 128.5, 128.5, 128.1, 128.0, 128.0, 128.0, 127.9, 127.7, 127.5, 127.4, 127.3, 125.9, 125.3 (d, $J_{\text{C-P}} = 5.9$ Hz), 124.3 (d, $J_{\text{C-P}} = 3.8$ Hz), 21.2, 18.8, 17.9 (d, $J_{\text{C-P}} = 10.3$ Hz), 17.6, 17.5, 16.0 ppm; $^{31}\text{P}\{1\text{H}\}$ NMR (121 MHz, CD_3CN): $\delta = 142.09$ ppm; $^{19}\text{F}\{1\text{H}\}$ NMR (376 MHz, CD_3CN): $\delta = (-110.34)$ - (-137.74) (m); IR: (neat, cm^{-1}) $\tilde{\nu} = 408, 438, 453, 479, 511, 528, 566, 653, 767, 784, 821, 838, 850, 886, 905, 964, 1194, 1417, 1443, 1485, 1600$ cm^{-1} ; HRMS: calcd m/z for $\text{C}_{65}\text{H}_{52}\text{N}_2\text{O}_2\text{P}^+ [\text{M}-\text{SbF}_6]^-$: 923.3761; found (ESI) 923.3761.

(R)-2-{2,6-Di(pyren-2-yl)dinaphtho[2,1-d:1',2'-f][1,3,2]dioxaphosphepin-4-yl}-1,3-di-mesityl-1H-imidazol-3-ium hexafluoroantimonate (178d):



Ar = 2-pyrenyl

Compound **178d** was prepared according to General Procedure **A** using (*R*)-3,3'-di(pyren-2-yl)-[1,1'-binaphthalene]-2,2'-diol (**173b**) (244.5 mg, 356 μmol 1.0 equiv.), pyridine (85 mg, 86.6 μL , 1.07 mmol, 3.0 equiv.) and PCl_3 (53.8 mg, 34.3 μL , 392 μmol , 1.1 equiv.) for the formation of the chlorophosphite. The chlorophosphite was then reacted with NaSbF_6 (277 mg, 1.07 mmol, 3.0 equiv.) and 1,3-bis(2,4,6-trimethylphenyl)-1,3-dihydro-2*H*-imidazol-2-ylidene (IMes) (103 mg, 0.338 mmol, 0.95 equiv.) to give the crude ligand. Column chromatography (DCM/EtOAc 100:1) yielded the ligand **178d** as a white solid (120 mg, 96 μmol , 28% yield).

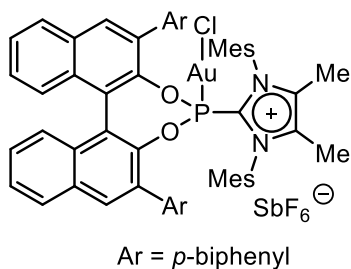
$[\alpha]_{24}^D$: -241.1 ($c = 0.10$, CH_2Cl_2); $^1\text{H NMR}$ (300 MHz, CD_3CN): δ 8.56 (s, 2H), 8.50 (s, 1H), 8.37 (d, $J = 4.3$ Hz, 2H), 8.33 (t, $J = 5.9$ Hz, 4H), 8.30-8.21 (m, 8H), 8.15 (t, $J = 7.0$ Hz, 2H), 8.10-8.08 (m, 2H), 8.05 (d, $J = 8.4$ Hz, 1H), 7.71 (t, $J = 7.5$ Hz, 1H), 7.55 (t, $J = 7.5$ Hz, 1H), 7.45 (t, $J = 7.8$ Hz, 1H), 7.30-7.22 (m, 2H), 7.16 (s, 1H), 6.92 (dd, $J = 8.1, 2.6$ Hz, 2H), 6.83 (s, 1H), 6.72 (s, 1H), 5.81 (s, 1H), 5.54 (s, 1H), 2.22 (s, 3H), 1.88 (s, 3H), 1.47 (s, 3H), 1.10 (s, 3H), 0.92 (s, 3H), -0.18 (s, 3H); $^{13}\text{C}\{1\text{H}\}$ NMR (126 MHz, CD_3CN): δ 146.5 (d, $J_{\text{C-P}} = 10.6$ Hz), 146.2, 146.1, 145.1, 143.0, 142.7, 142.6, 141.4, 138.3, 135.8, 135.7, 135.6, 135.5, 135.2, 135.0 (d, $J_{\text{C-P}} = 2.4$ Hz), 134.6,

134.2, 133.9, 133.7, 133.6, 133.4, 132.8, 132.7, 132.6 (d, $J_{C-P} = 5.5$ Hz), 132.3, 132.2, 132.1, 131.7, 131.1, 130.9, 130.8, 130.6, 130.2, 132.0 (d, $J_{C-P} = 5.2$ Hz), 129.9, 129.7, 129.5, 129.4, 129.3, 129.2, 129.1, 128.9, 128.4, 128.2, 128.1, 128.0, 127.9, 127.8, 127.7, 127.6, 127.5, 127.3, 127.0, 126.9 (d, $J_{C-P} = 2.3$ Hz), 126.7, 126.6, 126.3 (d, $J_{C-P} = 7.4$ Hz), 125.9, 125.6, 125.4 (d, $J_{C-P} = 5.5$ Hz), 125.1, 125.0 (d, $J_{C-P} = 6.6$ Hz), 124.8, 124.5 (d, $J_{C-P} = 3.5$ Hz), 123.8, 122.8, 21.3 (d, $J_{C-P} = 12.9$ Hz), 21.2, 18.7, 18.0, 17.5, 15.1 ppm; $^{31}\text{P}\{^1\text{H}\}$ NMR (121 MHz, CD_3CN): δ 142.25 ppm; $^{19}\text{F}\{^1\text{H}\}$ NMR (471 MHz, CD_3CN): $\delta = (-113.75)$ - (-134.29) (m) ppm; IR: (neat, cm^{-1}) $\tilde{\nu} = 416, 461, 440, 463, 471, 489, 658, 678, 712, 753, 801, 819, 834, 844, 867, 880, 919, 945, 999, 1030, 1084, 1151, 1206, 1217, 1227, 1306, 1365, 1414, 1443, 1493, 1546, 1599, 1727, 1738$ cm^{-1} ; HRMS: calcd m/z for $\text{C}_{73}\text{H}_{52}\text{N}_2\text{O}_2\text{P}^+ [\text{M}-\text{SbF}_6]^-$: 1019.3761; found (ESI) 1019.3753.

General Procedure B for the preparation of Au(I)-catalysts

According to the published procedure,^[218] a dried Schlenk flask equipped with a magnetic stirring bar and rubber septum was charged with the cationic phosphonite (1.0 equiv.) and dichloromethane (0.03 M), then cooled to -20 °C. To the Schlenk flask was then added (dimethyl sulfide)gold(I) chloride (1.0 equiv.) as a solid. The resulting solution was allowed to stir at -20 °C for 10 minutes, before warming to room temperature and stirring for between 30 minutes and one hour. The solvent was removed *in vacuo*, and the product dried under high vacuum.

Compound **162a**

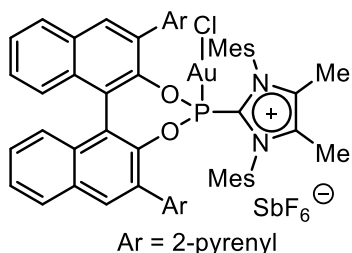


Prepared as a pale yellow solid (149 mg, 105 μmol , 99% yield) from compound **178a** (124.7 mg, 105 μmol , 1.0 equiv.), chloro(dimethyl sulfide)gold(I) (32.4 mg, 110 μmol , 1.05 equiv.) in dichloromethane (1.5 mL) according to General Procedure B. $[\alpha]_{20}^D: -45.0$ ($c = 0.1$, CH_2Cl_2); ^1H NMR: (300 MHz, CD_3CN) $\delta = 8.28$ (s, 1H), 8.25 – 8.18 (m, 2H), 8.04 (d, $J = 8.3$ Hz, 1H), 7.84 –

7.64 (m, 12H), 7.54 (dddd, $J = 8.2, 6.8, 2.3, 1.2$ Hz, 6H), 7.48 – 7.35 (m, 4H), 7.22 (ddd, $J = 8.4, 6.9, 1.3$ Hz, 1H), 7.05 (s, 2H), 6.95 (d, $J = 8.4$ Hz, 1H), 6.79 (d, $J = 1.9$ Hz, 1H), 6.73 (d, $J = 8.7$ Hz, 1H), 5.70 (s, 1H), 2.36 (s, 3H), 1.87 (s, 3H), 1.86 (s, 3H), 1.82 (s, 3H), 1.68 (s, 3H), 1.55 (s, 3H), 1.50 (s, 3H), 1.22 (s, 3H) ppm; $^{13}\text{C}\{^1\text{H}\}$ NMR: (101 MHz, CD_3CN) $\delta = 145.4$ (d, $J_{C-P} = 16.2$ Hz), 144.9 (d, $J_{C-P} = 7.1$ Hz), 144.5, 142.7, 142.4, 142.0, 141.0, 140.8, 138.1 (d, $J_{C-P} = 3.0$ Hz), 137.3 (d, $J_{C-P} = 2.0$ Hz), 136.1, 135.9, 135.5, 135.2, 135.0, 134.4, 134.1, 134.0, 133.9, 133.7 (d, $J_{C-P} = 1.0$ Hz), 133.6 (d, $J_{C-P} = 3.0$ Hz), 133.3, 133.3, 133.1 (d, $J_{C-P} = 3.0$ Hz), 132.8, 132.6, 132.3 (d, $J_{C-P} = 3.0$

Hz), 131.4, 130.9, 130.6, 130.1, 129.7, 129.5, 128.9, 128.6, 128.4, 128.3, 128.3, 128.1, 128.1, 128.0, 127.9, 127.9, 127.7, 127.6, 125.4 (d, $J_{C-P} = 4.0$ Hz), 122.3 (d, $J_{C-P} = 4.0$ Hz), 21.5, 21.2, 20.2, 18.9, 17.8, 16.5, 9.9, 9.6 ppm; $^{31}\text{P}\{^1\text{H}\}$ NMR: (121 MHz, CD_3CN) $\delta = 112.5$ ppm; $^{19}\text{F}\{^1\text{H}\}$ NMR: (376 MHz, CD_3CN) $\delta = -124.0$ (oct, $J_{F-^{123}\text{Sb}} = 1049.0$ Hz), -124.0 (sext, $J_{F-^{121}\text{Sb}} = 1932.6$ Hz) ppm; IR: (neat, cm^{-1}) $\tilde{\nu} = 499, 510, 539, 562, 612, 655, 698, 735, 754, 767, 844, 876, 891, 961, 1146, 1184$ cm^{-1} ; HR-MS: calcd m/z for $\text{C}_{67}\text{H}_{56}\text{AuClN}_2\text{O}_2\text{P}^+ [\text{M}-\text{SbF}_6]^-$: 1183.3428; found (ESI) 1183.3432.

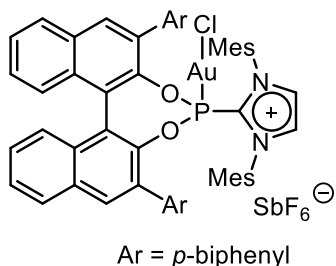
Compound **162b**



Prepared as a pale yellow solid (95 mg, 62.6 μmol , 96% yield) from compound **178b** (84.0 mg, 65.4 μmol , 1.0 equiv.), chloro(dimethyl sulfide)gold(I) (20.2 mg, 68.5 μmol , 1.05 equiv.) in dichloromethane (2.0 mL) according to General Procedure B.

$[\alpha]_{20}^D$: -58.0 ($c = 0.05$, CH_2Cl_2); ^1H NMR: (300 MHz, CD_3CN) $\delta = 8.61$ (d, $J = 1.2$ Hz, 2H), 8.53 – 8.46 (m, 3H), 8.32 (dd, $J = 7.7, 5.8$ Hz, 5H), 8.25 (d, $J = 3.6$ Hz, 5H), 8.21 (s, 2H), 8.15 – 8.02 (m, 5H), 7.72 (t, $J = 7.5$ Hz, 1H), 7.59 (t, $J = 7.6$ Hz, 1H), 7.48 (ddd, $J = 8.2, 6.9, 1.2$ Hz, 1H), 7.29 (td, $J = 7.7, 7.1, 1.5$ Hz, 1H), 7.04 (d, $J = 8.5$ Hz, 1H), 6.87 (d, $J = 9.3$ Hz, 2H), 6.63 (s, 1H), 6.39 (s, 1H), 5.77 (s, 1H), 2.21 (s, 3H), 1.73 (s, 3H), 1.63 (s, 3H), 1.57 (s, 3H), 1.51 (s, 3H), 1.38 (s, 3H), 0.34 (s, 3H), 0.07 (s, 3H) ppm; $^{13}\text{C}\{^1\text{H}\}$ NMR: (101 MHz, CD_3CN) $\delta = 145.6$ (d, $J_{C-P} = 16.2$ Hz), 145.2 (d, $J_{C-P} = 6.1$ Hz), 144.3, 142.7, 137.8, 137.0, 135.4, 134.5 (d, $J_{C-P} = 7.1$ Hz), 134.3, 134.1, 133.8, 133.8, 133.8, 133.3, 133.3, 133.1, 132.8, 132.7, 132.5, 132.4, 132.2, 132.1, 131.8, 130.4, 129.8, 129.6 (d, $J_{C-P} = 5.1$ Hz), 129.4, 129.3, 129.1, 128.8, 128.6, 128.4, 128.4, 128.3, 128.1, 128.1, 127.9, 127.8, 127.8, 127.7, 127.2, 126.7, 126.5, 125.2 (d, $J_{C-P} = 4.0$ Hz), 125.0, 124.8, 124.8, 122.4 (d, $J_{C-P} = 4.0$ Hz), 21.4, 21.2, 20.3, 18.5, 16.4, 15.3, 9.4 ppm; $^{31}\text{P}\{^1\text{H}\}$ NMR: (121 MHz, CD_3CN) $\delta = 112.6$ ppm; $^{19}\text{F}\{^1\text{H}\}$ NMR: (376 MHz, CD_3CN) $\delta = -124.0$ (oct, $J_{F-^{123}\text{Sb}} = 1045.3$ Hz), -124.0 (sext, $J_{F-^{121}\text{Sb}} = 1932.6$ Hz) ppm; IR: (neat, cm^{-1}) $\tilde{\nu} = 499, 540, 563, 575, 582, 586, 589, 605, 654, 712, 751, 821, 844, 871, 874, 879, 928, 2359$ cm^{-1} ; HR-MS: calcd m/z for $\text{C}_{75}\text{H}_{56}\text{AuClN}_2\text{O}_2\text{P}^+ [\text{M}-\text{SbF}_6]^-$: 1279.3428; found (ESI) 1279.3414.

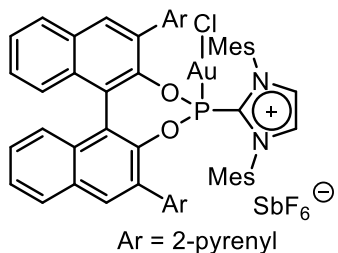
Compound **162c**



Prepared as a yellow solid (150 mg, 108 μmol , 94% yield) from compound **178c** (132 mg, 113.8 μmol , 1.0 equiv.), chloro(dimethyl sulfide)gold(I) (34.0 mg, 115.4 μmol , 1.01 equiv.) in dichloromethane (3.6 mL) according to General Procedure B.

$[\alpha]_{20}^D$: -30.5 ($c = 0.11$, CH_2Cl_2); $^1\text{H NMR}$ (300 MHz, CD_3CN): δ 8.29 (s, 1H), 8.24 (d, $J = 7.5$ Hz, 2H), 8.06 (d, $J = 8.4$ Hz, 1H), 7.86-7.68 (m, 15H), 7.61-7.50 (m, 5H), 7.50-7.38 (m, 3H), 7.26 (t, $J = 7.8$ Hz, 1H), 6.98 (d, $J = 11.5$ Hz, 3H), 6.76 (d, $J = 8.6$ Hz, 2H), 5.73 (s, 1H), 2.34 (s, 3H), 1.70 (s, 3H), 1.65 (s, 3H), 1.53 (s, 3H), 1.27 (s, 3H) ppm. $^{13}\text{C}\{^1\text{H}\}$ NMR (126 MHz, CD_3CN): $\delta = 145.3$ (d, $J_{\text{C-P}} = 16.4$ Hz), 144.7, 142.7, 142.5, 142.2, 141.1, 140.9, 137.5, 137.2, 135.7 (d, $J_{\text{C-P}} = 10.1$ Hz), 135.3, 135.1, 135.0, 134.1, 133.7, 133.6, 133.5 (d, $J_{\text{C-P}} = 3.1$ Hz), 133.4, 133.2 (d, $J_{\text{C-P}} = 1.9$ Hz), 132.8, 132.6, 132.3, 132.1 (d, $J_{\text{C-P}} = 2.7$ Hz), 131.6, 131.4, 130.9 (d, $J_{\text{C-P}} = 3.7$ Hz), 130.7, 130.6, 130.1, 130.0, 129.8, 129.5, 129.3, 129.0, 129.0, 128.7, 128.5, 128.5, 128.4, 128.2, 128.1, 128.1, 128.0, 127.8 (d, $J_{\text{C-P}} = 5.1$ Hz), 125.5 (d, $J_{\text{C-P}} = 4.1$ Hz), 122.5 (d, $J_{\text{C-P}} = 3.1$ Hz), 21.4, 21.2, 20.0, 18.9, 17.6, 16.3 ppm; $^{31}\text{P}\{^1\text{H}\}$ NMR (121 MHz, CD_3CN): $\delta = 112.84$ ppm; $^{19}\text{F}\{^1\text{H}\}$ NMR (471 MHz, CD_3CN): $\delta = (-113.60)$ - (-134.47) (m) ppm; IR: (neat, cm^{-1}) $\tilde{\nu} = 515, 540, 582, 605, 655, 732, 844, 882, 929, 962, 994, 1028, 1085, 1149, 1180, 1224, 1309, 1445, 1599$ cm^{-1} ; HRMS: calcd m/z for $\text{C}_{65}\text{H}_{52}\text{AuClN}_2\text{O}_2\text{P}^+ [\text{M-SbF}_6]^-$: 1155.3115; found (ESI) 1155.3158.

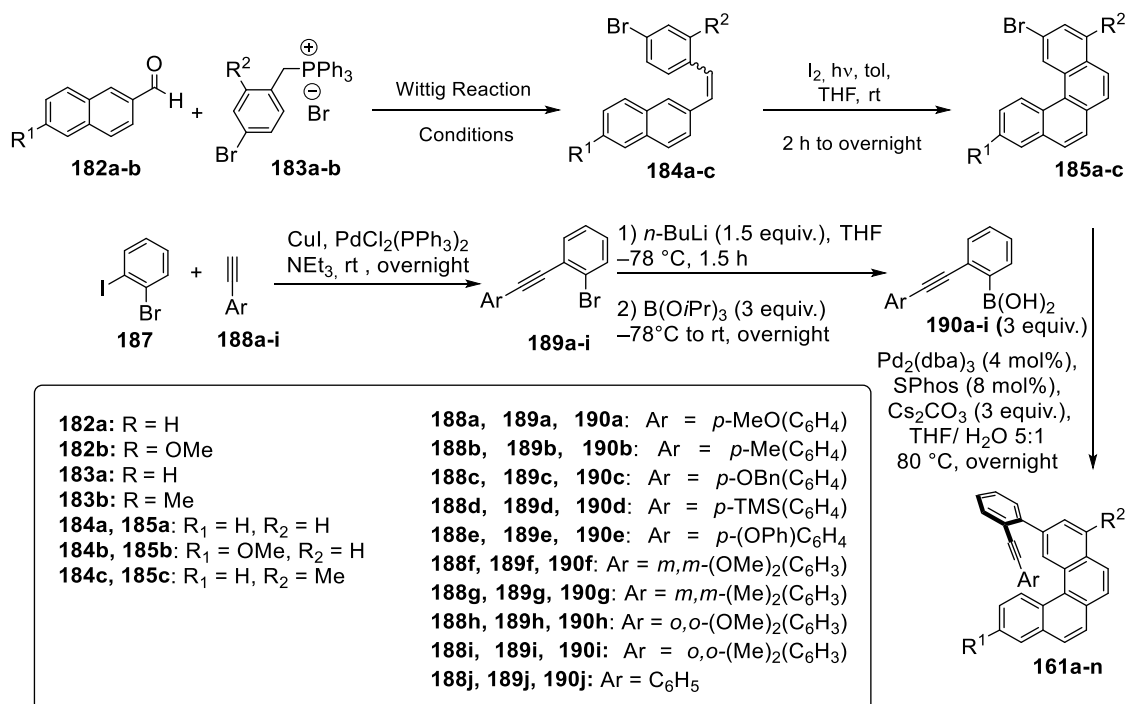
Compound 162d



Prepared as a yellow solid (140 mg, 94.1 μmol , 99% yield) from compound **4h** (120 mg, 95.5 μmol , 1.0 equiv.), chloro(dimethyl sulfide)gold(I) (29.7 mg, 100.8 μmol , 1.05 equiv.) in dichloromethane (3.2 mL) according to General Procedure B.

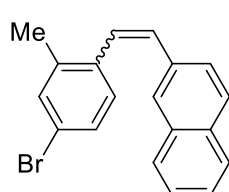
$[\alpha]_{20}^D$: -54.8 ($c = 0.23$, CH_2Cl_2); $^1\text{H NMR}$ (300 MHz, CD_3CN): δ 8.65 (s, 2H), 8.56 (s, 3H), 8.42 (s, 1H), 8.38 (s, 1H), 8.35 (s, 2H), 8.32 (s, 2H), 8.31-8.23 (m, 6H), 8.19-8.09 (m, 5H), 7.76 (t, $J = 7.5$ Hz, 1H), 7.65 (t, $J = 7.6$ Hz, 1H), 7.57 (s, 1H), 7.50 (s, 1H), 7.34 (t, $J = 7.8$ Hz, 2H), 7.09 (d, $J = 8.5$ Hz, 1H), 6.91 (d, $J = 8.7$ Hz, 1H), 6.86 (s, 1H), 6.57 (s, 1H), 6.40 (s, 1H), 5.86 (s, 1H), 2.20 (s, 3H), 1.77 (s, 3H), 1.67 (s, 3H), 1.65 (s, 3H), 0.39 (s, 3H), 0.18 (s, 3H) ppm. $^{13}\text{C}\{^1\text{H}\}$ NMR (126 MHz, CD_3CN): δ 145.6 (d, $J_{\text{C-P}} = 16.6$ Hz), 145.0 (d, $J_{\text{C-P}} = 6.6$ Hz), 144.4, 142.8, 137.1, 136.7, 135.2, 135.2, 134.8, 134.7, 134.5, 134.2 (d, $J_{\text{C-P}} = 3.3$ Hz), 134.2, 133.9, 133.8, 133.4 (d, $J_{\text{C-P}} = 2.0$ Hz), 133.3 (d, $J_{\text{C-P}} = 1.3$ Hz), 133.0, 132.6, 132.5 (d, $J_{\text{C-P}} = 2.9$ Hz), 132.3, 132.2, 132.0 (d, $J_{\text{C-P}} = 2.7$ Hz), 131.9, 131.4, 131.2, 130.4 (d, $J_{\text{C-P}} = 4.1$ Hz), 130.2, 129.9, 129.7, 129.6, 129.5, 129.4, 129.3, 128.9, 128.7, 128.6, 128.3, 128.1, 127.9, 127.9, 127.8, 127.2, 126.8, 126.6, 125.3 (d, $J_{\text{C-P}} = 4.4$ Hz), 125.1, 124.9, 124.9, 122.6 (d, $J_{\text{C-P}} = 3.9$ Hz), 21.3, 21.2, 20.1, 18.5, 16.2, 15.2 ppm; $^{31}\text{P}\{^1\text{H}\}$ NMR (121 MHz, CD_3CN): δ 112.69 ppm; $^{19}\text{F}\{^1\text{H}\}$ NMR (471 MHz, CD_3CN): δ (-112.98)-(-135.61) (m) ppm; IR: (neat, cm^{-1}) $\tilde{\nu} = 514, 582, 653, 712, 802, 844, 879, 928, 995, 1026, 1085, 1148, 1180, 1222, 1259, 1359, 1406, 1444, 1598$ cm^{-1} ; HRMS: calcd m/z for $\text{C}_{73}\text{H}_{52}\text{AuClN}_2\text{O}_2\text{P}^+ [\text{M-SbF}_6]^-$: 1251.3115; found (ESI) 1251.3132.

6.2.2. Synthesis of precursors **161a-n**



Scheme 56. Synthesis of the substituted [4]helicene-containing substrates **161a-n** via consecutive Wittig reaction, Mallory photocyclization and Suzuki coupling.

2-(4-Bromo-2-methylstyryl)naphthalene (**184c**):



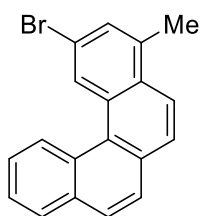
(4-Bromo-2-methylbenzyl)triphenylphosphonium bromide (**183b**) (2.00 g, 3.80 mmol, 1.1 equiv.) was placed in a dry flask under inert atmosphere. Anhydrous THF (35 mL) was added, and the resulting suspension was stirred at 0 °C. *n*-BuLi (1.7 mL 2.5 M, 4.25 mmol, 1.23 equiv.) was added dropwise and the red mixture was stirred at rt for 2 h. The reaction mixture was cooled to 0 °C, and 2-naphthaldehyde (540 mg, 3.46 mmol, 1 equiv.) was added as a solution in dry THF (7 mL) dropwise. The mixture was allowed to warm up to rt and then stirred at 60 °C for 60 h. The reaction was quenched by addition of water (10 mL). The biphasic mixture was extracted with EtOAc (20 mL), and the aqueous phase re-extracted with Et₂O (2 × 20 mL). The combined organic layers were dried over MgSO₄, filtered and concentrated in vacuo. The residue was purified by column chromatography (SiO₂, 0 to 10% EtOAc in pentane) to afford the olefin **184c** as a 3:2 mixture of *E* and *Z* isomers (917 mg, 2.84 mmol, 82%). ¹H NMR: (300 MHz, CDCl₃): mixture of two isomers (33:67) δ = 7.93 – 7.67 (m, 6H), 7.59 (dd, *J* = 25.7, 8.8 Hz, 2H), 7.44 (ddt, *J* = 14.1, 9.5, 7.1 Hz, 6H), 7.33 – 7.19 (m, 2H), 7.18 – 7.01 (m, 3H), 6.93 – 6.74 (m, 1H), 6.65 (d, *J* = 12.1 Hz, 1H), 2.49 (s, 2H), 2.32 (s, 3H) ppm; ¹³C NMR: (101 MHz, CDCl₃) δ = 138.6, 137.9, 136.0, 135.4, 134.8, 134.3, 133.7, 133.4, 133.2, 133.1, 133.0, 132.6, 131.2, 130.7, 130.7, 130.6, 130.1, 129.3, 128.8, 128.5, 128.4, 128.4, 128.3, 128.0, 127.9, 127.7, 127.6, 126.8, 126.8, 126.5, 126.4, 126.3, 126.1, 126.1, 126.06, 125.8, 125.6, 123.5, 121.2, 121.0, 35.4, 20.0, 19.8,

14.0 ppm; **IR**: (neat, cm^{-1}) $\tilde{\nu}$ = 1588, 1503, 1478, 1444, 1390, 1379, 1366, 1273, 1180, 1107, 1084, 959, 901, 886, 868, 859, 849, 772, 763, 745, 717, 664, 640, 620, 605, 567, 549, 531, 445, 415; **HR-MS**: calcd m/z for $\text{C}_{19}\text{H}_{15}\text{Br}^+$ [M^+]: 322.0352; found (ESI) 322.0353.

General Procedure C for Oxidative Photocyclization Reactions

The respective stilbene (1.0 equiv.) as well as iodine (2.2 equiv.) were dissolved in THF; the solutions were added into the photoreactor filled with degassed toluene (450 mL, due to reactor design). After 2 to 24 hours of irradiation (reaction control *via* TLC) the reaction was quenched with $\text{Na}_2\text{S}_2\text{O}_3$ (aq., sat., 250 mL), the phases were separated and the organic phase dried over Na_2SO_4 . After removal of the volatiles the crude mixture was subjected to column chromatography (conditions see individual cases) to yield the desired [4]helicenes.

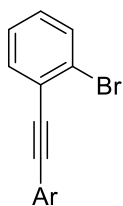
2-Bromo-4-methylbenzo[*c*]phenanthrene (**185c**):



Compound **185c** was prepared from stilbene **184c** (880 mg, 2.72 mmol, 1.00 equiv.) and iodine (1.49 g, 5.87 mmol, 2.16 equiv.) according to General Procedure **C**. After purification by column chromatography (SiO_2 , pentane) the compound **185c** was obtained as a white solid (510 mg, 1.59 mmol, 58%).

^1H NMR (400 MHz, CDCl_3) δ 9.15 (s, 1H), 9.03 (d, J = 8.4 Hz, 1H), 8.04 (d, J = 7.8 Hz, 1H), 7.99 – 7.86 (m, 2H), 7.77 (dq, J = 13.7, 7.5, 6.1 Hz, 3H), 7.69 (t, J = 7.4 Hz, 1H), 7.60 (s, 1H), 2.75 (d, J = 3.9 Hz, 3H) ppm; **^{13}C NMR** (101 MHz, CDCl_3) δ 136.6, 133.6, 131.5, 131.0, 130.9, 130.1, 129.8, 128.7, 128.5, 128.0, 127.8, 127.0, 126.8, 126.5, 126.5, 126.1, 122.9, 120.1, 20.0 ppm; **IR**: (neat, cm^{-1}) $\tilde{\nu}$ = 1602, 1583, 1563, 1484, 1451, 1434, 1401, 1392, 1369, 1358, 1338, 1165, 1133, 1110, 1096, 1038, 1032, 896, 884, 869, 852, 834, 821, 806, 799, 788, 775, 743, 731, 692, 660, 612, 595, 578, 547, 530, 520, 510, 490, 459, 447, 423, 411; **HR-MS**: calcd m/z for $\text{C}_{19}\text{H}_{13}\text{Br}^+$ [M^+]: 320.0195; found (ESI) 320.0191.

1-[[4-(Benzyloxy)phenyl]thynyl]-2-bromobenzene (**189c**):

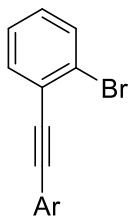


A suspension of 2-bromiodobenzene (**187**) (1.01 g, 0.46 mL, 3.57 mmol, 1 equiv.), $\text{PdCl}_2(\text{PPh}_3)_2$ (50.1 mg, 71.3 μmol , 2 mol%), CuI (20.3 mg, 106.5 μmol , 3 mol%) in NEt_3 (15 mL) was degassed with nitrogen stream for 5 minutes. After 10 min, a solution of 1-(benzyloxy)-4-ethynylbenzene (**188c**) ($\text{Ar} = p\text{-BnO}(\text{C}_6\text{H}_4)$) (880 g, 4.23 mmol, 1.18 equiv.) in NEt_3 (5 mL) was added dropwise over 5 min via syringe, and the reaction mixture was stirred overnight. After complete consumption of the 2-bromiodobenzene (**187**), as monitored by TLC, the reaction mixture was filtered

through a pad of celite and extracted with ethyl acetate (3 × 10 mL). The combined organic extracts were washed with a saturated solution of NH₄Cl (2 × 10 mL), water (2 × 10 mL), dried over MgSO₄, and the organic solvent was removed in *vacuo*. Column chromatography (SiO₂, pentane) yielded the desired arylacetylene **189c** as a white solid (974 mg, 2.68 mmol, 75%).

¹H NMR (300 MHz, CDCl₃) δ = 7.63 (dd, *J* = 8.0, 1.2 Hz, 1H), 7.59 – 7.51 (m, 3H), 7.43 (tdd, *J* = 10.4, 7.5, 5.6 Hz, 5H), 7.34 – 7.27 (m, 1H), 7.22 – 7.14 (m, 1H), 7.03 – 6.96 (m, 2H), 5.12 (s, 2H) ppm; ¹³C{¹H} NMR: (101 MHz, CDCl₃) δ = 159.1, 136.5, 133.2, 133.0, 132.4, 129.0, 128.7, 128.1, 127.5, 127.0, 125.7, 125.5, 115.30, 115.0, 94.0, 87.0, 70.0 ppm; IR: (neat, cm⁻¹) $\tilde{\nu}$ = 2215, 1603, 1583, 1568, 1507, 1460, 1452, 1431, 1415, 1380, 1311, 1285, 1244, 1172, 1146, 1117, 1107, 1078, 1039, 1024, 987, 971, 958, 941, 904, 862, 850, 811, 708, 651, 622, 596, 544, 529, 518, 501, 469, 454, 436, 420, 411; HR-MS: calcd *m/z* for C₂₁H₁₅BrO⁺ [M]⁺: 362.0301; found (ESI) 362.0298.

2-[(2-Bromophenyl)ethynyl]1,3-dimethoxybenzene (**189h**):

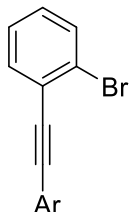


Ar = *o,o*-(MeO)₂(C₆H₃)

A suspension of 2-bromoiodobenzene (**187**) (492 mg, 0.22 mL, 1.74 mmol, 1 equiv.), PdCl₂(PPh₃)₂ (24.0 mg, 34.1 μmol, 2 mol%), CuI (10.0 mg, 52.5 μmol, 2 mol%) in NEt₃ (10 mL) was degassed with nitrogen stream for 5 minutes. After 10 min, a solution of 2-ethynyl-1,3-dimethoxybenzene (**188h**) (309 mg, 1.91 mmol, 1.1 equiv.) in NEt₃ (5 mL) was added dropwise over 5 min via syringe, and the reaction mixture was stirred overnight. After complete consumption of the 2-bromoiodobenzene, as monitored by TLC, the reaction mixture was filtered through a pad of celite and extracted with ethyl acetate (3 × 10 mL). The organic layer was washed with a saturated solution of NH₄Cl (2 × 10 mL), water (2 × 10 mL), dried over MgSO₄, and the organic solvent was removed in *vacuo*. Column chromatography (SiO₂, pentane) yielded the desired arylacetylene a white solid (287 mg, 0.90 mmol, 52%).

¹H NMR (400 MHz, CDCl₃) δ = 7.74 – 7.54 (m, 2H), 7.42 – 7.26 (m, 2H), 7.19 (td, *J* = 7.8, 1.7 Hz, 1H), 6.61 (d, *J* = 8.4 Hz, 2H), 3.96 (s, 6H); ¹³C{¹H} NMR: (101 MHz, CDCl₃) δ = 161.7, 133.5, 132.4, 130.2, 129.0, 126.9, 126.2, 125.3, 103.6, 101.5, 96.2, 86.8, 56.2 ppm; IR: (neat, cm⁻¹) $\tilde{\nu}$ = 3734, 3726, 3709, 3628, 1592, 1581, 1558, 1489, 1473, 1460, 1432, 1300, 1255, 1110, 1042, 1027, 777, 754, 725, 679, 650; HR-MS: calcd *m/z* for C₁₆H₁₂BrO₂⁺ [M-H]⁺: 316.0015; found (EI) 315.0015. HR-MS: calcd *m/z* for C₁₆H₁₃BrO₂⁺: 315.0015; found (EI) 315.0015.

2-[(2-bromophenyl)ethynyl]-1,3-dimethylbenzene (**189i**):



Ar = *o,o*-(Me)₂(C₆H₃)

A suspension of 2-bromoiodobenzene **187** (441 mg, 0.2 mL, 1.56 mmol, 1 equiv.), PdCl₂(PPh₃)₂ (21.9 mg, 31.2 μmol, 2 mol%), CuI (9.0 mg, 47.2 μmol, 3 mol%) in NEt₃ (10 mL) was degassed with nitrogen stream for 5 minutes. After 10 min, a solution of 2-ethynyl-1,3-dimethylbenzene (**188i**) (225 mg, 1.72 mmol, 1.1 equiv.) in NEt₃ (2 mL) was added dropwise over 5 min via syringe, and the reaction mixture was stirred overnight. After complete consumption of the 2-bromoiodobenzene, as monitored by TLC, the reaction mixture was filtered through a pad of celite and extracted with ethyl acetate (3 × 10 × mL), dried over MgSO₄, and the organic solvent was removed in *vacuo*. Column chromatography (SiO₂, pentane) yielded the desired arylacetylene a white solid (228 mg, 0.80 mmol, 51%).

¹H NMR (400 MHz, CDCl₃) δ = 7.66 (dd, *J* = 8.1, 1.2 Hz, 1H), 7.62 (dd, *J* = 7.6, 1.7 Hz, 1H), 7.32 (td, *J* = 7.6, 1.2 Hz, 1H), 7.24 – 7.16 (m, 2H), 7.12 (d, *J* = 7.5 Hz, 2H), 2.62 (s, 6H); ¹³C{¹H} NMR: (101 MHz, CDCl₃) δ = 140.8, 133.4, 132.6, 129.2, 128.3, 127.1, 126.9, 126.1, 125.2, 122.7, 96.3, 92.0, 21.4; IR: (neat, cm⁻¹) $\tilde{\nu}$ = 3734, 3726, 2360, 1558, 1473, 1433, 1420, 1115, 1042, 1025, 769, 750, 731, 712, 678, 663, 517; HR-MS: calcd *m/z* for C₁₆H₁₃Br⁺ [M]⁺: 284.0195; found (EI) 284.0194.

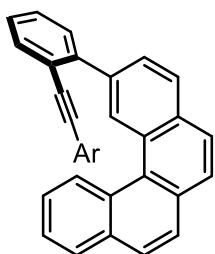
General Procedure D for the preparation of Boronic Acids **190**

A dried Schlenk flask equipped with a magnetic stirring bar was charged with the respective arylbromide **189a-i** (1.0 equiv.), which was then dissolved in THF and cooled to –78 °C. *n*-Butyllithium (1.3 equiv.) was added dropwise over 10 min. The mixture was stirred at –78 °C for 1 h, then at –40 °C for 1h. After cooling to –78 °C again, triisopropylborate (1.5 equiv.) was added, and the reaction mixture was allowed to reach room temperature overnight, while maintaining vigorous stirring. The reaction was quenched by the addition of aqueous HCl (2 M). The phases were separated, and the aqueous phase was extracted with ether (3 × 50 mL). The combined organic phases were dried over Na₂SO₄ and the solvents removed *in vacuo*. The crude boronic acids **190a-i** were filtered through a silica pad washing with EtOAc and used without further purification.

General Procedure E for Suzuki-Miyaura Cross-Coupling Reactions

A Schlenk flask equipped with a magnetic stirring bar was loaded with the respective bromide (1 equiv.), the respective boronic acid **190a-i** (1.5 equiv.), the base (Cs_2CO_3 , 3 equiv.), $\text{Pd}_2(\text{dba})_3$ (4 mol%) and SPhos (8 mol%). A thoroughly degassed mixture of THF and H_2O (10:1, 0.02 M) was added. The solution was placed in a pre-heated oil bath and stirred at 80 °C overnight. After cooling to room temperature, the mixture was eluted through a plug of silica gel using DCM. Column chromatography (SiO_2 , EtOAc in pentane) yielded the desired alkyne-decorated [5]helicene precursors **161a-n**.

2-[2-[(4-Methoxyphenyl)ethynyl]phenyl]benzo[c]phenanthrene (**161a**):

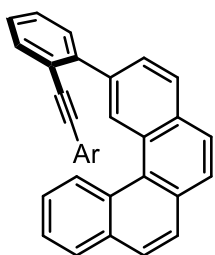


Ar = *p*-MeO(C_6H_4)

Prepared from 2-bromobenzo[c]phenanthrene (**185a**) (208 mg, 677 μmol , 1.0 equiv.), **190a** (256 mg, 1.02 mmol, 1.5 equiv.), $\text{Pd}_2(\text{dba})_3$ (25.0 mg, 27.3 μmol , 4 mol%), SPhos (22.2 mg, 54.1 μmol , 8 mol%), Cs_2CO_3 (664 mg, 2.04 mmol, 3.0 equiv.) and the solvent mixture (34 mL) according to General Procedure E. Column chromatography (SiO_2 , 0 to 5% EtOAc in pentane) yielded the product **161a** as a yellow solid (234 mg, 538.5 μmol , 80%).

$^1\text{H NMR}$ (400 MHz, CDCl_3) δ = 9.45 (dd, J = 1.7, 0.8 Hz, 1H), 9.29 (d, J = 8.5 Hz, 1H), 8.14 (d, J = 8.3 Hz, 1H), 8.03 – 7.87 (m, 6H), 7.81 – 7.71 (m, 1H), 7.59 – 7.52 (m, 2H), 7.52 – 7.35 (m, 3H), 7.19 – 7.12 (m, 2H), 6.72 – 6.63 (m, 2H), 3.75 (s, 3H) ppm; $^{13}\text{C NMR}$ (101 MHz, CDCl_3) δ = 159.4, 143.8, 138.7, 133.4, 133.1, 132.9, 132.7, 131.2, 130.3, 130.12, 130.05, 128.7, 128.33, 128.28, 128.14, 128.13, 127.7, 127.67, 127.5, 127.4, 127.2, 127.1, 127.0, 126.8, 126.3, 125.9, 122.3, 115.3, 113.8, 92.5, 88.4, 55.2 ppm; IR: (neat, cm^{-1}) $\tilde{\nu}$ = 3049, 3014, 2960, 2930, 2908, 2836, 2206, 1604, 1568, 1508, 1475, 1463, 1457, 1440, 1426, 1395, 1303, 1287, 1246, 1173, 1161, 1146, 1106, 1076, 1058, 1027, 984, 965, 952, 912, 871, 844, 828, 791, 754, 718, 707, 695, 681, 654, 641, 619, 588, 578, 566, 547, 529, 496, 483, 460, 443, 422, 407; HR-MS: calcd m/z for $\text{C}_{33}\text{H}_{23}\text{O}^+$ $[\text{M}+\text{H}]^+$: 435.1743; found (ESI) 435.1739.

2-[2-(*p*-Tolylethynyl)phenyl]benzo[c]phenanthrene (**161b**):



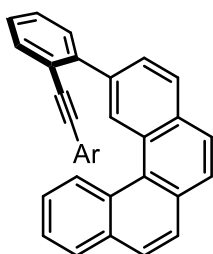
Ar = *p*-Me(C_6H_4)

Prepared from 2-bromobenzo[c]phenanthrene (**185a**) (208 mg, 677 μmol , 1.0 equiv.), **190b** (240 mg, 1.01 mmol, 1.49 equiv.), $\text{Pd}_2(\text{dba})_3$ (25.0 mg, 27.3 μmol , 4 mol%), SPhos (22.2 mg, 54.1 μmol , 8 mol%), Cs_2CO_3 (664 mg, 2.04 mmol, 3.0 equiv.) and the solvent mixture (34 mL) according to

General Procedure E. Column chromatography (SiO₂, 0 to 5% EtOAc in pentane) yielded the product as a yellow solid (170 mg, 406.1 μmol, 60%).

¹H NMR (300 MHz, CDCl₃) δ = 9.44 (dd, *J* = 1.7, 0.9 Hz, 1H), 9.29 (d, *J* = 8.6 Hz, 1H), 8.13 (d, *J* = 8.3 Hz, 1H), 8.06 – 7.82 (m, 6H), 7.82 – 7.70 (m, 1H), 7.63 – 7.35 (m, 5H), 7.18 – 7.05 (m, 2H), 7.01 – 6.91 (m, 2H), 2.28 (s, 3H) ppm; ¹³C NMR (101 MHz, CDCl₃) δ = 144.0, 138.7, 138.2, 133.4, 133.3, 132.7, 131.3, 131.2, 130.3, 130.14, 130.05, 128.9, 128.7, 128.5, 128.3, 128.2, 128.1, 127.7, 127.5, 127.4, 127.2, 127.1, 127.0, 126.8, 126.3, 125.9, 122.2, 120.1, 92.7, 89.0, 21.4 ppm; IR: (neat, cm⁻¹) $\tilde{\nu}$ = 2372, 2354, 2319, 1509, 1475, 1443, 1424, 910, 843, 827, 814, 794, 753, 707, 680, 619, 588, 577, 532, 517, 497, 416; HR-MS: calcd *m/z* for C₃₃H₂₂⁺ [M]⁺: 418.1716; found (ESI) 418.1713.

2-(2-{[4-(Benzyloxy)phenyl]ethynyl}phenyl)benzo[*c*]phenanthrene (161c):

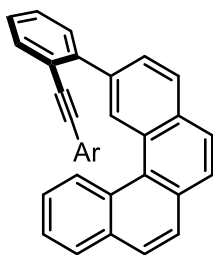


Ar = *p*-BnO(C₆H₄)

Prepared from 2-bromobenzo[*c*]phenanthrene (**185a**) (208 mg, 677 μmol, 1.0 equiv.), **190c** (335 mg, 1.021 mmol, 1.51 equiv.), Pd₂(dba)₃ (25.0 mg, 27.3 μmol, 4 mol%), SPhos (22.2 mg, 54.1 μmol, 8 mol%), Cs₂CO₃ (664 mg, 2.04 mmol, 3.0 equiv.) and the solvent mixture (34 mL) according to General Procedure E. Column chromatography (SiO₂, 0 to 5% EtOAc in pentane) yielded the product as a yellow solid (192 mg, 376 μmol, 56%).

¹H NMR (300 MHz, CDCl₃) δ = 9.47 (dd, *J* = 1.7, 0.8 Hz, 1H), 9.29 (dd, *J* = 8.4, 1.3 Hz, 1H), 8.14 (d, *J* = 8.3 Hz, 1H), 7.88 (s, 6H), 7.81 – 7.70 (m, 1H), 7.62 – 7.30 (m, 10H), 7.21 – 7.09 (m, 2H), 6.75 (d, *J* = 8.9 Hz, 2H), 5.00 (s, 2H) ppm; ¹³C NMR (101 MHz, CDCl₃) δ = 158.6, 143.8, 138.7, 136.6, 133.4, 133.1, 132.9, 132.7, 131.2, 130.3, 130.13, 130.05, 128.7, 128.6, 128.4, 128.3, 128.2, 128.1, 127.7, 127.5, 127.41, 127.39, 127.2, 127.1, 127.0, 126.8, 126.3, 125.9, 122.3, 115.6, 114.7, 92.5, 88.5, 69.9 ppm; IR: (neat, cm⁻¹) $\tilde{\nu}$ = 1602, 1506, 1475, 1453, 1283, 1240, 1224, 1173, 1146, 1107, 1023, 1003, 910, 843, 827, 794, 753, 712, 694, 681, 667, 644, 618, 600, 587, 577, 565, 550, 535, 522, 513, 497, 482, 457, 440, 413; HR-MS: calcd *m/z* for C₃₉H₂₆O⁺ [M]⁺: 510.1978; found (ESI) 510.1975.

4-{[2-(Benzo[*c*]phenanthren-2-yl)phenyl]ethynyl}phenyltrimethylsilane (161d):



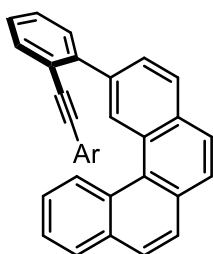
Ar = *p*-(Me₃Si)(C₆H₄)

Prepared from 2-bromobenzo[*c*]phenanthrene **185a** (135 mg, 439.4 μmol, 1.0 equiv.), **190d** (194 mg, 659.3 μmol, 1.5 equiv.), Pd₂(dba)₃ (16.1 mg, 17.6 μmol, 4 mol%), SPhos (14.5 mg, 35.3 μmol, 8 mol%), Cs₂CO₃ (430 mg, 1.32 mmol, 3.0 equiv.) and the solvent mixture (22 mL) according to General Procedure E. Column chromatography (SiO₂,

0 to 5% EtOAc in pentane) yielded the product **161d** as a yellow solid (184 mg, 385.9 μmol , 88%).

$^1\text{H NMR}$ (300 MHz, CDCl_3) δ = 9.43 (dd, J = 1.7, 0.8 Hz, 1H), 9.27 (d, J = 8.4 Hz, 1H), 8.13 (d, J = 8.3 Hz, 1H), 8.06 – 7.83 (m, 6H), 7.82 – 7.74 (m, 1H), 7.59 – 7.36 (m, 5H), 7.36 – 7.28 (m, 2H), 7.26 – 7.15 (m, 2H), 0.22 (s, 9H) ppm; $^{13}\text{C NMR}$ (101 MHz, CDCl_3) δ = 144.2, 140.8, 138.6, 133.4, 133.3, 133.0, 132.7, 131.2, 130.4, 130.3, 130.2, 130.1, 128.63, 128.64, 128.4, 128.1, 128.09, 127.7, 127.5, 127.4, 127.21, 127.15, 127.1, 126.8, 126.3, 125.9, 123.4, 122.0, 92.7, 90.0, - 1.29 ppm; **IR**: (neat) $\tilde{\nu}$ = 1594, 1475, 1246, 1108, 1095, 818, 794, 777, 753, 715, 695, 681, 633, 619, 595, 576, 563, 550, 536, 523, 499, 487, 472, 440, 410 cm^{-1} ; **HR-MS**: calcd m/z for $\text{C}_{35}\text{H}_{28}\text{Si}^+$ $[\text{M}]^+$: 476.1955; found (ESI) 476.1951.

2-{2-[(4-Phenoxyphenyl)ethynyl]phenyl}benzo[*c*]phenanthrene (**161e**):

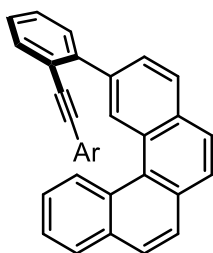


Ar = *p*-PhO(C_6H_4)

Prepared from 2-bromobenzo[*c*]phenanthrene (**185a**) (135 mg, 439.4 μmol , 1.0 equiv.), **190e** (218 mg, 693.9 μmol , 1.58 equiv.), $\text{Pd}_2(\text{dba})_3$ (16.1 mg, 17.6 μmol , 4 mol%), SPhos (14.5 mg, 35.3 μmol , 8 mol%), Cs_2CO_3 (430 mg, 1.32 mmol, 3.0 equiv.) and the solvent mixture (22 mL) according to General Procedure E. Column chromatography (SiO_2 , 0 to 5% EtOAc in pentane) yielded the product **161e** as a yellow solid (184 mg, 370.5 μmol , 84%).

$^1\text{H NMR}$ (400 MHz, CDCl_3) δ 9.50 – 9.44 (m, 1H), 9.28 (d, J = 8.5 Hz, 1H), 8.14 (d, J = 8.2 Hz, 1H), 8.05 – 7.82 (m, 6H), 7.77 (dd, J = 7.5, 1.6 Hz, 1H), 7.63 – 7.40 (m, 5H), 7.37 – 7.29 (m, 2H), 7.22 – 7.07 (m, 3H), 7.00 – 6.91 (m, 2H), 6.82 – 6.72 (m, 2H) ppm; $^{13}\text{C NMR}$ (101 MHz, CDCl_3) δ = 157.3, 156.5, 144.0, 138.6, 133.4, 133.2, 133.0, 132.7, 131.2, 130.3, 130.13, 130.05, 129.8, 128.7, 128.5, 128.4, 128.2, 128.1, 127.6, 127.5, 127.4, 127.22, 127.16, 127.1, 126.8, 126.3, 125.9, 123.7, 122.1, 119.2, 118.3, 117.8, 92.1, 89.1 ppm; **IR**: (neat, cm^{-1}) $\tilde{\nu}$ = 1731, 1586, 1504, 1486, 1445, 1357, 1277, 1236, 1196, 1164, 1102, 1070, 1023, 1012, 962, 953, 910, 868, 841, 794, 774, 751, 707, 691, 666, 619, 600, 588, 577, 566, 552, 532, 523, 487, 441, 415; **HR-MS**: calcd m/z for $\text{C}_{38}\text{H}_{24}\text{O}^+$ $[\text{M}]^+$: 496.1822; found (ESI) 496.1820.

2-{2-[3,5-Dimethoxyphenyl]ethynyl]phenyl}benzo[*c*]phenanthrene (**161f**):



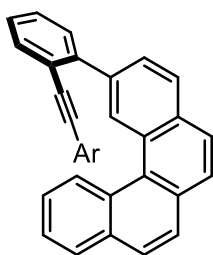
Ar = *m,m*-(OMe) $_2$ (C_6H_3)

Prepared from 2-bromobenzo[*c*]phenanthrene (**185a**) (135 mg, 439.4 μmol , 1.0 equiv.), **190f** (186 mg, 659.3 μmol , 1.5 equiv.), $\text{Pd}_2(\text{dba})_3$ (16.1 mg, 17.6 μmol , 4 mol%), SPhos (14.5 mg, 35.3 μmol , 8 mol%), Cs_2CO_3 (430 mg, 1.32 mmol, 3.0 equiv.) and the solvent

mixture (22 mL) according to General Procedure E. Column chromatography (SiO₂, 0 to 5% EtOAc in pentane) yielded the product **161f** as a yellow solid (109 mg, 234.6 μmol, 53%).

¹H NMR (400 MHz, CDCl₃) δ = 9.46 – 9.39 (m, 1H), 9.30 (dt, *J* = 7.9, 1.1 Hz, 1H), 8.14 (dd, *J* = 8.2, 1.2 Hz, 1H), 8.05 – 7.83 (m, 6H), 7.79 (dd, *J* = 7.5, 1.5 Hz, 1H), 7.61 – 7.55 (m, 2H), 7.54 – 7.38 (m, 3H), 6.41 – 6.29 (m, 3H), 3.55 (d, *J* = 1.2 Hz, 6H) ppm; ¹³C NMR (101 MHz, CDCl₃) δ: 160.3, 144.5, 138.7, 133.5, 133.2, 132.7, 131.3, 130.3, 130.1, 130.0, 128.71, 128.65, 128.5, 128.2, 128.0, 127.62, 127.58, 127.4, 127.21, 127.17, 127.1, 126.8, 126.4, 125.9, 124.5, 121.9, 109.0, 101.9, 92.5, 89.3, 55.2 ppm; IR: (neat, cm⁻¹) $\tilde{\nu}$ = 2373, 2352, 2346, 2331, 2321, 1583, 1478, 1446, 1416, 1355, 1321, 1267, 1250, 1235, 1202, 1153, 1139, 1062, 1028, 959, 927, 915, 902, 868, 858, 845, 819, 796, 762, 749, 737, 715, 700, 680, 619, 594, 578, 556, 542, 526, 487, 477, 470, 443, 414; HR-MS: calcd *m/z* for C₃₄H₂₅O₂⁺ [M+H]⁺: 465.1849; found (ESI) 465.1845.

2-{2-[(3,5-Dimethylphenyl)ethynyl]phenyl}benzo[*c*]phenanthrene (161g):

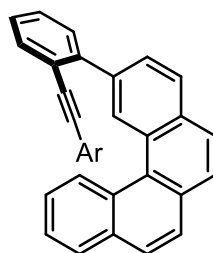


Ar = *m,m*-(Me)₂(C₆H₃)

Prepared from 2-bromobenzo[*c*]phenanthrene (**185a**) (81.6 mg, 265.6 μmol, 1.0 equiv.), **190g** (100 mg, 399.8 μmol, 1.5 equiv.), Pd₂(dba)₃ (9.9 mg, 10.8 μmol, 4 mol%), SPhos (8.9 mg, 21.7 μmol, 8.2 mol%), Cs₂CO₃ (261 mg, 801 μmol, 3.0 equiv.) and the solvent mixture (14 mL) according to General Procedure E. Column chromatography (SiO₂, 0 to 5% EtOAc in pentane) yielded the product **161g** as a yellow solid (67 mg, 154.8 μmol, 58%).

¹H NMR (300 MHz, CDCl₃) δ = 9.49 (d, *J* = 1.6 Hz, 1H), 9.26 (d, *J* = 8.2 Hz, 1H), 8.14 (d, *J* = 8.3 Hz, 1H), 8.03 – 7.83 (m, 6H), 7.75 (dd, *J* = 7.4, 1.6 Hz, 1H), 7.61 – 7.52 (m, 3H), 7.49 – 7.35 (m, 2H), 6.92 – 6.64 (m, 3H), 2.12 (d, *J* = 0.7 Hz, 6H) ppm; ¹³C NMR (101 MHz, CDCl₃) δ = 144.0, 138.6, 137.6, 133.4, 133.3, 132.7, 131.2, 130.3, 130.1, 130.03, 129.99, 129.0, 128.7, 128.5, 128.4, 128.2, 128.1, 127.7, 127.66, 127.55, 127.4, 127.2, 127.10, 127.05, 126.8, 126.3, 125.9, 122.7, 122.1, 92.9, 88.8, 21.0 ppm; IR: (neat, cm⁻¹) $\tilde{\nu}$ = 1596, 1479, 1444, 1425, 1029, 909, 843, 827, 794, 753, 687, 619, 595, 577, 542, 522, 494; HR-MS: calcd *m/z* for C₃₄H₂₃⁺ [M-H]⁺: 431.1794; found (ESI) 432.1869.

2-{2-[(2,6-Dimethoxyphenyl)ethynyl]phenyl}benzo[*c*]phenanthrene (161h):



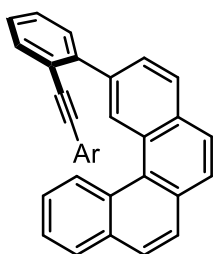
Ar = *o,o*-(OMe)₂(C₆H₃)

Prepared from 2-bromobenzo[*c*]phenanthrene (**185a**) (57 mg, 185.5 μmol, 1.0 equiv.), **190h** (80 mg, 283.5 μmol, 1.53 equiv.), Pd₂(dba)₃ (7.8 mg, 8.5 μmol, 4.8 mol%), SPhos (6.1 mg, 14.8 μmol, 8 mol%), Cs₂CO₃ (184 mg, 565 μmol, 3.0 equiv.) and the solvent mixture (11

mL) according to General Procedure E. Column chromatography (SiO₂, 0 to 5% EtOAc in pentane) yielded the product **161h** as a yellow solid (72.4 mg, 155.8 μmol, 84%).

¹H NMR (400 MHz, CDCl₃) δ = 9.43 (s, 1H), 9.35 (d, *J* = 8.4 Hz, 1H), 8.12 (d, *J* = 8.2 Hz, 1H), 8.05 (d, *J* = 7.9 Hz, 1H), 7.98 (d, *J* = 8.3 Hz, 2H), 7.91 (d, *J* = 8.8 Hz, 2H), 7.86 (t, *J* = 7.8 Hz, 2H), 7.53 (p, *J* = 6.3 Hz, 2H), 7.43 (qd, *J* = 7.7, 5.3 Hz, 3H), 7.09 (t, *J* = 8.3 Hz, 1H), 6.36 (d, *J* = 8.3 Hz, 2H), 3.49 (s, 6H) ppm; ¹³C NMR (101 MHz, CDCl₃) δ = 161.4, 143.9, 139.0, 133.4, 133.3, 132.7, 131.1, 130.4, 130.2, 130.1, 129.6, 129.0, 128.4, 128.2, 128.0, 127.9, 127.8, 127.5, 127.2, 127.0, 126.9, 126.7, 126.1, 125.8, 122.9, 103.3, 101.8, 97.9, 85.4, 55.7 ppm; IR: (neat, cm⁻¹) $\tilde{\nu}$ = 2359, 1479, 901, 845, 796, 775, 764, 753, 681, 619, 578, 550, 514, 494; HR-MS: calcd *m/z* for C₃₄H₂₃O₂⁺ [M-H]⁺: 463.1693; found (EI) 431.1685.

2-[2-[(2,6-Dimethylphenyl)ethynyl]phenyl]benzo[*c*]phenanthrene (**161i**):

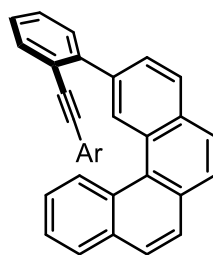


Ar = *o,o*-(Me)₂(C₆H₃)

Prepared from 2-bromobenzo[*c*]phenanthrene (**185a**) (135.1 mg, 440 μmol, 1.0 equiv.), **190i** (165 mg, 660 μmol, 1.5 equiv.), Pd₂(dba)₃ (16.1 mg, 17.6 μmol, 4 mol%), SPhos (14.5 mg, 35.3 μmol, 8 mol%), Cs₂CO₃ (430 mg, 1.32 mmol, 3.0 equiv.) and the solvent mixture (25 mL) according to General Procedure E. Column chromatography (SiO₂, 0 to 5% EtOAc in pentane) yielded the product **161i** as a white solid (160 mg, 370 μmol, 84%).

¹H NMR (300 MHz, CDCl₃) δ = 9.34 (s, 1H), 9.17 (d, *J* = 8.6 Hz, 1H), 8.10 (d, *J* = 8.2 Hz, 1H), 8.05 – 7.85 (m, 6H), 7.83 – 7.77 (m, 1H), 7.62 – 7.38 (m, 5H), 6.99 (dd, *J* = 8.4, 6.6 Hz, 1H), 6.94 – 6.81 (m, 2H), 2.12 (s, 6H) ppm; ¹³C NMR (101 MHz, CDCl₃) δ = 144.1, 140.3, 139.0, 133.4, 133.2, 132.7, 131.2, 130.3, 130.1, 130.1, 128.6, 128.41, 128.39, 128.3, 128.0, 127.7, 127.59, 127.55, 127.4, 127.22, 127.16, 127.0, 126.8, 126.5, 126.2, 125.9, 122.9, 122.8, 97.6, 90.4, 20.6 ppm; IR: (neat, cm⁻¹) $\tilde{\nu}$ = 3049, 2918, 1598, 1469, 1421, 1370, 1245, 1111, 1025, 901, 845, 793, 764, 751, 619, 576, 513, 494; HR-MS: calcd *m/z* for C₃₄H₂₃⁺ [M-H]⁺: 431.1794; found (EI) 431.1795.

2-[2-(Phenylethynyl)phenyl]benzo[*c*]phenanthrene (**161j**):



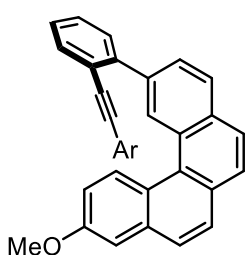
Ar = C₆H₅

Prepared from 2-bromobenzo[*c*]phenanthrene (**185a**) (208 mg, 677.1 μmol, 1.0 equiv.), **190j** (226 mg, 1.02 mmol, 1.5 equiv.), Pd₂(dba)₃ (25.0 mg, 27.3 μmol, 4 mol%), SPhos (22.2 mg, 54.1 μmol, 8 mol%), Cs₂CO₃ (664 mg, 2.04 mmol, 3.0 equiv.) and the solvent mixture (39 mL) according to General Procedure E. Column chromatography (SiO₂, 0 to 5% EtOAc in pentane) yielded the product **161j** as a yellow solid (178 mg, 440 μmol,

65%).

$^1\text{H NMR}$ (400 MHz, CDCl_3) δ = 9.46 (d, J = 1.6 Hz, 1H), 9.28 (d, J = 8.6 Hz, 1H), 8.17 – 8.10 (m, 1H), 8.04 – 7.84 (m, 6H), 7.79 (dd, J = 7.5, 1.7 Hz, 1H), 7.61 – 7.53 (m, 2H), 7.52 – 7.39 (m, 3H), 7.26 – 7.10 (m, 5H) ppm; $^{13}\text{C NMR}$ (101 MHz, CDCl_3) (one overlapping peak) δ = 144.1, 138.6, 133.44, 133.35, 132.8, 131.4, 131.2, 130.3, 130.2, 130.1, 128.68, 128.66, 128.4, 128.2, 128.1, 128.1, 127.7, 127.5, 127.4, 127.22, 127.17, 127.1, 126.8, 126.3, 125.9, 123.2, 122.0, 92.4, 89.7 ppm; **IR**: (neat, cm^{-1}) $\tilde{\nu}$ = 1597, 1491, 1474, 1441, 1156, 1107, 911, 841, 827, 793, 688, 666, 619, 590, 576, 566, 533, 523, 497, 489, 411; **HR-MS**: calcd m/z for $\text{C}_{32}\text{H}_{19}^+$ $[\text{M}-\text{H}]^+$: 403.1481; found (EI) 403.1480.

10-Methoxy-2-[2-[(4-methoxyphenyl)ethynyl]phenyl]benzo[*c*]phenanthrene (**161k**):

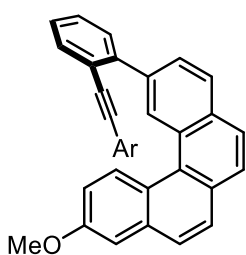


Ar = *p*-MeO(C_6H_4)

Prepared from **185b** (114 mg, 338.1 μmol , 1.0 equiv.), **190a** (128 mg, 507.7 μmol , 1.5 equiv.), $\text{Pd}_2(\text{dba})_3$ (12.5 mg, 13.7 μmol , 4.1 mol%), SPhos (11.3 mg, 27.5 μmol , 8.1 mol%), Cs_2CO_3 (344 mg, 1.06 mmol, 3.1 equiv.) and the solvent mixture (22 mL) according to General Procedure E. Column chromatography (SiO_2 , 0 to 5% EtOAc in pentane) yielded the product **161k** as a yellow solid (137 mg, 294.9 μmol , 87%).

$^1\text{H-NMR}$: (400 MHz, CDCl_3) δ = 9.38 (d, J = 1.6 Hz, 1H), 9.19 (d, J = 9.3 Hz, 1H), 8.12 (d, J = 8.2 Hz, 1H), 7.97 – 7.86 (m, 3H), 7.84 (s, 2H), 7.77 (dd, J = 7.5, 1.6 Hz, 1H), 7.58 – 7.52 (m, 1H), 7.51 – 7.40 (m, 2H), 7.36 (d, J = 2.8 Hz, 1H), 7.24 – 7.05 (m, 3H), 6.75 – 6.63 (m, 2H), 3.96 (s, 3H), 3.75 (s, 3H) ppm; $^{13}\text{C}\{\text{H}\}\text{-NMR}$: (101 MHz, CDCl_3) δ = 159.4, 157.5, 143.9, 138.5, 135.0, 133.1, 132.9, 132.8, 130.1, 129.91, 129.87, 129.7, 128.7, 128.3, 128.1, 128.0, 127.41, 127.35, 127.11, 127.07, 126.8, 126.2, 125.1, 122.3, 117.0, 115.3, 113.8, 108.1, 92.5, 88.5, 55.4, 55.2 ppm; **IR**: (neat, cm^{-1}) $\tilde{\nu}$ = 1623, 1604, 1567, 1508, 1476, 1455, 1428, 1396, 1355, 1303, 1286, 1264, 1246, 1195, 1173, 1146, 1106, 1029, 962, 932, 907, 854, 829, 784, 757, 737, 718, 693, 682, 664, 652, 638, 598, 574, 534, 525, 504, 486, 434, 416; **HR-MS**: calcd m/z for $\text{C}_{34}\text{H}_{25}\text{O}_2^+$ $[\text{M}+\text{H}]^+$: 465.1849; found (ESI) 465.1847.

10-Methoxy-2-[2-(*p*-tolylethynyl)phenyl]benzo[*c*]phenanthrene (**161l**):

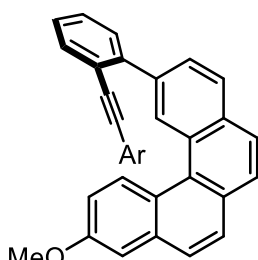


Ar = *p*-Me(C_6H_4)

Prepared from **185b** (100 mg, 296.5 μmol , 1.0 equiv.), **190b** (105 mg, 444.7 μmol , 1.5 equiv.), $\text{Pd}_2(\text{dba})_3$ (11.0 mg, 12.0 μmol , 4 mol%), SPhos (9.9 mg, 24 μmol , 8.1 mol%), Cs_2CO_3 (293 mg, 0.9 mmol, 3.0 equiv.) and the solvent mixture (15 mL) according to General Procedure E. Column chromatography (SiO_2 , 0 to 5% EtOAc in pentane) yielded the product **161l** as a yellow solid (60 mg, 133.7 μmol , 45%).

$^1\text{H NMR}$: (400 MHz, CDCl_3) δ = 9.36 (s, 1H), 9.18 (d, J = 9.3 Hz, 1H), 8.11 (d, J = 8.2 Hz, 1H), 7.98 – 7.90 (m, 2H), 7.87 (s, 1H), 7.84 (s, 2H), 7.77 (dd, J = 7.7, 1.4 Hz, 1H), 7.55 (dd, J = 7.7, 1.4 Hz, 1H), 7.49 – 7.39 (m, 2H), 7.36 (d, J = 2.8 Hz, 1H), 7.14 (d, J = 8.1 Hz, 2H), 7.10 (dd, J = 9.3, 2.8 Hz, 1H), 6.97 (d, J = 7.7 Hz, 2H), 3.96 (s, 3H), 2.28 (s, 3H) ppm; $^{13}\text{C}\{\text{H}\}\text{-NMR}$: (101 MHz, CDCl_3) 157.5, 144.0, 138.5, 138.2, 135.0, 133.2, 132.8, 131.3, 130.1, 129.91, 129.88, 129.7, 128.9, 128.7, 128.4, 128.1, 128.0, 127.4, 127.4, 127.10, 127.06, 126.8, 126.2, 125.0, 122.1, 120.1, 116.9, 108.1, 92.6, 89.1, 55.4, 21.4 ppm; **IR**: (neat, cm^{-1}) $\tilde{\nu}$ = 2928, 2835, 1623, 1609, 1508, 1476, 1453, 1427, 1396, 1355, 1263, 1234, 1194, 1161, 1108, 1033, 962, 950, 932, 907, 785, 756, 707, 694, 681, 665, 649, 637, 598, 573, 533, 520, 501, 465, 447, 433, 417, 407; **HR-MS**: calcd m/z for $\text{C}_{34}\text{H}_{24}\text{O}^+$ $[\text{M}]^+$: 448.1822; found (ESI) 448.1822.

2-(2-([4-(Benzyloxy)phenyl]ethynyl)phenyl)-10-methoxybenzo[*c*]phenanthrene (**161m**):

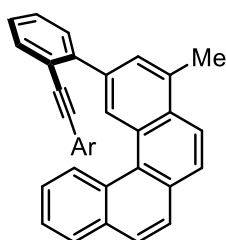


Ar = *p*-BnO(C_6H_4)

Prepared from **185b** (100 mg, 296.5 μmol , 1.0 equiv.), **190c** (164 mg, 499.7 μmol , 1.68 equiv.), $\text{Pd}_2(\text{dba})_3$ (11.0 mg, 12.0 μmol , 4 mol%), SPhos (9.9 mg, 24.1 μmol , 8.1 mol%), Cs_2CO_3 (293 mg, 899.2 μmol , 3.0 equiv.) and the solvent mixture (15 mL) according to general procedure E. Column chromatography (SiO_2 , 0 to 5% EtOAc in pentane) yielded the product **161m** as a yellow solid (96.5 mg, 178.5 μmol , 60%).

NMR (400 MHz, CDCl_3) δ = 9.40 (d, J = 1.8 Hz, 1H), 9.20 (dd, J = 9.2, 1.9 Hz, 1H), 8.12 (dd, J = 8.3, 2.0 Hz, 1H), 7.99 – 7.90 (m, 2H), 7.89 – 7.81 (m, 3H), 7.77 (dt, J = 7.6, 1.9 Hz, 1H), 7.56 (dt, J = 7.8, 1.8 Hz, 1H), 7.51 – 7.41 (m, 2H), 7.41 – 7.31 (m, 6H), 7.15 (ddt, J = 21.5, 9.3, 2.6 Hz, 3H), 6.76 (dd, J = 8.8, 2.1 Hz, 2H), 5.00 (d, J = 1.9 Hz, 2H), 3.96 (d, J = 2.0 Hz, 3H) ppm; $^{13}\text{C NMR}$ (101 MHz, CDCl_3) δ = 158.5, 157.5, 143.9, 138.5, 136.6, 135.0, 133.1, 132.9, 132.8, 130.0, 129.9, 129.9, 129.7, 128.7, 128.6, 128.3, 128.11, 128.05, 128.0, 127.45, 127.42, 127.35, 127.11, 127.07, 126.8, 126.2, 125.0, 122.3, 117.0, 115.6, 114.8, 108.1, 92.4, 88.5, 69.9, 55.37; **IR**: (neat, cm^{-1}) $\tilde{\nu}$ = 1604, 1507, 1477, 1454, 1427, 1356, 1284, 1264, 1235, 1195, 1173, 1147, 1107, 1028, 908, 842, 828, 785, 754, 735, 694, 682, 665, 638, 601, 574, 537, 518, 504, 484, 456, 450, 431, 422, 417, 407; **HR-MS**: calcd m/z for $\text{C}_{40}\text{H}_{29}\text{O}_2^+$ $[\text{M}+\text{H}]^+$: 541.2162; found (ESI) 541.2157.

2-(2-((4-methoxyphenyl)ethynyl)phenyl)-4-methylbenzo[*c*]phenanthrene (**161n**):



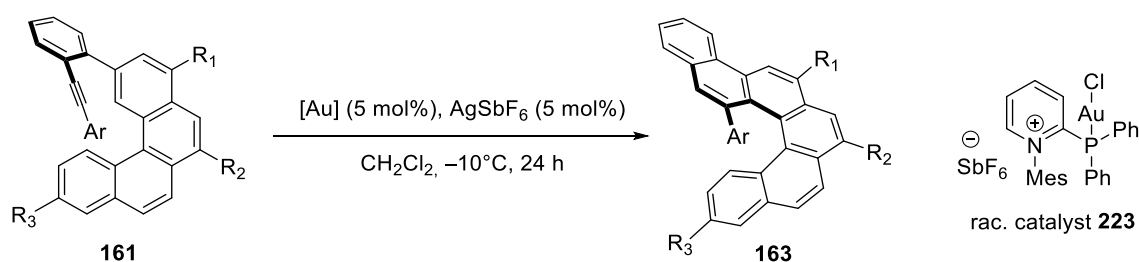
Ar = *p*-MeO(C_6H_4)

Prepared from **185c** (150 mg, 466.9 μmol , 1.0 equiv.), **190a** (177 mg, 702.1 μmol , 1.5 equiv.), $\text{Pd}_2(\text{dba})_3$ (17.0 mg, 18.7 μmol , 4 mol%), SPhos (22.2 mg, 54.0 μmol , 11.6 mol%), Cs_2CO_3 (664 mg, 2.04 mmol, 4.4 equiv.) and the solvent mixture (34 mL) according to general procedure E.

Column chromatography (SiO₂, 0 to 5% EtOAc in pentane) yielded the product as a yellow solid (178 mg, 396.8 μmol, 85%).

¹H NMR (300 MHz, CDCl₃) δ = 9.31 (s, 1H), 9.27 (d, J = 8.6 Hz, 1H), 8.20 (d, J = 8.8 Hz, 1H), 8.00 (d, J = 6.4 Hz, 1H), 7.95 – 7.82 (m, 4H), 7.76 (dd, J = 7.5, 1.6 Hz, 1H), 7.60 – 7.51 (m, 2H), 7.50 – 7.35 (m, 3H), 7.16 (d, J = 8.8 Hz, 2H), 6.68 (d, J = 8.8 Hz, 2H), 3.75 (s, 3H), 2.94 (s, 3H) ppm; ¹³C NMR (101 MHz, CDCl₃) δ = 159.4, 143.9, 138.0, 134.1, 133.5, 133.1, 132.9, 131.6, 130.8, 130.4, 130.3, 130.0, 128.6, 128.5, 128.3, 128.2, 128.16, 127.4, 127.1, 127.0, 126.8, 126.7, 126.2, 125.9, 123.1, 122.3, 115.4, 113.8, 93.0, 88.5, 55.2, 20.4 ppm; IR: (neat, cm⁻¹) $\tilde{\nu}$ = 1604, 1567, 1509, 1478, 1461, 1439, 1415, 1401, 1302, 1286, 1246, 1173, 1161, 1146, 1133, 1106, 1028, 909, 885, 872, 829, 809, 795, 783, 752, 716, 709, 679, 642, 629, 603, 593, 577, 530, 505, 492; HR-MS: calcd *m/z* for C₃₄H₂₅O⁺ [M+H]⁺: 449.1900; found (ESI) 449.1912.

6.2.3. Au(I) Catalyzed Hydroarylation towards [5]Helicenes



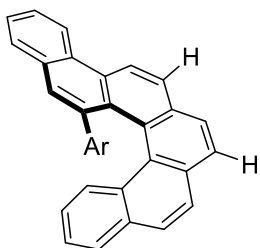
Scheme 57. Enantioselective Au(I)-catalyzed cycloisomerization reaction.

General Procedure F for Gold-catalyzed Cycloisomerization Reactions

In a Schlenk flask equipped with a stirring bar, the respective substrate (25 μmol) and the Au(I) precatalyst (5 mol%) were thoroughly dried *in vacuo* for 30 min. The mixture was dissolved in DCM (0.5 mL) and cooled to the desired temperature (-10 °C). A freshly prepared solution of AgSbF₆ (0.05 M in DCM, 5 mol%) was added. After stirring for 24 h, the mixture was filtered through a plug of silica to give a mixture of the desired helicene and the corresponding dibenzo[*a,m*]tetraphene. Further purification by preparative HPLC gave the desired helicenes.

As a reference for the determination of the helicenes' enantiomeric excesses, racemic reactions were carried out with gold catalyst **223** employing the general procedure described above but stirring the reaction mixture at room temperature instead.

9-(4-Methoxyphenyl)naphtho[2,1-c]chrysene (**163a**):



Ar = *p*-MeO(C₆H₄)

Prepared from **161a** (10.8 mg, 24.9 μmol, 1.0 equiv.), **162b** (1.9 mg, 1.25 μmol, 5 mol%) and AgSbF₆ (0.43 mg, 1.25 μmol, 5 mol%, 0.05 M in DCM) in DCM (0.5 mL) according to General Procedure F. The crude mixture was obtained as a yellow solid (9.5 mg, 88% yield), **163a**:**191a**: >99:1, >95% conversion (determined by NMR), 95% enantiomeric excess.

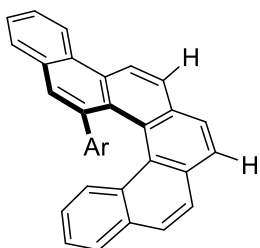
The *ee* was determined by chiral SFC: on SFC-IA3, modifier 35% *i*-propanol at 1.7 mL min⁻¹ and backpressure regulator set to 2000 psi, 310 K; major enantiomer *t_R* = 1.76 min, minor enantiomer *t_R* = 3.87 min.

[α]₂₄^D: (95% *ee*) +1561.70 (*c* = 1.07, DCM); ¹H NMR (300 MHz, CDCl₃) δ = 8.91 (d, *J* = 8.7 Hz, 1H), 8.87 (d, *J* = 8.1 Hz, 1H), 8.17 (d, *J* = 8.6 Hz, 1H), 8.00 (dd, *J* = 8.0, 1.7 Hz, 2H), 7.88 (d, *J* = 8.2 Hz, 2H), 7.85 – 7.80 (m, 2H), 7.79 – 7.61 (m, 4H), 7.59 – 7.50 (m, 2H), 7.38 (ddd, *J* = 8.0, 6.9, 1.2 Hz, 1H), 7.16 (ddd, *J* = 8.4, 6.9, 1.4 Hz, 1H), 5.99 (br s, 2H), 3.62 (s, 3H) ppm; ¹³C NMR (101 MHz, CDCl₃) δ = 157.0, 139.2, 135.1, 132.5, 132.0, 131.5, 131.1, 130.4, 130.1, 129.8, 128.7, 128.6, 128.4, 128.01, 127.97, 127.5, 127.2, 127.0, 126.7, 126.5, 126.4, 126.1, 125.4, 125.3, 125.1, 124.9, 123.3, 121.6, 55.3 ppm; IR: (neat, cm⁻¹) $\tilde{\nu}$ = 1604, 1507, 1483, 1464, 1438, 1316, 1284, 1242, 1207, 1175, 1145, 1110, 1033, 946, 902, 889, 834, 828, 793, 772, 763, 743, 731, 701, 660, 641, 625, 591, 577, 558, 549, 538, 513, 473, 449, 439, 428, 418; HR-MS: calcd *m/z* for C₃₃H₂₂O⁺ [M]⁺: 434.1665; found (ESI) 434.1600.

Synthesis of compound **163a**, reaction scaled up to 250 μmol

Substrate **161a** (108 mg, 248.5 μmol, 1.0 equiv.), **162b** (18.9 mg, 12.46 μmol, 5 mol%) and AgSbF₆ (4.26 mg, 12.48 μmol, 5 mol%, 0.05 M in DCM) in DCM (3 mL) were stirred according to General Procedure F at – 10 °C for 18 h. Column chromatography (SiO₂, 0 to 5% EtOAc in pentane) yielded the product as a yellow solid (88.6 mg, 0.21 mmol, 82%), **161a**:**191a**: 97:3, *ee* = 92%.

9-(*p*-Tolyl)naphtho[2,1-c]chrysene (**163b**):



Ar = *p*-Me(C₆H₄)

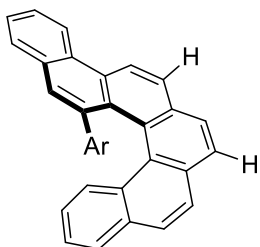
Prepared from **161b** (10.5 mg, 25.1 μmol, 1.0 equiv.), **162b** (1.9 mg, 1.25 μmol, 5 mol%) and AgSbF₆ (0.43 mg, 1.25 μmol, 5 mol%, 0.05 M in DCM) in DCM (0.5 mL) according to General Procedure F. The crude

mixture was obtained as a yellow solid, **163b:191b**: >99:1, >95% conversion (determined by NMR), 97% enantiomeric excess.

The analytically pure sample of **163b** (9.5 mg, 90% yield) was obtained by semi-preparative HPLC; separation conditions: MeCN/H₂O = 80/20 to 100/0 over 20min, 1.0 mL min⁻¹, 295 K; helicene t_R = 23.3 min. The ee was determined by chiral SFC: on SFC-IA3, modifier 30% *i*-propanol at 1.7 mL min⁻¹ and backpressure regulator set to 2000 psi, 300 K; major enantiomer t_R = 2.09 min, minor enantiomer t_R = 4.46 min.

[α]₂₄^D: (97% ee) +182.4 (c = 0.04, DCM); ¹H NMR (400 MHz, CDCl₃) δ = 8.89 (dd, *J* = 14.3, 8.5 Hz, 2H), 8.17 (d, *J* = 8.6 Hz, 1H), 8.03 – 7.94 (m, 2H), 7.88 (d, *J* = 8.2 Hz, 1H), 7.83 – 7.64 (m, 4H), 7.64 – 7.55 (m, 2H), 7.50 (d, *J* = 8.5 Hz, 1H), 7.37 (ddd, *J* = 8.0, 6.8, 1.3 Hz, 1H), 7.15 (ddd, *J* = 8.5, 6.8, 1.5 Hz, 1H), 6.88 – 5.36 (br s, 4H), 2.06 (s, 3H) ppm; ¹³C NMR (101 MHz, CDCl₃) δ = 139.7, 139.3, 134.4, 132.4, 132.0, 131.4, 131.0, 130.3, 130.0, 129.9, 128.8, 128.77, 128.5, 128.0, 127.3, 127.1, 126.9, 126.81, 126.78, 126.7, 126.5, 126.4, 126.0, 125.3, 125.1, 124.8, 123.3, 121.6, 20.7 ppm; IR: (neat, cm⁻¹) $\tilde{\nu}$ = 1692, 1599, 1509, 1260, 1245, 1145, 1112, 1075, 1031, 1021, 979, 947, 905, 837, 817, 794, 763, 743, 731, 702, 669, 659, 642, 625, 591, 579, 551, 534, 520, 512, 493, 473, 458, 450, 442; HR-MS: calcd *m/z* for C₃₃H₂₂: [M]⁺: 417.1716; found (ESI) 418.1712.

9[-(Benzyloxy)phenyl]naphtho[2,1-*c*]chrysene (**163c**):



Ar = *p*-BnO(C₆H₄)

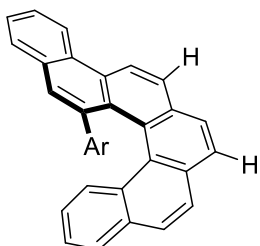
Prepared from **161c** (12.8 mg, 25 μmol, 1.0 equiv.), **162b** (1.9 mg, 1.25 μmol, 5 mol%) and AgSbF₆ (0.43 mg, 1.25 μmol, 5 mol%, 0.05 M in DCM) in DCM (0.5 mL) according to General Procedure F. The crude mixture was obtained as a yellow solid, **163c:191c**: >99:1, >95% conversion (determined by NMR), 95% enantiomeric excess.

The analytically pure sample of **163c** (9.1 mg, 71% yield) was obtained by semi-preparative HPLC; separation conditions: MeCN/H₂O = 90/10 to 100/0 over 20 min, 1.0 mL min⁻¹, 295 K; helicene t_R = 17.6 min. The ee was determined by chiral SFC: on SFC-IA3, modifier 35% *i*-propanol at 1.7 mL min⁻¹ and backpressure regulator set to 2000 psi, 300 K; major enantiomer t_R = 3.50 min, minor enantiomer t_R = 8.51 min.

[α]₂₄^D: (95% ee) +812.5 (c = 0.39, DCM); ¹H NMR (300 MHz, CDCl₃) δ = 8.88 (dd, *J* = 11.0, 8.4 Hz, 2H), 8.17 (d, *J* = 8.6 Hz, 1H), 7.99 (dd, *J* = 8.0, 1.7 Hz, 2H), 7.91 – 7.60 (m, 5H), 7.60 – 7.29 (m, 9H), 7.14 (ddd, *J* = 8.4, 6.8, 1.4 Hz, 1H), 6.19 (br s, 4H), 4.89 (s, 2H) ppm; ¹³C NMR (101 MHz, CDCl₃) δ = 156.3, 139.2, 137.5, 135.3, 132.4, 132.0, 131.4, 131.0, 130.4, 130.1, 129.8, 128.7,

128.7, 128.5, 128.4, 128.0, 127.95, 127.8, 127.5, 127.3, 127.2, 127.0, 126.7, 126.5, 126.4, 126.1, 125.31, 125.27, 125.1, 124.9, 123.3, 121.6, 69.9 ppm; **IR**: (neat, cm^{-1}) $\tilde{\nu}$ = 1604, 1506, 1484, 1465, 1454, 1440, 1314, 1287, 1278, 1238, 1223, 1174, 1145, 1111, 1080, 1016, 947, 903, 864, 834, 825, 794, 773, 764, 727, 695, 680, 660, 641, 615, 590, 577, 550, 539, 513, 472, 448, 419, 408; **HR-MS**: calcd m/z for $\text{C}_{39}\text{H}_{26}\text{O}^+$ $[\text{M}]^+$: 510.1978; found (ESI) 510.1975.

Trimethyl[4-(naphtho[2,1-c]chrysen-9-yl)phenyl]silane (**163d**):



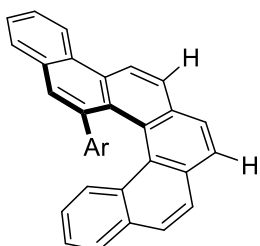
Prepared from **161d** (11.9 mg, 25 μmol , 1.0 equiv.), **162b** (1.9 mg, 1.25 μmol , 5 mol%) and AgSbF_6 (0.43 mg, 1.25 μmol , 5 mol%, 0.05 M in DCM) in DCM (0.5 mL) according to General Procedure **F**. The crude mixture was obtained as a yellow solid, **163d**:**191d**: >99:1, >95% conversion (determined by NMR), 95% enantiomeric excess.

Ar = *p*-(Me_3Si)(C_6H_4)

The analytically pure sample of **163d** (10.7 mg, 90% yield) was obtained by semi-preparative HPLC; separation conditions: MeCN/ H_2O = 90/10 to 100/0 over 10 min, 1.0 mL min^{-1} , 295 K; helicene t_R = 22.0 min. The *ee* was determined by chiral SFC: on SFC-IG3, modifier 35% ethanol at 1.7 mL min^{-1} , and backpressure regulator set to 2000 psi, 300 K; major enantiomer t_R = 1.43 min, minor enantiomer t_R = 2.70 min.

$[\alpha]_{24}^D$: (95% *ee*) +1103.9 (c = 0.34, DCM); **^1H NMR** (400 MHz, CDCl_3) δ = 8.90 (dd, J = 15.2, 8.5 Hz, 2H), 8.19 (d, J = 8.6 Hz, 1H), 8.04 – 7.96 (m, 2H), 7.88 (d, J = 8.2 Hz, 1H), 7.79 (ddd, J = 15.3, 8.2, 1.3 Hz, 2H), 7.70 (ddd, J = 7.9, 6.9, 1.2 Hz, 1H), 7.65 – 7.59 (m, 2H), 7.54 (dd, J = 8.1, 1.3 Hz, 1H), 7.44 – 7.33 (m, 2H), 7.15 (ddd, J = 8.3, 6.9, 1.4 Hz, 1H), 7.04 – 6.20 (s br, 3H), 5.65 (s br, 1H), 0.20 (s, 9H) ppm; **^{13}C NMR** (101 MHz, CDCl_3) δ 142.4, 139.6, 136.2, 132.4, 132.0, 131.4, 130.9, 130.4, 130.0, 129.97, 129.1, 128.8, 128.6, 127.7, 127.5, 127.2, 127.17, 126.9, 126.8, 126.7, 126.5, 126.2, 126.1, 125.3, 125.0, 124.7, 123.4, 121.6, -1.2 ppm; **IR**: (neat) $\tilde{\nu}$ = 1244, 1109, 1031, 832, 817, 793, 776, 764, 742, 726, 704, 693, 657, 641, 627, 592, 577, 549, 537, 516, 496, 472, 407 cm^{-1} ; **HR-MS**: calcd m/z for $\text{C}_{35}\text{H}_{28}\text{Si}^+$ $[\text{M}]^+$: 476.1955; found (ESI) 476.1954.

9-(4-Phenoxyphenyl)naphtho[2,1-c]chrysene (**163e**):



Ar = *p*-PhO(C_6H_4)

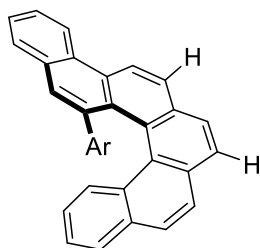
Prepared from **161e** (12.4 mg, 25 μmol , 1.0 equiv.), **162b** (1.9 mg, 1.25 μmol , 5 mol%) and AgSbF_6 (0.43 mg, 1.25 μmol , 5 mol%, 0.05 M in DCM) in DCM (0.5 mL) according to General Procedure **F**. The crude mixture was obtained as a yellow solid, **161e**:**191e**: >99:1, >95% conversion (determined by NMR), 97% enantiomeric excess.

The analytically pure sample of **163e** (11.1 mg, 90% yield) was

obtained by semi-preparative HPLC; separation conditions: MeCN/H₂O = 90/10 to 100/0 over 20min, 1.0 mL min⁻¹, 295 K; helicene t_R = 20.1 min. The ee was determined by chiral SFC: on SFC-IA3, modifier 25% *i*-propanol at 2.25 mL min⁻¹ and backpressure regulator set to 3000 psi, 300 K; major enantiomer t_R = 3.14 min, minor enantiomer t_R = 5.51 min.

[α]₂₄^D: (97% ee) +789.8 (*c* = 0.47, DCM); ¹H NMR (300 MHz, CDCl₃) δ = 8.90 (dd, *J* = 11.8, 8.4 Hz, 2H), 8.19 (d, *J* = 8.6 Hz, 1H), 8.01 (dd, *J* = 8.0, 1.9 Hz, 2H), 7.94 – 7.85 (m, 2H), 7.82 – 7.63 (m, 5H), 7.58 (s, 1H), 7.41 (ddt, *J* = 8.1, 7.0, 2.2 Hz, 3H), 7.25 – 7.08 (m, 2H), 6.92 – 6.82 (m, 2H), 6.80 – 6.58 (s br, 1H), 6.44 (s br, 1H), 6.19 – 5.93 (s br, 1H), 5.68 (s br, 1H) ppm; ¹³C NMR (101 MHz, CDCl₃) δ = 157.9, 154.1, 139.0, 138.0, 132.4, 132.1, 131.3, 131.1, 130.4, 130.2, 129.9, 129.4, 129.0, 128.7, 128.5, 128.3, 127.8, 127.5, 127.3, 127.03, 127.00, 126.9, 126.7, 126.6, 126.2, 125.6, 125.5, 125.2, 125.1, 123.4, 122.5, 121.7, 118.1 ppm; IR: (neat, cm⁻¹) $\tilde{\nu}$ = 1587, 1504, 1487, 1439, 1229, 1166, 1146, 1103, 1073, 1026, 1015, 947, 903, 866, 835, 793, 765, 745, 727, 690, 660, 641, 605, 586, 577, 565, 550, 533, 522, 511, 499, 492, 473, 451, 442, 430, 420, 410; HR-MS: calcd *m/z* for C₃₈H₂₄O: [M]⁺: 496.1822; found (ESI) 496.1818.

9-(3,5-Dimethoxyphenyl)naphtho[2,1-*c*]chrysene (163f):



Ar = *m,m*-(MeO)₂(C₆H₃)

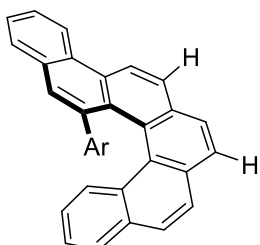
Prepared from **161f** (11.6 mg, 25 μ mol, 1.0 equiv.), **162b** (1.9 mg, 1.25 μ mol, 5 mol%) and AgSbF₆ (0.43 mg, 1.25 μ mol, 5 mol%, 0.05 M in DCM) in DCM (0.5 mL) according to General Procedure **F**. The crude mixture was obtained as a yellow solid, **163f:191f**: >99:1, >95% conversion (determined by NMR), 68% enantiomeric excess.

The analytically pure sample of **163f** (8.9 mg, 77% yield) was obtained by semi-preparative HPLC; separation conditions: MeCN/H₂O = 90/10 to 100/0 over 20min, 1.0 mL min⁻¹, 295 K; helicene t_R = 10.7 min. The ee was determined by chiral SFC: on SFC-IG3, modifier 25% *i*-propanol at 2.25 mL min⁻¹ and backpressure regulator set to 3000 psi, 310 K; major enantiomer t_R = 2.29 min, minor enantiomer t_R = 3.35 min.

[α]₂₄^D: (68% ee) +1252.1 (*c* = 0.46, DCM); ¹H NMR (300 MHz, CDCl₃) δ = 8.89 (dd, *J* = 10.8, 8.4 Hz, 2H), 8.19 (d, *J* = 8.6 Hz, 1H), 8.07 – 7.94 (m, 2H), 7.93 – 7.80 (m, 2H), 7.80 – 7.66 (m, 4H), 7.65 – 7.53 (m, 2H), 7.42 (ddd, *J* = 8.0, 6.8, 1.2 Hz, 1H), 7.16 (ddd, *J* = 8.3, 6.8, 1.4 Hz, 1H), 5.87 (t, *J* = 2.2 Hz, 2H), 4.80 (s br, 1H), 3.67 (s br, 3H), 3.08 (s br, 3H) ppm; ¹³C NMR (101 MHz, CDCl₃) δ 144.0, 139.4, 132.3, 131.9, 131.8, 130.6, 130.4, 130.0, 129.8, 129.2, 128.9, 128.6, 127.8, 127.5, 127.3, 127.3, 127.0, 126.8, 126.5, 126.2, 125.5, 125.1, 125.1, 124.7, 123.3, 121.6, 110.0, 105.8, 105.2, 99.1, 55.0, 54.6. IR: (neat, cm⁻¹) $\tilde{\nu}$ = 1597, 1523, 1481, 1458, 1449, 1438, 1421, 1403, 1384, 1330, 1299, 1255, 1194, 1185, 1146, 1117, 1075, 1058, 1038, 1029, 996, 977, 952,

897, 880, 867, 854, 833, 791, 760, 748, 714, 693, 678, 658, 650, 634, 616, 599, 590, 577, 567, 550, 520, 472, 462, 446, 437, 419, 411 cm^{-1} . **HR-MS**: calcd m/z for $\text{C}_{34}\text{H}_{25}\text{O}_2^+$ $[\text{M}+\text{H}]^+$: 465.1849; found (ESI) 465.1853.

9-(3,5-Dimethylphenyl)naphtho[2,1-c]chrysene (**163g**):



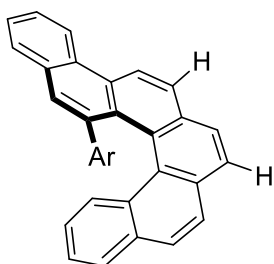
Prepared from **161g** (10.8 mg, 25 μmol , 1.0 equiv.), **162b** (1.9 mg, 1.25 μmol , 5 mol%) and AgSbF_6 (0.43 mg, 1.25 μmol , 5 mol%, 0.05 M in DCM) in DCM (0.5 mL) according to General Procedure F. The crude mixture was obtained as a yellow solid, **163g:191g**: >99:1, >99% conversion (determined by NMR), 68% enantiomeric excess.

Ar = *m,m*-(Me)₂(C₆H₃)

The analytically pure sample of **163g** (8.6 mg, 80% yield) was obtained by semi-preparative HPLC; separation conditions: MeCN/H₂O = 90/10 to 100/0 over 20min, 1.0 mL min⁻¹, 295 K; helicene t_R = 20.4 min. The *ee* was determined by chiral HPLC: IA-3, Hex/IPA = 95/5, isocratic, 20 min, 1.0 mL min⁻¹, 298 K, 256 nm; major enantiomer t_R = 3.8 min, minor enantiomer t_R = 5.6 min.

$[\alpha]_{24}^D$: (68% *ee*) +918.7 (c = 0.43, DCM); **¹H NMR** (400 MHz, CDCl₃) δ = 8.90 (dt, J = 13.5, 5.7 Hz, 2H), 8.18 (dd, J = 8.5, 3.2 Hz, 1H), 8.05 – 7.94 (m, 2H), 7.93 – 7.55 (m, 7H), 7.51 (dd, J = 8.5, 3.2 Hz, 1H), 7.39 (t, J = 7.4 Hz, 1H), 7.22 – 7.09 (m, 1H), 6.34 (s, 2H), 5.21 (s br, 1H), 2.06 (s br, 3H), 1.59 (s br, J = 15.6 Hz, 3H) ppm. **¹³C NMR** (101 MHz, CDCl₃) δ 141.7, 139.6, 132.4, 131.9, 131.7, 130.2, 129.9, 129.7, 129.1, 128.9, 128.5, 128.0, 127.4, 127.1, 127.01, 126.96, 126.8, 126.7, 126.6, 126.3, 126.0, 125.7, 125.3, 125.2, 124.4, 123.3, 121.6, 21.1. **IR**: (neat, cm^{-1}) $\tilde{\nu}$ = 1600, 1465, 1437, 1370, 1323, 1258, 1090, 1065, 1030, 976, 960, 942, 903, 885, 862, 853, 837, 816, 791, 769, 762, 750, 741, 714, 696, 676, 666, 654, 643, 617, 607, 588, 581, 547, 524, 499, 471, 455, 437, 427, 418, 409, 401; **HR-MS**: calcd m/z for $\text{C}_{34}\text{H}_{24}^+$ $[\text{M}]^+$: 432.1873; found (ESI) 432.1874.

9-(2,6-Dimethoxyphenyl)naphtho[2,1-c]chrysene (**163h**):



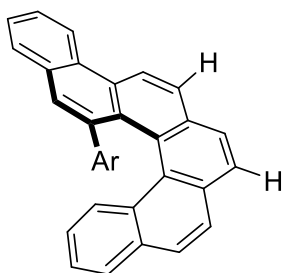
Prepared from **161h** (10.8 mg, 23.2 μmol , 1.0 equiv.), **162b** (1.9 mg, 1.25 μmol , 5.4 mol%) and AgSbF_6 (0.43 mg, 1.25 μmol , 5.4 mol%, 0.05 M in DCM) in DCM (0.5 mL) according to General Procedure F. The crude was as a yellow solid, **163h:191h**: >75:25, >45% conversion (determined by NMR), 0% enantiomeric excess.

Ar = *o,o*-(MeO)₂(C₆H₃) The analytically pure sample of **163h** (3.8 mg, 35% yield) was obtained by semi-preparative HPLC; separation conditions: MeCN/H₂O = 90/10 to 100/0 over

20 min, 1.0 mL min⁻¹, 295 K. The *ee* was determined by chiral HPLC: IG-3 SFC, CO₂/EtOH = 80/20, isocratic, 20 min, 2.25 mL min⁻¹, 310 K; major enantiomer *t_R* = 4.15 min, minor enantiomer *t_R* = 2.51 min.

¹H NMR (400 MHz, CDCl₃) δ = 8.87 (dd, *J* = 8.5, 1.7 Hz, 2H), 8.12 – 7.99 (m, 2H), 7.99 – 7.89 (m, 2H), 7.84 (d, *J* = 2.0 Hz, 1H), 7.81 – 7.70 (m, 2H), 7.70 – 7.62 (m, 1H), 7.62 – 7.56 (m, 2H), 7.52 (d, *J* = 8.6 Hz, 1H), 7.35 – 7.29 (m, 1H), 7.10 (ddt, *J* = 8.4, 6.9, 1.6 Hz, 1H), 6.66 (dd, *J* = 9.1, 7.5 Hz, 1H), 5.96 (d, *J* = 8.4 Hz, 1H), 5.63 (d, *J* = 7.3 Hz, 1H), 3.46 (s, 3H), 2.49 (s, 3H) ppm; ¹³C NMR (101 MHz, CDCl₃) δ = (two overlapping peaks) 155.7, 154.8, 132.0, 131.7, 131.5, 131.1, 130.7, 130.5, 130.2, 130.1, 129.8, 129.2, 128.6, 128.1, 127.5, 127.1, 127.0, 126.9, 126.7, 126.7, 126.5, 126.1, 125.9, 125.6, 124.3, 123.4, 122.0, 118.9, 102.9, 102.5, 54.4, 54.2. IR: (neat, cm⁻¹) $\tilde{\nu}$ = 3733, 3627, 2360, 1578, 1471, 1246, 1109, 1024, 838, 747, 659; HR-MS: calcd *m/z* for C₃₄H₂₄O₂[M+H]⁺: 465.1849; found (ESI) 465.1847.

9-Phenylnaphtho[2,1-c]chrysene (**163j**):



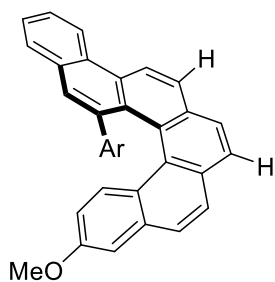
Ar = Ph

Prepared from **161j** (10.1 mg, 25 μmol, 1.0 equiv.), **162b** (1.9 mg, 1.25 μmol, 5 mol%) and AgSbF₆ (0.43 mg, 1.25 μmol, 5 mol%, 0.05 M in DCM) in DCM (0.5 mL) according to General Procedure F. The crude mixture was obtained as a yellow solid, **163j**:**191j**: >99:1, 16% conversion (determined by NMR), 94% enantiomeric excess.

The analytically pure sample of **163j** (1.5 mg, 15% yield) was obtained by semi-preparative HPLC; separation conditions: MeCN/H₂O = 90/10 to 100/0 over 20 min, 1.0 mL min⁻¹, 295 K. The *ee* was determined by chiral HPLC: IA-3, Hex/IPA = 95/5, isocratic, 20 min, 1.0 mL min⁻¹, 298 K, 256 nm; major enantiomer *t_R* = 1.7 min, minor enantiomer *t_R* = 3.6 min.

[α]₂₄^D: (94% *ee*) +1082 (*c* = 0.43, DCM); ¹H NMR (400 MHz, CDCl₃) δ = 8.93 (s, 1H), 8.91 – 8.84 (m, 1H), 8.19 (d, *J* = 8.6 Hz, 1H), 8.00 (dd, *J* = 8.4, 2.6 Hz, 2H), 7.89 (d, *J* = 8.2 Hz, 1H), 7.83 (d, *J* = 8.4 Hz, 1H), 7.80 – 7.73 (m, 1H), 7.70 (t, *J* = 7.4 Hz, 1H), 7.66 – 7.55 (m, 3H), 7.50 (d, *J* = 8.5 Hz, 1H), 7.38 (t, *J* = 7.4 Hz, 1H), 7.17 (ddd, *J* = 8.3, 6.7, 1.4 Hz, 1H), 6.99 – 6.17 (m, 4H), 5.68 (br. s, 1H) ppm; ¹³C NMR (101 MHz, CDCl₃) δ = (two overlapping peaks) 142.2, 139.7, 132.4, 132.0, 131.5, 130.9, 130.4, 130.1, 129.9, 129.2, 128.8, 128.6, 127.7, 127.5, 127.2, 127.1, 127.0, 126.9, 126.8, 126.7, 126.5, 126.1, 125.4, 125.1, 125.0, 124.8, 123.4, 121.6 ppm IR: (neat, cm⁻¹) $\tilde{\nu}$ = 3732, 3599, 2454, 2925, 2831, 1575, 1472, 1246, 1109, 1033, 837, 808, 747, 697, 670, 660; HR-MS: calcd *m/z* for C₃₂H₂₀⁺ [M]⁺: 404.1560; found (EI) 404.1562.

6-Methoxy-9-(4-methoxyphenyl)naphtho[2,1-c]chrysene (163k):



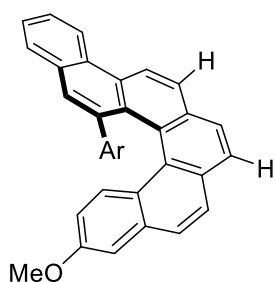
Ar = *p*-MeO(C₆H₄)

Prepared from **161k** (11.6 mg, 25 μmol, 1.0 equiv.), **162b** (1.9 mg, 1.25 μmol, 5 mol%) and AgSbF₆ (0.43 mg, 1.25 μmol, 5 mol%, 0.05 M in DCM) in DCM (0.5 mL) according to General Procedure **F**. The crude mixture was obtained as a yellow solid, **161k**:**191k**: 93:7, >95% conversion (determined by NMR), 93% enantiomeric excess.

The analytically pure sample of **163k** (6.3 mg, 54% yield) was obtained by semi-preparative HPLC; separation conditions: MeCN/H₂O = 90/10 to 100/0 over 20 min, 1.0 mL min⁻¹, 295 K; helicene t_R = 12.0 min. The *ee* was determined by chiral SFC: on SFC-IA3, with 20% *i*-propanol at 2.25 mL min⁻¹ and 3000 psi bpr, 310 K; major enantiomer t_R = 2.84 min, minor enantiomer t_R = 5.57 min.

[α]_D²⁴: (93% *ee*) +981.70 (*c* = 0.31, DCM); ¹H NMR (400 MHz, CDCl₃) δ = 8.87 (dd, *J* = 11.8, 8.4 Hz, 2H), 8.16 (d, *J* = 8.5 Hz, 1H), 7.96 (dd, *J* = 22.1, 8.0 Hz, 2H), 7.86 (d, *J* = 8.2 Hz, 1H), 7.71 (ddt, *J* = 21.8, 15.1, 7.6 Hz, 3H), 7.63 (s, 1H), 7.57 (s, 1H), 7.47 (d, *J* = 8.5 Hz, 1H), 7.01 (d, *J* = 2.6 Hz, 1H), 6.83 (dd, *J* = 9.2, 2.6 Hz, 1H), 6.69 – 5.39 (s br, 4H), 3.96 (s, 3H), 3.64 (s, 3H) ppm; ¹³C NMR (101 MHz, CDCl₃) δ = 157.6, 157.1, 139.1, 135.1, 133.0, 132.4, 132.1, 130.3, 129.8, 129.1, 128.9, 128.6, 128.4, 128.3, 128.1, 127.8, 127.2, 126.7, 126.5, 126.43, 126.39, 126.2, 125.5, 125.2, 124.9, 123.3, 121.6, 116.3, 107.0, 55.5, 55.3 ppm; IR: (neat, cm⁻¹) $\tilde{\nu}$ = 1618, 1606, 1508, 1480, 1470, 1270, 1244, 1176, 1033, 851, 830, 750, 734, 672, 657, 418, 405; HR-MS: calcd *m/z* for C₃₄H₂₄O₂⁺ [M]⁺: 464.1771; found (ESI) 464.1767.

6-Methoxy-9-(*p*-tolyl)naphtho[2,1-c]chrysene (163l):



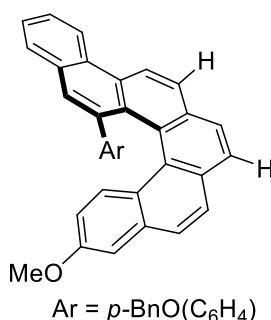
Ar = *p*-Me(C₆H₄)

Prepared from **161l** (11.2 mg, 25 μmol, 1.0 equiv.), **162b** (1.9 mg, 1.25 μmol, 5 mol%) and AgSbF₆ (0.43 mg, 1.25 μmol, 5 mol%, 0.05 M in DCM) in DCM (0.5 mL) according to General Procedure **F**. The crude mixture was obtained as a yellow solid, **163l**:**191l**: >99:1, >95% conversion (determined by NMR), 88% enantiomeric excess.

The analytically pure sample of **163l** (7.8 mg, 70% yield) was obtained by semi-preparative HPLC; separation conditions: MeCN/H₂O = 80/20 to 100/0 over 20min, 1.0 mL min⁻¹, 295 K; helicene t_R = 21.2 min. The *ee* was determined by chiral SFC: on SFC-IA3, modifier 35% *i*-propanol at 2.25 mL min⁻¹ and backpressure regulator set to 3000 psi, 300 K; major enantiomer t_R = 1.70 min, minor enantiomer t_R = 3.53 min.

$[\alpha]_{24}^D$: (88% *ee*) +1090.10 (*c* = 0.29, DCM); $^1\text{H NMR}$ (400 MHz, CDCl_3) δ = 8.87 (dd, *J* = 10.9, 8.4 Hz, 2H), 8.15 (d, *J* = 8.5 Hz, 1H), 7.96 (dd, *J* = 23.7, 8.1 Hz, 2H), 7.85 (d, *J* = 8.1 Hz, 1H), 7.78 – 7.65 (m, 3H), 7.64 – 7.54 (m, 2H), 7.42 (d, *J* = 8.4 Hz, 1H), 6.98 (d, *J* = 2.8 Hz, 1H), 6.83 (dd, *J* = 9.1, 2.7 Hz, 1H), 6.73 – 4.98 (s br, 4H), 3.96 (s, 3H), 2.08 (s, 3H) ppm. $^{13}\text{C NMR}$ (101 MHz, CDCl_3) δ = 157.5, 139.5, 139.3, 134.4, 132.9, 132.4, 132.1, 130.2, 129.8, 128.9, 128.8, 128.5, 128.4, 128.0, 127.2, 126.64, 126.61, 126.5, 126.4, 126.2, 126.1, 125.4, 125.1, 124.9, 123.3, 121.5, 116.2, 107.0, 55.5, 20.7. **IR**: (neat, cm^{-1}) $\tilde{\nu}$ = 1619, 1605, 1525, 1510, 1496, 1480, 1469, 1447, 1430, 1406, 1352, 1269, 1237, 1194, 1169, 1144, 1115, 1072, 1053, 1031, 954, 903, 849, 832, 815, 789, 748, 731, 723, 703, 656, 625, 607, 595, 582, 568, 551, 543, 531, 510, 494, 481, 450, 427, 413; **HR-MS**: calcd *m/z* for $\text{C}_{34}\text{H}_{25}\text{O}^+$ [$\text{M}+\text{H}$] $^+$: 449.1900; found (ESI) 449.1898.

9-[4-(Benzyloxy)phenyl]-6-methoxynaphtho[2,1-c]chrysene (163m):

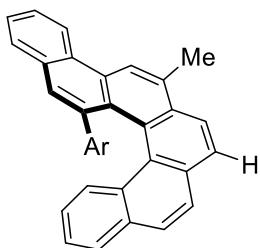


Prepared from **161m** (13.5 mg, 25 μmol , 1.0 equiv.), **162b** (1.9 mg, 1.25 μmol , 5 mol%) and AgSbF_6 (0.43 mg, 1.25 μmol , 5 mol%, 0.05 M in DCM) in DCM (0.5 mL) according to General Procedure F. The crude mixture was obtained as a yellow solid, **163m**:**191m**: 94:6, >95% conversion (determined by NMR), 88% enantiomeric excess.

The analytically pure sample of **163m** (10.4 mg, 77% yield) was obtained by semi-preparative HPLC; separation conditions: MeCN/ H_2O = 90/10 to 100/0 over 20min, 1.0 mL min^{-1} , 295 K; helicene t_R = 16.7 min. The *ee* was determined by chiral SFC: on SFC-IA3, modifier 35% *i*-propanol at 2.25 mL min^{-1} and backpressure regulator set to 3000 psi, 300 K; major enantiomer t_R = 1.92 min, minor enantiomer t_R = 3.42 min.

$[\alpha]_{24}^D$: (88% *ee*) +911.5 (*c* = 0.32, DCM); $^1\text{H NMR}$ (300 MHz, CDCl_3) δ = 8.86 (t, *J* = 8.5 Hz, 2H), 8.15 (d, *J* = 8.6 Hz, 1H), 8.05 – 7.81 (m, 3H), 7.75 (ddd, *J* = 8.4, 6.9, 1.6 Hz, 1H), 7.70 – 7.59 (m, 3H), 7.55 (s, 1H), 7.51 – 7.34 (m, 6H), 6.89 (d, *J* = 2.7 Hz, 1H), 6.81 (dd, *J* = 9.1, 2.7 Hz, 1H), 6.60 – 5.45 (br s, 4H), 4.91 (s, 2H), 3.89 (s, 3H) ppm. $^{13}\text{C NMR}$ (101 MHz, CDCl_3) δ = 157.5, 156.3, 139.0, 137.6, 135.4, 132.9, 132.4, 132.1, 130.2, 129.8, 129.0, 128.8, 128.63, 128.56, 128.4, 128.3, 128.1, 127.8, 127.2, 127.1, 126.7, 126.5, 126.4, 126.4, 126.2, 125.5, 125.1, 124.9, 123.3, 121.5, 116.3, 107.0, 69.8, 55.4. **IR**: (neat, cm^{-1}) $\tilde{\nu}$ = 1604, 1559, 1524, 1506, 1480, 1469, 1454, 1430, 1407, 1352, 1314, 1269, 1236, 1224, 1195, 1173, 1145, 1114, 1073, 1053, 1027, 952, 904, 849, 824, 811, 787, 747, 727, 695, 657, 649, 626, 607, 595, 582, 568, 554, 535, 516, 509, 499, 481, 454, 433, 424, 407; **HR-MS**: calcd *m/z* for $\text{C}_{40}\text{H}_{28}\text{O}_2^+$ [M] $^+$: 540.2084; found (ESI) 540.2081.

9-(4-Methoxyphenyl)-16-methylnaphtho[2,1-c]chrysene **163n**



Prepared from **161n** (11.2 mg, 25 μmol , 1.0 equiv.), **162b** (1.9 mg, 1.25 μmol , 5 mol%) and AgSbF_6 (0.43 mg, 1.25 μmol , 5 mol%, 0.05 M in DCM) in DCM (0.5 mL) according to general procedure **F**. The crude mixture was obtained as a green solid, **163n:191n**: 97:3, >99% conversion (determined by NMR), 98% enantiomeric excess.

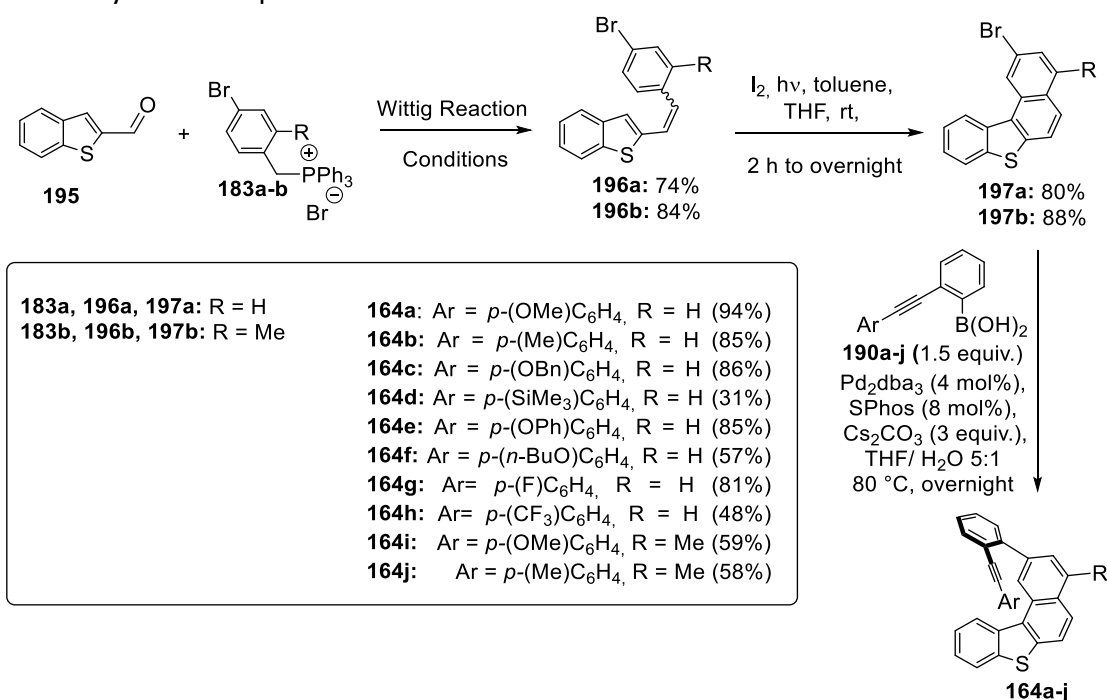
Ar = *p*-MeO(C₆H₄)

The analytically pure sample of **163n** (7.3 mg, 65% yield) was obtained by semi-preparative HPLC; separation conditions: MeCN/H₂O = 90/10 to 100/0 over 20 min, 1.0 mL min⁻¹, 295 K; helicene t_R = 15.557 min, isomer t_R = 20.6 min. The *ee* was determined by chiral HPLC: IA-3, Hex/IPA = 95/5, 20 min, 1.0 mL min⁻¹, 298 K, 256 nm; major enantiomer t_R = 3.1 min, minor enantiomer t_R = 7.9 min.

$[\alpha]_{24}^D$: (98% *ee*) +977.1 (c = 0.36, DCM); ¹H NMR (300 MHz, CDCl₃) δ = 8.87 (d, J = 8.2 Hz, 1H), 8.74 (s, 1H), 8.18 (d, J = 8.4 Hz, 1H), 8.00 – 7.85 (m, 2H), 7.79 – 7.59 (m, 5H), 7.58 – 7.45 (m, 2H), 7.37 (ddd, J = 8.0, 6.9, 1.2 Hz, 1H), 7.14 (ddd, J = 8.3, 6.8, 1.4 Hz, 1H), 6.28 (s br, J = 111.6 Hz, 4H), 3.64 (s, 3H), 3.06 (d, J = 0.9 Hz, 3H). ¹³C NMR (101 MHz, CDCl₃) δ = 157.0, 139.2, 135.2, 132.6, 132.4, 131.7, 131.6, 131.2, 129.8, 129.7, 129.4, 128.8, 128.4, 127.9, 127.5, 127.1, 127.03, 126.98, 126.9, 126.6, 126.3, 125.5, 125.3, 125.26, 124.8, 123.3, 122.14, 122.10, 55.3, 20.4. IR: (neat, cm⁻¹) $\tilde{\nu}$ = 2372, 2351, 2319, 1604, 1509, 1484, 1462, 1450, 1441, 1435, 1288, 1242, 1172, 1157, 1128, 1104, 1068, 1032, 959, 949, 906, 892, 865, 831, 816, 797, 781, 766, 741, 731, 705, 670, 666, 652, 640, 631, 620, 600, 589, 577, 551, 539, 530, 508, 482, 453, 438, 424, 416, 405; HR-MS: calcd m/z for C₃₄H₂₄O⁺ [M]⁺: 448.1822; found (ESI) 448.1822.

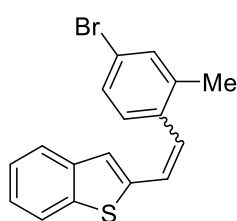
6.3. Enantioselective synthesis of thia[5]helicenes

6.3.1. Synthesis of precursors



Scheme 58. Synthesis of the precursors of thia[5]helicenes – substituted thia[4]helicenes **164a-j** via consecutive Wittig reaction, Mallory photocyclization and Suzuki coupling.

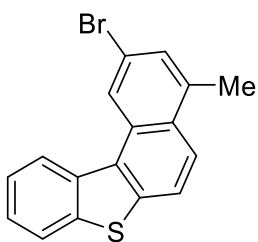
***E,Z*-2-(4-Bromo-2-methylstyryl)benzo[*b*]thiophene (196b):**



(4-Bromo-2-methylbenzyl)triphenylphosphonium bromide (**183b**) (2.0 g, 3.80 mmol, 1.1 equiv.) was placed in a dry flask under inert atmosphere. Anhydrous THF (35 mL) was added and the resulting suspension was stirred at 0 °C. *n*-BuLi (1.7 mL 2.5M, 4.16 mmol, 1.2 equiv.) was added dropwise, and the red mixture was stirred at rt for 2 h. The solution was cooled to 0 °C and commercially available benzo[*b*]thiophene-2-carbaldehyde **195** (560 mg, 3.45 mmol, 1 equiv.) was added dropwise as a solution in dry THF (7 mL). The reaction mixture was allowed to warm up to rt, then stirred at 60 °C overnight and cooled down to rt. The reaction was quenched by addition of water (10 mL). The biphasic mixture was extracted with EtOAc (20 mL) and the aqueous phase re-extracted with Et₂O (2 × 20 mL). The combined organic extracts were dried over MgSO₄, filtered and concentrated in vacuo. The residue was purified by column chromatography (SiO₂, 0 to 10% EtOAc in pentane) to afford the olefin as a mixture of *E*- and *Z*-diastereomers (950 mg, 2.89 mmol, 84%). ¹H NMR: (300 MHz, CDCl₃): mixture of two isomers (2:3) δ = 7.82 – 7.75 (m, 1H), 7.73 – 7.68 (m, 1H), 7.63 (dd, *J* = 11.1, 7.2 Hz, 1H), 7.45 (d, *J* = 9.1 Hz, 2H), 7.37 – 7.29 (m, 5H), 7.24 – 7.07 (m, 4H), 6.90 (d, *J* = 11.8 Hz, 1H), 6.57 (d, *J* = 11.7 Hz, 1H), 2.42 (s, 3H), 2.25 (s, 2H) ppm; ¹³C NMR: (101 MHz, CDCl₃) δ =

142.8, 140.4, 140.2, 139.8, 139.0, 138.9, 138.7, 137.9, 135.3, 134.6, 133.3, 133.0, 131.0, 129.3, 129.1, 128.8, 127.3, 126.7, 125.5, 125.3, 124.9, 124.7, 124.6, 124.3, 124.0, 123.7, 123.5, 122.3, 122.2, 122.1, 121.9, 121.6, 19.73, 19.69 ppm; IR: (neat, cm^{-1}) $\tilde{\nu}$ = 1587, 1474, 1455, 1431, 1374, 1212, 1098, 952, 935, 859, 847, 830, 793, 745, 725, 681, 658, 591, 572, 550, 530, 510; HR-MS: calcd m/z for $\text{C}_{17}\text{H}_{13}\text{BrS}^+$ $[\text{M}]^+$: 327.9916; found (EI) 327.9913.

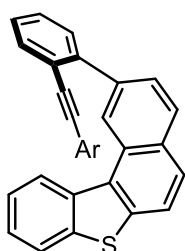
2-Bromo-4-methylbenzo[*b*]naphtho[1,2-*d*]thiophene (**197b**):



Compound **197b** was prepared from **196b** (800 mg, 2.43 mmol, 1.0 equiv.) and iodine (680 mg, 2.68 mmol, 1.1 equiv.) according to General Procedure **C** described above. After purification by column chromatography (SiO_2 , pentane) the compound **197b** was obtained as a white solid (700 mg, 2.14 mmol, 88%).

$^1\text{H NMR}$ (300 MHz, CDCl_3) δ = 8.87 (s, 1H), 8.63 (d, J = 8.2 Hz, 1H), 7.95 (d, J = 7.9 Hz, 1H), 7.83 (q, J = 8.9 Hz, 2H), 7.59 – 7.44 (m, 3H), 2.66 (s, 3H) ppm; $^{13}\text{C NMR}$ (101 MHz, CDCl_3) δ = 139.8, 139.3, 137.7, 136.3, 131.8, 129.5, 129.2, 128.7, 125.6, 125.1, 124.7, 124.0, 123.5, 123.3, 121.3, 121.2, 20.2 ppm; IR: (neat, cm^{-1}) $\tilde{\nu}$ = 1598, 1581, 1541, 1503, 1457, 1438, 1393, 1373, 1358, 1308, 1289, 1213, 1157, 1145, 1105, 1074, 1028, 925, 868, 846, 822, 802, 791, 769, 736, 713, 678, 656, 622, 605, 566, 545, 516, 499, 474, 416; HR-MS: calcd m/z for $\text{C}_{17}\text{H}_{11}\text{BrS}^+$ $[\text{M}]^+$: 325.9756; found (ESI) 325.9759.

2-{2-[(4-Methoxyphenyl)ethynyl]phenyl}benzo[*b*]naphtho[1,2-*d*]thiophene (**164a**):

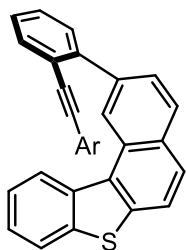


Prepared from 2-bromobenzo[*b*]naphtho[1,2-*d*]thiophene (**197a**) (136 mg, 434.2 μmol , 1.0 equiv.), **190a** (166 mg, 658.5 μmol , 1.52 equiv.), $\text{Pd}_2(\text{dba})_3$ (15.9 mg, 17.4 μmol , 4 mol%), SPhos (14.2 mg, 34.7 μmol , 8 mol%), Cs_2CO_3 (429 mg, 1.32 mmol, 3.0 equiv.) and the solvent mixture (25 mL) according to General Procedure **E**. Column chromatography (SiO_2 , 0 to 5% EtOAc in pentane) yielded the product as a yellow solid (180 mg, 408.5 μmol , 94%).

$^1\text{H NMR}$ (300 MHz, CDCl_3) δ = 9.39 (d, J = 1.7 Hz, 1H), 8.96 – 8.84 (m, 1H), 8.11 (d, J = 8.3 Hz, 1H), 8.03 – 7.86 (m, 4H), 7.76 (dd, J = 7.4, 1.6 Hz, 1H), 7.64 (dd, J = 7.6, 1.5 Hz, 1H), 7.55 – 7.44 (m, 2H), 7.44 – 7.34 (m, 2H), 7.14 (d, J = 8.8 Hz, 2H), 6.61 (d, J = 8.8 Hz, 2H), 3.70 (s, 3H) ppm; $^{13}\text{C NMR}$ (101 MHz, CDCl_3) δ = 159.5, 143.6, 139.6, 139.3, 138.8, 136.6, 133.2, 132.9, 131.2, 130.4, 130.1, 129.4, 128.9, 128.4, 127.6, 127.3, 126.6, 125.3, 124.9, 124.9, 124.0, 123.0, 122.3, 121.2, 115.2, 113.7, 92.8, 88.2, 55.2 ppm; IR: (neat, cm^{-1}) $\tilde{\nu}$ = 3059, 2209, 1604, 1486, 1460,

1437, 1362, 1288, 1246, 1174, 1144, 1031, 922, 834, 779, 757, 716, 601, 519, 503, 489, 418;
HR-MS: calcd m/z for $C_{31}H_{20}OS^+$ $[M]^+$: 440.1229; found (EI) 440.1226.

2-[2-(*p*-Tolylethynyl)phenyl]benzo[*b*]naphtho[1,2-*d*]thiophene (**164b**):

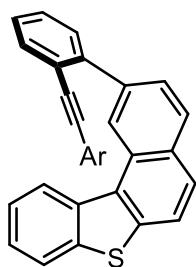


Ar = *p*-Me(C_6H_4)

Prepared from 2-bromobenzo[*b*]naphtho[1,2-*d*]thiophene (**197a**) (116 mg, 370.3 μ mol, 1.0 equiv.), **190b** (132 mg, 559.1 μ mol, 1.51 equiv.), $Pd_2(dba)_3$ (13.5 mg, 14.7 μ mol, 4 mol%), SPhos (12.1 mg, 29.5 μ mol, 8 mol%), Cs_2CO_3 (361 mg, 1.11 mmol, 3.0 equiv.) and the solvent mixture (21 mL) according to General Procedure E. Column chromatography (SiO₂, 0 to 5% EtOAc in pentane) yielded the product **164b** as a yellow solid (133 mg, 313.2 μ mol, 85%).

¹H NMR (400 MHz, $CDCl_3$) δ = 9.37 (s, 1H), 8.94 – 8.87 (m, 1H), 8.10 (d, J = 8.4 Hz, 1H), 8.02 – 7.87 (m, 4H), 7.77 (dd, J = 7.7, 1.4 Hz, 1H), 7.64 (dd, J = 7.7, 1.4 Hz, 1H), 7.50 (td, J = 7.6, 1.5 Hz, 1H), 7.47 – 7.37 (m, 3H), 7.13 – 7.06 (m, 2H), 6.90 (d, J = 8.0 Hz, 2H), 2.23 (s, 3H) ppm; **¹³C NMR** (101 MHz, $CDCl_3$) δ = 143.8, 139.6, 139.3, 138.8, 138.2, 136.6, 133.3, 131.4, 131.2, 130.4, 130.1, 129.4, 128.9, 128.8, 128.6, 127.6, 127.4, 126.6, 125.3, 125.0, 124.9, 124.1, 123.0, 122.2, 121.3, 120.0, 92.9, 88.8, 21.4 ppm; **IR:** (neat, cm^{-1}) $\tilde{\nu}$ = 1509, 1481, 1437, 1362, 1214, 1142, 922, 843, 812, 778, 757, 711, 674, 651, 621, 600, 587, 514, 492, 479, 418; **HR-MS:** calcd m/z for $C_{31}H_{20}S^+$ $[M]^+$: 424.1280; found (EI) 424.1279.

2-(2-[4-(Benzyloxy)phenyl]ethynyl)phenyl]benzo[*b*]naphtho[1,2-*d*]thiophene (**164c**):



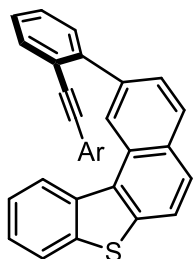
Ar = *p*-BnO(C_6H_4)

Prepared from 2-bromobenzo[*b*]naphtho[1,2-*d*]thiophene (**197a**) (136 mg, 434.2 μ mol, 1.0 equiv.), **190c** (216 mg, 658.2 μ mol, 1.52 equiv.), $Pd_2(dba)_3$ (14.5 mg, 15.8 μ mol, 3.6 mol%), SPhos (14.5 mg, 35.3 μ mol, 8.1 mol%), Cs_2CO_3 (429 mg, 3 mmol, 3.0 equiv.) and the solvent mixture (25 mL) according to General Procedure E. Column chromatography (SiO₂, 0 to 5% EtOAc in pentane) yielded the product **164c** as a yellow solid (194 mg, 375.4 μ mol, 86%).

¹H NMR (400 MHz, $CDCl_3$) δ = 9.38 (s, 1H), 8.91 (d, J = 6.8 Hz, 1H), 8.11 (d, J = 8.3 Hz, 1H), 7.99 – 7.94 (m, 3H), 7.93 – 7.86 (m, 1H), 7.75 (d, J = 7.6 Hz, 1H), 7.64 (d, J = 7.7 Hz, 1H), 7.49 (t, J = 7.3 Hz, 1H), 7.42 (td, J = 6.4, 3.5 Hz, 3H), 7.35 (d, J = 4.3 Hz, 4H), 7.32 – 7.27 (m, 1H), 7.13 (d, J = 8.5 Hz, 2H), 6.68 (d, J = 8.6 Hz, 2H), 4.95 (s, 2H) ppm; **¹³C NMR** (101 MHz, $CDCl_3$) δ = 158.7, 143.6, 139.6, 139.3, 138.8, 136.6, 136.6, 133.2, 132.9, 131.2, 130.4, 130.1, 129.4, 128.9, 128.6, 128.4, 128.4, 127.6, 127.4, 127.3, 126.6, 125.3, 124.9, 124.9, 124.0, 123.0, 122.2, 121.2, 115.5, 114.6,

92.7, 88.3, 69.9 ppm; **IR:** (neat, cm^{-1}) $\tilde{\nu}$ = 3729, 3024, 2348, 1608, 1592, 1569, 1509, 1454, 1377, 1361, 1311, 1287, 1253, 1212, 1173, 1143, 1103, 1028, 947, 922, 872, 827, 807, 775, 754, 742, 728, 712, 690, 674, 653, 598, 583, 523, 503, 475, 418; **HR-MS:** calcd m/z for $\text{C}_{37}\text{H}_{25}\text{OS}^+$ $[\text{M}+\text{H}]^+$: 517.1621; found (ESI) 517.1613.

(4-{{2-(Benzo[b]naphtho[1,2-d]thiophen-2-yl)phenyl}ethynyl}phenyl)trimethylsilane (164d):

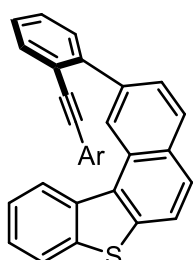


Ar = *p*-(Me_3Si)(C_6H_4)

Prepared from 2-bromobenzo[*b*]naphtho[1,2-*d*]thiophene (**197a**) (165 mg, 526.8 μmol , 1.0 equiv.), **190d** (221 mg, 751.1 μmol , 1.43 equiv.), Pd_2dba_3 (18.3 mg, 20.0 μmol , 3.8 mol%), SPhos (16.4 mg, 39.9 μmol , 7.6 mol%), Cs_2CO_3 (487 mg, 1.49 mmol, 2.8 equiv.) and the solvent mixture (28 mL) according to General Procedure E. Column chromatography (SiO_2 , 0 to 5% EtOAc in pentane) yielded the product as a yellow solid (80 mg, 165.7 μmol , 31%).

^1H NMR (400 MHz, CDCl_3) δ = 9.38 (d, J = 1.6 Hz, 1H), 8.96 – 8.85 (m, 1H), 8.13 (d, J = 8.4 Hz, 1H), 8.05 – 7.90 (m, 4H), 7.81 (dd, J = 7.6, 1.5 Hz, 1H), 7.75 – 7.64 (m, 1H), 7.54 (td, J = 7.6, 1.5 Hz, 1H), 7.50 – 7.36 (m, 3H), 7.28 (s, 2H), 7.21 (d, J = 8.1 Hz, 2H), 0.21 (s, 9H) ppm. **^{13}C NMR** (101 MHz, CDCl_3) δ = 143.9, 140.9, 139.6, 139.2, 138.8, 136.6, 133.4, 132.9, 131.2, 130.5, 130.4, 130.1, 129.4, 128.9, 128.8, 127.6, 127.4, 126.6, 125.2, 124.9, 124.8, 124.0, 123.4, 123.0, 122.0, 121.3, 92.9, 89.9, -1.3 ppm; **IR:** (neat, cm^{-1}) $\tilde{\nu}$ = 1713, 1591, 1506, 1477, 1457, 1438, 1360, 1244, 1214, 1145, 1106, 1067, 923, 858, 838, 820, 777, 757, 749, 720, 697, 677, 653, 634, 622, 601, 592, 573, 541, 531, 515, 502, 418; **HR-MS:** calcd m/z for $\text{C}_{33}\text{H}_{26}\text{KSSi}^+$ $[\text{M}+\text{K}]^+$: 521.1156; found (ESI) 521.1146.

2-2-{{(4-Phenoxyphenyl)ethynyl}phenyl}benzo[*b*]naphtho[1,2-*d*]thiophene (164e):



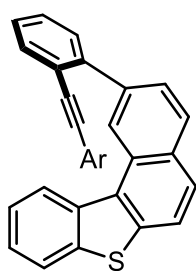
Ar = *p*-PhO(C_6H_4)

Prepared from 2-bromobenzo[*b*]naphtho[1,2-*d*]thiophene (**197a**) (165 mg, 526.8 μmol , 1.0 equiv.), **190e** (235 mg, 748.1 μmol , 1.42 equiv.), Pd_2dba_3 (18.3 mg, 20.0 μmol , 3.8 mol%), SPhos (16.4 mg, 39.9 μmol , 7.6 mol%), Cs_2CO_3 (487 mg, 1.49 mmol, 2.83 equiv.) and the solvent mixture (28 mL) according to General Procedure E. Column chromatography (SiO_2 , 0 to 5% EtOAc in pentane) yielded the product **164e** as a yellow solid (226 mg, 449.6 μmol , 85%).

^1H NMR (400 MHz, CDCl_3) δ = 9.40 (s, 1H), 8.90 (d, J = 7.8 Hz, 1H), 8.11 (d, J = 8.4 Hz, 1H), 7.98 (d, J = 7.8 Hz, 2H), 7.95 (s, 1H), 7.90 (d, J = 8.4 Hz, 1H), 7.77 (d, J = 7.6 Hz, 1H), 7.65 (d, J = 7.7 Hz, 1H), 7.51 (t, J = 7.6 Hz, 1H), 7.47 – 7.39 (m, 3H), 7.30 (t, J = 7.8 Hz, 2H), 7.15 (s, 2H), 7.10 (t,

$J = 7.4$ Hz, 1H), 6.89 (d, $J = 8.0$ Hz, 2H), 6.70 (d, $J = 8.3$ Hz, 2H) ppm; ^{13}C NMR (101 MHz, CDCl_3) $\delta = 157.3, 156.5, 143.7, 139.7, 139.2, 138.9, 136.6, 133.2, 133.1, 131.2, 130.4, 130.1, 129.8, 129.4, 129.0, 128.7, 127.6, 127.4, 126.5, 125.2, 124.9, 124.8, 124.1, 123.7, 123.0, 122.0, 121.3, 119.2, 118.3, 117.7, 92.4, 89.0$ ppm; IR: (neat, cm^{-1}) $\tilde{\nu} = 3057, 2925, 2320, 1586, 1505, 1486, 1362, 1231, 1163, 1103, 1068, 1023, 871, 834, 777, 747, 721, 691, 623, 599, 503, 418$; HR-MS: calcd m/z for $\text{C}_{36}\text{H}_{22}\text{KOS}^+$ $[\text{M}+\text{K}]^+$: 541.1023; found (ESI) 541.1018.

2-(2-((4-butoxyphenyl)ethynyl)phenyl)benzo[*b*]naphtho[1,2-*d*]thiophene (164f):

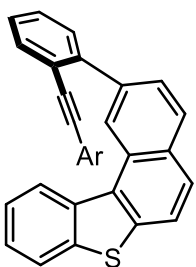


Ar = p -(n -BuO) C_6H_4

Prepared from 2-bromobenzo[*b*]naphtho[1,2-*d*]thiophene (**197a**) (136 mg, 434.2 μmol , 1.0 equiv.), **190f** (194 mg, 687.6 μmol , 1.58 equiv.), Pd_2dba_3 (16.1 mg, 17.6 μmol , 4 mol%), SPhos (14.5 mg, 35.3 μmol , 8.1 mol%), Cs_2CO_3 (429 mg, 1.32 mmol, 3.0 equiv.) and the solvent mixture (25 mL) according to General Procedure E. Column chromatography (SiO_2 , 0 to 5% EtOAc in pentane) yielded the product as a white solid (120 mg, 248.6 μmol , 57%).

^1H NMR (400 MHz, CDCl_3) $\delta = 9.39$ (s, 1H), 8.96 – 8.85 (m, 1H), 8.11 (d, $J = 8.4$ Hz, 1H), 8.00 – 7.93 (m, 3H), 7.92 – 7.86 (m, 1H), 7.76 (dd, $J = 7.6, 1.5$ Hz, 1H), 7.64 (dd, $J = 7.4, 1.5$ Hz, 1H), 7.55 – 7.35 (m, 4H), 7.12 (d, $J = 8.7$ Hz, 2H), 6.60 (d, $J = 8.7$ Hz, 2H), 3.84 (t, $J = 6.5$ Hz, 2H), 1.69 (dq, $J = 8.2, 6.5$ Hz, 2H), 1.52 – 1.34 (m, 2H), 0.94 (t, $J = 7.4$ Hz, 3H) ppm; ^{13}C NMR (101 MHz, CDCl_3) $\delta = 159.1, 143.6, 139.6, 139.4, 138.8, 136.6, 133.2, 132.9, 131.2, 130.4, 130.1, 129.4, 128.9, 128.4, 127.6, 127.4, 126.6, 125.3, 125.0, 124.9, 124.1, 123.0, 122.3, 121.2, 115.0, 114.3, 92.9, 88.1, 67.7, 31.2, 19.2, 13.8$ ppm; IR: (neat, cm^{-1}) $\tilde{\nu} = 2954, 2928, 2869, 1604, 1593, 1566, 1508, 1462, 1441, 1427, 1377, 1362, 1304, 1284, 1242, 1213, 1196, 1173, 1144, 1105, 1065, 1041, 1024, 1006, 966, 949, 921, 876, 829, 805, 778, 747, 722, 646, 622, 599, 587, 561, 533, 521, 503, 489, 477, 443, 425, 412, 404$; HR-MS: calcd m/z for $\text{C}_{36}\text{H}_{26}\text{NaOS}^+$ $[\text{M}+\text{Na}]^+$: 505.1597; found (ESI) 505.1590.

2-(2-(((4-Fluorophenyl)ethynyl)phenyl)benzo[*b*]naphtho[1,2-*d*]thiophene (164g):



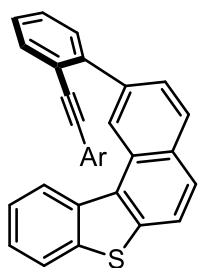
Ar = p -F(C_6H_4)

Prepared from 2-bromobenzo[*b*]naphtho[1,2-*d*]thiophene (**197a**) (136 mg, 434.2 μmol , 1.0 equiv.), **190g** (158 mg, 631.7 μmol , 1.45 equiv.), Pd_2dba_3 (16.1 mg, 17.6 μmol , 4 mol%), SPhos (14.5 mg, 35.3 μmol , 8.1 mol%), Cs_2CO_3 (429 mg, 1.32 mmol, 3.0 equiv.) and the solvent mixture (25 mL) according to General Procedure E. Column chromatography (SiO_2 , 0 to 5% EtOAc in pentane) yielded the product **164g** as a yellow solid (150 mg, 350 μmol ,

81%).

$^1\text{H NMR}$ (400 MHz, CDCl_3) δ = 9.44 (s, 1H), 8.93 (d, J = 7.3 Hz, 1H), 8.11 (d, J = 8.4 Hz, 1H), 8.04 – 7.93 (m, 3H), 7.90 (d, J = 8.4 Hz, 1H), 7.81 (d, J = 7.6 Hz, 1H), 7.68 (d, J = 6.3 Hz, 1H), 7.54 (t, J = 6.8 Hz, 1H), 7.45 (q, J = 6.7 Hz, 3H), 7.24 – 7.17 (m, 2H), 6.80 (t, J = 8.7 Hz, 2H) ppm; $^{13}\text{C NMR}$ (101 MHz, CDCl_3) δ = 162.4 (d, J_{CF} = 255.7 Hz), 143.9, 139.7, 139.2, 139.0, 136.6, 133.42, 133.40 (d, J_{CF} = 8.2 Hz), 131.3, 130.4, 130.2, 129.4, 129.0 (d, J_{CF} = 11.8 Hz), 127.5 (d, J_{CF} = 17.0 Hz), 126.5, 125.4, 124.9, 124.1, 123.2, 121.8, 121.4, 119.25 (d, J_{CF} = 3.5), 115.4 (d, J_{CF} = 22.2 Hz), 91.71, 89.4 (d, J_{CF} = 1.4 Hz) ppm; $^{19}\text{F NMR}$ (377 MHz, CDCl_3) δ = –111.1 ppm; **IR**: (neat, cm^{-1}) $\tilde{\nu}$ = 2954, 2928, 1603, 1592, 1507, 1462, 1442, 1428, 1362, 1304, 1284, 1243, 1221, 1213, 1173, 1154, 1144, 1105, 1065, 1024, 965, 921, 877, 831, 801, 778, 748, 722, 647, 623, 599, 585, 561, 532, 520, 502, 478, 458, 449, 441, 427, 418, 406; **HR-MS**: calcd m/z for $\text{C}_{30}\text{H}_{18}\text{FS}^+$ $[\text{M}+\text{H}]^+$: 429.1108; found (EI) 429.1100.

2-(2-([4-(Trifluoromethyl)phenyl]ethynyl)phenyl)benzo[*b*]naphtho[1,2-*d*]thiophene (**164h**):

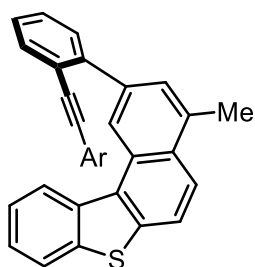


Ar = *p*-(CF_3) C_6H_4

Prepared from 2-bromobenzo[*b*]naphtho[1,2-*d*]thiophene (**197a**) (136 mg, 434.2 μmol , 1.0 equiv.), **190h** (191 mg, 677.1 μmol , 1.56 equiv.), Pd_2dba_3 (16.1 mg, 17.6 μmol , 4 mol%), SPhos (14.5 mg, 35.3 μmol , 8.1 mol%), Cs_2CO_3 (429 mg, 1.32 mmol, 3.0 equiv.) and the solvent mixture (25 mL) according to General Procedure E. Column chromatography (SiO_2 , 0 to 5% EtOAc in pentane) yielded the product **164h** as a yellow solid (100 mg, 209 μmol , 48%).

$^1\text{H NMR}$ (400 MHz, CDCl_3) δ = 9.40 (s, 1H), 8.88 (d, J = 7.8 Hz, 1H), 8.12 (d, J = 8.3 Hz, 1H), 8.03 – 7.93 (m, 3H), 7.88 (dd, J = 8.4, 1.6 Hz, 1H), 7.81 (dd, J = 7.7, 1.4 Hz, 1H), 7.69 (dd, J = 7.8, 1.3 Hz, 1H), 7.56 (td, J = 7.6, 1.4 Hz, 1H), 7.50 – 7.36 (m, 3H), 7.35 – 7.25 (m, 4H) ppm; $^{13}\text{C NMR}$ (101 MHz, CDCl_3) δ = 144.3, 139.7, 139.0, 139.0, 136.5, 133.6, 131.6, 131.3, 130.4, 130.2, 129.7 (q, J_{CF} = 32.9 Hz), 129.4, 129.3, 129.1, 127.6, 127.5, 126.9, 126.4, 125.4, 125.0 (q, J_{CF} = 3.6 Hz), 124.80, 124.75, 124.1, 123.9 (q, J_{CF} = 272.2 Hz), 123.2, 121.5, 121.3, 92.0, 91.3 ppm; $^{19}\text{F NMR}$ (377 MHz, CDCl_3) δ = –62.9 ppm; **IR**: (neat, cm^{-1}) $\tilde{\nu}$ = 1605, 1593, 1508, 1478, 1460, 1445, 1363, 1321, 1285, 1268, 1247, 1168, 1155, 1124, 1105, 1065, 1030, 906, 836, 808, 777, 756, 723, 647, 638, 599, 580, 565, 501, 490, 441, 419; **HR-MS**: calcd m/z for $\text{C}_{31}\text{H}_{18}\text{F}_3\text{S}^+$ $[\text{M}+\text{H}]^+$: 479.1076; found (EI) 479.1072.

2-[(4-Methoxyphenyl)ethynyl]phenyl-4-methylbenzo[*b*]naphtho[1,2-*d*]thiophene (164i):

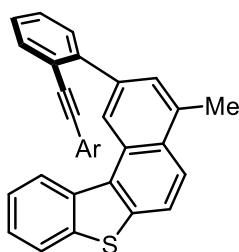


Ar = *p*-MeO(C₆H₄)

Prepared from **197b** (146 mg, 446.1 μmol, 1.0 equiv.), **190a** (169 mg, 670.4 μmol, 1.5 equiv.), Pd₂dba₃ (16.1 mg, 17.6 μmol, 3.9 mol%), SPhos (14.5 mg, 35.3 μmol, 7.9 mol%), Cs₂CO₃ (429 mg, 1.32 mmol, 2.96 equiv.) and the solvent mixture (25 mL) according to General Procedure E. Column chromatography (SiO₂, 0 to 5% EtOAc in pentane) yielded the product **164i** as a yellow solid (120 mg, 263.9 μmol, 59%).

¹H NMR (400 MHz, CDCl₃) δ = 9.30 (s, 1H), 8.92 (d, *J* = 7.0 Hz, 1H), 8.15 (d, *J* = 8.9 Hz, 1H), 8.03 – 7.92 (m, 2H), 7.76 (d, *J* = 8.9 Hz, 2H), 7.64 (d, *J* = 7.6 Hz, 1H), 7.54 – 7.35 (m, 4H), 7.13 (d, *J* = 8.5 Hz, 2H), 6.61 (d, *J* = 8.5 Hz, 2H), 3.70 (s, 3H), 2.89 (s, 3H) ppm; ¹³C NMR (101 MHz, CDCl₃) δ = 159.5, 143.6, 139.7, 138.8, 138.5, 136.8, 135.0, 133.2, 132.9, 130.7, 130.2, 130.02, 130.00, 128.4, 127.7, 127.26, 125.27, 125.2, 124.8, 123.5, 123.0, 122.5, 122.2, 121.0, 115.3, 113.7, 92.8, 88.3, 55.2, 20.7 ppm; IR: (neat, cm⁻¹) $\tilde{\nu}$ = 2954, 2930, 1603, 1592, 1566, 1507, 1477, 1462, 1440, 1379, 1362, 1303, 1285, 1244, 1213, 1173, 1154, 1144, 1105, 1067, 1025, 966, 949, 922, 878, 865, 831, 806, 777, 755, 747, 722, 674, 660, 644, 623, 615, 583, 562, 531, 520, 501, 486, 427, 421; HR-MS: calcd *m/z* for C₃₂H₂₃OS⁺ [M+H]⁺: 455.1464; found (ESI) 455.1455.

4-Methyl-2-[2-(*p*-tolylethynyl)phenyl]benzo[*b*]naphtho[1,2-*d*]thiophene (164j):

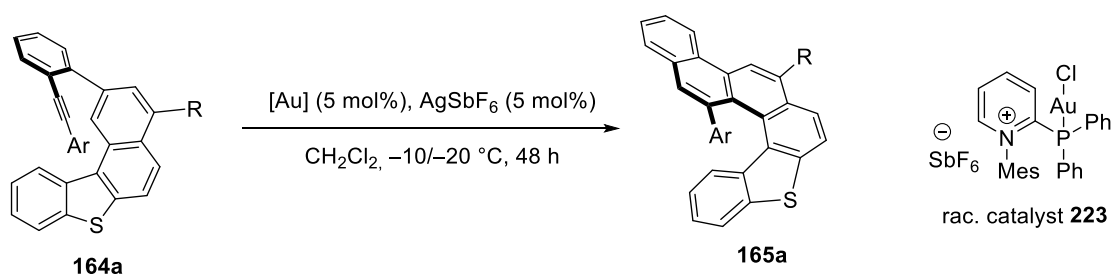


Ar = *p*-Me(C₆H₄)

Prepared from **197b** (100 mg, 305.5 μmol, 1.0 equiv.), **190b** (108 mg, 457.4 μmol, 1.5 equiv.), Pd₂dba₃ (11.3 mg, 12.3 μmol, 4 mol%), SPhos (10.2 mg, 24.8 μmol, 8.1 mol%), Cs₂CO₃ (302 mg, 926.8 μmol, 3.0 equiv.) and the solvent mixture (18 mL) according to General Procedure E. Column chromatography (SiO₂, 0 to 5% EtOAc in pentane) yielded the product **164j** as a white solid (78 mg, 177.8 μmol, 58%).

¹H NMR (400 MHz, CDCl₃) δ = 9.29 (s, 1H), 8.93 (d, *J* = 9.4 Hz, 1H), 8.15 (d, *J* = 8.9 Hz, 1H), 8.02 – 7.93 (m, 2H), 7.77 (d, *J* = 7.8 Hz, 2H), 7.65 (d, *J* = 6.3 Hz, 1H), 7.50 (td, *J* = 7.6, 1.5 Hz, 1H), 7.47 – 7.36 (m, 3H), 7.10 (d, *J* = 8.1 Hz, 2H), 6.90 (d, *J* = 7.9 Hz, 2H), 2.89 (s, 3H), 2.23 (s, 3H) ppm; ¹³C NMR (101 MHz, CDCl₃) δ = 143.8, 139.7, 138.8, 138.5, 138.2, 136.8, 135.0, 133.3, 131.4, 130.7, 130.2, 130.02, 130.00, 128.8, 128.6, 127.7, 127.3, 125.3, 125.2, 124.8, 123.5, 123.0, 122.5, 122.1, 121.0, 120.1, 92.9, 89.0, 21.4, 20.7 ppm; IR: (neat, cm⁻¹) $\tilde{\nu}$ = 2023, 1508, 1479, 1464, 1439, 1295, 1271, 1240, 1160, 1144, 1120, 1074, 1065, 1045, 1026, 944, 812, 804, 749, 736, 727, 710, 637, 613, 576, 561, 550, 521, 513, 505, 488, 478, 470, 459, 444, 420, 412; HR-MS: calcd *m/z* for [C₃₂H₂₃S⁺ [M+H]⁺: 439.1515; found (ESI) 439.1514.

6.3.2. Au(I)-Catalyzed Hydroarylation towards Thia[5]helicenes



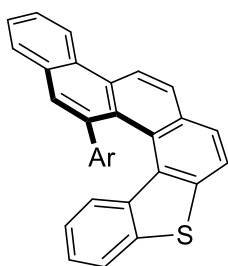
Scheme 569. Enantioselective Au(I)-catalyzed cycloisomerization reaction.

General Procedure F for Gold-catalysed Cycloisomerization Reactions

In a Schlenk flask equipped with a stirring bar, the respective substrate (25 μ mol) and the Au(I) precatalyst (5 mol%) were thoroughly dried *in vacuo* for 30 min. The mixture was dissolved in DCM (0.5 mL) and cooled to the indicated temperature ($-10\text{ }^\circ C$). A freshly prepared solution of $AgSbF_6$ (0.05 M in DCM, 5 mol%) was added. After 48 h stirring, the reaction mixture was filtered through a plug of silica to give a solution of the desired helicene **165** as a mixture with the corresponding dibenzo[*a,m*]tetraphene. Further purification by preparative HPLC gave the isolated helicenes.

As reference for the determination of the helicenes' enantiomeric excesses, racemic reactions were carried out with gold catalyst **223** employing the general setup described above but stirring the reaction mixture at room temperature instead.

14-(4-Methoxyphenyl)benzo[*b*]chryseno[4,3-*d*]thiophene (**165a**):

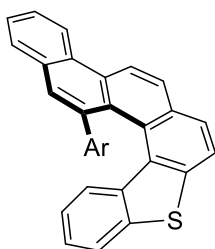


Prepared from **164a** (11.0 mg, 25 μ mol, 1.0 equiv.), **162c** (1.8 mg, 1.29 μ mol, 5.1 mol%) and $AgSbF_6$ (0.43 mg, 1.25 μ mol, 5 mol%, 0.05 M in DCM) in DCM (0.5 mL) according to General Procedure F. The crude mixture was obtained as a yellow solid, **165a**:**198a**: >99:1, >99% conversion (determined by NMR), 91% enantiomeric excess.

Ar = *p*-MeO(C₆H₄) The analytically pure sample of **165a** (10.6 mg, 96% yield) was obtained by semi-preparative HPLC; separation conditions: MeCN/H₂O 90-10, gradient to 100-0, 1.0 mL min⁻¹ over 20 min, 295 K. The *ee* was determined by chiral SFC: on SFC-IA3, CO₂/IPA = 80/20 isocratic at 2.5 mL min⁻¹ and backpressure regulator set to 3000 psi, 310 K; major enantiomer t_R = 2.84 min, minor enantiomer t_R = 8.13 min.

$[\alpha]_{20}^D$: (91% *ee*) +1113° (*c* = 0.10, DCM); $^1\text{H NMR}$ (400 MHz, CDCl_3) δ = 8.78 (d, *J* = 7.9 Hz, 1H), 8.73 (d, *J* = 8.7 Hz, 1H), 8.12 – 8.01 (m, 3H), 7.92 (s, 2H), 7.83 – 7.64 (m, 3H), 7.59 (d, *J* = 7.9 Hz, 1H), 7.27 – 7.18 (m, 1H), 7.17 – 7.09 (m, 1H), 6.71 (s br, 2H), 6.23 (s, 2H), 3.58 (s, 3H) ppm; $^{13}\text{C NMR}$ (101 MHz, CDCl_3) δ = 157.9, 139.6, 138.2, 137.8, 137.4, 134.7, 132.7, 132.4, 131.5, 130.4, 129.8, 129.4, 128.4, 127.9, 127.1, 126.9, 126.5, 126.1, 126.0, 125.31, 125.25, 124.6, 123.4, 122.9, 121.8, 121.5, 120.7, 111.9, 55.2 ppm; **IR**: (neat, 418 cm^{-1}) $\tilde{\nu}$ = 3050, 1603, 1507, 1435, 1284, 1244, 1180, 1153, 1109, 1029, 930, 894, 827, 781, 761, 729, 699, 671, 648, 637, 621, 587, 570, 556, 539, 512, 471, 451, 431; **HR-MS**: calcd *m/z* for $\text{C}_{31}\text{H}_{20}\text{OS}^+$ [*M*] $^+$: 440.1229; found (EI) 440.1225.

14-(*p*-Tolyl)benzo[*b*]chryseno[4,3-*d*]thiophene (**165b**):

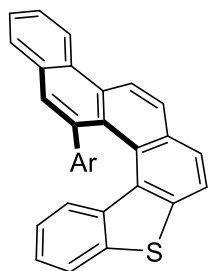


Prepared from **164b** (10.6 mg, 25 μmol , 1.0 equiv.), **162c** (1.8 mg, 1.29 μmol , 5.2 mol%) and AgSbF_6 (0.43 mg, 1.25 μmol , 5 mol%, 0.05 M in DCM) in DCM (0.5 mL) according to General Procedure F. The crude mixture was obtained as a yellow solid, **165b:198b**: >99:1, >99% conversion (determined by NMR), 96% enantiomeric excess.

Ar = *p*-Me(C_6H_4) The analytically pure sample of **165b** (10.4 mg, 98% yield) was obtained by semi-preparative HPLC; separation conditions: MeCN/ H_2O 80-20, gradient to 100-0 over 20 min, 1.0 mL min^{-1} , 295 K. The *ee* was determined by chiral SFC: on SFC-IA3, CO_2/IPA = 70/30 isocratic at 2.5 mL min^{-1} and backpressure regulator set to 3000 psi, 310 K; major enantiomer t_R = 1.23 min, minor enantiomer t_R = 2.94 min.

$[\alpha]_{23}^D$: (96% *ee*) +1652° (*c* = 0.15, DCM); $^1\text{H NMR}$ (400 MHz, CDCl_3) δ = 8.79 (d, *J* = 8.0 Hz, 1H), 8.73 (d, *J* = 8.7 Hz, 1H), 8.13 – 8.00 (m, 3H), 7.92 (s, 2H), 7.79 (s, 1H), 7.77 – 7.65 (m, 2H), 7.57 (d, *J* = 7.9 Hz, 1H), 7.22 (ddd, *J* = 8.1, 7.1, 1.2 Hz, 1H), 7.13 (ddd, *J* = 8.2, 7.1, 1.2 Hz, 1H), 6.93 – 6.05 (m, 4H), 2.02 (s, 3H) ppm; $^{13}\text{C NMR}$ (101 MHz, CDCl_3) δ = 140.0, 139.1, 138.1, 137.7, 137.3, 135.7, 132.7, 132.5, 131.5, 130.4, 129.5, 128.6, 128.5, 128.2, 127.1, 127.0, 126.9, 126.6, 126.1, 126.0, 125.3, 125.2, 124.7, 123.4, 122.9, 121.6, 121.5, 120.7, 20.8 ppm; **IR**: (neat, cm^{-1}) $\tilde{\nu}$ = 2918, 1590, 1508, 1488, 1465, 1458, 1439, 1406, 1388, 1341, 1316, 1040, 932, 849, 838, 818, 810, 775, 742, 727, 647, 598, 588, 500, 475, 465, 434, 420, 406; **HR-MS**: calcd *m/z* for $\text{C}_{31}\text{H}_{21}\text{S}^+$ [*M*+*H*] $^+$: 425.1359; found (ESI) 425.1355.

14-[4-(Benzyloxy)phenyl]benzo[*b*]chryseno[4,3-*d*]thiophene (165c):



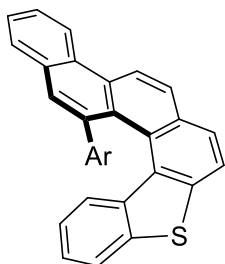
Ar = *p*-BnO(C₆H₄)

Prepared from **164c** (12.9 mg, 25 μmol, 1.0 equiv.), **162c** (1.8 mg, 1.29 μmol, 5 mol%) and AgSbF₆ (0.43 mg, 1.25 μmol, 5 mol%, 0.05 M in DCM) in DCM (0.5 mL) according to General Procedure F. The crude mixture was obtained as a yellow solid, **165c:198c**: >99:1, >99% conversion (determined by NMR), 96% enantiomeric excess.

The analytically pure sample of **165c** (11.7 mg, 91% yield) was obtained by semi-preparative HPLC; separation conditions: MeCN-H₂O 95-5, gradient to 100-0 over 30 min, 1.0 mL min⁻¹, 295 K. The *ee* was determined by chiral SFC: on SFC-IA3, CO₂/IPA = 65/35 isocratic at 2.5 mL min⁻¹ and backpressure regulator set to 3000 psi, 310 K; major enantiomer *t*_R = 1.94 min, minor enantiomer *t*_R = 5.63 min.

[*a*]_D²⁴: (96% *ee*) +1307° (*c* = 0.06, DCM); ¹H NMR (400 MHz, CDCl₃) δ = 8.78 (d, *J* = 8.1 Hz, 1H), 8.73 (d, *J* = 8.6 Hz, 1H), 8.06 (dd, *J* = 16.7, 8.3 Hz, 3H), 7.92 (s, 2H), 7.78 (s, 1H), 7.76 – 7.64 (m, 2H), 7.56 (d, *J* = 7.9 Hz, 1H), 7.42 – 7.29 (m, 5H), 7.24 – 7.09 (m, 2H), 6.99 – 5.92 (m, 4H), 4.84 (s, 2H) ppm; ¹³C NMR (101 MHz, CDCl₃) δ = 157.1, 139.6, 138.1, 137.8, 137.3, 137.2, 135.0, 132.7, 132.4, 131.5, 130.4, 129.8, 129.4, 128.5, 128.4, 128.0, 127.8, 127.2, 127.1, 126.9, 126.5, 126.02, 125.97, 125.3, 125.2, 124.6, 123.4, 122.9, 121.8, 121.5, 120.7, 113.0, 69.8 ppm; IR: (neat, cm⁻¹) $\tilde{\nu}$ = 1708, 1603, 1508, 1442, 1241, 1219, 1177, 1154, 1026, 894, 826, 781, 759, 746, 730, 698, 648, 637, 588, 571, 539, 512, 471, 432; HR-MS: calcd *m/z* for C₃₇H₂₅OS⁺ [M+H]⁺: 517.1621; found (ESI) 517.1611.

[4-(Benzo[*b*]chryseno[4,3-*d*]thiophen-14-yl)phenyl]trimethylsilane (165d):



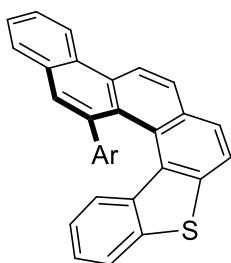
Ar = *p*-(Me₃Si)(C₆H₄)

Prepared from **164d** (12.1 mg, 25 μmol, 1.0 equiv.), **162c** (1.8 mg, 1.29 μmol, 5 mol%) and AgSbF₆ (0.43 mg, 1.25 μmol, 5 mol%, 0.05 M in DCM) in DCM (0.5 mL) according to general Procedure F. The crude mixture was obtained as a yellow solid, **165d:198d**: >99:1, >99% conversion (determined by NMR), 99% enantiomeric excess.

The analytically pure sample of **165d** (9.7 mg, 80% yield) was obtained by semi-preparative HPLC; separation conditions: MeCN/H₂O 80:20, gradient to 100:0 over 20 min, 1.0 mL min⁻¹, 295 K. The *ee* was determined by chiral SFC: on SFC-IA3, CO₂/IPA = 70/30 isocratic at 2.5 mL min⁻¹ and backpressure regulator set to 3000 psi, 310 K; major enantiomer *t*_R = 1.23 min, minor enantiomer *t*_R = 2.94 min.

$[\alpha]_{24}^D$: (99% *ee*) +1741° (*c* = 0.15, CHCl₃); ¹H NMR (400 MHz, CDCl₃) δ = 8.80 (d, *J* = 8.1 Hz, 1H), 8.74 (d, *J* = 8.7 Hz, 1H), 8.10 (d, *J* = 8.7 Hz, 1H), 8.05 (dd, *J* = 7.7, 1.3 Hz, 1H), 7.96 (d, *J* = 8.2 Hz, 1H), 7.92 (s, 2H), 7.84 (s, 1H), 7.78 – 7.67 (m, 2H), 7.49 (d, *J* = 7.9 Hz, 1H), 7.24 – 7.16 (m, 1H), 7.13 – 7.08 (m, 1H), 6.78 (collapsed m, 4H), 0.11 (s, 9H) ppm; ¹³C NMR (101 MHz, CDCl₃) δ = 142.1, 140.0, 138.4, 137.9, 137.8, 137.3, 132.7, 131.6, 131.1, 130.5, 129.8, 128.7, 128.4, 128.3, 127.3, 127.1, 126.9, 126.1, 126.0, 125.4, 125.2, 124.7, 123.6, 123.0, 121.8, 121.7, 120.9, –1.3 ppm; IR: (neat, cm⁻¹) $\tilde{\nu}$ = 3054, 2949, 1719, 1688, 1589, 1580, 1442, 1335, 1315, 1245, 1155, 1110, 1068, 1060, 1038, 948, 931, 895, 851, 836, 821, 780, 759, 729, 694, 647, 626, 590, 572, 536, 522, 504, 478, 466, 456, 447, 437, 428, 420; HR-MS: calcd *m/z* for C₃₃H₂₇SSi⁺ [M+H]⁺: 483.1597; found (ESI) 483.1595.

14-(4-Phenoxyphenyl)benzo[*b*]chryseno[4,3-*d*]thiophene (165e):

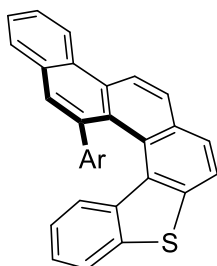


Prepared from **164e** (10.0 mg, 20 μmol, 1.0 equiv.), **162c** (1.8 mg, 1.29 μmol, 6.5 mol%) and AgSbF₆ (0.43 mg, 1.25 μmol, 6.25 mol%, 0.05 M in DCM) in DCM (0.5 mL) according to General Procedure F. The crude mixture was obtained as a yellow solid, **165e:198e**: >99:1, >99% conversion (determined by NMR), 97% enantiomeric excess.

Ar = *p*-PhO(C₆H₄) The analytically pure sample of **165e** (9.7 mg, 97% yield) was obtained by semi-preparative HPLC; separation conditions: MeCN/H₂O 90-10, gradient to 100:0 over 10 min, 1.0 mL min⁻¹, 295 K. The *ee* was determined by chiral SFC: on SFC-IA3, CO₂/IPA = 70/30 isocratic at 2.5 mL min⁻¹ and backpressure regulator set to 3000 psi, 310 K; major enantiomer *t*_R = 1.98 min, minor enantiomer *t*_R = 3.74 min.

$[\alpha]_{24}^D$: (97% *ee*) +1169° (*c* = 0.07, DCM); ¹H NMR (400 MHz, CDCl₃) δ = 8.85 (d, *J* = 8.1 Hz, 1H), 8.79 (d, *J* = 8.6 Hz, 1H), 8.18 – 8.07 (m, 3H), 7.98 (s, 2H), 7.87 (s, 1H), 7.83 – 7.71 (m, 3H), 7.43 – 7.35 (m, 2H), 7.31 (t, *J* = 6.9 Hz, 3H), 7.21 (t, *J* = 7.7 Hz, 1H), 7.15 – 7.07 (m, 1H), 6.72 (d, *J* = 7.4 Hz, 2H), 6.41 (s, br 2H) ppm; ¹³C NMR (101 MHz, CDCl₃) δ = 158.3, 154.8, 139.2, 138.1, 137.9, 137.8, 137.3, 132.6, 132.4, 131.6, 130.5, 130.1, 129.6, 129.4, 128.5, 128.3, 127.3, 127.1, 126.8, 126.2, 126.0, 125.6, 125.1, 124.8, 123.5, 123.2, 122.4, 121.8, 121.7, 120.8, 118.2, 117.6 ppm; IR: (neat, cm⁻¹) $\tilde{\nu}$ = 2920, 1590, 1504, 1487, 1467, 1459, 1441, 1393, 1320, 1230, 1200, 1103, 1041, 886, 868, 849, 838, 830, 812, 785, 778, 739, 698, 685, 649, 606, 597, 585, 532, 505, 487, 476, 466, 435; HR-MS: calcd *m/z* for C₃₆H₂₃OS⁺ [M+H]⁺: 503.1464; found (ESI) 503.1451.

14-(4-Butoxyphenyl)benzo[*b*]chryseno[4,3-*d*]thiophene (165f):

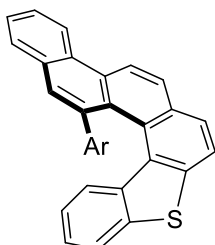


Prepared from **164f** (12.1 mg, 25 μmol , 1.0 equiv.), **162c** (1.8 mg, 1.29 μmol , 5.2 mol%) and AgSbF_6 (0.43 mg, 1.25 μmol , 5 mol%, 0.05 M in DCM) in DCM (0.5 mL) according to General Procedure F. The crude mixture was obtained as a yellow solid, **165f:198f**: >99:1, >99% conversion (determined by NMR), 97% enantiomeric excess.

Ar = *p*-(*n*-BuO) C_6H_4 The analytically pure sample of **165f** (12.0 mg, 99% yield) was obtained by semi-preparative HPLC; separation conditions: MeCN/ H_2O 95:5, gradient to 100:0 over 5 min, 1.0 mL min^{-1} , 295 K. The *ee* was determined by chiral SFC: on SFC-IA3, CO_2/IPA = 70/30 isocratic at 2.5 mL min^{-1} and backpressure regulator set to 3000 psi, 310 K; major enantiomer t_{R} = 1.53 min, minor enantiomer t_{R} = 4.52 min.

$[\alpha]_{\text{D}}^{24}$: (97% *ee*) +1559° (c = 0.07, DCM); $^1\text{H NMR}$ (400 MHz, CDCl_3) δ = 8.80 (dd, J = 7.9, 0.9 Hz, 1H), 8.76 (d, J = 8.8 Hz, 1H), 8.12 (d, J = 8.6 Hz, 1H), 8.09 – 8.03 (m, 2H), 7.96 (s, 2H), 7.79 (s, 1H), 7.76 – 7.67 (m, 2H), 7.61 (dq, J = 8.0, 0.7 Hz, 1H), 7.25 (ddd, J = 8.1, 7.1, 1.2 Hz, 1H), 7.15 (ddd, J = 8.2, 7.1, 1.2 Hz, 1H), 7.11 – 5.55 (m, 4H), 3.77 – 3.67 (m, 2H), 1.65 – 1.56 (m, 2H), 1.44 – 1.34 (m, 2H), 0.95 (t, J = 7.3 Hz, 3H) ppm; $^{13}\text{C NMR}$ (101 MHz, CDCl_3) δ = 157.8, 140.0, 138.5, 138.2, 137.7, 134.9, 133.1, 132.7, 131.9, 130.9, 130.1, 129.7, 128.7, 128.2, 127.5, 127.4, 126.9, 126.5, 126.4, 125.7, 125.6, 125.0, 123.7, 123.4, 122.1, 121.9, 121.1, 113.0, 68.0, 31.5, 19.5, 14.0 ppm; IR: (neat, cm^{-1}) $\tilde{\nu}$ = 3054, 2955, 2929, 2869, 1605, 1580, 1508, 1466, 1459, 1443, 1407, 1389, 1382, 1338, 1316, 1305, 1283, 1277, 1262, 1240, 1220, 1176, 1159, 1143, 1125, 1112, 1068, 1040, 1027, 1010, 973, 948, 931, 894, 882, 850, 826, 781, 759, 731, 701, 670, 649, 631, 600, 598, 573, 539, 516, 476, 465, 456, 435, 420; HR-MS: calcd m/z for $[\text{C}_{34}\text{H}_{27}\text{OS}^+ [\text{M}+\text{H}]^+$: 483.1777; found (ESI) 483.1765.

14-(4-Fluorophenyl)benzo[*b*]chryseno[4,3-*d*]thiophene (165g):



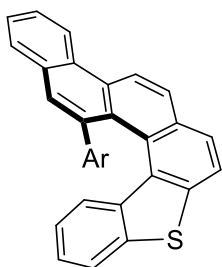
Prepared from **164g** (10.7 mg, 25 μmol , 1.0 equiv.), **162c** (1.8 mg, 1.29 μmol , 5 mol%) and AgSbF_6 (0.43 mg, 1.25 μmol , 5 mol%, 0.05 M in DCM) in DCM (0.5 mL) according to General Procedure F. The crude mixture was obtained as a yellow solid, **165g:198g** >99:1, >99% conversion (determined by NMR), 93% enantiomeric excess.

Ar = *p*-F(C_6H_4) The analytically pure sample of **165g** (3.7 mg, 35% yield) was obtained by semi-preparative HPLC; separation conditions: MeCN/ H_2O 90-10, gradient to 100-0 over 10 min, 1.0 mL min^{-1} , 295 K. The *ee* was determined by chiral SFC: on SFC-IA3, CO_2/IPA = 70/30

isocratic at 2.5 mL min⁻¹ and backpressure regulator set to 3000 psi, 310 K; major enantiomer $t_R = 1.00$ min, minor enantiomer $t_R = 1.70$ min.

$[\alpha]_{24}^D$: (93% *ee*) +1599° ($c = 0.23$, DCM); ¹H NMR (400 MHz, CDCl₃) $\delta = 8.87 - 8.82$ (m, 1H), 8.78 (d, $J = 8.6$ Hz, 1H), 8.14 (d, $J = 8.7$ Hz, 1H), 8.10 - 8.04 (m, 2H), 7.98 (s, 2H), 7.84 - 7.71 (m, 3H), 7.66 (dt, $J = 8.0, 0.9$ Hz, 1H), 7.28 (dd, $J = 8.0, 1.2$ Hz, 2H), 7.18 (ddd, $J = 8.2, 7.1, 1.2$ Hz, 1H), 6.41 (s, 3H) ppm; ¹³C NMR (101 MHz, CDCl₃) $\delta = 162.4, 160.0, 138.9, 138.3, 138.03$ (d, $J_{CF} = 3.3$ Hz), 137.95, 137.2, 132.5, 132.3, 131.6, 130.4, 130.15, 129.6, 128.50, 128.45, 127.3, 127.1, 126.9, 126.1, 125.8, 125.4, 124.9, 124.4, 123.5, 123.0, 122.1, 121.7, 120.8, 113.3 (d, $J_{CF} = 1.8$ Hz) ppm; ¹⁹F NMR (377 MHz, CDCl₃) $\delta = -116.45$ ppm; IR: (neat, 420 cm⁻¹) $\tilde{\nu} = 1592, 1505, 1488, 1466, 1458, 1442, 1407, 1319, 1214, 1198, 895, 852, 829, 812, 778, 751, 742, 732, 687, 648, 598, 587, 572, 533, 507, 493, 477, 468, 457, 436$; HR-MS: calcd m/z for C₃₀H₁₇FS⁺ [M]⁺: 428.1030; found (EI) 428.1030.

14-[4-(Trifluoromethyl)phenyl]benzo[*b*]chryseno[4,3-*d*]thiophene (165h):

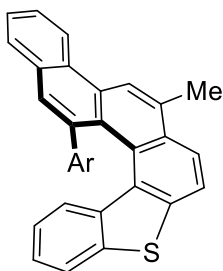


Prepared from **164h** (12.0 mg, 25 μ mol, 1.0 equiv.), **162c** (1.8 mg, 1.29 μ mol, 5 mol%) and AgSbF₆ (0.43 mg, 1.25 μ mol, 5 mol%, 0.05 M in DCM) in DCM (0.5 mL) according to General Procedure F. The crude mixture was obtained as a yellow solid, **165h:198h**: >99:1, >99% conversion (determined by NMR), 68% enantiomeric excess.

Ar = *p*-(CF₃)C₆H₄ The analytically pure sample of **165g** (11.4 mg, 95% yield) was obtained by semi-preparative HPLC; separation conditions: MeCN/H₂O 80-20, gradient to 100-0 over 30 min, 1.0 mL min⁻¹, 295 K. The *ee* was determined by chiral SFC: on SFC-IA3, CO₂/IPA = 70/30 isocratic at 2.5 mL min⁻¹ and backpressure regulator set to 3000 psi, 310 K; major enantiomer $t_R = 0.65$ min, minor enantiomer $t_R = 1.20$ min.

¹H NMR (300 MHz, CDCl₃) $\delta = 8.81$ (d, $J = 8.2$ Hz, 1H), 8.75 (d, $J = 8.7$ Hz, 1H), 8.12 (d, $J = 8.7$ Hz, 1H), 8.07 (dd, $J = 7.8, 1.6$ Hz, 1H), 7.97 (d, $J = 8.1$ Hz, 1H), 7.94 (s, 2H), 7.84 - 7.73 (m, 2H), 7.71 (d, $J = 7.0$ Hz, 1H), 7.58 (d, $J = 7.9$ Hz, 1H), 7.22 (d, $J = 7.9$ Hz, 1H), 7.17 - 7.08 (m, 1H), 6.89 (s br, 4H) ppm; ¹³C NMR (101 MHz, CDCl₃) $\delta = 145.4, 138.42, 138.36, 138.1, 136.9, 132.4, 132.2, 131.6, 130.4, 129.9, 128.9, 128.8, 128.7, 128.3, 128.0, 127.7, 127.5, 127.3, 127.22, 126.16, 125.54, 125.50, 125.4, 124.5, 124.3, 123.5, 123.1, 122.7, 122.1, 121.8, 120.8, 120.0$ ppm; ¹⁹F NMR (377 MHz, CDCl₃) $\delta = -62.89$ ppm; IR: (neat, cm⁻¹) $\tilde{\nu} = 3853, 3749, 3734, 3725, 3709, 3691, 3676, 3648, 3628, 3607, 3597, 2359, 1615, 1558, 1540, 1520, 1507, 1498, 1110, 1066, 907, 848, 836, 829, 781, 740, 732, 648$; HR-MS: calcd m/z for C₃₁H₁₇F₃S⁺ [M]⁺: 478.0998; found (EI) 478.0997.

14-(4-Methoxyphenyl)-6-methylbenzo[*b*]chryseno[4,3-*d*]thiophene (165i):

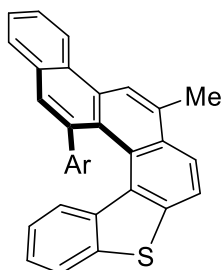


Prepared from **164i** (11.4 mg, 25 μmol , 1.0 equiv.), **162c** (1.8 mg, 1.29 μmol , 5.2 mol%) and AgSbF_6 (4.29 mg, 1.25 μmol , 5 mol%, 0.05 M in DCM) in DCM (0.5 mL) according to General Procedure F. The crude mixture was obtained as a yellow solid, **165i**:**198i**: >99:1, >99% conversion (determined by NMR), 91% enantiomeric excess.

Ar = *p*-MeO(C₆H₄) The analytically pure sample of **165i** (11.1 mg, 97% yield) was obtained by semi-preparative HPLC; separation conditions: MeCN/H₂O 90:10, gradient to 100:0 over 10 min, 1.0 mL min⁻¹, 295 K. The *ee* was determined by chiral SFC: on SFC-IA3, CO₂/IPA = 70/30 isocratic at 2.5 mL min⁻¹ and backpressure regulator set to 3000 psi, 310 K; major enantiomer t_R = 1.25 min, minor enantiomer t_R = 3.92 min.

$[\alpha]_{24}^D$: (91% *ee*) +1515° (c = 0.16, DCM); ¹H NMR (400 MHz, CDCl₃) δ = 8.78 (d, J = 8.1 Hz, 1H), 8.56 (s, 1H), 8.09 (d, J = 8.6 Hz, 1H), 7.98 (dt, J = 16.4, 8.3 Hz, 3H), 7.69 (h, J = 7.0 Hz, 3H), 7.58 (d, J = 7.9 Hz, 1H), 7.22 (t, J = 7.5 Hz, 1H), 7.11 (t, J = 7.6 Hz, 1H), 6.65 (collapsed m, 2H), 6.22 (s br, 2H), 3.58 (s, 3H), 2.97 (s, 3H) ppm; ¹³C NMR (101 MHz, CDCl₃) δ = 157.8, 139.6, 138.2, 137.6, 137.4, 134.8, 133.2, 132.8, 132.6, 131.1, 130.2, 129.7, 129.0, 128.4, 127.1, 126.8, 126.5, 126.3, 125.3, 124.6, 124.2, 123.3, 123.0, 122.1, 121.8, 121.3, 121.2, 111.9, 55.2, 20.5 ppm; IR: (neat, cm⁻¹) $\tilde{\nu}$ = 1607, 1509, 1460, 1388, 862, 848, 831, 816, 774, 647, 599, 585, 505, 495, 487, 470, 458, 441, 422, 406; HR-MS: calcd m/z for C₃₂H₂₃SO⁺ [M+H]⁺: 455.1464; found (ESI) 455.1453.

6-Methyl-14-(*p*-tolyl)benzo[*b*]chryseno[4,3-*d*]thiophene (165j):



Prepared from **164j** (11.0 mg, 25 μmol , 1.0 equiv.), **162c** (1.8 mg, 1.29 μmol , 5.2 mol%) and AgSbF_6 (0.43 mg, 1.25 μmol , 5 mol%, 0.05 M in DCM) in DCM (0.5 mL) according to General Procedure F. The crude mixture was obtained as a yellow solid, **165j**:**198j**: >99:1, >99% conversion (determined by NMR), 95% enantiomeric excess.

Ar = *p*-Me(C₆H₄) The analytically pure sample of **165j** (10.6 mg, 96% yield) was obtained by semi-preparative HPLC; separation conditions: MeCN/H₂O 90:10, gradient to 100:0 over 10 min, 1.0 mL min⁻¹, 295 K. The *ee* was determined by chiral SFC: on SFC-IA3, CO₂/IPA = 70/30 isocratic at 2.5 mL min⁻¹ and backpressure regulator set to 3000 psi, 310 K; major enantiomer t_R = 1.12 min, minor enantiomer t_R = 3.02 min.

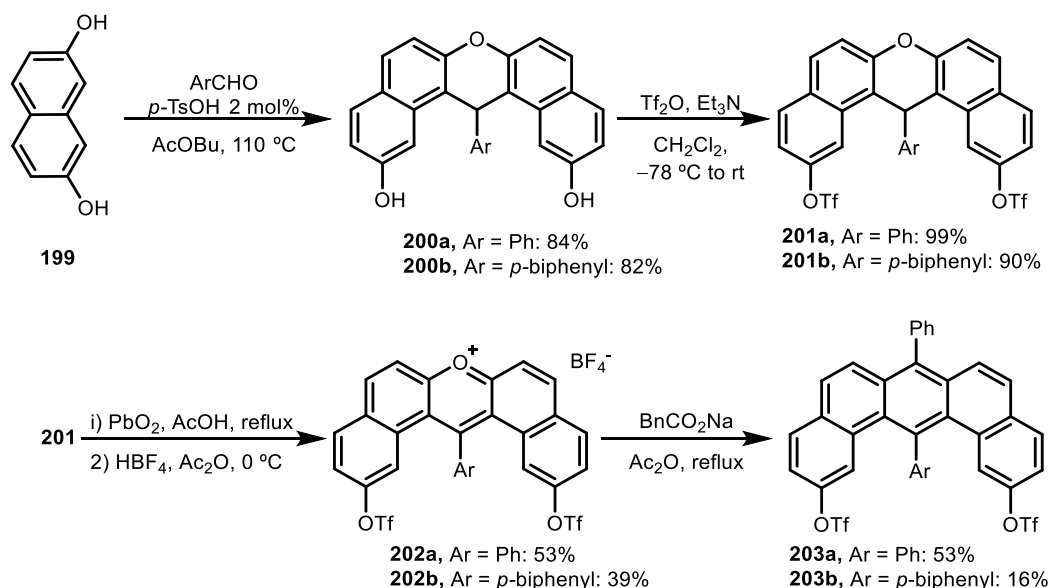
$[\mathbf{a}]_{24}^D$: (95% *ee*) +1334° (*c* = 0.10, DCM); $^1\text{H NMR}$ (400 MHz, CDCl_3) δ = 8.79 (d, *J* = 8.2 Hz, 1H), 8.56 (s, 1H), 8.09 (d, *J* = 8.6 Hz, 1H), 8.01 (dd, *J* = 8.1, 3.3 Hz, 2H), 7.95 (d, *J* = 8.5 Hz, 1H), 7.77 – 7.63 (m, 3H), 7.56 (d, *J* = 7.9 Hz, 1H), 7.21 (t, *J* = 7.5 Hz, 1H), 7.11 (t, *J* = 7.6 Hz, 1H), 6.46 (d, *J* = 7.4 Hz, 4H), 2.97 (s, 3H), 2.03 (s, 3H) ppm; $^{13}\text{C NMR}$ (101 MHz, CDCl_3) δ = 140.0, 139.2, 138.1, 137.6, 137.3, 135.5, 133.2, 132.79, 132.76, 131.1, 130.1, 129.2, 128.5, 128.44, 127.41, 126.9, 126.8, 126.5, 126.4, 125.3, 124.6, 124.2, 123.3, 123.0, 122.1, 121.7, 121.3, 121.2, 20.8, 20.4 ppm; **IR**: (neat, cm^{-1}) $\tilde{\nu}$ = 2920, 1590, 1559, 1506, 1487, 1459, 1440, 1408, 1388, 1362, 1341, 1320, 1200, 1040, 886, 868, 849, 838, 830, 813, 777, 740, 730, 686, 647, 607, 597, 585, 531, 504, 497, 488, 477, 467; **HR-MS**: calcd *m/z* for $\text{C}_{32}\text{H}_{23}\text{S}^+$ $[\text{M}+\text{H}]^+$: 439.1515; found (ESI) 439.1501.

6.4. Synthesis of in-Fjord substituted expanded helicenes

6.4.1. Synthesis of the starting materials

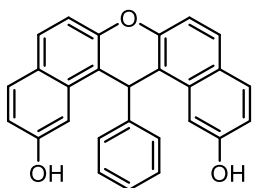
Synthesis of benzo[*m*]tetraphene core

The synthesis of benzo[*m*]tetraphene cores **203a-b** was carried out by a modification of a synthetic route previously reported by Müllen, Fasel, Räder and co-workers.^[238,239] The Scheme 60 below summarizes the sequence.



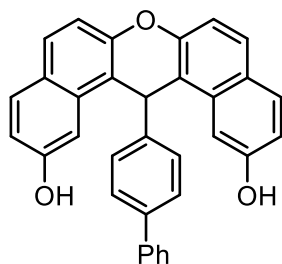
Scheme 57: Synthesis of the benzo[*m*]tetraphene core platform.

14-Phenyl-14*H*-dibenzo[*a,j*]xanthene-2,12-diol (**200a**):



A round-bottom flask equipped with a stirring bar was charged with 2,7-dihydroxynaphthalene (**199**) (32.03 g, 200 mmol, 2 equiv.) and butyl acetate (200 mL) under ambient atmosphere. After 5 minutes, *p*-TsOH×H₂O (380 mg, 2.0 mmol, 2 mol%) was added, followed by freshly distilled benzaldehyde (10.61 g, 10.2 mL, 100 mmol, 1.0 equiv.). The reaction mixture was heated to 110 °C in a pre-heated oil bath and stirred for 32 h at this temperature with TLC monitoring, then allowed to cool down to room temperature. The excess of solvent was removed under vacuo. The oily residue was then triturated with diethyl ether, the formed solid was filtered off and washed thoroughly with cold diethyl ether (3 × 20 mL). A first crop of pure diol **200a** (26.53 g, 68 mmol, 68%) was obtained as a brown solid. The filtrate was concentrated, and the process repeated twice affording additional crop of 6.44 g (overall yield 32.97 g, 84 mmol, 84%). ¹H NMR: (400 MHz, acetone-*d*₆) δ = 8.73 (s, 2H), 7.86 (d, *J* = 2.3 Hz, 2H), 7.81 – 7.72 (m, 4H), 7.63 – 7.57 (m, 2H), 7.29 (d, *J* = 8.8 Hz, 2H), 7.16 (t, *J* = 7.8 Hz, 2H), 7.06 (dd, *J* = 8.8, 2.3 Hz, 2H), 7.03 – 6.96 (m, 1H), 6.27 (s, 1H) ppm; ¹³C NMR: (100 MHz, acetone-*d*₆) δ = 157.3, 150.1, 146.3, 134.2, 131.3, 129.7, 129.3, 129.2, 127.2, 126.8, 117.2, 117.1, 115.5, 106.6, 38.9 ppm; IR: (neat, cm⁻¹) $\tilde{\nu}$ = 3345, 1704, 1637, 1518, 1445, 1394, 1232, 1040, 927, 825, 757, 703, 614, 507; HR-MS: calcd *m/z* for C₂₇H₁₉O₃ [M+H]⁺: 391.1329; found (ESI) 391.1324.

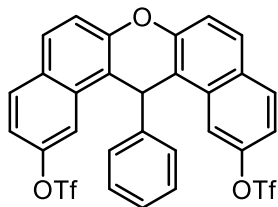
14-([1,1'-Biphenyl]-4-yl)-14*H*-dibenzo[*a,j*]xanthene-2,12-diol (**200b**):



A round-bottom flask was charged with 2,7-dihydroxynaphthalene (**199**) (17.3 g, 108.0 mmol, 2 equiv.), *p*-TsOH×H₂O (513.6 mg, 2.7 mmol, 5 mol%), [1,1'-biphenyl]-4-carbaldehyde (9.84 g, 54.0 mmol, 1 equiv.) and butyl acetate (100 mL). The reaction mixture was stirred at 130 °C for 36 h with TLC monitoring. Once complete conversion was observed, the mixture was allowed to cool down to room temperature. Then, volatiles were removed under reduced pressure and washed with a hexane:Et₂O 1:1 mixture. Compound **200b** (20.56 g, 44.1 mmol, 82%) was obtained as a white solid. ¹H NMR: (400 MHz, DMSO-*d*₆) δ = 9.94 (s, 2H), 7.83 – 7.73 (m, 6H), 7.61 (d, *J* = 7.9 Hz, 2H), 7.51 – 7.45 (m, 4H), 7.33 (dq, *J* = 18.6, 6.5, 5.6 Hz, 5H), 7.03 (dd, *J* = 8.8, 2.1 Hz, 2H), 6.20 (s, 1H) ppm; ¹³C NMR: (100 MHz, DMSO-*d*₆) δ = 157.0, 149.0, 144.7, 140.2, 138.8, 133.2, 130.8, 129.2, 129.1, 129.0, 127.7, 127.2, 127.0, 125.5, 117.0, 115.9, 114.6, 105.6, 37.3 ppm; IR: (neat, cm⁻¹) $\tilde{\nu}$ = 3191, 3026, 2891, 1634, 1615, 1598, 1517, 1486, 1447, 1396, 1257, 1231, 1208, 1158,

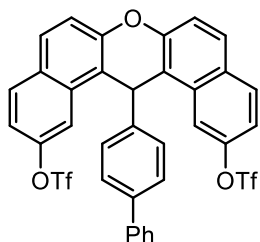
1135, 1074, 1007, 914, 851, 827, 758, 742, 723, 693, 665, 608, 518, 502, 454, 440, 431, 411;
HR-MS: calcd m/z for $C_{33}H_{23}O_3$ $[M+H]^+$: 467.1642; found (ESI) 467.1630.

14-Phenyl-14H-dibenzo[*a,j*]xanthene-2,12-diyl bis(trifluoromethanesulfonate) (201a):



In a 500-mL double-necked round-bottom flask equipped with an oval stirring bar, diol **200a** (17.57 g, 45 mmol, 1 equiv.) was suspended in anhydrous dichloromethane (150 mL). The suspension was vigorously stirred for 5 min and triethylamine (27.3 g, 37.6 mL, 270 mmol, 6.0 equiv.) was added. The obtained dark-brown solution was cooled down to -78 °C and after stirring for 5 min at that temperature, trifluoromethanesulfonic anhydride (28.2 g, 16.8 mL, 100 mmol, 2.2 equiv.) was added dropwise. After an additional 15 min, the bath was removed and the reaction mixture was allowed to reach room temperature. The reaction was monitored by TLC until complete consumption of the starting material was observed. After approximately 1 h, the reaction was quenched by addition of HCl 2 M solution (50 mL). The insoluble solid formed was dissolved by addition of chloroform (100 mL) and the aqueous acidic phase was extracted with $CHCl_3$ (3×100 mL), washed with 2 M HCl (2×100 mL), water (100 mL) and 1 M NaOH (2×100 mL). The combined organic layers were dried over Na_2SO_4 , filtered over a silica plug and concentrated in vacuo affording **201a** (29.22 g, 44.6 mmol, 99%) as a white solid, which was pure enough to continue the desired synthesis. **1H NMR:** (400 MHz, $CDCl_3$) δ = 8.24 (d, J = 2.4 Hz, 2H), 7.93 – 7.83 (m, 4H), 7.56 (d, J = 8.9 Hz, 2H), 7.50 – 7.44 (m, 2H), 7.33 (dd, J = 8.9, 2.4 Hz, 2H), 7.22 (t, J = 7.7 Hz, 2H), 7.12 – 7.04 (m, 1H), 6.16 (s, 1H) ppm; **^{13}C NMR:** (100 MHz, $CDCl_3$) δ = 149.2, 148.2, 143.4, 131.9, 131.3, 130.1, 129.1, 128.9, 128.1, 127.1, 119.3, 118.9 (q, J_{CF} = 321.2 Hz), 118.0, 116.9, 114.6, 38.7 ppm; **^{19}F NMR:** (282 MHz, $CDCl_3$) δ (ppm) = -72.7 ; **IR:** (neat, cm^{-1}) $\tilde{\nu}$ = 1596, 1518, 1416, 1198, 1137, 1008, 885, 833, 702, 589; **HR-MS:** calcd m/z for $C_{29}H_{16}F_6NaO_7S_2^+$ $[M+Na]^+$: 677.0134; found (ESI) 677.0122.

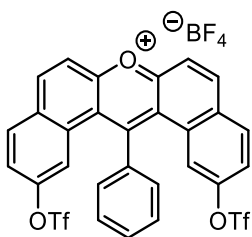
14-([1,1'-Biphenyl]-4-yl)-14H-dibenzo[*a,j*]xanthene-2,12-diyl bis(trifluoromethanesulfonate) (201b):



Compound **200b** (7.0 g, 15 mmol, 1 equiv.) was suspended in anhydrous CH_2Cl_2 (75 mL) under N_2 atmosphere, then NEt_3 (9.1 g, 12.5 mL, 90 mmol, 6 equiv.) was added at room temperature. The brown solution formed was allowed to stir for 5 min. Then, the reaction mixture was cooled down to -78 °C, and trifluoromethanesulfonic anhydride (9.52 g, 5.7 mL, 33.7 mmol, 2.25 equiv.) was added dropwise. Once the addition was finished, the reaction mixture was allowed to stir for an

additional 10 min at $-78\text{ }^{\circ}\text{C}$, then the cooling bath was removed, and the mixture was allowed to warm up to room temperature. Once the starting material was consumed (1 h), the reaction was quenched by addition of aqueous NH_4Cl saturated solution. Then additional CH_2Cl_2 was added in order to dissolve any solid, and the aqueous phase was extracted twice. The combined organic layers were washed with 1 M HCl ($2 \times 40\text{ mL}$), water ($2 \times 30\text{ mL}$), 1 M NaOH ($2 \times 30\text{ mL}$), dried over Na_2SO_4 and evaporated under reduced pressure, affording almost pure product **201b**, which was additionally purified by column chromatography on silica gel (cyclohexane/ CH_2Cl_2 1:1) to deliver pure ditriflate **201b** as a brown solid (9.86 g, 13.5 mmol, 90%). **$^1\text{H NMR}$** : (400 MHz, CDCl_3) $\delta = 8.29$ (d, $J = 2.4\text{ Hz}$, 2H), 7.91 (d, $J = 8.9\text{ Hz}$, 2H), 7.86 (d, $J = 9.0\text{ Hz}$, 2H), 7.58 (d, $J = 8.9\text{ Hz}$, 2H), 7.53 (d, $J = 8.3\text{ Hz}$, 2H), 7.46 – 7.41 (m, 3H), 7.39 – 7.32 (m, 4H), 7.29 (d, $J = 6.7\text{ Hz}$, 2H), 6.21 (s, 1H) ppm; **$^{13}\text{C NMR}$** : (100 MHz, CDCl_3) $\delta = 149.3$, 148.3, 142.4, 140.3, 140.0, 131.9, 131.4, 130.1, 129.2, 128.7, 128.5, 127.7, 127.3, 126.9, 119.3, 118.9 (q, $J_{\text{CF}} = 321.2\text{ Hz}$), 118.1, 116.8, 114.6, 38.4 ppm; **$^{19}\text{F NMR}$** : (377 MHz, CDCl_3) δ (ppm) = -72.5 ; **IR**: (neat, cm^{-1}) $\tilde{\nu} = 3837$, 3412, 1747, 1563, 1225, 1172, 979, 771, 707, 607, 598, 558, 545, 518, 510, 502, 455, 442, 432, 423, 413; **HR-MS**: calcd m/z for $\text{C}_{35}\text{H}_{20}\text{F}_6\text{NaO}_7\text{S}_2^+$ $[\text{M}+\text{Na}]^+$: 753.0447; found (ESI) 753.0434.

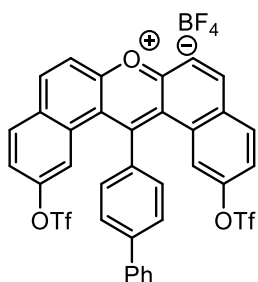
14-([1,1'-Biphenyl]-4-yl)-2,12-bis{[(trifluoromethyl)sulfonyl]oxy}dibenzo[*a,j*]xanthen-7-ium tetrafluoroborate (202a):



A 500-mL round-bottom flask equipped with an oval stirring bar was charged with **201a** (20.0 g, 30.56 mmol, 1 equiv.) and glacial acetic acid (200 mL). The obtained solution was vigorously stirred for 5 min, and PbO_2 (10.95 g, 45.8 mmol, 1.5 equiv.) was added in one portion. The flask was then immersed in a pre-heated oil bath and stirred under reflux. The reaction was monitored by TLC, and after 24 h, a second portion of PbO_2 (7.3 g, 1.0 equiv., 30.52 mmol) was added. The reaction mixture was allowed to stir for another 24 h, then it was allowed to cool down to room temperature and poured into ice. The beige solid formed was collected by filtration, washed with water and dried under vacuum (10^{-3} mbar) at $80\text{ }^{\circ}\text{C}$. Once dried, the solid was immediately used in the next step. Thus, under N_2 atmosphere, a round-bottom flask was charged with the solid intermediate, acetic anhydride (90 mL) and anhydrous toluene (60 mL). The mixture was cooled down to $0\text{ }^{\circ}\text{C}$ in an ice-water bath, and HBF_4 (48% w/w in water; ca. 20 mL, 153 mmol, 5 equiv.) was added dropwise until no further precipitation was observed. The bright orange solid formed was filtered and washed with anhydrous diethyl ether affording pyrylium salt **202a** as a bright orange solid (11.9 g, 16.1 mmol, 53%). **$^1\text{H NMR}$** : (400 MHz, CD_2Cl_2) $\delta = 8.85 - 8.75$ (m, 2H), 8.34 (d, $J = 8.5\text{ Hz}$, 2H), 8.23 (d, $J = 8.8\text{ Hz}$, 2H), 7.95 (d, $J = 7.8\text{ Hz}$, 3H), 7.73 – 7.59 (m, 2H), 7.55 (d, $J = 8.1\text{ Hz}$, 2H), 6.95 (d, J

= 1.9 Hz, 2H) ppm; ^{13}C NMR: (100 MHz, CD_2Cl_2) δ = 169.1, 160.5, 149.7, 146.7, 136.6, 134.0, 133.2, 132.7, 132.1, 130.4, 125.8, 123.2, 122.8 (q, J_{CF} = 320.5 Hz), 122.1, 121.3, 119.2 ppm; ^{19}F NMR: (282 MHz, $\text{DMSO}-d_6$) δ (ppm) = -72.7, -148.2; IR: (neat, cm^{-1}) $\tilde{\nu}$ = 1599, 1518, 1419, 1337, 1203, 1136, 1004, 888, 837, 704, 625, 501; HR-MS: calcd m/z for $\text{C}_{29}\text{H}_{15}\text{F}_6\text{O}_7\text{S}_2^+$ [$\text{M}-\text{BF}_4$] $^+$: 653.0158; found 653.0152.

14-([1,1'-Biphenyl]-4-yl)-2,12-bis{[(trifluoromethyl)sulfonyl]oxy}dibenzo[*a,j*]xanthen-7-ium tetrafluoroborate (202b):

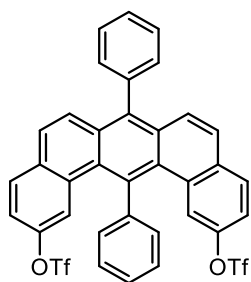


Under open air, a round-bottom flask was charged with the compound **201b** (9.76 g, 13.36 mmol, 1 equiv.) and glacial acetic acid (120 mL).

Then, the mixture was stirred under reflux in a pre-heated oil bath and PbO_2 (10 g, 41.8 mmol, 3.13 equiv.) was added in one portion. The reaction mixture was allowed to stir under reflux for 24 h until complete conversion of **201b** was observed by TLC. After that, the

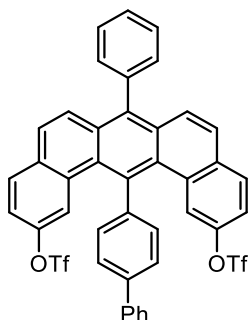
mixture was allowed to cool down to room temperature and poured into a beaker with ice. The precipitate was collected by filtration, washed with water and dried under high vacuum at 80 °C to remove the remaining solvent. The black fine powder obtained was immediately used in the next reaction. Thus, a two-neck round-bottom flask was charged under N_2 atmosphere with the black fine powder obtained in the previous step, anhydrous toluene (32 mL) and acetic anhydride (40 mL). The obtained solution was cooled down to 0 °C and HBF_4 (48% w/w in water, 10.15 mL, 77 mmol, 5 equiv.) was added dropwise until no more formation of precipitate was observed (30 min to 1 h). The dark orange solid obtained was filtered under N_2 atmosphere and dried by washing with anhydrous Et_2O (2×25 mL) affording pure salt **202b** (4.23 g, 5.18 mmol, 39% over two steps) as a dark orange solid. ^1H NMR: (400 MHz, CD_2Cl_2) δ = 8.90 (dt, J = 9.1, 0.7 Hz, 2H), 8.45 (d, J = 9.2 Hz, 2H), 8.34 (d, J = 8.8 Hz, 2H), 8.27 – 8.17 (m, 2H), 7.89 – 7.81 (m, 2H), 7.74 – 7.66 (m, 4H), 7.60 (tt, J = 6.8, 0.9 Hz, 2H), 7.55 – 7.50 (m, 1H), 7.32 – 7.28 (m, 2H) ppm; ^{13}C NMR: (100 MHz, CD_2Cl_2) δ = 168.8, 160.5, 149.7, 146.6, 146.2, 138.9, 135.1, 134.0, 132.1, 131.7, 130.4, 129.0, 128.8, 127.6, 126.4, 123.2, 122.2, 121.5, 119.2, 118.5 (q, J_{CF} = 320.4 Hz) ppm; ^{19}F NMR: (282 MHz, $\text{DMSO}-d_6$) δ (ppm) = -73.2, -153.1; IR: (neat, cm^{-1}) $\tilde{\nu}$ = 3541, 3086, 1618, 1587, 1553, 1511, 1469, 1421, 1374, 1334, 1247, 1207, 1135, 1056, 1028, 934, 884, 848, 808, 781, 762, 748, 736, 695, 668, 630, 608, 592, 541, 522; HR-MS: calcd m/z for $\text{C}_{35}\text{H}_{19}\text{F}_6\text{O}_7\text{S}_2^+$ [$\text{M}-\text{BF}_4$] $^+$: 729.0471; found 729.0456.

7,14-Diphenylbenzo[*m*]tetraphene-2,12-diyl bis(trifluoromethanesulfonate) (**203a**):



A two-neck round-bottom flask under nitrogen atmosphere was charged with pyrylium salt **202a** (10.00 g, 13.5 mmol, 1.0 equiv.), sodium phenylacetate (8.12 g, 51.35 mmol, 3.8 equiv.) and acetic anhydride (150 mL). The flask was immersed into a pre-heated oil bath and heated under reflux for 12 h. During the course of the reaction CO₂ gas evolution was observed. After 12 h, the mixture was allowed to cool down to room temperature, and a precipitate was formed. The latter was filtered off and washed with MeOH, affording crude **203a** almost pure as a grey solid. The solid was subsequently dissolved in chloroform and precipitated by addition of hexane affording analytically pure **203a** (5.20 g, 7.16 mmol, 53%) as a white solid. ¹H NMR: (400 MHz, CDCl₃) δ = 7.84 (d, *J* = 8.7 Hz, 2H), 7.81 – 7.55 (m, 10H), 7.55 – 7.49 (m, 2H), 7.47 (dd, *J* = 7.2, 1.8 Hz, 2H), 7.35 (dd, *J* = 8.6, 2.4 Hz, 2H), 7.19 (d, *J* = 2.4 Hz, 2H) ppm; ¹³C NMR: (101 MHz, CDCl₃) δ = 145.8, 143.3, 138.8, 138.6, 138.2, 133.3, 132.1, 131.7, 131.6, 130.9, 130.6, 129.7, 129.4, 128.7, 128.1, 127.4, 126.9, 126.8, 122.1, 119.5, 118.6 (q, *J* = 320.8 Hz) ppm; ¹⁹F NMR: (377 MHz, CDCl₃) δ (ppm) = -73.3; IR: (neat, cm⁻¹) $\tilde{\nu}$ = 3006, 1601, 1512, 1424, 1211, 1136, 1023, 915, 841, 763, 703, 597; HR-MS: calcd *m/z* for C₃₆H₂₀F₆NaO₆S₂⁺ [M+Na]⁺: 749.0498; found (ESI) 749.0498.

14-([1,1'-Biphenyl]-4-yl)-7-phenylbenzo[*m*]tetraphene-2,12-diyl bis(trifluoromethanesulfonate) (**203b**):

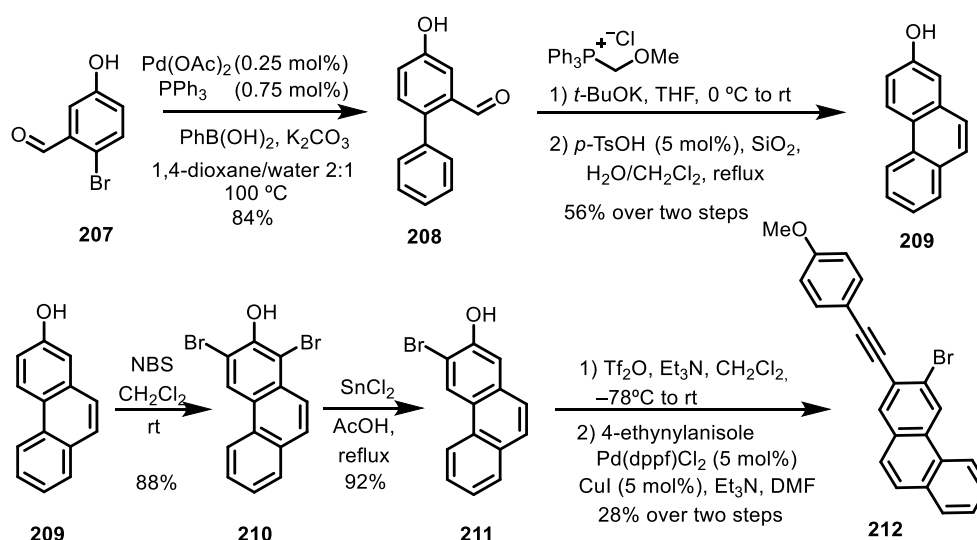


Under inert atmosphere, a two-neck round-bottom flask was charged with pyrylium salt **202b** (4.23 g, 5.18 mmol, 1 equiv.), sodium-2-phenylacetate (4.1 g, 25.8 mmol, 5 equiv.) and acetic anhydride (52 mL). The flask was immersed into a pre-heated oil bath, and the reaction mixture was stirred under reflux for 12 h. During the course of the reaction gas evolution was observed. After 12 h, the mixture was allowed to cool down to room temperature, and a precipitate was formed. The solid was filtered off and washed thoroughly with MeOH, affording **203b** as a grey solid in almost pure form. Final by column chromatography on silica gel (eluent hexane/CHCl₃ 2:1) furnished analytically pure **203b** (670 mg, 0.835 mmol, 16%). ¹H NMR: (400 MHz, CDCl₃) δ = 7.94 (d, *J* = 7.8 Hz, 2H), 7.84 (dd, *J* = 17.0, 8.1 Hz, 4H), 7.61 (dt, *J* = 26.4, 8.1 Hz, 11H), 7.48 (dt, *J* = 10.4, 5.2 Hz, 3H), 7.42 – 7.32 (m, 4H) ppm; ¹³C NMR: (101 MHz, CDCl₃) δ = 145.8, 143.1, 142.1, 140.6, 138.8, 138.18, 138.16, 133.4, 132.1, 131.8, 131.3, 130.7, 130.4, 129.7, 128.8, 128.1, 127.7, 127.6, 127.5, 126.9, 126.8, 122.2, 120.1, 119.6, 116.9 ppm; ¹⁹F NMR: (377 MHz, CDCl₃) δ (ppm) = -73.3; IR: (neat, cm⁻¹) $\tilde{\nu}$ = 3038, 2055, 1601, 1487, 1425, 1390, 1333, 1214,

1137, 1023, 951, 932, 916, 897, 885, 842, 831, 763, 747, 717, 698, 647, 627, 597, 565; **HR-MS**: calcd m/z for $C_{42}H_{25}F_6O_6S_2^+$ $[M+H]^+$: 803.0991; found (ESI) 803.0978.

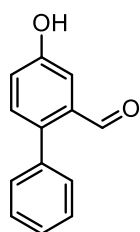
Synthesis of bromoethynylarene precursors

The bromoethynylarenes 1-bromo-2-[(4-methoxyphenyl)ethynyl]benzene **189a**^[267] and 1-bromo-2-[(4-methoxyphenyl)ethynyl]naphthalene, precursor of compound **205**^[274], were synthesized according to previously published procedures, as stated in the beginning of this Section. On the other hand, 3-bromo-2-[(4-methoxyphenyl)ethynyl]phenanthrene **212** was prepared as shown below in Scheme 58:



Scheme 58: Synthesis of the bromoethynylarene **212**.

4-Hydroxy-[1,1'-biphenyl]-2-carbaldehyde (**208**):

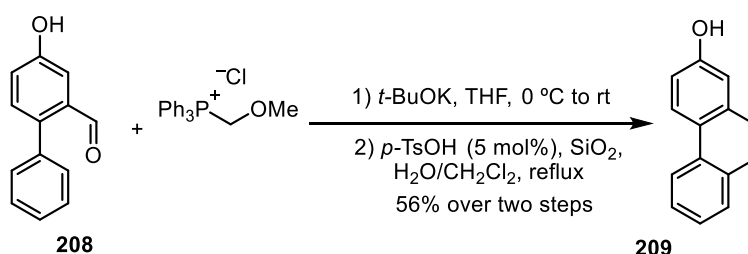


A round-bottom flask equipped with a magnetic stirring bar was charged with 2-bromo-5-hydroxybenzaldehyde (**207**) (5.03 g, 25.0 mmol, 1.0 equiv.), benzenboronic acid (6.10 g, 50.0 mmol, 2.0 equiv.), palladium acetate (14 mg, 62.4 μ mol, 0.25 mol%), triphenylphosphine (49 mg, 187 μ mol, 0.75 mol%), potassium carbonate (12.09 g, 87.5 mmol, 3.5 equiv.), degassed 1,4-dioxane (50 mL) and degassed water (25 mL). The reaction mixture was stirred under reflux using an oil bath and the reaction was monitored by TLC until complete consumption of the starting material was achieved. After 17 h, the reaction mixture was allowed to cool down and the reaction was quenched by dropwise addition of 2 M HCl aqueous solution (100 mL). The excess of 1,4-dioxane was partially evaporated in vacuo, and the aqueous residue was extracted with

ethyl acetate (4 × 60 mL). The combined organic phases were washed with 2 M HCl (50 mL), brine (2 × 100 mL), dried over sodium sulfate, filtered and concentrated in vacuo. The residue was purified by column chromatography on silica gel (gradient hexane/ethyl acetate 4:1 to 2:1) affording pure product **208** as a beige solid (4.18 g, 21.09 mmol, 84%).

¹H NMR: (400 MHz, CDCl₃) δ = 9.95 (s, 1H), 7.54 (d, *J* = 2.8 Hz, 1H), 7.51 – 7.41 (m, 3H), 7.41 – 7.32 (m, 3H), 7.20 (dd, *J* = 8.4, 2.8 Hz, 1H), 5.57 (s, 1H) ppm; ¹³C NMR: (101 MHz, CDCl₃) δ = 192.5, 155.4, 139.2, 137.4, 134.6, 132.5, 130.2, 128.4, 127.9, 121.4, 113.0 ppm; IR: (neat, cm⁻¹) $\tilde{\nu}$ = 3209, 2861, 2774, 2651, 1650, 1581, 1513, 1471, 1398, 1269, 1098, 998, 810, 762, 629, 574, 527; HR-MS: calcd *m/z* for C₁₃H₁₀O₂⁺ [M]⁺: 198.0675; found (EI) 198.0682.

2-Phenanthrenol (**209**):

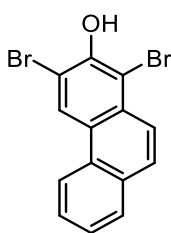


Scheme 59: Synthesis of 2-Phenanthrenol (**209**).

A two-neck round-bottom flask equipped with a magnetic stirring bar was charged with thoroughly powdered (methoxymethyl)triphenylphosphonium chloride (13.71 g, 40.0 mmol, 2.0 equiv.), which was suspended in anhydrous THF (100 mL). The mixture was cooled down, and a previously prepared solution of *t*-BuOK (4.49 g, 40 mmol, 2.0 equiv.) in anhydrous THF (50 mL) was added dropwise over 15 min at 0 °C. Once the addition was finished, the colored solution was allowed to stir for 2 h. After that, a solution of both 4'-hydroxy-[1,1'-biphenyl]-2-carbaldehyde (**208**) (3.96 g, 20 mmol, 1.0 equiv.) and *t*-BuOK (2.24 g, 20 mmol, 1.0 equiv.) in THF (40 mL) was added dropwise to the ylide solution at 0 °C. The reaction mixture thus obtained was allowed to stir at room temperature for 15 h. After that, the reaction was quenched by addition of 2 M HCl (40 mL). The excess of THF was removed in vacuo, and the residue was extracted with ethyl acetate (3 × 100 mL). The combined organic phases were washed with aqueous 2 M HCl (20 mL), brine (2 × 60 mL), dried over Na₂SO₄, filtered and concentrated in vacuo. The crude thus obtained was dissolved in CH₂Cl₂ (150 mL), and then *p*-toluenesulfonic acid monohydrate (190 mg, 1.0 mmol, 5 mol%), SiO₂ (1 g) and water (0.5 mL) were added. That reaction mixture was stirred under reflux over a period of 24 h and after that concentrated. The residue was purified by column chromatography on silica gel (hexane/ethyl acetate 5:1 to 3:1) affording pure compound **209** as a white solid (2.17 g, 11.2 mmol, 56% over

two steps). **¹H NMR:** (400 MHz, CDCl₃) δ = 8.65 – 8.55 (m, 2H), 7.88 (d, *J* = 7.8 Hz, 1H), 7.74 (d, *J* = 8.9 Hz, 1H), 7.69 – 7.61 (m, 2H), 7.56 (tt, *J* = 7.7, 1.0 Hz, 1H), 7.28 – 7.21 (m, 2H), 5.08 (s, 1H) ppm; **¹³C NMR:** (101 MHz, CDCl₃) δ = 154.3, 133.7, 131.2, 130.6, 128.7, 127.9, 126.9, 126.2, 125.8, 124.9, 124.8, 122.2, 116.7, 111.9 ppm; **IR:** (neat, cm⁻¹) $\tilde{\nu}$ = 3253, 3051, 1615, 1569, 1525, 1442, 1303, 1244, 1164, 1034, 947, 871, 810, 746, 625, 575; **HR-MS:** calcd *m/z* for C₁₄H₁₀O⁺ [M]⁺: 194.0726; found (EI) 194.0730.

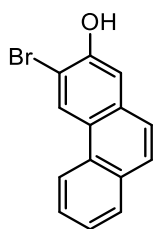
1,3-Dibromo-2-phenanthrol (**210**):



2-Phenanthrenol (**209**) (0.810 g, 4.17 mmol, 1.0 equiv.) was dissolved in CH₂Cl₂ (16 mL, 0.2 M) at room temperature. Then, recrystallized NBS (1.77 g, 10.0 mmol, 2.4 equiv.) was added in portions over 30 min. The reaction mixture was protected from light and allowed to stir at room temperature over 20 h before the reaction being quenched by addition of water (30 mL).

The mixture was extracted with CH₂Cl₂ (3 × 30 mL) and the combined organic phases were washed with aqueous Na₂S₂O₃ (2 × 30 mL) and water (40 mL), dried with Na₂SO₄, filtered and finally concentrated in vacuo affording the crude product. Purification by column chromatography on silica gel (hexane/ethyl acetate 20:1) delivered pure product **210** as a white solid (1.30 g, 3.69 mmol, 88%). **¹H NMR:** (400 MHz, CDCl₃) δ = 8.81 (s, 1H), 8.49 (d, *J* = 8.3 Hz, 1H), 8.00 (d, *J* = 9.2 Hz, 1H), 7.88 (dd, *J* = 7.9, 1.5 Hz, 1H), 7.83 (d, *J* = 9.2 Hz, 1H), 7.67 (ddd, *J* = 8.4, 7.0, 1.5 Hz, 1H), 7.60 (ddd, *J* = 8.1, 7.0, 1.2 Hz, 1H), 6.24 (s, 1H) ppm; **¹³C NMR:** (101 MHz, CDCl₃) δ = 148.0, 131.1, 130.9, 129.7, 129.1, 128.9, 127.7, 127.0, 126.8, 126.4, 124.5, 122.4, 110.2, 108.6 ppm; **IR:** (neat, cm⁻¹) $\tilde{\nu}$ = 3414, 3051, 1916, 1747, 1580, 1518, 1380, 1246, 1175, 1048, 991, 942, 874, 810, 737, 603, 530; **HR-MS:** calcd *m/z* for C₁₄H₈Br₂O⁺ [M]⁺: 351.8916; found (EI) 351.8918.

3-Bromophenanthren-2-ol (**211**):

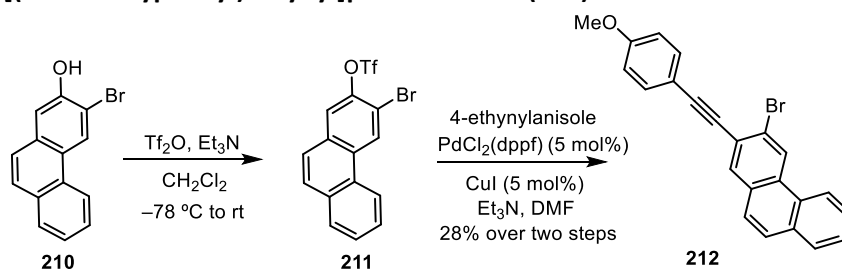


A round-bottom flask was charged with 1,3-dibromo-2-phenanthrenol (**210**) (1.30 g, 3.69 mmol, 1.0 equiv.) and subsequently AcOH (50 mL) was added. The reaction mixture was then heated to reflux, and at this temperature SnCl₂ (7.0 g, 36.9 mmol, 10.0 equiv.) was added in portions over a period of 3 h. After 48 h under reflux, the reaction mixture was allowed to cool down to room

temperature and was poured into ice. The mixture was acidified to pH ≈ 1 by addition of 1 M HCl (100 mL) and extracted with CH₂Cl₂ (3 × 50 mL). The combined organic extracts were washed with 1 M HCl (2 × 50 mL) and water (50 mL), dried over Na₂SO₄ and concentrated in vacuo. The crude product was purified by column chromatography on silica gel (hexane/ethyl

acetate 20:1 to 10:1) affording pure product **211** (0.93 g, 3.40 mmol, 92%) as a white solid. **¹H NMR:** (400 MHz, CDCl₃) δ = 8.81 (s, 1H), 8.50 (d, *J* = 8.6 Hz, 1H), 7.87 (dd, *J* = 7.9, 1.5 Hz, 1H), 7.74 (d, *J* = 8.9 Hz, 1H), 7.66 (ddd, *J* = 8.4, 7.0, 1.5 Hz, 1H), 7.63 – 7.56 (m, 2H), 7.47 (s, 1H), 5.73 (s, 1H) ppm; **¹³C NMR:** (101 MHz, CDCl₃) δ = 150.6, 133.3, 131.3, 129.5, 128.8, 128.3, 127.2, 126.8, 126.4, 125.9, 125.8, 122.2, 112.8, 111.8 ppm; **IR:** (neat, cm⁻¹) $\tilde{\nu}$ = 3314, 3051, 2710, 1593, 1530, 1455, 1400, 1263, 1200, 1103, 1017, 969, 856, 805, 747, 701, 602, 543; **HR-MS:** calcd *m/z* for C₁₄H₉BrO⁺ [M]⁺: 271.9831; found (EI) 271.9830.

3-Bromo-2-[(4-methoxyphenyl)ethynyl]phenanthrene (**212**):



Scheme 60: Synthesis of 3-bromo-2-[(4-methoxyphenyl)ethynyl]phenanthrene (**212**).

Under nitrogen atmosphere, 3-bromo-2-phenanthrol (**211**) (864 mg, 3.16 mmol, 1.0 equiv.) was dissolved in anhydrous CH₂Cl₂ (10 mL) and triethylamine (960 mg, 1.32 mL, 9.49 mmol, 3.0 equiv.) was added to the solution. The reaction mixture was cooled down to –78 °C, and trifluoromethanesulfonic anhydride (1.25 g, 0.75 mL, 4.43 mmol, 1.4 equiv.) was added dropwise. Subsequently, the cooling bath was removed, the reaction mixture was allowed to warm up to room temperature, and the reaction was quenched by addition of 1 M HCl (20 mL). Then the mixture was extracted with CH₂Cl₂ (3 × 25 mL), and the combined organic phases were washed with 1 M HCl (3 × 20 mL), water (20 mL) and 1 M NaOH (30 mL), dried over Na₂SO₄, and finally concentrated in vacuo to afford crude 3-bromophenanthren-2-yl trifluoromethanesulfonate, which was pure enough to be used in the next step.

Under nitrogen atmosphere, a Schlenk flask was charged with crude 3-bromophenanthren-2-yl trifluoromethanesulfonate (1.21 g, 3.0 mmol), DMF (12.5 mL) and triethylamine (2.9 g, 4.0 mL, 39.5 mmol). The obtained solution was then degassed by passing nitrogen gas over 10 min. After that, PdCl₂(dppf) (110 mg, 149 μmol, 5 mol%) and 4-ethynylanisole (0.548 g, 4.15 mmol, 1.4 equiv.) were added. The mixture was initially allowed to stir at room temperature for 5 min, then cooled down to 0 °C, and at that temperature CuI (28.4 mg, 149 μmol, 5 mol%) was added in one portion. The bath was removed, and the reaction mixture was allowed to stir at room temperature for 17 h until complete consumption of the starting materials was observed. The reaction was then quenched by addition of 1 M HCl (20 mL) at 0 °C, and the mixture was extracted with ethyl acetate (3 × 30 mL). The combined organic phases were

washed with 1 M HCl (2 × 20 mL) and brine (2 × 20 mL), dried over sodium sulfate and concentrated in vacuo. The crude product was purified by column chromatography on silica gel (hexane/dichloromethane 4:1 to 2:1) affording pure product **212** as a white solid (341 mg, 0.88 mmol, 28% over two steps). **¹H NMR:** (400 MHz, CDCl₃) δ = 8.93 (s, 1H), 8.59 (d, *J* = 8.2 Hz, 1H), 8.10 (s, 1H), 7.91 (dd, *J* = 7.8, 1.6 Hz, 1H), 7.78 (d, *J* = 8.9 Hz, 1H), 7.75 – 7.56 (m, 5H), 7.01 – 6.89 (m, 2H), 3.88 (s, 3H) ppm; **¹³C NMR:** (101 MHz, CDCl₃) δ = 160.1, 133.4, 133.0, 132.5, 130.9, 130.8, 129.1, 128.8, 128.1, 127.6, 127.3, 126.7, 126.0, 123.8, 123.4, 123.0, 115.2, 114.3, 94.4, 87.2, 55.5 ppm; **IR:** (neat, cm⁻¹) $\tilde{\nu}$ = 3015, 2971, 2843, 2365, 2206, 2160, 1898, 1826, 1774, 1598, 1515, 1444, 1254, 1175, 1112, 1034, 986, 828, 755, 663, 551; **HR-MS:** calcd for C₂₃H₁₅BrO⁺ [M]⁺: 386.0301; found (EI) 386.0312.

Coupling of building blocks

General Procedure G for the Synthesis of Arylzinc Reagents **204-206**

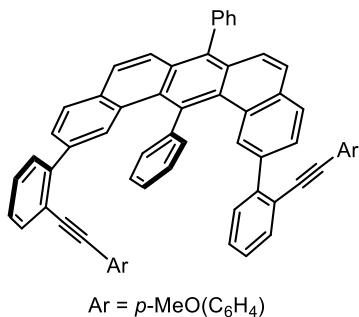
In a Schlenk flask, the bromoethynyl arene (1.0 equiv.) was dissolved in anhydrous THF (0.25 M) under nitrogen atmosphere. The solution was cooled down to –70 °C, and *n*-BuLi (2.5 M in hexanes, 1.05 equiv.) was added dropwise. The reaction mixture was stirred for 40 min, during which the formation of a precipitate was observed; then it was allowed to warm up to –50 °C and a freshly prepared solution of ZnBr₂ in anhydrous THF (1 M, 1.3 equiv.) was added dropwise. After vigorous stirring at –50 °C over 60 min, the cooling bath was removed, and the reaction mixture was allowed to warm up to room temperature. After stirring the reaction mixture at room temperature for an additional 3 h, the excess of solvent was partially evaporated in vacuo affording a concentrated solution of the organozinc compound suitable for use in the Negishi cross-coupling reaction.

General Procedure H for Negishi cross-coupling

An oven-dried microwave vial was equipped with a magnetic stirring bar and charged with the respective benzo[*m*]tetraphene-2,12-diyl bis(trifluoromethanesulfonate) derivative **203** (1.0 equiv.), Pd₂(dba)₃ (2.5 mol%) and SPhos (15 mol%). The microwave vial was crimped on top with a PFT rubber septum. Then, it was evacuated and refilled with nitrogen (twice). After that, anhydrous THF (0.16–0.25 M) was added followed by the respective organozinc **204-206** solution (5.0 equiv.). Subsequently, the vial was heated under microwave irradiation at 110 °C for 30 min. After detecting complete consumption of the starting material, the reaction was quenched by addition of MeOH (0.2 mL) and filtered over a pad of Celite, which was

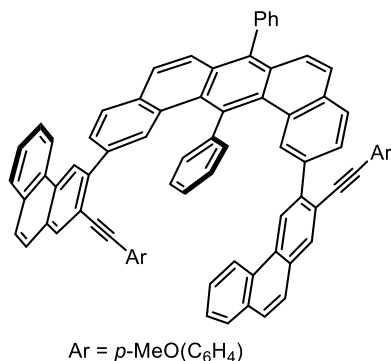
additionally washed with THF (10 mL) and CH₂Cl₂ (30 mL). The filtrate was concentrated and purified by column chromatography on silica gel (cyclohexane/ethyl acetate 20:1 to 3:1).

2,12-Bis{2-[(4-methoxyphenyl)ethynyl]phenyl}-7,14-diphenylbenzo[*m*]tetraphene (213):



Compound **213** was prepared according to the General Procedures **G** and **H**, affording a crude that was purified by column chromatography on silica gel (cyclohexane/ethyl acetate 10:1 to 4:1) to deliver the desired pure product as a pale yellow solid (115 mg, 0.14 mmol, 68%). ¹H NMR: (500 MHz, CDCl₃) δ = 7.88 (dd, *J* = 8.0, 1.6 Hz, 2H), 7.81 (d, *J* = 8.1 Hz, 2H), 7.66 – 7.56 (m, 7H), 7.54 – 7.43 (m, 10H), 7.26 – 7.22 (m, 5H), 7.13 – 7.08 (m, 4H), 6.90 – 6.85 (m, 2H), 6.72 – 6.65 (m, 4H), 3.74 (s, 6H) ppm; ¹³C NMR: (125 MHz, CDCl₃) δ = 159.5, 145.8, 143.5, 139.7, 137.6, 137.3, 136.3, 133.1, 132.8, 132.5, 132.2, 130.90, 130.87, 130.2, 130.1, 128.7, 128.5, 127.9, 127.82, 127.78, 127.7, 127.2, 126.9, 126.8, 125.6, 121.8, 115.7, 113.9, 113.9, 92.2, 88.4, 55.4 ppm; IR: (neat, cm⁻¹) $\tilde{\nu}$ = 3014, 2965, 2838, 2217, 2033, 1903, 1602, 1654, 1632, 1578, 1506, 1439, 1247, 1175, 1108, 1023, 948, 835, 754, 678, 636, 532; HR-MS: calcd *m/z* for C₆₄H₄₃O₂ [M+H]⁺: 843.3258; found (ESI) 843.3252.

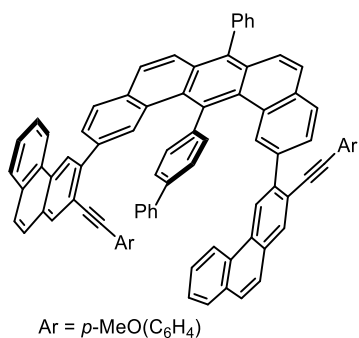
2,12-Bis{2-[(4-methoxyphenyl)ethynyl]phenanthren-3-yl}-7,14-diphenylbenzo[*m*]tetraphene (214):



Compound **214** was prepared according to the General Procedures **G** and **H** just described above, affording a crude that was purified by column chromatography on silica gel (cyclohexane/ethyl acetate 10:1 to 4:1). Compound **214** is obtained as a beige solid (161 mg, 0.15 mmol, 77%). ¹H NMR: (400 MHz, CDCl₃) δ = 8.57 (dd, *J* = 7.9, 1.5 Hz, 2H), 8.13 (s, 2H), 7.96 (s, 2H), 7.87 (dd, *J* = 7.7, 1.6 Hz, 2H), 7.85 – 7.76 (m, 4H), 7.71 (d, *J* = 8.8 Hz, 2H), 7.68 – 7.64 (m, 3H), 7.64 – 7.59 (m, 7H), 7.58 (dd, *J* = 3.4, 1.6 Hz, 2H), 7.57 – 7.52 (m, 5H), 7.50 (d, *J* = 9.0 Hz, 2H), 7.35 (t, *J* = 7.7 Hz, 2H), 7.08 – 6.97 (m, 5H), 6.70 – 6.58 (m, 4H), 3.74 (s, 6H) ppm; ¹³C NMR: (100 MHz, CDCl₃) δ = 159.2, 145.0, 141.5, 139.5, 137.5, 137.1, 136.6, 133.0, 132.6, 132.30, 132.26, 132.0, 131.9, 130.9, 130.7, 130.5, 130.08, 130.06, 129.9, 129.4, 128.6, 128.5, 128.4, 128.3, 128.0, 127.6, 127.3, 127.2, 126.9, 126.8, 126.4, 126.2, 125.5, 123.31, 123.28, 121.0, 115.5, 113.6, 93.4, 88.7, 54.8 ppm; IR: (neat, cm⁻¹) $\tilde{\nu}$ = 3042, 3007, 2933, 2835, 2198, 1634, 1618, 1589, 1544, 1507, 1491, 1435, 1353, 1246,

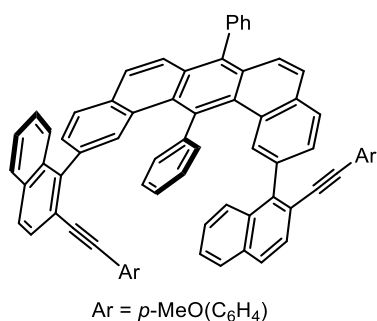
1167, 1104, 1026, 978, 821, 747, 645, 523; **HR-MS**: calcd m/z for $C_{80}H_{51}O_2$ $[M+H]^+$: 1043.3884; found (ESI) 1043.3880.

14-([1,1'-Biphenyl]-4-yl)-2,12-bis{2-[(4-methoxyphenyl)ethynyl]phenanthren-3-yl}-7-phenylbenzo[*m*]tetraphene (215):



Compound **215** was prepared according to the General Procedure H, affording a crude that was purified by column chromatography on silica gel (cyclohexane/ethyl acetate 10:1 to 4:1). Compound **215** is obtained as an orange solid (550 mg, 0.49 mmol, 66%). **¹H NMR**: (400 MHz, CS₂/C₆D₁₂ 5:1) δ = 8.28 (d, J = 8.3 Hz, 2H), 8.15 (s, 2H), 7.80 – 7.72 (m, 8H), 7.70 – 7.48 (m, 13H), 7.48 – 7.41 (m, 4H), 7.34 (ddd, J = 8.0, 6.9, 1.2 Hz, 2H), 7.27 – 7.17 (m, 2H), 7.14 (ddd, J = 8.4, 6.9, 1.4 Hz, 2H), 6.96 – 6.85 (m, 4H), 6.62 (td, J = 7.4, 1.3 Hz, 1H), 6.58 – 6.43 (m, 4H), 6.29 (td, J = 7.6, 1.6 Hz, 2H), 6.00 (dt, J = 8.2, 1.5 Hz, 2H), 3.68 (s, 6H) ppm; **¹³C NMR**: (101 MHz, CS₂/C₆D₁₂ 5:1) δ = 160.0, 144.5, 142.3, 142.2, 140.6, 140.5, 138.6, 138.0, 137.6, 133.7, 133.4, 133.2, 132.9, 132.8, 132.4, 132.2, 131.6, 131.2, 131.0, 130.6, 130.2, 130.0, 129.3, 129.3, 129.0, 128.6, 128.3, 128.1, 127.9, 127.9, 127.3, 127.2, 127.1, 126.9, 126.8, 126.4, 123.6, 123.4, 121.5, 116.6, 114.3, 94.2, 89.7, 55.2 ppm (one more signal is overlapped); **IR**: (neat, cm⁻¹) $\tilde{\nu}$ = 1597, 1512, 1486, 1449, 1396, 1318, 1268, 1248, 1198, 1134, 1074, 1051, 1026, 1007, 950, 914, 889, 829, 808, 759, 743.424, 721.247, 690, 670, 662, 641, 608, 595, 517, 506; **HR-MS**: calcd m/z for $C_{86}H_{55}O_2$ $[M+H]^+$: 1119.4197; found (ESI) 1119.4171.

2,12-Bis{2-[(4-methoxyphenyl)ethynyl]naphthalen-1-yl}-7,14-diphenylbenzo[*m*]tetraphene (216):

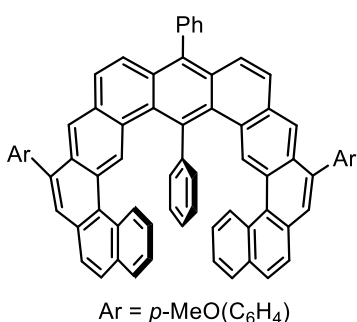


Compound **216** was prepared according to General Procedure H, affording a crude that was purified by column chromatography on silica gel (cyclohexane/ethyl acetate 10:1 to 4:1). Compound **216** is obtained as an orange solid (172 mg, 0.18 mmol, 91%). **¹H NMR**: (400 MHz, CDCl₃) δ = 7.84 (dd, J = 8.1, 1.7 Hz, 2H), 7.78 – 7.70 (m, 2H), 7.68 – 7.60 (m, 7H), 7.57 (td, J = 7.8, 7.2, 1.8 Hz, 2H), 7.52 (d, J = 9.1 Hz, 3H), 7.46 (dd, J = 8.5, 4.3 Hz, 2H), 7.42 (ddd, J = 7.9, 3.3, 1.6 Hz, 2H), 7.37 – 7.29 (m, 3H), 7.25 – 7.14 (m, 6H), 6.83 – 6.76 (m, 4H), 6.73 (t, J = 7.7 Hz, 1H), 6.56 (dq, J = 9.5, 2.9 Hz, 4H), 6.34 – 6.22 (m, 2H), 3.66 (s, 6H) ppm; **¹³C NMR**: (100 MHz, CDCl₃) δ = 159.3, 144.32, 144.29, 143.2, 143.1, 139.90, 139.89, 138.51, 138.49, 137.09, 137.06, 135.3, 135.2, 132.99, 132.96, 132.8, 132.74, 132.71, 132.61, 132.57, 132.2, 132.03, 132.00, 131.9, 130.9, 130.82, 130.75, 130.5,

130.3, 128.74, 128.70, 128.6, 128.4, 128.3, 127.84, 127.78, 127.73, 127.67, 127.65, 127.5, 127.4, 127.3, 127.2, 127.1, 127.0, 126.9, 126.1, 125.9, 125.4, 120.5, 120.4, 115.7, 113.84, 113.82, 113.7, 93.5, 93.4, 89.1, 89.1, 55.3 ppm; **IR:** (neat, cm^{-1}) $\tilde{\nu}$ = 3053, 3008, 2964, 2894, 2835, 2199, 1590, 1548, 1507, 1456, 1401, 1322, 1285, 1246, 1167, 1105, 1026, 978, 918, 869, 820, 747, 655, 608, 531; **HR-MS:** calcd m/z for $\text{C}_{72}\text{H}_{47}\text{O}_2$ $[\text{M}+\text{H}]^+$: 943.3571; found (ESI) 943.3564.

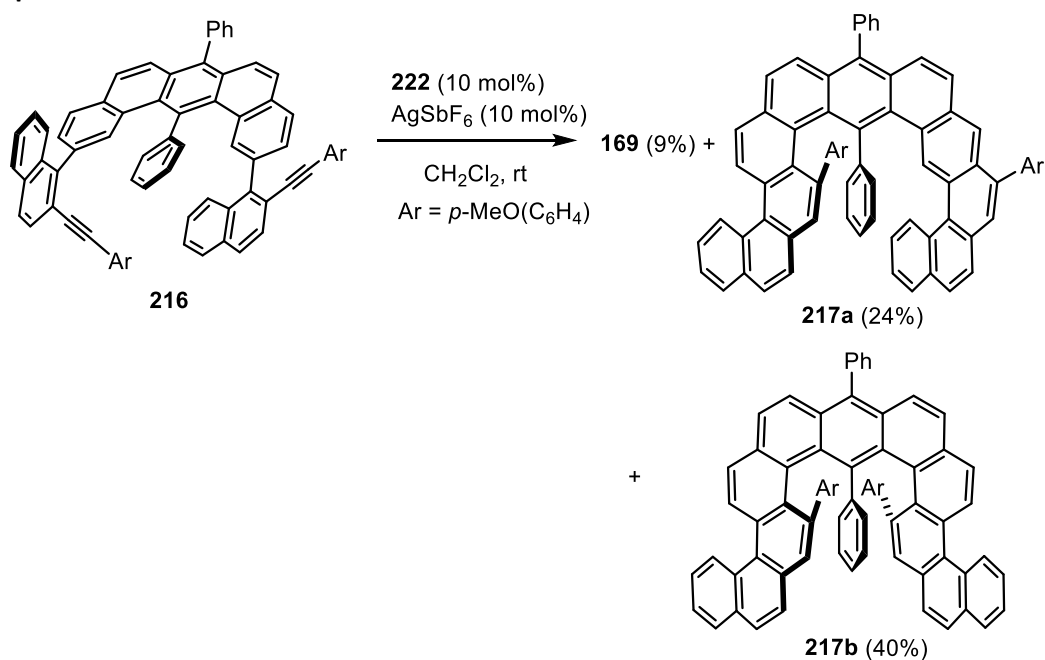
6.4.2. Synthesis of Expanded Helicenes

Compound 169:



A freshly prepared stock solution of AgSbF_6 (0.045 M) in anhydrous CH_2Cl_2 (100 μL , 4.5 μmol , 10 mol%) was added to a solution of gold catalyst **218** (3.9 mg, 4.5 μmol , 10 mol%) in anhydrous CH_2Cl_2 (0.4 mL). The mixture was allowed to stir for 5 min at rt at 0 °C. Then, the suspension thus obtained was transferred to a stirred solution of alkyne **216** (42 mg, 44.5 μmol , 1.0 equiv.) in PhF (1.5 mL), and stirred at 4 °C until complete consumption of the starting materials was observed (4 days). Subsequently, the obtained yellow-greenish precipitate was stirred with CH_2Cl_2 (40 mL) and filtered through a pad of Celite, which was thoroughly washed with more CH_2Cl_2 (2 \times 20 mL). Concentration of that crude in vacuo afforded a solid that was further purified by column chromatography on silica gel (cyclohexane: CH_2Cl_2 2:1 to 1:1). Helicene **169** is obtained as a bright yellow solid (26 mg, 27.6 μmol , 62%). **¹H NMR:** (400 MHz, CDCl_3) δ = 9.08 (s, 2H), 8.42 (s, 2H), 8.20 (d, J = 8.5 Hz, 2H), 7.82 (d, J = 8.5 Hz, 2H), 7.79 (d, J = 8.2 Hz, 2H), 7.72 (d, J = 8.5 Hz, 2H), 7.70 – 7.60 (m, 13H), 7.48 (d, J = 8.9 Hz, 2H), 7.34 (t, J = 7.0 Hz, 2H), 7.24 – 7.19 (m, 4H), 7.16 (d, J = 8.3 Hz, 4H), 6.22 (t, J = 7.6 Hz, 2H), 5.78 (t, J = 7.6 Hz, 1H), 3.98 (s, 6H) ppm; **¹³C NMR:** (101 MHz, CDCl_3) δ = 159.3, 142.8, 139.6, 138.2, 137.7, 137.3, 133.2, 132.9, 132.3, 131.9, 131.4, 131.0, 130.8, 130.4, 130.3, 130.1, 130.0, 129.5, 128.7, 128.3, 128.2, 128.0, 127.9, 127.88, 127.85, 127.5, 127.1, 126.5, 126.4, 126.2, 125.8, 125.4, 125.1, 124.0, 114.2, 114.1, 55.6 ppm; **IR:** (neat, cm^{-1}) $\tilde{\nu}$ = 3161, 3120, 3074, 1755, 1625, 1599, 1518, 1445, 1419, 1394, 1337, 1203, 1136, 1004, 888, 837, 739, 704, 642, 625, 501; **HR-MS:** calcd m/z for $\text{C}_{72}\text{H}_{46}\text{O}_2\text{Na}^+$ $[\text{M}+\text{Na}]^+$: 965.3390; found (ESI) 965.3393.

Compounds **217a** and **217b**:



Scheme 61: Synthesis of expanded helicenes **217a** and **217b**.

A freshly prepared stock solution of AgSbF_6 (0.045 M) in anhydrous CH_2Cl_2 (100 μL , 4.5 μmol , 10 mol%) was added to a solution of catalyst **222** (4.0 mg, 4.5 μmol , 10 mol%) in anhydrous CH_2Cl_2 (0.4 mL). The mixture was allowed to stir for 5 min at rt and then added to a solution of alkyne **216** (42 mg, 44.5 μmol , 1.0 equiv.) in CH_2Cl_2 (1.5 mL). The reaction was monitored by TLC until complete consumption of the starting materials was observed. After 3 h, the obtained yellow-greenish solid was stirred with CH_2Cl_2 (40 mL) and filtered through a pad of Celite. The cake was thoroughly washed with more CH_2Cl_2 (2×20 mL) and the combined filtrate was concentrated. The residue thus obtained was purified by column chromatography on silica gel (cyclohexane/ CH_2Cl_2 2:1 to 1:1) affording pure expanded helicene **169** (4 mg, 4.2 μmol , 9%) and a second fraction containing a mixture of helicenes **217a** and **217b**. This mixture was separated by flash column chromatography on silica gel (cyclohexane/ethyl acetate 7:1 to 2:1) affording pure **217b** (17 mg, 18.0 μmol , 40%) as a first fraction and pure **217a** (10 mg, 10.6 μmol , 24%) as the second one; both as bright yellow solids.

Compound **217a**

^1H NMR: (400 MHz, $\text{CS}_2/\text{cyclohexane-d}_{12}$ = 20:1) δ = 8.91 – 8.83 (m, 2H), 8.63 (s, 1H), 8.16 (s, 1H), 7.84 (dd, J = 8.0, 1.5 Hz, 1H), 7.76 (d, J = 8.4 Hz, 1H), 7.72 (d, J = 8.5 Hz, 1H), 7.69 – 7.46 (m, 17H), 7.44 – 7.38 (m, 2H), 7.31 (d, J = 9.1 Hz, 1H), 7.19 – 7.11 (m, 2H), 7.06 – 6.99 (m, 3H), 6.96 (ddd, J = 8.4, 6.8, 1.4 Hz, 1H), 6.89 (s, 1H), 6.28 (dd, J = 7.6, 1.7 Hz, 1H), 6.15 (d, J = 8.2 Hz, 2H), 6.06 (t, J = 7.5 Hz, 1H), 5.93 (t, J = 7.5 Hz, 1H), 5.54 (t, J = 7.4 Hz, 1H), 3.90 (s, 3H), 3.47 (s, 3H)

ppm; **¹³C NMR**: (101 MHz, CS₂/cyclohexane-d₁₂ = 20:1) δ = 159.6, 158.3, 140.5, 139.4, 139.0, 138.3, 137.4, 134.8, 133.7, 133.44, 133.35, 133.30, 133.25, 132.7, 132.4, 132.3, 132.1, 131.55, 131.54, 131.47, 131.2, 130.7, 130.64, 130.61, 130.5, 130.4, 130.14, 130.11, 129.8, 129.0, 128.9, 128.7, 128.6, 128.6, 128.3, 128.21, 128.16, 128.13, 128.10, 128.09, 128.07, 128.04, 127.97, 127.7, 127.30, 127.25, 127.2, 126.93, 126.91, 126.6, 126.5, 126.32, 126.29, 126.2, 126.0, 125.9, 125.8, 125.7, 125.2, 124.1, 124.0, 114.3, 112.4, 55.1, 54.8 ppm; **IR**: (neat, cm⁻¹) $\tilde{\nu}$ = 3072, 2974, 1604, 1594, 1544, 1516, 1437, 1370, 1352, 1269, 1260, 1223, 1192, 1151, 1095, 1019, 947, 798, 714, 671, 620, 541; **HR-MS**: calcd *m/z* for C₇₂H₄₆NaO₂⁺ [M+Na]⁺: 965.3390; found (ESI) 965.3386.

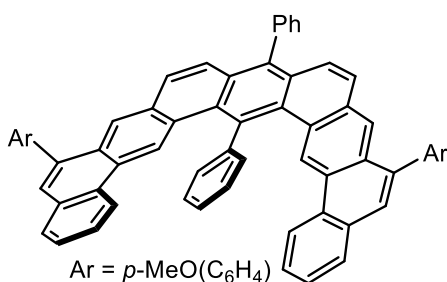
Chiral resolution of both enantiomers was achieved through chiral semi-preparative HPLC by using Daicel Chiralpak IC, 10.0 × 250mm 5 micron particle chromatographic column; isocratic flow rate 4.75 mL min⁻¹; hexane/isopropanol 90:10; enantiomer (+)-**217a**: t_R = 5.3 min; enantiomer (-)-**217a**: t_R = 8.5 min; [α]₂₄^D = 834.53° (c = 0.04, CH₂Cl₂).

Compound **217b**

¹H NMR: (400 MHz, CDCl₃) δ = 9.36 – 9.09 (m, 2H), 8.97 (d, *J* = 8.5 Hz, 2H), 7.92 (dd, *J* = 8.2, 1.5 Hz, 2H), 7.81 (d, *J* = 8.5 Hz, 2H), 7.76 – 7.53 (m, 15H), 7.36 (t, *J* = 8.5 Hz, 4H), 6.75 (s, 2H), 6.26 – 6.02 (m, 8H), 5.77 (t, *J* = 7.6 Hz, 2H), 5.55 (t, *J* = 7.3 Hz, 1H), 3.56 (s, 6H) ppm; **¹³C NMR**: (101 MHz, CDCl₃) δ = 157.6, 138.7, 137.8, 136.5, 135.8, 134.4, 133.4, 133.32, 133.25, 132.7, 131.9, 130.8, 130.3, 130.2, 130.1, 129.53, 129.52, 129.48, 128.6, 128.5, 128.1, 128.0, 127.7, 127.6, 126.7, 126.6, 126.1, 125.6, 125.4, 125.0, 124.59, 124.55, 123.7, 111.4, 55.1 ppm; **IR**: (neat, cm⁻¹) $\tilde{\nu}$ = 3177, 3053, 2927, 2834, 1910, 1869, 1684, 1603, 1508, 1439, 1373, 1244, 1163, 1027, 907, 815, 745, 699, 604, 525; **HR-MS**: calcd *m/z* for C₇₂H₄₆O₂Na⁺ [M+Na]⁺: 965.3390; found (ESI) 965.3395.

Chiral resolution of both enantiomers was achieved through chiral semi-preparative HPLC by using Daicel Chiralpak IC, 10.0 × 250mm 5 micron particle chromatographic column; flow rate 4.75 mL min⁻¹; hexane/isopropanol 95:5; enantiomer (+)-**217b**: t_R = 7.0 min; enantiomer (-)-**217b**: t_R = 9.9 min. [α]₂₄^D = 1029.00° (c = 0.04, CHCl₃).

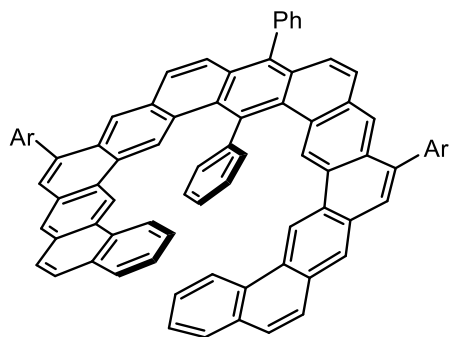
2,10-Bis(4-methoxyphenyl)-6,17-diphenylbenzo[a]phenanthro[2,3-o]pentaphene (166):



A freshly prepared stock 0.045 M solution of AgSbF₆ in anhydrous CH₂Cl₂ (100 μL, 4.5 μmol, 10 mol %) was added to a solution gold catalyst **218** (3.9 mg, 4.5 μmol, 10 mol%) in anhydrous CH₂Cl₂ (0.4 mL). The

mixture was allowed to stir for 5 min at rt and then added to a previously prepared solution of diyne **213** (38 mg, 45.1 μmol , 1.0 equiv.) in PhF (1.5 mL), at 0 °C. After stirring for 10 min, the ice bath was removed. The reaction mixture was allowed to stir at room temperature until complete consumption of the starting material was observed by TLC (14 h). The thus obtained yellow-greenish solid was dissolved in CH_2Cl_2 (20 mL) and filtered through a celite plug and the cake was thoroughly washed with more CH_2Cl_2 (2×20 mL). After evaporation of the solvent, crude **166** was purified by column chromatography on silica gel (cyclohexane/ CH_2Cl_2 2:1 to 1:1) affording helicene **166** (25 mg, 29.7 μmol , 66%) as a yellow solid. $^1\text{H NMR}$: (400 MHz, $\text{CS}_2/\text{CDCl}_3$ 7:1) δ = 8.90 (s, 2H), 8.24 (s, 2H), 7.85 (d, J = 6.8 Hz, 2H), 7.80 – 7.75 (m, 3H), 7.72 (dd, J = 14.2, 7.0 Hz, 2H), 7.67 – 7.47 (m, 17H), 7.41 (dd, J = 19.3, 8.4 Hz, 4H), 7.08 (d, J = 8.5 Hz, 4H), 3.96 (s, 6H) ppm; $^{13}\text{C NMR}$: (101 MHz, $\text{CS}_2/\text{CDCl}_3$ 7:1) δ = 159.9, 146.4, 139.9, 139.32, 139.31, 138.4, 133.4, 133.3, 133.1, 132.6, 132.3, 131.8, 131.3, 130.8, 130.6, 130.2, 129.4, 129.2, 129.1, 129.0, 128.5, 128.4, 127.7, 127.4, 126.6, 126.5, 126.3, 125.9, 124.1, 114.6, 55.8 ppm; **IR**: (neat, cm^{-1}) $\tilde{\nu}$ = 2977, 1610, 1591, 1549, 1512, 1450, 1415, 1323, 1285, 1257, 1180, 1142, 1105, 1033, 979, 866, 813, 769, 744, 666, 558, 530; **HR-MS**: calcd m/z for $\text{C}_{64}\text{H}_{42}\text{NaO}_2^+$ $[\text{M}+\text{Na}]^+$: 865.3077; found (ESI) 865.3072.

Compound 167:



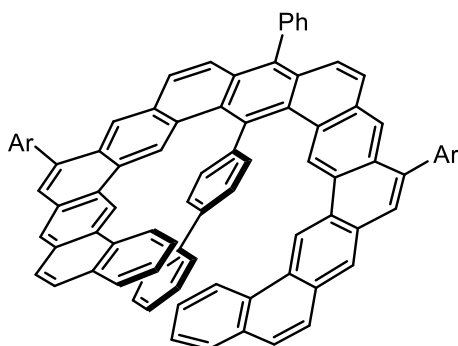
Ar = *p*-MeO(C_6H_4)

A freshly prepared stock solution of AgSbF_6 (0.02 M) in anhydrous CH_2Cl_2 (100 μL , 2.0 μmol , 10 mol%) was added to a solution of gold catalyst **218** (1.7 mg, 2.0 μmol , 10 mol%) in anhydrous CH_2Cl_2 (0.4 mL). The mixture was allowed to stir for 5 min at rt and then added dropwise to a previously prepared solution of alkyne **214** (21 mg, 20.1 μmol , 1.0 equiv.) in PhF (1.0 mL) and CH_2Cl_2 (0.5 mL). After stirring the mixture for

24 h, the obtained yellow-greenish solid was treated with CH_2Cl_2 (30 mL) and filtered through a pad of Celite. The cake was thoroughly washed with more CH_2Cl_2 (2×20 mL). The combined filtrate was concentrated in rotatory evaporator and purified by column chromatography on silica gel (cyclohexane/ CH_2Cl_2 2:1 to 1:1) affording pure helicene **200** (15 mg, 14.4 μmol , 72%) as a bright yellow solid. $^1\text{H NMR}$: (400 MHz, $\text{CS}_2/\text{CDCl}_3$ 5:1) δ = 9.12 (s, 2H), 8.91 (s, 2H), 8.76 (d, J = 8.9 Hz, 2H), 8.32 (s, 2H), 8.16 (s, 2H), 7.94 (d, J = 6.9 Hz, 2H), 7.73 – 7.48 (m, 25H), 7.45 (t, J = 7.3 Hz, 2H), 7.18 (d, J = 8.5 Hz, 4H), 6.97 (t, J = 7.1 Hz, 1H), 4.01 (s, 6H) ppm; $^{13}\text{C NMR}$: (101 MHz, $\text{CS}_2/\text{CDCl}_3$ 7:1) δ = 159.3, 144.3, 139.3, 138.0, 137.9, 137.1, 133.0, 132.8, 132.5, 132.3, 131.9, 131.6, 131.2, 130.9, 130.8, 130.6, 130.4, 130.0, 129.04, 128.96, 128.9, 128.8, 128.7,

128.6, 128.5, 127.89, 127.86, 127.9, 127.5, 127.1, 127.1, 126.8, 126.7, 126.1, 126.0, 125.7, 125.5, 123.9, 116.6, 114.1, 55.3 ppm; **IR**: (neat, cm^{-1}) $\tilde{\nu}$ = 3102, 3014, 2965, 2837, 1604, 1581, 1506, 1466, 1440, 1321, 1289, 1247, 1175, 1147, 1108, 1042, 1023, 1001, 961, 950, 835, 817, 784, 709, 678, 635, 547, 532; **HR-MS**: calcd m/z for $\text{C}_{80}\text{H}_{50}\text{NaO}_2^+$ $[\text{M}+\text{Na}]^+$: 1065.3703; found (ESI) 1065.3697.

Compound 168:



Ar = *p*-(OMe) C_6H_4

A freshly prepared CH_2Cl_2 stock solution of AgSbF_6 (59 μL , 0.045 M, 2.63 μmol , 0.2 equiv.) was added to a solution of gold catalyst **218** (2.26 mg, 2.62 μmol , 0.2 equiv.) in 1,1,2,2-tetrachloroethane (TCE) (0.2 mL). The mixture was allowed to stir 5 min at rt and then added to a solution of substrate **215** (14.7 mg, 13.13 μmol , 1 equiv.) in TCE (0.6 mL). Additional 0.2 mL of TCE were added in order to improve solubility. The

reaction mixture was allowed to stir 1 h and then it was filtered through a plug of silica to give a solution of the desired helicene **168**. The product was obtained as a yellow powder (6.5 mg, 5.81 μmol , 44%) after column chromatography (cyclohexane:toluene 1:1). **^1H NMR**: (500 MHz, $\text{CS}_2/\text{C}_6\text{D}_{12}$ 5:1) δ = 9.26 (s, 2H), 9.02 (s, 2H), 8.58 (d, J = 8.0 Hz, 2H), 8.23 (s, 2H), 8.09 (s, 2H), 8.03 (d, J = 8.1 Hz, 2H), 7.72 (d, J = 8.1 Hz, 2H), 7.65 – 7.47 (m, 16H), 7.45 (d, J = 8.8 Hz, 2H), 7.41 (d, J = 8.9 Hz, 2H), 7.32 – 7.22 (m, 5H), 7.05 (d, J = 8.6 Hz, 4H), 6.34 (tt, J = 7.2, 1.3 Hz, 1H), 6.13 – 6.06 (m, 2H), 6.06 – 6.00 (m, 2H), 3.92 (s, 6H) ppm; **^{13}C NMR**: (126 MHz, $\text{CS}_2/\text{C}_6\text{D}_{12}$ 5:1) δ = 159.6, 143.5, 142.2, 141.1, 139.4, 139.2, 138.5, 137.8, 137.3, 133.2, 133.2, 133.1, 132.5, 132.1, 131.4, 131.2, 131.1, 131.0, 130.8, 130.5, 130.4, 129.31, 129.30, 129.2, 129.0, 128.9, 128.5, 128.2, 128.1, 127.7, 127.5, 127.49, 127.4, 126.8, 126.8, 126.7, 126.5, 126.4, 126.4, 126.1, 125.8, 123.4, 116.8, 114.3, 55.1 ppm; **IR**: (neat, cm^{-1}) $\tilde{\nu}$ = 3420, 3097, 1750, 1571, 1228, 1195, 1175, 978, 760, 744, 596, 553, 536, 516, 503, 494, 485, 470, 455, 439, 432, 424, 413; **HR-MS**: calcd m/z for $\text{C}_{86}\text{H}_{54}\text{NaO}_2^+$ $[\text{M}+\text{Na}]^+$: 1141.4016; found (ESI) 1141.3980.

6.4.3. Fluorescence quantum yield (Φ_F)

The relative determination of the fluorescence quantum yield (Φ_F) in a series of solvents was determined according to the formula presented below:

$$\Phi_x = \Phi_r \frac{\text{Grad}_x n_x^2}{\text{Grad}_r n_r^2}$$

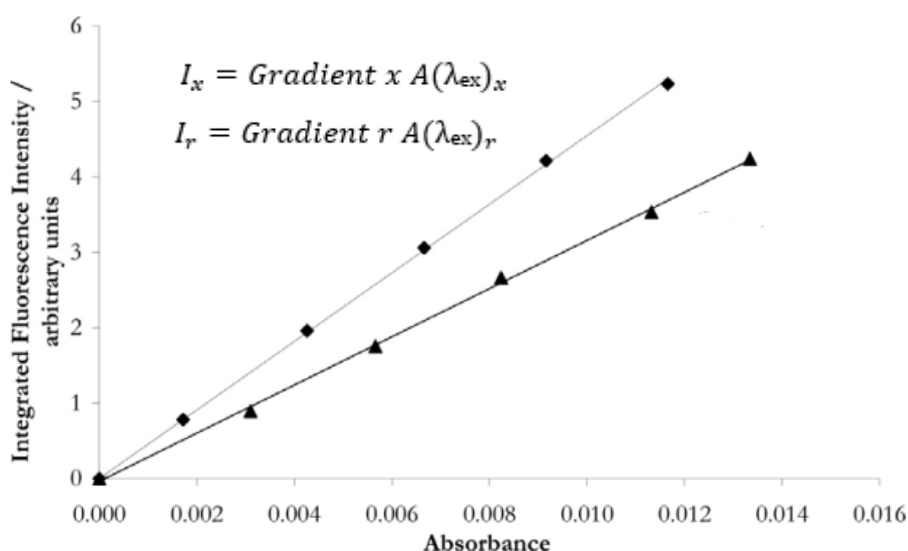


Figure 50. Linear plots of two samples. The gradient of each sample is proportional to that sample's fluorescence quantum yield.^[278]

The subscripts x and r refer respectively to sample x and reference (standard) fluorophore r with known quantum yield Φ_r in a specific solvent; I stands for the spectrally corrected, integrated fluorescence spectra; $A(\lambda_{\text{ex}})$ denotes the absorbance at the used excitation wavelength λ_{ex} and at a specified concentration; n represents the refractive index of the solvent (in principle at the average emission wavelength). To minimize inner filter effects, the absorbance at the excitation wavelength λ_{ex} was kept under 0.1. The measurements were performed using 10×10 mm cuvettes. Quinine in 0.1 M H_2SO_4 was used as fluorescence quantum yield reference ($\Phi_r = 0.54$) for compounds **167-169** and **217a-b**; 9,10-diphenylanthracene in cyclohexane was used as fluorescence quantum yield reference ($\Phi_r = 1.00$) for compound **166**.

6.5. Theoretical calculations

6.5.1. DID Visualization

DID visualization^[251] enabled us to pinpoint which parts of the molecule provide significant stabilization to the conformation through London dispersion forces. SCS-LMP2/cc-pVTZ^[252,275] implemented in Molpro 2020.1^[276] was used to calculate the interactions which are then used to weight the orbital densities for plotting. Before doing the DID calculation, molecules examined were partitioned into several Sections. This approach allows us to visualize intramolecular interactions based on the location of the occupied and virtual spaces (using the projected atomic orbitals mapping to atomic centers). The partitioning scheme adapted are the following:

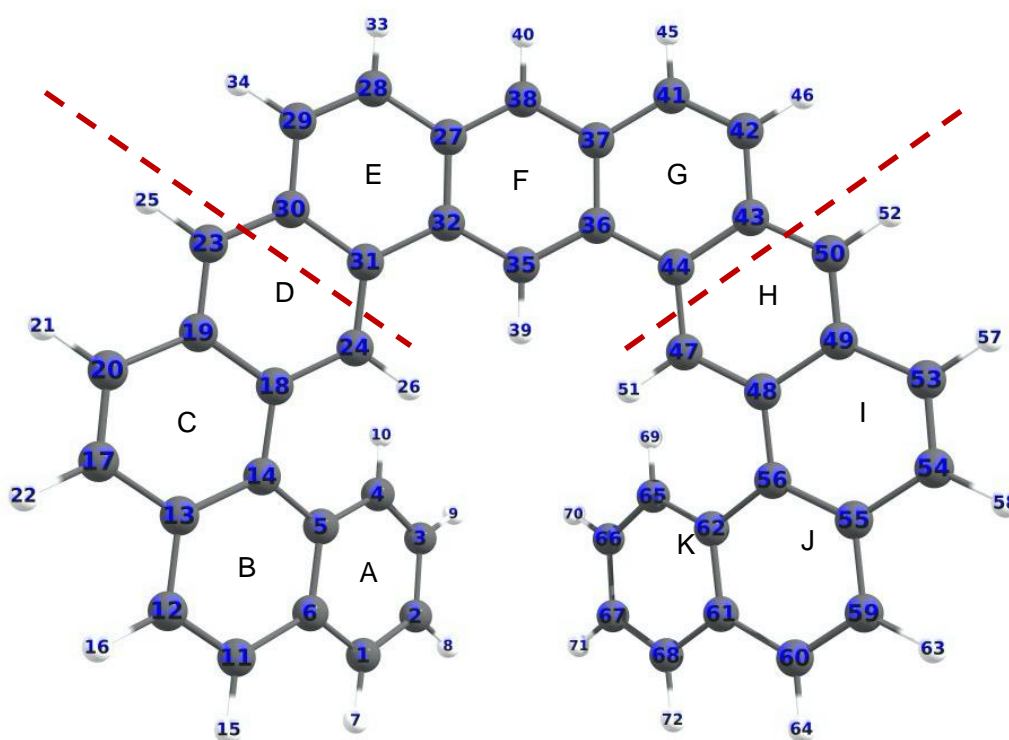


Figure 51. Partitioning scheme of system **169_H**.

The molecular system **169_H** was partitioned as shown in Figure 51. Rings A to D were considered as one region (arm 1, atoms 1-26) and rings H to K was another region (arm 2, atoms 47-72). The rings E-G were considered as backbone and any density contribution coming from that region was not accounted for. This means that only the density contribution from arm 1 and arm 2 were examined in this DID calculation. The red broken line indicates the boundary of the partitioning within the system.

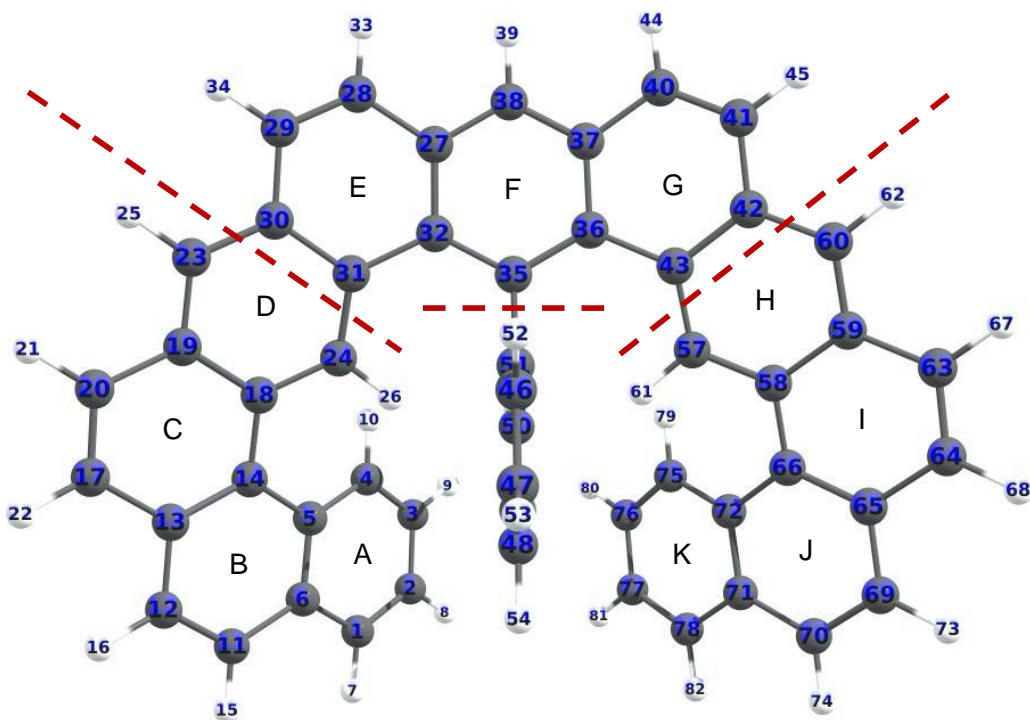


Figure 52. Partitioning scheme of system **169_{ph}**.

In the case of **169_{ph}**, similar partitioning scheme with **169_H** was adapted, except that this time there is a phenyl substituent in the middle of the helicene. Boundaries of each region was indicated by the red broken lines. In contrast to **169_H** where two regions were considered, here we examined three regions, i.e., arm 1 (rings A-D, atoms 1-26), phenyl substituent (atoms 46-56) and arm 2 (rings H-K, atoms 57-82). The DID visualization in this system shows the interaction of arm 1 with the phenyl substituent and the interaction of the arm 2 with phenyl substituent (Figure 52).

In order to display the dispersion contributions, the densities were rendered using ParaView 5.4.0 (64-bit, Linux).^[277] A uniform density range was used in the visualization, i.e., 0.00024 – 0.6 ea_0^{-3} .

6.5.2. Nudged elastic band calculations

Nudged elastic band calculations (NEB) were performed with the program package Orca 4.2.1.^[250] The energy barriers as listed in the text are provided by the electronic energy difference between the global structural minimum and the NEB climbing image (CI). Deviations to optimized transition states (e.g., compounds **166_{ph}** and **169_H**) were found to be below 2 kJ/mol. The convergence tolerance for the maximum component of the atomic force acting on the CI was set to 5×10^{-4} Hartree/Bohr, allowing for a tight convergence close to the maximum. The data which provides the basis for the figures of this study as well as the structures for the helicenes intermediate states are provided in a published dataset under <https://doi.org/10.25625/LX8RSZ>. Alternatively, the raw coordinates can be found at the end of this Section.

6.5.3. Computed absorption spectra

The absorption spectra of compounds **166-168** were computed with simplified time-dependent density functional theory (sTD-DFT) with the ω B97X functional and the def2-TZVP basis set (references provided in main manuscript). Excitations were considered up to a threshold of 10.0 eV, including configurations above a coupling threshold of 1.0×10^{-4} and below 20.0 eV. A comparison between experimental and computed absorption spectra is provided in Figure 53. All computed values were shifted by 1 eV.

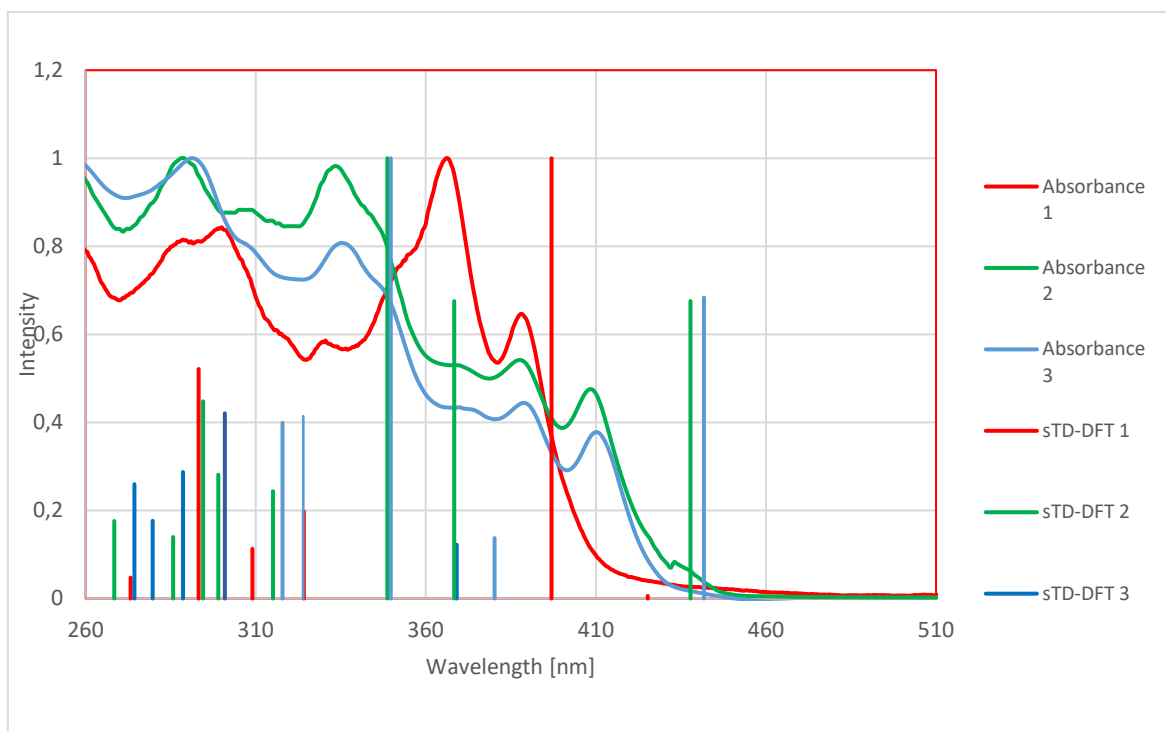


Figure 53. Comparison between experimentally measured absorption spectra (bands) and sTD-DFT computed absorption peaks. Both sets of data have been normalized.

Coordinates:

166_{Ph} MINO PBEh3c optimized

C	-0.18446652973481	1.14866856065460	-4.12835488088368
C	-0.59056228036100	0.61204270223458	-5.32721063078328
C	-0.03886174566948	1.06598803709963	-6.52822638136570
C	0.91569242859652	2.05282566914916	-6.50195107845338
C	2.34651568400000	3.63628448402761	-5.27569015131694
C	1.34367176990155	2.61325462693446	-5.28806624388749
C	0.78668595057115	2.16108634209838	-4.07253424308376
C	1.24664858538365	2.74489857837849	-2.82505031033194
C	0.75710529487032	2.33748529545018	-1.58504132744772
H	0.42409169189897	3.81148286957271	4.02916099593550
C	2.43712104457030	4.70491697246100	0.72902324604785
C	1.82636843566533	4.43768687113954	1.89348252266718
C	0.96433925733001	3.30006124114938	2.03176631136155
C	0.34197263592794	3.06722446011854	3.24506939518449
C	-0.38320883222529	1.91415409924735	3.48458328644358
C	-1.14000018453717	1.79938044262996	4.69719760238016
C	-1.85199194100269	0.69430961977246	4.96617645186170
C	-0.14852451766137	-4.19289152735651	0.92033409453462
C	0.06635296055110	-5.39476653016204	0.28803194854881
C	-0.56744758687682	-6.55552871971442	0.73922591773425
C	-1.41267350528877	-6.48581898484044	1.81901113765995
H	-3.46330418877559	-4.01689935434809	5.07783807828847
C	-2.78399776283282	-4.04880766676315	4.23502709995074
C	-2.54109658234704	-5.20923654338973	3.59421924949546

C	-1.64598217249825	-5.26799208254484	2.47759307229569
C	-1.00175932529917	-4.09385908377774	2.03090852191434
C	-0.66976011280930	-1.63943079039056	2.33307085137496
C	-1.25945319828813	-2.84191520514397	2.72052230750981
C	-2.14954861847862	-2.83557103116254	3.82094482336247
C	-2.34994368953871	-1.64483241659249	4.50825138910120
C	-1.74256809888726	-0.45929346544123	4.12359001857607
C	-0.93231714144646	-0.42006770793310	2.95141372240094
C	-0.37591946235741	0.87107493356770	2.52041279286474
C	-1.22078294245011	-0.25536617534662	-0.31438378406252
C	-1.32363089520065	-1.20972783620543	-1.31541813360394
C	-0.17864633011677	-1.76911241729258	-1.86590029377398
C	1.06892835967827	-1.37415501870251	-1.40250299097352
C	1.17101213939953	-0.43027745668452	-0.39165288686665
C	0.02700097040787	0.14267164992873	0.15951360326115
C	0.13554565456297	1.16120743140691	1.23371909454252
C	0.74752865584563	2.40534002032161	0.95013714640202
C	1.20463441466244	2.85631714366249	-0.37292477842128
C	2.11729398911325	3.94961042844919	-0.44534269082562
C	2.62868644470829	4.34844188349291	-1.67094666048867
C	2.23498546552405	3.75722163860691	-2.86473394573275
C	2.77283170475641	4.18314246332188	-4.11999867417617
H	3.52954142026640	4.95777580666914	-4.12346756371513
H	-0.62232188961436	0.76193981436741	-3.21914421972584
H	-1.33936820815407	-0.16888678518462	-5.33529808909760
H	-0.35789184456823	0.64053714845391	-7.47042728062910
H	1.35374130563664	2.41071541020730	-7.42583399991880

H	2.75876318748815	3.96456915691273	-6.22212211811267
H	-0.02579431598305	1.60284368053359	-1.57747834168747
H	3.12950580867550	5.53267363693091	0.64131005398921
H	2.00401580313903	5.05295379004555	2.76677692489183
H	-1.15516233886831	2.64762434453522	5.36988543309462
H	-2.46627504610847	0.63261069352510	5.85587490846482
H	0.34800922829030	-3.31635577995967	0.52977075286907
H	0.72834104409241	-5.43630019960324	-0.56690929800426
H	-0.39748393046862	-7.49960113527011	0.23881809435856
H	-1.91570851943061	-7.37687508615126	2.17503425216111
H	-3.02547934965063	-6.12338740040019	3.91529524637811
H	0.04583104407721	-1.66690413286834	1.53331118188263
H	-2.97696448718300	-1.64573924949203	5.39305262508743
H	-2.11492376519339	0.17902301422771	0.11397805823738
H	-2.30055511625024	-1.51833118844745	-1.66341953594333
H	-0.25640697568500	-2.50977554495662	-2.65051846212023
H	1.96659145395869	-1.80019367433128	-1.83091683510693
H	2.14495970129619	-0.12153068439082	-0.03389716732000
H	3.33646989699536	5.16938591356321	-1.69796921525471

166_{Ph} TS1 PBEh3c optimized

C	0.87136246167504	0.67635382761101	-4.17526705490299
C	0.84055194944691	-0.02781848649482	-5.35551328454856
C	1.24149616749592	0.57673060799332	-6.54912010634955
C	1.66967210268283	1.88118220764830	-6.53021305914116
C	2.15960703625373	3.97339048614497	-5.33954903737164
C	1.70755331474102	2.61489118242644	-5.33411759168892
C	1.29929955918379	2.01026428468660	-4.12425830645435

C	1.33936451845657	2.78318268939293	-2.89239168366528
C	0.94623461695480	2.26396189638877	-1.65336609586504
H	0.39142029145379	3.81741688584975	4.02026376420090
C	1.51177841117991	5.20345759285350	0.56444798815914
C	1.13744709809292	4.76975674003882	1.77072961873379
C	0.67295291743031	3.42860853789803	1.95476918800350
C	0.31439230964673	3.07310879630323	3.23649915222924
C	-0.13606604429484	1.81405013031519	3.56744161679085
C	-0.47207174603968	1.59705034674179	4.94162092312367
C	-0.90660625595711	0.40508955403399	5.35864804049006
C	-1.30154874136203	-4.07732048751112	0.55259891861933
C	-1.48603226412094	-5.20462844824176	-0.21217135318893
C	-1.91984485840478	-6.39433352332846	0.37718392987606
C	-2.16383598156341	-6.42440332321290	1.72808304626662
H	-2.31175238428504	-4.28673591171463	5.76570325071715
C	-2.10011947966912	-4.24467980714367	4.70439871395477
C	-2.25653970823599	-5.33348426901838	3.92791525048671
C	-1.98329093763704	-5.28182049743344	2.52348175363050
C	-1.53818971914972	-4.07765095413533	1.93409928726952
C	-0.89700528259360	-1.67605760717625	2.26903531098935
C	-1.35320891752152	-2.90099177875443	2.76925263448291
C	-1.64760264777838	-3.00841675506583	4.14611208161913
C	-1.47996637965510	-1.88471970263145	4.93714503504268
C	-1.03751540637190	-0.67376467710571	4.43128682470024
C	-0.72078196862521	-0.52295089608200	3.04125590245677
C	-0.24326345047624	0.80558829753380	2.56827116775919
C	-1.16363783556683	-0.01479951669256	-0.53816083106903

C	-1.24944705224659	-0.96978351597494	-1.54095996854699
C	-0.14838193659315	-1.76160756034409	-1.84303614629712
C	1.03678229957837	-1.59703145595020	-1.13772612081798
C	1.12141965939065	-0.64094647051679	-0.13575467442398
C	0.02268102114324	0.15654274910119	0.17071430762201
C	0.11831887479614	1.17860036316607	1.24144303016041
C	0.57679189787220	2.48261404591256	0.89496888887289
C	0.97587501156472	2.97880633392056	-0.45107981830211
C	1.43939899749115	4.33073555546145	-0.56437788891804
C	1.82983005276763	4.85324546279090	-1.78598312243537
C	1.79552855163564	4.11807599997670	-2.95841454021268
C	2.20328695973563	4.69303444084572	-4.20253235222245
H	2.54669696214762	5.72022400540397	-4.21014540113169
H	0.55823994571223	0.17790443962963	-3.27310718033869
H	0.50257894679636	-1.05607704662476	-5.35484233772920
H	1.21303293482055	0.02301615576086	-7.47818350550049
H	1.98433064593321	2.36334195632870	-7.44777648664652
H	2.46663310020652	4.41155253367662	-6.28131320642544
H	0.59892901941901	1.25233205811444	-1.65185935671913
H	1.86798407639164	6.21493898501287	0.41528306408504
H	1.17861294394068	5.41750832122272	2.63706242007195
H	-0.36354204430171	2.42588962826261	5.62945445693281
H	-1.16206092750627	0.23009144278420	6.39604086234742
H	-0.97018285491694	-3.17615236486579	0.06436838002069
H	-1.29546514575452	-5.16446589402066	-1.27683431504553
H	-2.06574249444328	-7.28104269755621	-0.22534388450137
H	-2.50520414499747	-7.33838557269269	2.19871261279667

H	-2.59848211336928	-6.26888835594496	4.35359209594672
H	-0.66876324603777	-1.64579234378320	1.22437694038733
H	-1.69948700290529	-1.95119392495984	5.99673912828995
H	-2.01810311111506	0.60532971447053	-0.29989085831123
H	-2.17442473524782	-1.09505164392957	-2.08798127602400
H	-0.21326859737691	-2.50632945053735	-2.62626853243878
H	1.89516975116785	-2.21352681094082	-1.36896729841844
H	2.04392982057321	-0.50833262752679	0.41438646267115
H	2.17225118834201	5.88131612220866	-1.82087937415446

167_{ph} MINO PBEh3c optimized

C	-4.09778672042776	3.80457095999704	0.11821319123050
C	-3.72935902269986	3.49760293959612	-1.16406804254181
C	-3.58861628173336	2.15347500704560	-1.53217813464039
C	-3.73891918077306	1.15592850328134	-0.60352933404748
C	-4.04036793180679	1.43921676749138	0.74641290394059
C	-4.30144070281597	2.79396128027833	1.07722274059790
C	-4.84414324202509	3.11577205749626	2.34966382327302
C	-5.18852384439011	2.13181171130968	3.21254198070165
C	-5.30452708381053	-0.23857412500151	3.84950958352521
C	-4.88980100763449	0.77137435723016	2.92997586524383
C	-4.19946099248426	0.42666326153428	1.76119569112134
C	-3.75539139589740	-3.23020539723461	2.38038674851312
C	2.65582898586382	-0.57685448830666	-1.34869787011288
H	5.38537883309776	0.54050713122196	-4.83763239330538
C	5.01539896533505	0.80494861218945	-3.85486775066170
C	5.27387690873668	2.01780226237742	-3.32072683458091

C	4.84564393636269	2.35180283025035	-2.00047151502399
C	5.11160424518686	3.65186637791421	-1.49205606421040
C	4.75079914794847	3.99696371725350	-0.23396030600624
C	3.73152248026542	0.71281658796494	1.16427862959244
C	3.56971772196713	1.03538383417668	2.48714639848708
C	3.66718304839380	2.36615986616574	2.91332751372855
C	4.00861305673834	3.33529140988882	2.00852128949994
C	4.22650952984809	3.01950183254160	0.65345611599104
C	4.00316233488426	1.69759729457130	0.18992512413463
C	4.17384816962769	1.40874092503534	-1.21295327162557
C	3.68798702627111	0.21258990219605	-1.86774183807446
C	4.18060982906711	-0.11470572454957	-3.15906725103532
C	3.79662455552660	-1.32187093140303	-3.73462195683547
C	1.74905383107345	-4.28624105250806	-3.08910205309710
C	2.60431090650672	-3.44939217249643	-3.69669055571619
C	2.85299636452365	-2.14897466632379	-3.15004854668745
C	2.16233459671558	-1.71362931835237	-1.97980446595986
C	-0.24344893611120	0.35686385165128	-1.12782166820652
C	-0.24667840540048	1.68703212889772	-0.74043691117036
C	-0.00525506145393	2.02976638353644	0.58163006538682
C	0.23675799105293	1.03390614165074	1.51621290376841
C	0.24153812144863	-0.29681786579438	1.13113010016269
C	0.00461345671427	-0.64674098982317	-0.19548953317216
C	-0.96917265311550	-2.94962347492231	-0.12128978191621
C	0.02132967429463	-2.06914651080985	-0.61248970417205
C	1.03012973126073	-2.51788201549477	-1.49495408194609
C	0.94440175733743	-3.84809831895185	-1.98472734535788

H	0.06769189340924	-5.77240905540161	-1.70944198347730
C	0.05592341614598	-4.73317901318669	-1.40047522886593
C	-0.84896990189693	-4.32966429640630	-0.43419405838166
C	-1.63879007212296	-5.31699898912970	0.24389950775775
C	-2.51406650212831	-4.96547419219980	1.19868881289119
C	-2.79421315736874	-3.58287194428041	1.44851131809646
C	-2.11592693232741	-2.56429593393067	0.71503677815839
C	-2.63514942897386	-1.27723943614472	0.80485822151242
C	-3.68437554548400	-0.92267203313571	1.66025077711072
C	-4.16765174085145	-1.91295217521264	2.55615375600183
C	-5.01925902840131	-1.54080790036496	3.63462624958228
H	-5.37828349921661	-2.30775013671952	4.30947851790652
H	-4.27258316733850	4.83424169715097	0.40600372039587
H	-3.59131982641952	4.28139622404210	-1.89696299499553
H	-3.37098505955283	1.89485392004939	-2.56011381296742
H	-3.67299005742165	0.13138216070805	-0.93699996330347
H	-5.03332547963250	4.15405413962214	2.59206622234689
H	-5.67647802080481	2.37059008824400	4.14956433614655
H	-5.88416190813993	0.06114982646518	4.71418976184508
H	-4.19689444866160	-4.00504083856615	2.99726573568023
H	2.20117451757920	-0.25618027689605	-0.43235634938650
H	5.84492895720254	2.75210668366352	-3.87557541192838
H	5.58900043894285	4.37375078052119	-2.14329859983900
H	4.91589501948311	5.00310783625015	0.13114036639000
H	3.70429076557360	-0.32900009880069	0.88281953442842
H	3.38226800101502	0.25001170547247	3.20743154509222
H	3.51829012802040	2.61641310508549	3.95549176146481

H	4.15329786896393	4.35894220734846	2.33332374613634
H	4.24736090242801	-1.62031942209666	-4.67465845749883
H	1.61000048861047	-5.29738558464844	-3.45077593089479
H	3.16157312901614	-3.76059669348263	-4.57155394771956
H	-0.42587897362844	0.09049057373786	-2.16132537436259
H	-0.43997086801316	2.45983763578604	-1.47192890214215
H	-0.00543275058802	3.06853882157640	0.88214077401376
H	0.43352245776578	1.29509685314113	2.54706447871500
H	0.42417346143795	-1.07472721668505	1.86203101156686
H	-1.47458102881140	-6.35859434208878	-0.00298146941043
H	-3.06532665805244	-5.71424627905167	1.75382590539529
H	-2.19166013322677	-0.49471928320703	0.22145618774382

[2]Ph TS1 PBEh3c optimized

C	-4.55377872447672	4.01955376546792	2.23743698248430
C	-3.25402132006683	4.30299186390069	1.93387780592391
C	-2.50071308020866	3.32121221765880	1.28618469375528
C	-2.99364501549168	2.05553599888531	1.09210094615282
C	-4.29570896812860	1.68681049786891	1.49110145254393
C	-5.10871370665747	2.75952261501735	1.95911621319842
C	-6.50446653775004	2.59396922737961	2.12066338927062
C	-7.04531777241333	1.37583164098805	1.94383111516598
C	-6.85911034208496	-0.99002218926811	2.10072684534381
C	-6.21239068894417	0.23741695748710	1.78353564756227
C	-4.83119089732409	0.33541800594072	1.51889781168438
C	-4.08479215935024	-3.27170509328190	2.11495554784419
C	2.77802529363090	-0.56621623615275	-1.47077705368569

H	5.46424182411773	-0.25159275704350	-5.16405408509479
C	5.07459609419641	0.24676570265532	-4.28520603573010
C	5.20806078765875	1.57935478877308	-4.11835358004431
C	4.80995715034832	2.20022615205868	-2.89581895044026
C	5.04891097689419	3.58702158028532	-2.70072655794084
C	4.86902434107692	4.16262114593233	-1.48781775883475
C	4.19136544135572	1.17293302367505	0.61743432504862
C	4.34670246956664	1.70147606819550	1.87176657647665
C	4.55550824753829	3.07686942860967	2.04341912934219
C	4.65489395600223	3.88776573871489	0.94394827038828
C	4.56104288263185	3.35854723855712	-0.35722131329437
C	4.27104284809664	1.98266969941949	-0.53554871933576
C	4.25446034229470	1.43464848880486	-1.86293576699955
C	3.79209728296241	0.10239167791992	-2.18022623258724
C	4.33211166602369	-0.51126670729653	-3.33645608158115
C	4.06916008700121	-1.85652135997357	-3.52820288049597
C	2.05791111686535	-4.62888380674950	-2.38843292963184
C	3.02959528890167	-3.94360836485818	-2.99171557967520
C	3.14579969192112	-2.53971310956690	-2.76061583971036
C	2.33916700490980	-1.85500461752805	-1.78694723713804
C	-0.09524332610704	0.40889085292109	-0.89980044329324
C	0.12974419132114	1.72617387402223	-0.52386910364430
C	0.59581476711649	2.01822856923562	0.75041389858354
C	0.79151095369183	0.99347038835564	1.66314375302199
C	0.57286911667452	-0.32284944985277	1.28611691104408
C	0.15786820519430	-0.63017591097599	-0.00769342511806
C	-0.97286810955793	-2.86440491504428	0.05332844123531

C	0.09482602573469	-2.05441562314064	-0.42660003274656
C	1.16419933246989	-2.57709463637589	-1.22598068907924
C	1.09928100537058	-3.95646092154161	-1.56646368995300
H	0.09100256099974	-5.80046141545692	-1.30569036738013
C	0.09281293060581	-4.74434424165738	-1.06440829729365
C	-0.88911686204254	-4.25903703032795	-0.23599797361698
C	-1.71425889343230	-5.25764194850024	0.36782144041456
C	-2.59685089107536	-4.90443467078142	1.29960085376637
C	-2.89366890090596	-3.51772046644943	1.47914051259995
C	-2.18755301660836	-2.45795457421488	0.83057960003329
C	-2.79043298167292	-1.18537570874540	0.90186783080972
C	-4.07260360731613	-0.93108037055327	1.46326604882378
C	-4.73553208014668	-2.05948987680453	2.02707839474317
C	-6.11883453770694	-2.07693763065212	2.34675344241202
H	-6.55689124908340	-2.99730526758842	2.70927421367646
H	-5.18530700236192	4.76313729855352	2.70471451183540
H	-2.82783161486902	5.26979710316700	2.16260219678929
H	-1.51125756627017	3.56178424391633	0.93156105958543
H	-2.35112324739787	1.36063788968061	0.58464835343158
H	-7.11778804157340	3.45050946464563	2.36769507027989
H	-8.11299832385937	1.22067549878876	2.02985820788177
H	-7.93144723308062	-0.99687097636938	2.24186928749394
H	-4.60519530284053	-4.10445788120368	2.57154629499896
H	2.30447232722927	-0.01540063344449	-0.67897613692560
H	5.68955380132281	2.18442971041635	-4.87660967748291
H	5.38511334906976	4.17580612715660	-3.54591669367093
H	5.03846567805424	5.22333488855891	-1.35116893202019

H	4.08385501086047	0.10329343452367	0.51297320385438
H	4.33524018972276	1.04296538446681	2.73007975331185
H	4.68233783649834	3.48648817102568	3.03649585719343
H	4.86542043054169	4.94370357733801	1.06154978501718
H	4.57936770030187	-2.39064150188610	-4.32206909614145
H	1.95205291055083	-5.69801615360509	-2.51951609451327
H	3.74991882652663	-4.42857531952392	-3.63763145962221
H	-0.41919935659612	0.17925884244391	-1.90676608267585
H	-0.04211445353550	2.52447916935806	-1.23409667350522
H	0.80758167259059	3.04061740461885	1.03541113980615
H	1.13414606839118	1.22084385249054	2.66382272933734
H	0.75443694489595	-1.12528639235680	1.98989206336915
H	-1.56333243066043	-6.29066452816909	0.08326261886824
H	-3.19691663563382	-5.63493181944317	1.82492297234147
H	-2.27335175249879	-0.38351516349564	0.41002427215765

167_{ph} INT1 PBEh3c optimized

C	-3.47745726467179	3.73706976420814	3.00980869795164
C	-2.49928133590537	3.36652962816267	3.89406407130558
C	-2.11406231946378	2.02111094289177	3.97821382192590
C	-2.66940777293873	1.08320273832438	3.14693778775835
C	-3.68990854688670	1.43008984533054	2.23689821473928
C	-4.12867455212297	2.77794163291341	2.21274252259718
C	-5.31035216367648	3.11752757698823	1.50008712376888
C	-6.12070217330549	2.13602188341674	1.03724877290851
C	-6.69347682155314	-0.25617815263890	0.86129863886253
C	-5.73423589578872	0.77062375008824	1.11440415757896

C	-4.43672474776325	0.43529276794061	1.51975719867158
C	-4.57379916891541	-3.23233297474342	1.07716219344865
C	2.70949933645260	-0.59078487607631	-1.39423396026059
H	5.42615256312271	-0.56680868864765	-5.08380838610941
C	4.93309533577993	0.01833242109951	-4.31752147568595
C	4.83999293896430	1.36151805263105	-4.41591021020567
C	4.31024815676694	2.13290365131412	-3.33747895139940
C	4.29552847021870	3.55165556455544	-3.41981104253214
C	4.01506657890711	4.31063424397568	-2.33343498270371
C	3.94145795440148	1.70257241580440	0.31526680314275
C	4.08668985599756	2.47807813269087	1.43601402780363
C	4.05982730215300	3.87675545028404	1.34332976782741
C	3.94084750959935	4.47131920679928	0.11520021788475
C	3.87959126166331	3.69728108041176	-1.05848476990947
C	3.82617613580101	2.28401720250131	-0.96514696127999
C	3.88197300956355	1.49833323003163	-2.16556333045004
C	3.63626702061654	0.07387415425462	-2.21814912193236
C	4.28703085004880	-0.65573883228316	-3.24163345806923
C	4.20997151528802	-2.03732856725276	-3.19033014285844
C	2.46770087668468	-4.81650082421998	-1.67314859332537
C	3.38858900756917	-4.12216537350723	-2.34421609281398
C	3.35662143292873	-2.69382281543506	-2.32338658701142
C	2.45145851445661	-1.96410589787979	-1.47858268256749
C	-0.36858791689069	0.16966795479627	-0.78909768555177
C	-0.38347019844942	1.52277547689960	-0.48190299062335
C	0.11745712440313	1.97084627683691	0.73158798434825
C	0.63378976702723	1.05959899890588	1.64064905378985

C	0.64679946628046	-0.29350332172552	1.33739007325294
C	0.14837649891707	-0.74889719196018	0.11891865689899
C	-0.89930776803090	-3.01997238931020	0.24299917384365
C	0.19344690309638	-2.20296310371106	-0.17406675711814
C	1.34225050254480	-2.72651706040967	-0.83866509337111
C	1.40890564367841	-4.14075148224529	-0.98634977796580
H	0.47336725695968	-6.00933805712017	-0.63395157572745
C	0.39719365229905	-4.93674831583554	-0.50061423558632
C	-0.74576207933040	-4.42554675788988	0.07114482136379
C	-1.75299179582190	-5.38148520021668	0.41738256499573
C	-2.96377175893519	-4.97675285720717	0.80372818513889
C	-3.24727273447258	-3.58003377146039	0.90456361491832
C	-2.22790285823423	-2.57753647317253	0.75724921773597
C	-2.64182241656495	-1.27358223379986	1.06422335278558
C	-3.98619042896641	-0.92062190068308	1.28708314035542
C	-4.98550381059405	-1.91335570299859	1.14905554291927
C	-6.35597297863278	-1.55573436733366	0.99743094521177
H	-7.09640664577926	-2.34094089592385	0.91180925157021
H	-3.81527993666149	4.76528241215768	2.96688627686590
H	-2.05914020253590	4.09918398631399	4.55727381125771
H	-1.40018362225400	1.71267224974051	4.73044273070553
H	-2.38813092597376	0.04577993900855	3.25954432498567
H	-5.60283793566715	4.15712489934457	1.42194813958917
H	-7.08454781043305	2.37735357578159	0.60599331601151
H	-7.71341940984257	0.03078380920469	0.63703034064870
H	-5.31880139166696	-4.01962697831970	1.08852275423381
H	2.14521754318020	0.02771767409685	-0.72055114051907

H	5.23985405942592	1.88145256920089	-5.27757180469788
H	4.52384854106569	4.01616726852760	-4.37153578944821
H	3.99016395530414	5.39086968381459	-2.40612075192542
H	4.01048497163852	0.62815246540566	0.40753281237251
H	4.26075013508047	2.00529150506825	2.39348103667774
H	4.18017909784629	4.48290633958531	2.23138950027003
H	3.96545057048838	5.55035331402069	0.02502264301542
H	4.79974053288209	-2.62723637397707	-3.88298725248965
H	2.46229101924827	-5.89901911744359	-1.68006230494852
H	4.16482887695273	-4.61552889917182	-2.91494532517159
H	-0.75543932933505	-0.17859463691821	-1.73782576042847
H	-0.78486851797301	2.23122044802542	-1.19406615814280
H	0.10774758367322	3.02559081435040	0.97053310371187
H	1.02693590357239	1.40537597146934	2.58730012175565
H	1.05061588050883	-1.00646841063344	2.04552282810928
H	-1.52003143460216	-6.43227277052561	0.30084005232579
H	-3.75543191468171	-5.68372297625670	1.01695638092410
H	-1.93232252773604	-0.46633472023997	1.07128538206562

167_{ph} TS2 PBEh3c optimized

C	-3.05302911111381	2.95139559211551	4.44634302688596
C	-1.99846832225609	2.29268546290920	5.02156521179684
C	-1.70597094227623	0.97900206922675	4.62933401607875
C	-2.43156686572209	0.37136429822589	3.63858713014631
C	-3.51529436498071	1.02687986034620	3.01659292050977
C	-3.85708325081587	2.32305571338582	3.47692508273577
C	-5.07239428851822	2.92211593857052	3.04755296910920

C	-5.97783397973430	2.19303570617828	2.35265212397529
C	-6.71858359897139	0.04692089977538	1.39796988028159
C	-5.67930423877383	0.87195871863087	1.92384708038240
C	-4.38743356590989	0.35819094818076	2.09226959157528
C	-4.81920136252434	-2.98877637897953	0.60547345482902
C	2.75179567445011	-0.48943775074693	-1.57396744020345
H	7.11738326269791	-1.32425367411376	-2.65496796438597
C	6.38378214481225	-0.53355673149351	-2.55966191406758
C	6.68595508489184	0.74950574964643	-2.78156004175740
C	5.66639778265223	1.73616869535083	-2.69978621017249
C	6.00758963246239	2.99066840551850	-3.26990692491481
C	5.11904303316208	4.00045056770239	-3.30382454267603
C	2.55121671795361	2.72392865186133	-0.95477004855166
C	1.88231023441974	3.89964292045312	-0.70497835261906
C	2.14965575864958	5.06428844446928	-1.43013054545299
C	3.15722685752819	5.03618978374920	-2.34997521725159
C	3.92410031743788	3.87726755644335	-2.55346213621347
C	3.58721466524981	2.65281952857989	-1.90676549407688
C	4.39197180701691	1.47042854442643	-2.15464445427787
C	4.02080651613275	0.05939130446289	-1.94318399551767
C	5.04277581019795	-0.88315983432082	-2.25549100618460
C	4.72786839808987	-2.21727528803412	-2.35729041671644
C	2.22135063915689	-4.73395658012187	-2.00714432964868
C	3.34559887595274	-4.11694089578139	-2.33754153428936
C	3.48656562625360	-2.72109489914580	-2.07362183198306
C	2.44617377841909	-1.87380642889781	-1.56413421588243
C	-0.66191667173071	0.33272502551505	-0.74063819549409

C	-0.80581369941605	1.60633777143421	-0.20850626521185
C	-0.27582821958807	1.90601811322803	1.03829225692249
C	0.45310449343623	0.94683029510125	1.72553980299253
C	0.59957975642047	-0.32572608021143	1.19284503320179
C	0.01377442990270	-0.65347045680031	-0.02800743882784
C	-1.11689424159710	-2.87390389947371	-0.14778796131420
C	0.03085570453419	-2.07154056379823	-0.47178785880943
C	1.18851578531190	-2.58857654111703	-1.13099016541968
C	1.17069298284022	-3.99807520708277	-1.37914578133750
H	0.14003050597259	-5.83608500715059	-1.21810101882287
C	0.09759827610438	-4.77293169224037	-1.01475612922234
C	-1.04077007721794	-4.25997399463969	-0.45171585967959
C	-2.10797132321093	-5.19639802502561	-0.27114591719832
C	-3.32449213084118	-4.76765579753900	0.05980829656185
C	-3.51946854139995	-3.38613399129705	0.36213275283957
C	-2.42685683192838	-2.44935114646688	0.42879497688623
C	-2.74418276193498	-1.23802456423898	1.04922057987342
C	-4.05380307257801	-0.87417703859231	1.41698103048445
C	-5.12945796353676	-1.71126785978032	1.03654111515207
C	-6.47173951176673	-1.23908391682943	1.07096596098260
H	-7.27135255426090	-1.90707145814470	0.77507156287675
H	-3.32031495284249	3.94752207945004	4.77697475423069
H	-1.42278006624864	2.76625050518861	5.80550815366038
H	-0.92281682119037	0.42492854361540	5.12970897864791
H	-2.21532653000509	-0.65697177127447	3.38853871240943
H	-5.30074999859881	3.93345536406967	3.35909876450012
H	-6.95208886753984	2.60420844663000	2.11687753304519

H	-7.72382334549327	0.44666921527240	1.34566471532281
H	-5.61745442162713	-3.70565526803919	0.44789894202502
H	1.95985223932642	0.19756682965828	-1.32612106898976
H	7.68550346211773	1.05389548939060	-3.05952965373876
H	6.98495598619339	3.08927263114076	-3.72598368321304
H	5.34621992791646	4.92871850151624	-3.81219073364264
H	2.31836568898741	1.86794362700979	-0.33809236623161
H	1.14787323478311	3.93105788896434	0.08257099567004
H	1.60699122150319	5.98150208962453	-1.23569410055604
H	3.42611090617051	5.92811087100300	-2.89970269936006
H	5.48775453887908	-2.89961529090940	-2.71708197316641
H	2.07088384976445	-5.79330487230901	-2.18096235243846
H	4.16946760220683	-4.63963322186440	-2.80874173311550
H	-1.11426848063397	0.08674078740984	-1.69261798982321
H	-1.35195149174241	2.36058472892908	-0.75920848951373
H	-0.42928298501404	2.88394872436518	1.47619129492908
H	0.88288881410613	1.18320831633350	2.69008807284122
H	1.14154705688888	-1.08519910982237	1.74192308550812
H	-1.90801033785670	-6.23999875395871	-0.47895876892009
H	-4.16739245980430	-5.44331357442498	0.12972995308368
H	-1.97637682975216	-0.50945364039215	1.23819700793689

167_{PH} MIN1 PBEh3c optimized

C	-1.76642510316439	2.60274439836221	4.60149159713189
C	-0.67802758163309	1.81283549791772	4.85889155382672
C	-0.65696376975284	0.49749202200864	4.37728334299852
C	-1.67365354259085	0.02755856441722	3.58636999900380

C	-2.77359620281325	0.83988929395280	3.23524031190122
C	-2.84533530819875	2.12406265191618	3.83348444559715
C	-4.04179580159711	2.88292742293493	3.72711400083885
C	-5.13611591671118	2.35100318449691	3.13397946534117
C	-6.25968837570589	0.54562323721999	1.89833360938019
C	-5.07504030131297	1.09139577463870	2.47825528429015
C	-3.86482696520267	0.39108362890623	2.40658319836828
C	-4.92587374634843	-2.43606649177184	0.20975285822753
C	2.54949339033646	-0.61800223494772	-1.52724594263948
H	7.11169045076757	-0.72300655057511	-1.29290260015766
C	6.22218712722377	-0.11556285130085	-1.40511271750261
C	6.28957141784379	1.23189128111589	-1.33739319144212
C	5.13501051855918	2.04297669521058	-1.55491572777462
C	5.24355240838884	3.45611888287623	-1.44678642940163
C	4.17949336677886	4.25829965638284	-1.68527134246285
C	1.73344724930212	1.83775928479357	-3.07964882962173
C	0.74736412952346	2.68709711862007	-3.51090599539705
C	0.81785470613466	4.05888582103722	-3.23571110899458
C	1.92201790359830	4.55819297673861	-2.59841184369964
C	2.96890137286259	3.71070162443940	-2.18777113113554
C	2.84859250777420	2.30689883025394	-2.35209291175520
C	3.90661634512893	1.45233186006402	-1.87448466413626
C	3.78254422109978	0.02197085090318	-1.69345277870658
C	4.95874056141476	-0.75803926918842	-1.54256701280653
C	4.83525986400863	-2.14288482892122	-1.48369165634676
C	2.32857934575040	-4.80991853428952	-1.54627752009832
C	3.52294517486733	-4.19821896280130	-1.52170700847430

C 3.60187103348599 -2.77061582443938 -1.43380557417571
C 2.41341755514468 -1.98741863768878 -1.32864534245987
C -0.74203998081177 0.30387514312425 -0.92346744845376
C -0.72216108050580 1.63738046954605 -0.54821367800647
C 0.02036293740907 2.04161734440071 0.55119901687422
C 0.74615114347884 1.10502138114899 1.27232810499105
C 0.72835379624514 -0.22868232560647 0.89870206406790
C -0.01840371868840 -0.64125474767327 -0.20134952211617
C -1.25042822216124 -2.79672614962867 -0.48482262650468
C -0.04404780353625 -2.06928432505922 -0.59833613996236
C 1.13778313497549 -2.67640794580614 -1.08020171777979
C 1.11578032259918 -4.07446647997175 -1.32841539182466
H -0.11492354868193 -5.78847614763437 -1.63684474074447
C -0.09480838316108 -4.74437599665292 -1.34499701857945
C -1.28024800698484 -4.12059665122410 -0.99792532297312
C -2.51986267506910 -4.82094572457490 -1.17606955047792
C -3.69089941137657 -4.24717442864830 -0.85897580234812
C -3.71698717316828 -2.98167926346543 -0.18811067795810
C -2.50052356332566 -2.29620015797883 0.10756241568509
C -2.58553338669779 -1.22883225766399 0.99477612288872
C -3.79310986200104 -0.73387711087584 1.49889677525352
C -4.99782645781338 -1.28524750495244 0.98864015425291
C -6.23884101101395 -0.63450224872149 1.24189798619289
H -7.15074232802908 -1.06708729813277 0.84942205761279
H -1.82949653970199 3.60041198617438 5.01925777901018
H 0.13834662431203 2.18412241053907 5.46424369900907
H 0.15980328883340 -0.16156519400096 4.64124280732838

H	-1.64907621358379	-1.00739951922967	3.27990889519679
H	-4.08389291498254	3.86333696769900	4.18524679099764
H	-6.07506671418702	2.89116630416399	3.12920127371210
H	-7.18981754208065	1.08519322376390	2.02881314696315
H	-5.84618800225529	-2.91953266313967	-0.09921986174769
H	1.67559312461974	0.00346765835902	-1.50662473808763
H	7.23514619074149	1.72462836567848	-1.14597285446722
H	6.19272036779302	3.87851866958834	-1.14024593248978
H	4.25743438613425	5.33058273102403	-1.55564399907446
H	1.67137503209924	0.79549564722632	-3.35424573575020
H	-0.08560596581567	2.29126158777275	-4.07691677741638
H	0.02815367469583	4.72223429061676	-3.56298996995171
H	2.02200917418700	5.62404425021504	-2.43232525163619
H	5.73285346984503	-2.75116511848413	-1.47199052207747
H	2.25519988239364	-5.88189556031748	-1.68183213269127
H	4.44061777057690	-4.76370888783686	-1.62442644384074
H	-1.32557930766946	-0.01239821097718	-1.77910154706348
H	-1.28521716155768	2.36420551277300	-1.11751929012781
H	0.03423589784460	3.08232950987136	0.84481699363435
H	1.32132489506898	1.41475468030896	2.13433492574189
H	1.30136123885479	-0.95839960842615	1.45699487741652
H	-2.48684268325888	-5.80912083674639	-1.61782683186905
H	-4.62933070266002	-4.75348495890046	-1.04827978368662
H	-1.68891402689142	-0.71916718494746	1.28742708516117

168_{Bi-Ph} MINO PBEh3c optimized

C	3.78645733251072	15.07096825869596	15.72027993739648
C	4.42758937556799	15.21892499362619	14.54750858120281

C	4.09898357431938	14.40248488677226	13.41511283172560
C	3.08793478564410	13.40991093795165	13.52281052087043
C	2.43099828823484	13.21478465593096	14.80982829837775
C	2.77347401214021	14.06999738976714	15.88536622013661
C	2.77231313625588	12.67092348970523	12.38889148019778
C	3.40599533053630	12.86160595690628	11.16208397202664
C	4.44449348266465	13.82403067643106	11.08247472655358
C	4.75996154969005	14.57485033981285	12.20853566883440
C	3.05045429685384	12.11610246849107	9.96769285200666
C	1.98723579323130	11.20102153820303	9.93256637269948
H	1.38258045740980	11.04391917885099	10.81334514528121
H	2.00609130999379	11.91410456254496	12.46037934813680
C	2.08640746035102	13.94371282541973	17.08299503827697
C	1.12408488849774	12.96396329310665	17.28244807109408
C	0.87381100822163	11.99843839885480	16.26719240337144
C	1.49118762074174	12.21145661627634	15.03397384452129
C	-0.05497281804721	10.89840774297235	16.56214511269571
C	-0.92204163467623	11.08722291955711	17.67196794775999
C	-0.70160535846434	12.14281516729370	18.61620078676837
C	0.32881602364727	12.99059948622177	18.47296798876653
C	-1.99016662040250	10.22765259294024	17.85425901723848
C	-2.15800656627004	9.09764280180143	17.07401143676560
C	-1.13700318042773	8.72177999459794	16.16067384623726
C	-0.13226590628719	9.67139713765918	15.86286440018261
C	-3.36550213637142	8.33455136521881	17.19197909962683
C	-3.55906647391633	7.23266802203110	16.45007953414877
C	-2.49246008052146	6.70195949442567	15.65513151716259

C	-1.24029812276999	7.37443926767921	15.58446726957747
C	-0.17644712597677	6.66473502113154	15.02677191629278
C	-0.31761737712899	5.41489140130286	14.42908834604616
C	-1.60732383519640	4.83174296152916	14.38406151613693
C	-2.65484448781112	5.47670015647304	15.02365951525686
C	-1.81108707508666	3.57744944816758	13.72009186061492
C	-0.78778293071978	2.93093951405685	13.13438639078846
C	0.54425792722808	3.46181653280366	13.17318244159223
C	0.80062657397184	4.69299739138795	13.83448168963073
C	2.11214555337578	5.15143053950484	13.87962535172105
C	3.17364029151940	4.46167720337643	13.29591226871530
C	2.89435013528156	3.25828395128856	12.59958966115635
C	1.58900626569109	2.78291407852000	12.56524010942183
H	2.32202191138911	6.08427648436078	14.38127114822863
H	4.19768049858668	6.61475283146006	14.66151852289285
C	4.93161854457778	6.06299081245342	14.09264688324673
C	4.54757842121762	4.92856485413026	13.36142594003159
H	-2.81178514849790	3.16407492931006	13.69409602030440
C	0.85691238504757	9.37766237316272	14.79819484112515
H	-2.71650329010927	10.44296899533938	18.62982376628185
H	4.02984788413855	15.70429594704113	16.56455445087891
C	3.78649189879816	12.32123508916535	8.78119289235689
C	1.68091392845587	10.49948407597237	8.79047729712643
C	5.15422191846399	14.00733705614321	9.85324499512293
H	5.54504108387575	15.31970220865916	12.14027943423720
H	5.19967798185061	15.96952984868985	14.43330824679083
H	2.28540712710186	14.64953951351978	17.88186664176474

H	0.80817765419396	7.09434894337945	15.07350607801488
H	-0.95114863082930	1.98783644690405	12.62760124164962
H	1.38013254427298	1.85342700153353	12.04706452229838
C	3.94970444256425	2.55559672897906	11.93605133929879
C	6.23788820381141	6.49203937259849	14.11837079460349
C	5.55160683718748	4.21440067437646	12.67319693834937
H	-3.62727108719294	4.99779196400032	15.05530790831797
H	-4.13555714907442	8.69883971645129	17.86057810994866
H	-4.49497961462696	6.68940608207490	16.49062236670649
H	-1.36092363809372	12.20513383193298	19.47291639600679
H	0.53301453645882	13.75055760419605	19.21681500838484
H	1.21883423309529	11.57901458434302	14.20809035413818
C	5.21392976253744	3.02047898833798	11.95773992121623
C	6.87893153823534	4.67052855829479	12.70659724448368
C	7.22330093864572	5.79636591979044	13.41299953414462
H	6.50310188858771	7.37042142678416	14.69269566062719
H	8.24968620161969	6.13743273034523	13.43179831776299
H	7.63505638063143	4.11556346444153	12.16455379727952
H	6.00288460503474	2.48910036601106	11.43981740619946
H	3.70783537900545	1.64280258948907	11.40563206164898
C	3.46157072285786	11.59332671111143	7.62544373283862
C	2.42797909443745	10.68921995465470	7.62477954384990
C	4.84922825265483	13.28160579443522	8.75987526867940
H	0.85354440793948	9.80175878449017	8.79564688276394
H	2.18797579359773	10.13413432751293	6.72767151047854
H	4.03948633603090	11.75870629118886	6.72419836798080
H	5.39941580583696	13.42188605125359	7.83742224712588

H	5.95071193733517	14.74049596074190	9.82115947895810
C	2.21657503191928	9.31179800232910	15.09449240089113
C	3.14417218883720	9.07305915682454	14.09216496411791
C	2.72432604893535	8.85259948097206	12.78781558318632
C	1.36902911071390	8.88981724304166	12.49126889401779
C	0.44319498429696	9.16948004177938	13.48452615355368
H	2.54834198525439	9.47844373557321	16.11161598938821
H	4.20047903897095	9.05953838701008	14.32631214200130
H	3.44718118229605	8.65731908843630	12.00737527730009
H	1.03393212849561	8.69830569462616	11.48033940544688
H	-0.61234396487670	9.20759962105922	13.24664273893839

168_{Bi-Ph} TS1 PEh3c optimized

C	0.06722374526689	7.02217090952257	1.26144094395189
C	0.82146258695500	7.21637320212792	0.17707272659371
C	1.23526735891263	6.10031985446959	-0.61373385316717
C	0.87618675493718	4.75423026826965	-0.28818884190918
C	-0.00756097780577	4.54123049089315	0.87735870499906
C	-0.35449331795587	5.70287280125132	1.61396821695439
C	1.40819003278914	3.75350041513064	-1.10710719369262
C	2.22506226787772	4.02557565213914	-2.22018637936801
C	2.48843004018907	5.37828050580030	-2.55309387857158
C	2.00617971677376	6.37434159115887	-1.72576980600853
C	2.81993488953598	3.00720326913877	-3.07452185445024
C	2.77676110770412	1.63834063436207	-2.77373211987266
H	2.31817446160522	1.31593683724400	-1.85043094527809
H	1.16987139176240	2.72279190051169	-0.87737776698081
C	-1.14744290206928	5.57494630426231	2.72749675980706

C	-1.64955170145731	4.36700200457581	3.15890684917834
C	-1.38536016744658	3.15446547035047	2.44220666867906
C	-0.54353270573635	3.30741741672164	1.31080642041304
C	-2.04923500872377	1.91800011259842	2.97767819214467
C	-2.831111114633554	2.10171119880174	4.15990493669359
C	-2.99694352475584	3.34603023142048	4.83856145047062
C	-2.43681510514312	4.44622316354799	4.34562010666242
C	-3.53223176901016	1.05680029439097	4.71126010773702
C	-3.56355280867055	-0.19954976434716	4.16028839705554
C	-2.78465047180866	-0.49033482150090	3.00489357250593
C	-2.02687130484174	0.59106017457064	2.45291255702350
C	-4.44480838228632	-1.12692453872357	4.79667443699226
C	-4.63308275516041	-2.33891625690707	4.27558845576608
C	-3.88246778445156	-2.73547567427132	3.12926492631416
C	-2.89948680193911	-1.89257888753366	2.51163413282800
C	-2.14066761144542	-2.51367472893542	1.50630215888435
C	-2.36183302235761	-3.82256855141145	1.05771920441387
C	-3.43961992883579	-4.55952960600991	1.59926005835425
C	-4.14079947688314	-4.00706462416325	2.64911340216493
C	-3.80756974627623	-5.84493978744145	1.08509983198339
C	-3.15045496125265	-6.37599175966190	0.04211406319463
C	-1.99187678018095	-5.72334409732191	-0.49280960710759
C	-1.53585484539465	-4.49172390929653	0.05772579206873
C	-0.27949292422595	-4.03568345439391	-0.32008500160879
C	0.52990028207705	-4.73280977380257	-1.21892446809695
C	-0.01359827667848	-5.86073781490719	-1.88357041269022
C	-1.26002624073146	-6.33456813046147	-1.49682236563995

H	0.09694481107980	-3.13443428600835	0.14395747171782
H	2.07046613455605	-2.88589008247856	0.07284379456711
C	2.60512304070416	-3.44456649088064	-0.68188024259263
C	1.92631451708643	-4.40974557102709	-1.44132059568157
H	-4.63864989530530	-6.36623266375746	1.54430277085784
C	-1.16413234013335	0.31836620773342	1.27919606245816
H	-4.12255157665621	1.24536291691643	5.60006407861604
H	-0.25246657854203	7.84699696203308	1.88562845592017
C	3.50270409211815	3.39856444628775	-4.25109733215365
C	3.33354361233228	0.69624443796193	-3.60842472917625
C	3.22252916570924	5.73366001843064	-3.72799572268304
H	2.23342250867714	7.40887862634071	-1.95909823708778
H	1.13918641986422	8.20728230155349	-0.12080314095397
H	-1.39739675820832	6.46637233975072	3.29067051347331
H	-1.34482899790852	-1.96638048069124	1.03564231656983
H	-3.43993304887709	-7.33488002517945	-0.36973207209213
H	-1.64303561261912	-7.24232723985993	-1.95025807739510
C	0.74843889973246	-6.53858184677270	-2.88712551375378
C	3.95495776596824	-3.23114298821277	-0.83458418309615
C	2.66694714855244	-5.15604452847138	-2.38328359307298
H	-4.92108171479709	-4.59079436560928	3.12420910416629
H	-4.97657690345872	-0.80027710706674	5.68092091579813
H	-5.32903596975983	-3.04295209825102	4.71325311973041
H	-3.60550412560420	3.36784102481288	5.73308424468905
H	-2.56363782091591	5.41191286060212	4.81767620940366
H	-0.29017892612147	2.43878034824510	0.72617496056723
C	2.02510217125466	-6.19069223576866	-3.13815932968383

C	4.04213250582685	-4.91745207082852	-2.53149345456440
C	4.68477111459211	-3.97646076998631	-1.76531896252858
H	4.45838747807796	-2.50242531801969	-0.21294317977201
H	5.75140411415660	-3.82614334020716	-1.86621481661775
H	4.60150386692560	-5.51258301153513	-3.24312113662014
H	2.60094908447347	-6.71610370592379	-3.88981310003254
H	0.28070715140112	-7.35109650573578	-3.42999125191648
C	4.04363221230563	2.42428402173918	-5.10222674875652
C	3.95835615031021	1.08849559862556	-4.79580164795581
C	3.68105441124380	4.78440858035337	-4.56251529278096
H	3.29714971998004	-0.35259199426690	-3.33976615587665
H	4.38382849282821	0.35026898530938	-5.46149713996284
H	4.54244497100830	2.75250844616345	-6.00685677150303
H	4.21228535248729	5.05338482996446	-5.46795077958289
H	3.38048269236269	6.78575277334698	-3.93628451714879
C	0.18118525009384	0.01792488837358	1.47244779212734
C	0.99378513688576	-0.28009065935433	0.38836539564558
C	0.46270474060611	-0.29645283949900	-0.89505490541457
C	-0.87128165749230	0.02998853855099	-1.09475025561650
C	-1.68051595653384	0.34083617842645	-0.01218587887103
H	0.58501840245836	0.01333059535099	2.47674528217642
H	2.04135839509550	-0.50411804505203	0.54544310385092
H	1.08535749232108	-0.56190437072663	-1.73928518167509
H	-1.28099068507269	0.03549019377706	-2.09566614866839
H	-2.72403264159576	0.58501999835130	-0.16264407643961

C	4.14098134237099	14.48090733613571	15.40833878845819
C	5.30338305723430	14.07905692095166	14.86279187561452
C	5.65749443371614	12.68911238944568	14.81650894287721
C	4.77431984293949	11.71628703624088	15.35719600304397
C	3.45556088470074	12.14177202870749	15.80670887575418
C	3.18050199995612	13.52639873018916	15.88029488927971
C	5.21409509085135	10.40072429459467	15.43063284274525
C	6.44568088486829	9.98975013590890	14.92478139201358
C	7.26072590212345	10.94898762053603	14.27169174592285
C	6.86191700982557	12.28095929382784	14.26273935016836
C	6.91587867693211	8.61948630803792	15.01615396688347
C	6.25529705086780	7.63812645741257	15.77161716010730
H	5.38645386403871	7.90443836883700	16.35617066705338
H	4.57643530672198	9.66668669071594	15.89937001862127
C	1.96670936223664	13.92692575971907	16.41557786795824
C	0.98032780736213	13.01804559502526	16.77423036356593
C	1.15597515673641	11.62711648029616	16.51145035274847
C	2.43689837421358	11.24052026838574	16.11008311448224
C	0.00217189223932	10.72801857250852	16.71670734969446
C	-1.06290728007347	11.25053138176672	17.49687858572678
C	-1.11720086906715	12.63010438554580	17.88014313425714
C	-0.18025580294788	13.49345405952652	17.46321103614423
C	-2.11695564102748	10.42891042673455	17.83940701586739
C	-2.25601794602385	9.15096199205412	17.33137517395993
C	-1.31522128196675	8.64295545935521	16.38864769142244
C	-0.16455221537103	9.43704265283588	16.15227640967706
C	-3.40725382710882	8.40701906234148	17.74155808388580

C	-3.70606191672788	7.23942972870798	17.16183281461197
C	-2.88707101031315	6.72892417520289	16.10732411528465
C	-1.66914823386203	7.36828538922741	15.71988316305037
C	-0.96043600802256	6.73739703600059	14.68408207640738
C	-1.40067495779009	5.58763046649234	14.02483063664367
C	-2.67107345289740	5.06177399344349	14.35584674836357
C	-3.35574561674127	5.62048471282980	15.41832797494681
C	-3.26380881825301	4.01983150790850	13.57032537535660
C	-2.63143342752712	3.53376455435450	12.48908026093345
C	-1.29783936293293	3.95240817145961	12.16785699671434
C	-0.63418639345074	4.91614267169889	12.97680766171237
C	0.72364794785607	5.12712550544180	12.75790703258770
C	1.43025505794734	4.47532081123222	11.74249015646761
C	0.71035091761940	3.65042197781009	10.84201405430121
C	-0.63007604194817	3.38640849025052	11.09407868498749
H	1.25382556612754	5.80539311826109	13.41324789902171
H	3.27074395836698	5.56201836308085	13.43835680080586
C	3.69883367885713	5.19636593991526	12.51899455113933
C	2.86719283578464	4.59237772214746	11.56650558525875
H	-4.25119214992958	3.66668419113064	13.84069737327241
C	0.90824879796629	8.95308804322495	15.25669406593895
H	-2.89417771187370	10.81810679278462	18.48718739380963
H	3.89467209059365	15.53379829092750	15.46966308795557
C	8.09767201564614	8.24943774847695	14.33967353589298
C	6.70606076151492	6.33899737970666	15.81382299911896
C	8.47323138277685	10.53505675968370	13.63391231605499
H	7.51148039551357	13.02188179879139	13.80990421579480

H	6.00724003284426	14.80338947353824	14.47146389315838
H	1.77864665268629	14.98401588519704	16.56724598913140
H	-0.04634531607485	7.17098430740192	14.32641766389424
H	-3.10088050931143	2.78381271548898	11.86457625168581
H	-1.16251505996428	2.69894403267304	10.44602558580826
C	1.36918837974233	3.08590970886317	9.70344248631369
C	5.05679756722839	5.30841825708550	12.32907072669486
C	3.47412932159948	4.03705076989753	10.41943769097466
H	-4.31595890550849	5.20326714716058	15.70049188065582
H	-4.03875579073476	8.82827074081056	18.51350828814911
H	-4.58649035782930	6.67973950616320	17.45207184049374
H	-1.97071552327846	12.96707088758459	18.45492508093314
H	-0.25549098449017	14.55070355795838	17.68420776373884
H	2.66040268063175	10.19521194124290	16.01599710891029
C	2.68079925657698	3.30024710373478	9.48244067622875
C	4.85876471045983	4.17238172236413	10.23125154412019
C	5.64285776814579	4.80699962153482	11.16390652375592
H	5.67179242657824	5.77583490978203	13.08872017888109
H	6.70943618068683	4.90125526348222	11.00878415983242
H	5.30702496821045	3.75115381199502	9.33950471588883
H	3.16568650855571	2.88543549070533	8.60746854875611
H	0.78501618275363	2.49009254028168	9.01292046421316
C	8.53630800752187	6.91616114937407	14.38391949022988
C	7.84925443986734	5.96680476331704	15.10068118816272
C	8.85731164998616	9.24324625196805	13.64145922713672
H	6.17812683331868	5.60605657547600	16.40979280600476
H	8.19836230837163	4.94335276046010	15.12902491617414

H	9.44148065306370	6.64601324349873	13.85343463433599
H	9.76685264829892	8.93829993176128	13.13865964196630
H	9.07071418680750	11.28200384438757	13.12584208056102
C	1.80997920570110	7.98879123799663	15.70037457958368
C	2.89202656335097	7.63683764200669	14.91125574621865
C	3.08941020370759	8.24698227887873	13.67790741196534
C	2.16955869906867	9.17456883448520	13.21625342637717
C	1.08099058422839	9.52345509380069	14.00138990947018
H	1.66537358901990	7.53205567297841	16.67161024967395
H	3.59664631970979	6.89588263494037	15.26606390741140
H	3.95394827617417	7.99526030965312	13.07948295455826
H	2.31154504484867	9.64018629300969	12.25047539241852
H	0.37710721679646	10.26978703923164	13.65629310116236

168_{Bi-Ph} TS2 PBEh3c optimized

C	1.96732968187128	6.31715903592709	0.96297902560653
C	3.17469946756803	5.88455242618282	0.55864214651605
C	3.51570090216459	4.49215293139397	0.61039566221576
C	2.57236512734486	3.54749820723677	1.09914067292147
C	1.22239598856657	4.00217865619575	1.41455081216646
C	0.95695463291182	5.39203124671658	1.38878540146615
C	2.98689710895767	2.22992813006940	1.24943939779849
C	4.25603510409801	1.78972593675169	0.87499827712485
C	5.15035907159583	2.72482134090656	0.29422969419056
C	4.76763665240704	4.05773557707173	0.20126176631538
C	4.68475795289504	0.40971025959002	1.01760573403514
C	3.90548421422455	-0.56724423026006	1.65621983146929

H	2.96966438376900	-0.29133778014865	2.12029467664874
H	2.29591634220492	1.51633301884672	1.67125156653401
C	-0.29219041535951	5.83312478718122	1.79592033578220
C	-1.31488850182324	4.95563725574837	2.12999284272694
C	-1.13302776506170	3.55051455397476	1.97056388073591
C	0.17072172673408	3.12861459976964	1.69289836913246
C	-2.30702720516197	2.67364819969907	2.15708564402257
C	-3.41287383416963	3.24147494188972	2.84209132198591
C	-3.48539678474281	4.64606010619662	3.11923106372862
C	-2.51961327825075	5.47682512034796	2.70196440228151
C	-4.47102305069776	2.42916273684762	3.20123720389020
C	-4.56829995474141	1.11069167458316	2.79242387422720
C	-3.59889245920654	0.56116486324315	1.90295791922153
C	-2.45219847949144	1.35213985740067	1.66391266479954
C	-5.68046959853395	0.34783061220284	3.26768306259945
C	-5.88426377606894	-0.89941437365333	2.82491942332130
C	-5.03943923773166	-1.45655873935573	1.81335134615663
C	-3.89706987768268	-0.76683582728830	1.30952507653417
C	-3.21258831018345	-1.40148286751520	0.25164152345807
C	-3.57879391455257	-2.63912487602843	-0.29524742412773
C	-4.73573049680819	-3.27189031680809	0.22847637269201
C	-5.41571486087401	-2.67446748542167	1.27269519322475
C	-5.25058674085320	-4.48392752375492	-0.33349920019268
C	-4.65319194526091	-5.05042033785860	-1.39223927113341
C	-3.45202204630578	-4.49562792490874	-1.93919803058826
C	-2.86174327810888	-3.31964319194579	-1.38828698495871
C	-1.62653405182823	-2.92640314715490	-1.91112026507545

C	-0.98171757659574	-3.62310295669194	-2.94837706011814
C	-1.64590402948640	-4.72621639113655	-3.53966782303910
C	-2.85469584468464	-5.14249872776464	-3.00656087809721
H	-1.13817728786110	-2.05248344700607	-1.49726548030414
H	0.87113002347308	-1.94125313081386	-1.88667824385485
C	1.18573044900005	-2.37572515189496	-2.82071989786203
C	0.34546514999384	-3.29874063410413	-3.45205549266769
H	-6.14620181715215	-4.91501653596279	0.09492884975819
C	-1.35293297349253	0.81384837771141	0.84543683444543
H	-5.27326090032225	2.84983208835830	3.79714591872333
H	1.72829290372863	7.37359377447394	0.95101181327230
C	5.93357497126690	0.01694399265952	0.48994515496620
C	4.30854684843972	-1.88074302816166	1.71857112202900
C	6.42376096552759	2.28774130772094	-0.19193167898943
H	5.46842425285388	4.77865231978880	-0.20552408426985
H	3.92354438056883	6.58532952570021	0.20923965851003
H	-0.47550984784448	6.89944304941566	1.87203172152849
H	-2.37781362398323	-0.90059744738099	-0.20252542260019
H	-5.05206835833138	-5.95098983195720	-1.84117689279794
H	-3.33887847871311	-6.01819229216112	-3.42417629349058
C	-1.07087124546522	-5.42256338504378	-4.65083483560548
C	2.42407944354078	-2.05361324086398	-3.32813100043792
C	0.85539231865113	-3.97538444094649	-4.58413834274045
H	-6.30491688108265	-3.15979447923194	1.65872260298943
H	-6.34304373315437	0.80193513157658	3.99334141957386
H	-6.71593689630593	-1.49035224217323	3.18644837598869
H	-4.37003371450050	5.02516414226634	3.61611311175992

H	-2.60409417245872	6.54756441581958	2.84324170529041
H	0.38296826108691	2.07522500507256	1.69342832721977
C	0.11111136749985	-5.04674691593515	-5.17052310152160
C	2.12088753043593	-3.63826605147768	-5.09031777040161
C	2.88956998753195	-2.67189298620122	-4.49155562703338
H	3.05122825143722	-1.33854125249488	-2.81125608408748
H	3.86046246196358	-2.41620695263678	-4.89651461338289
H	2.49578379185230	-4.17617198574173	-5.95368816912446
H	0.53965251766078	-5.57845625685357	-6.01221852241387
H	-1.61340067008965	-6.26429281503162	-5.06371350714423
C	6.33078344778520	-1.32750054166052	0.56662214322875
C	5.52739375294281	-2.27118432256280	1.15786742471517
C	6.78932764851670	0.99313448293461	-0.11528543980902
H	3.68035669012291	-2.61320767904536	2.20861309295716
H	5.83852103712925	-3.30638552212930	1.19909785779775
H	7.28841005237432	-1.61345278335540	0.14876473629513
H	7.74673963523681	0.66908534862547	-0.50449813023730
H	7.08387746593088	3.01876385282204	-0.64272117975646
C	-0.52607104984789	-0.18613535240648	1.34704604617229
C	0.59597836931581	-0.57131302067685	0.63456554199484
C	0.90799351387349	0.05871985300134	-0.56423114270514
C	0.03436996279641	0.98785706872818	-1.10941671344068
C	-1.09879134565469	1.35930686354710	-0.40623119886332
H	-0.76022365431271	-0.64088361580233	2.30185878183928
H	1.24066861297166	-1.34988103763868	1.01914198858843
H	1.83412478590855	-0.17687564078653	-1.06938841332253
H	0.24569136266203	1.43659083219593	-2.07027119643530

H -1.77263660655452 2.10959320944225 -0.80036500254323

169_H MINO PBEh3c optimized

C -6.99533736099968 14.99213144290005 15.83929890627503

C -6.38677290932696 14.85999536523512 14.62118619846469

C -6.45675673357270 13.63121825040747 13.95403565617669

C -7.06879814886629 12.55259643451318 14.53922179344542

C -7.63266820952965 12.62525986628089 15.83428391741288

C -7.64793547346655 13.90417068429610 16.45086304578551

C -8.38693446834770 14.10260588429852 17.64709578371318

C -9.13816282259276 13.10108591661727 18.16023671925786

C -9.96436001208117 10.79131573192577 18.13067678211605

C -9.11241415673914 11.80066496019694 17.58923865513956

C -8.27462056605939 11.51744464995128 16.50273482185379

C -8.94471098993114 7.83967495366216 16.19982554653302

C -2.64744481583919 10.46969917373387 12.75675576525973

H 1.02231228812183 11.26190161159115 10.15792788729807

C 0.30578966920022 11.66592301896582 10.86226127795424

C 0.25982163056567 12.99055893342052 11.11907067829301

C -0.63227693964289 13.52681579266987 12.09640720454596

C -0.64609408304736 14.92838641308312 12.32937773311379

C -1.43942995780798 15.46921904641820 13.28347266137522

C -2.71073721888371 12.43822761845993 15.01384941482680

C -3.36547180929497 13.00311313855267 16.07813728444971

C -3.48328921252453 14.39449765302765 16.18401062953163

C -2.87695193891767 15.18964197241347 15.25014814017725

C -2.18032428872582 14.63262627541077 14.16004177823993

C	-2.15265794636147	13.22510101023514	13.97985274518974
C	-1.47250815782536	12.67961765832687	12.82935902189836
C	-1.59057033473009	11.30553029221134	12.38827229959483
C	-0.64120389997907	10.78738399818213	11.46317046157607
C	-0.70145911395912	9.44362098116182	11.10121246581993
C	-2.72828801285782	6.40821647340105	11.60280359823983
C	-1.73438008031080	7.21576652330913	11.18958521620368
C	-1.69738397746516	8.60027866202163	11.56559440006226
C	-2.72412480064853	9.13467081540963	12.38886355600710
H	-4.86647726055771	9.74083957395411	13.92857036399466
C	-5.86560306543537	7.86823511803770	14.07660597187279
C	-4.84720431559430	8.70327625239596	13.63213472579335
C	-3.80530094966925	8.26194849634230	12.82503324299256
C	-3.79096334923660	6.90042253153950	12.43255935427763
H	-4.79418790881957	5.01829526422902	12.56020989344109
C	-4.80813104560116	6.05907285955130	12.86463536478825
C	-5.84091790624096	6.50871320106610	13.67726843528145
C	-6.87733166426603	5.61703175244219	14.11421961003072
C	-7.87750347995643	6.04524453936958	14.90593923145146
C	-7.94897923520596	7.41165761073401	15.33795496099049
C	-6.95474014396255	8.33694791875662	14.92236122530028
C	-7.06380045042821	9.65544463774931	15.33960715211792
C	-8.12257296714006	10.12855825083028	16.11875918251677
C	-9.03652159604756	9.16220821568886	16.62615049657510
C	-9.97897762530504	9.54043874108571	17.62477220997622
H	-10.66381590527627	8.79492865151856	18.00890564608296
H	-7.00846101795637	15.95168866473668	16.34272732564379

H	-5.88515172616827	15.70029682501660	14.16173816638902
H	-6.04198652927702	13.53294987342013	12.95978850653449
H	-7.16850636463655	11.65106679250527	13.95447471927109
H	-8.38698454223428	15.08348300585200	18.10641912836180
H	-9.76016621186131	13.26970347143037	19.03075882500055
H	-10.62889466328412	11.06216668691692	18.94176804062029
H	-9.65991274473803	7.11859767391163	16.58020270371070
H	-3.46118406560748	10.90671330509721	13.31151260777490
H	0.93167172248301	13.67053084843160	10.61000501817682
H	-0.02024242866841	15.56203596516660	11.71324892941970
H	-1.47238762426657	16.54180435730395	13.43096146378880
H	-2.56752002415516	11.36831585849847	15.01250774106535
H	-3.77484757646604	12.36847787838469	16.85286317089265
H	-4.01853098905437	14.83177282611767	17.01541522871322
H	-2.90152001944135	16.26811715273670	15.35224369056758
H	0.04199223476152	9.05288575544485	10.41538335306392
H	-2.74307956389281	5.36430749041547	11.31479657761485
H	-0.93864043257558	6.83046298446386	10.56411621742557
H	-6.83561457026840	4.58370255482236	13.79261834279158
H	-8.64963987327656	5.36077409609061	15.23507957288021
H	-6.27183926822558	10.34458111565412	15.09936155697785

169_H TS1 PBEh3c optimized

C	-2.50670356476297	4.19538654084888	1.50761084476734
C	-1.43693337065321	4.11234318643239	0.66372062714242
C	-0.99213548539730	2.84327458106320	0.28913528559512
C	-1.61954031997606	1.71261173311607	0.74480715063633

C	-2.74634617873732	1.73382454451953	1.60419765433495
C	-3.16353058570558	3.04411406811483	1.98639394169383
C	-4.25513667760236	3.23364168943877	2.86756033709848
C	-4.91960145958650	2.16784550335444	3.35270070914923
C	-5.37098149180243	-0.18570097553735	3.53587093235253
C	-4.55917836762125	0.84664822326137	2.98004191235427
C	-3.48612071396237	0.57637247332808	2.10767494602948
C	-3.95977863509982	-3.18081474737206	2.02182722270857
C	2.22223259792916	-0.54228625832539	-1.59916929800527
H	5.59936480430242	0.34010922008658	-4.54166325833713
C	4.96404177887654	0.71946705059345	-3.75102161953722
C	4.94274640889435	2.03597557793347	-3.45283896838429
C	4.16292777755719	2.53730911057932	-2.36701845065251
C	4.16996147935543	3.93133130792646	-2.09134437558992
C	3.48915143094368	4.43788771075427	-1.03676879960929
C	2.44429701127499	1.34367223478349	0.73387725052327
C	1.92921606681470	1.87054857096965	1.89040313121828
C	1.81542892143622	3.25712588357889	2.05376109839131
C	2.29595970978586	4.08619307200355	1.07714911777231
C	2.86051050844642	3.56901442429089	-0.10578250780500
C	2.87059705232866	2.16815272581423	-0.33337707099446
C	3.41215434645372	1.66283609179582	-1.57195780842622
C	3.24269709076542	0.30385940301773	-2.04174988896484
C	4.08919403194727	-0.18115569304314	-3.07765771337974
C	3.99694270474274	-1.51532499864912	-3.46626017555325
C	2.04997217352199	-4.57642755260601	-2.83259197109427
C	2.99438093497807	-3.75279911061578	-3.32226543426554

C	3.04954005760491	-2.37298960036855	-2.93228021737775
C	2.09529407148921	-1.86010026774436	-2.01300282087626
H	0.00404556400085	-1.26326702416731	-0.40082006460869
C	-0.97867290425866	-3.14320409757370	-0.21114284126852
C	0.01708568886459	-2.30200853095422	-0.69498543671754
C	1.03633142552747	-2.73816912635852	-1.53366689301087
C	1.04321495094541	-4.09918406548939	-1.92791194768680
H	0.09394516740289	-6.00070337093381	-1.71314434540802
C	0.07137226679305	-4.95506311382909	-1.42649974290333
C	-0.92684681727479	-4.51434487666387	-0.56740323433840
C	-1.89297795025049	-5.43144231595508	-0.03174834304166
C	-2.85233886827832	-5.01599000449479	0.81484141535474
C	-2.96584987923452	-3.63261442562243	1.17643922037403
C	-2.05979123830412	-2.68135897815359	0.65101614068717
C	-2.24249432923756	-1.34130806964243	0.96113146700446
C	-3.25242840128936	-0.83825370018456	1.79047136220411
C	-4.11723860784446	-1.83485978124344	2.34564287249587
C	-5.16871992549990	-1.47768829036325	3.23019084984884
H	-5.79722017384964	-2.25679363699527	3.64252998011648
H	-2.87643231192629	5.16173267504191	1.82845648872683
H	-0.93839054232253	5.00085630282075	0.30134707853591
H	-0.13310736508105	2.74147374382957	-0.36092185420620
H	-1.17759987651476	0.79792036289174	0.41193347635351
H	-4.54266563273687	4.24136543653578	3.13970121772155
H	-5.75511343599405	2.29927088669485	4.02855497315733
H	-6.17233915197478	0.10130592410057	4.20514765501633
H	-4.65541528403859	-3.89509076591728	2.44833084599793

H	1.47875391106002	-0.12871848941611	-0.93738845011687
H	5.55394541294018	2.73411125805825	-4.01124179556608
H	4.71891975937394	4.58701975989796	-2.75587039225650
H	3.46872317961855	5.50509671451897	-0.85334850954322
H	2.58039139248316	0.27435624511578	0.67332217249767
H	1.61995765722387	1.20748997578251	2.68716085892571
H	1.37657805347359	3.66400650255325	2.95420367145170
H	2.27340536980372	5.16078009471697	1.21403069211361
H	4.67180149565041	-1.88655280041538	-4.22941061838298
H	2.02647343151033	-5.61931723875353	-3.12353726649445
H	3.73968994190963	-4.12292268780638	-4.01542154545090
H	-1.82467530798274	-6.47406393740533	-0.31680325378172
H	-3.56725827366526	-5.71767556068106	1.22658204169423
H	-1.55768249956468	-0.66813671688262	0.50025027158992

169_H INT1 PBEh3c optimized

C	-2.77441407213951	4.32121753774217	0.27891139207833
C	-1.43161515857454	4.13868863922834	0.09183753924421
C	-0.84548320597038	2.92868231516943	0.48491513934683
C	-1.61806962893515	1.90726913668544	0.97492073690923
C	-3.02366933586831	2.01929214356863	1.08037555859093
C	-3.58268220938244	3.29428387657724	0.80494058491255
C	-4.94131886591923	3.55369680446992	1.12502153718965
C	-5.68815107773826	2.60978464237106	1.74269325174988
C	-6.01165755243687	0.33693463298876	2.60214904704133
C	-5.18158112691300	1.29917726460074	1.95317932293764
C	-3.89355809967260	0.95414232367876	1.52172024888668

C	-4.08741141718266	-2.74590310816455	2.14106511936520
C	2.30333629362735	-0.32377003796638	-1.28053533344464
H	5.65809706375481	0.46463324139463	-4.27349137891525
C	5.03920517791039	0.86288786172790	-3.47901886558385
C	5.03202715732342	2.18545680657960	-3.20589124271693
C	4.28590843023784	2.70975693844131	-2.10707224669112
C	4.32494876818535	4.10436021820242	-1.83657678805610
C	3.69539143623950	4.62450602890249	-0.75681543244509
C	2.66425178741365	1.54698436263349	1.05291944868944
C	2.23005259393683	2.08041875837861	2.23994403907341
C	2.15941196655515	3.46921761361183	2.41446812716964
C	2.60025918364455	4.29244319041405	1.41364927009879
C	3.09183067237968	3.76746502391248	0.20179198280742
C	3.05963234257683	2.36775793050247	-0.02901289904742
C	3.54235197704572	1.85332416976032	-1.28696678901856
C	3.33821812819430	0.49511646778740	-1.74078660750499
C	4.17159254575297	-0.01953273615023	-2.77242355470913
C	4.08069851553421	-1.36743798180261	-3.11140300437466
C	2.19021324611274	-4.41746313287312	-2.27605943900466
C	3.11067851442077	-3.60893628869371	-2.83284333145665
C	3.13641050815580	-2.20447820610979	-2.54010522533659
C	2.16654238950036	-1.65033579419401	-1.66179084903262
H	-0.06588154875300	-0.94861918165161	-0.28017551095424
C	-0.98156302127090	-2.84044818459158	0.06607786513603
C	0.00896853453672	-2.01341890059877	-0.45179666066909
C	1.09358706417331	-2.50291093669105	-1.17115013433928
C	1.15497755247140	-3.89485624478595	-1.43017289938786

H	0.28878639330329	-5.80376823229004	-1.01349768903910
C	0.20766114324721	-4.73372309897608	-0.85684162846275
C	-0.83693930025795	-4.24174467692553	-0.08520135363526
C	-1.75428960590661	-5.12671976343610	0.57576736533308
C	-2.75312468642446	-4.64970251398602	1.34151893294207
C	-2.98897039092291	-3.23819759715049	1.45828143599095
C	-2.13764348676447	-2.32522216679289	0.78370937528408
C	-2.45801042570834	-0.97608516624552	0.80033393689859
C	-3.53967821755124	-0.45247596493937	1.51671951519271
C	-4.39243222287481	-1.38663808918342	2.17295595295634
C	-5.61143479899991	-0.94155825986308	2.75977583210775
H	-6.23578835543587	-1.65799356238167	3.27883672891050
H	-3.23526088048533	5.27299188841553	0.04395602133713
H	-0.81796276824591	4.93264603513945	-0.31224611075198
H	0.22682444648447	2.80621812585956	0.42678154705079
H	-1.11891565342425	1.02536118066548	1.34716117110610
H	-5.35118459183975	4.53421294831053	0.91566843888595
H	-6.70140664411426	2.82783463124083	2.05646213091224
H	-6.97294032622327	0.66066751357210	2.98147774843197
H	-4.76350617846351	-3.44129684096408	2.62602991255642
H	1.56654988260376	0.11099403338986	-0.62301186160725
H	5.63599862662267	2.86902050150373	-3.78955704851992
H	4.86027842378494	4.74934397688844	-2.52240965290719
H	3.70289129337693	5.69192953600405	-0.57407130525465
H	2.76009296544004	0.47430648455526	0.97628934900704
H	1.95412616147080	1.42034699847182	3.05155711230485
H	1.78806949818214	3.88233779142253	3.34221168585828

H	2.60600559673353	5.36657117736172	1.55448577752889
H	4.75992807218046	-1.76878372913948	-3.85523649634542
H	2.20103340273457	-5.48148381584240	-2.47761117592812
H	3.86847019725563	-4.01271725881344	-3.49278043618906
H	-1.60923179134542	-6.19427131410073	0.46406760111985
H	-3.42150296404951	-5.32792333643864	1.85755171264932
H	-1.90012834330948	-0.31626463038805	0.15710345573735

169_H TS2 PBEh3c optimized

C	-2.27699487475333	3.91533462006034	2.47336569976643
C	-1.07392076856792	3.49845976262101	2.97275016946003
C	-0.80012901585804	2.12647364346073	3.04815155278880
C	-1.69408463319898	1.20765213382496	2.56492769951536
C	-2.92520979445772	1.60404145826452	1.99703002545387
C	-3.23552217212494	2.98790014739982	2.02126354836270
C	-4.54353495648040	3.42125066600084	1.67895629861561
C	-5.52187495259352	2.51472506189238	1.44674054995335
C	-6.31213792618936	0.19151417838675	1.28404847275768
C	-5.23806461818549	1.12298096897775	1.41150188154279
C	-3.91965916229388	0.66907625601767	1.53961956608717
C	-4.49400138419683	-2.99431996215125	1.11661130067530
C	2.42200515226527	-0.58661793041906	-1.31936566335040
H	5.65838638439660	-0.19399138616147	-4.51602602158469
C	5.01448913675616	0.31956787519060	-3.81265410288203
C	4.86186222287524	1.65971936352739	-3.86429272387355
C	4.09000728305111	2.34888542331473	-2.88103793167857
C	3.99736170434625	3.76533319058647	-2.93360639307660

C	3.37651081795805	4.46157266654342	-1.95250764336581
C	2.74604612789239	1.78748212861360	0.54984090979753
C	2.37326015607943	2.53778980282951	1.63375074718397
C	2.20454359649832	3.92406949379315	1.51941708154375
C	2.47974454655002	4.53761633113182	0.32838030632986
C	2.91848209166855	3.79561795968793	-0.78524758318398
C	2.99585157058264	2.38129545712366	-0.70753145001242
C	3.46390074870576	1.63950063409788	-1.84892091660290
C	3.38082207653248	0.19987089163951	-1.97218045967023
C	4.25582338028013	-0.45067466896654	-2.88428824491212
C	4.30171058332302	-1.84027732552575	-2.90196611658758
C	2.61387713386220	-4.80290702378788	-1.55214924142164
C	3.52738690737103	-4.04034343137845	-2.17468165942234
C	3.42414382274047	-2.61071535262169	-2.16032596252922
C	2.38750973000756	-1.97195935527823	-1.42260665463208
H	0.03309808151015	-1.21137426228593	-0.26483434065624
C	-0.88086126827269	-3.09255940830338	0.16379152349597
C	0.16335130514632	-2.28482387021896	-0.28781138060986
C	1.33370140481397	-2.80183481164282	-0.84418769817346
C	1.47293051658799	-4.21210448853730	-0.91429834265323
H	0.56981616384870	-6.09860127126840	-0.49573605801696
C	0.45938300895220	-5.02205048461933	-0.42689755036292
C	-0.71989911462249	-4.49970089172094	0.08038796901789
C	-1.79218060485749	-5.38090451410843	0.44249143408945
C	-2.99722350739131	-4.89640542119469	0.78430956425885
C	-3.22423637046386	-3.48351675256821	0.86745415072044
C	-2.15552440462028	-2.56889934738719	0.64881820748910

C	-2.39465925308637	-1.22073758707959	0.88478776651000
C	-3.65269794298052	-0.72450999795475	1.25270603696016
C	-4.74653594862694	-1.63284944603449	1.24274046220068
C	-6.08169436931679	-1.13840198024320	1.29014256831186
H	-6.90119136550673	-1.84560313790802	1.26529365158847
H	-2.52642543604131	4.96931767391844	2.45657997846592
H	-0.35703322053491	4.21858827898523	3.34287418887353
H	0.11331910560441	1.78202771201645	3.51288797671817
H	-1.47290820686561	0.15835308216428	2.69207912053486
H	-4.76105557721553	4.48214740803494	1.67527301636719
H	-6.54034438685485	2.83973177452952	1.27281072894659
H	-7.32417177310216	0.57404377617856	1.23472862473044
H	-5.32248254159774	-3.69080471708376	1.18028292068496
H	1.64806132350382	-0.08265097235491	-0.75864230385626
H	5.36728298277123	2.24274320515918	-4.62416559863543
H	4.43164854603835	4.28035987584206	-3.78150800507177
H	3.28683842803844	5.53910144104518	-2.01297387286236
H	2.92316937634613	0.73145474834553	0.68953922501187
H	2.23588894165689	2.05435734987309	2.59120469109815
H	1.90090380656393	4.50809973042825	2.37775298495266
H	2.40440786730565	5.61446007074217	0.23882845163495
H	5.02479724446228	-2.33348995001482	-3.54215957266222
H	2.69793626141303	-5.88257726580898	-1.55982050580741
H	4.36121790790049	-4.49133656792742	-2.69778825474116
H	-1.62041950778508	-6.44876466273047	0.38751875472095
H	-3.82072797888706	-5.56422745690798	1.00477499523940
H	-1.59407040867654	-0.51198054005499	0.73379745043874

7. Literature

- [1] Gingras M, *Chem. Soc. Rev.* **2013**, *42*, 1051–1095.
- [2] Y. Shen, C. F. Chen, *Chem. Rev.* **2012**, *112*, 1463–1535.
- [3] I. G. Stará, I. Stary, *Phenanthrenes, Helicenes, and Other Angular Acenes*, Thieme, Stuttgart, **2009**.
- [4] N. Hoffmann, *J. Photochem. Photobiol. C Photochem. Rev.* **2014**, *19*, 1–19.
- [5] J. Meisenheimer, K. Witte, *Berichte der deutschen chemischen Gesellschaft* **1903**, *36*, 4153–4164.
- [6] R. Weitzenböck, H. Lieb, *Monatsh. Chem.* **1912**, *33*, 549–565.
- [7] W. E. Bachmann, R. O. Edgerton Vol, *J. Am. Chem. Soc.* **1940**, *62*, 2970–2973.
- [8] M. Newman, D. Lednicer, *J. Am. Chem. Soc.* **1956**, *78*, 4765–4770.
- [9] R. H. Martin, *Angew. Chem. Int. Ed. Engl.* **1974**, *13*, 649–659.
- [10] K. Dhbaibi, L. Favereau, J. Crassous, *Chem. Rev.* **2019**, *119*, 8846–8953.
- [11] S. Moussa, F. Aloui, B. ben Hassine, *Synth. Commun.* **2011**, *41*, 1006–1016.
- [12] S. Moussa, F. Aloui, P. Retailleau, B. ben Hassine, *Synth. Commun.* **2012**, *42*, 1010–1018.
- [13] G. Pieters, A. Gaucher, S. Marque, F. Maurel, P. Lesot, D. Prim, *J. Org. Chem.* **2010**, *75*, 2096–2098.
- [14] S. Cauteruccio, E. Licandro, M. Panigati, G. D'Alfonso, S. Maiorana, *Coord. Chem. Rev.* **2019**, *386*, 119–137.
- [15] Y.-H. Tian, G. Park, M. Kertesz, *Chem. Mater.* **2008**, *20*, 3266–3277.
- [16] R. Kumar, D. K. Maity, *Int. Quantum J. Chem.* **2021**, *121*, e26450.
- [17] P. Sehnal, I. G. Stará, D. Šaman, M. Tichý, J. Míšek, J. Cvačka, L. Rulíšek, J. Chocholoušová, J. Vacek, G. Goryl, M. Szymonski, I. Císařová, I. Starý, *Proc. Natl. Acad. Sci. U. S. A.* **2009**, *106*, 13169–13174.
- [18] C. Chen, Y. Shen, *Helicene Chemistry: From Synthesis to Applications*, Springer, Berlin, Heidelberg, **2016**.
- [19] M. Gingras, G. Félix, R. Peresutti, *Chem. Soc. Rev.* **2013**, *42*, 1007–1050.
- [20] R. S. Cahn, C. Ingold, V. Prelog, *Angew. Chem. Int. Ed. Engl.* **1966**, *5*, 385–415.
- [21] P. Ravat, *Chem. – Eur. J.* **2021**, *27*, 3957–3967.
- [22] M. B. Groen, H. Wynberg, *J. Am. Chem. Soc.* **1971**, *93*, 2968–2974.
- [23] C. M. Kemp, S. F. Mason, *Tetrahedron* **1966**, *22*, 629–635.

- [24] D. Lightner, D. Hefelfinger, G. Frank, T. Powers, K. Trueblood, *Nat. Phys. Sci.* **1971**, *232*, 124–125.
- [25] KP Meurer, F Vögtle, in *Top. Curr. Chem.*, **1985**, pp. 1–76.
- [26] H Wynberg, *Acc. Chem. Res.* **1971**, *4*, 65–73.
- [27] R Kuroda, *J. Chem. Soc. Perkin Trans* **1982**, *2*, 789–794.
- [28] K. Yamamoto, M. Okazumi, H. Suemune, K. Usui, *Org. Lett.* **2013**, *15*, 1806–1809.
- [29] C. Goedicke, H. Stegemeyer, *Tetrahedron Lett.* **1970**, *11*, 937–940.
- [30] H. Marom, S. Pogodin, I. Agranat, *Polycyclic Aromat. Compd.* **2007**, *27*, 295–310.
- [31] P. Ravat, R. Hinkelmann, D. Steinebrunner, A. Prescimone, I. Bodoky, M. Juriček, *Org. Lett.* **2017**, *19*, 3707–3710.
- [32] J. Barroso, J. L. Cabellos, S. Pan, F. Murillo, X. Zarate, M. A. Fernandez-Herrera, G. Merino, *Chem. Commun.* **2017**, *54*, 188–191.
- [33] R. H. Martin, M. J. Marchant, *Tetrahedron Lett.* **1972**, *13*, 3707–3708.
- [34] R. H. Martin, M. J. Marchant, *Tetrahedron* **1974**, *30*, 347–349.
- [35] H. J. Lindner, *Tetrahedron* **1975**, *31*, 281–284.
- [36] R. H. Janke, G. Haufe, E. U. Würthwein, J. H. Borkent, *J Am Chem Soc* **1996**, *118*, 6031–6035.
- [37] F. Lebon, G. Longhi, F. Gangemi, S. Abbate, J. Priess, M. Juza, C. Bazzini, T. Caronna, A. Mele, *J. Phys. Chem. A* **2004**, *108*, 11752–11761.
- [38] M. P. Johansson, M. Patzschke, *Chem. – Eur. J.* **2009**, *15*, 13210–13218.
- [39] G. R. Kiel, K. L. Bay, A. E. Samkian, N. J. Schuster, J. B. Lin, R. C. Handford, C. Nuckolls, K. N. Houk, T. D. Tilley, *J. Am. Chem. Soc.* **2020**, *142*, 11084–11091.
- [40] B. Liu, M. Böckmann, W. Jiang, N. L. Doltsinis, Z. Wang, *J. Am. Chem. Soc.* **2020**, *142*, 7092–7099.
- [41] K. Fujise, E. Tsurumaki, G. Fukuhara, N. Hara, Y. Imai, S. Toyota, *Chem. Asian J.* **2020**, *15*, 2456–2461.
- [42] K. Fujise, E. Tsurumaki, K. Wakamatsu, S. Toyota, *Chem. – Eur. J.* **2021**, *27*, 4548–4552.
- [43] G. R. Kiel, S. C. Patel, P. W. Smith, D. S. Levine, T. D. Tilley, *J. Am. Chem. Soc.* **2017**, *139*, 18456–18459.
- [44] G. R. Kiel, K. L. Bay, A. E. Samkian, N. J. Schuster, J. B. Lin, R. C. Handford, C. Nuckolls, K. N. Houk, T. D. Tilley, *J. Am. Chem. Soc.* **2020**, *142*, 11084–11091.
- [45] Y. Nakakuki, T. Hirose, K. Matsuda, *J. Am. Chem. Soc.* **2018**, *140*, 15461–15469.
- [46] D. Reger, P. Haines, K. Y. Amsharov, J. A. Schmidt, T. Ullrich, S. Bönisch, F. Hampel, A. Görling, J. Nelson, K. E. Jelfs, D. M. Guldi, N. Jux, *Angew. Chem. Int. Ed.* **2021**, *60*, 18073–18081.

- [47] S. Obenland, W. Schmidt, *J. Am. Chem. Soc.* **1975**, *97*, 6633–6638.
- [48] B. M. Deb, G. Kavu, *Can. J. Chem.* **1980**, *58*, 258–262.
- [49] J. M. Schulman, R. L. Disch, *J. Phys. Chem. A* **1999**, *103*, 6669–6672.
- [50] G. Portella, J. Poater, J. M. Bofill, P. Alemany, M. Solà, *J. Org. Chem.* **2005**, *70*, 2509–2521.
- [51] C. A. Liberko, L. L. Miller, T. J. Katz, L. Liu, *J. Am. Chem. Soc.* **1993**, *115*, 2478–2482.
- [52] K. Górski, K. Noworyta, J. Mech-Piskorz, *RSC Adv.* **2020**, *10*, 42363–42377.
- [53] T. Fujikawa, Y. Segawa, K. Itami, *J. Am. Chem. Soc.* **2015**, *137*, 7768.
- [54] T. Fujikawa, Y. Segawa, K. Itami, *J. Org. Chem.* **2017**, *82*, 7745–7749.
- [55] J. B. Birks, D. J. S. Birch, E. Cordemans, E. vander Donckt, *Chem. Phys. Lett.* **1976**, *43*, 33–36.
- [56] C. Kitamura, Y. Tanigawa, T. Kobayashi, H. Naito, H. Kurata, T. Kawase, *Tetrahedron* **2012**, *68*, 1688–1694.
- [57] H. Kubo, T. Hirose, K. Matsuda, *Org. Lett.* **2017**, *19*, 1776–1779.
- [58] H. Oyama, K. Nakano, T. Harada, R. Kuroda, M. Naito, K. Nobusawa, K. Nozaki, *Org. Lett.* **2013**, *15*, 2104–2107.
- [59] T. Mori, *Chem. Rev.* **2021**, *121*, 2373–2412.
- [60] W. L. Zhao, M. Li, H. Y. Lu, C. F. Chen, *Chem. Commun.* **2019**, *55*, 13793–13803.
- [61] F. Furche, R. Ahlrichs, C. Wachsmann, E. Weber, A. Sobanski, F. Vögtle, S. Grimme, *J. Am. Chem. Soc.* **2000**, *122*, 1717–1724.
- [62] X. Liu, P. Yu, L. Xu, J. Yang, J. Shi, Z. Wang, Y. Cheng, H. Wang, *J. Org. Chem.* **2013**, *78*, 6316–6321.
- [63] T. R. Kelly, I. Tellitu, J. P. Sestelo, *Angew. Chem. Int. Ed. Engl.* **1997**, *36*, 1866–1868.
- [64] T. Blythe, D. Bloor, *Electrical Properties of Polymers*, Cambridge University Press, New York, **2005**.
- [65] W. Warta, N. Karl, *Phys. Rev. B* **1985**, *32*, 1172.
- [66] I. M. Rutenberg, O. A. Scherman, R. H. Grubbs, W. Jiang, E. Garfunkel, Z. Bao, *J. Am. Chem. Soc.* **2004**, *126*, 4062–4063.
- [67] V. Podzorov, E. Menard, A. Borissov, V. Kiryukhin, J. A. Rogers, M. E. Gershenson, *Phys. Rev. Lett.* **2004**, *93*, 086602.
- [68] L. Shan, D. Liu, H. Li, X. Xu, B. Shan, J.-B. Xu, Q. Miao, L. Shan, D. Liu, X. Xu, B. Shan, Q. Miao, H. Li, J. Xu, *Adv. Mater.* **2015**, *27*, 3418–3423.
- [69] J. Luo, X. Xu, R. Mao, Q. Miao, *J. Am. Chem. Soc.* **2012**, *134*, 13796–13803.
- [70] T. Fujikawa, N. Mitoma, A. Wakamiya, A. Saeki, Y. Segawa, K. Itami, *Org. Biomol. Chem.* **2017**, *15*, 4697–4703.

- [71] C. Li, Y. Yang, Q. Miao, *Chem. Asian J.* **2018**, *13*, 884–894.
- [72] T. J. Katz, W. Slusarek, *J. Am. Chem. Soc.* **1979**, *101*, 4259–4267.
- [73] K. Yamamoto, T. Ikeda, T. Kitsuki, Y. Okamoto, H. Chikamatsu, M. Nakazaki, *J. Chem. Soc., Perkin Trans. 1* **1990**, 271–276.
- [74] Y. Dai, T. J. Katz, *J. Org. Chem.* **1997**, *62*, 1274–1285.
- [75] Y. Dai, T. J. Katz, D. A. Nichols, *Angew. Chem. Int. Ed. Engl.* **1996**, *35*, 2109–2111.
- [76] M. Nakazaki, K. Yamamoto, T. Ikeda, T. Kitsuki, Y. Okamoto, *J. Chem. Soc., Chem. Commun.* **1983**, 787–788.
- [77] S. Honzawa, H. Okubo, S. Anzai, M. Yamaguchi, K. Tsumoto, I. Kumagai, *Bioorg. Med. Chem.* **2002**, *10*, 3213–3218.
- [78] G. Bredig, P. S. Fiske, *Biochem. Z.* **1912**, *46*, 7–23.
- [79] B. B. Hassine, M. Gorsane, J. Pecher, R. H. Martin, *Bull. Soc. Chim. Belg.* **1985**, *94*, 597–603.
- [80] B. B. Hassine, M. Gorsane, J. Pecher, R. H. Martin, *Bull. Soc. Chim. Belg.* **1985**, *94*, 759–769.
- [81] B. B. Hassine, M. Gorsane, F. Geerts-Evrard, J. Pecher, R. H. Martin, D. Castelet, *Bull. Soc. Chim. Belg.* **1986**, *95*, 547–556.
- [82] B. B. Hassine, M. Gorsane, J. Pecher, R. H. Martin, *Bull. Soc. Chim. Belg.* **1986**, *95*, 557–566.
- [83] B. B. Hassine, M. Gorsane, J. Pecher, R. H. Martin, *Bull. Soc. Chim. Belg.* **1987**, *96*, 801–808.
- [84] M. T. Reetz, E. W. Beuttenmüller, R. Goddard, *Tetrahedron Lett.* **1997**, *38*, 3211–3214.
- [85] K. Yamamoto, T. Shimizu, K. Igawa, K. Tomooka, G. Hirai, H. Suemune, K. Usui, *Sci. Rep.* **2016**, *6*, 36211.
- [86] E. Licandro, S. Cauteruccio, D. Dova, *Adv. Heterocycl. Chem.* **2016**, *118*, 1–46.
- [87] I. Takemura, R. Sone, H. Nishide, *Polym. Adv. Technol.* **2008**, *19*, 1092–1096.
- [88] K. E. S. Phillips, T. J. Katz, S. Jockusch, A. J. Lovinger, N. J. Turro, *J. Am. Chem. Soc.* **2001**, *123*, 11900–11907.
- [89] Y. Yamamoto, H. Sakai, J. Yuasa, Y. Araki, T. Wada, T. Sakanoue, T. Takenobu, T. Kawai, T. Hasobe, *Chem. – Eur. J.* **2016**, *22*, 4263–4273.
- [90] M. Scholz, M. Mühlstädt, F. Dietz, *Tetrahedron Lett.* **1967**, *8*, 665–668.
- [91] M. Flammang-Barbieux, J. Nasielski, R. Martin, *Tetrahedron Lett.* **1967**, *8*, 743–744.
- [92] F. B. Mallory, C. W. Mallory, *Photocyclization of Stilbenes and Related Molecules, in Org. React.* **1984**, *30*, 1–456.
- [93] D. de Keukeleire, S.-L. He, *Chem. Rev.* **1993**, *93*, 359–380.

- [94] R. H. Martin, M. Flammang-Barbieux, J. P. Cosyn, M. Gelbcke, *Tetrahedron Lett.* **1968**, *9*, 3507–3510.
- [95] A. Sudhakar, T. J. Katz, *Tetrahedron Lett.* **1986**, *27*, 2231–2234.
- [96] L. Liu, T. J. Katz, *Tetrahedron Lett.* **1991**, *32*, 6831–6834.
- [97] L. Liu, B. Yang, T. J. Katz, M. K. Poindexter, *J. Org. Chem.* **1991**, *56*, 3769–3775.
- [98] J. H. Dopper, D. Oudman, H. Wynberg, *J. Am. Chem. Soc.* **1973**, *95*, 3692–3698.
- [99] H. Wynberg, M. B. Groen, H. Schadenberg, *J. Org. Chem.* **1971**, *36*, 2797–2809.
- [100] O. Diels, K. Alder, *Liebigs Ann. Chem.* **1928**, *460*, 98–122.
- [101] H. A. Weidlich, *Ber. dtsch. chem. Ges.* **1938**, *71*, 1203–1209.
- [102] L. Minuti, A. Taticchi, A. Marrocchi, E. Gacs-Baitz, *Tetrahedron* **1997**, *53*, 6873–6878.
- [103] Z. Y. Wang, Y. Qi, T. Bender, J. Gao, *Macromolecules* **1997**, *30*, 764–769.
- [104] Y. Altman, D. Ginsburg, *J. Chem. Soc.* **1959**, 466–468.
- [105] F. Bell, D. H. Waring, *J. Chem. Soc.* **1949**, 2689–2693.
- [106] L. Liu, T. J. Katz, *Tetrahedron Lett.* **1990**, *31*, 3983–3986.
- [107] M. S. Newman, L. M. Joshel, *J. Am. Chem. Soc.* **1938**, *60*, 485–488.
- [108] M. Yamaguchi, H. Okubo, M. Hirama, *Chem. Commun.* **1996**, 1771–1772.
- [109] M. Newman, M. Wolf, *J. Chem. Soc.* **1952**, *62*, 2326.
- [110] M. S. Newman, D. Lednicer, *J. Am. Chem. Soc.* **1956**, *78*, 4765–4770.
- [111] X. Xiang, L. T. Scott, *Org. Lett.* **2007**, *9*, 3937–3940.
- [112] M. Shimizu, I. Nagao, Y. Tomioka, T. Hiyama, *Angew. Chem. Int. Ed.* **2008**, *47*, 8096–8099.
- [113] F. Aloui, S. Moussa, B. ben Hassine, *Tetrahedron Lett.* **2012**, *53*, 3216–3219.
- [114] B. Milde, M. Leibelng, M. Pawliczek, J. Grunenberg, P. G. Jones, D. B. Werz, *Angew. Chem. Int. Ed.* **2015**, *54*, 1331–1335.
- [115] K. Kamikawa, I. Takemoto, S. Takemoto, H. Matsuzaka, *J. Org. Chem.* **2007**, *72*, 7406–7408.
- [116] D. Peña, A. Cobas, D. Pérez, E. Guitián, L. Castedo, *Org. Lett.* **2000**, *2*, 1629–1632.
- [117] S. K. Collins, A. Grandbois, M. P. Vachon, J. Côté, *Angew. Chem. Int. Ed.* **2006**, *45*, 2923–2926.
- [118] J. Storch, J. Sýkora, J. Čermak, J. Karban, I. Císařová, A. Růžička, *J. Org. Chem.* **2009**, *74*, 3090–3093.
- [119] F. Dubois, M. Gingras, *Tetrahedron Lett.* **1998**, *39*, 5039–5040.
- [120] M. Miyasaka, A. Rajca, M. Pink, S. Rajca, *Chem. – Eur. J.* **2004**, *10*, 6531–6539.

- [121] Z. Wang, J. Shi, J. Wang, C. Li, X. Tian, Y. Cheng, H. Wang, *Org. Lett.* **2010**, *12*, 456–459.
- [122] S. I. Weissman, *J. Org. Chem.* **1976**, *41*, 4040–4041.
- [123] M. C. Carreño, R. Hernández-Sánchez, J. Mahugo, A. Urbano, *J. Org. Chem.* **1999**, *64*, 1387–1390.
- [124] M. C. Carreño, S. García-Cerrada, A. Urbano, *J. Am. Chem. Soc.* **2001**, *123*, 7929–7930.
- [125] M. C. Carreño, M. González-López, A. Urbano, *Chem. Commun.* **2005**, 611–613.
- [126] F. Teplý, I. G. Stará, I. Starý, A. Kollárovič, D. Šaman, Š. Vyskočil, P. Fiedler, *J. Org. Chem.* **2003**, *68*, 5193–5197.
- [127] I. G. Stará, I. Starý, *Acc. Chem. Res.* **2020**, *53*, 144–158.
- [128] I. G. Stará, Z. Alexandrová, F. Teplý, P. Sehnal, I. Starý, D. Šaman, M. Buděšínský, J. Cvačka, *Org. Lett.* **2005**, *7*, 2547–2550.
- [129] A. Jančařík, J. Rybáček, K. Cocq, J. Vacek Chocholoušová, J. Vacek, R. Pohl, L. Bednárová, P. Fiedler, I. Císařová, I. G. Stará, I. Starý, *Angew. Chem. Int. Ed.* **2013**, *125*, 10154–10159.
- [130] R. Yamano, Y. Shibata, K. Tanaka, *Chem. – Eur. J.* **2018**, *24*, 6364–6370.
- [131] M. Satoh, Y. Shibata, K. Tanaka, *Chem. – Eur. J.* **2018**, *24*, 5434–5438.
- [132] M. F. Hawthorne, D. C. Young, P. M. Garrett, D. A. Owen, S. G. Schwerin, F. N. Tebbe, P. A. Wegner, *J. Am. Chem. Soc.* **1970**, *90*, 862–868.
- [133] K. Tanaka, H. Suzuki, H. Osuga, *Tetrahedron Lett.* **1997**, *38*, 457–460.
- [134] K. Tanaka, H. Suzuki, H. Osuga, *J. Org. Chem.* **1997**, *62*, 4465–4470.
- [135] G. C. Bond, P. A. Sermon, G. Webb, D. A. Buchanan, P. B. Wells, *J. Chem. Soc., Chem. Comm.* **1973**, 444b–4445.
- [136] G. J. Hutchings, *J. Catal.* **1985**, *96*, 292–295.
- [137] M. Haruta, T. Kobayashi, H. Sano, N. Yamada, *Chem. Lett.* **1987**, *16*, 405–408.
- [138] W. Zi, F. Dean Toste, *Chem. Soc. Rev.* **2016**, *45*, 4567.
- [139] A. Fürstner, *Chem. Soc. Rev.* **2009**, *38*, 3208–3221.
- [140] A. Fürstner, P. W. Davies, *Angew. Chem. Int. Ed.* **2007**, *46*, 3410–3449.
- [141] C. Nevado, A. M. Echavarren, *Synthesis* **2005**, *2*, 167–182.
- [142] J. Tian, Y. Chen, M. Vayer, A. Djurovic, R. Guillot, R. Guermazi, S. Dagorne, C. Bour, V. Gandon, *Chem. – Eur. J.* **2020**, *26*, 12831–12838.
- [143] B. Ranieri, I. Escofet, A. M. Echavarren, *Org. Biomol. Chem.* **2015**, *13*, 7103–7118.
- [144] R. Dorel, A. M. Echavarren, *Chem. Rev.* **2015**, *115*, 9028–9072.
- [145] C. Obradors, A. M. Echavarren, *Acc. Chem. Res.* **2013**, *47*, 902–912.
- [146] Z. Li, C. Brouwer, C. He, *Chem. Rev.* **2008**, *108*, 3239–3265.

- [147] R. J. Harris, R. A. Widenhoefer, *Chem. Soc. Rev.* **2016**, *45*, 4533–4551.
- [148] D. J. Gorin, B. D. Sherry, F. D. Toste, *Chem. Rev.* **2008**, *108*, 3351–3378.
- [149] M. J. S. Dewar, *Bull. Soc. Chim. Fr.* **1951**, *18*, C71–C79.
- [150] J. Chatt, L. Duncanson, *J. Chem. Soc.* **1953**, 2939–2947.
- [151] C. J. V. Halliday, J. M. Lynam, *Dalton Trans.* **2016**, *45*, 12611–12626.
- [152] B. W. Davies, R. J. Puddephatt, N. C. Payne, *Can. J. Chem.* **1972**, *50*, 2276–2284.
- [153] M. S. Nechaev, V. M. Rayón, G. Frenking, *J. Phys. Chem.* **2004**, *108*, 3134–3142.
- [154] R. Hertwig, W. Koch, D. Schröder, H. Schwarz, J. Hrusak, P. Schwerdtfeger, *J. Phys. Chem.* **1996**, *100*, 12253–12260.
- [155] H. Ito, T. Yajima, J. -i. Tateiwa, A. Hosomi, *Chem. Commun.* **2000**, 981–982.
- [156] R. T. Baker, J. C. Calabrese, S. A. Westcott, *J. Organomet. Chem.* **1995**, *498*, 109–117.
- [157] Y. Liu, F. Song, S. Guo, *J. Am. Chem. Soc.* **2006**, *128*, 11332–11333.
- [158] D. Xing, B. Guan, G. Cai, Z. Fang, L. Yang, Z. Shi, *Org. Lett.* **2006**, *8*, 693–696.
- [159] F. Gasparrini, M. Giovannoli, D. Misiti, G. Natile, G. Palmieri, *Tetrahedron* **1983**, *39*, 3181–3184.
- [160] M. Sawamura, Y. Ito, *Chem. Rev.* **1992**, *92*, 857–871.
- [161] T. Hayashi, M. Sawamura, Y. Ito, *Tetrahedron* **1992**, *48*, 1999–2012.
- [162] Y. Ito, M. Sawamura, T. Hayashi, *J. Am. Chem. Soc.* **1986**, *108*, 6405–6406.
- [163] M. R. Luzung, J. P. Markham, F. D. Toste, *J. Am. Chem. Soc.* **2004**, *126*, 10858–10859.
- [164] M. Mato, A. Franchino, C. García-Morales, A. M. Echavarren, *Chem. Rev.* **2021**, *121*, 8613–8684.
- [165] K. A. Owens, J. A. Berson, *J. Am. Chem. Soc.* **1990**, *112*, 5973–5985.
- [166] B. D. Sherry, F. D. Toste, *J. Am. Chem. Soc.* **2004**, *126*, 15978–15979.
- [167] P. Peltier, R. Euzen, R. Daniellou, C. Nugier-Chauvin, V. Ferrières, *Carbohydr. Res.* **2008**, *343*, 1897–1923.
- [168] A. Das, N. T. Patil, *Chem. – Eur. J.* **2022**, *28*, e202104371.
- [169] C.-Y. Wu, T. Horibe, C. B. Jacobsen, F. D. Toste, *Nature* **2015**, *517*, 449–454.
- [170] J. Yang, Y. Zhu, A. K. W. Tse, X. Zhou, Y. Chen, Y. C. Tse, K. M. C. Wong, C. Y. Ho, *Chem. Commun.* **2019**, *55*, 4471–4474.
- [171] G. Zhou, F. Liu, J. Zhang, *Chem. – Eur. J.* **2011**, *17*, 3101–3104.
- [172] T. Shibuya, K. Nakamura, K. Tanaka, *Beilstein J. Org. Chem.* **2011**, *7*, 944–950.
- [173] M. Satoh, Y. Shibata, Y. Kimura, K. Tanaka, *Eur. J. Org. Chem.* **2016**, *2016*, 4465–4469.

- [174] A. Martínez, P. García-García, M. A. Fernández-Rodríguez, F. Rodríguez, R. Sanz, *Angew. Chem. Int. Ed.* **2010**, *49*, 4633–4637.
- [175] H. Zheng, R. J. Felix, M. R. Gagné, *Org. Lett.* **2014**, *16*, 2272–2275.
- [176] M. J. Campbell, F. D. Toste, *Chem. Sci.* **2011**, *2*, 1369–1378.
- [177] S. G. Sethofer, T. Mayer, F. D. Toste, *J. Am. Chem. Soc.* **2010**, *132*, 8276–8277.
- [178] K. Kong, J. A. Enquist, M. E. McCallum, G. M. Smith, T. Matsumaru, E. Menhaji-Klotz, J. L. Wood, *J. Am. Chem. Soc.* **2013**, *135*, 10890–10893.
- [179] A. de Meijere, S. Bräse, M. Oestreich, *Metal Catalyzed Cross-Coupling Reactions and More*, Wiley-VCH Verlag, Weinheim, Germany, **2013**.
- [180] Á. Kozma, T. Deden, J. Carreras, C. Wille, J. Petušková, J. Rust, M. Alcarazo, *Chem. – Eur. J.* **2014**, *20*, 2208–2214.
- [181] J. Carreras, G. Gopakumar, L. Gu, A. Gimeno, P. Linowski, J. Petrušková, W. Thiel, M. Alcarazo, *J. Am. Chem. Soc.* **2013**, *135*, 18815–18823.
- [182] L. D. M. Nicholls, M. Alcarazo, *Chem. Lett.* **2018**, *48*, 1–13.
- [183] E. N. Jacobsen, A. Pfaltz, H. Yamamoto, *Comprehensive Asymmetric Catalysis*, Springer Verlag, **1999**.
- [184] T. P. Yoon, E. N. Jacobsen, *Science (1979)* **2003**, *299*, 1691–1693.
- [185] M. Alcarazo, *Chem. – Eur. J.* **2014**, *20*, 7868–7877.
- [186] E. Haldón, Á. Kozma, H. Tinnermann, L. Gu, R. Goddard, M. Alcarazo, *Dalton Trans.* **2016**, *45*, 1872–1876.
- [187] A. G. Orpen, N. G. Connelly, *Organometallics* **1990**, *9*, 1206–1210.
- [188] D. G. Gilheany, *Chem. Rev.* **1994**, *94*, 1339–1374.
- [189] Y. Jean, *Molecular Orbitals of Transition Metal Complexes*, Oxford University Press, Oxford, **2005**.
- [190] C. A. Tolman, *Chem. Rev.* **1977**, *77*, 313–348.
- [191] D. Setiawan, R. Kalescky, E. Kraka, D. Cremer, *Inorg. Chem.* **2016**, *55*, 2332–2344.
- [192] A. v. Zakharov, Y. v. Vishnevskiy, N. Allefeld, J. Bader, B. Kurscheid, S. Steinhauer, B. Hoge, B. Neumann, H. G. Stammler, R. J. F. Berger, N. W. Mitzel, *Eur. J. Inorg. Chem.* **2013**, 3392–3404.
- [193] H. Tinnermann, C. Wille, M. Alcarazo, *Angew. Chem. Int. Ed.* **2014**, *53*, 8732–8736.
- [194] M. Alcarazo, *Acc. Chem. Res.* **2016**, *49*, 1797–1805.
- [195] C. A. Tolman, *Chem Rev* **1977**, *77*, 313–348.
- [196] S. Hussein, D. Priester, P. Beet, J. Cottom, S. J. Hart, T. James, R. J. Thatcher, A. C. Whitwood, J. M. Slattery, *Chem. – Eur. J.* **2019**, *25*, 2262–2271.
- [197] M. Dalal, Dalal Institute, **2017**.

- [198] A. B. P. Lever, *Inorg. Chem* **1990**, *29*, 1271–1285.
- [199] X. Marset, A. Khoshnood, L. Sotorríos, E. Gómez-Bengoia, D. A. Alonso, D. J. Ramón, *ChemCatChem* **2017**, *9*, 1269–1275.
- [200] P. Wasserscheid, H. Waffenschmidt, P. Machnitzki, K. W. Kottsieper, O. Stelzer, *Chem. Commun.* **2001**, 451–452.
- [201] K. W. Kottsieper, O. Stelzer, P. Wasserscheid, *J. Mol. Catal. A: Chem.* **2001**, *175*, 285–288.
- [202] C. J. Rugen, M. Alcarazo, *Synlett* **2022**, *33*, 16–26.
- [203] S. Saleh, E. Fayad, M. Azouri, J. C. Hierso, J. Andrieu, M. Picquet, *Adv. Synth. Catal.* **2009**, *351*, 1621–1628.
- [204] J. Li, J. Peng, Y. Bai, G. Zhang, G. Lai, X. Li, *J. Organomet. Chem.* **2010**, *695*, 431–436.
- [205] C. C. Brasse, U. Englert, A. Salzer, H. Waffenschmidt, P. Wasserscheid, *Organometallics* **2000**, *19*, 3818–3823.
- [206] J. Sirieix, M. Oßberger, B. Betzemeier, P. Knochel, *Synlett* **2000**, *11*, 1613–1615.
- [207] A. Zieliński, X. Marset, C. Golz, L. M. Wolf, M. Alcarazo, *Angew. Chem. Int. Ed.* **2020**, *59*, 23299–23305.
- [208] X. Marset, M. Recort-Fornals, M. Kpante, A. Zieliński, C. Golz, L. M. Wolf, M. Alcarazo, *Adv. Synth. Catal.* **2021**, *363*, 3546–3553.
- [209] C. Maaliki, C. Lepetit, Y. Canac, C. Bijani, C. Duhayon, R. Chauvin, *Chem. – Eur. J.* **2012**, *18*, 7705–7714.
- [210] L. Gu, L. M. Wolf, A. Zieliński, W. Thiel, M. Alcarazo, *J. Am. Chem. Soc.* **2017**, *139*, 4948–4953.
- [211] J. Carreras, M. Patil, W. Thiel, M. Alcarazo, *J. Am. Chem. Soc.* **2012**, *134*, 16753–16758.
- [212] Y. García-Rodeja, I. Fernández, *Organometallics* **2017**, *36*, 460–466.
- [213] J. W. Dube, Y. Zheng, W. Thiel, M. Alcarazo, *J. Am. Chem. Soc.* **2016**, *138*, 6869–6877.
- [214] J. Carreras, M. Patil, W. Thiel, M. Alcarazo, *J. Am. Chem. Soc.* **2012**, *134*, 16753–16758.
- [215] H. Teller, S. Flügge, R. Goddard, A. Fürstner, *Angew. Chem. Int. Ed.* **2010**, *49*, 1949–1953.
- [216] H. Teller, M. Corbet, L. Mantilli, G. Gopakumar, R. Goddard, W. Thiel, A. Fürstner, *J. Am. Chem. Soc.* **2012**, *134*, 15331–15342.
- [217] E. González-Fernández, L. D. M. Nicholls, L. D. Schaaf, C. Farès, C. W. Lehmann, M. Alcarazo, *J. Am. Chem. Soc.* **2017**, *139*, 1428–1431.
- [218] L. D. M. Nicholls, M. Marx, T. Hartung, E. González-Fernández, C. Golz, M. Alcarazo, *ACS Catal.* **2018**, *8*, 6079–6085.
- [219] T. Hartung, R. Machleid, M. Simon, C. Golz, M. Alcarazo, *Angew. Chem. Int. Ed.* **2020**, *59*, 5660–5664.

- [220] V. Pelliccioli, T. Hartung, M. Simon, C. Golz, E. Licandro, S. Cauteruccio, M. Alcarazo, *Angew. Chem. Int. Ed.* **2022**, *61*, e202114577.
- [221] J. Zhang, M. Simon, C. Golz, M. Alcarazo, *Angew. Chem. Int. Ed.* **2020**, *59*, 5647–5650.
- [222] R. Noyori, I. Tomino, Y. Tanimoto, *J. Am. Chem. Soc.* **1979**, *101*, 3129–3131.
- [223] Y. Chen, S. Yekta, A. K. Yudin, *Chem. Rev.* **2003**, *103*, 3212.
- [224] I. Ahmed, D. A. Clark, *Org. Lett.* **2014**, *16*, 4332–4335.
- [225] P. Wipf, J. K. Jung, *J. Org. Chem.* **2000**, *65*, 6319–6337.
- [226] A. J. Arduengo III, H. v. Rasika Dias, R. L. Harlow, M. Kline, *J. Am. Chem. Soc.* **1992**, *114*, 5530–5534.
- [227] K. B. Simonsen, K. v. Gothelf, K. A. Jørgensen, *J. Org. Chem.* **1998**, *63*, 7536–7538.
- [228] P. S. J. Kaib, L. Schreyer, S. Lee, R. Properzi, B. List, *Angew. Chem. Int. Ed.* **2016**, *55*, 13200–13203.
- [229] K. Hirano, S. Urban, C. Wang, F. Glorius, *Org. Lett.* **2009**, *11*, 1019–1022.
- [230] L. S. Rocha (Patrikeeva), I. P. Beletskaya, *Russ. Chem. Bull.* **2014**, *63*, 2686–2688.
- [231] H. R. Talele, A. R. Chaudhary, P. R. Patel, A. v Bedekar, *Arkivoc* **2011**, *IX*, 15–37.
- [232] K. B. Jørgensen, *Molecules* **2010**, *15*, 4334–4358.
- [233] G. Zichen, Bachelor Thesis, Georg-August Universität Göttingen, **2020**.
- [234] C. Röhlich, A. S. Wirth, K. Köhler, *Chem. – Eur. J.* **2012**, *18*, 15485–15494.
- [235] Y. Nakai, T. Mori, Y. Inoue, *J. Phys. Chem. A* **2012**, *116*, 7372–7385.
- [236] B. A. Brown, C. M. Kemp, S. F. Mason, *J. Chem. Soc. A* **1971**, 751–755.
- [237] C. Mahler, U. Müller, W. M. Müller, V. Enkelmann, C. Moon, G. Brunklaus, H. Zimmermann, S. H. Höger, *Chem. Commun.* **2008**, 4816–4818.
- [238] W. Zhang, Z. Chen, B. Yang, X.-Y. Wang, R. Berger, A. Narita, G. B. Barin, P. Ruffieux, R. Fasel, X. Feng, H. J. Räder, K. Müller, *Anal. Chem* **2017**, *89*, 7485–7492.
- [239] P. Ruffieux, S. Wang, B. Yang, C. Sánchez-Sánchez, J. Liu, T. Dienel, L. Talirz, P. Shinde, C. A. Pignedoli, D. Passerone, T. Dumslaff, X. Feng, K. Müllen, R. Fasel, *Nature* **2016**, *531*, 489–493.
- [240] P. Walla, C. O. Kappe, *Chem. Commun.* **2004**, 564–565.
- [241] M. Genov, A. Almorín, P. Espinet, *Tetrahedron Asymmetry* **2007**, *18*, 625–627.
- [242] K. Mori, T. Murase, M. Fujita, *Angew. Chem. Int. Ed.* **2015**, *54*, 6847–6851.
- [243] S. Grimme, J. G. Brandenburg, C. Bannwarth, A. Hansen, *J. Chem. Phys.* **2015**, *143*, 054107.
- [244] S. Grimme, *J. Chem. Phys* **2006**, *124*, 34108.
- [245] S. Grimme, S. Ehrlich, L. Goerigk, *J. Comp. Chem.* **2011**, *32*, 1456–1465.

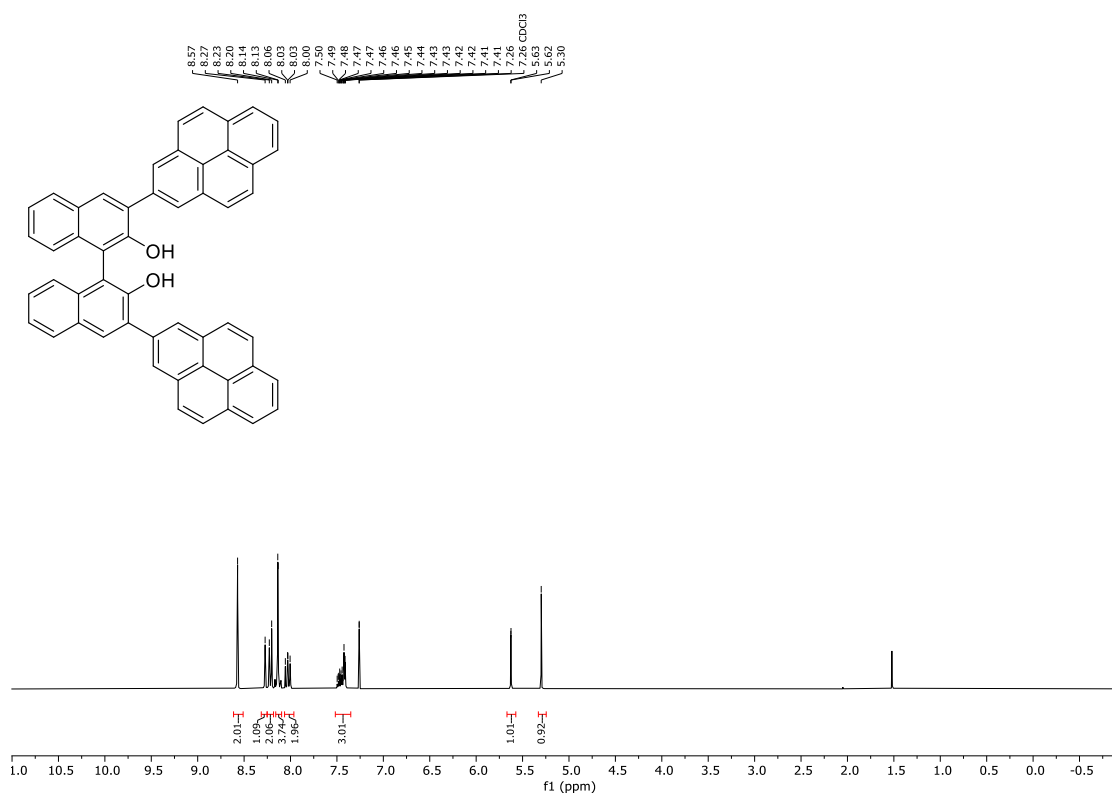
- [246] S. Grimme, J. Antony, S. Ehrlich, H. Krieg, *J. Chem. Phys.* **2010**, *132*, 154104.
- [247] F. Weigend, R. Ahlrichs, *Phys. Chem. Chem. Phys.* **2005**, *7*, 3297–3305.
- [248] F. Weigend, *Phys. Chem. Chem. Phys.* **2006**, *8*, 1057–1065.
- [249] A. Hellweg, C. Hättig, S. Höfener, W. Klopper, A. Hellweg, W. Klopper, *Theor. Chem. Acc.* **2007**, *117*, 587–597.
- [250] F. Neese, *Comp. Mol. Sci.* **2012**, *2*, 73–78.
- [251] A. Wuttke, R. A. Mata, *J. Comp. Chem.* **2017**, *38*, 15–23.
- [252] S. Grimme, *J. Chem. Phys.* **2003**, *118*, 9095.
- [253] M. Andrejic, R. A. Mata, *Phys. Chem. Chem. Phys.* **2013**, *15*, 18115–18122.
- [254] C. Bannwarth, S. Grimme, *Comp. Theor. Chem.* **2014**, *1040–1041*, 45–53.
- [255] J.-D. Chai, M. Head-Gordon, *J. Chem. Phys.* **2008**, *128*, 084106.
- [256] C. Bannwarth, J. Seibert, S. Grimme, *Chirality* **2016**, *28*, 365–369.
- [257] A. Bedi, O. Gidron, *Acc. Chem. Res.* **2019**, *52*, 2482–2490.
- [258] A. Bedi, L. J. W. Shimon, O. Gidron, *J. Am. Chem. Soc.* **2018**, *140*, 8086–8090.
- [259] K. Yavari, P. Aillard, Y. Zhang, F. Nuter, P. Retailleau, A. Voituriez, A. Marinetti, *Angew. Chem. Int. Ed.* **2014**, *53*, 861–865.
- [260] Q. Lefebvre, M. Jentsch, M. Rueping, *Beilstein J. Org. Chem.* **2013**, *9*, 1883–1890.
- [261] G. F. Zha, W. Y. Fang, Y. G. Li, J. Leng, X. Chen, H. L. Qin, *J. Am. Chem. Soc.* **2018**, *140*, 17666–17673.
- [262] Q. Chen, F. Gao, H. Tang, M. Yao, Q. Zhao, Y. Shi, Y. Dang, C. Cao, *ACS Catal.* **2019**, *9*, 3730–3736.
- [263] T. Kimachi, T. Ogata, M. Doe, M. Sakanaka, A. Nishiuchi, M. Aomatsu, M. Tanaka, M. Shimizu, N. Yoshioka, K. Kubota, Y. Teraoka, C. Nakajima, S. Takahashi, *Heterocycles* **2019**, *99*, 534–548.
- [264] Z.-F. Xu, H. Dai, L. Shan, C.-Y. Li, *Org. Lett.* **2018**, *20*, 1054–1057.
- [265] S. Jabeen, R. A. Khera, J. Iqbal, M. Asgher, *Russ. J. Org. Chem.* **2019**, *55*, 1416–1422.
- [266] L. Jin, W. Hao, J. Xu, N. Sun, B. Hu, Z. Shen, W. Mo, X. Hu, *Chem. Commun.* **2017**, *53*, 4124–4127.
- [267] A. C. Shaikh, D. S. Ranade, P. R. Rajamohanam, P. P. Kulkarni, N. T. Patil, *Angew. Chem. Int. Ed.* **2017**, *56*, 757–761.
- [268] A. K. Verma, R. R. Jha, R. Chaudhary, R. K. Tiwari, K. Siva, K. S. K. Reddy, A. Danodia, *J. Org. Chem.* **2012**, *77*, 8191–8205.
- [269] H. Li, J. L. Petersen, K. K. Wang, *J. Org. Chem.* **2001**, *66*, 7804–7810.
- [270] R. D. Mule, A. C. Shaikh, A. B. Gade Ab, N. T. Patil, R. Li, / Chemcomm, C. Communication, *Chemical Communications* **2018**, *54*, 11909–11912.

- [271] H. Yamada, S. Yamaguchi, *Patent Application JP 2008156261 A*, **2008**, 2008156261.
- [272] C. Ge, G. Wang, P. Wu, C. Chen, *Org. Lett.* **2019**, *21*, 5010–5014.
- [273] H. Tinnermann, L. D. M. Nicholls, T. Johannsen, C. Wille, C. Golz, R. Goddard, M. Alcarazo, **2018**, DOI 10.1021/acscatal.8b03271.
- [274] M. Satoh, Y. Shibata, K. Tanaka, *Chem. – Eur. J.* **2018**, *24*, 5434–5438.
- [275] T. H. Dunning Jr., *J. Chem. Phys.* **1989**, *90*, 1007–1023.
- [276] H. J. Werner, P. J. Knowles, G. Knizia, F. R. Manby, M. Schütz, *MOLPRO, version 2020.1, a package of ab initio programs, 2020*, see <http://www.molpro.net>. **n.d.**, DOI 10.1002/WCMS.82.
- [277] J. Ahrens, B. Geveci, C. Law, *ParaView: An End-User Tool for Large-Data Visualization*, Elsevier Inc., **2005**.
- [278] “https://www.horiba.com/en_en/applications/materials/material-research/quantum-dots/recording-fluorescence-quantum-yields/”

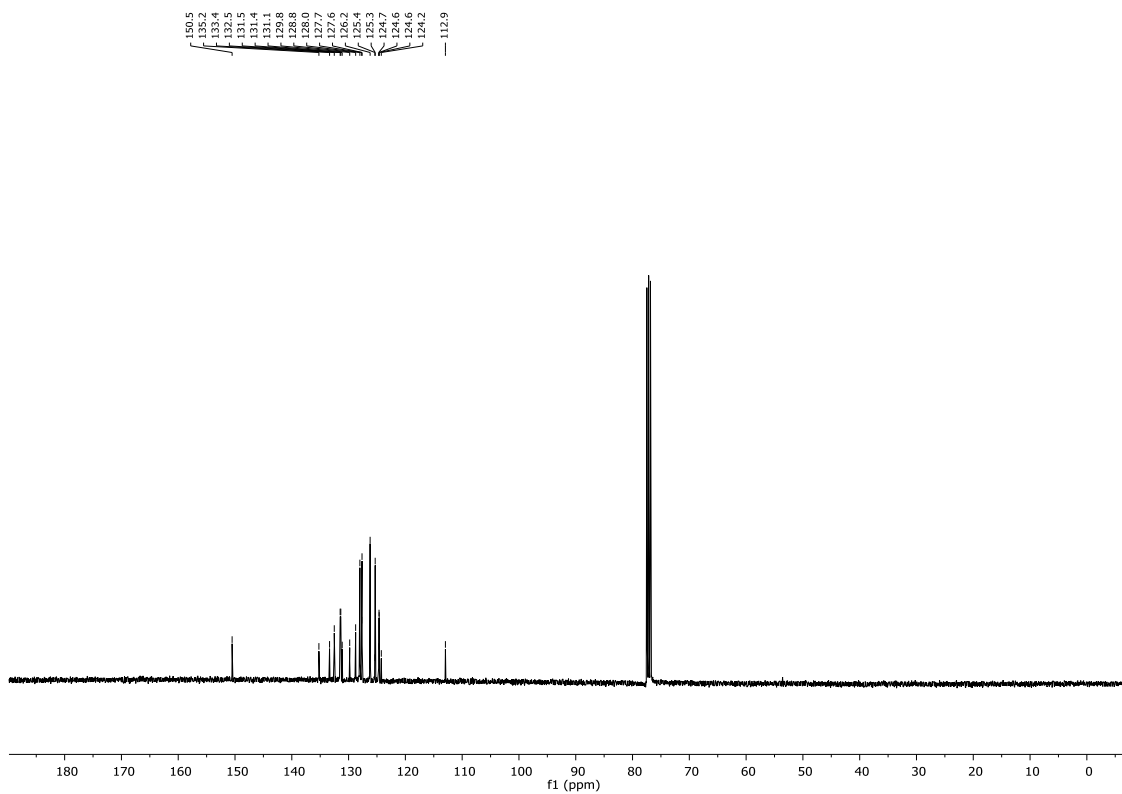
8. Appendix

8.1. NMR Spectra

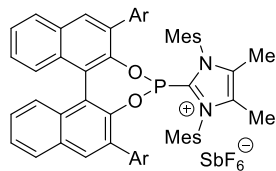
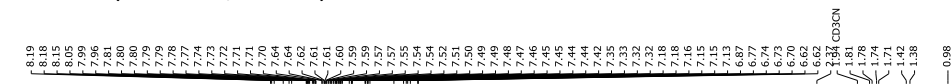
^1H NMR: (400 MHz, CDCl_3) **173b**



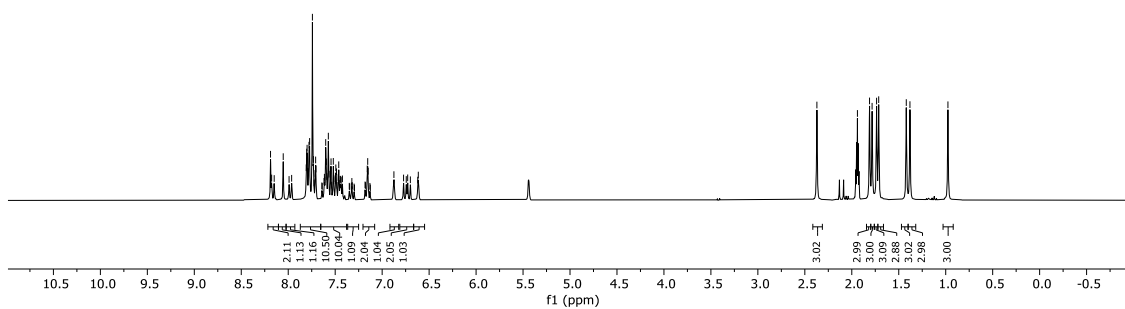
$^{13}\text{C}\{\text{H}\}$ NMR: (101 MHz, CDCl_3) **173b**



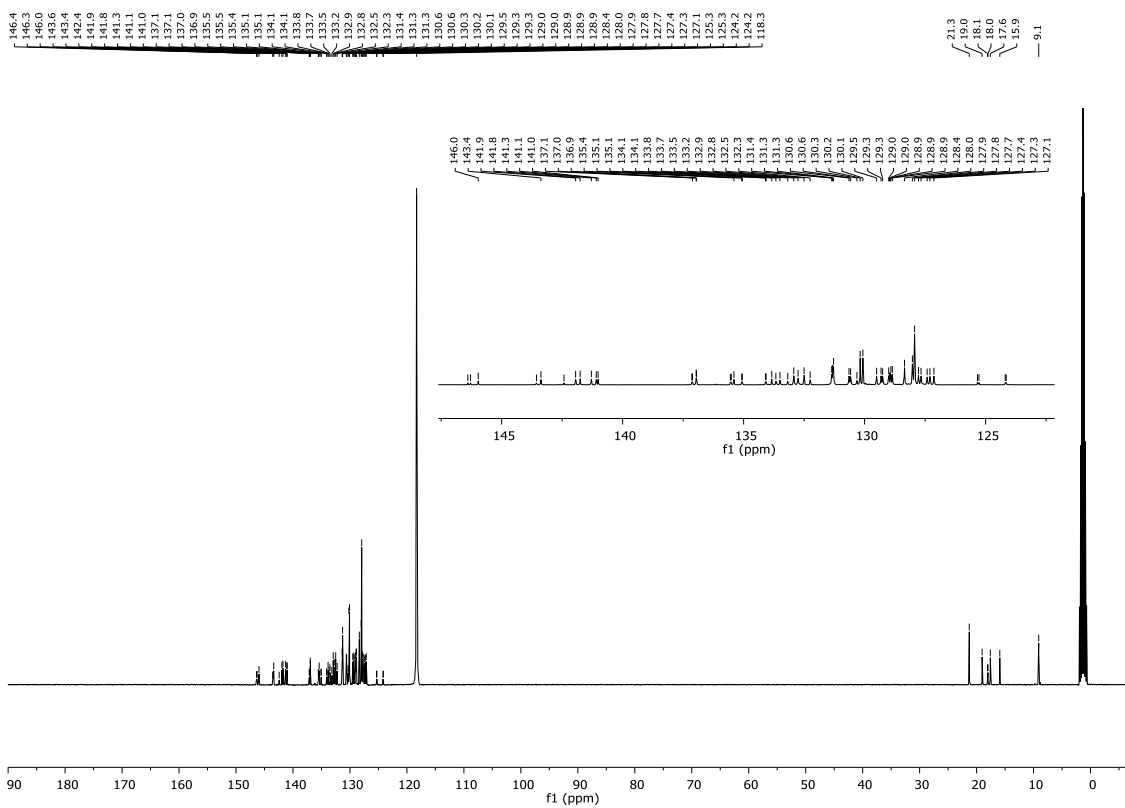
¹H NMR: (400 MHz, CD₃CN) **178a**



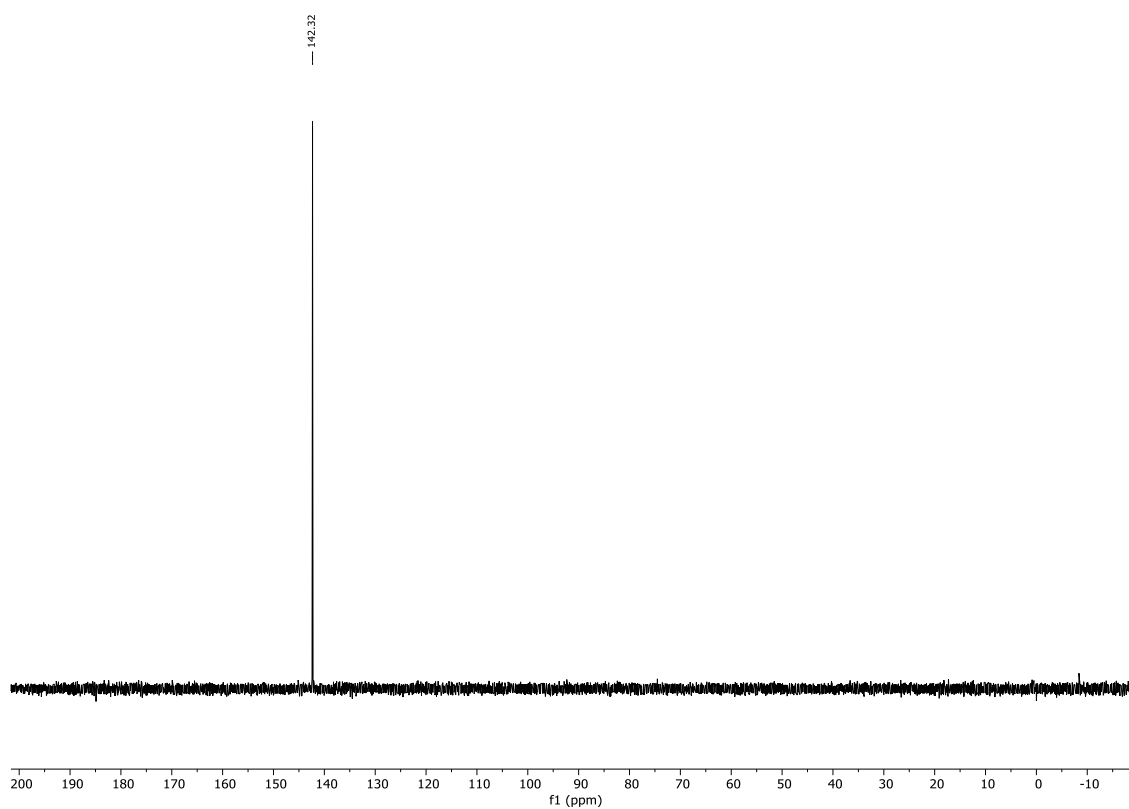
Ar = *p*-biphenyl



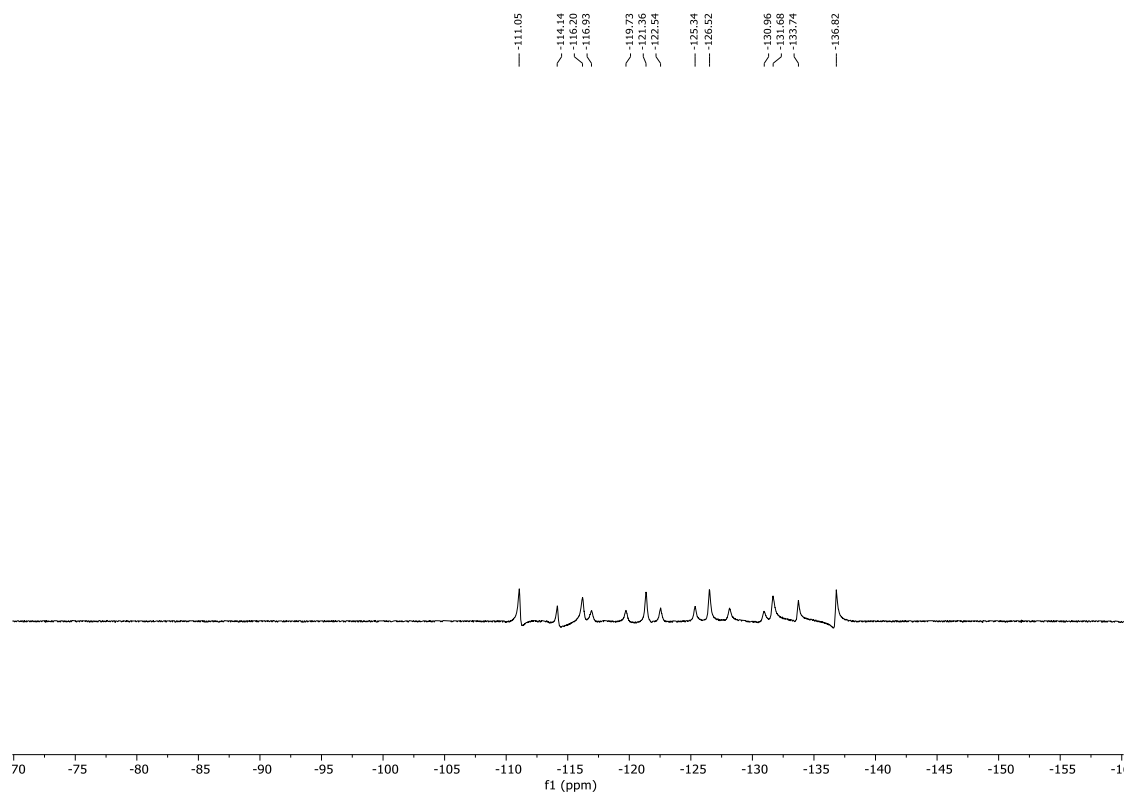
¹³C{H} NMR: (101 MHz, CD₃CN) **178a**



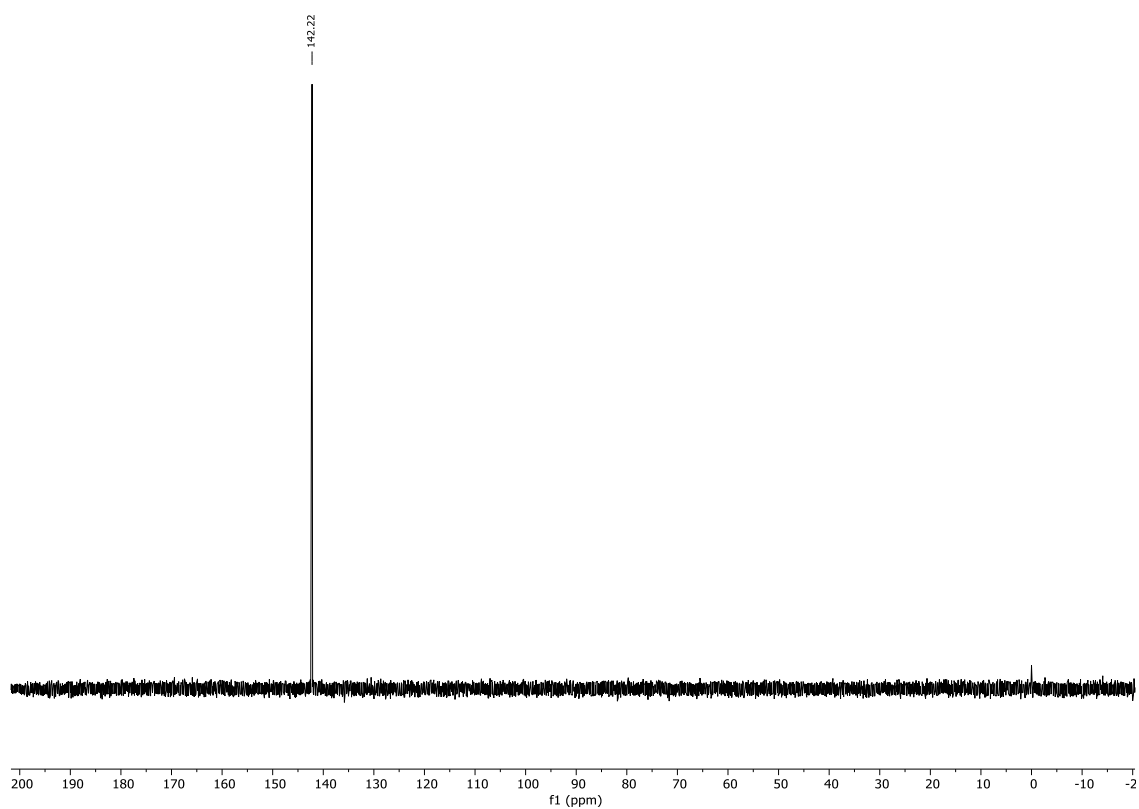
$^{31}\text{P}\{\text{H}\}$ NMR: (162 MHz, CD_3CN) **178a**



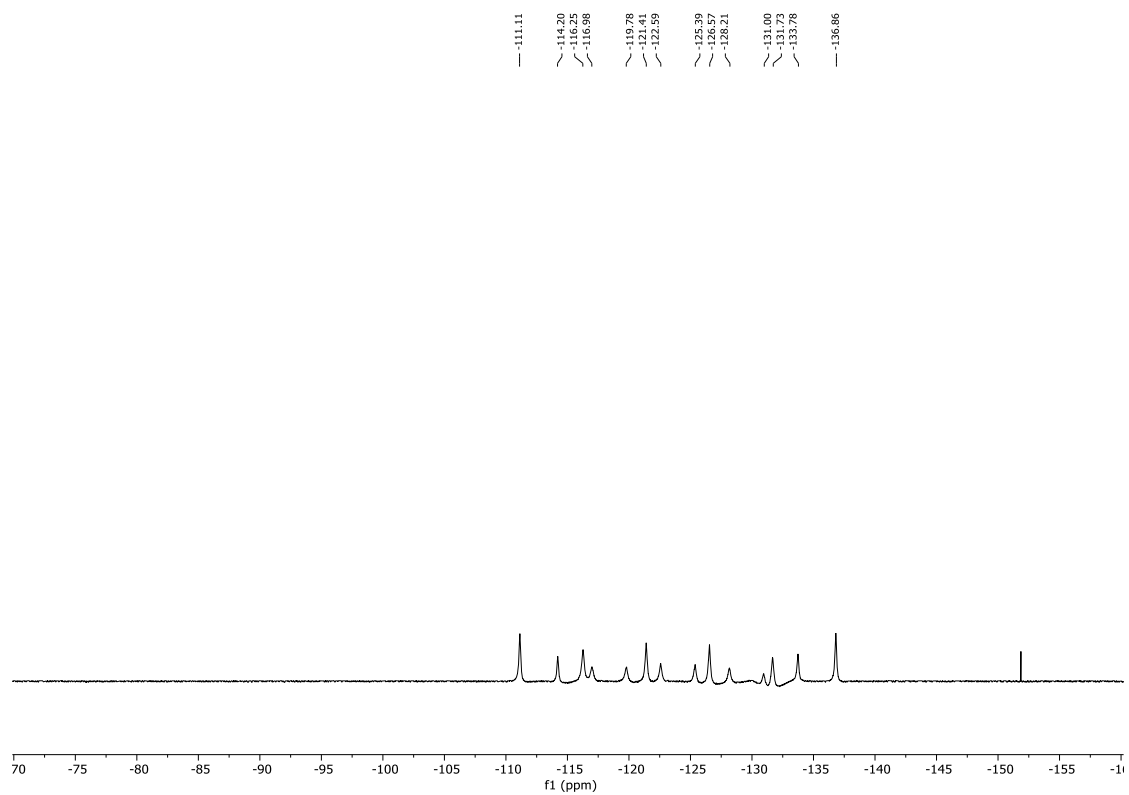
^{19}F NMR: (376 MHz, CD_3CN) **178a**



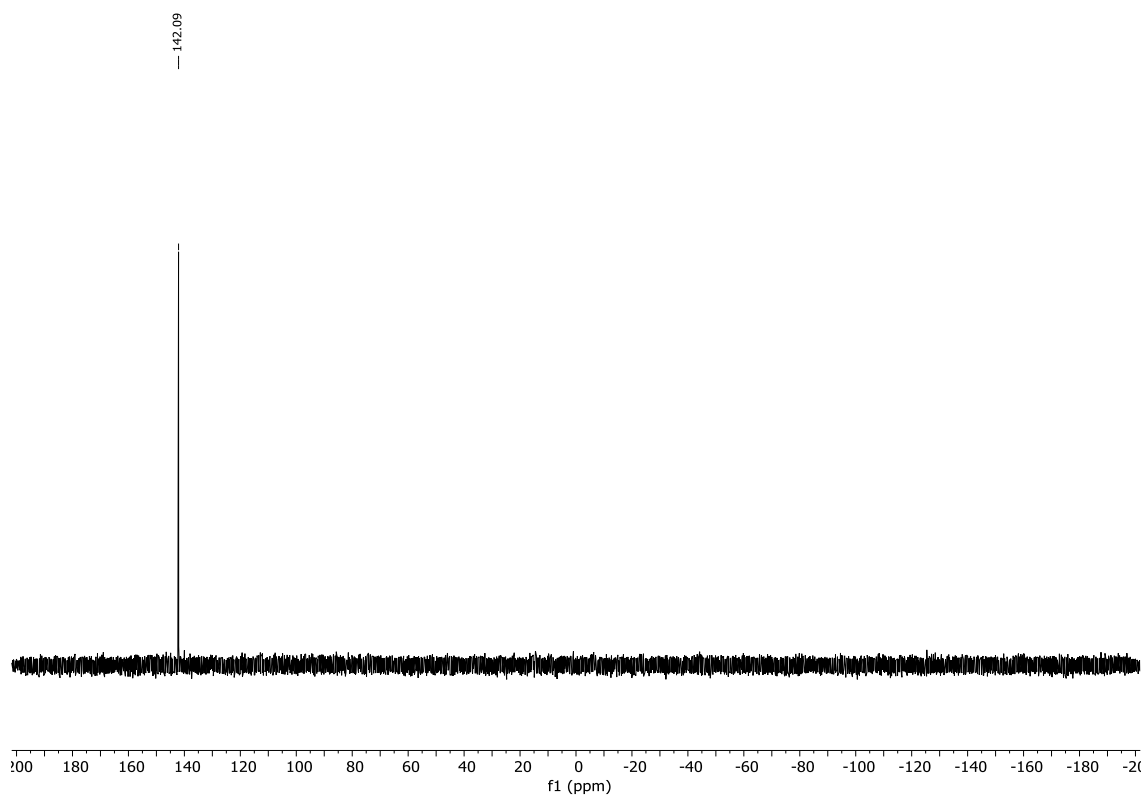
$^{31}\text{P}\{\text{H}\}$ NMR: (162 MHz, CD_3CN) **178b**



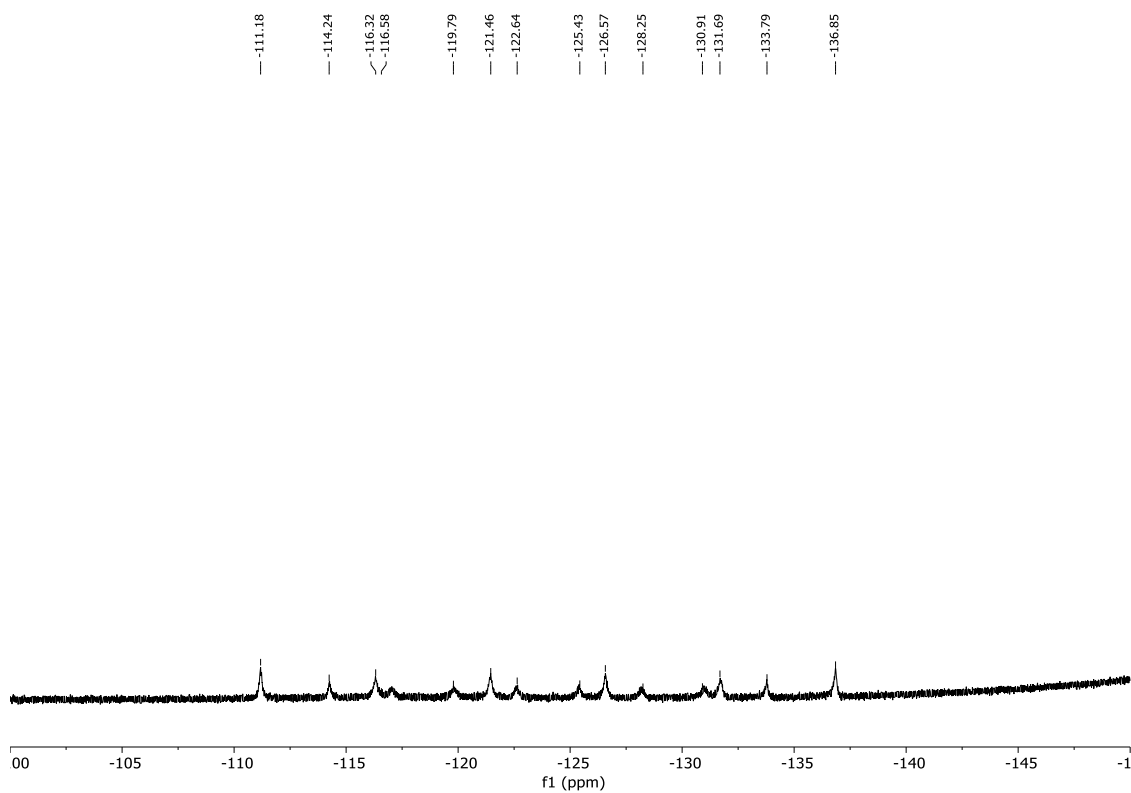
^{19}F NMR: (376 MHz, CD_3CN) **178b**



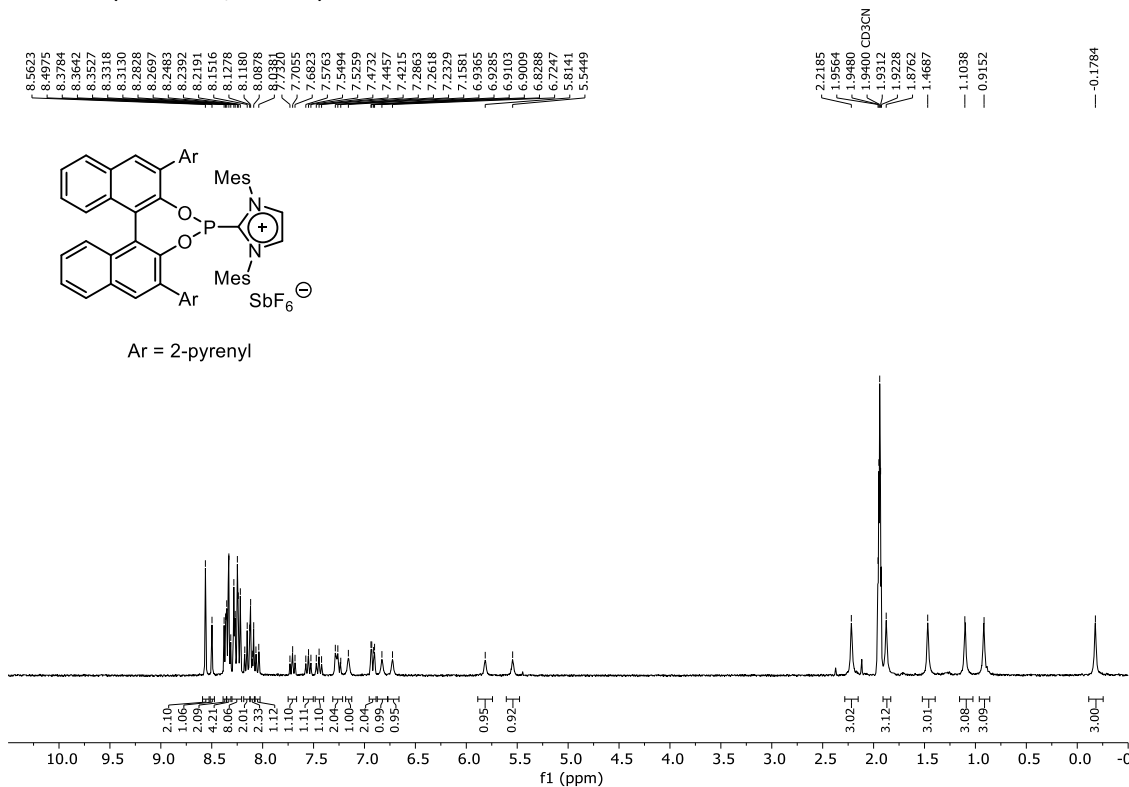
$^{31}\text{P}\{\text{H}\}$ NMR: (121 MHz, CD_3CN) **178c**



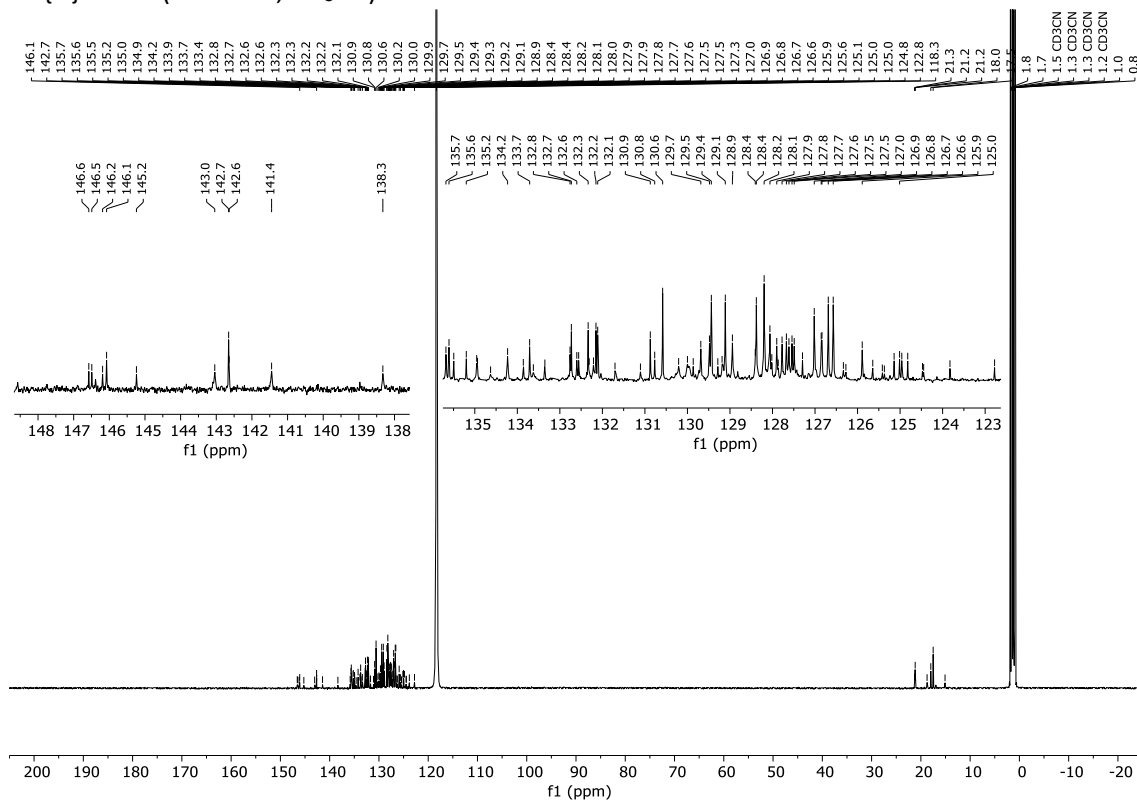
^{19}F NMR: (376 MHz, CD_3CN) **178c**



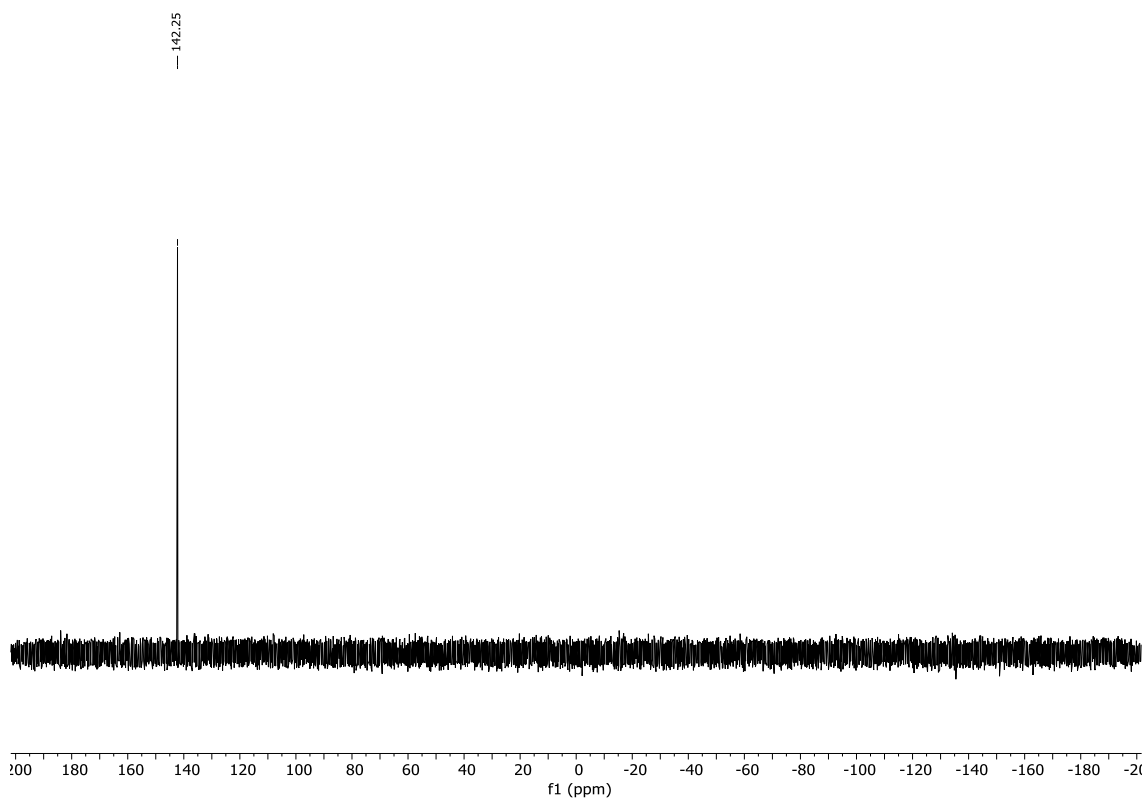
¹H NMR: (300 MHz, CD₃CN) **178d**



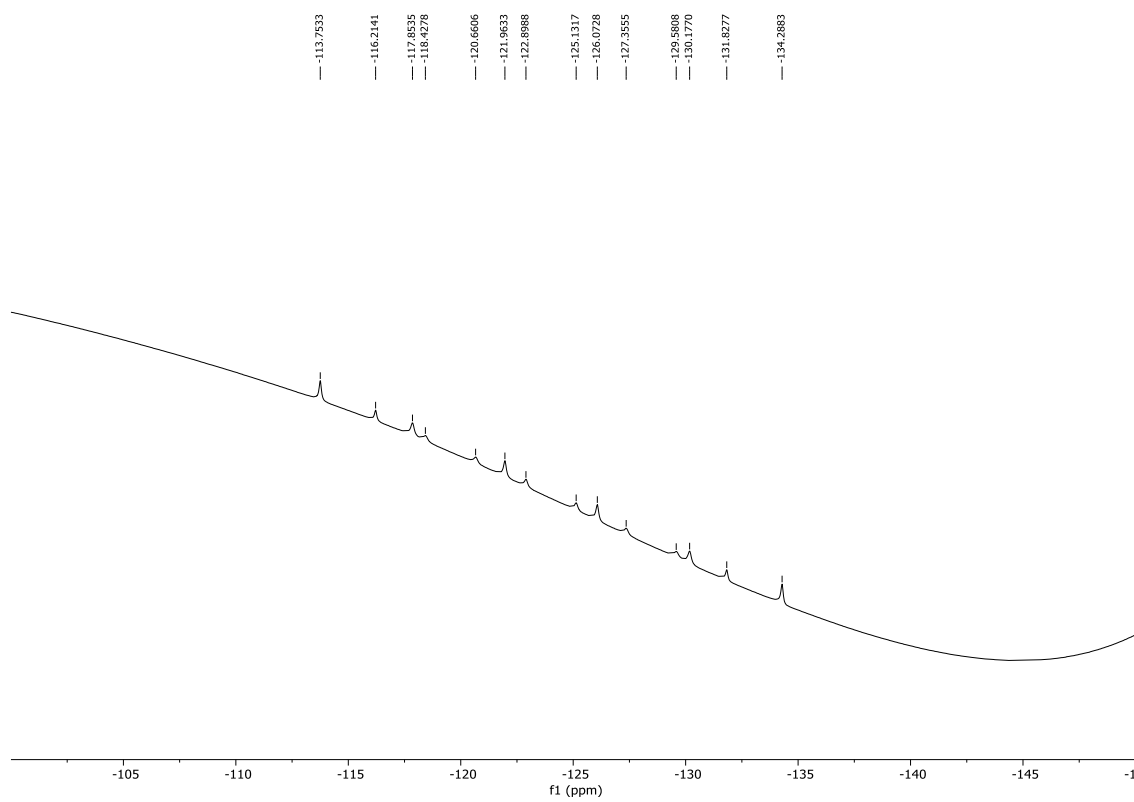
¹³C{H} NMR: (126 MHz, CD₃CN) **178d**



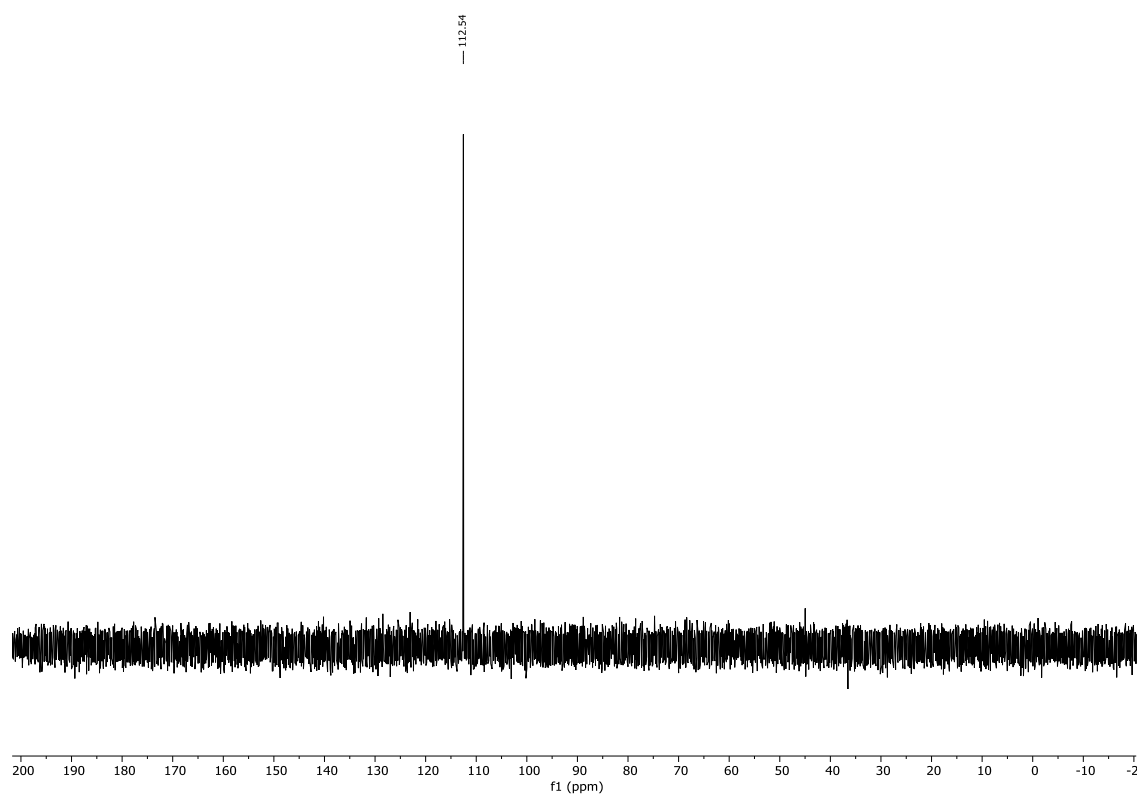
$^{31}\text{P}\{\text{H}\}$ NMR: (121 MHz, CD_3CN) **178d**



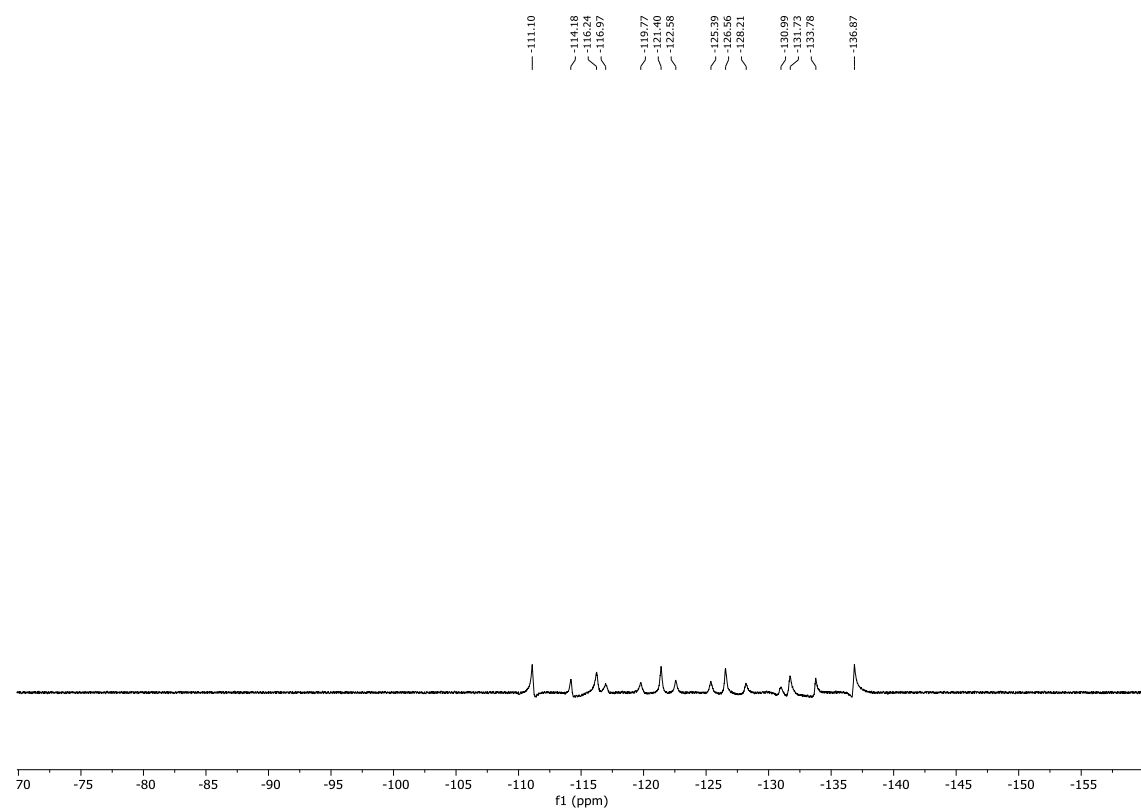
^{19}F NMR: (471 MHz, CD_3CN) **178d**



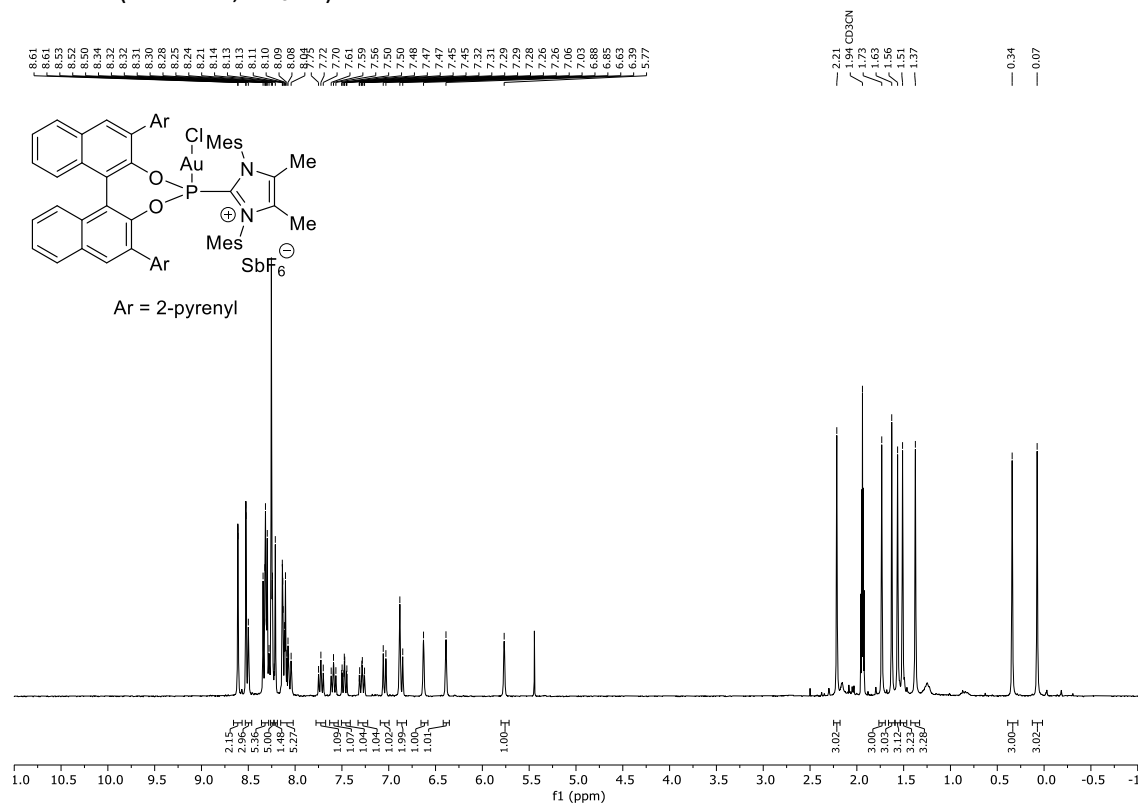
$^{31}\text{P}\{\text{H}\}$ NMR: (162 MHz, CD_3CN) **162a**



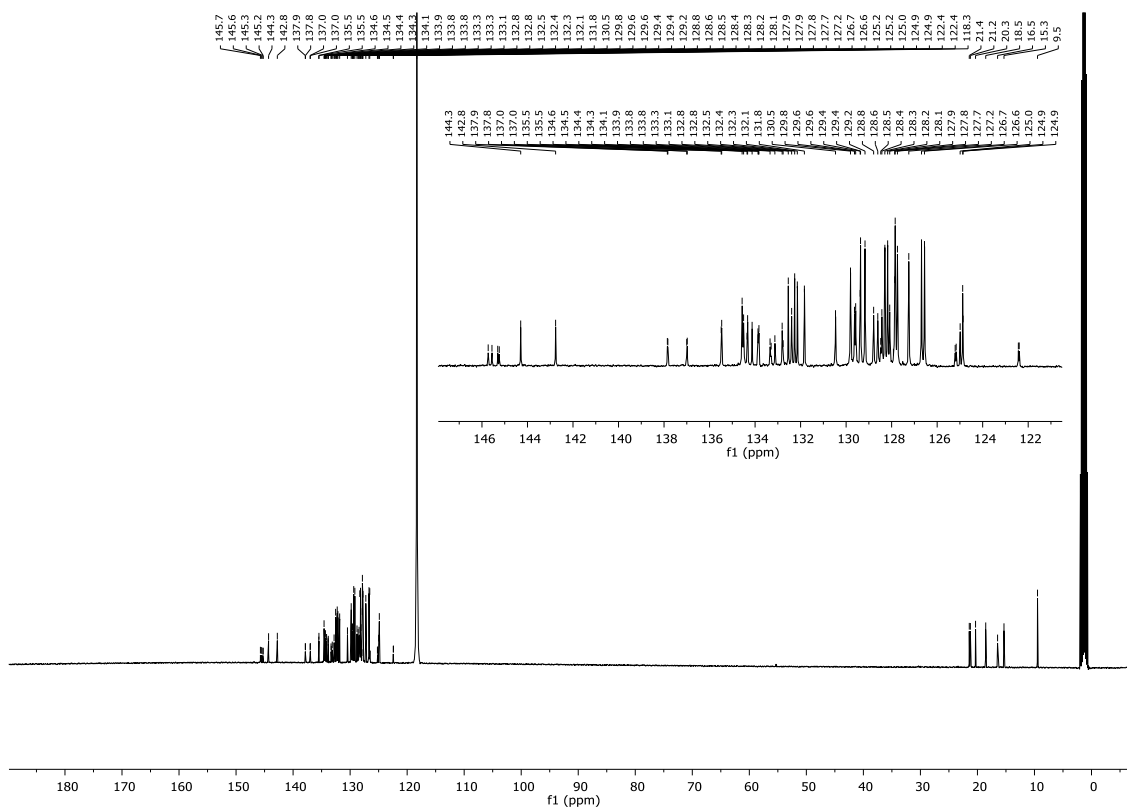
^{19}F NMR: (376 MHz, CD_3CN) **162a**



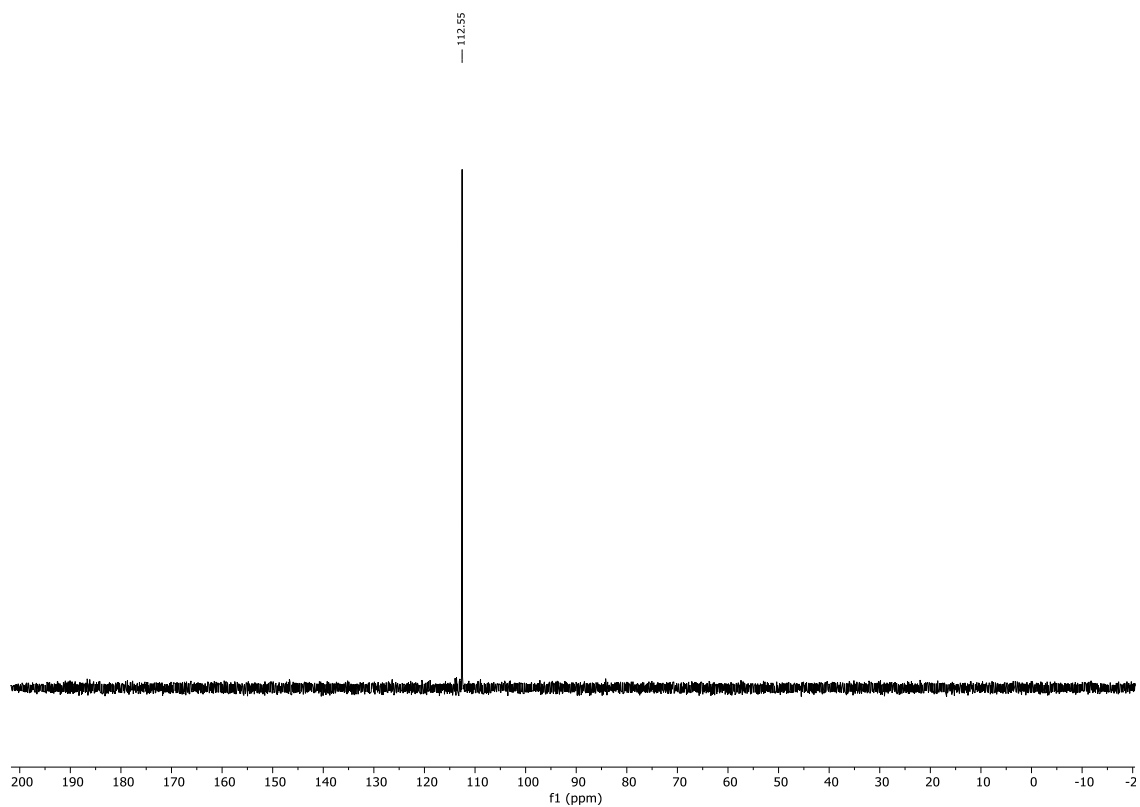
¹H NMR: (400 MHz, CD₃CN) **162b**



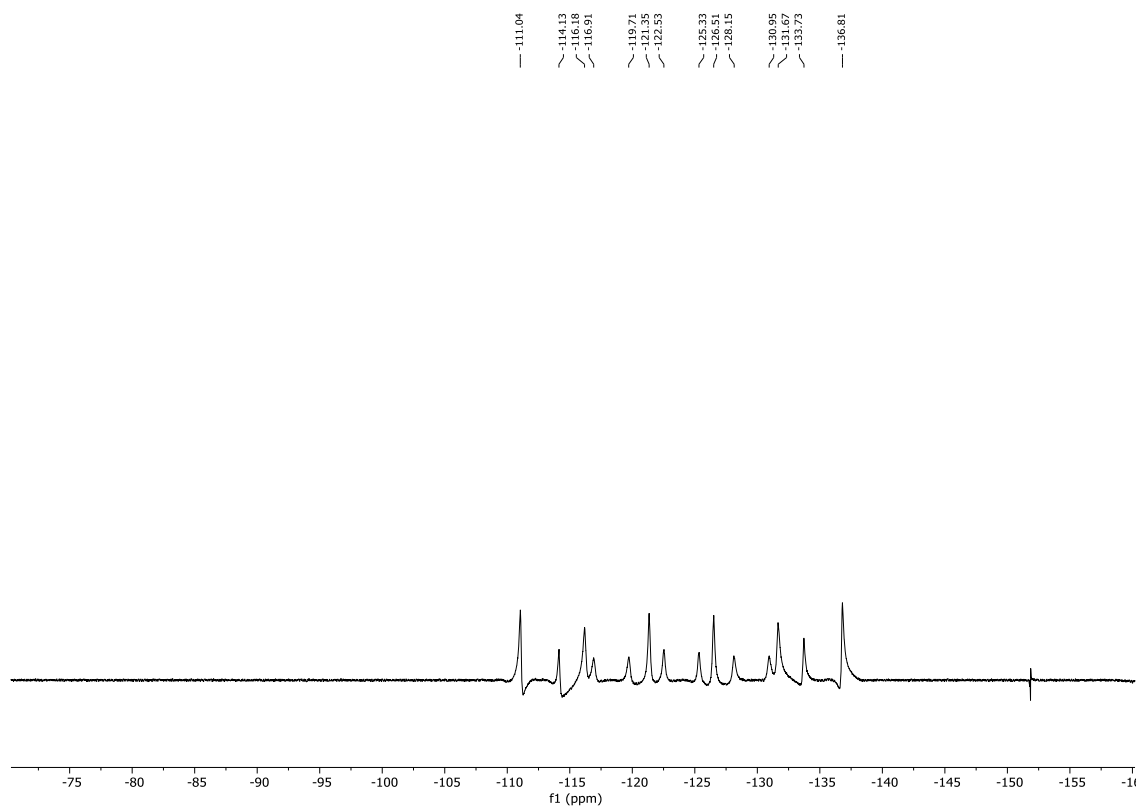
¹³C{H} NMR: (101 MHz, CD₃CN) **162b**



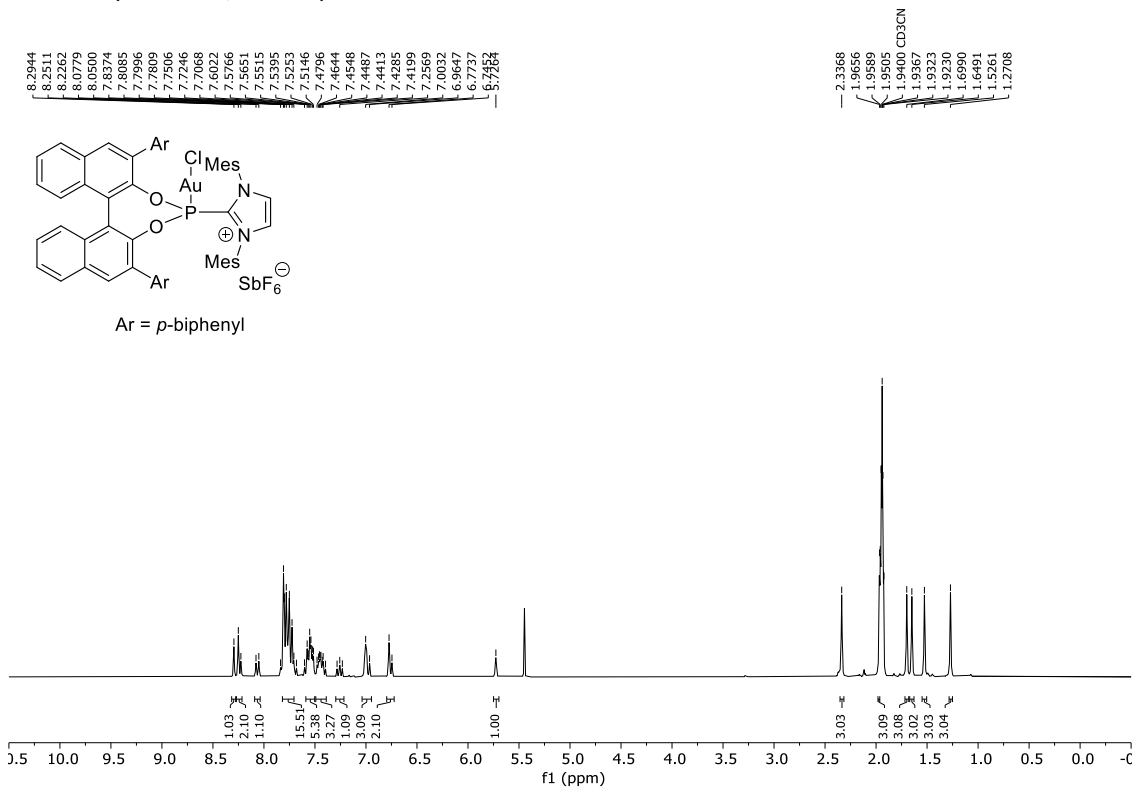
$^{31}\text{P}\{\text{H}\}$ NMR: (162 MHz, CD_3CN) **162b**



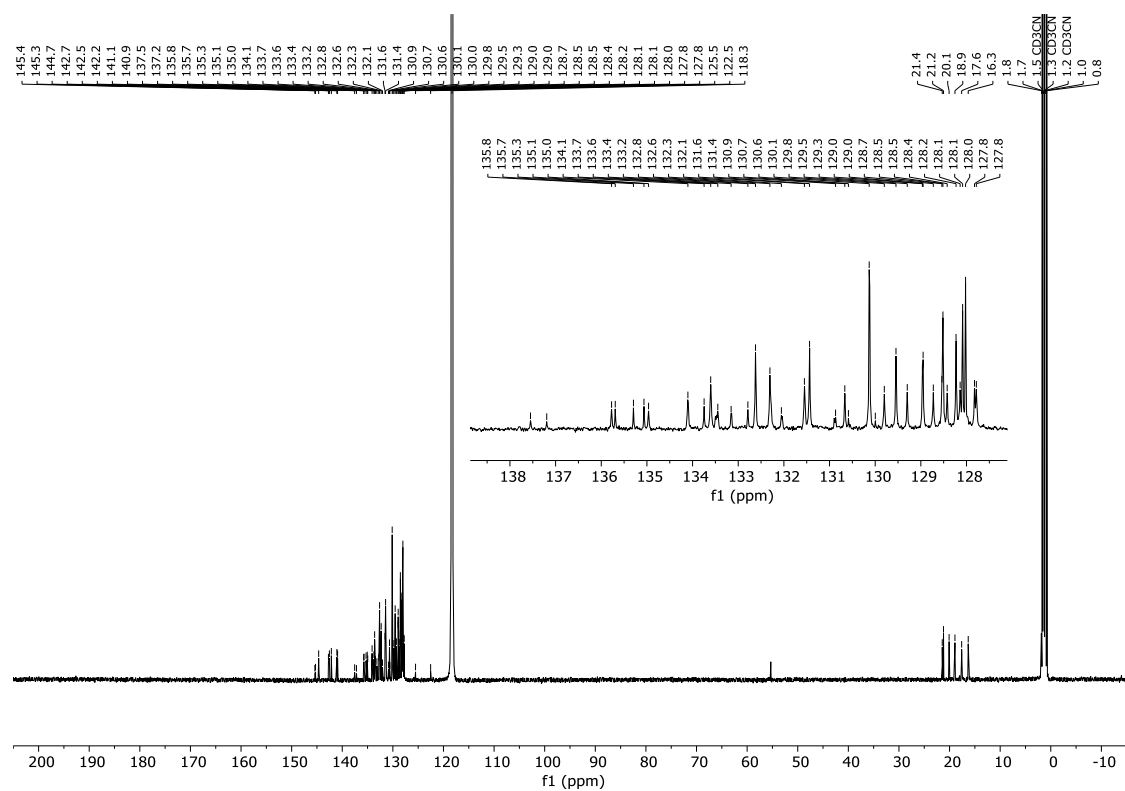
^{19}F NMR: (376 MHz, CD_3CN) **162b**



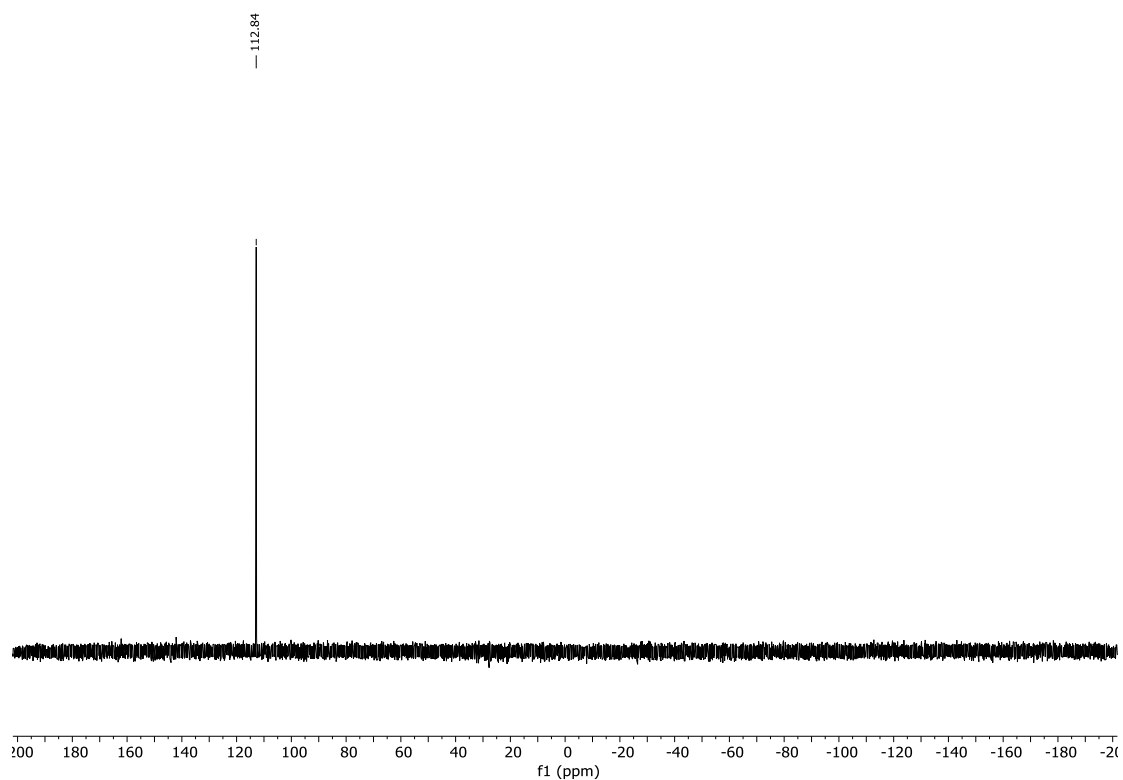
¹H NMR: (300 MHz, CD₃CN) **162c**



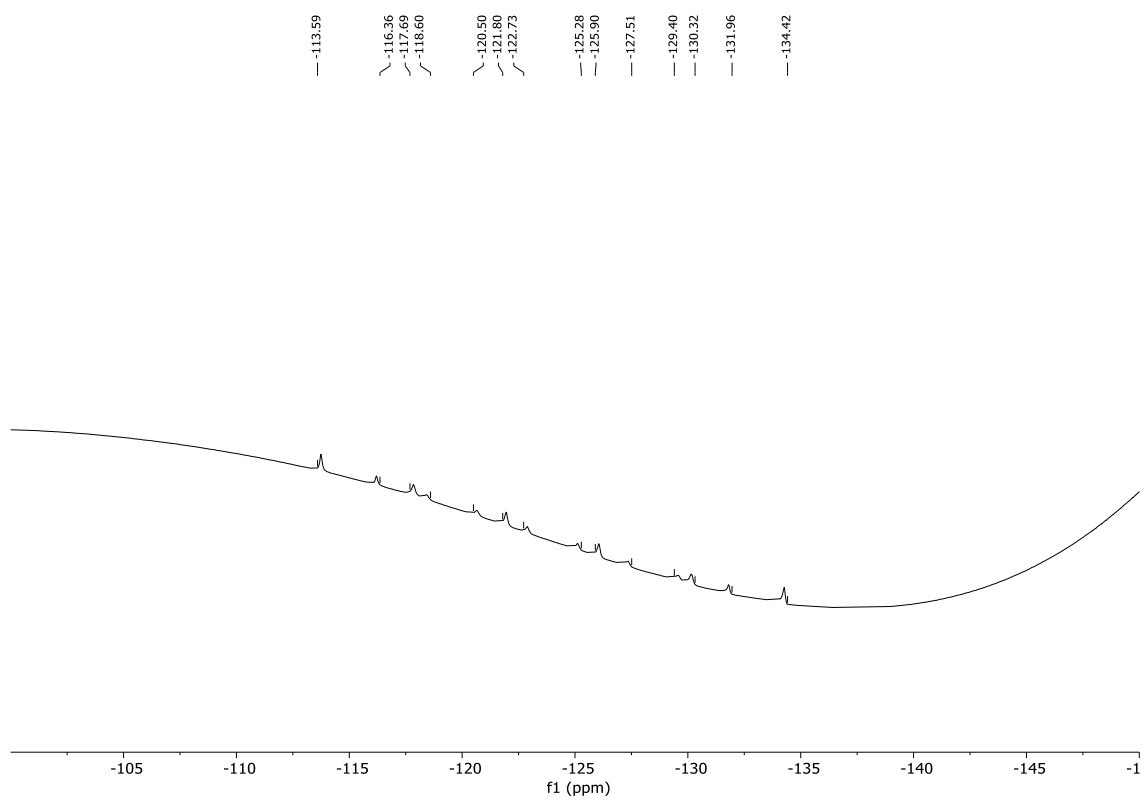
¹³C{H} NMR: (126 MHz, CD₃CN) **162c**



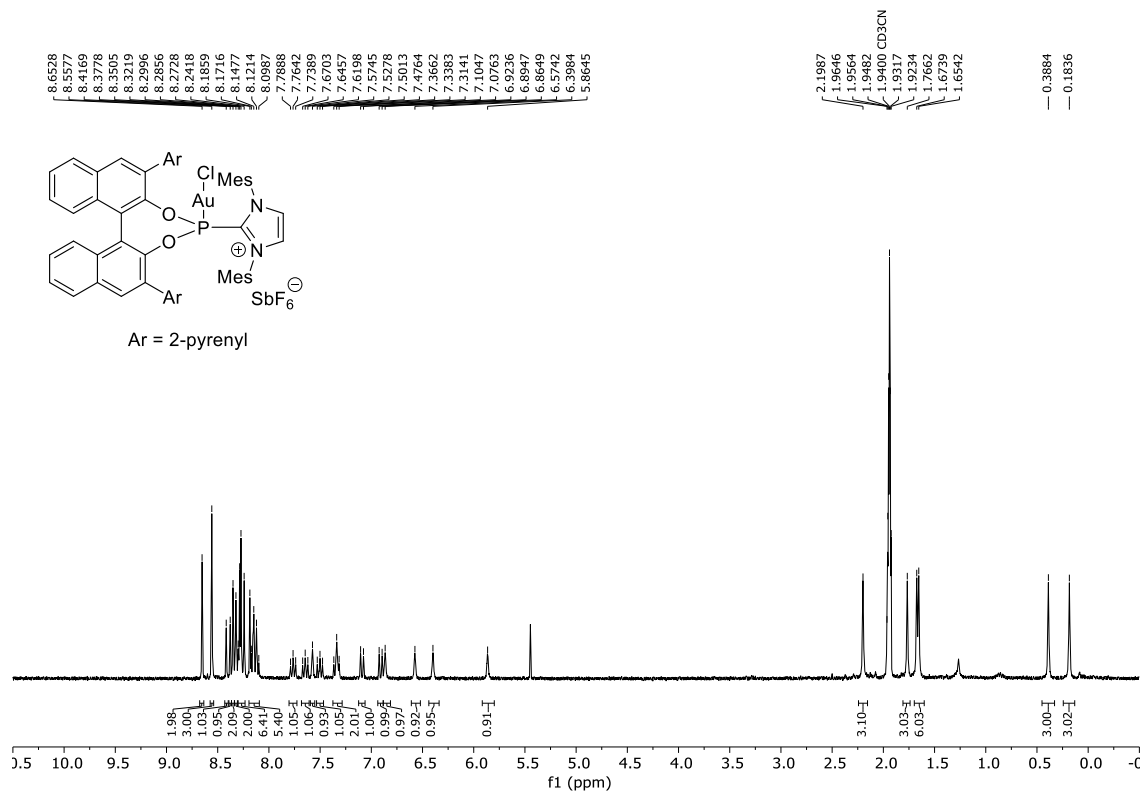
$^{31}\text{P}\{\text{H}\}$ NMR: (121 MHz, CD_3CN) **162c**



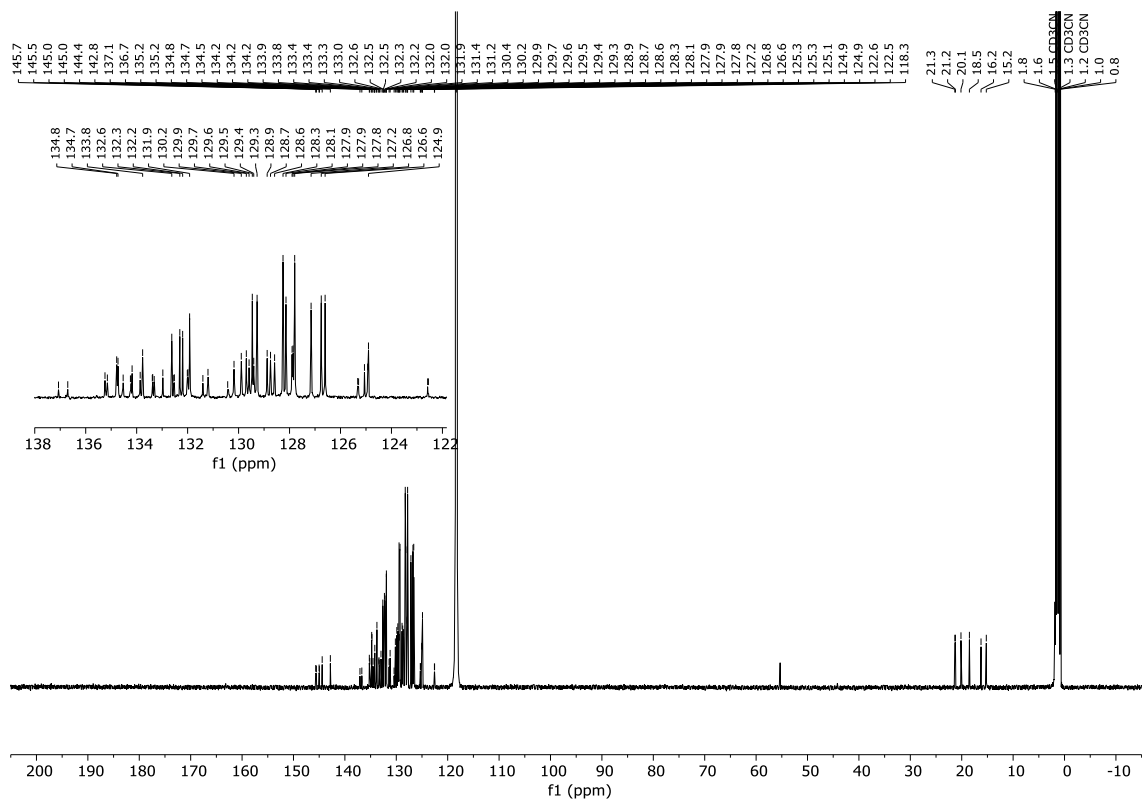
^{19}F NMR: (471 MHz, CD_3CN) **162c**



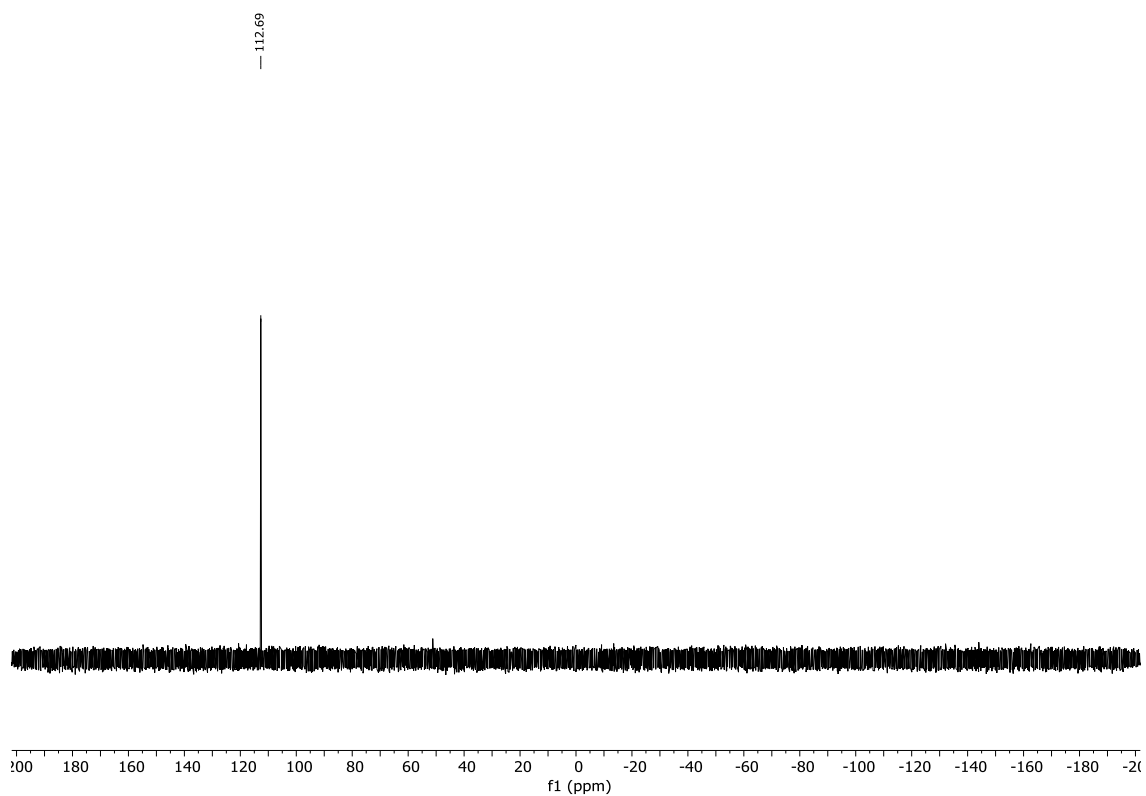
¹H NMR: (300 MHz, CD₃CN) **162d**



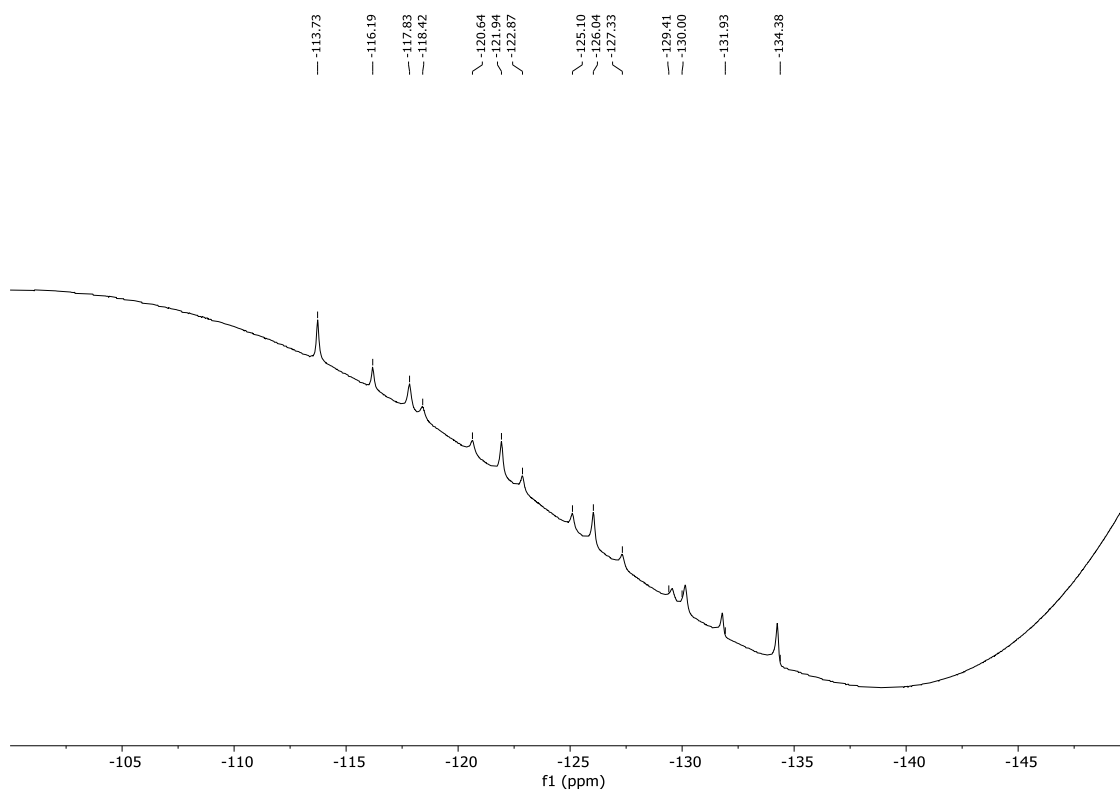
¹³C{H} NMR: (126 MHz, CD₃CN) **162d**



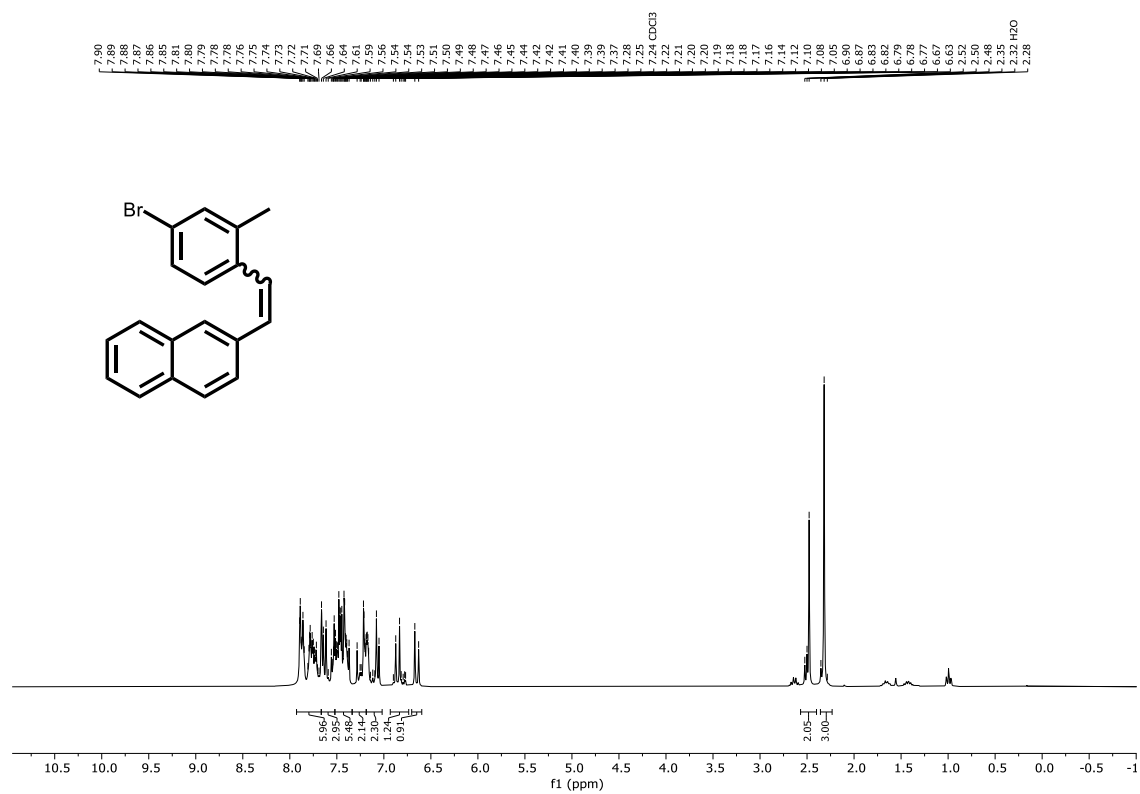
$^{31}\text{P}\{\text{H}\}$ NMR: (121 MHz, CD_3CN) **162d**



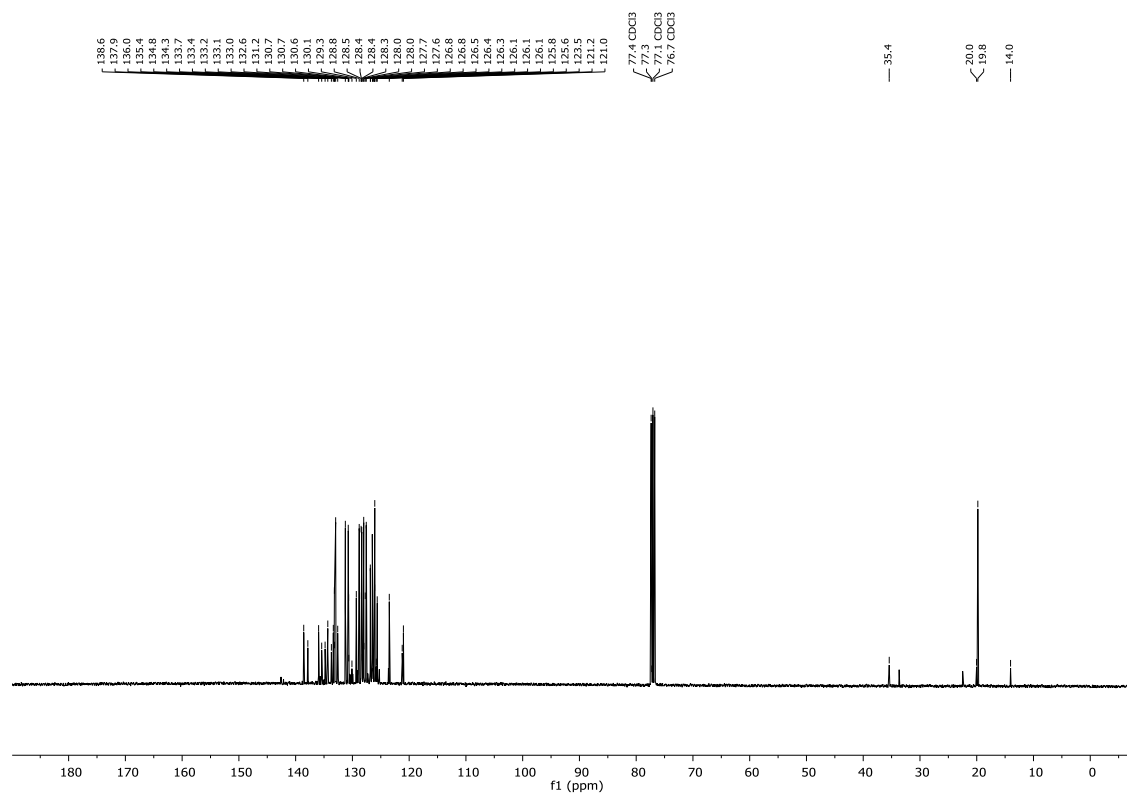
^{19}F NMR: (471 MHz, CD_3CN) **162d**



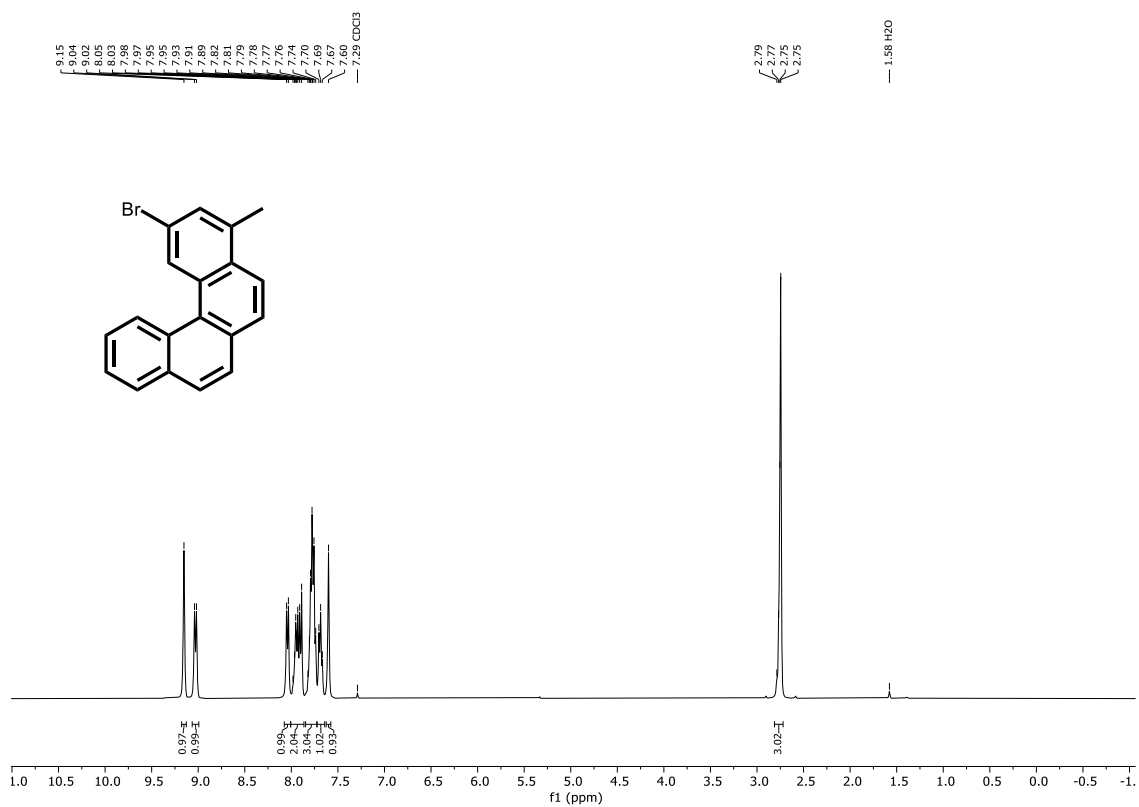
^1H NMR: (400 MHz, CDCl_3) **184c**



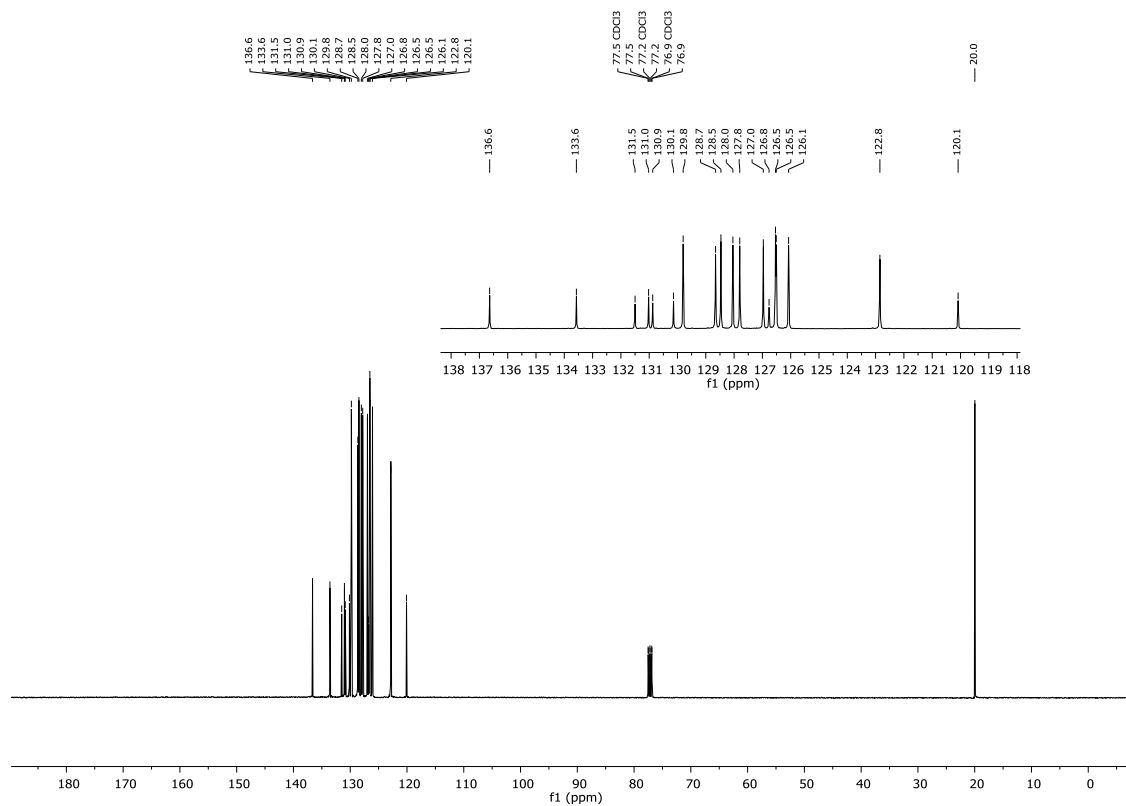
$^{13}\text{C}\{^1\text{H}\}$ NMR: (101 MHz, CDCl_3) **184c**



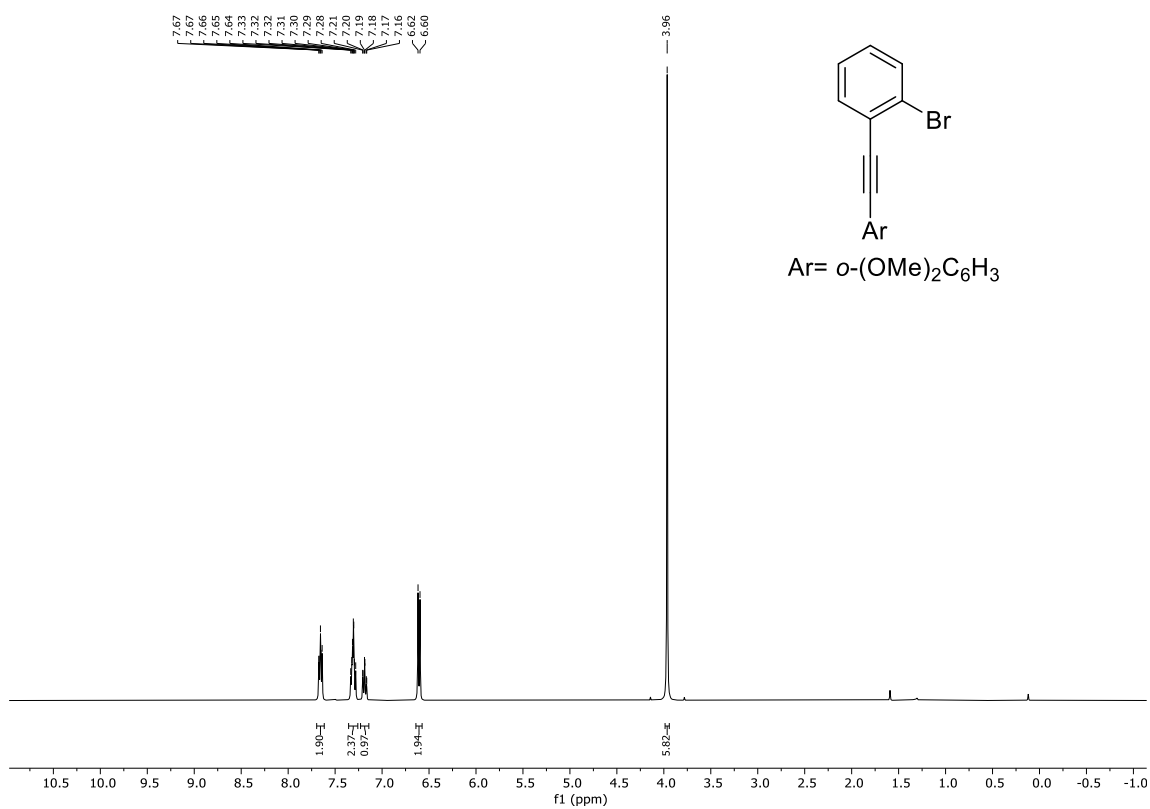
^1H NMR: (400 MHz, CDCl_3) **185c**



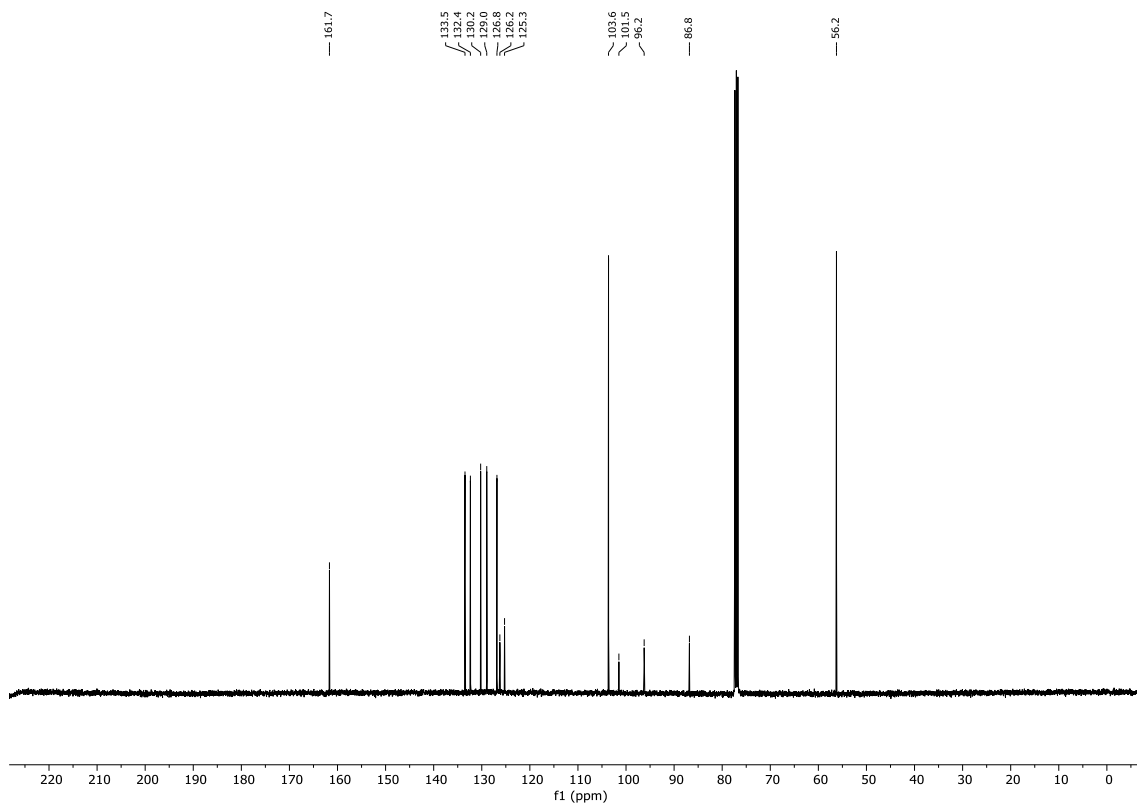
$^{13}\text{C}\{^1\text{H}\}$ NMR: (101 MHz, CDCl_3) **185c**



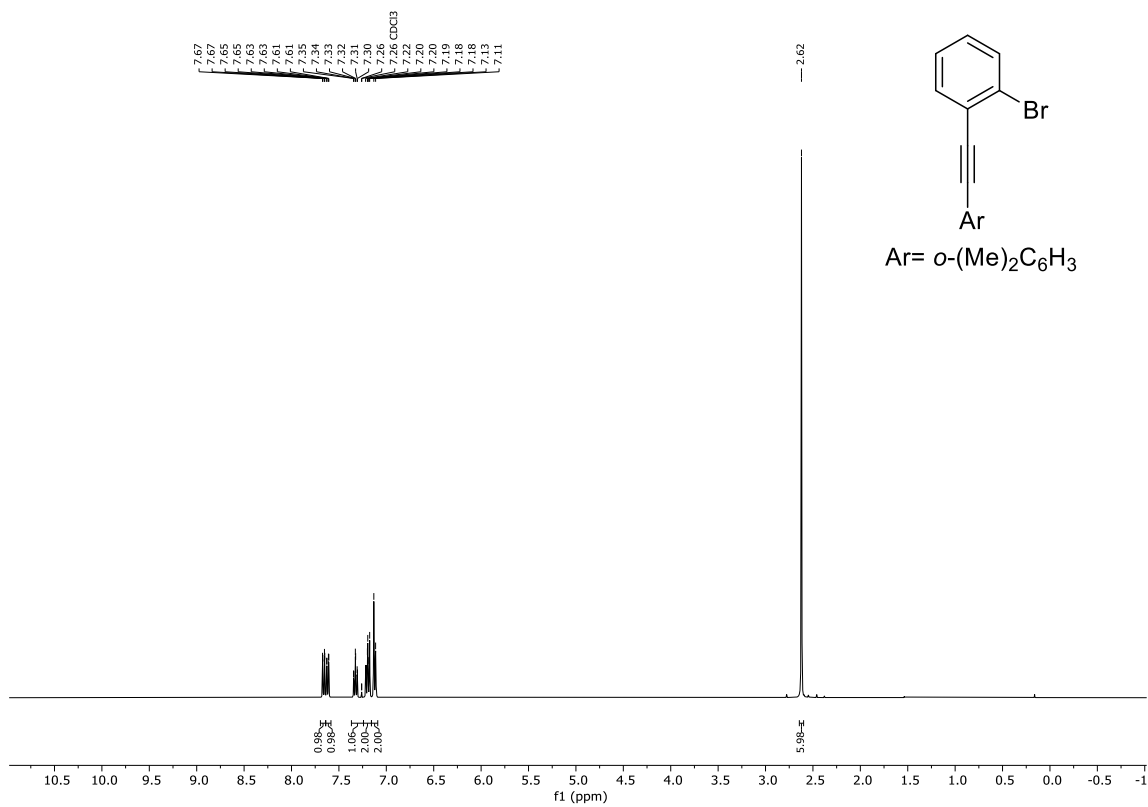
¹H NMR: (400 MHz, CDCl₃) **189h**



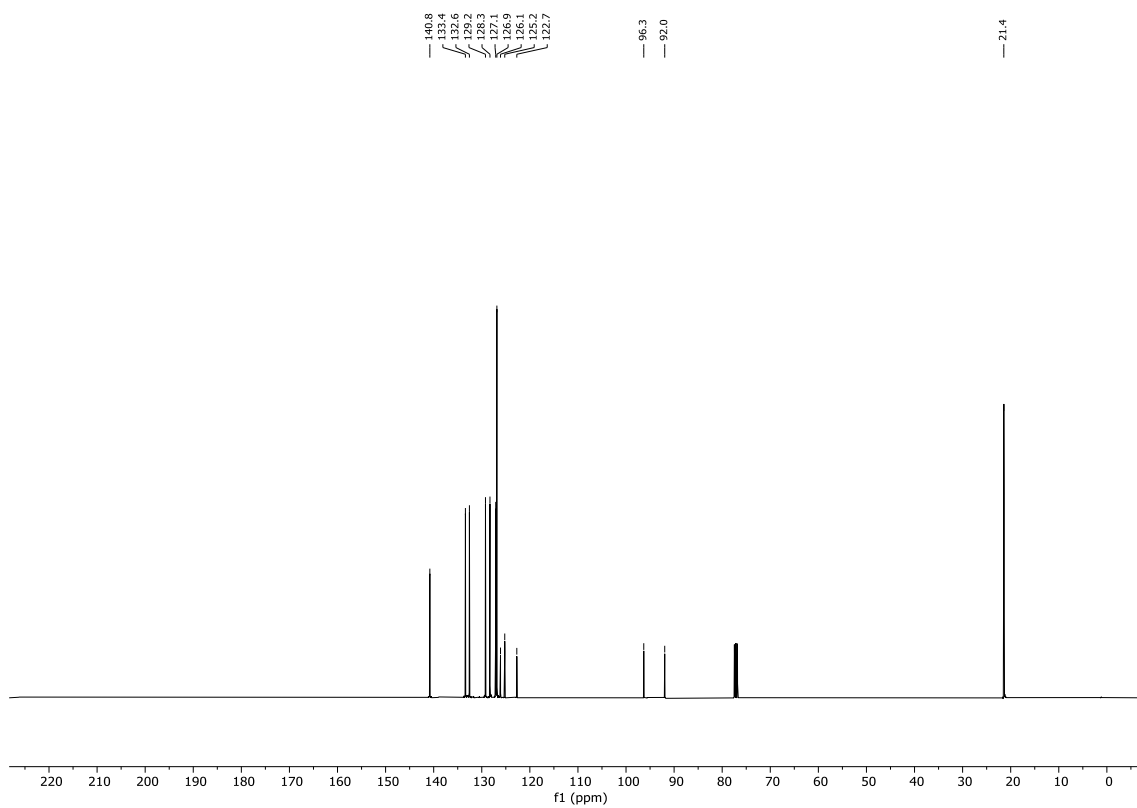
¹³C{H} NMR: (101 MHz, CDCl₃) **189h**



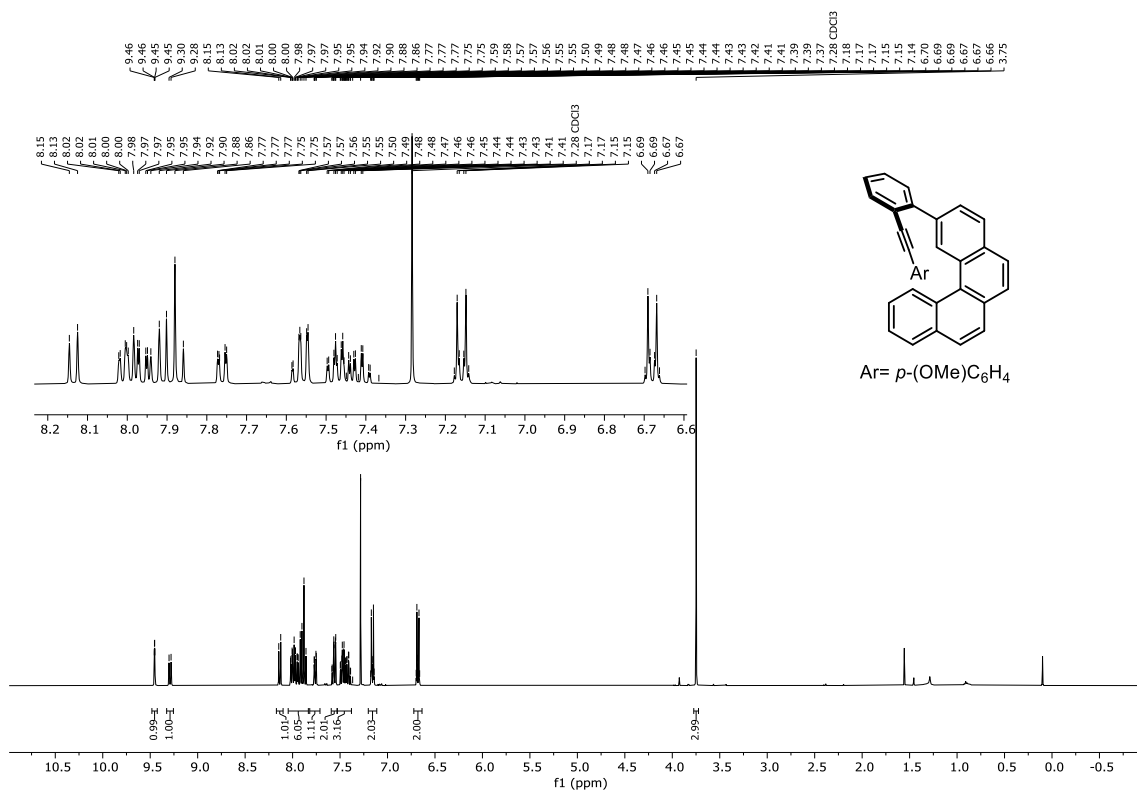
^1H NMR: (400 MHz, CDCl_3) **189i**



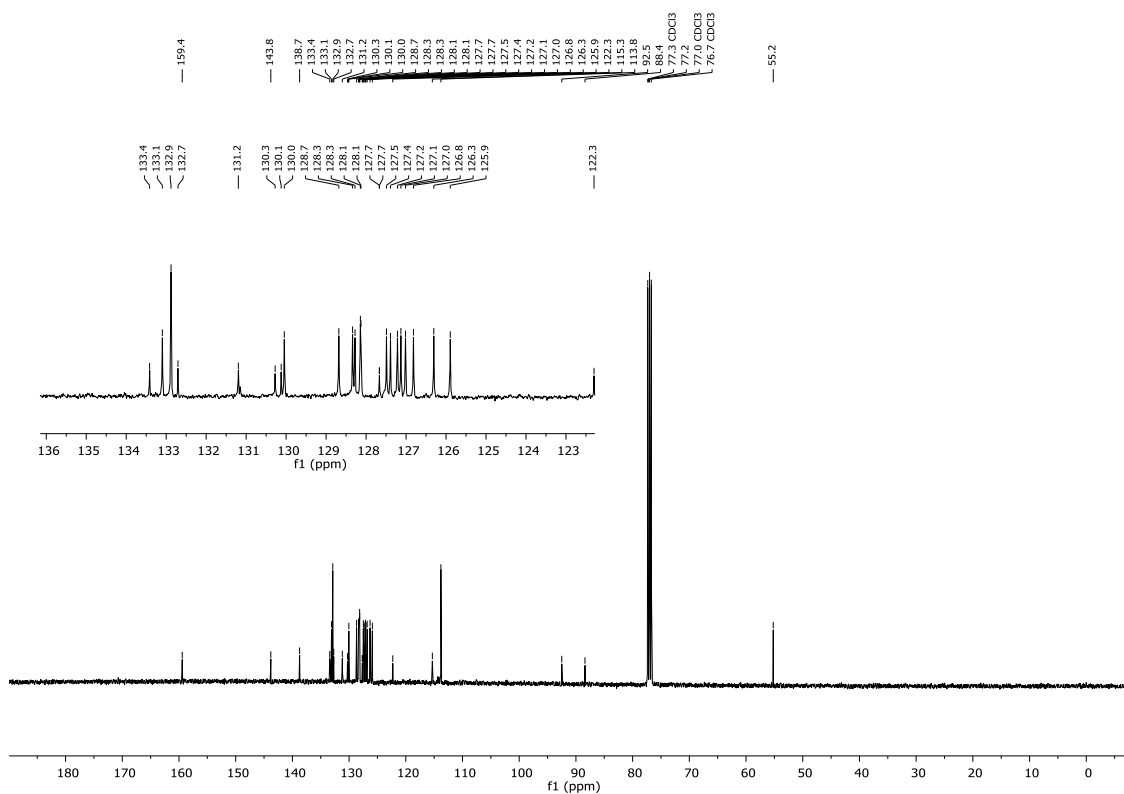
$^{13}\text{C}\{\text{H}\}$ NMR: (101 MHz, CDCl_3) **189i**



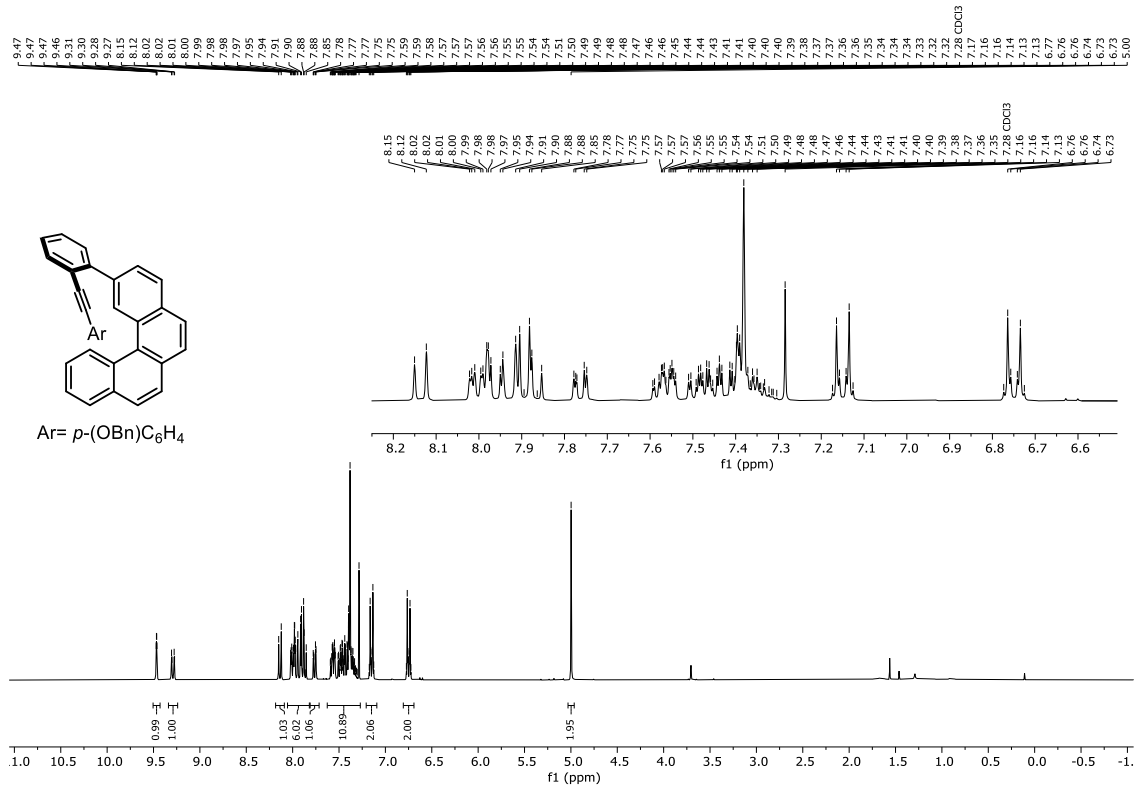
¹H NMR: (400 MHz, CDCl₃) **161a**



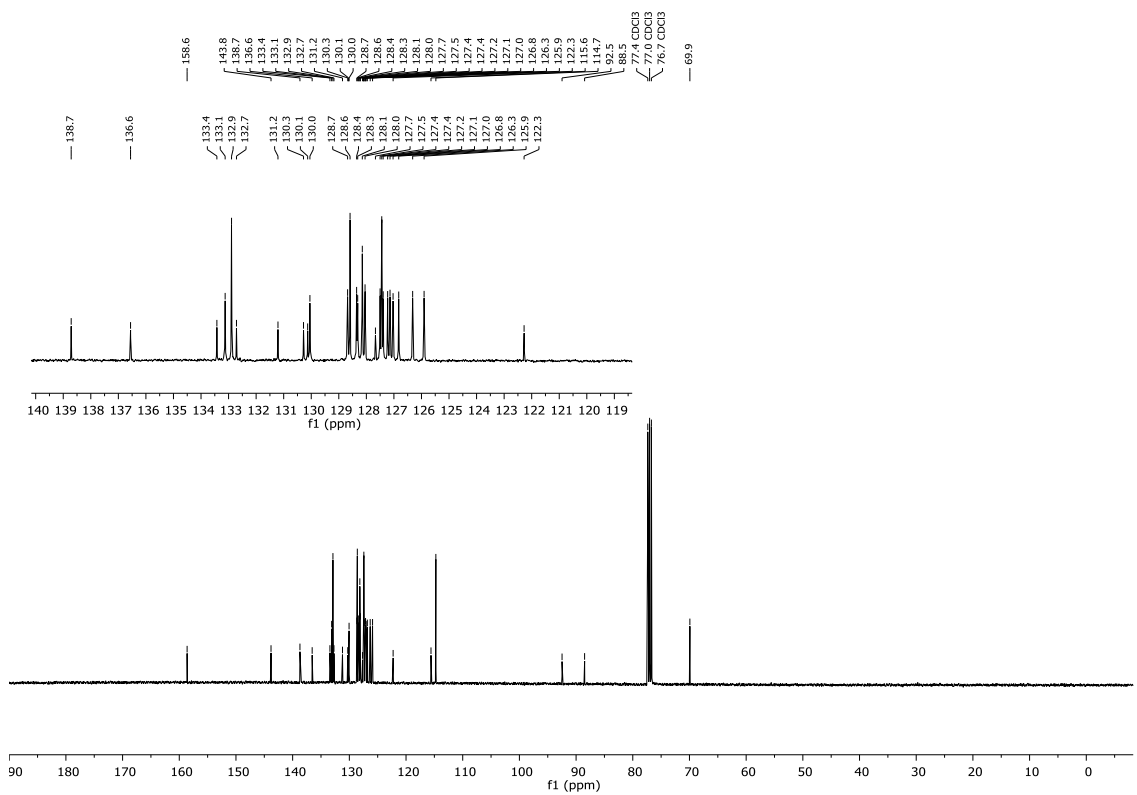
¹³C{¹H} NMR: (101 MHz, CDCl₃) **161a**



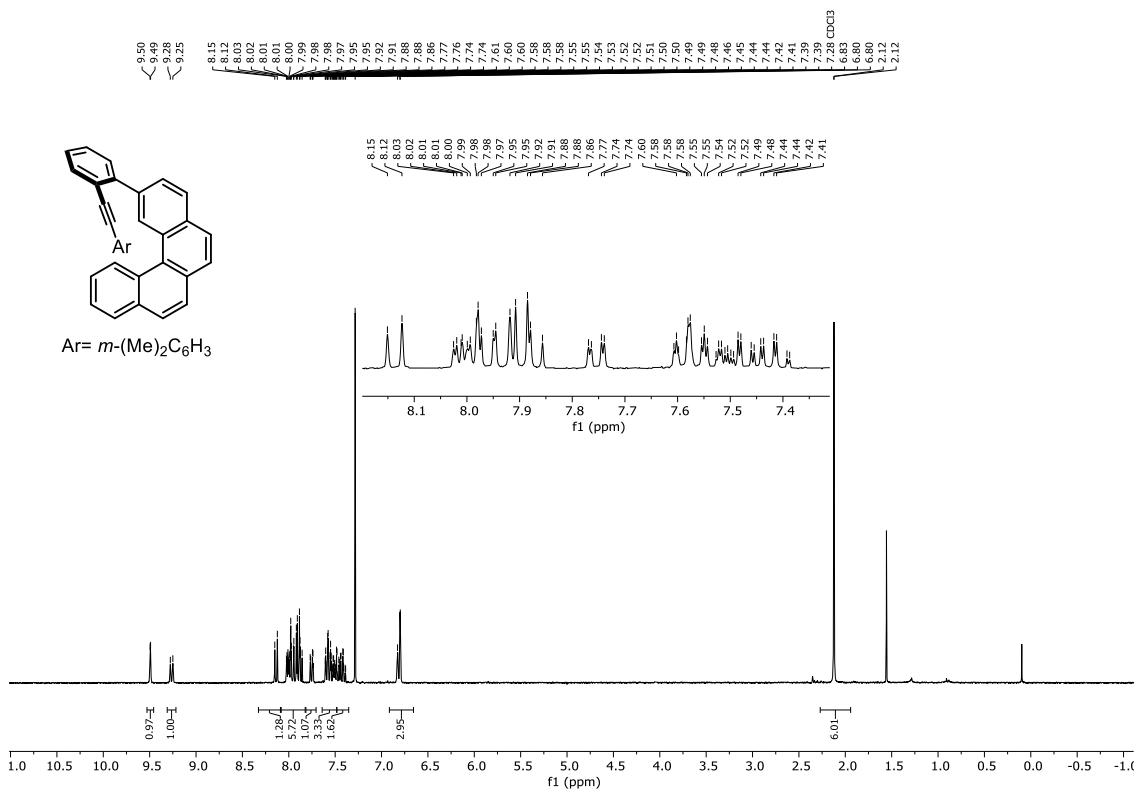
¹H NMR: (400 MHz, CDCl₃) **161c**



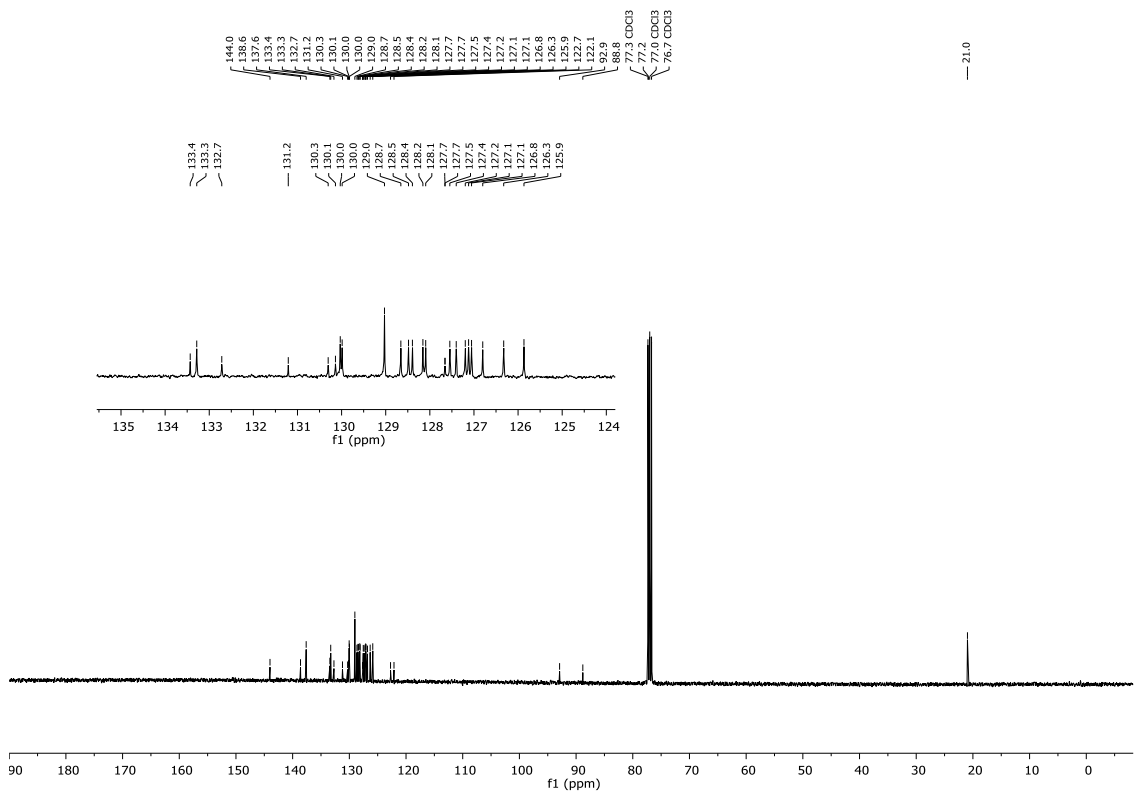
¹³C{H} NMR: (101 MHz, CDCl₃) **161c**



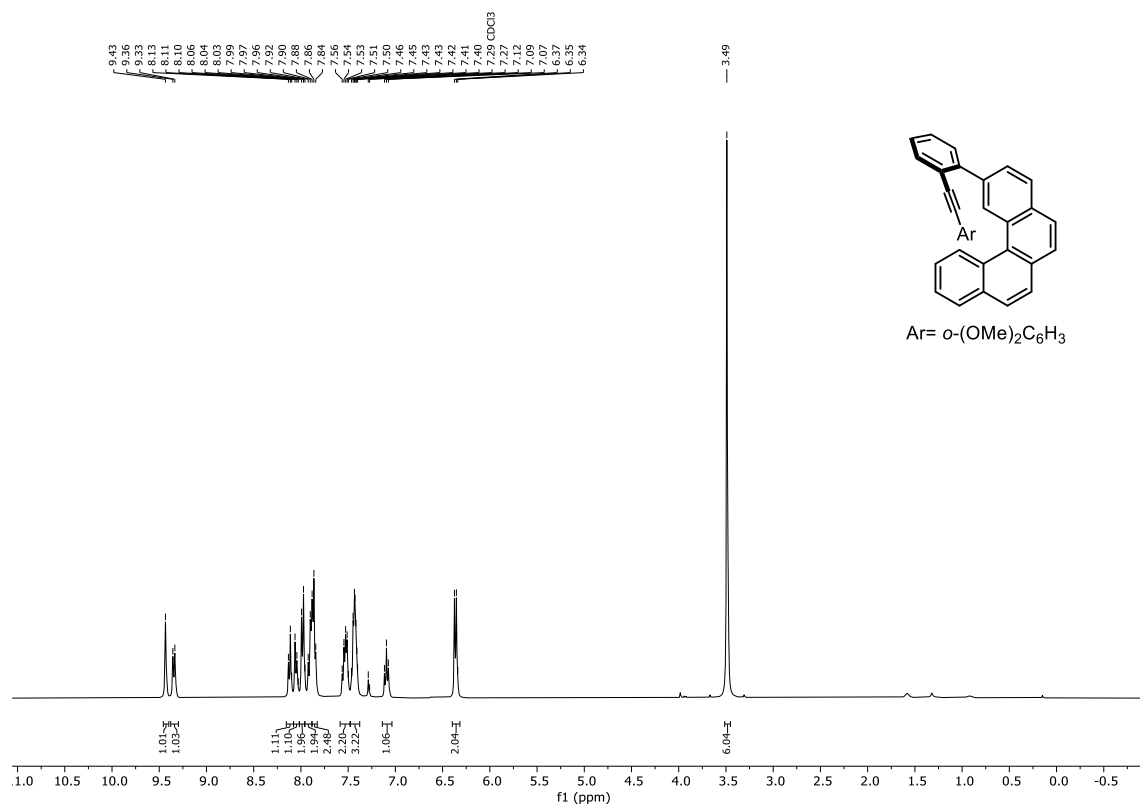
¹H NMR: (400 MHz, CDCl₃) **161g**



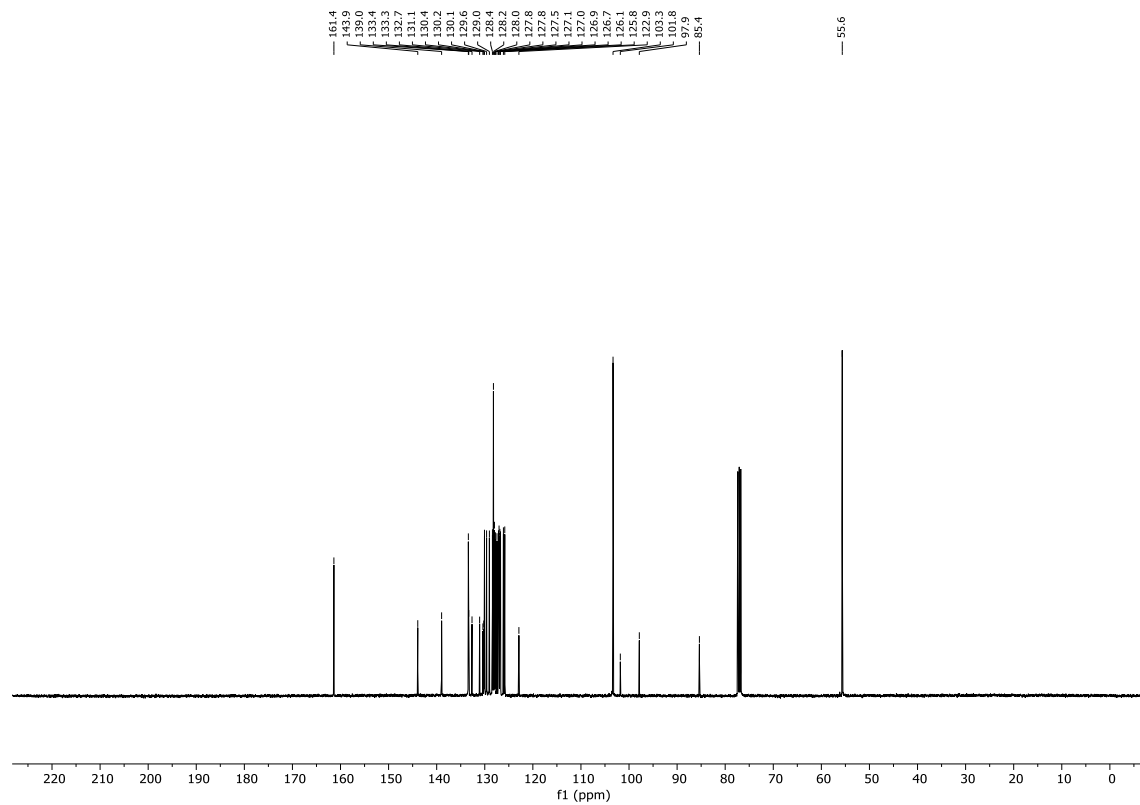
¹³C{H} NMR: (101 MHz, CDCl₃) **161g**



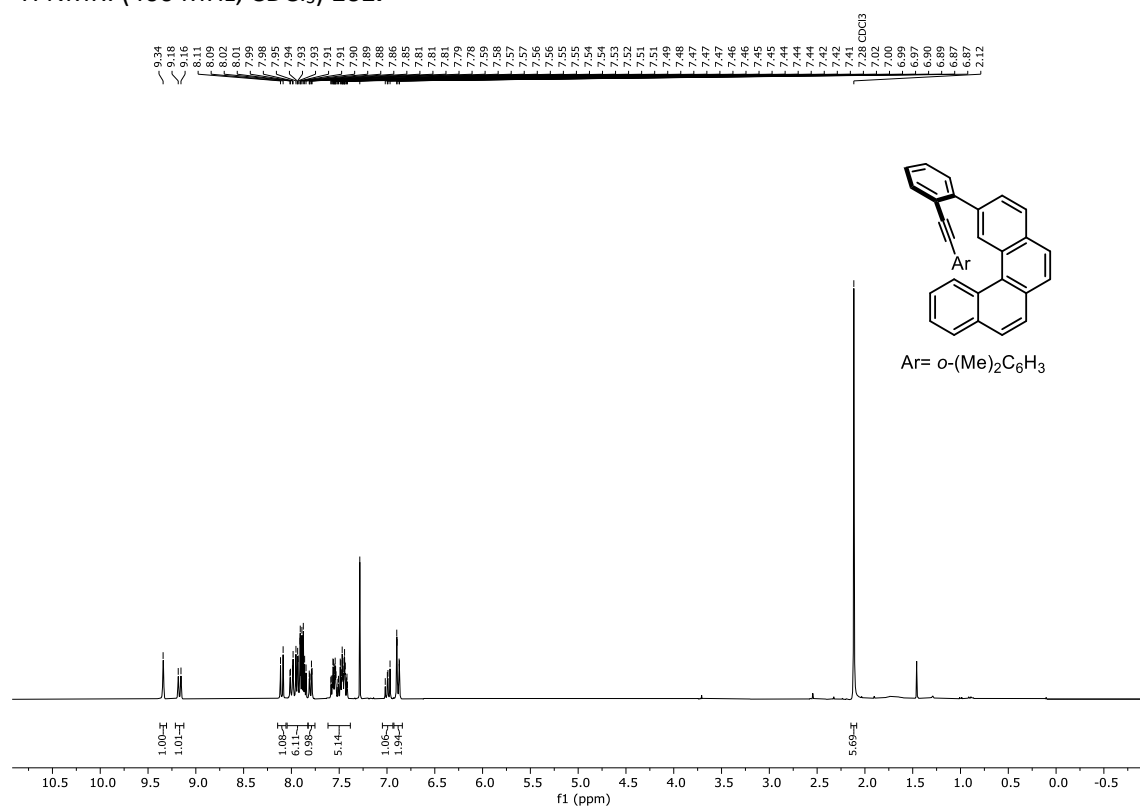
¹H NMR: (400 MHz, CDCl₃) **161h**



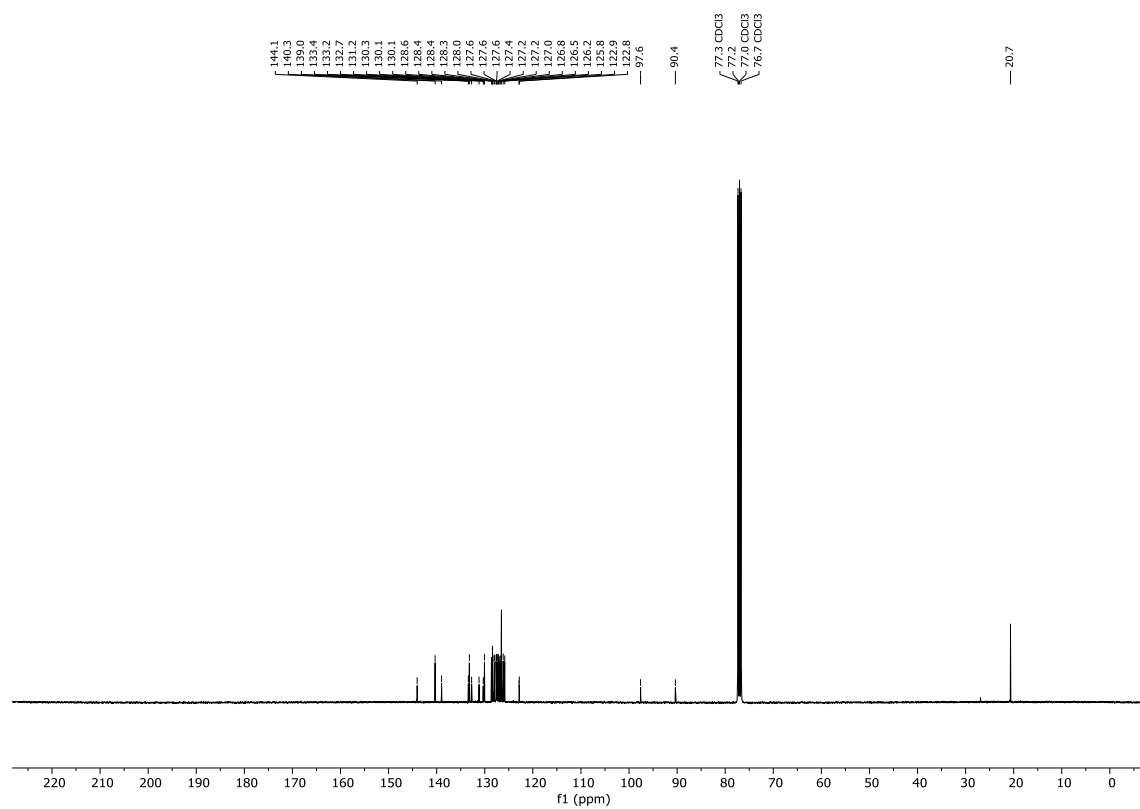
¹³C{H} NMR: (101 MHz, CDCl₃) **161h**



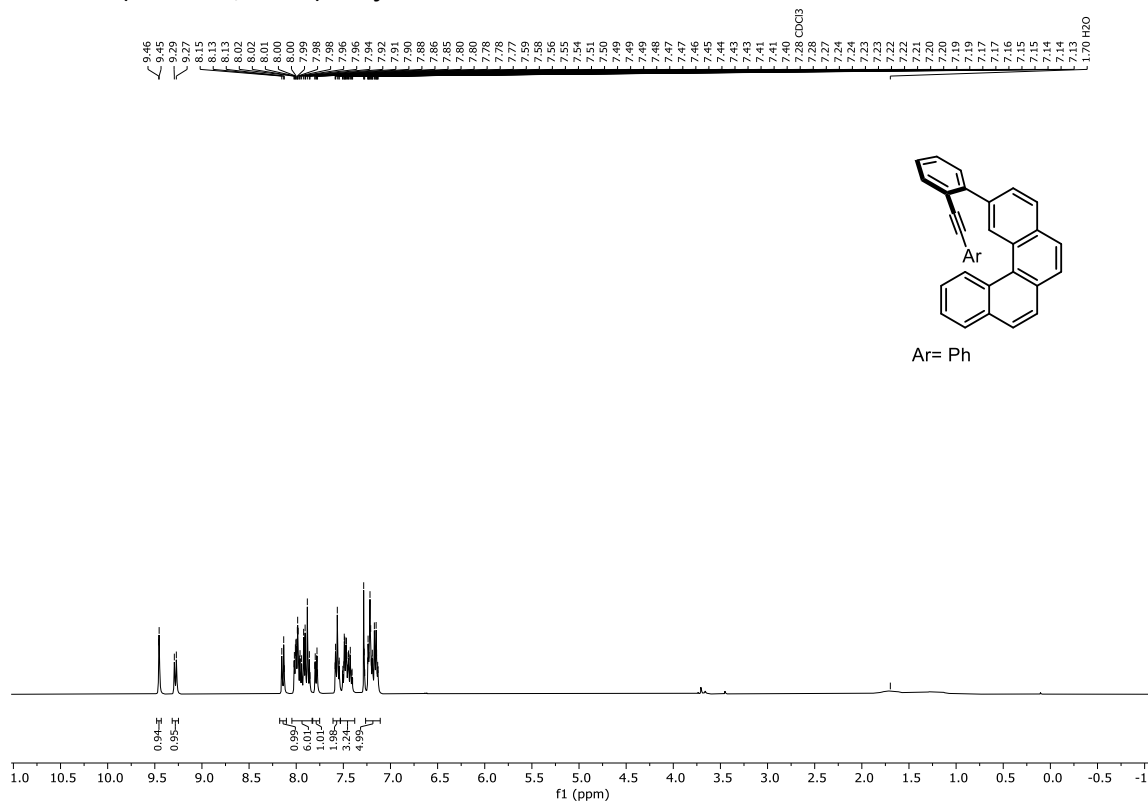
¹H NMR: (400 MHz, CDCl₃) **161i**



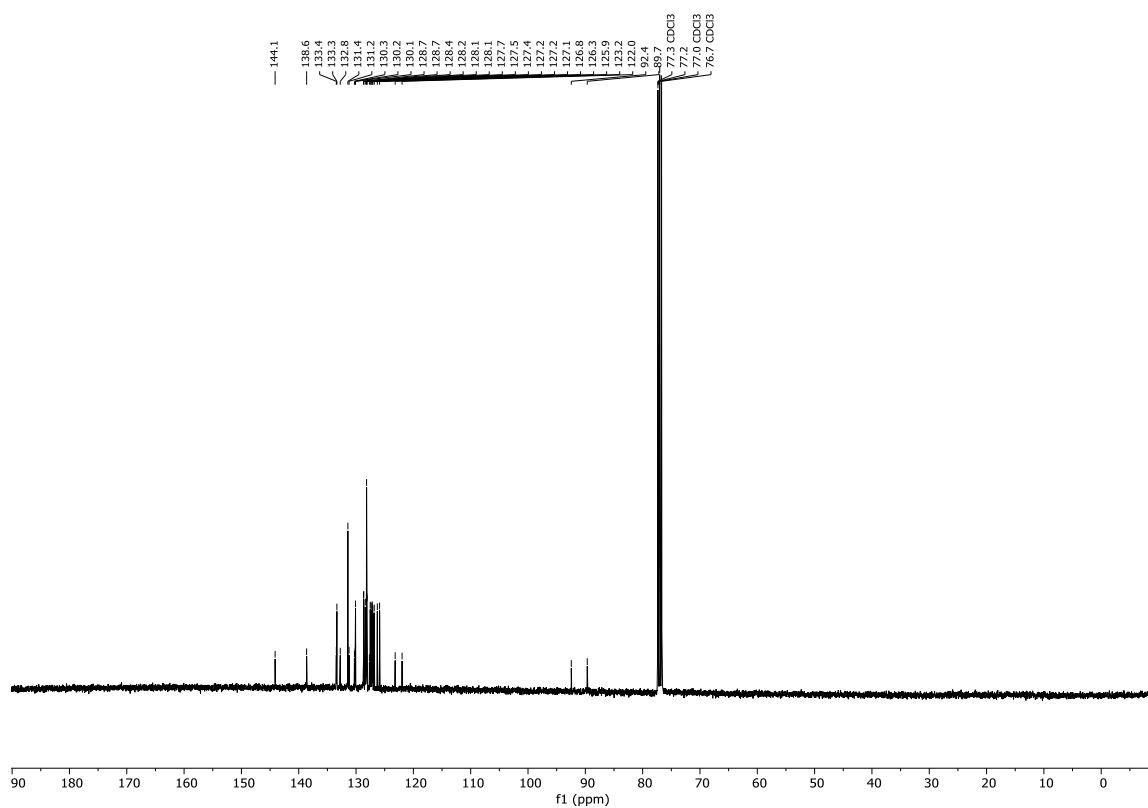
¹³C{H} NMR: (101 MHz, CDCl₃) **161i**



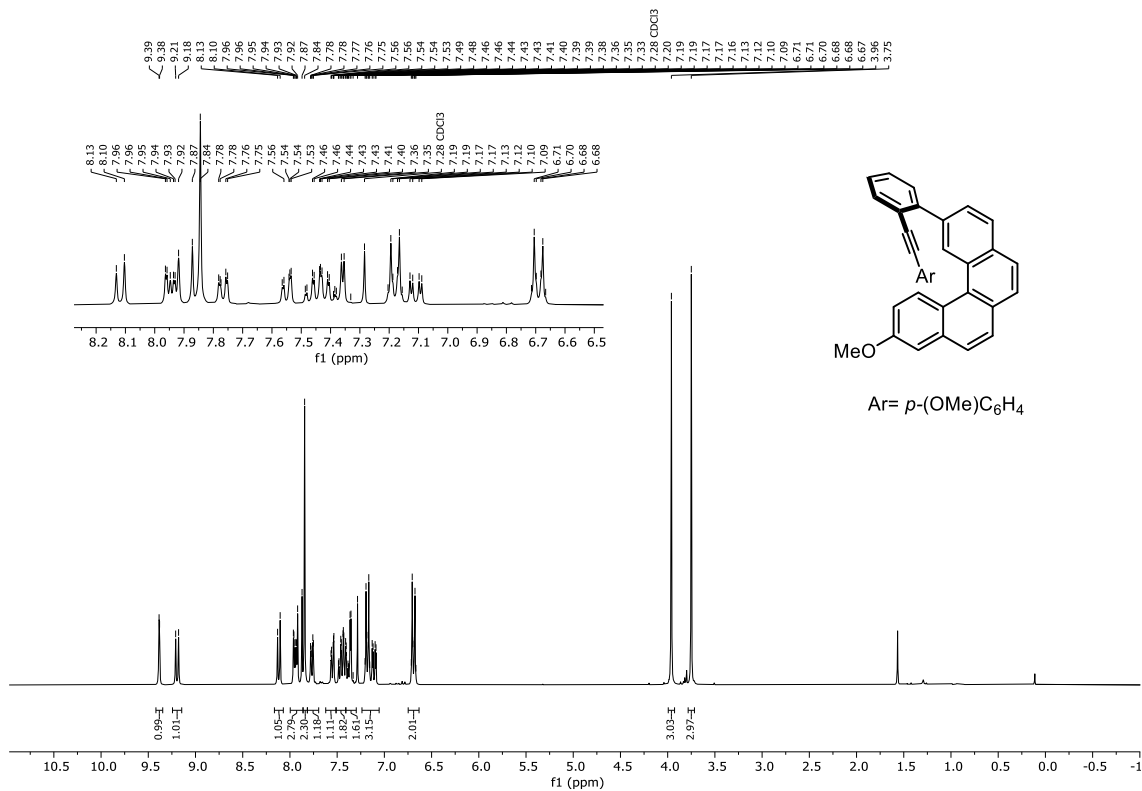
¹H NMR: (400 MHz, CDCl₃) **161j**



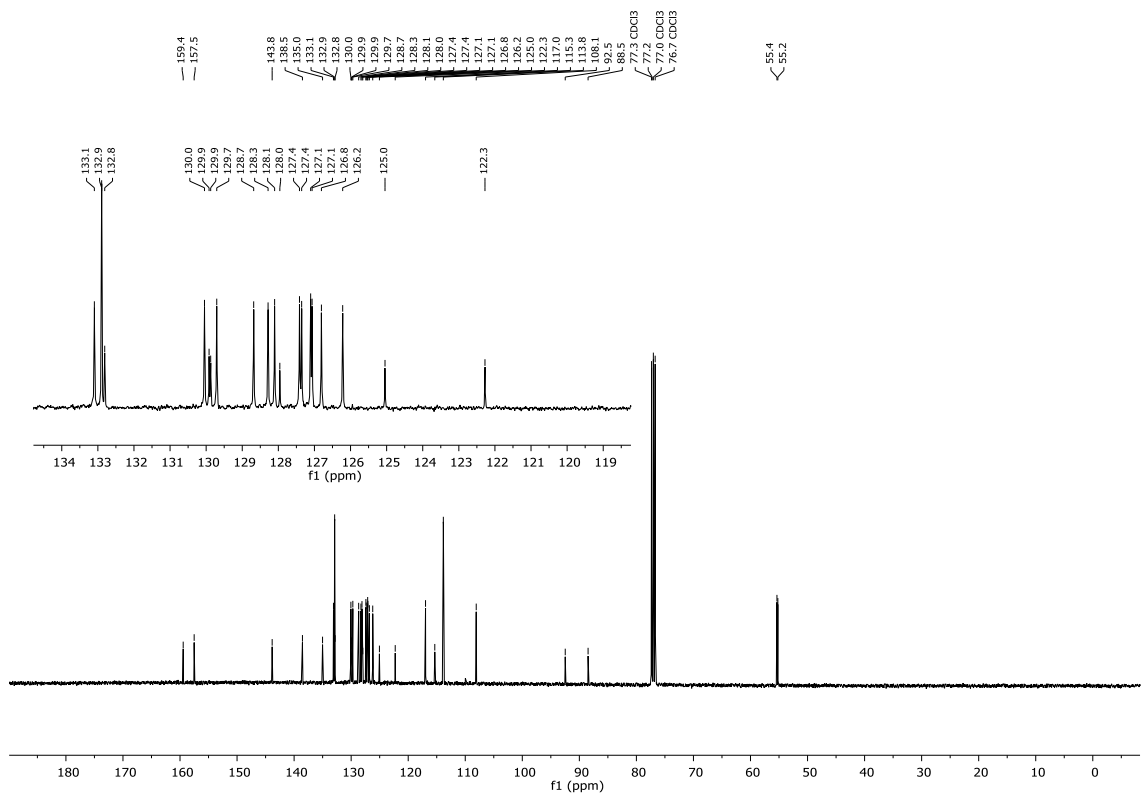
¹³C{H} NMR: (101 MHz, CDCl₃) **161j**



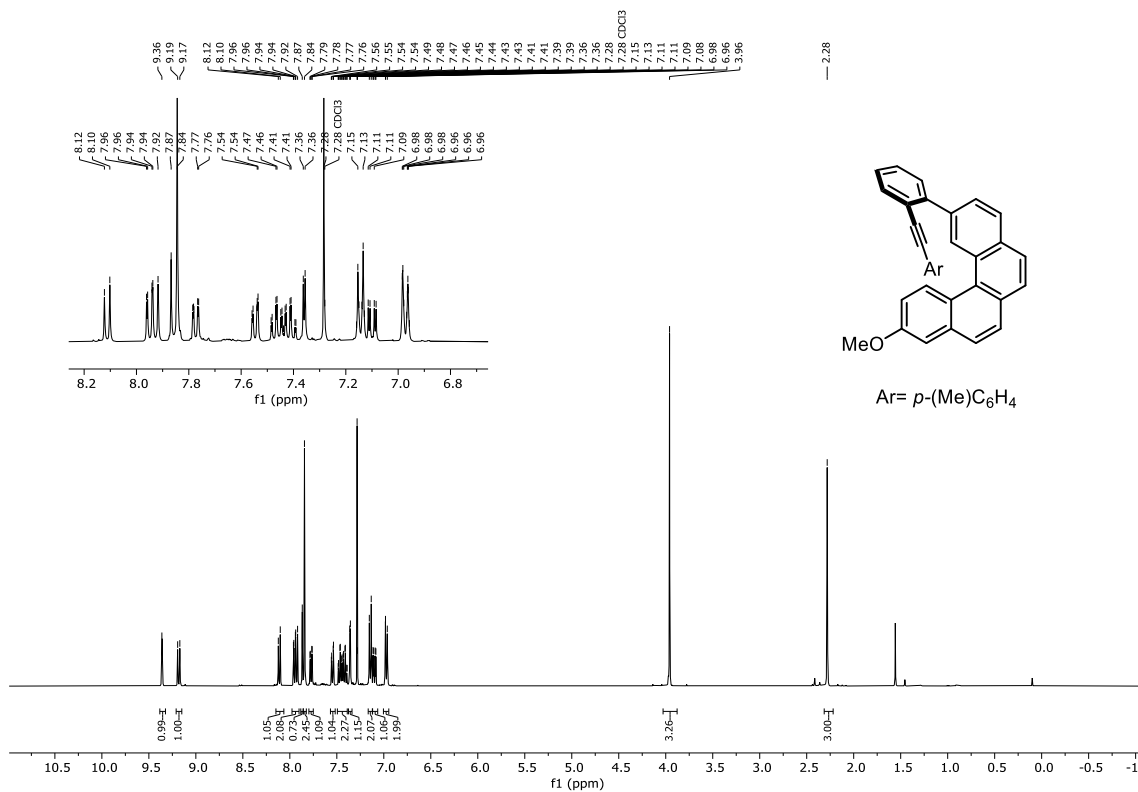
¹H NMR: (400 MHz, CDCl₃) **161k**



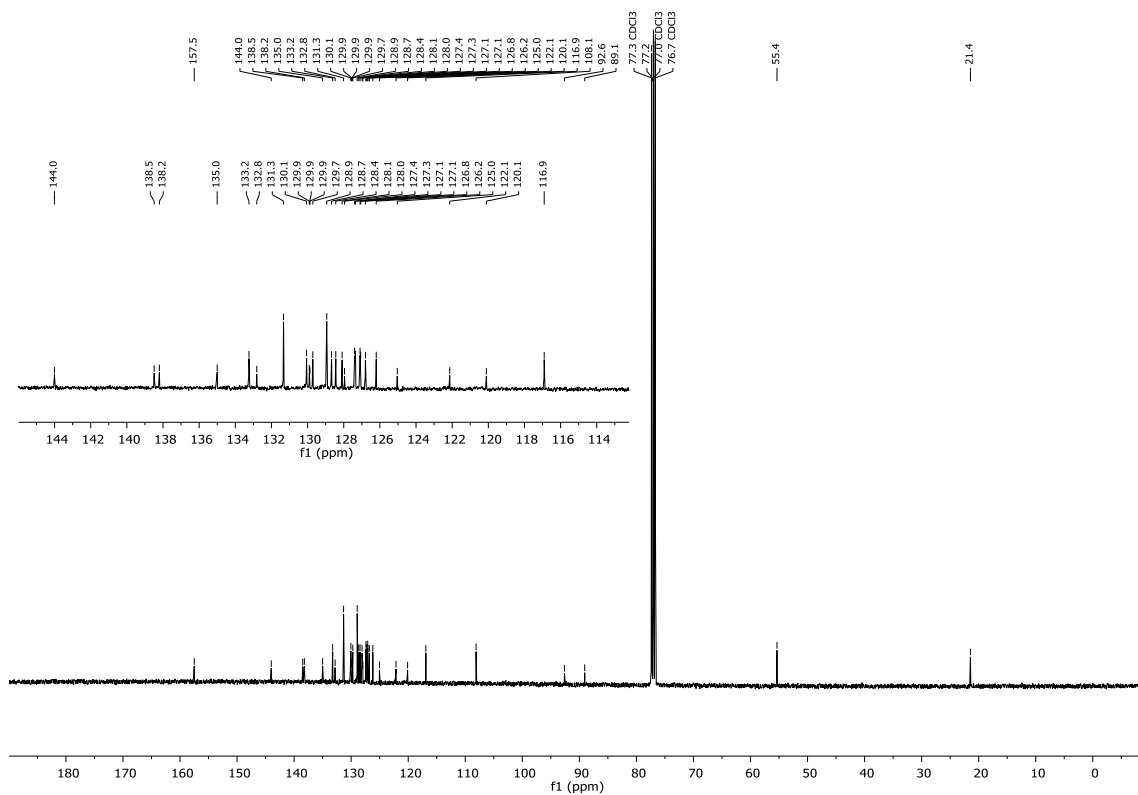
¹³C{H} NMR: (101 MHz, CDCl₃) **161k**



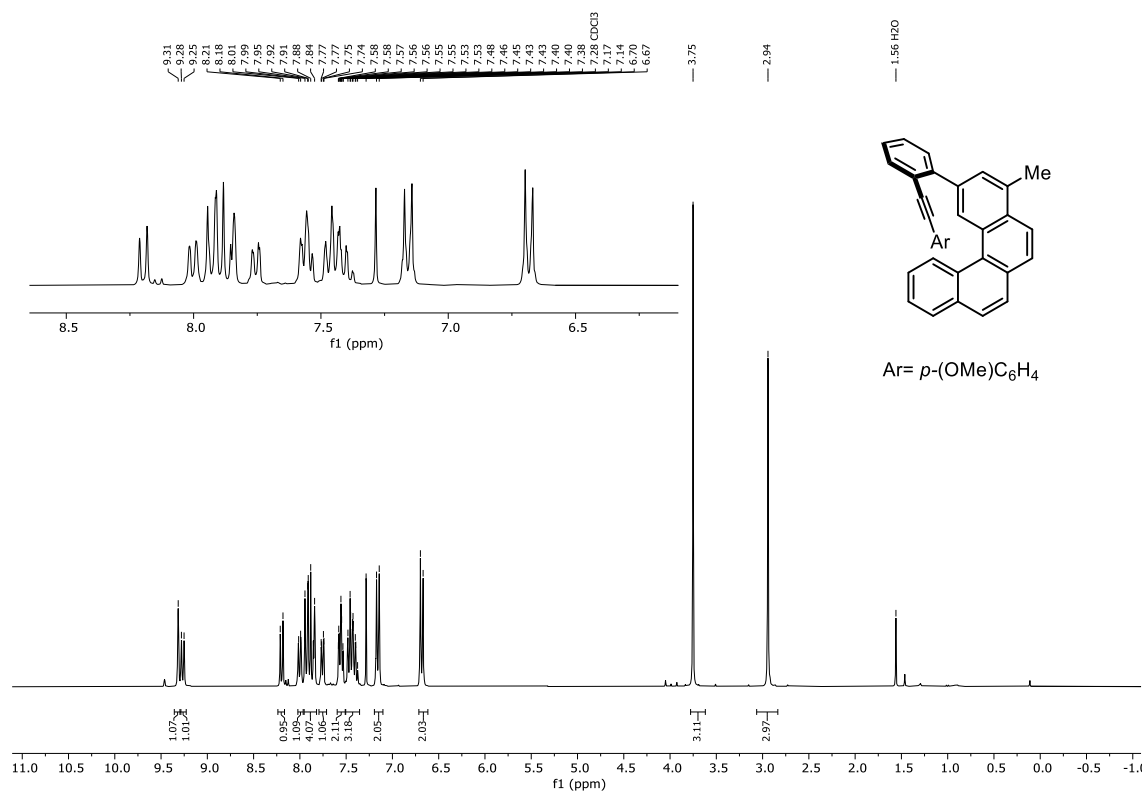
¹H NMR: (400 MHz, CDCl₃) 161I



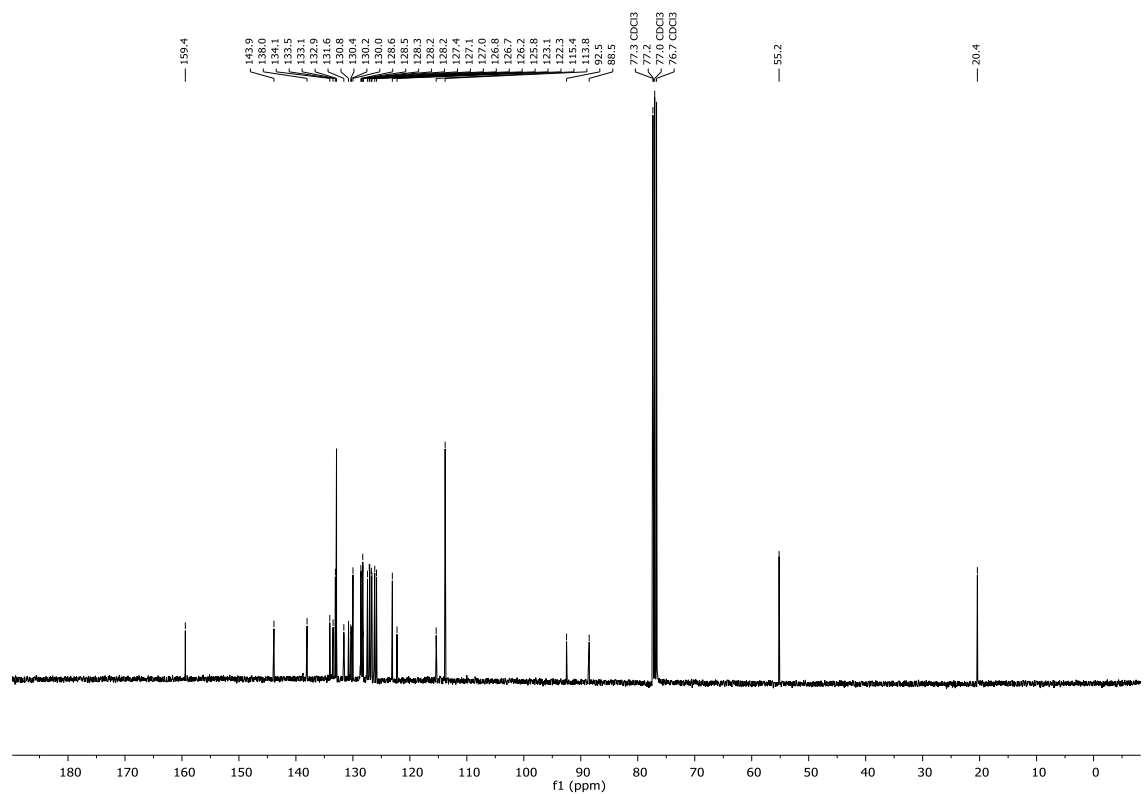
¹³C{H} NMR: (101 MHz, CDCl₃) 161I



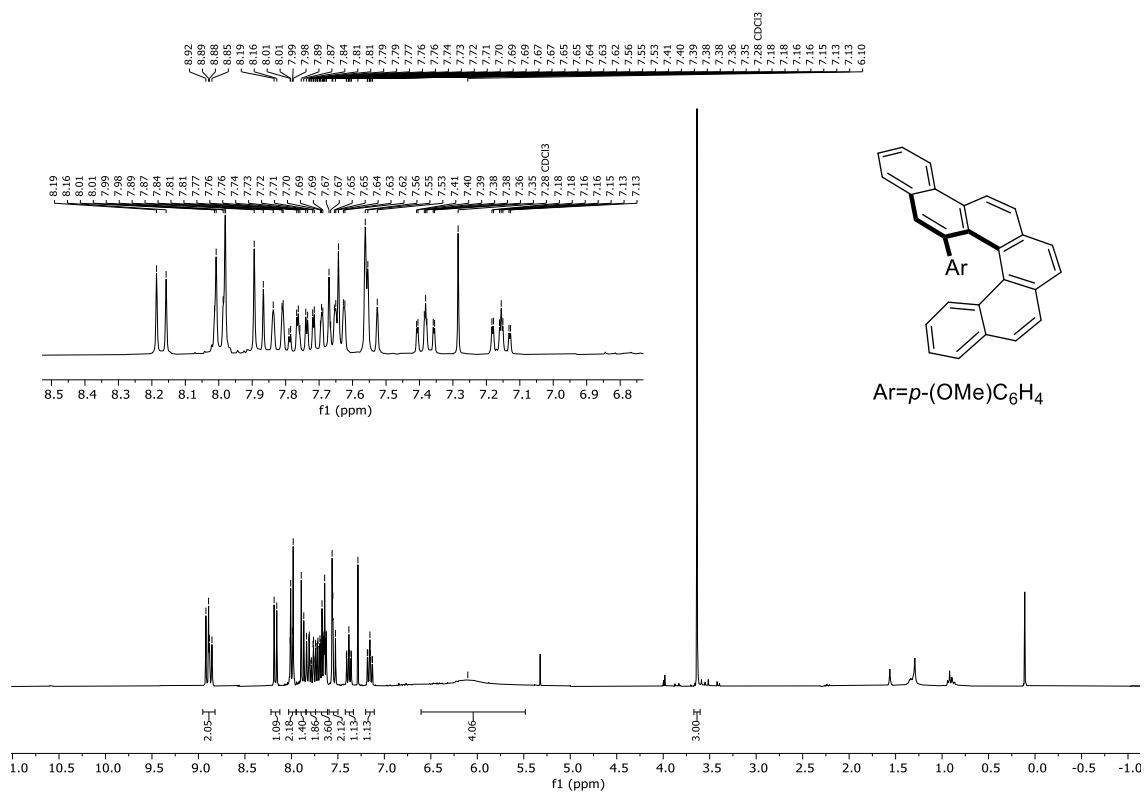
^1H NMR: (400 MHz, CDCl_3) **161n**



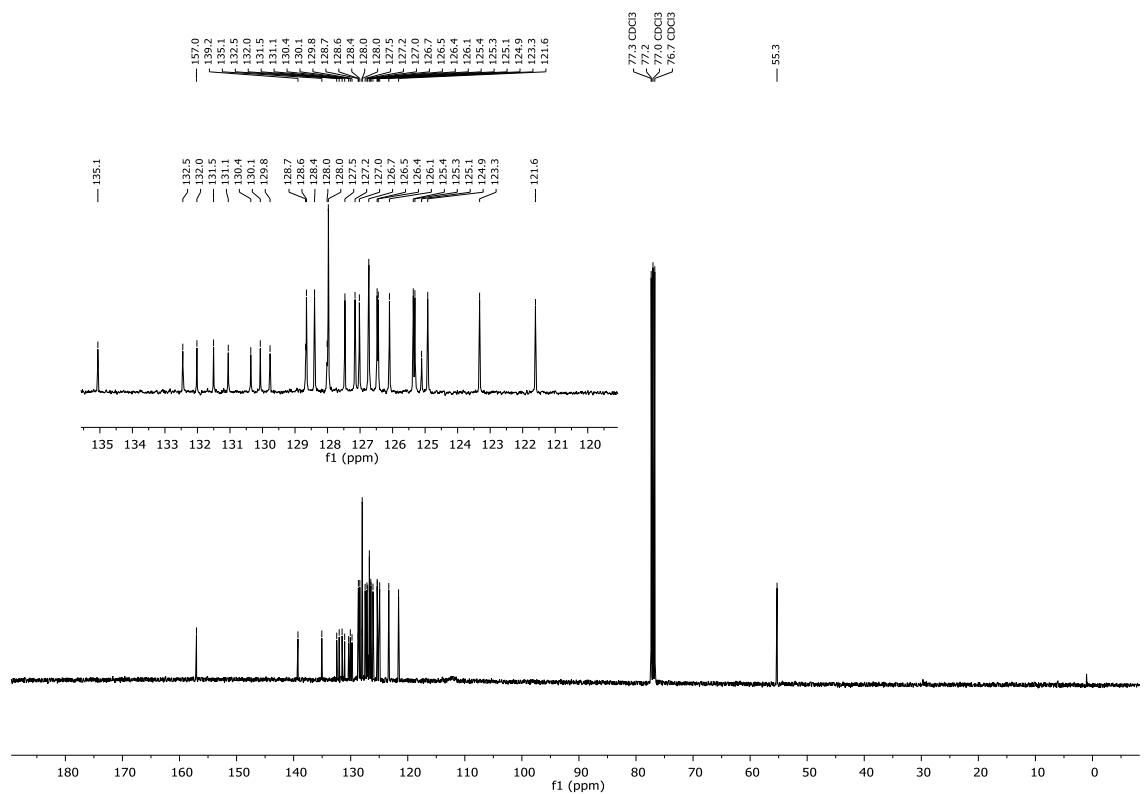
$^{13}\text{C}\{^1\text{H}\}$ NMR: (101 MHz, CDCl_3) **161n**



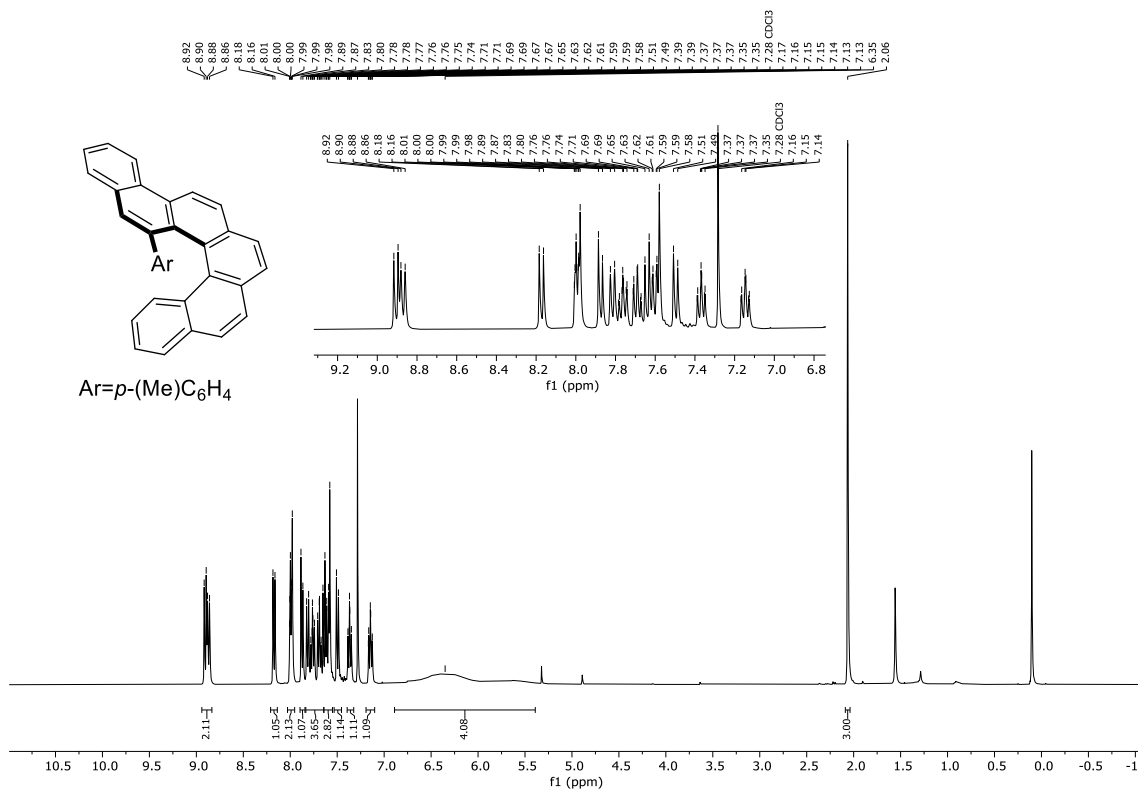
^1H NMR: (400 MHz, CDCl_3) **163a**



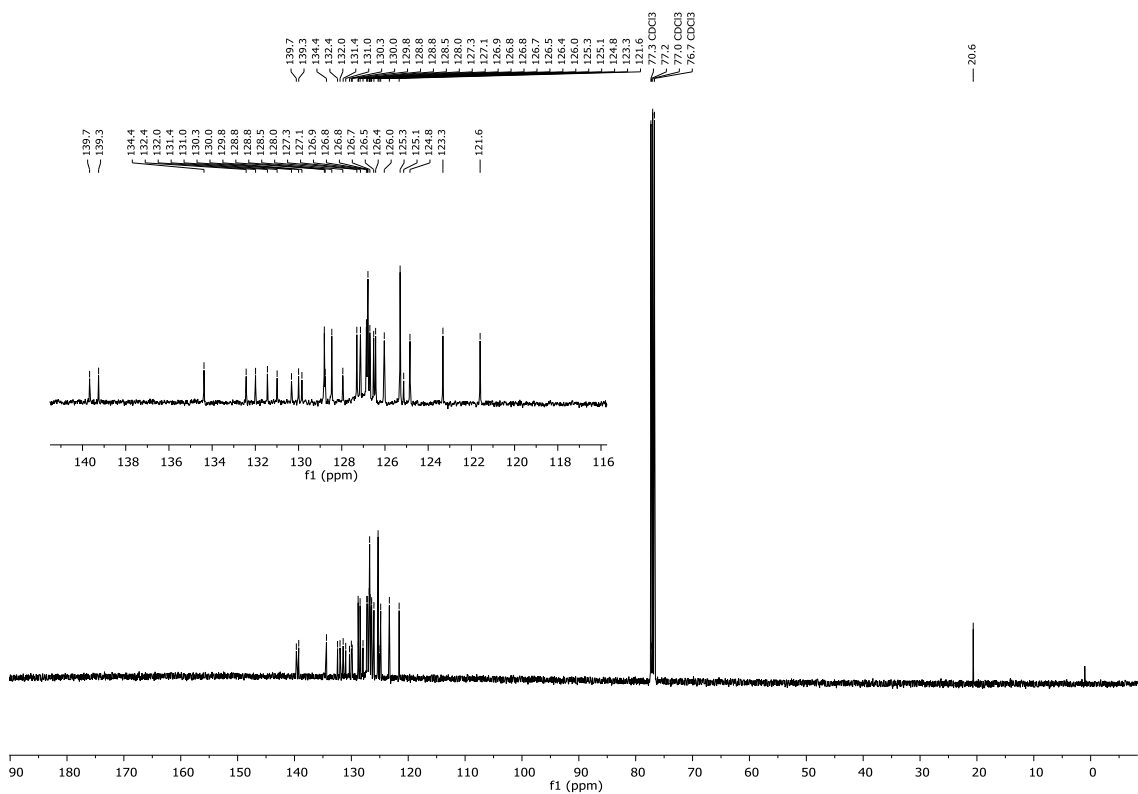
$^{13}\text{C}\{^1\text{H}\}$ NMR: (101 MHz, CDCl_3) **163a**



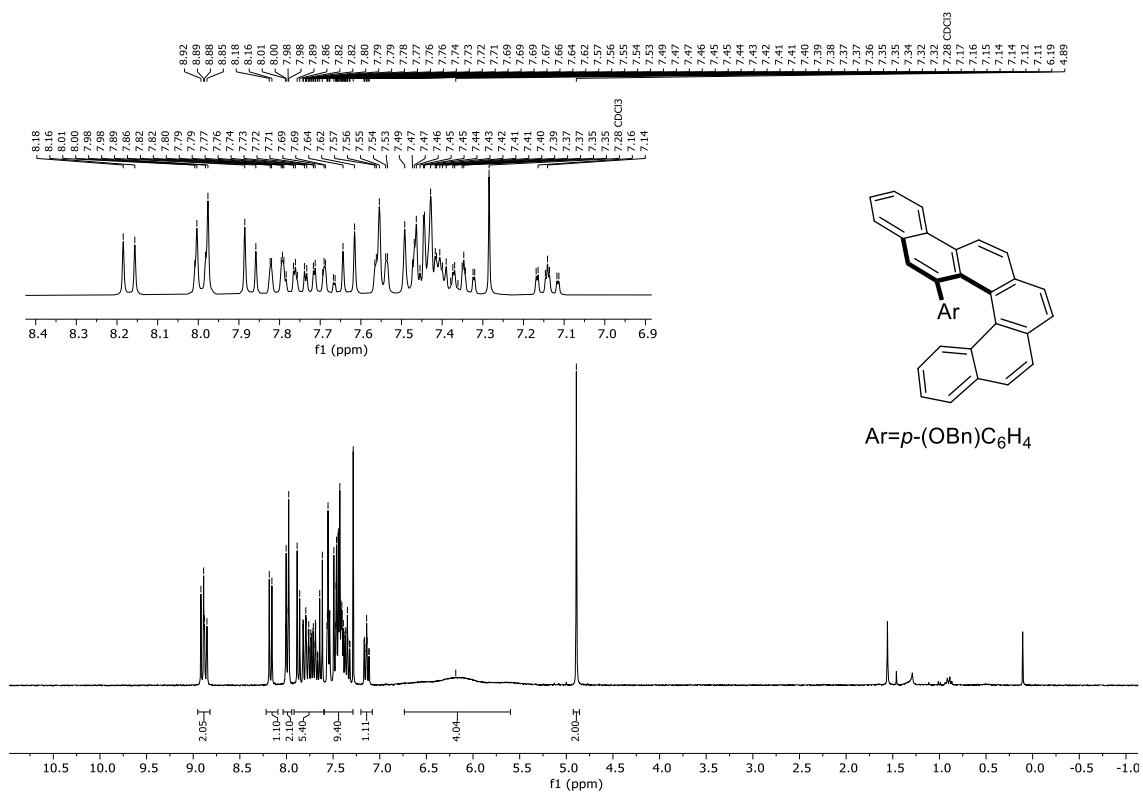
¹H NMR: (400 MHz, CDCl₃) **163b**



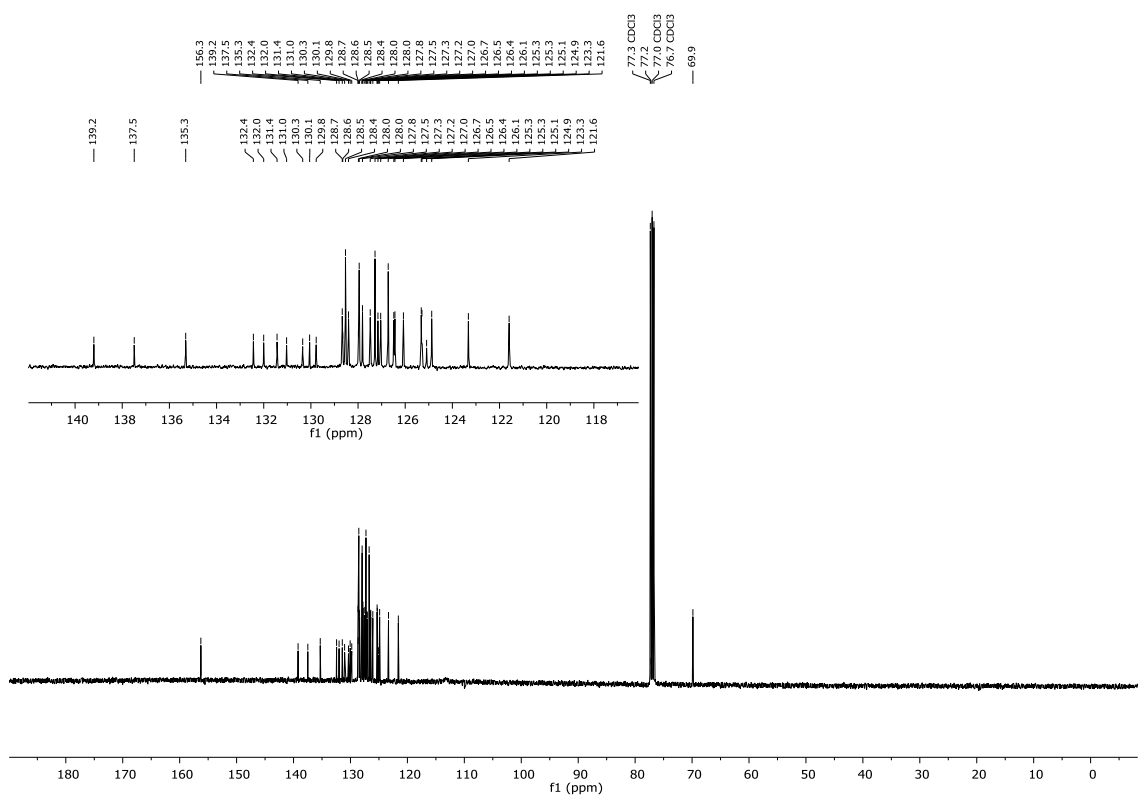
¹³C{H} NMR: (101 MHz, CDCl₃) **163b**



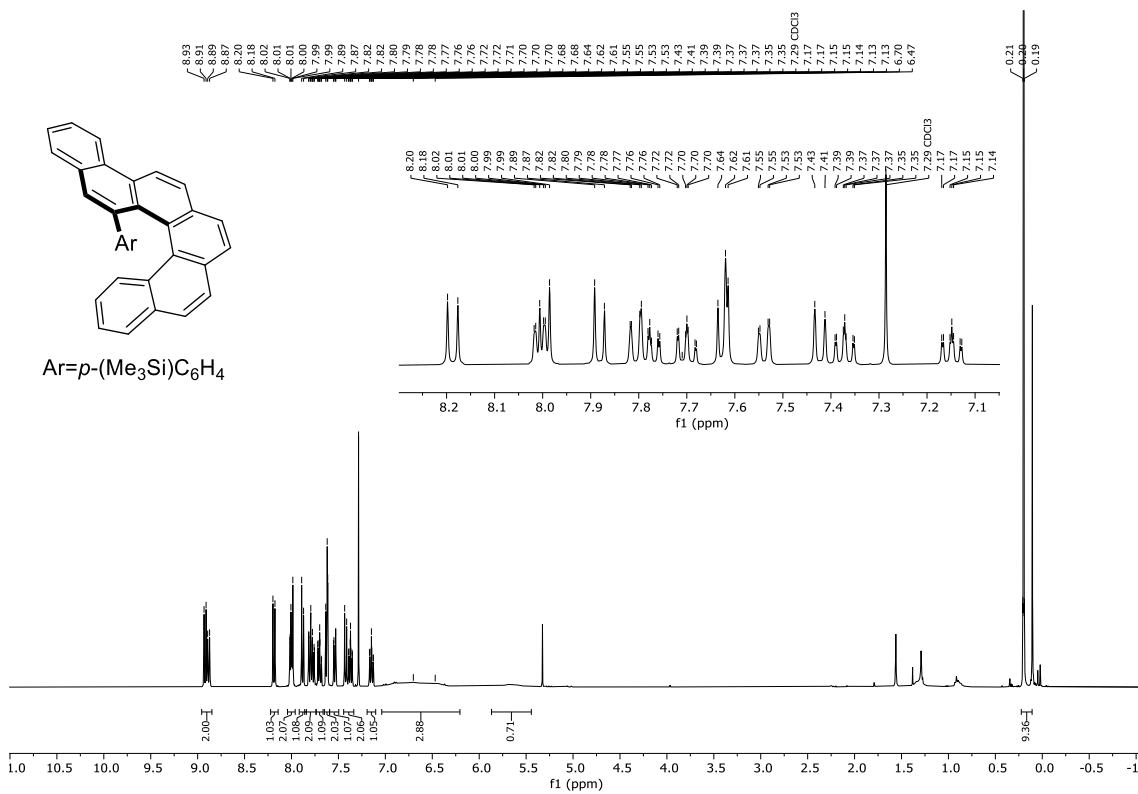
¹H NMR: (400 MHz, CDCl₃) **163c**



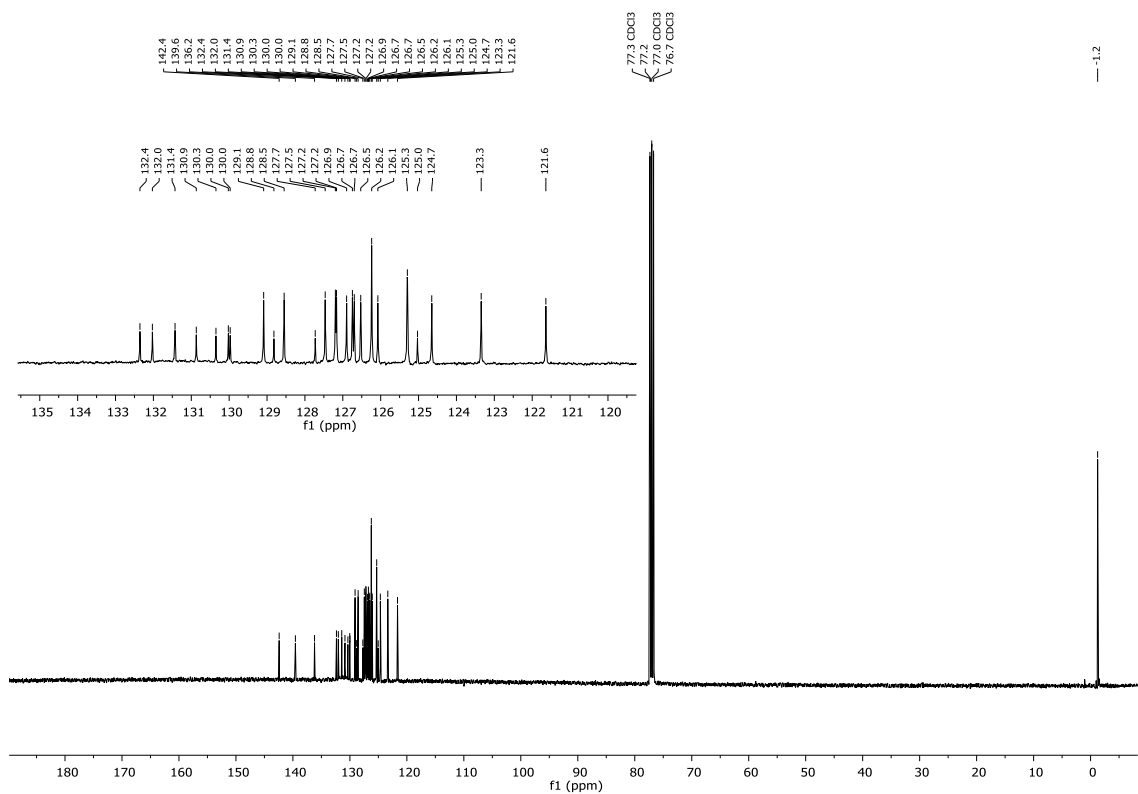
¹³C{¹H} NMR: (101 MHz, CDCl₃) **163c**



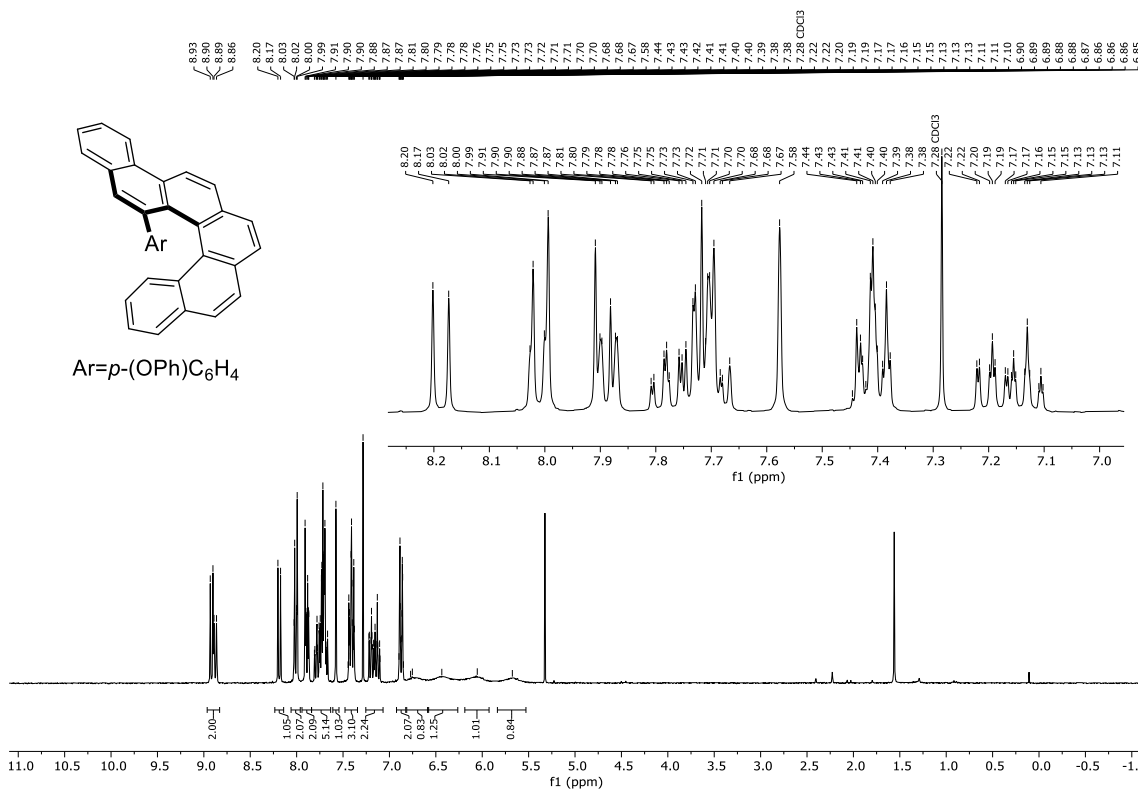
¹H NMR: (400 MHz, CDCl₃) **163d**



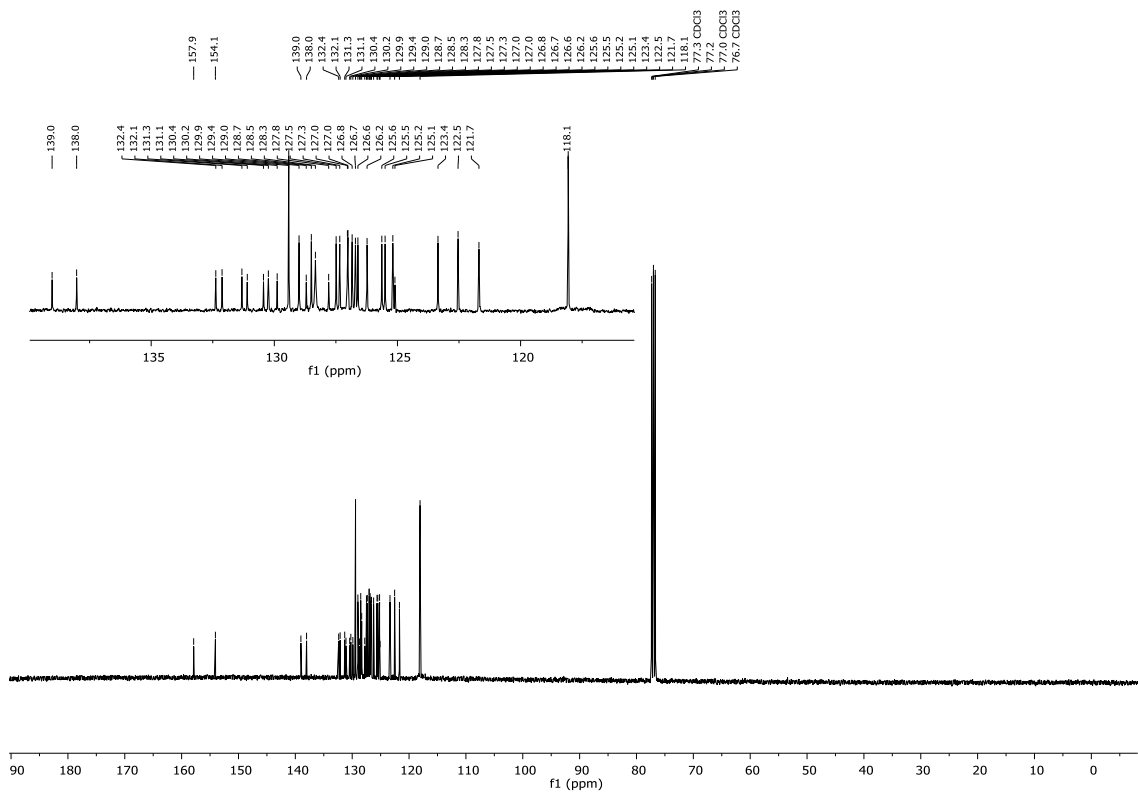
¹³C{H} NMR: (101 MHz, CDCl₃) **163d**



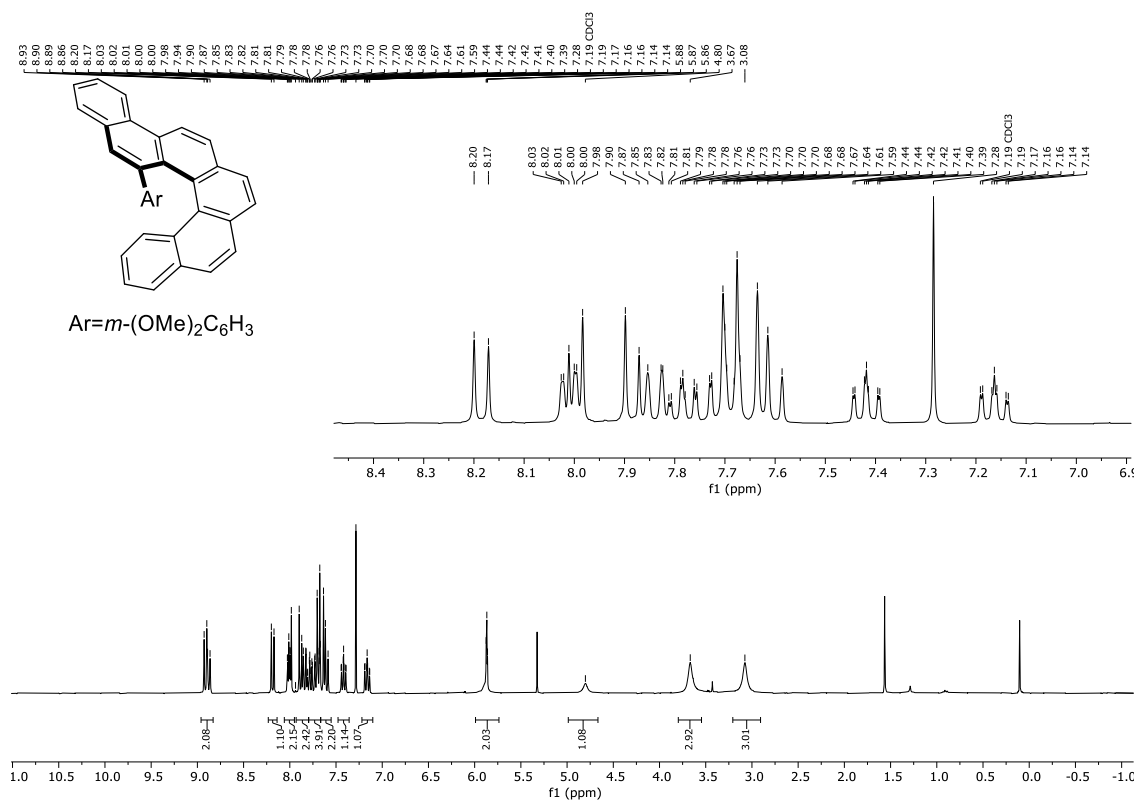
¹H NMR: (400 MHz, CDCl₃) **163e**



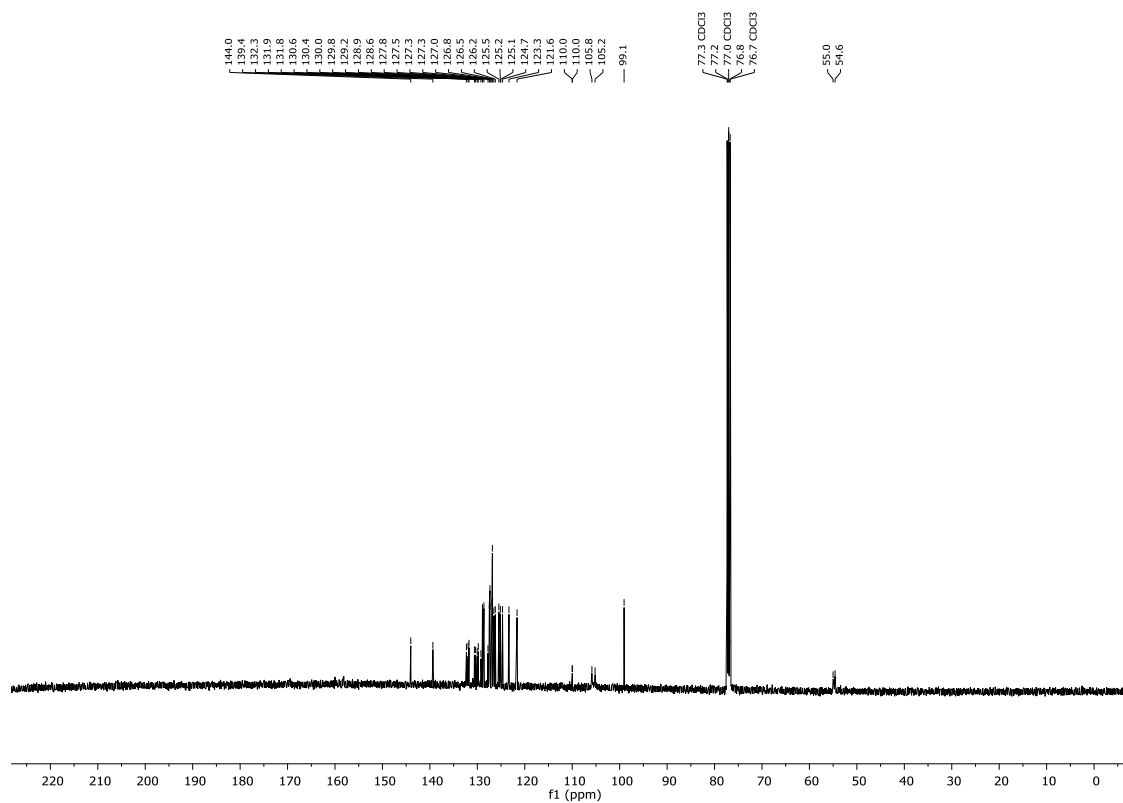
¹³C{H} NMR: (101 MHz, CDCl₃) **163e**



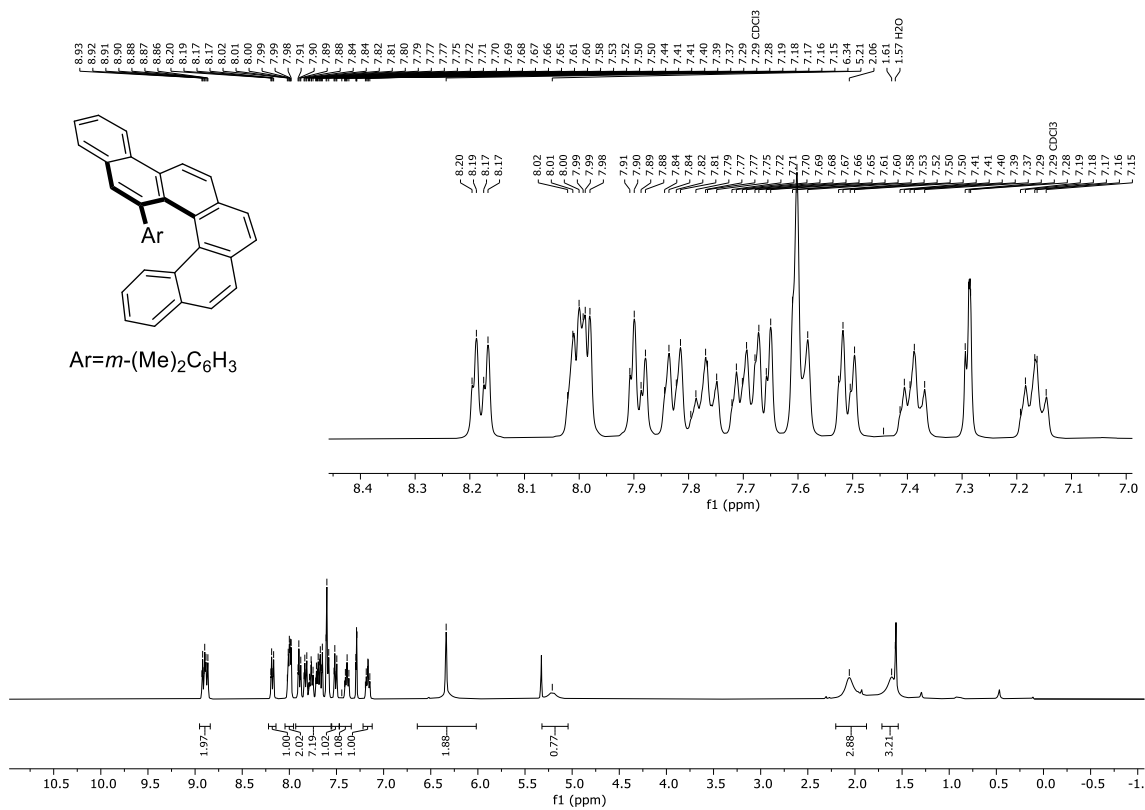
¹H NMR: (400 MHz, CDCl₃) **163f**



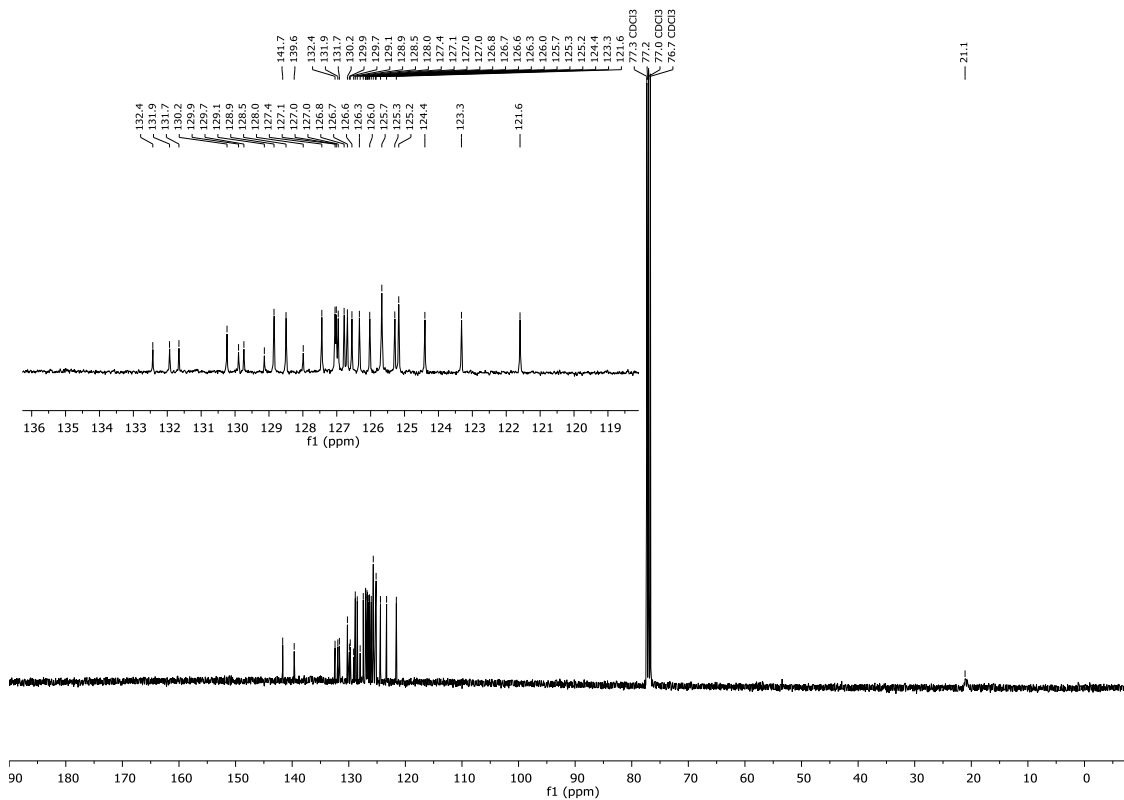
¹³C{H} NMR: (101 MHz, CDCl₃) **163f**



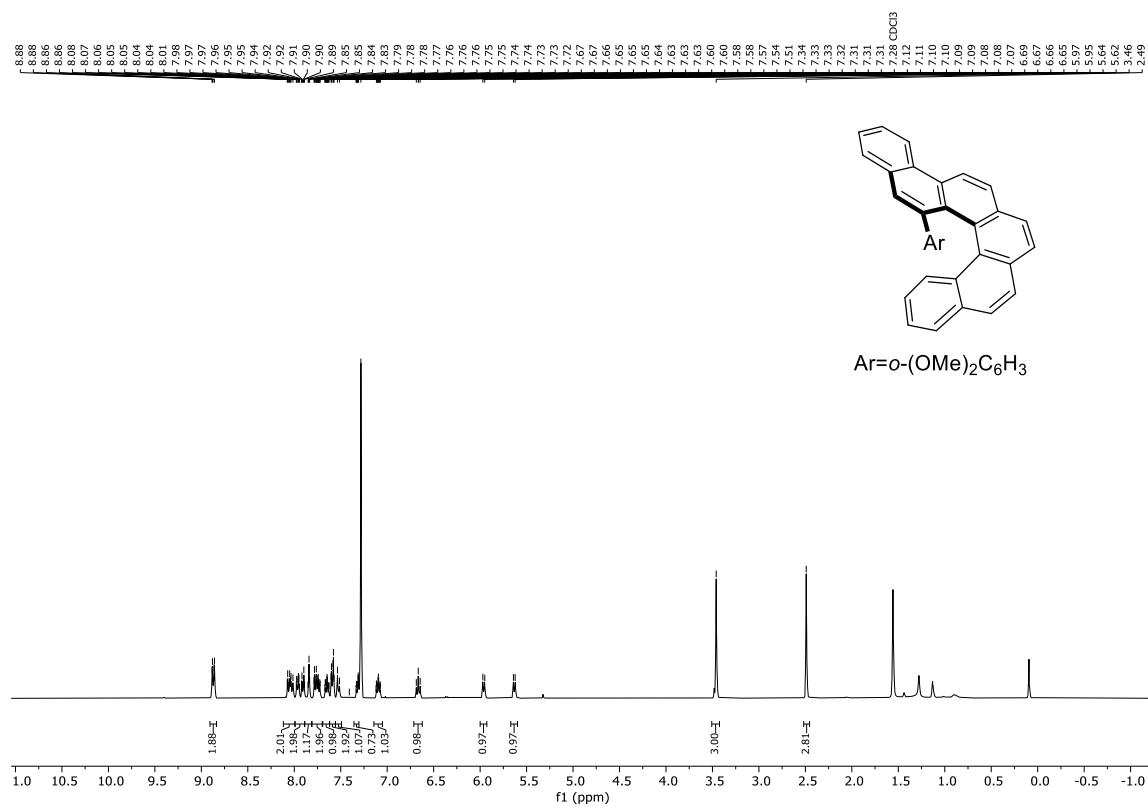
¹H NMR: (400 MHz, CDCl₃) **163g**



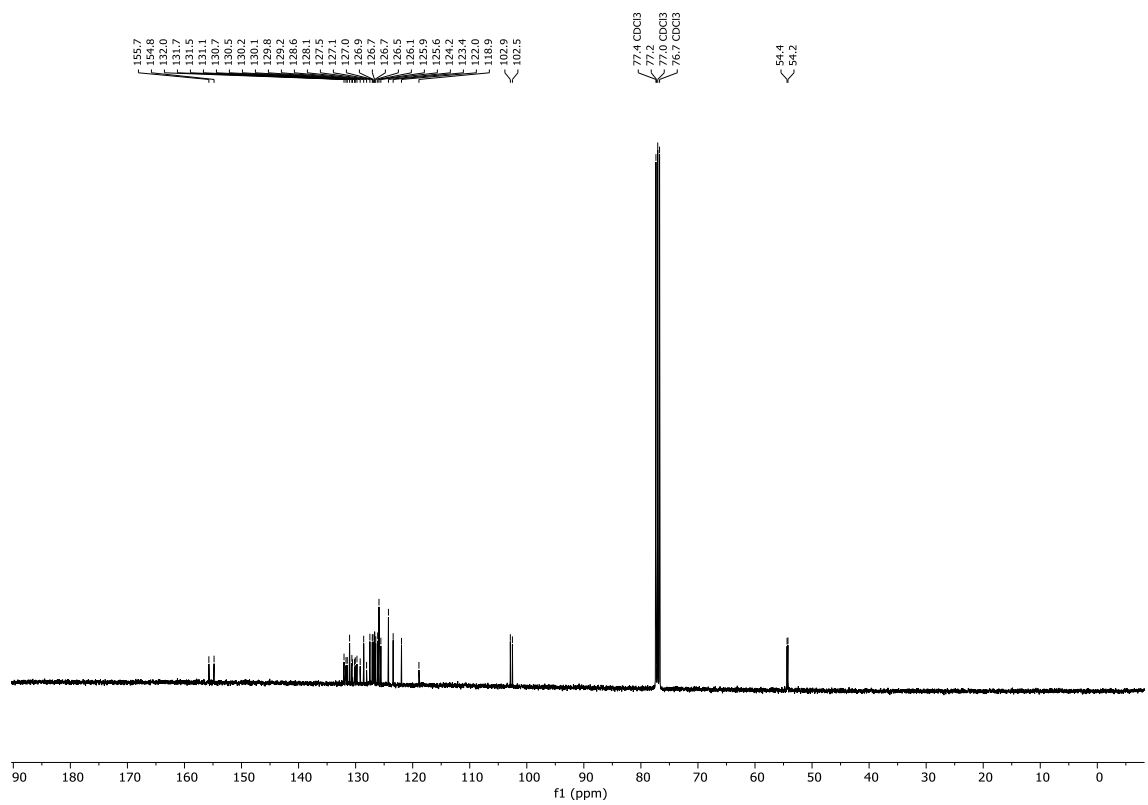
¹³C{H} NMR: (101 MHz, CDCl₃) **163g**



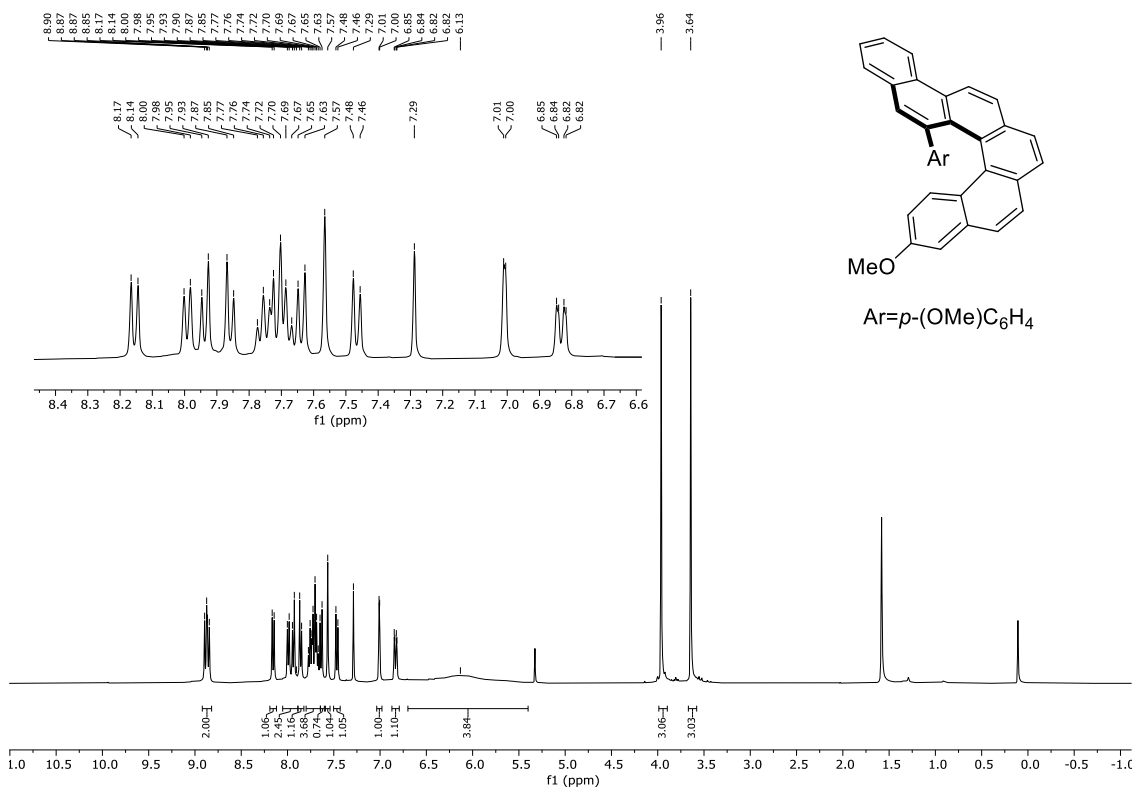
¹H NMR: (400 MHz, CDCl₃) **163h**



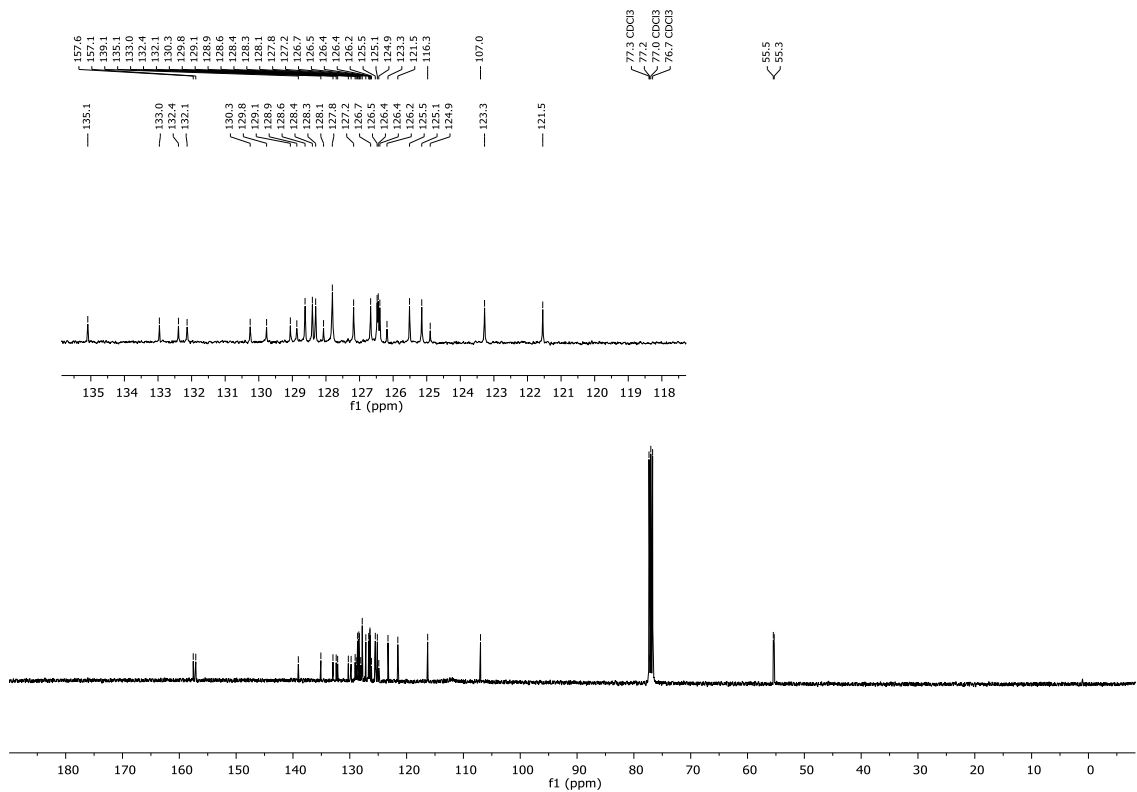
¹³C{H} NMR: (101 MHz, CDCl₃) **163h**



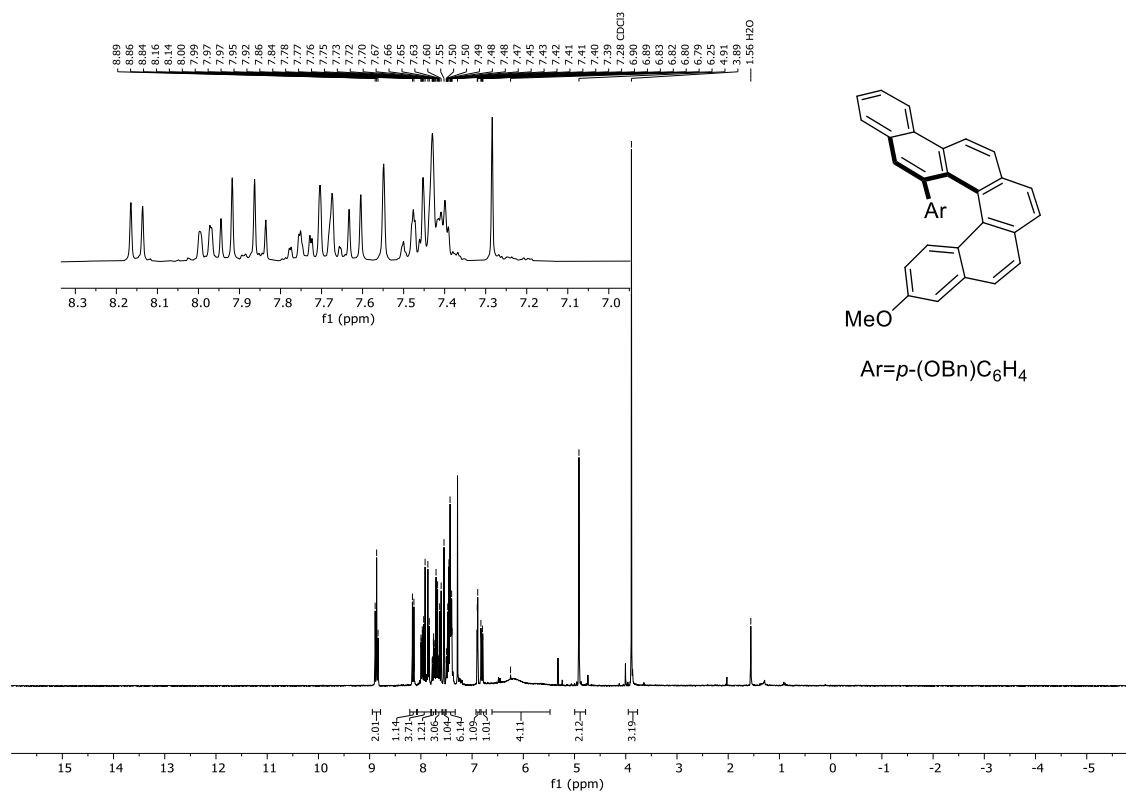
¹H NMR: (400 MHz, CDCl₃) **163k**



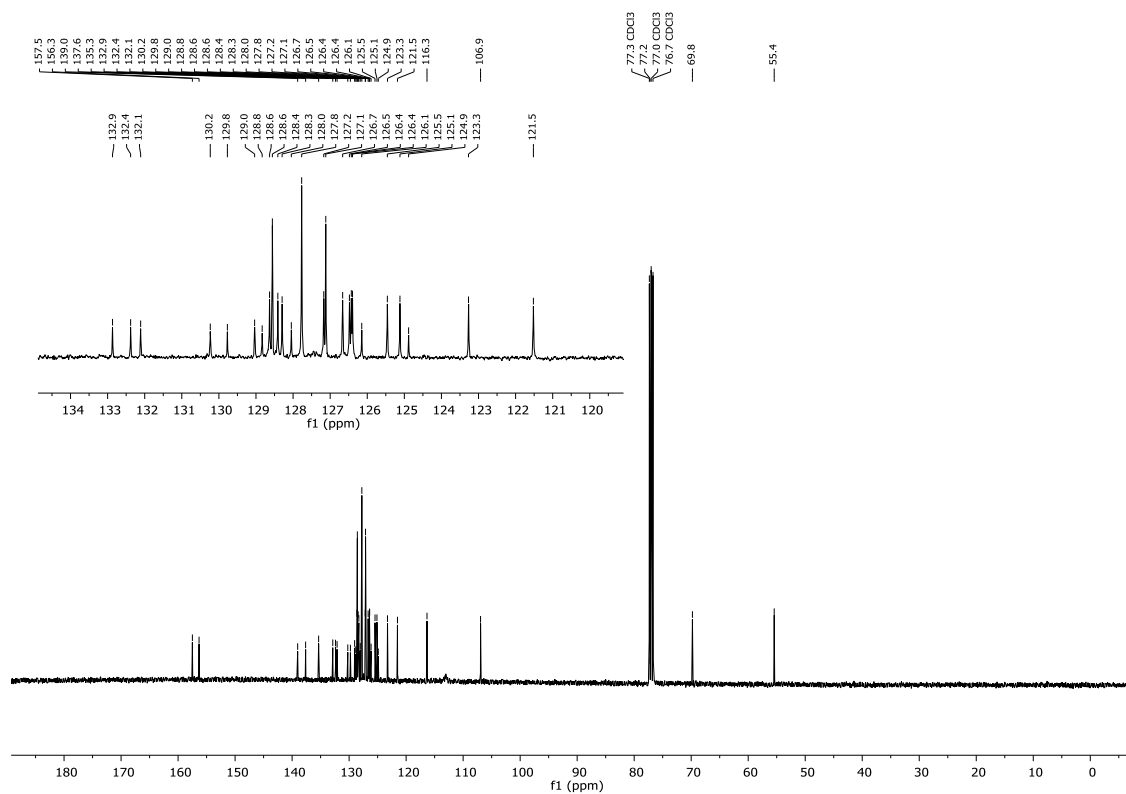
¹³C{H} NMR: (101 MHz, CDCl₃) **163k**



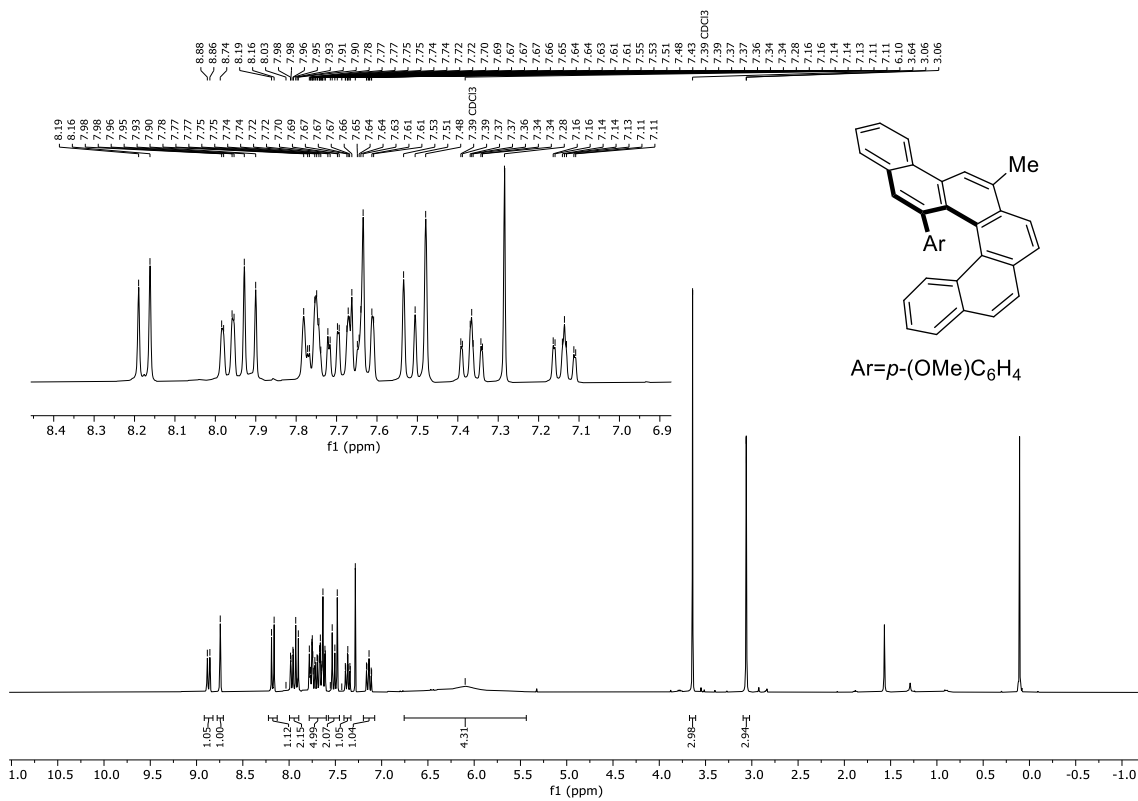
¹H NMR: (400 MHz, CDCl₃) **163m**



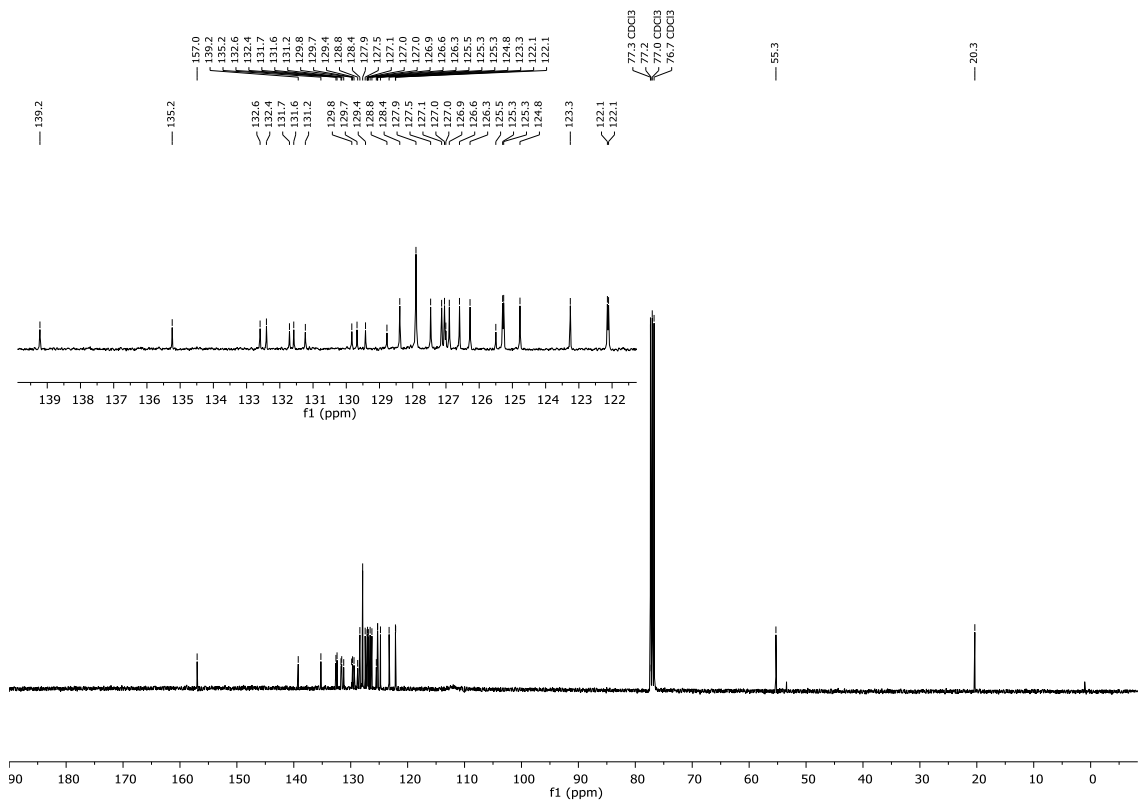
¹³C{H} NMR: (101 MHz, CDCl₃) **163m**



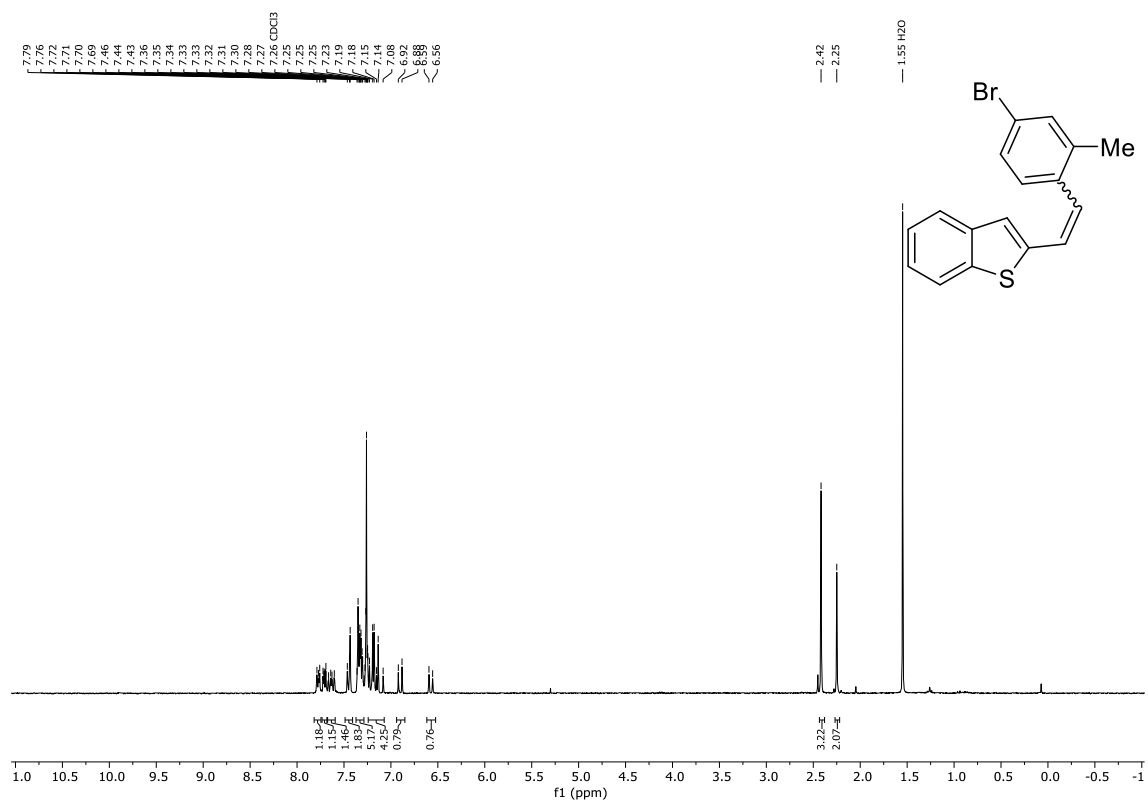
¹H NMR: (400 MHz, CDCl₃) **163n**



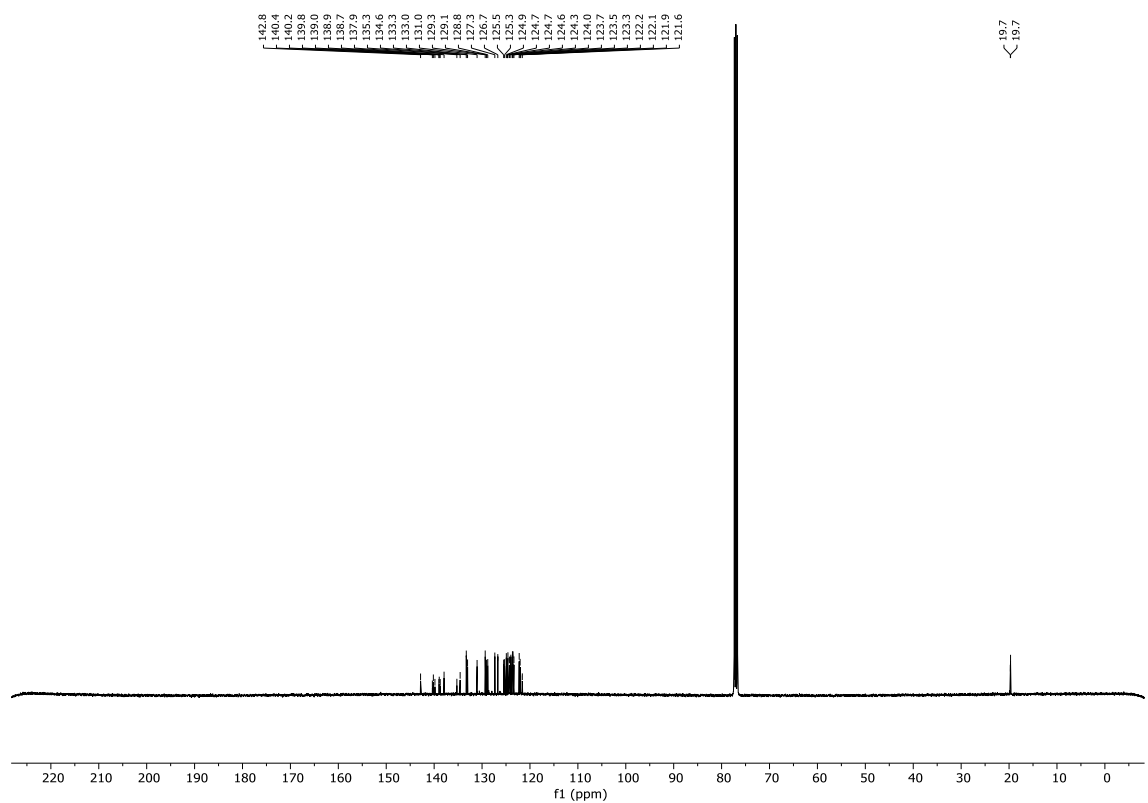
¹³C{¹H} NMR: (101 MHz, CDCl₃) **163n**



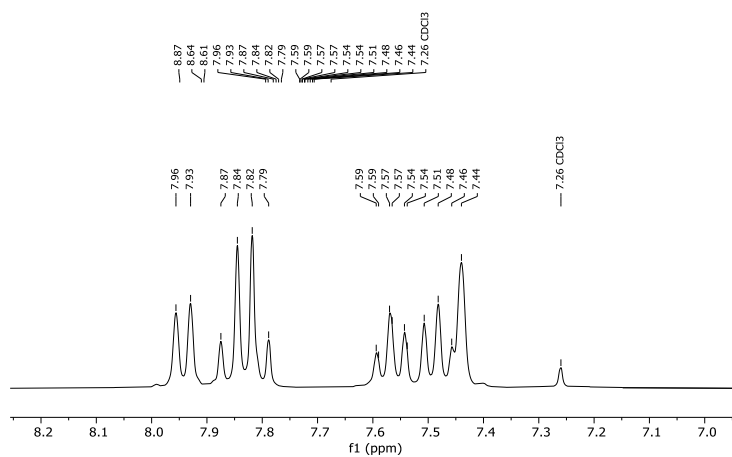
¹H NMR: (300 MHz, CDCl₃) **196b**



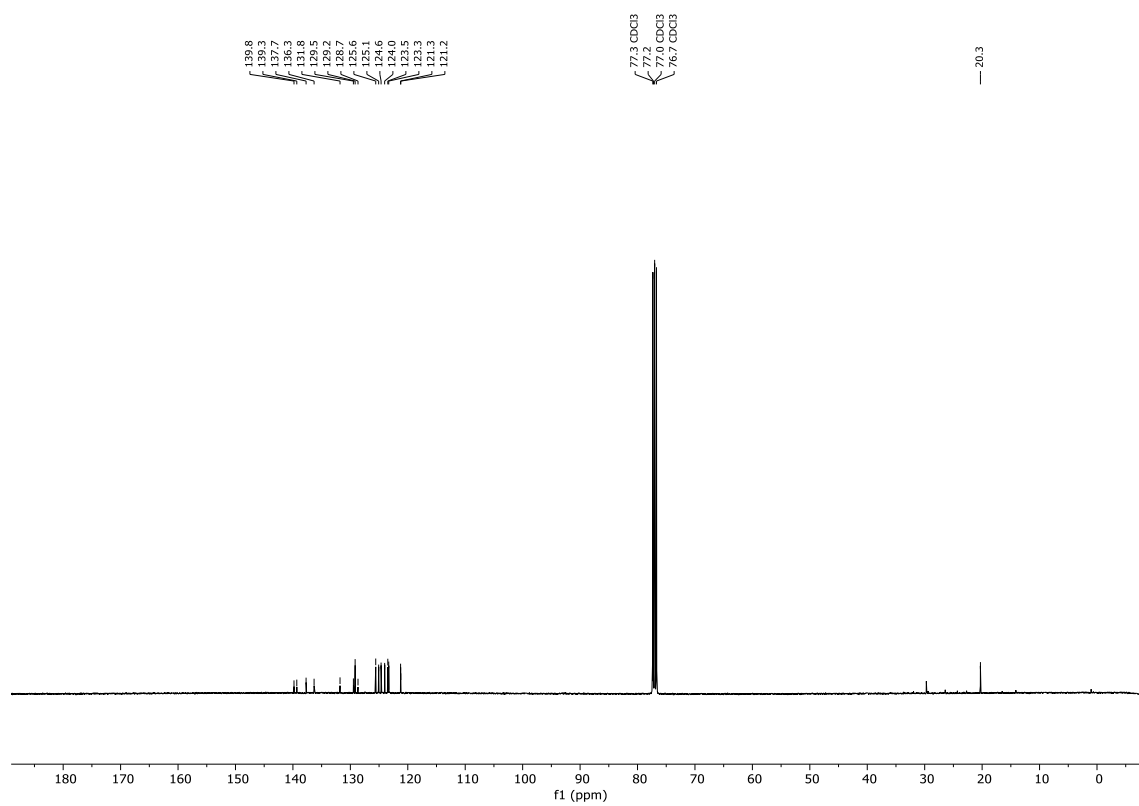
¹³C{H} NMR: (101 MHz, CDCl₃) **196b**



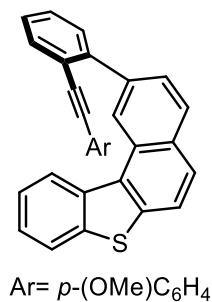
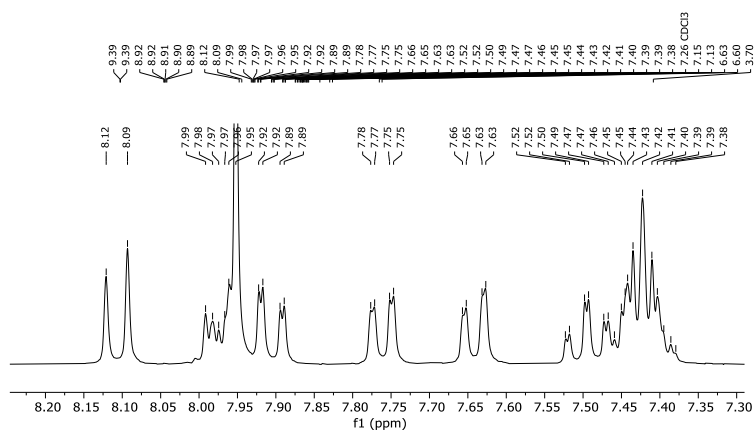
^1H NMR: (300 MHz, CDCl_3) **197b**



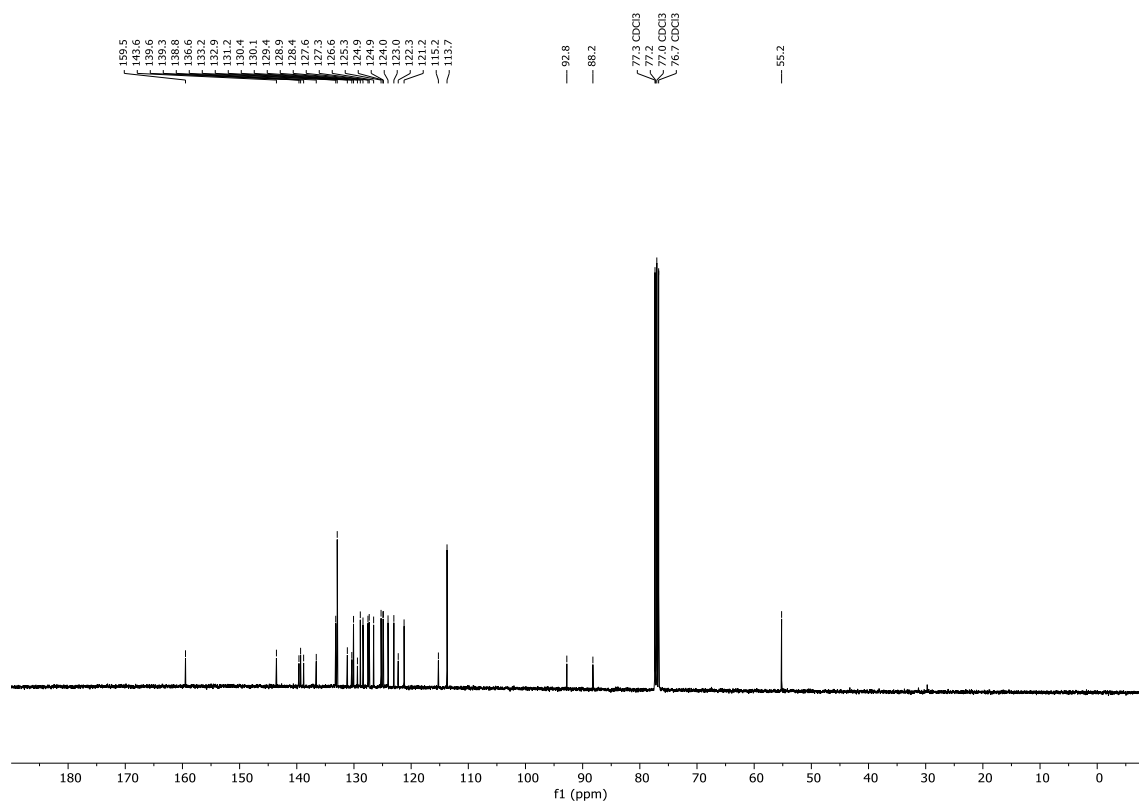
$^{13}\text{C}\{\text{H}\}$ NMR: (101 MHz, CDCl_3) **197b**



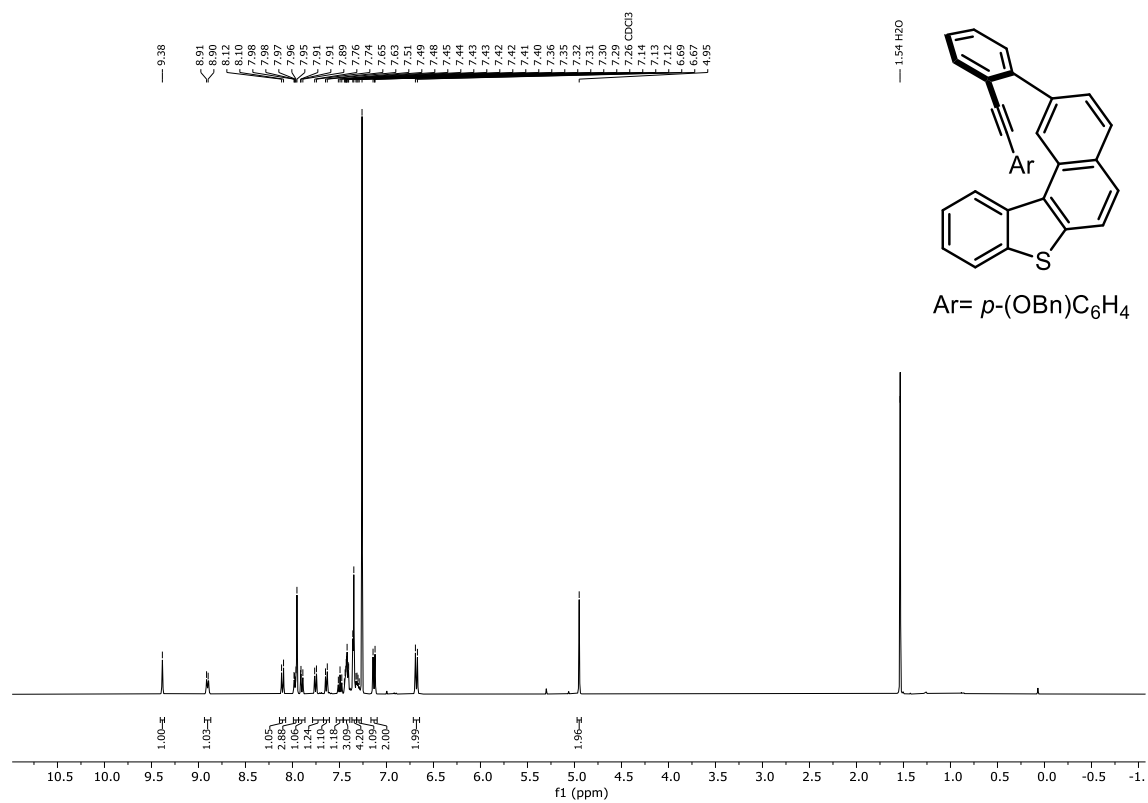
^1H NMR: (300 MHz, CDCl_3) **164a**



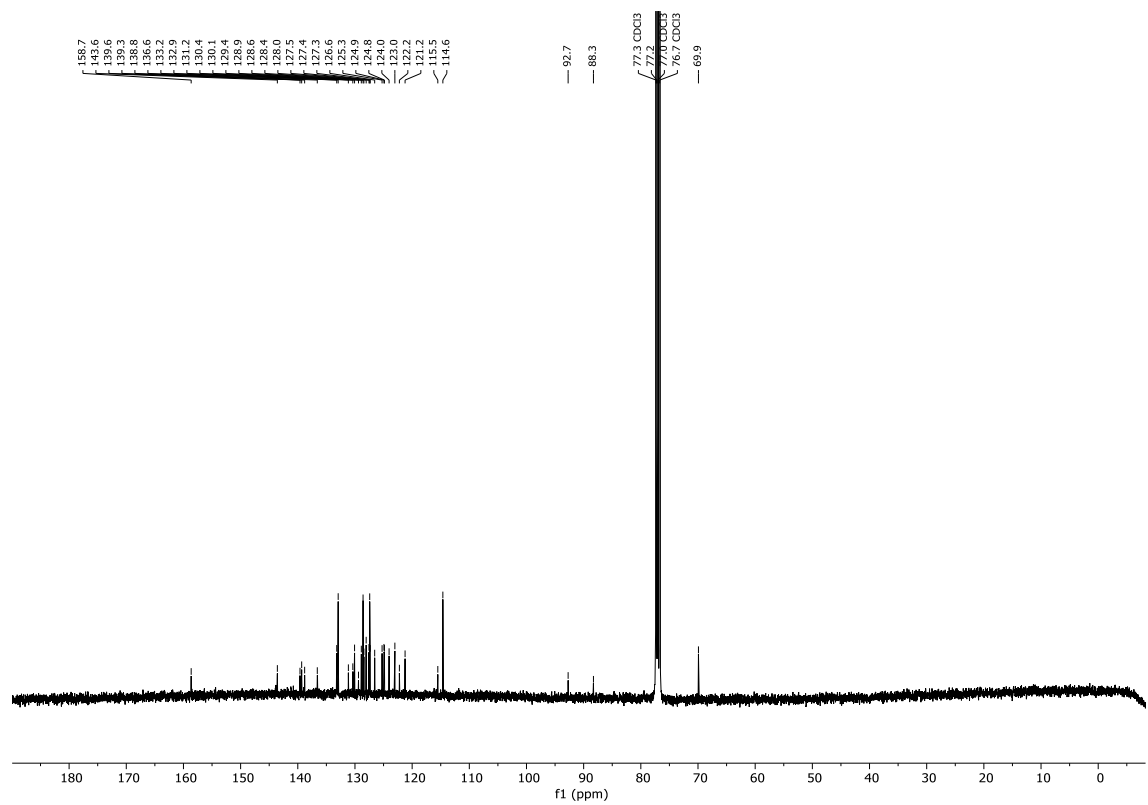
$^{13}\text{C}\{^1\text{H}\}$ NMR: (101 MHz, CDCl_3) **164a**



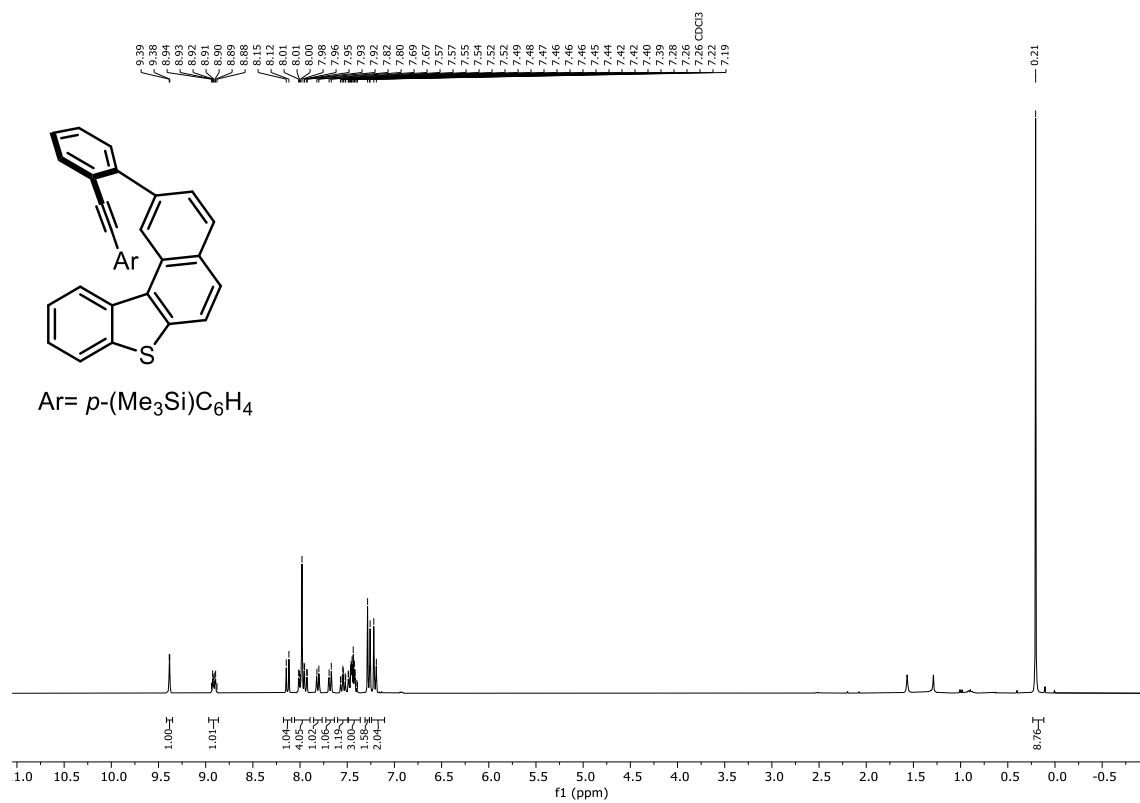
¹H NMR: (400 MHz, CDCl₃) **164c**



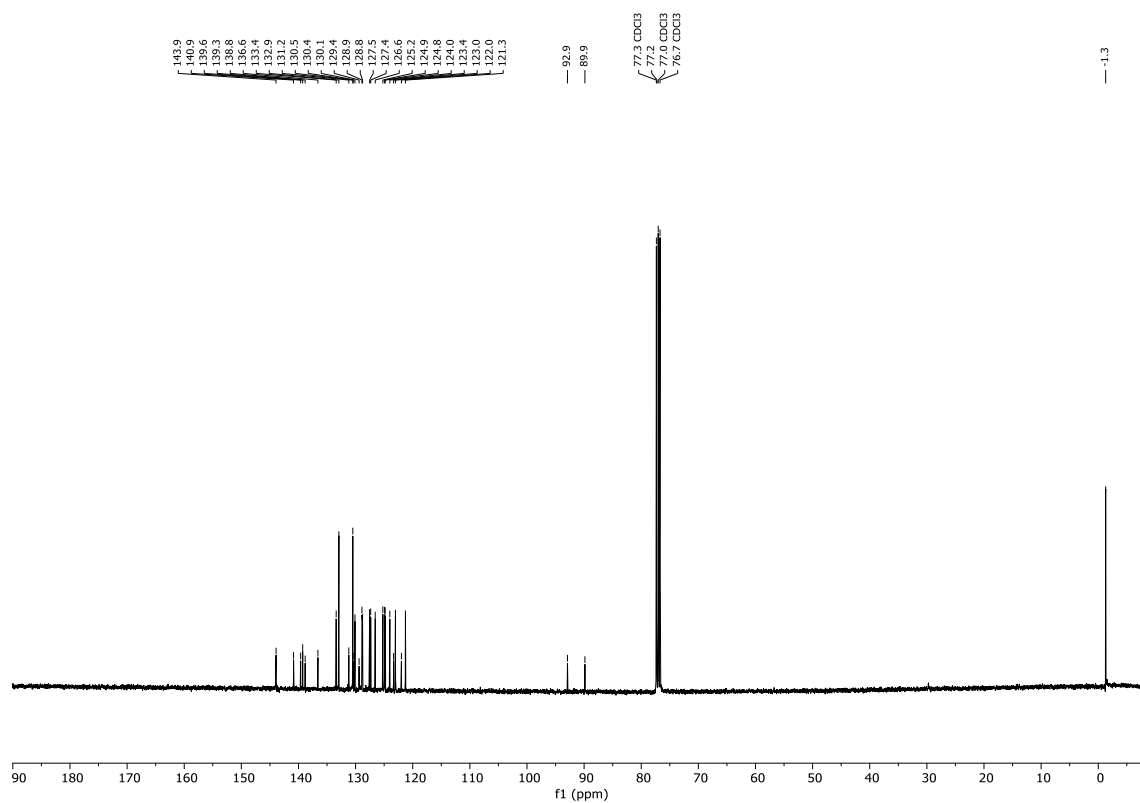
¹³C{H} NMR: (101 MHz, CDCl₃) **164c**



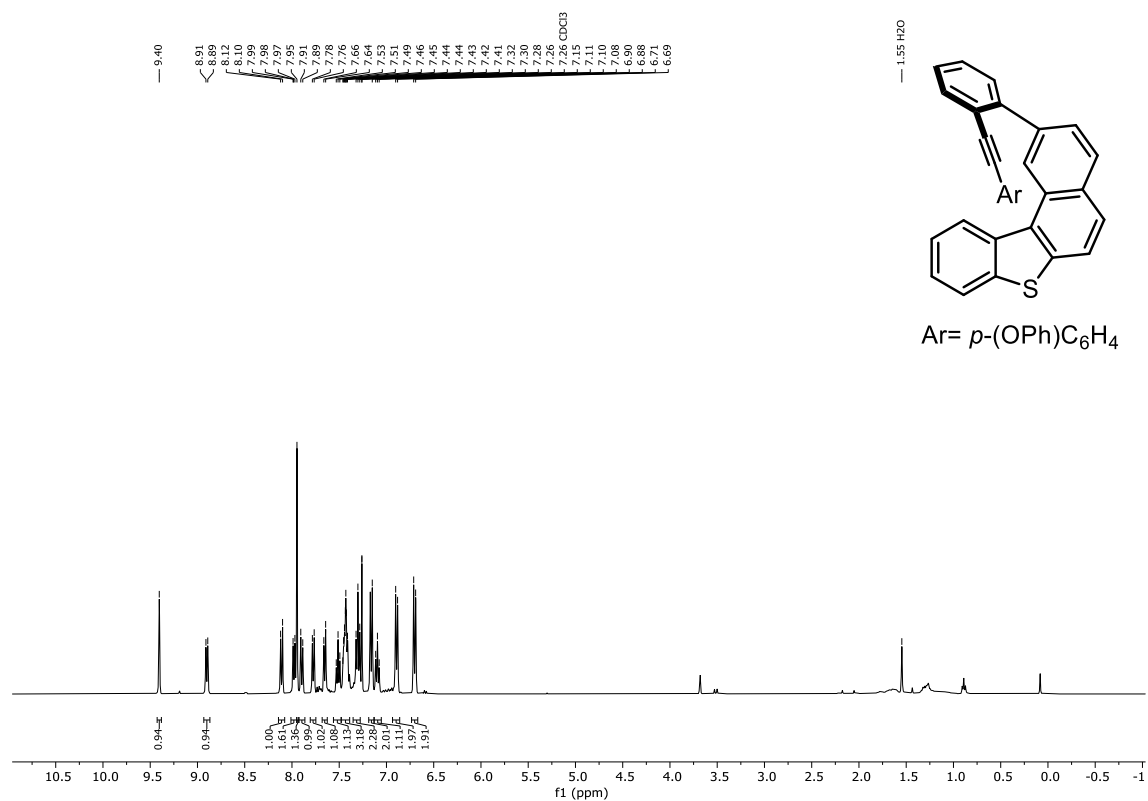
¹H NMR: (400 MHz, CDCl₃) **164d**



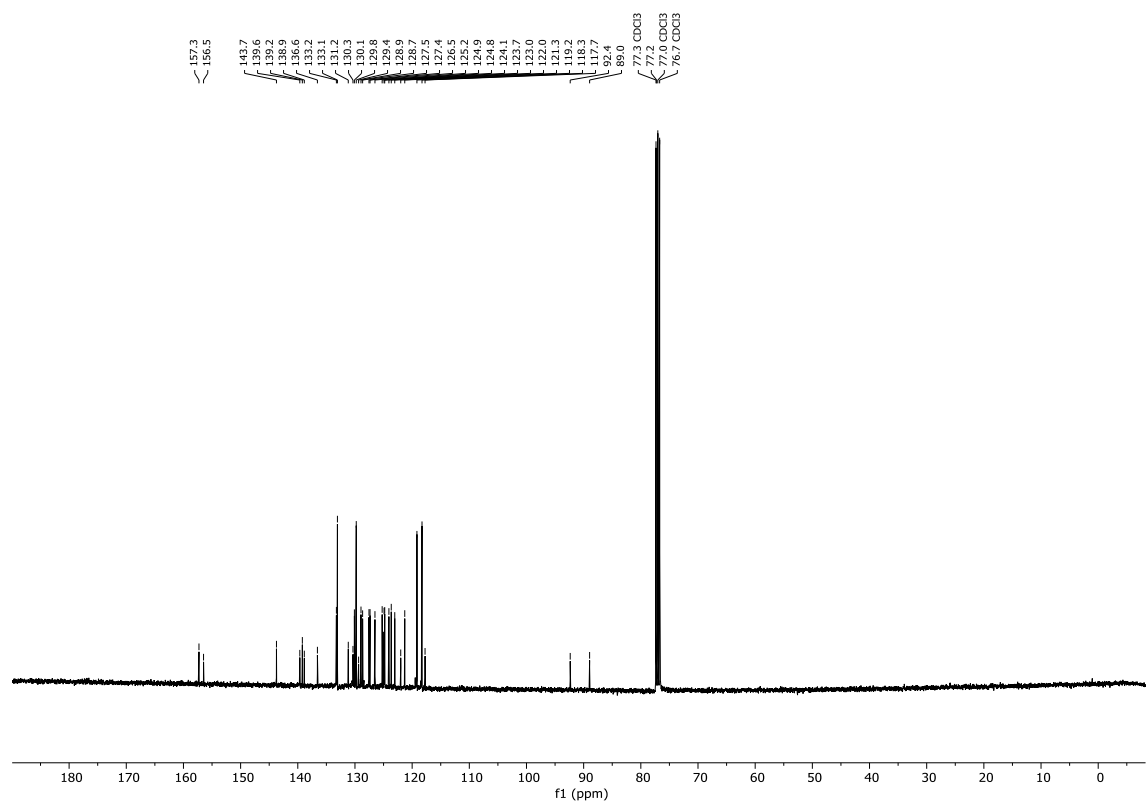
¹³C{¹H} NMR: (101 MHz, CDCl₃) **164d**



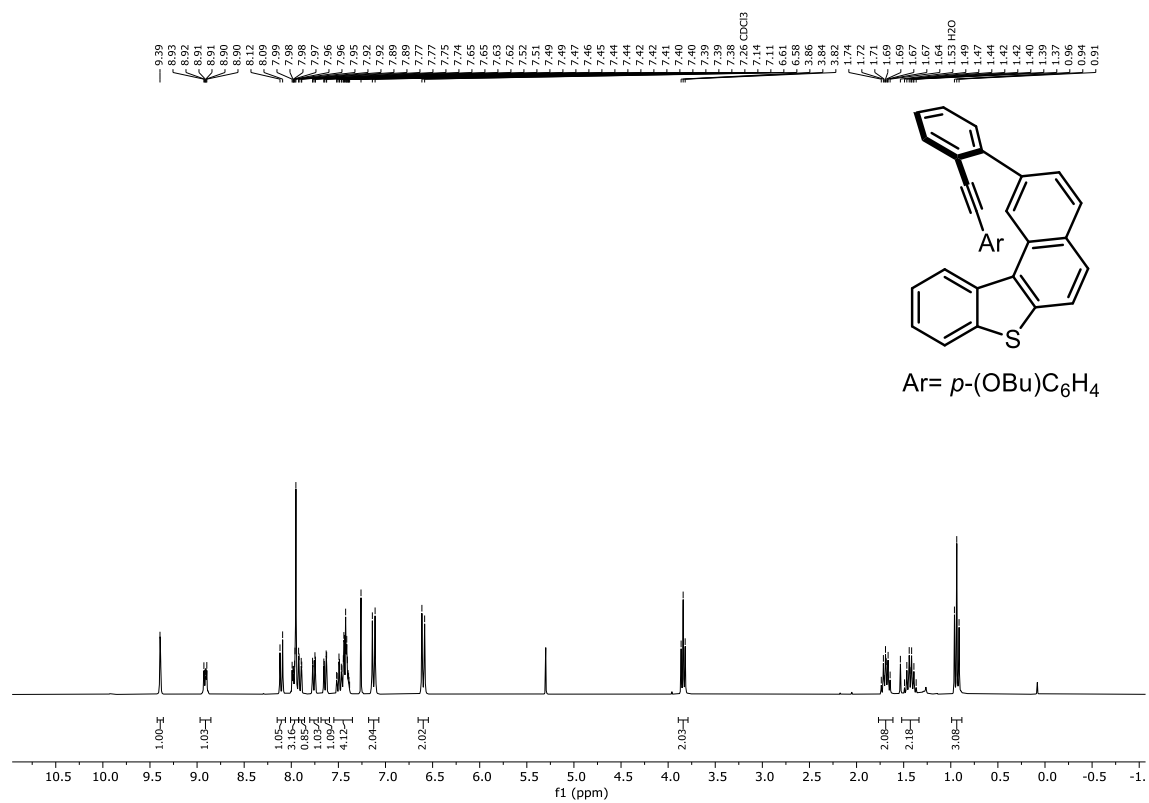
^1H NMR: (400 MHz, CDCl_3) **164e**



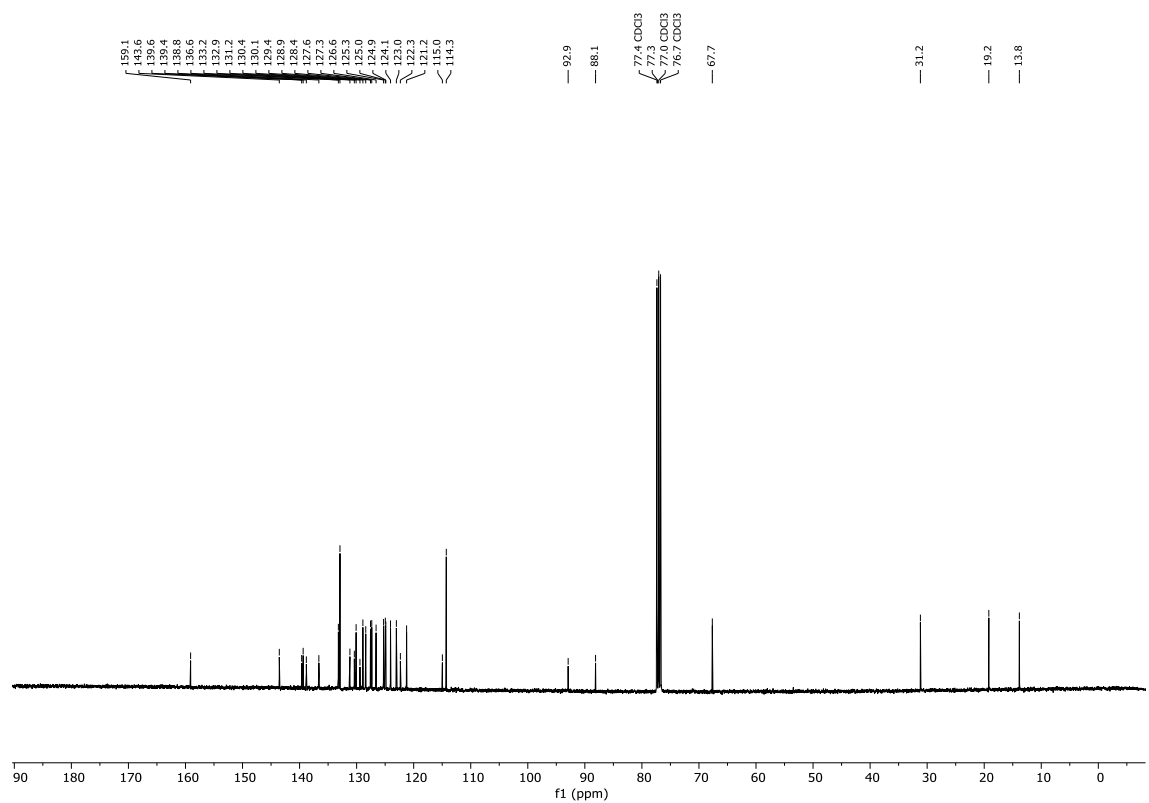
$^{13}\text{C}\{^1\text{H}\}$ NMR: (101 MHz, CDCl_3) **164e**



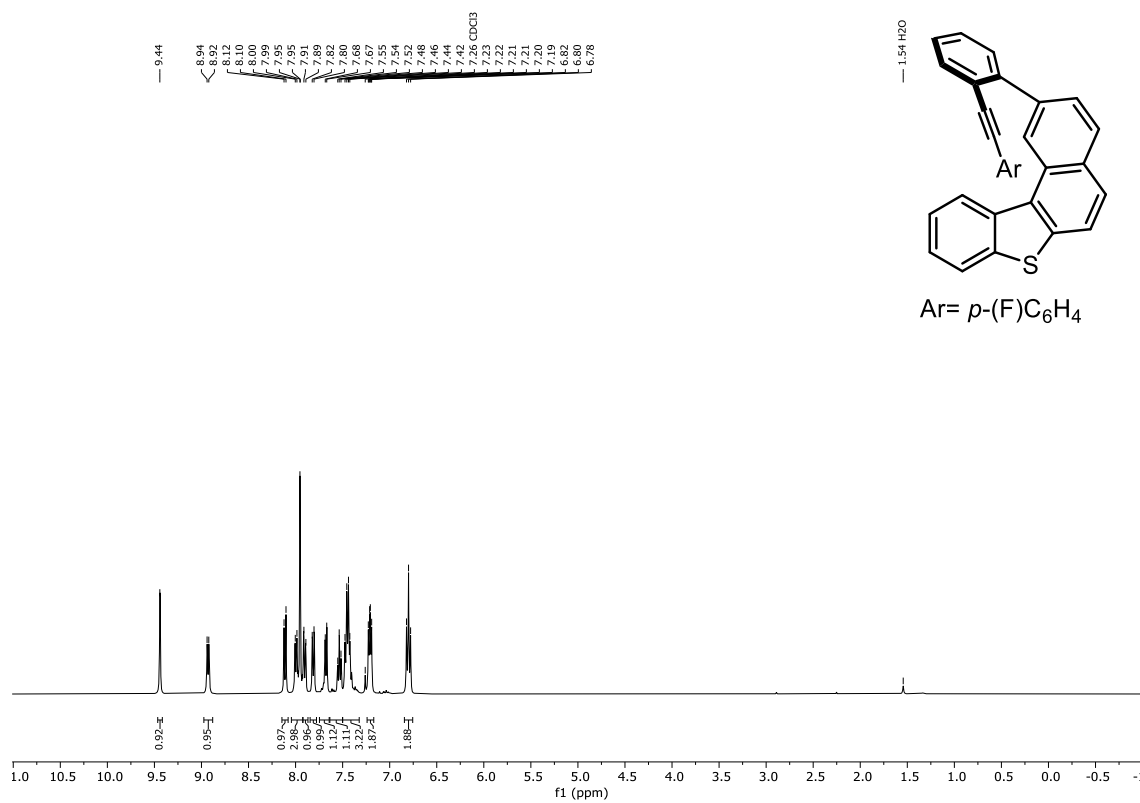
^1H NMR: (400 MHz, CDCl_3) **164f**



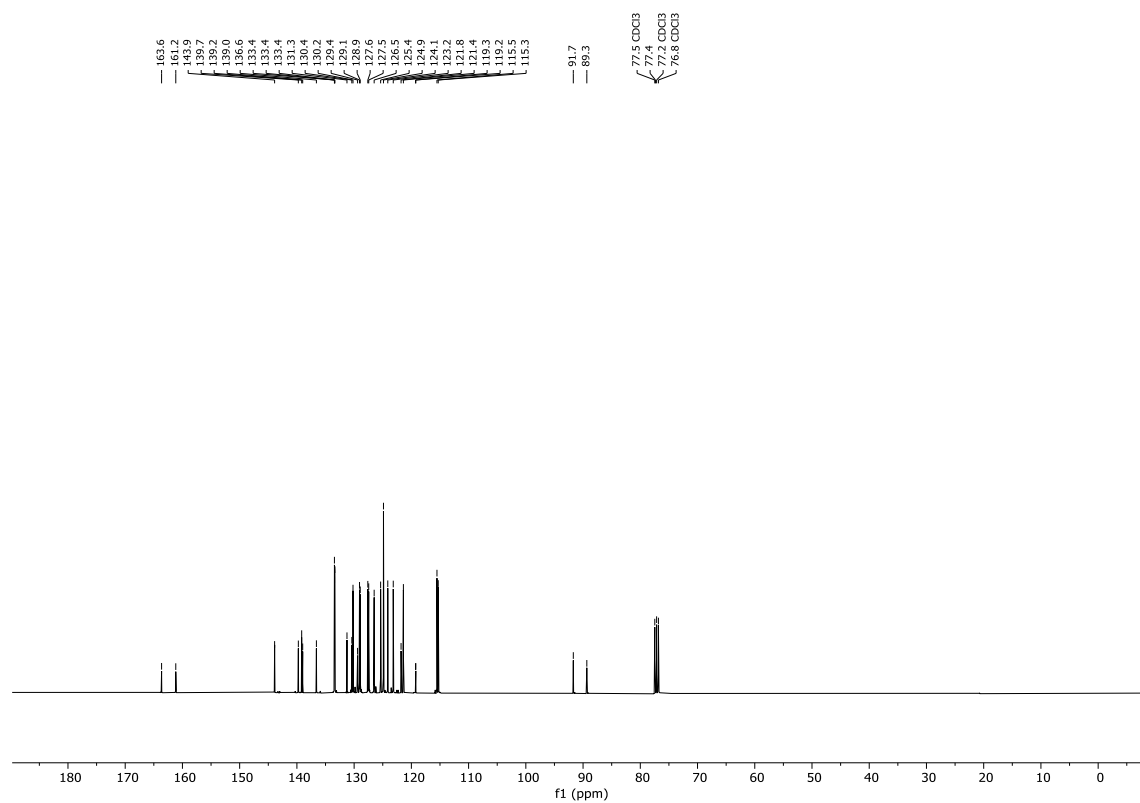
$^{13}\text{C}\{^1\text{H}\}$ NMR: (101 MHz, CDCl_3) **164f**



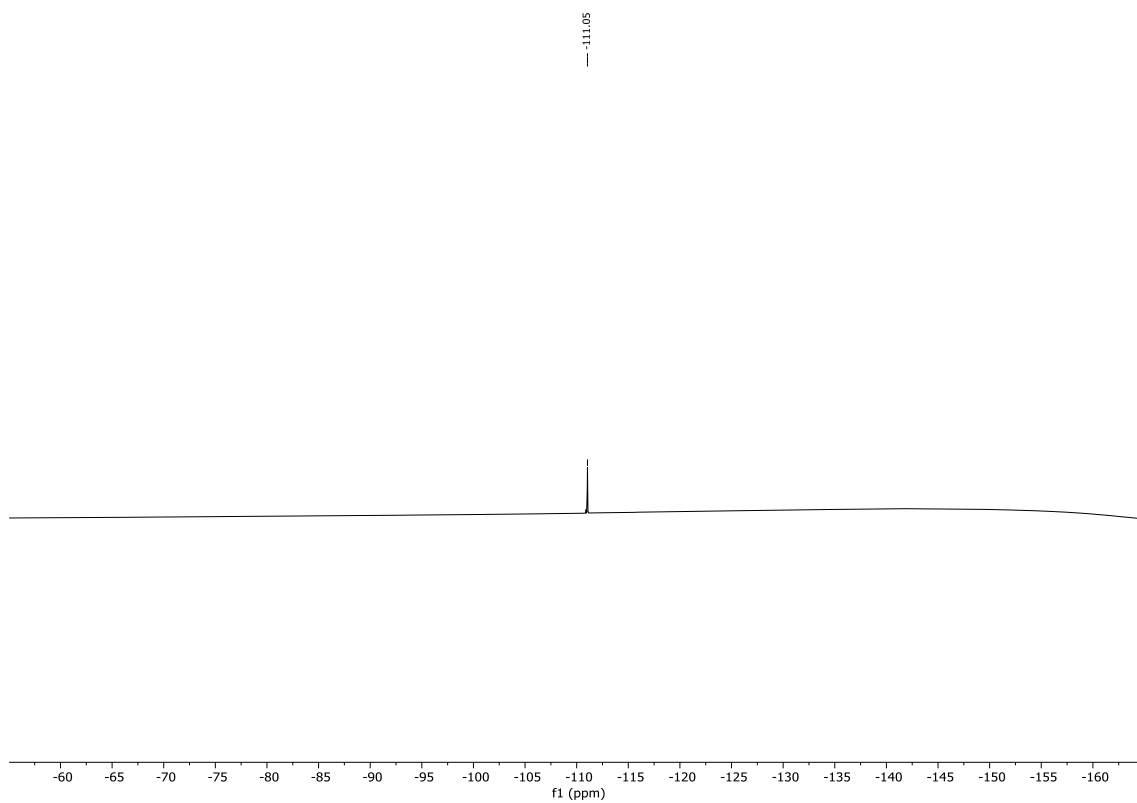
^1H NMR: (400 MHz, CDCl_3) **164g**



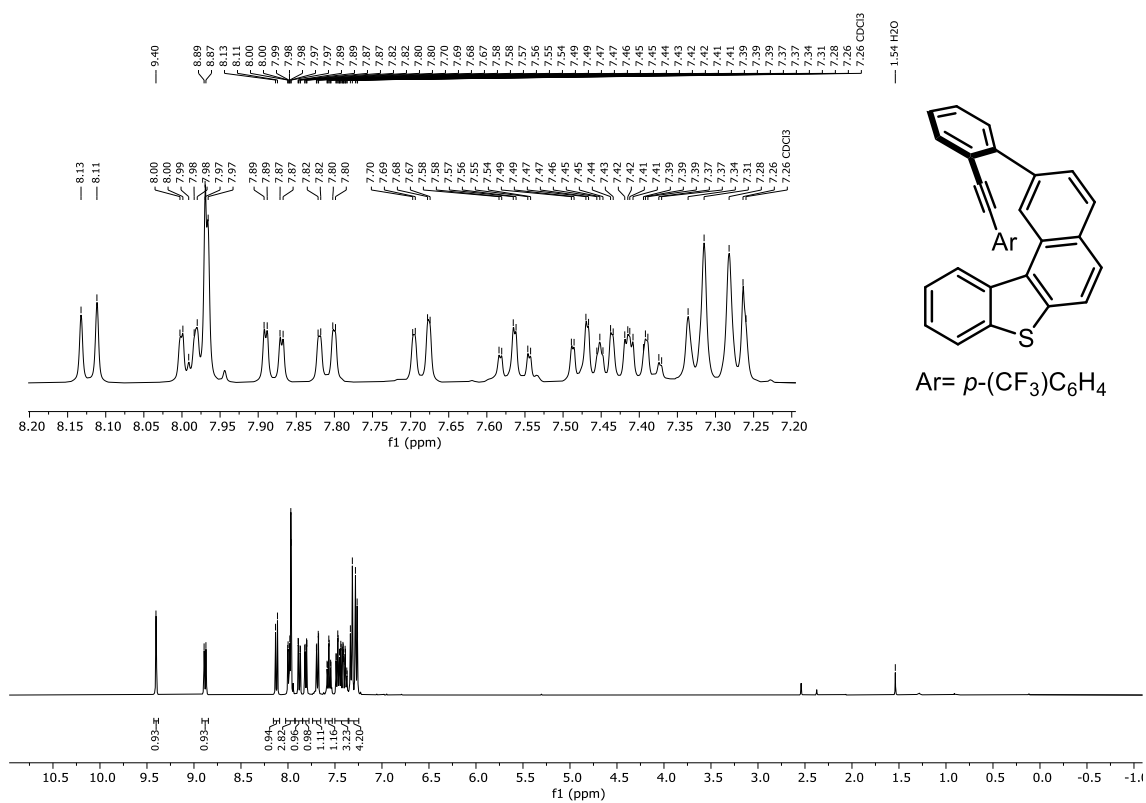
$^{13}\text{C}\{^1\text{H}\}$ NMR: (101 MHz, CDCl_3) **164g**



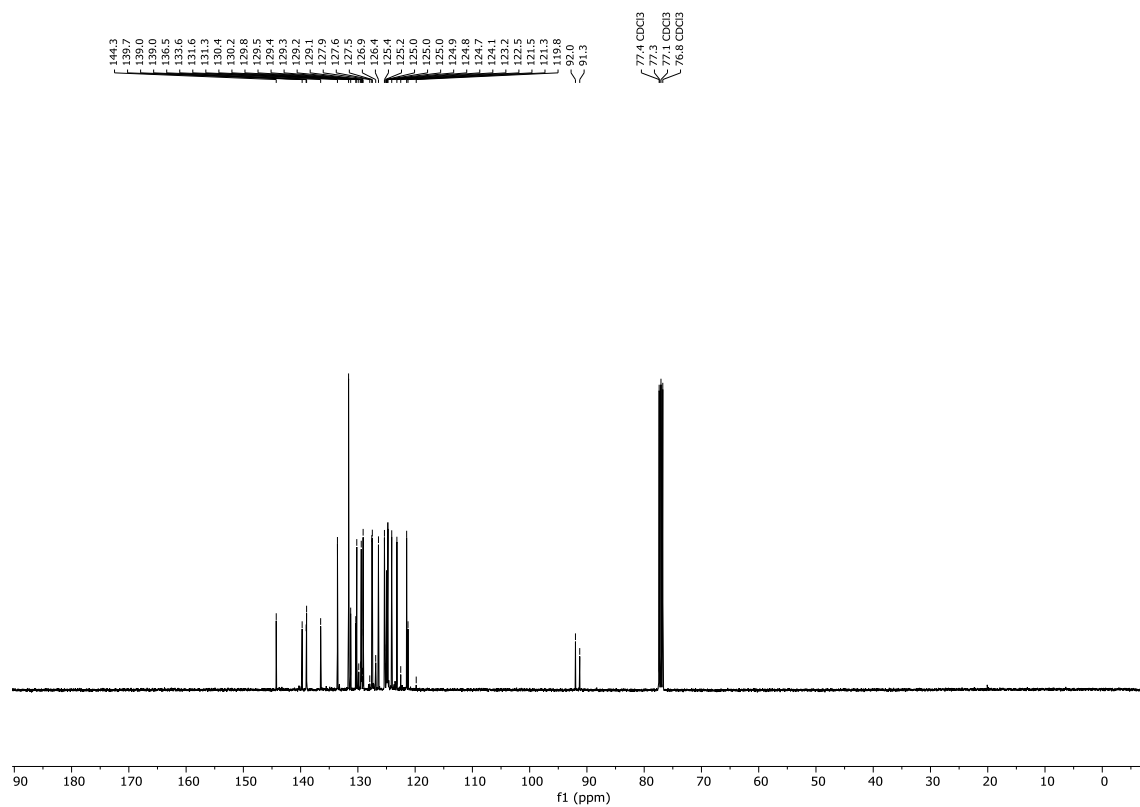
^{19}F NMR: (377 MHz, CDCl_3) **164g**



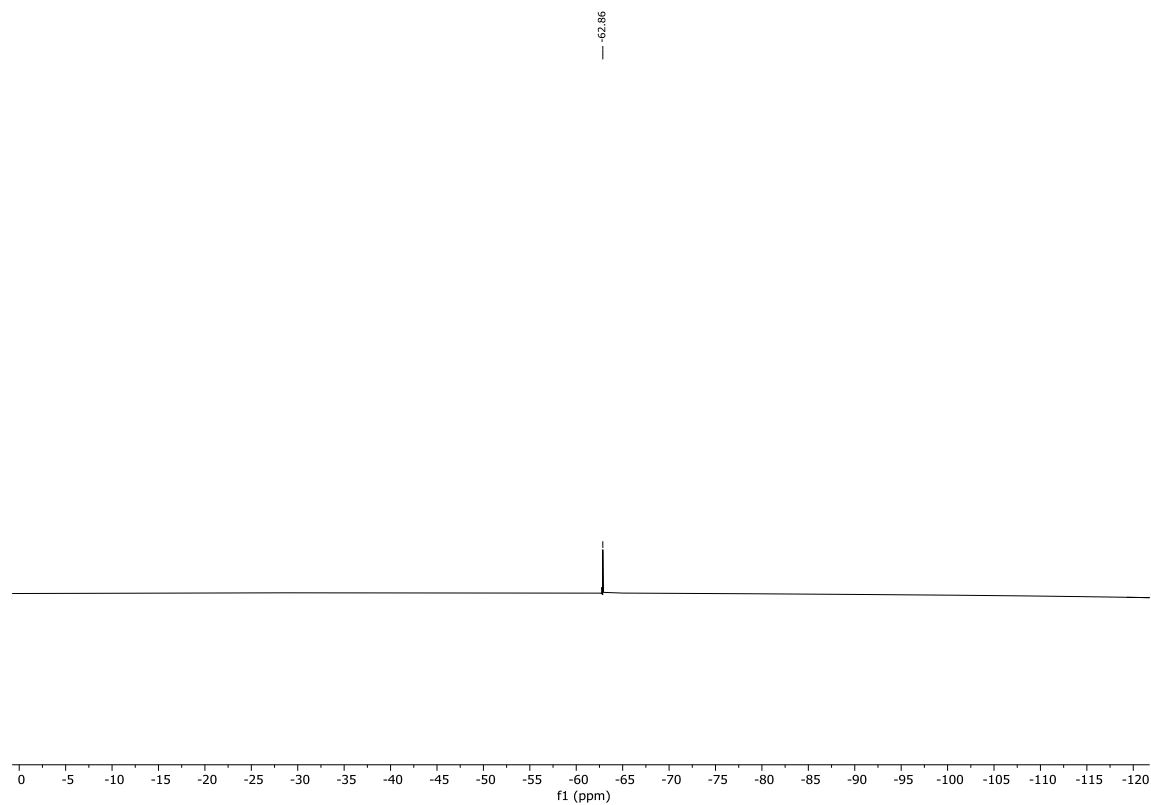
^1H NMR: (400 MHz, CDCl_3) **164h**



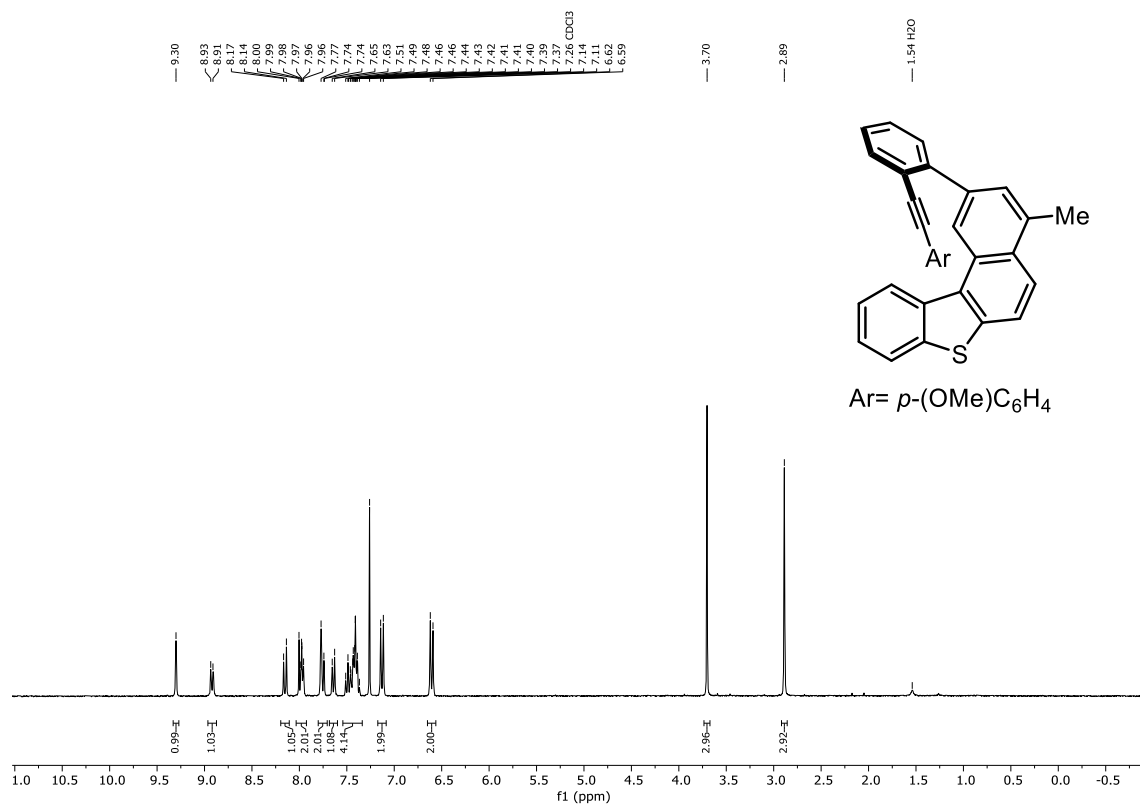
$^{13}\text{C}\{\text{H}\}$ NMR: (101 MHz, CDCl_3) **164h**



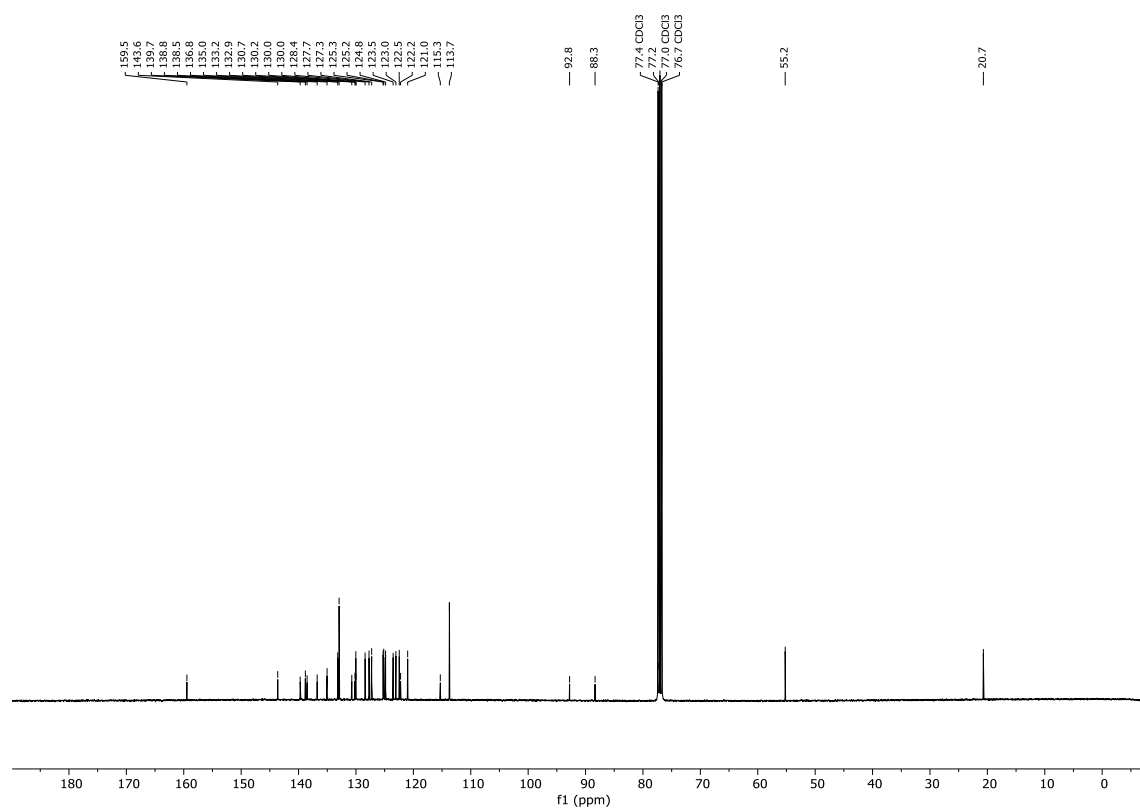
^{19}F NMR: (377 MHz, CDCl_3) **164h**



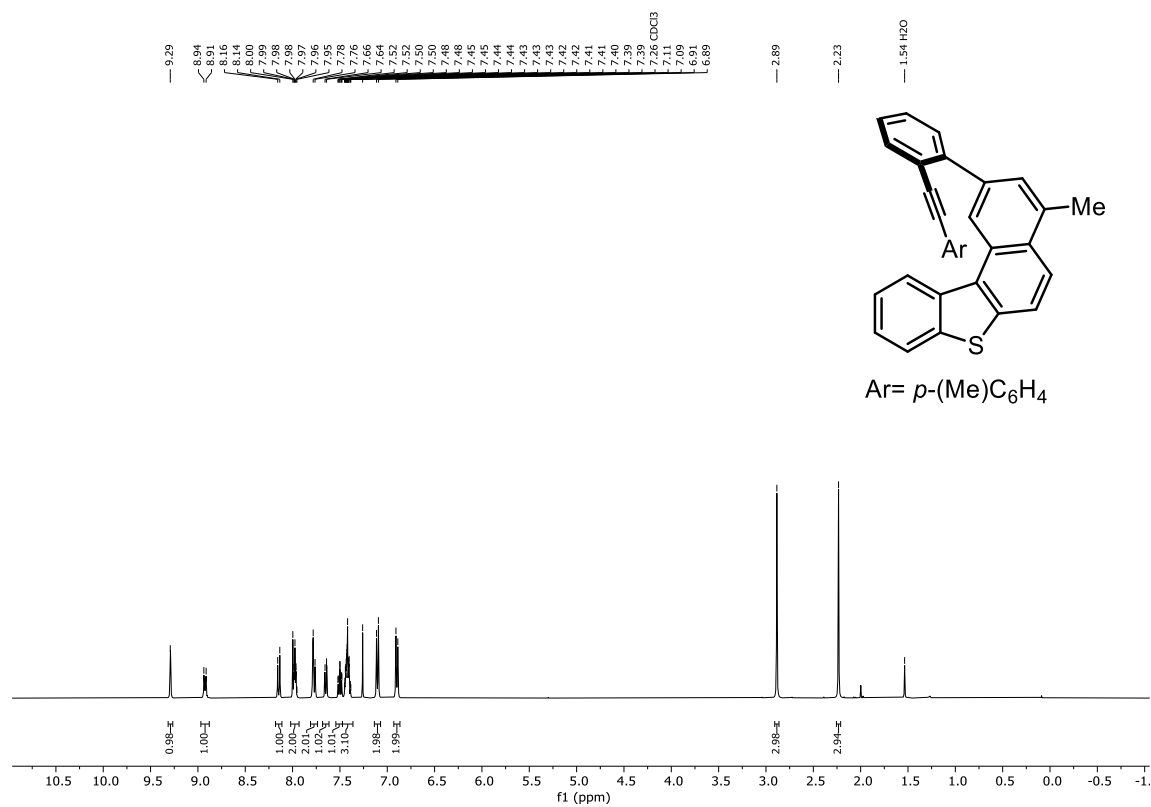
^1H NMR: (400 MHz, CDCl_3) **164i**



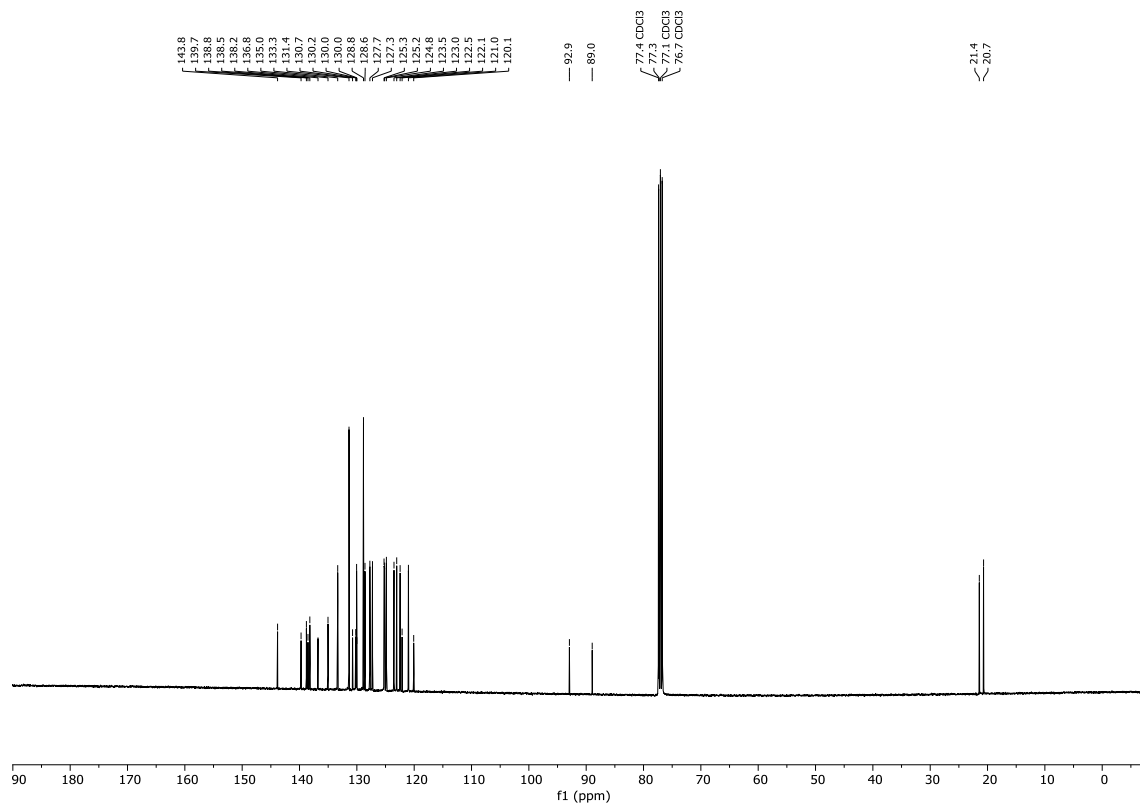
$^{13}\text{C}\{^1\text{H}\}$ NMR: (101 MHz, CDCl_3) **164i**



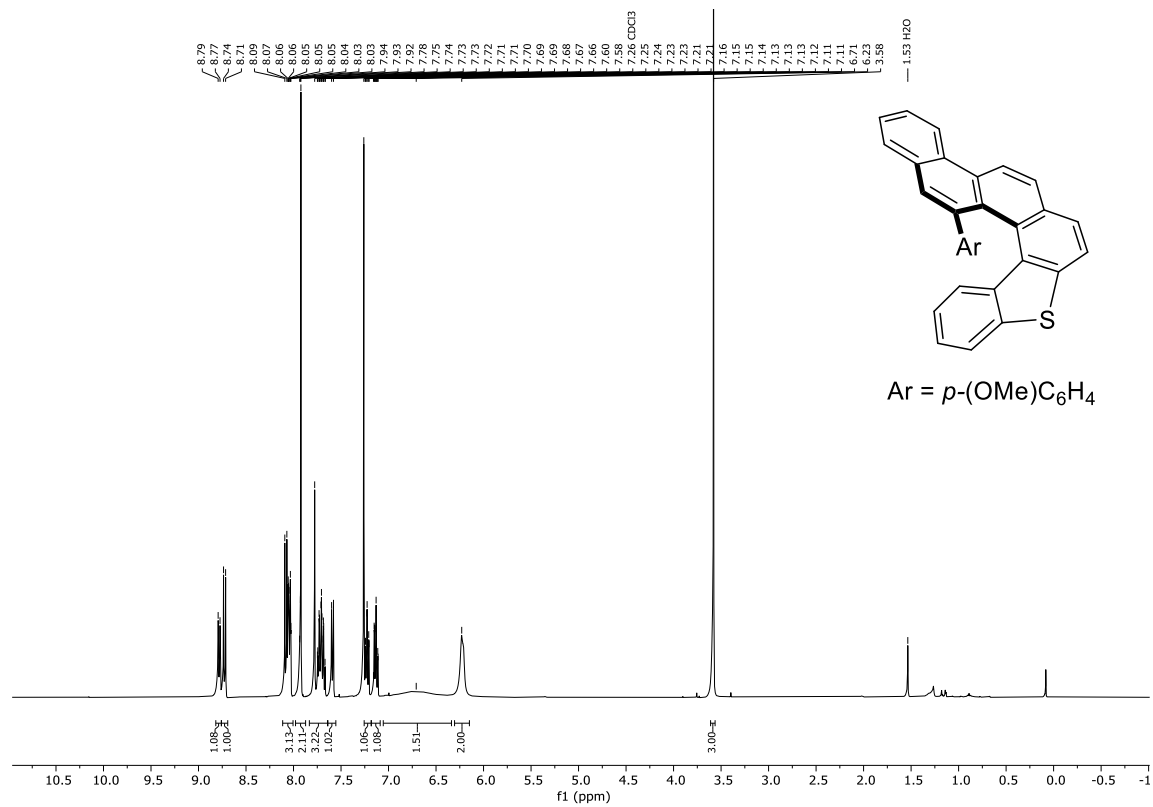
^1H NMR: (400 MHz, CDCl_3) **164j**



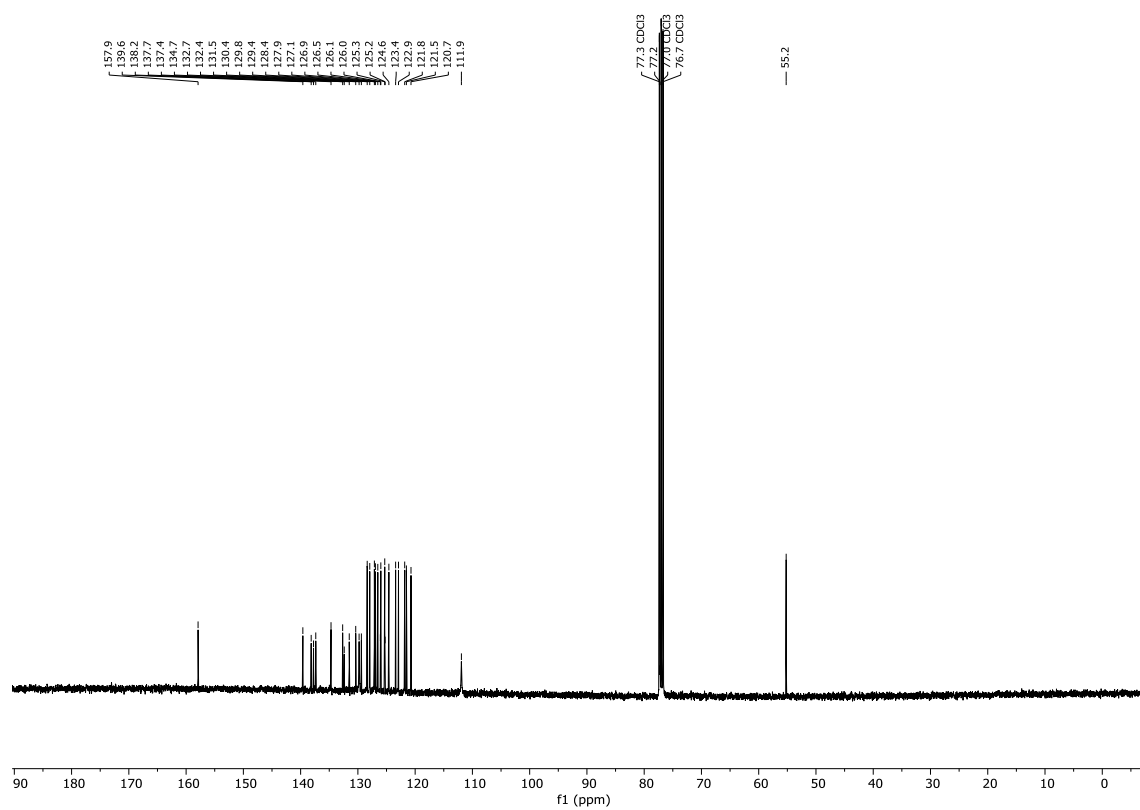
$^{13}\text{C}\{^1\text{H}\}$ NMR: (101 MHz, CDCl_3) **164j**



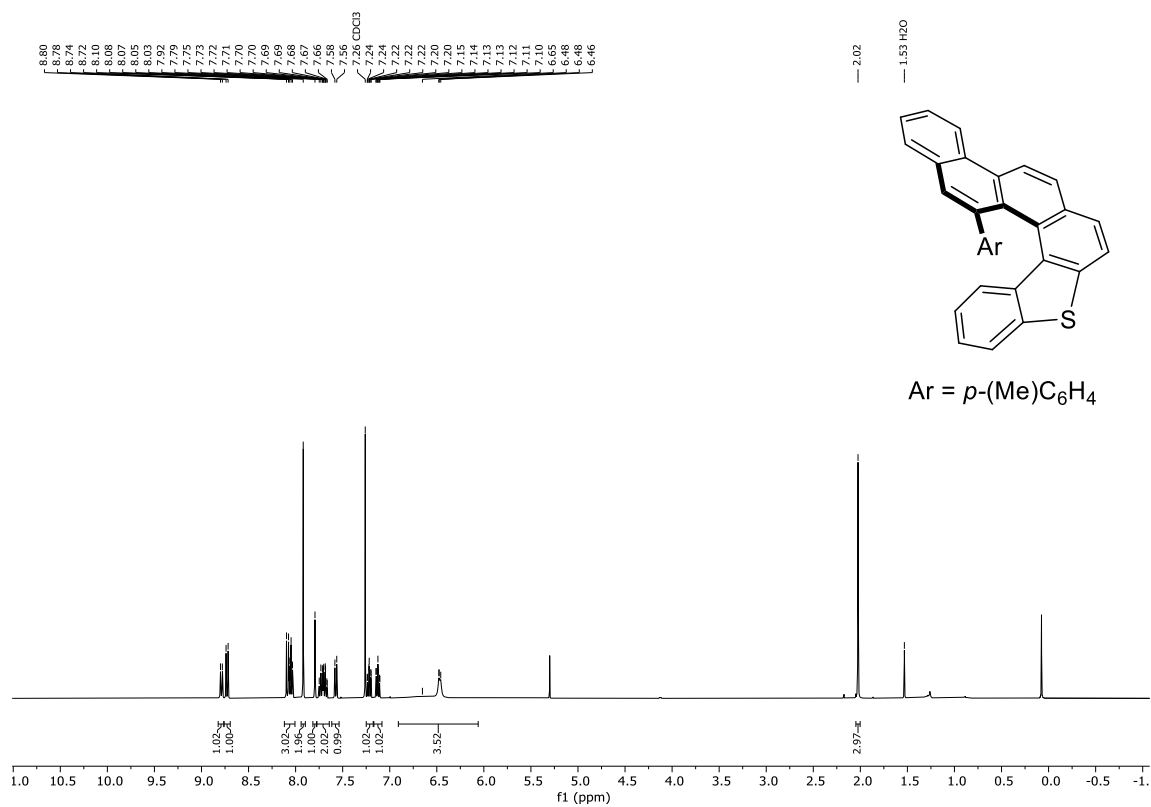
^1H NMR: (400 MHz, CDCl_3) **165a**



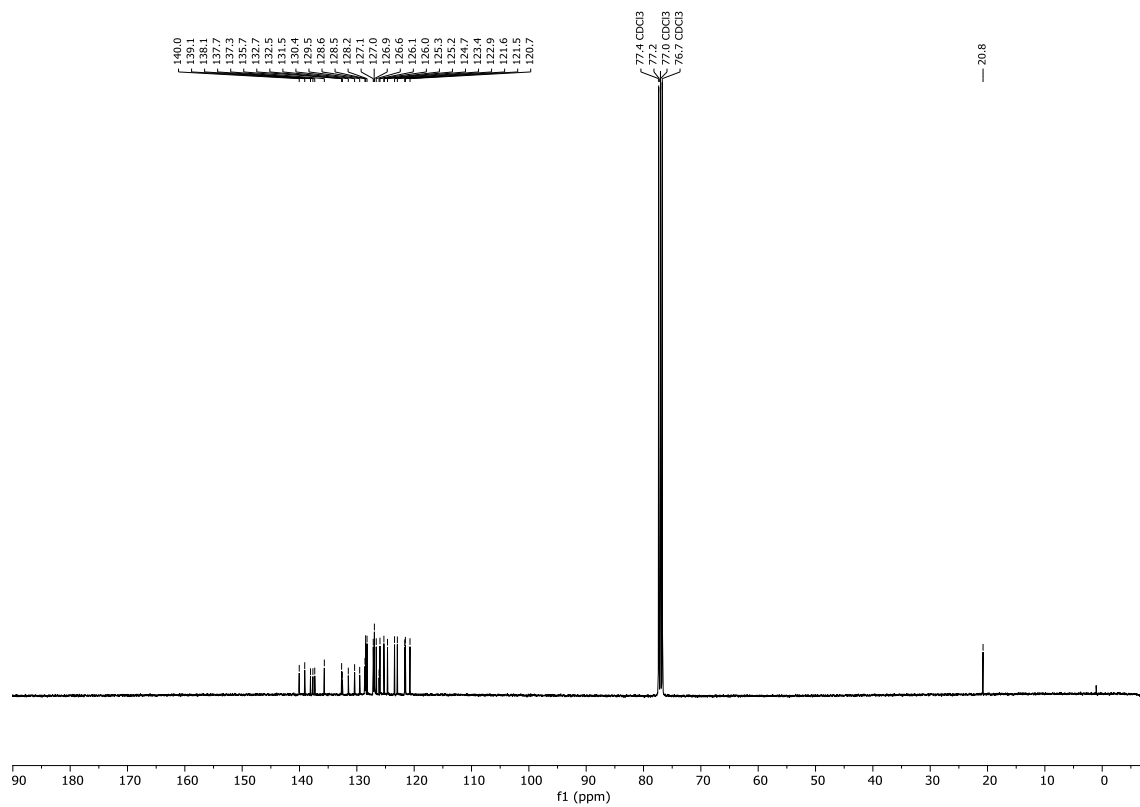
$^{13}\text{C}\{^1\text{H}\}$ NMR: (101 MHz, CDCl_3) **165a**



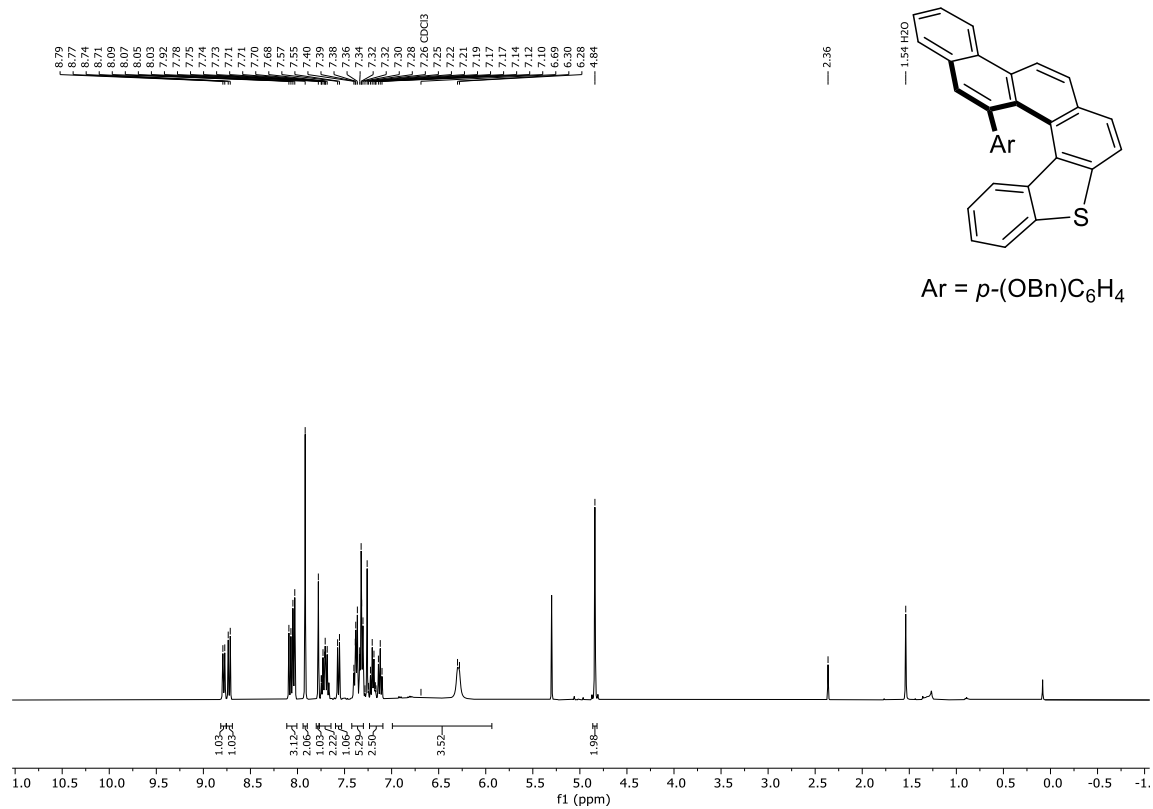
¹H NMR: (400 MHz, CDCl₃) **165b**



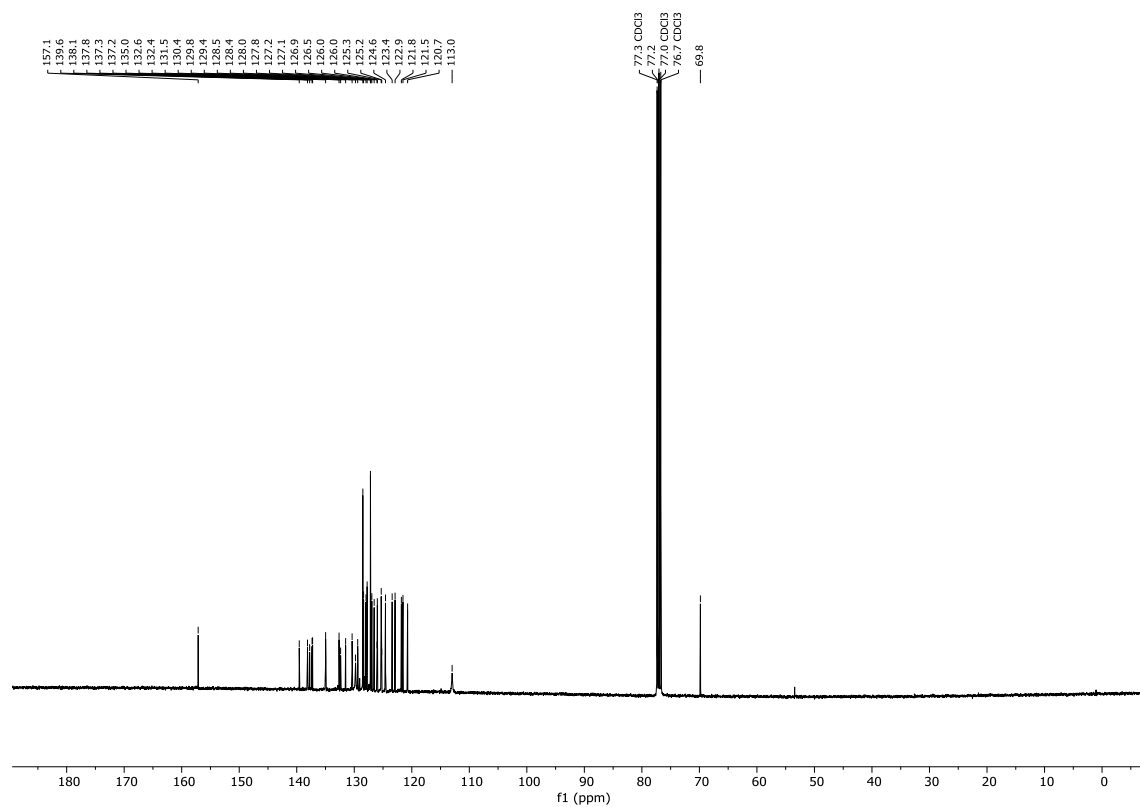
¹³C{H} NMR: (101 MHz, CDCl₃) **165b**



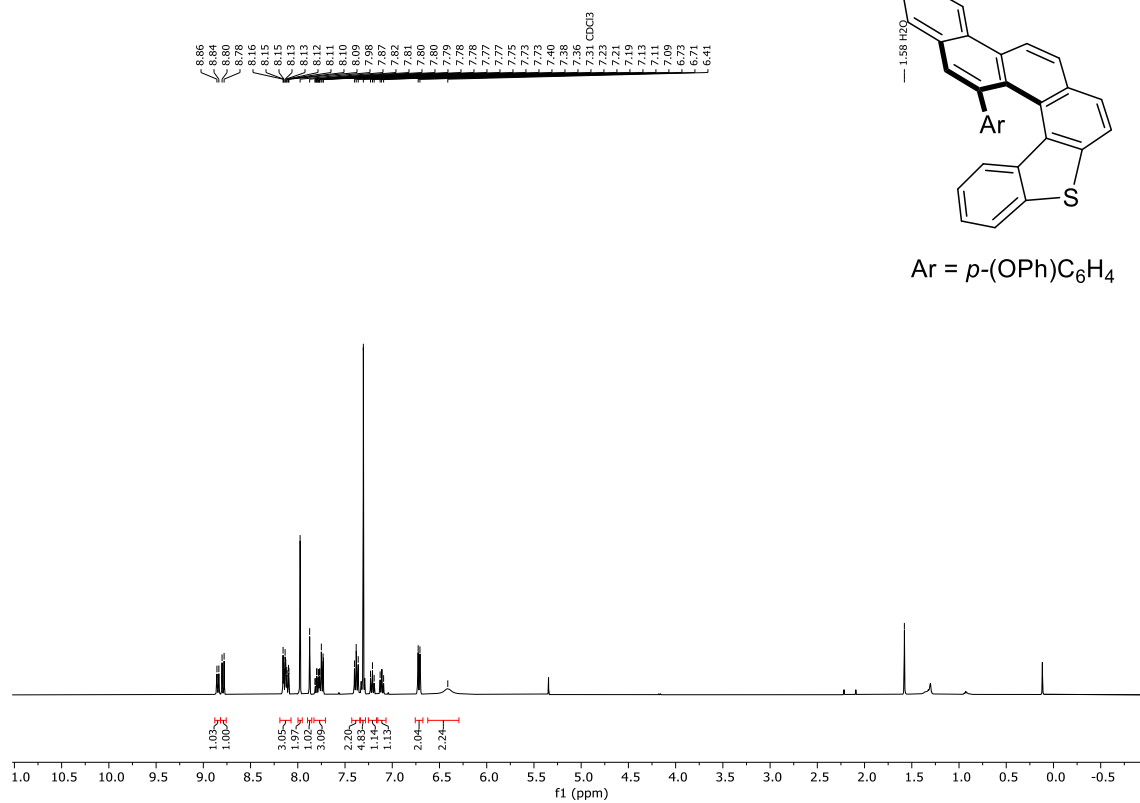
^1H NMR: (400 MHz, CDCl_3) **165c**



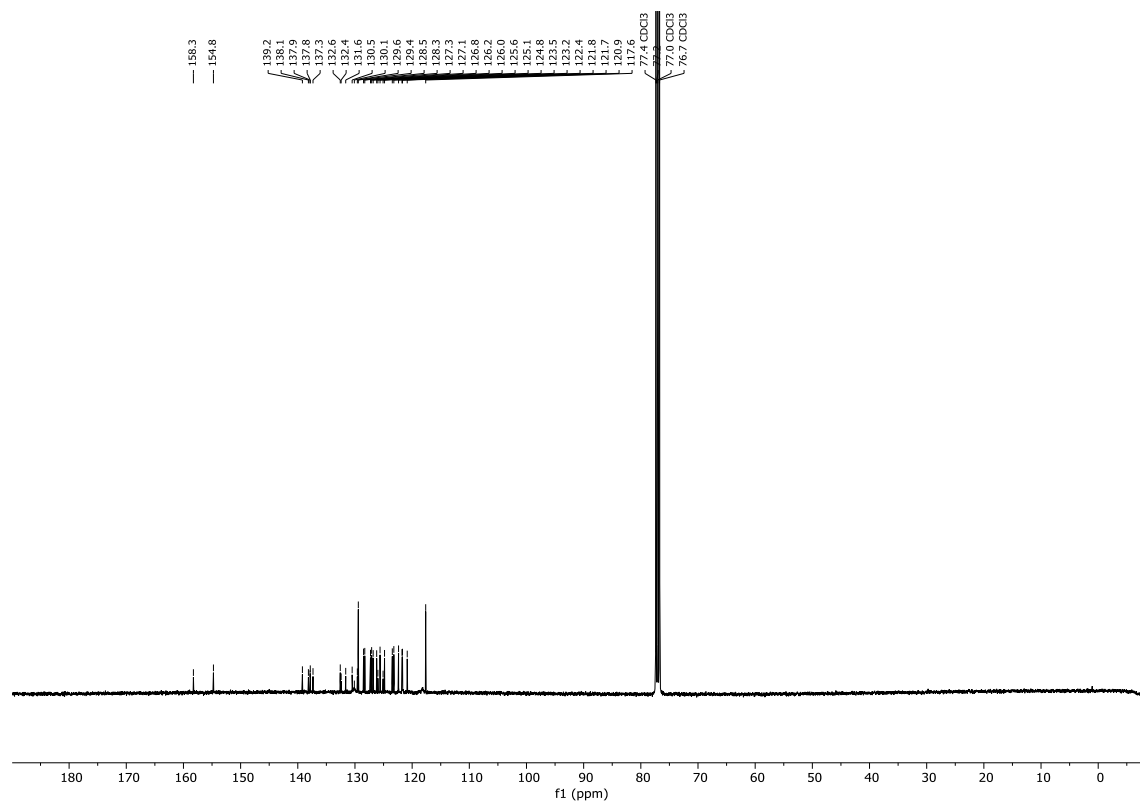
$^{13}\text{C}\{\text{H}\}$ NMR: (101 MHz, CDCl_3) **165c**



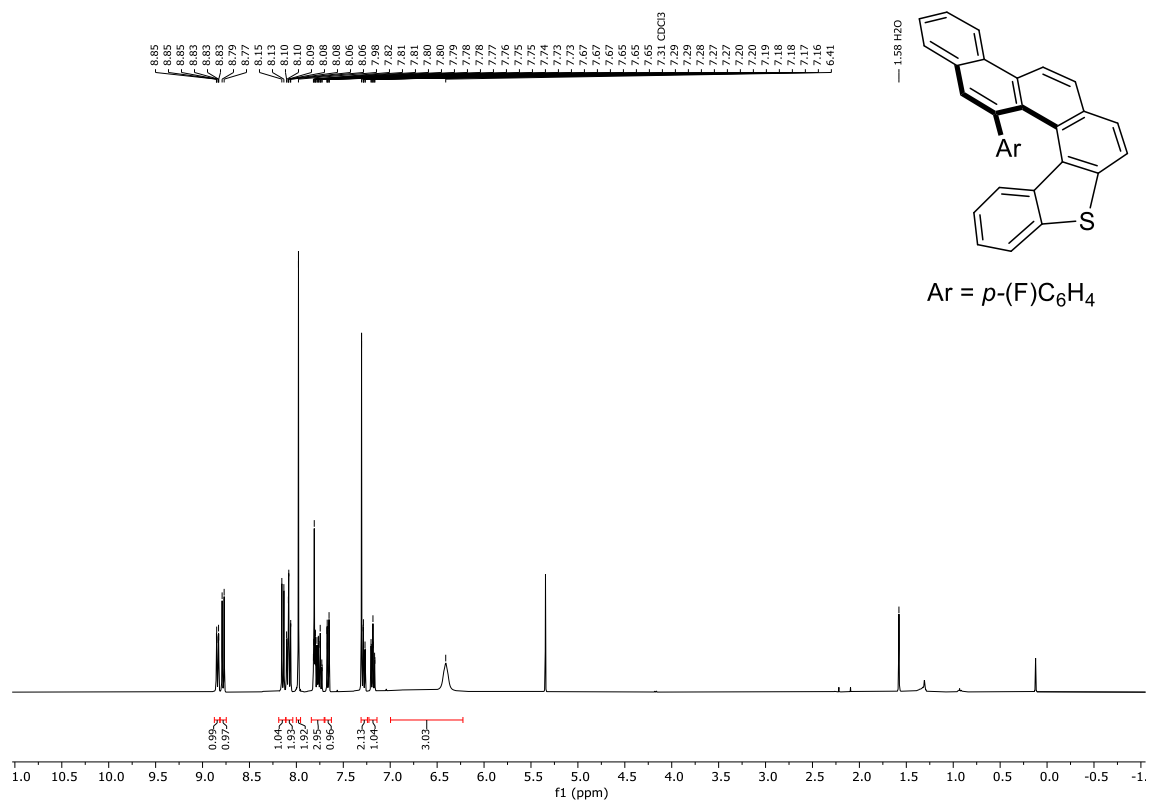
^1H NMR: (400 MHz, CDCl_3) **165e**



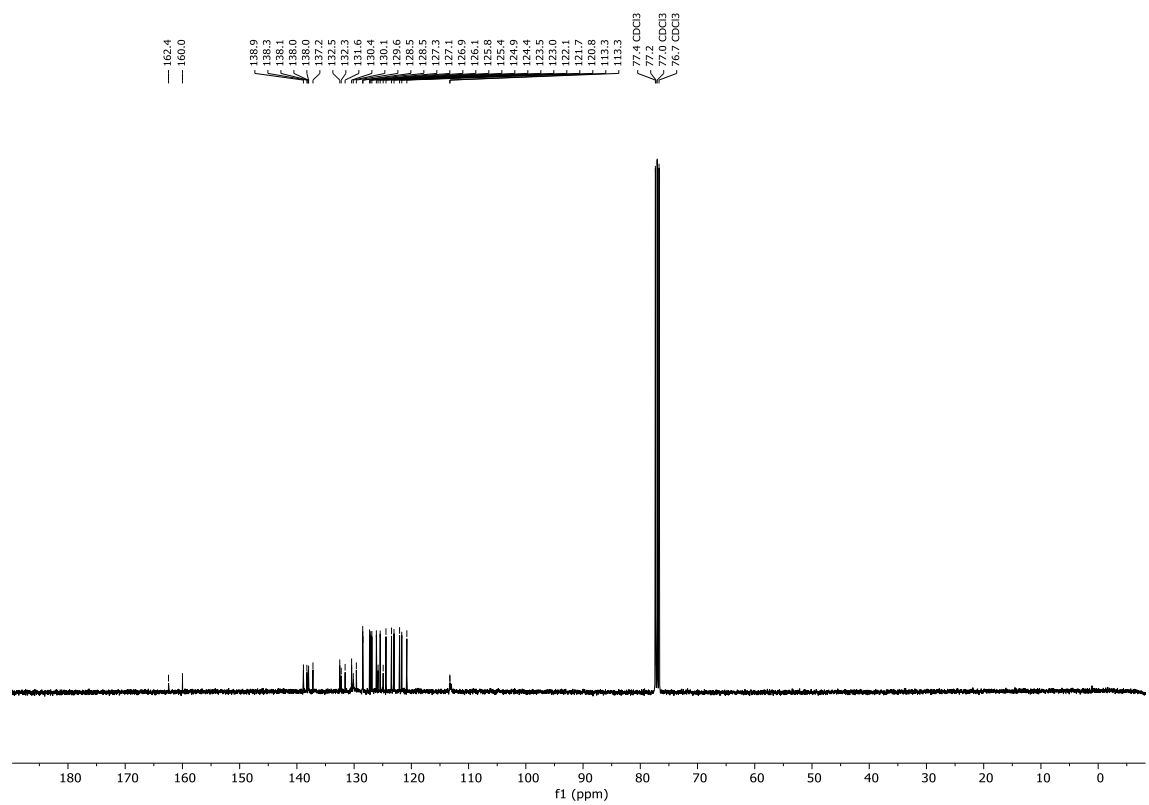
$^{13}\text{C}\{\text{H}\}$ NMR: (101 MHz, CDCl_3) **165e**



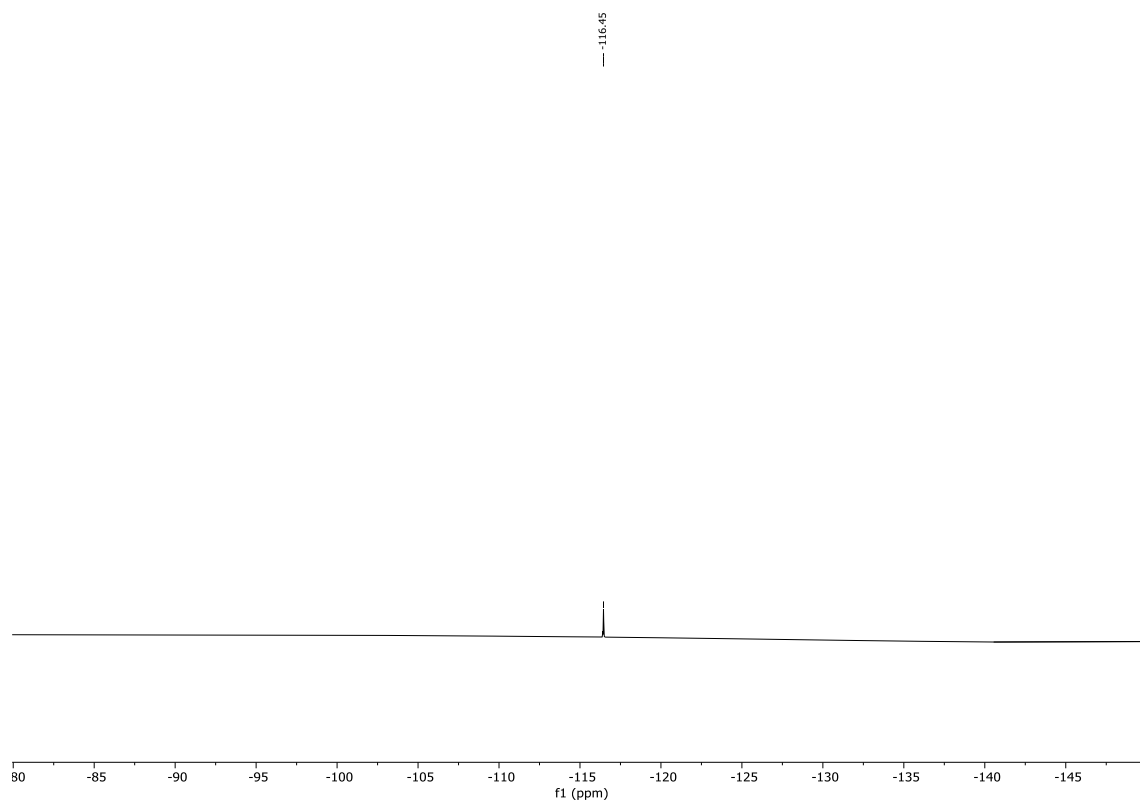
^1H NMR: (400 MHz, CDCl_3) 165g



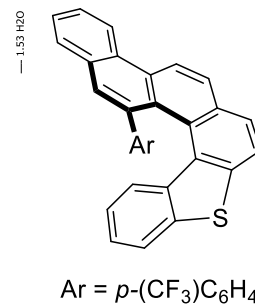
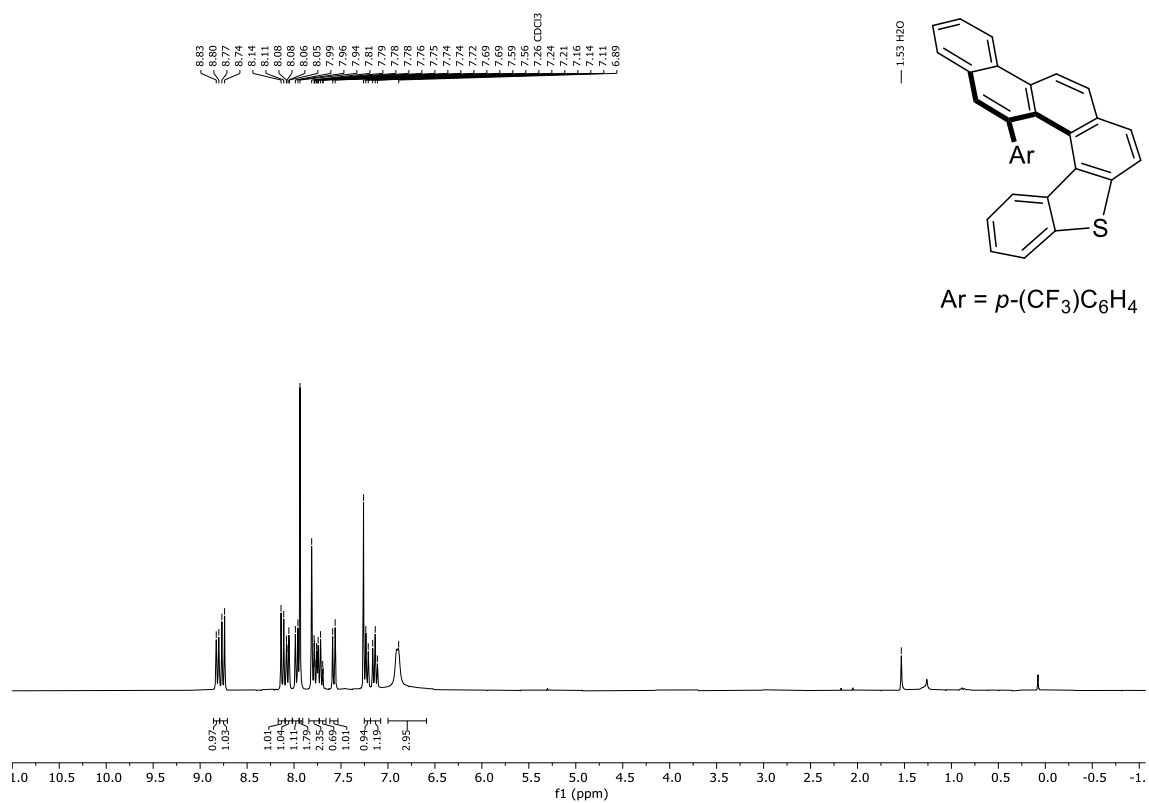
$^{13}\text{C}\{^1\text{H}\}$ NMR: (101 MHz, CDCl_3) 165g



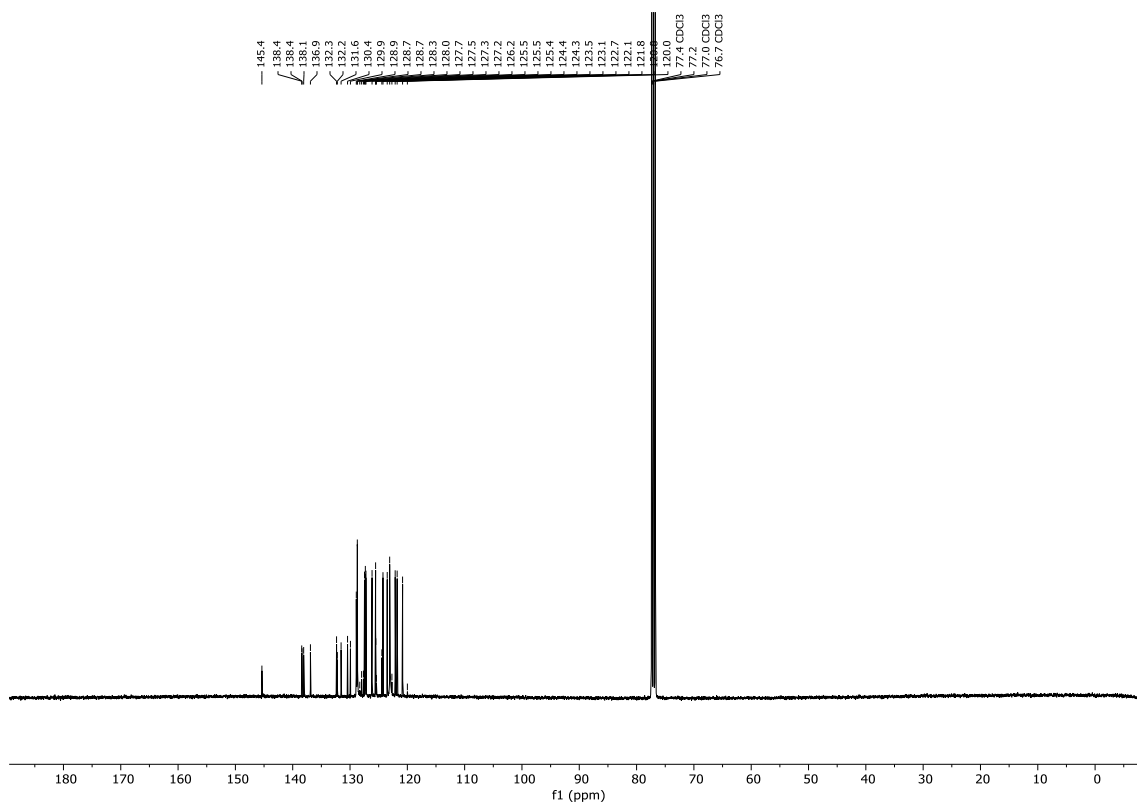
^{19}F NMR: (377 MHz, CDCl_3) **165g**



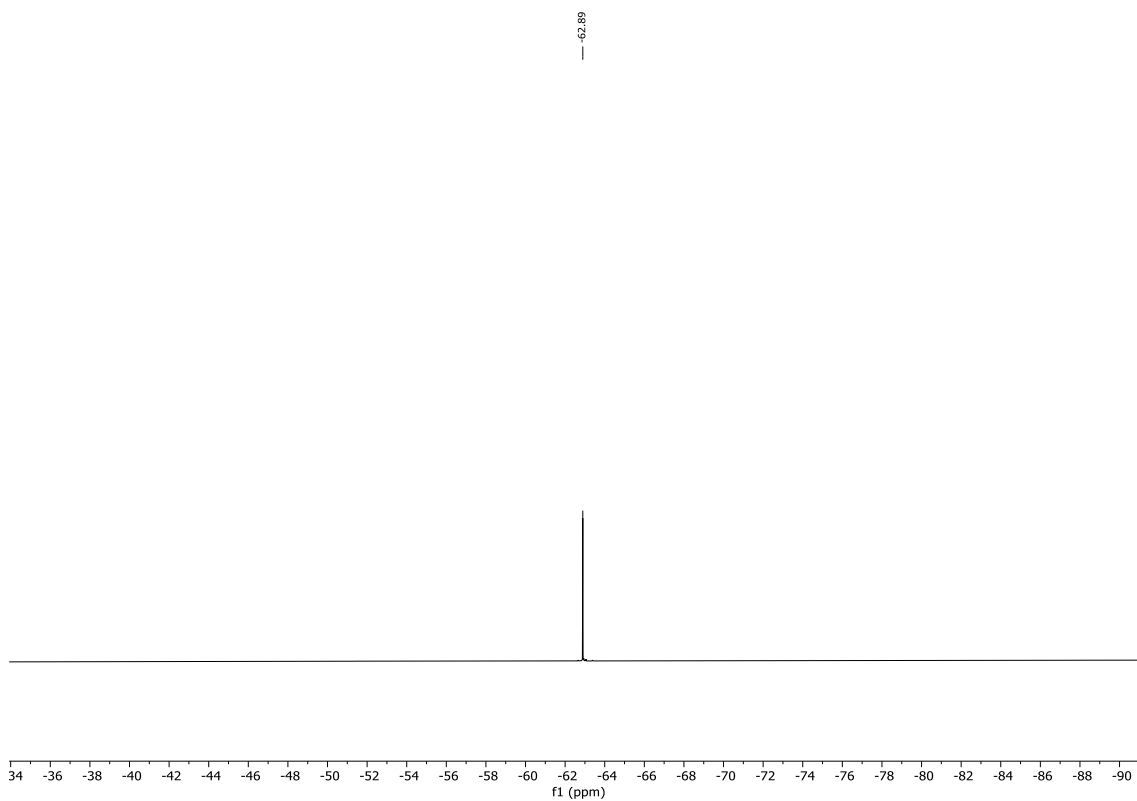
^1H NMR: (400 MHz, CDCl_3) **165h**



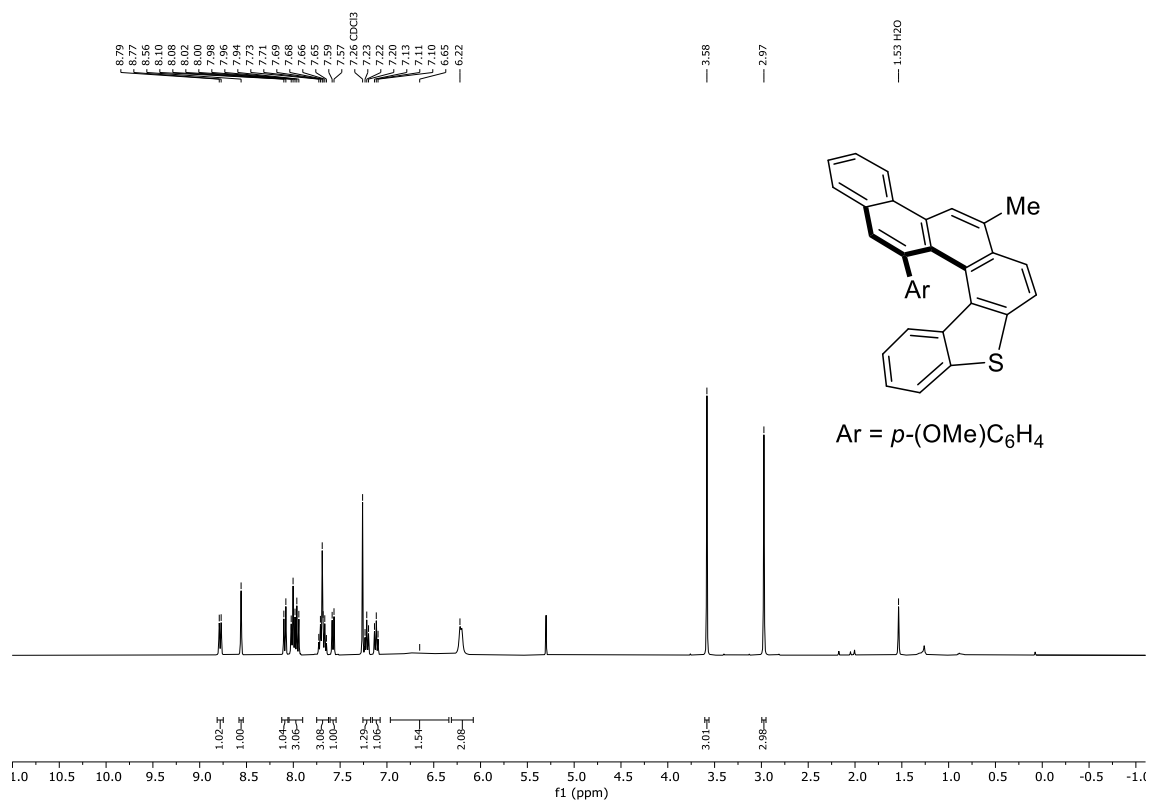
$^{13}\text{C}\{\text{H}\}$ NMR: (101 MHz, CDCl_3) **165h**



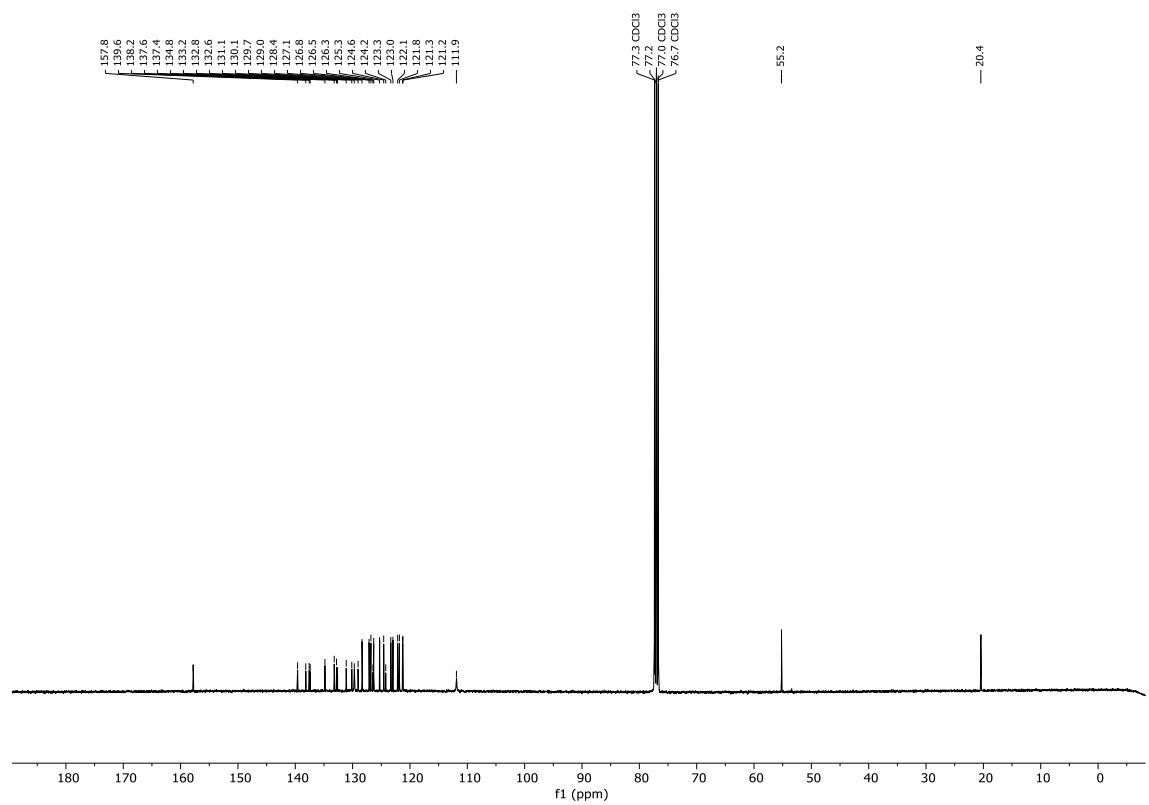
^{19}F NMR: (377 MHz, CDCl_3) **165h**



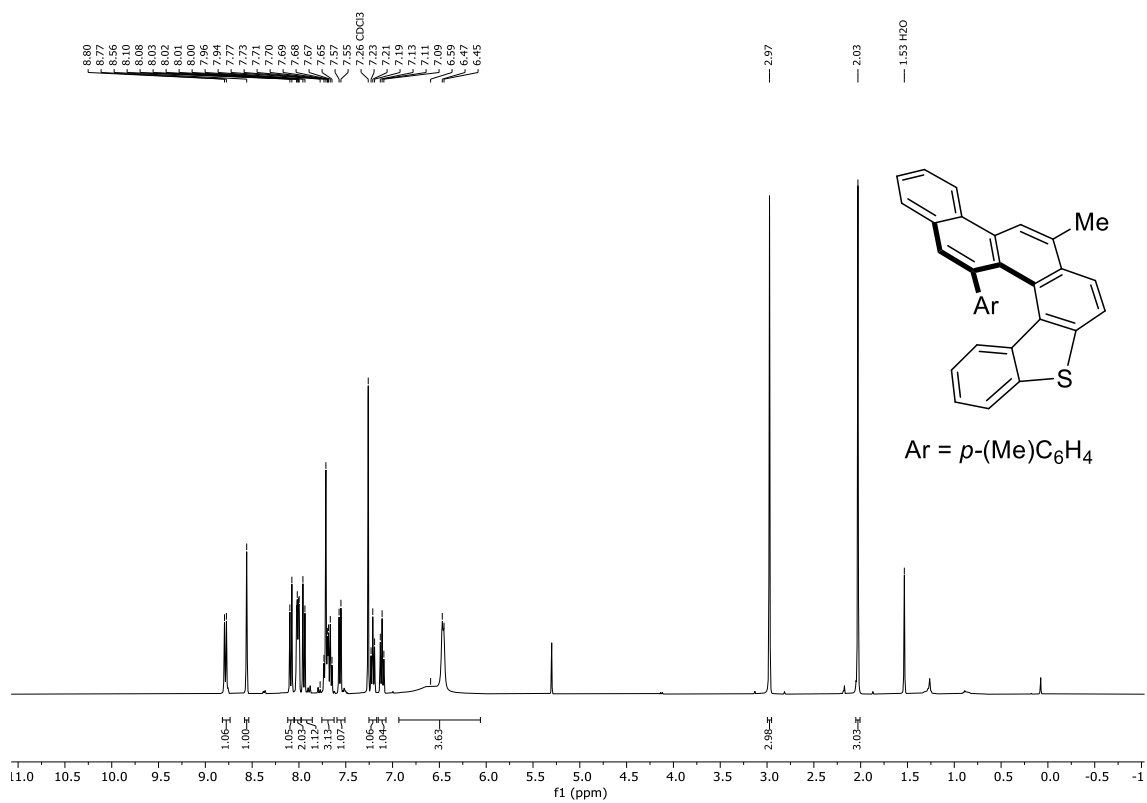
^1H NMR: (400 MHz, CDCl_3) **165i**



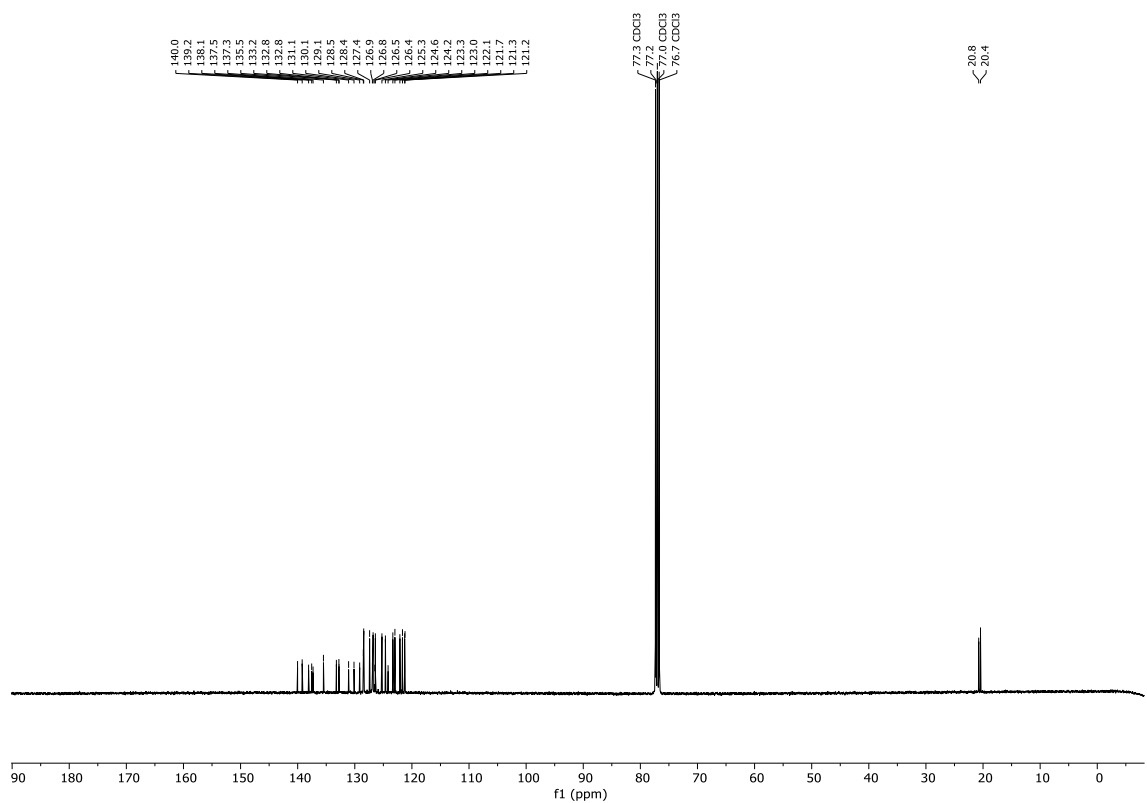
$^{13}\text{C}\{^1\text{H}\}$ NMR: (101 MHz, CDCl_3) **165i**



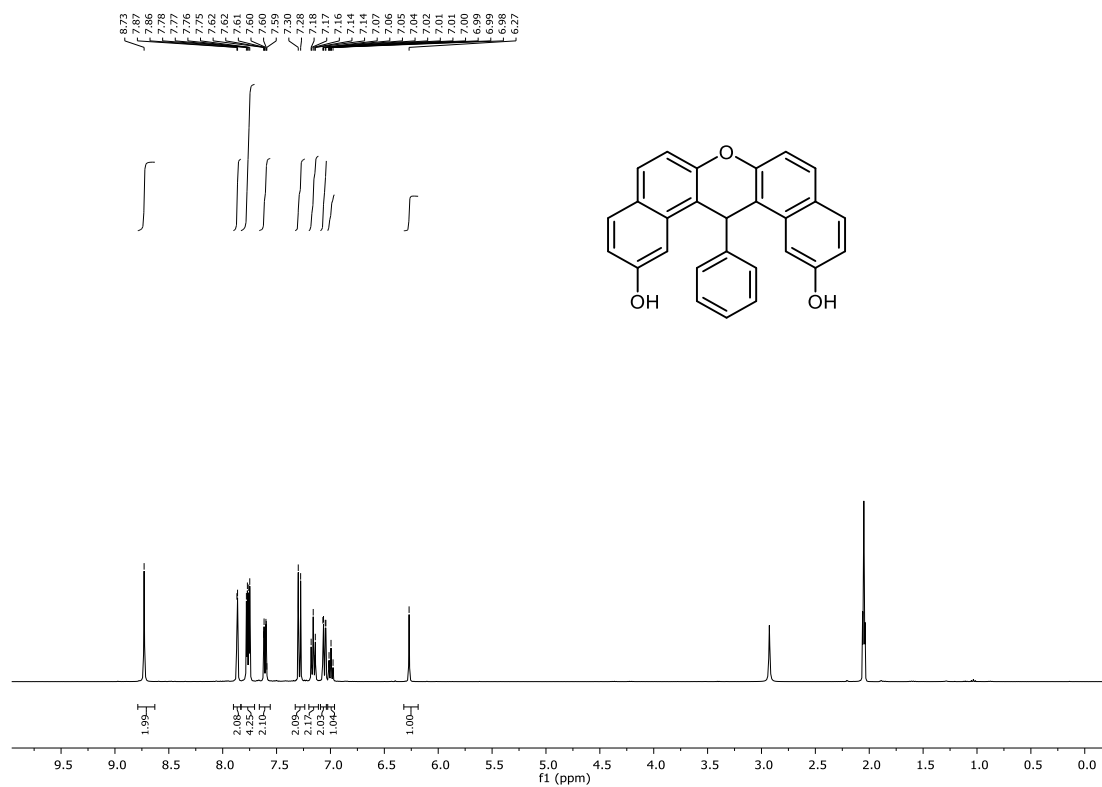
^1H NMR: (400 MHz, CDCl_3) **165j**



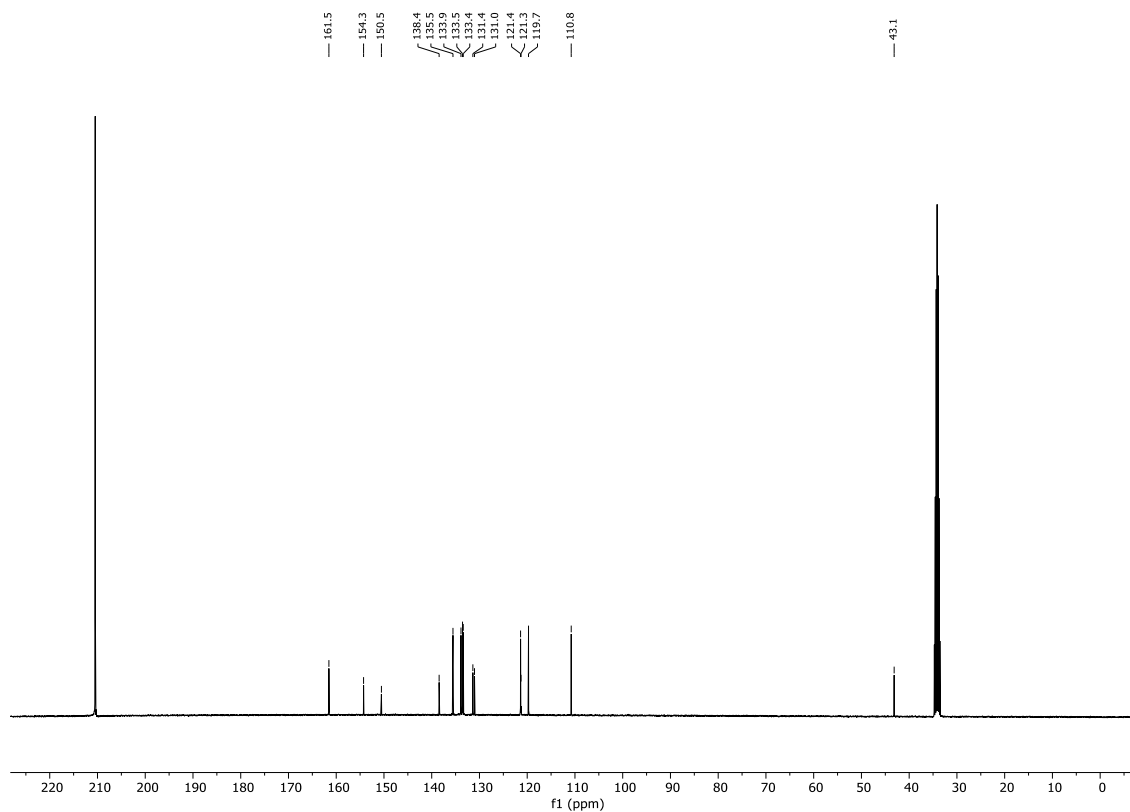
$^{13}\text{C}\{^1\text{H}\}$ NMR: (101 MHz, CDCl_3) **165j**



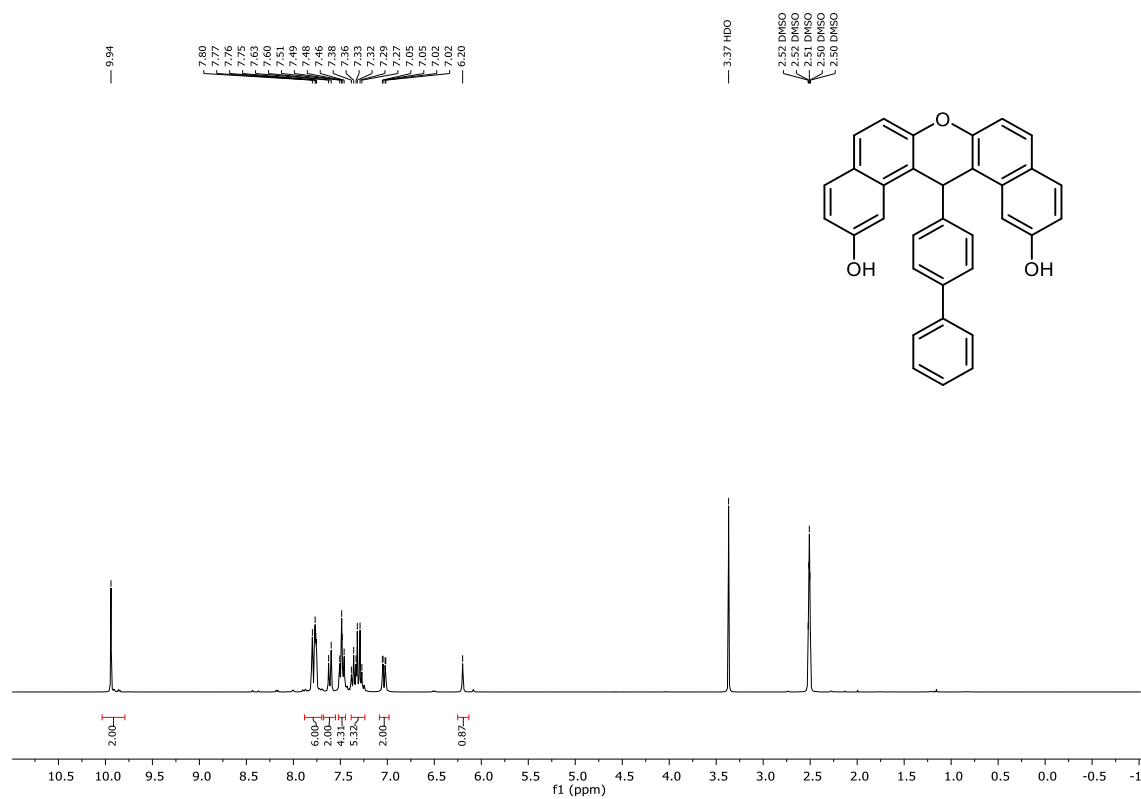
¹H NMR: (400 MHz, acetone-d₆) **200a**



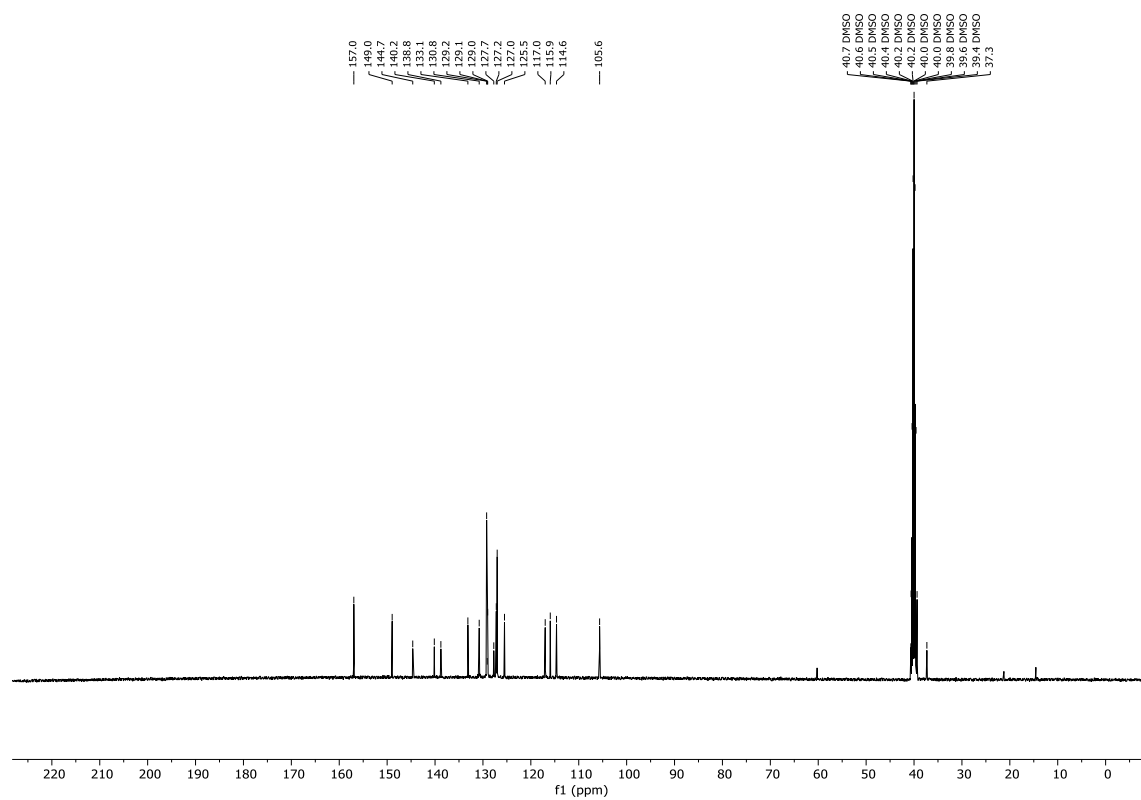
¹³C{H} NMR: (100 MHz, acetone-d₆) **200a**



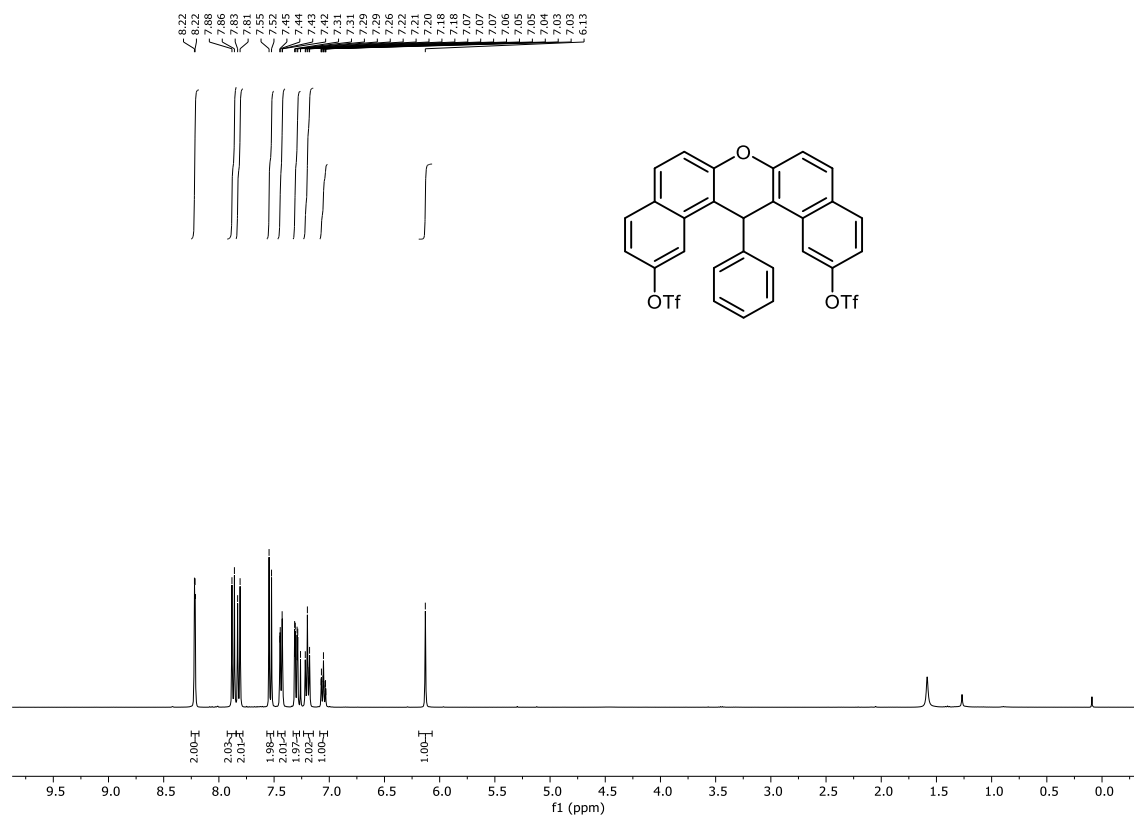
¹H NMR: (300 MHz, DMSO-d₆) **200b**



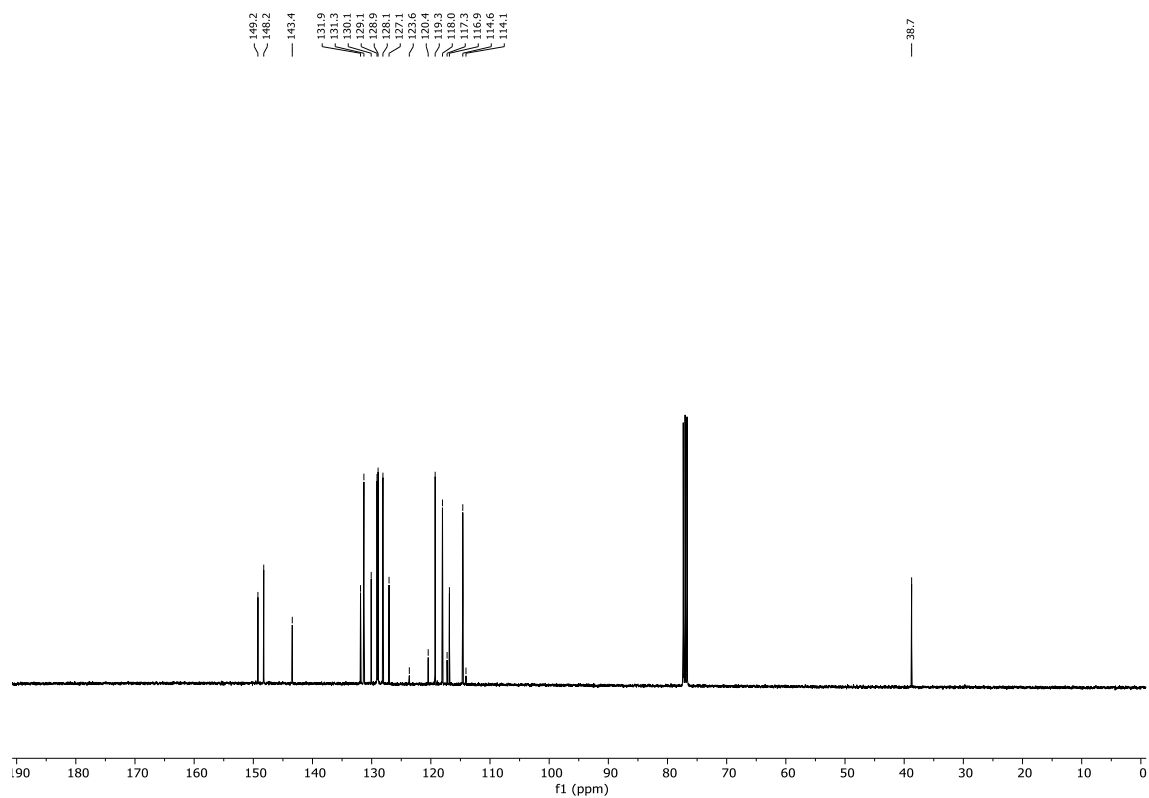
¹³C{H} NMR: (101 MHz, DMSO-d₆) **200b**



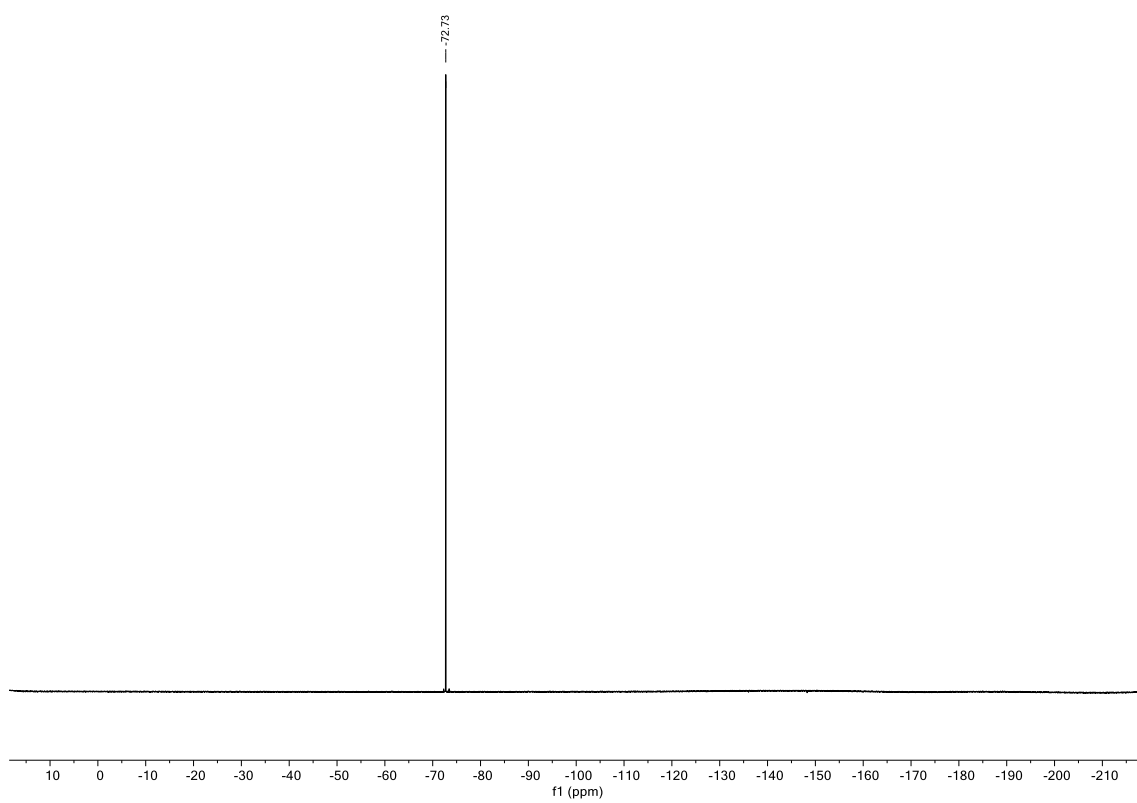
¹H NMR: (400 MHz, CDCl₃) **201a**



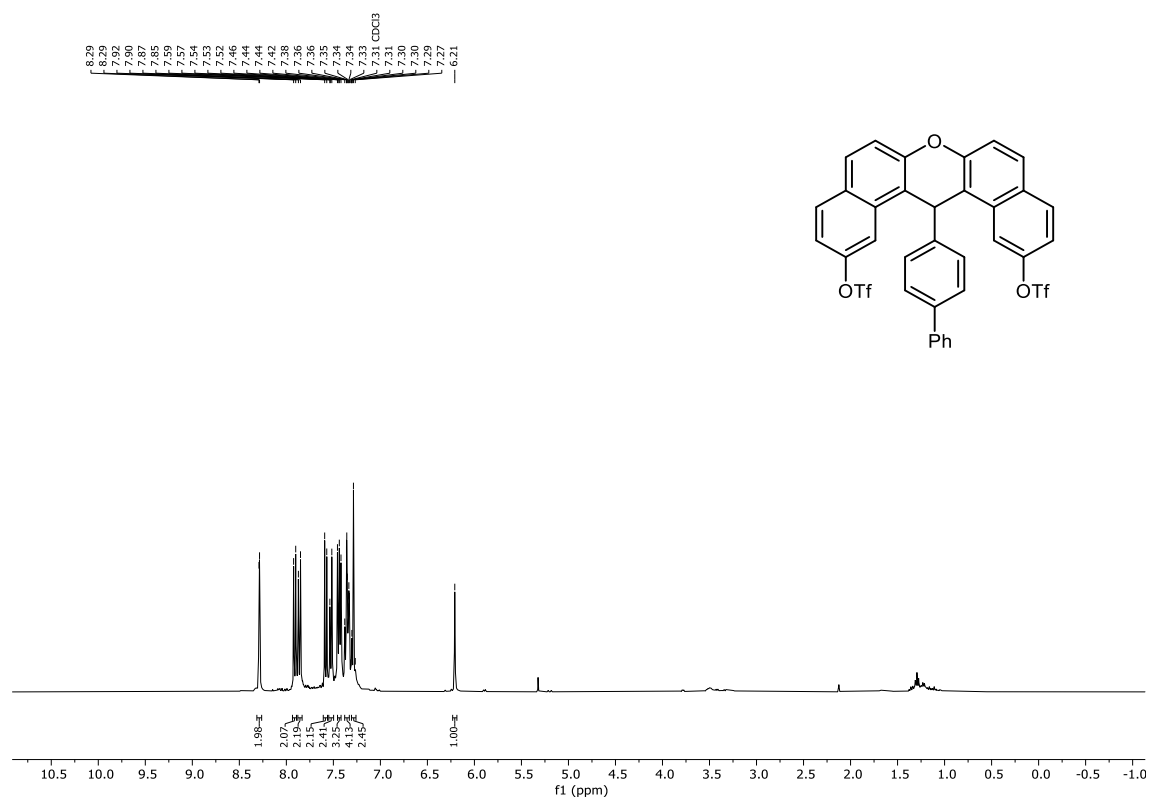
¹³C{H} NMR: (100 MHz, CDCl₃) **201a**



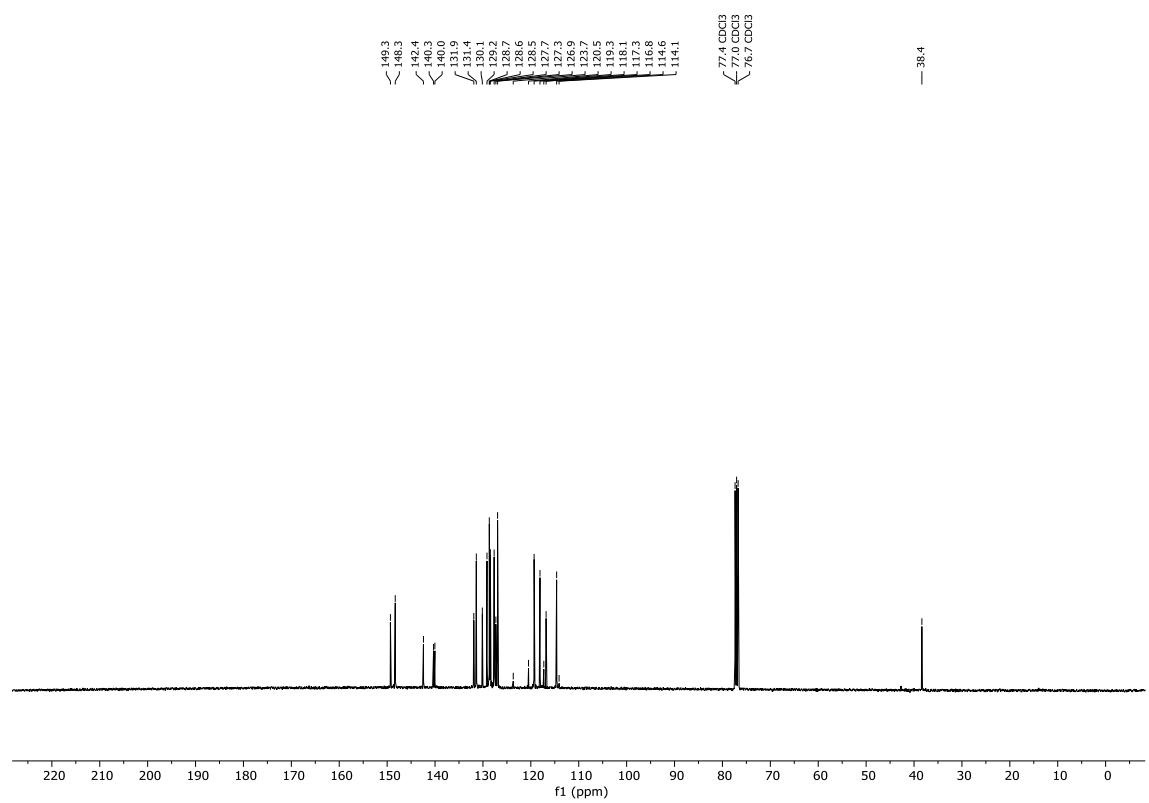
^{19}F NMR: (282 MHz, CDCl_3) **201a**



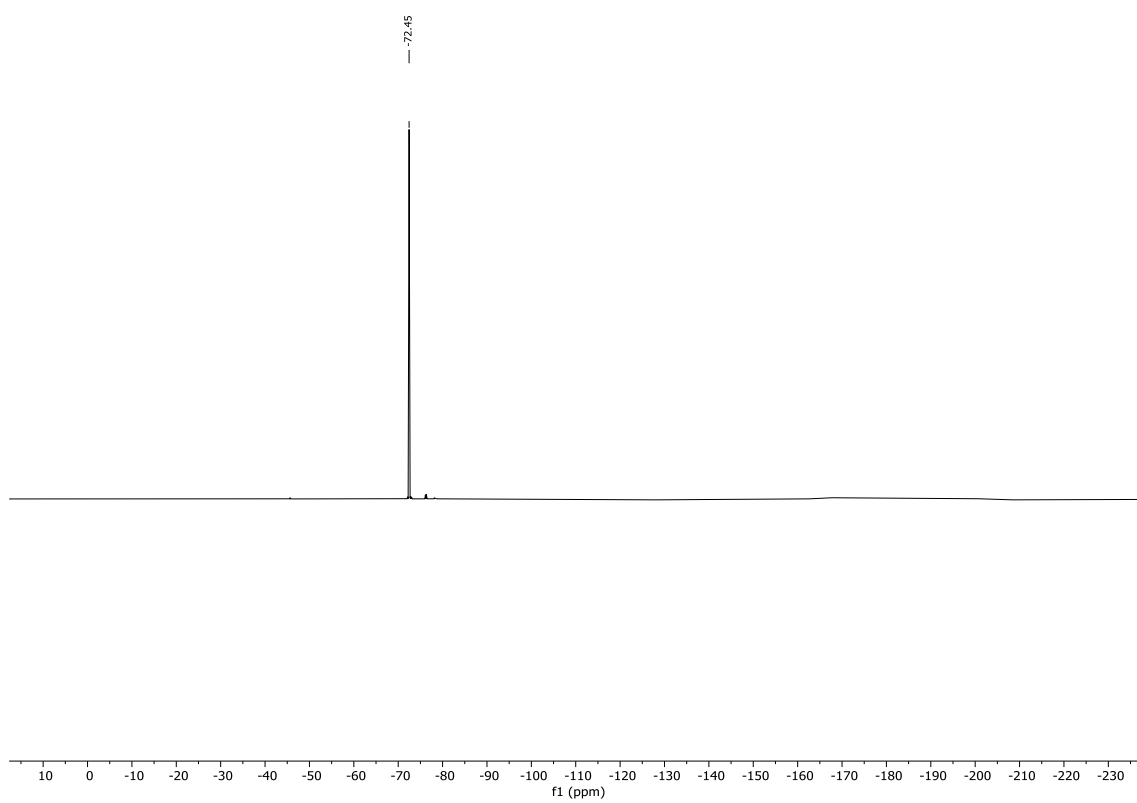
^1H NMR: (400 MHz, CDCl_3) **201b**



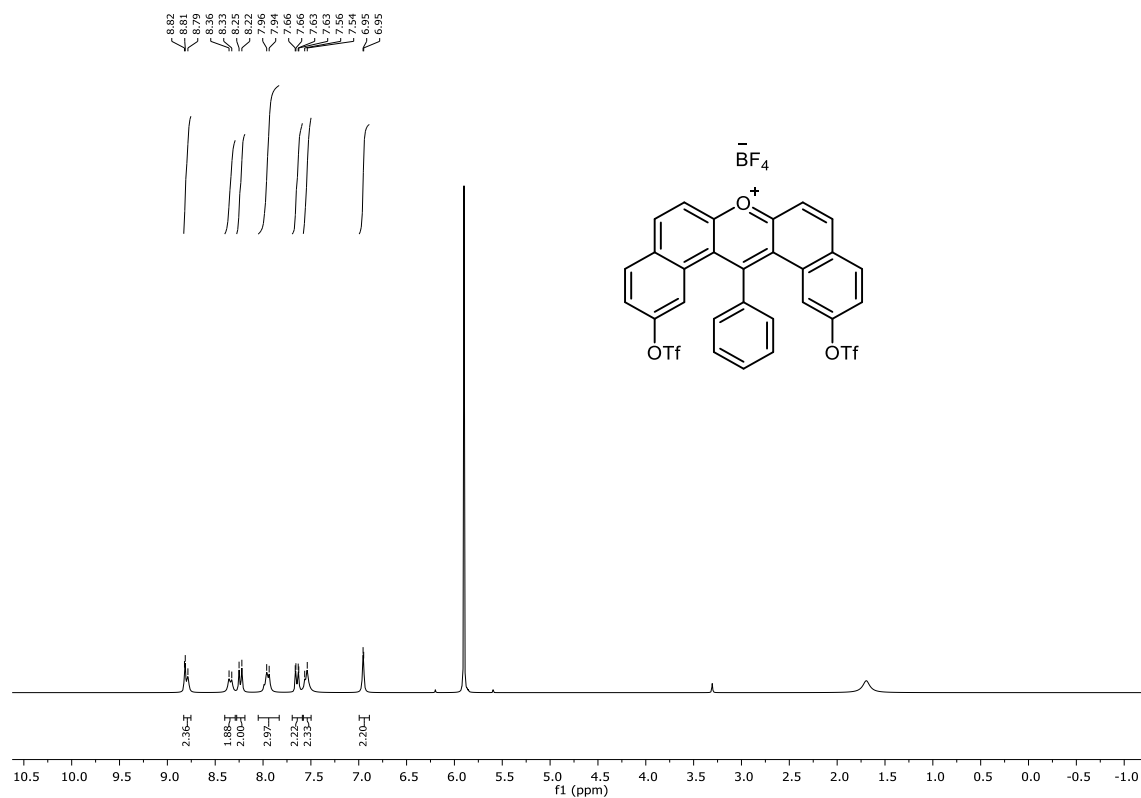
^{13}C NMR: (101 MHz, CDCl_3) **201b**



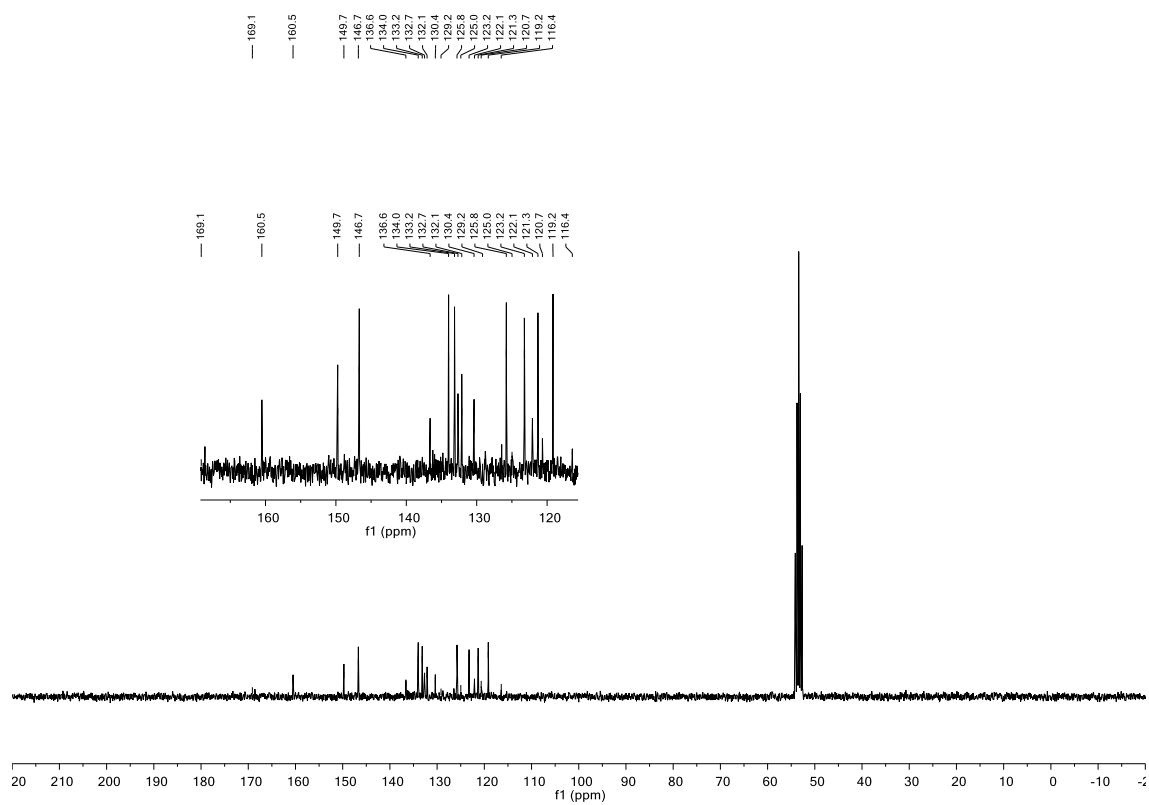
^{19}F NMR: (377 MHz, CDCl_3) **201b**



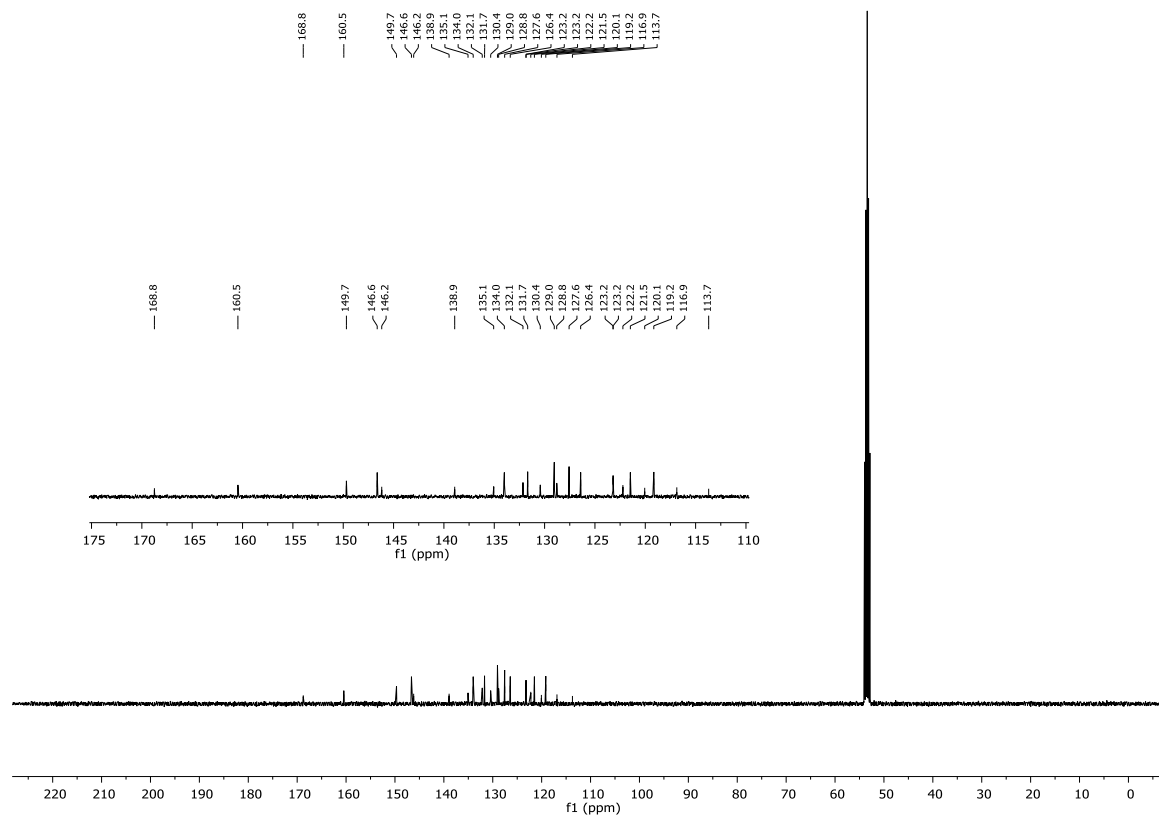
^1H NMR: (400 MHz, 1,1,2,2-tetrachloroethane- d_2) **202a**



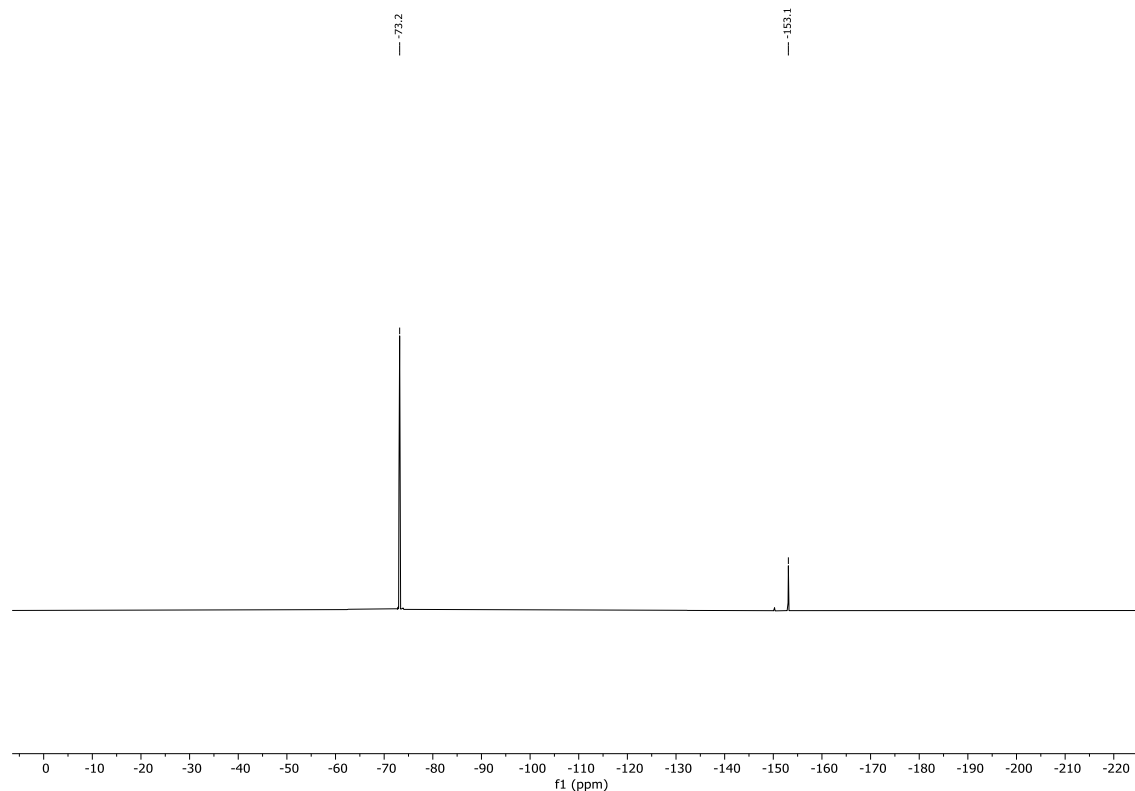
$^{13}\text{C}\{^1\text{H}\}$ NMR: (75 MHz, CD_2Cl_2) **202a**



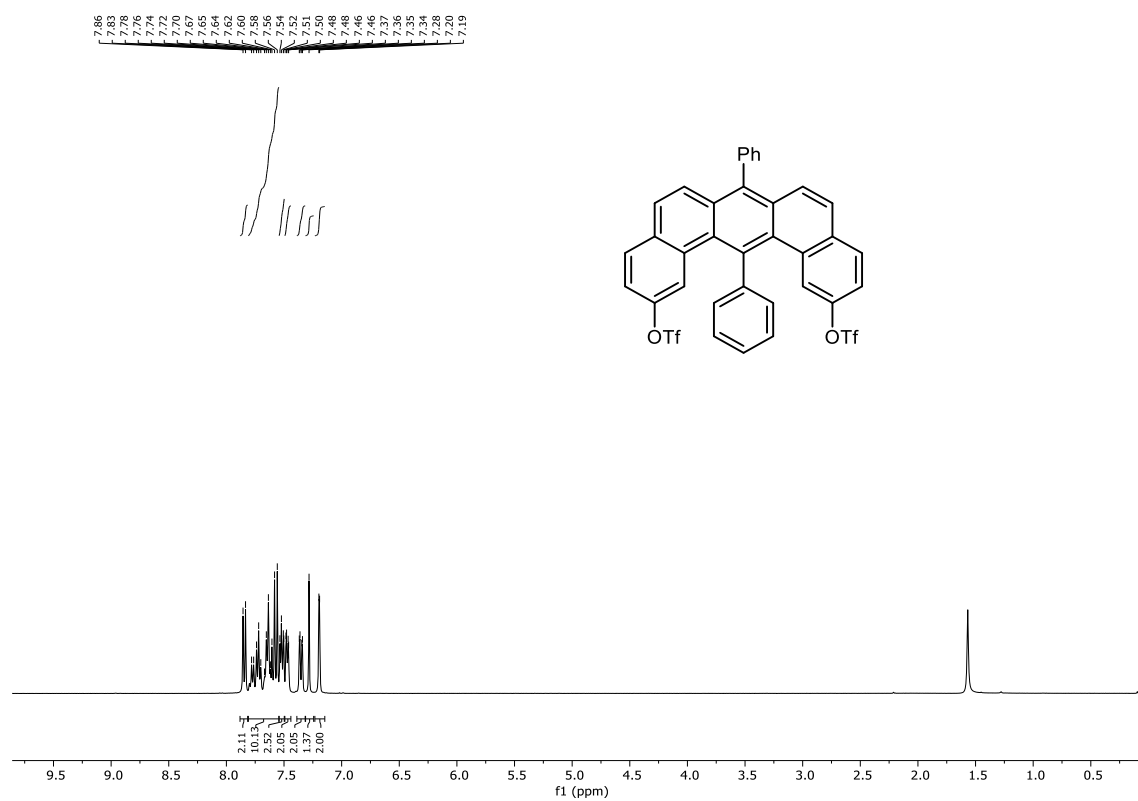
$^{13}\text{C}\{\text{H}\}$ NMR: (101 MHz, CD_2Cl_2) **202b**



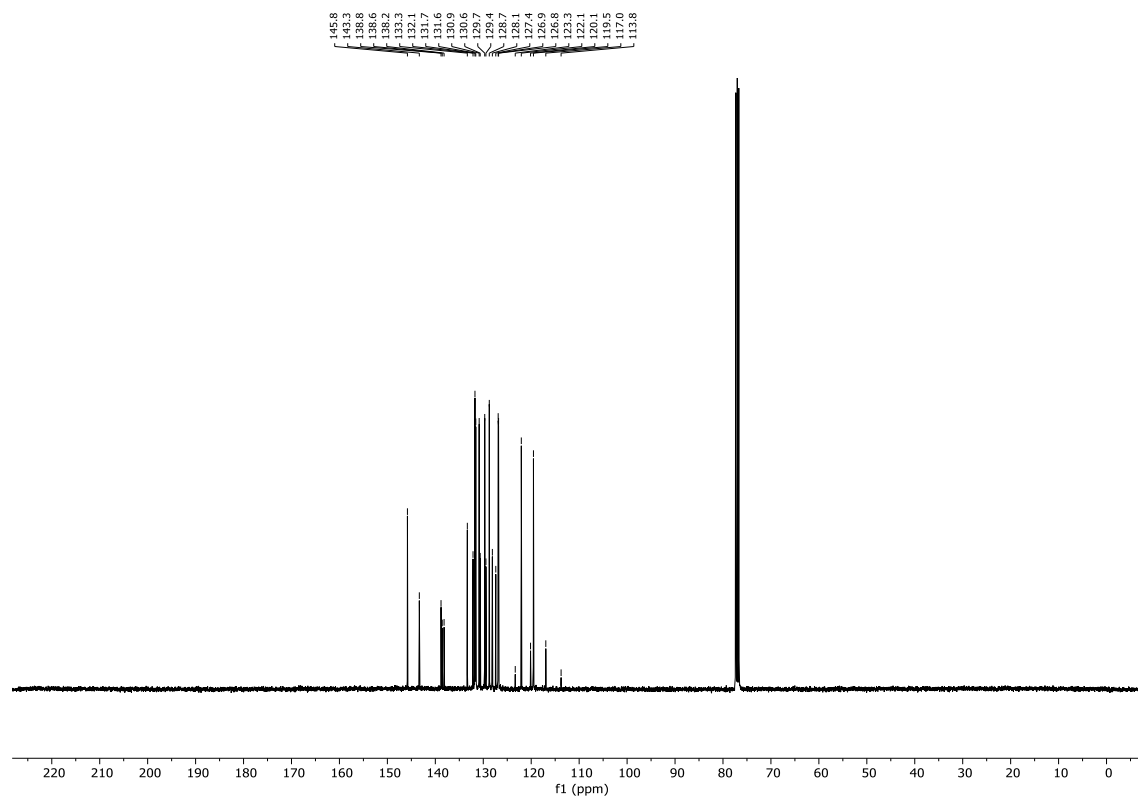
^{19}F NMR (377 MHz, CDCl_3) **202b**



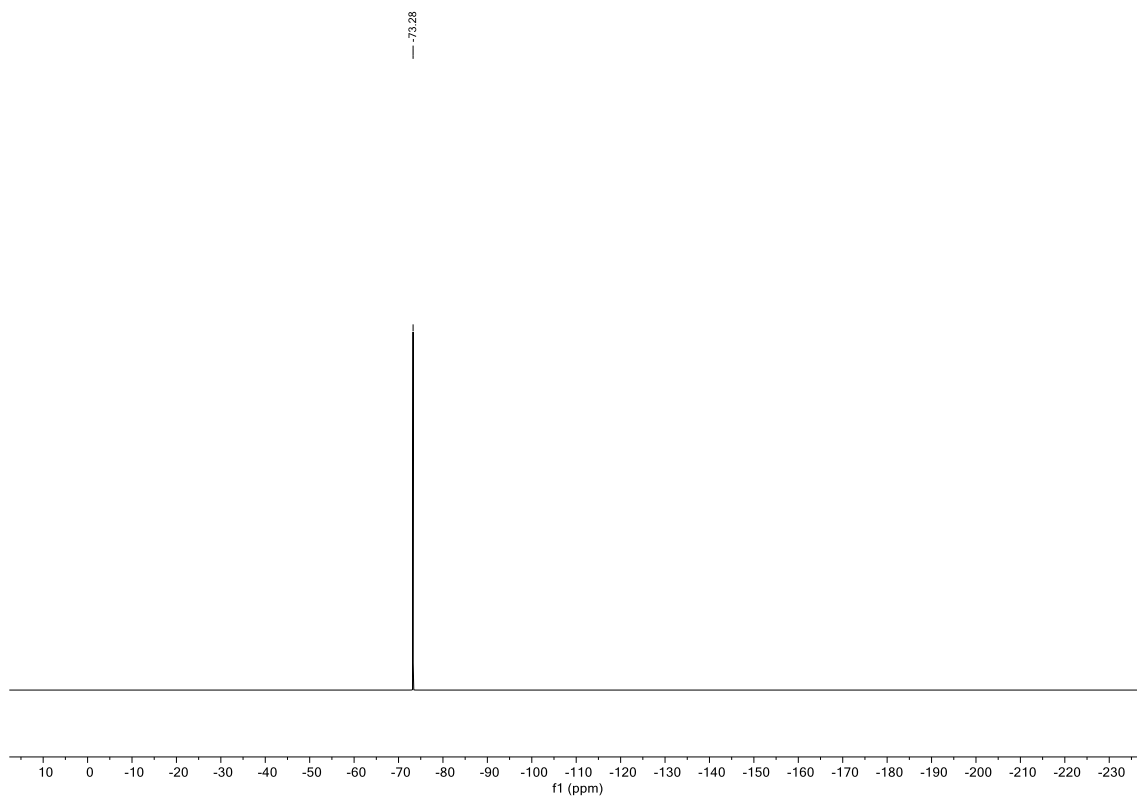
^1H NMR: (400 MHz, CDCl_3) **203a**



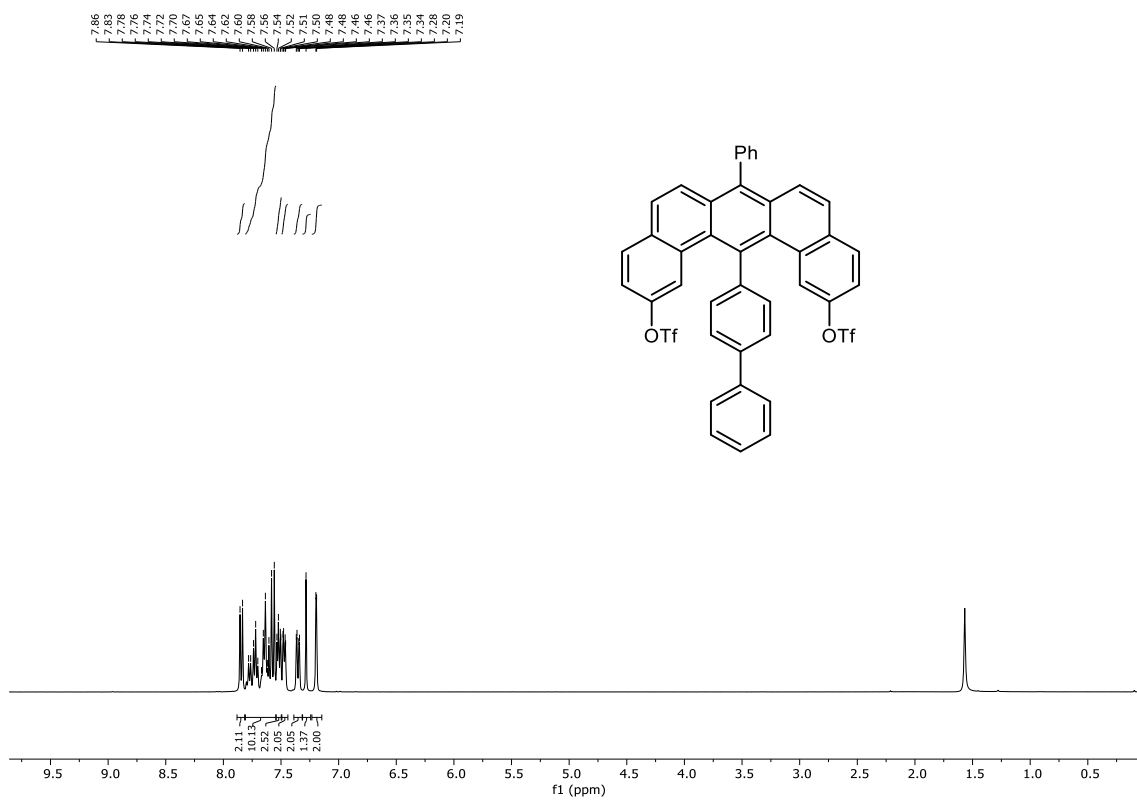
$^{13}\text{C}\{\text{H}\}$ NMR: (100 MHz, CDCl_3) **203a**



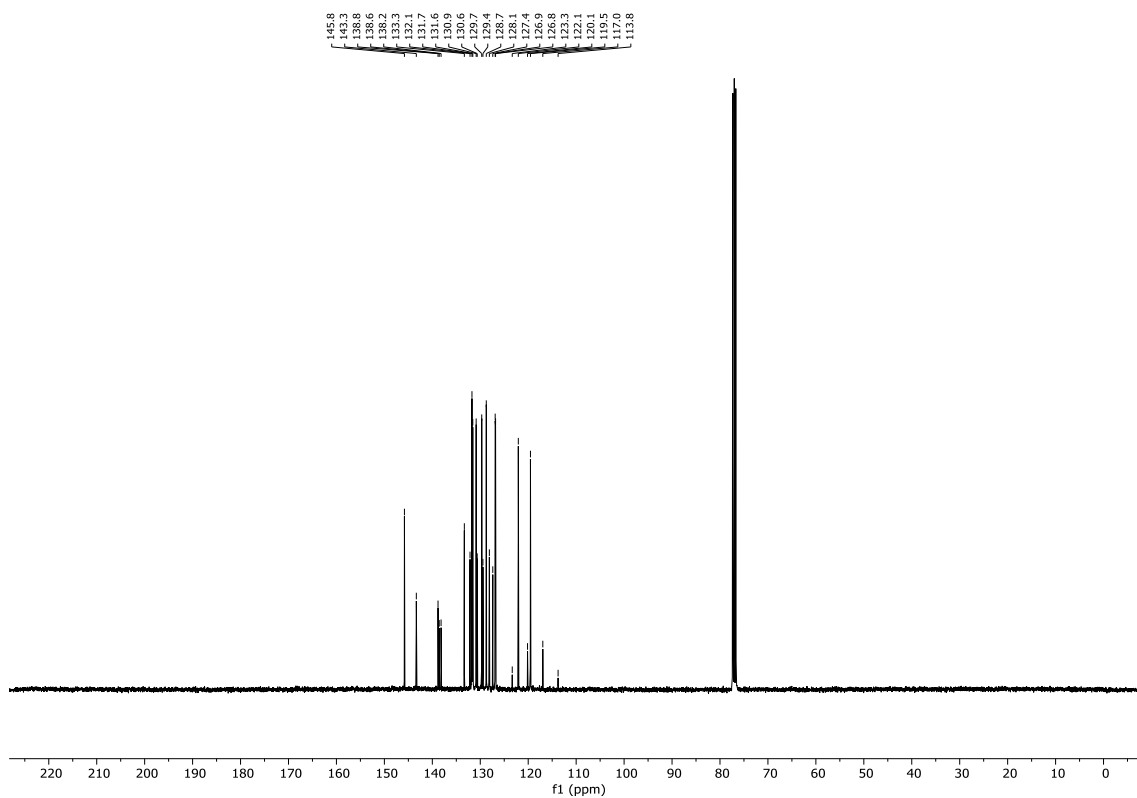
^{19}F NMR: (377 MHz, CDCl_3) **203a**



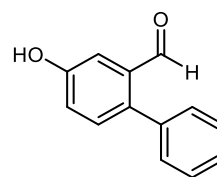
^1H NMR: (400 MHz, CDCl_3) **203b**



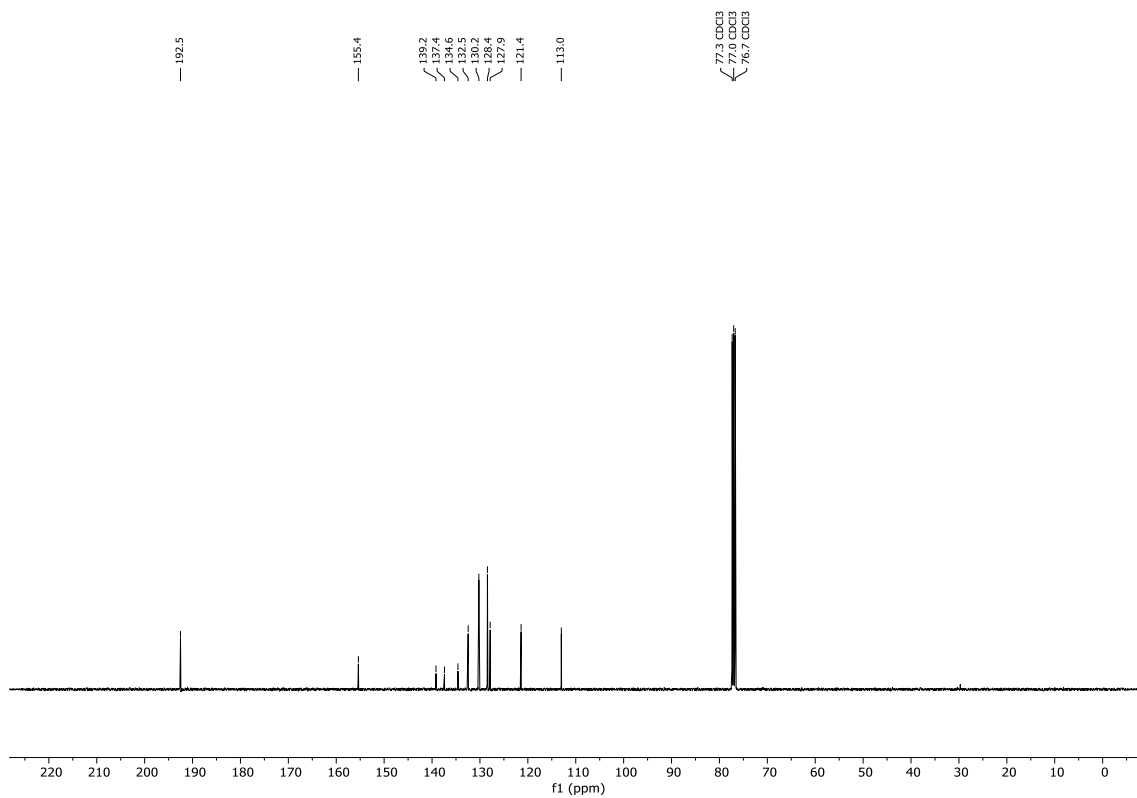
$^{13}\text{C}\{\text{H}\}$ NMR: (100 MHz, CDCl_3) **203b**



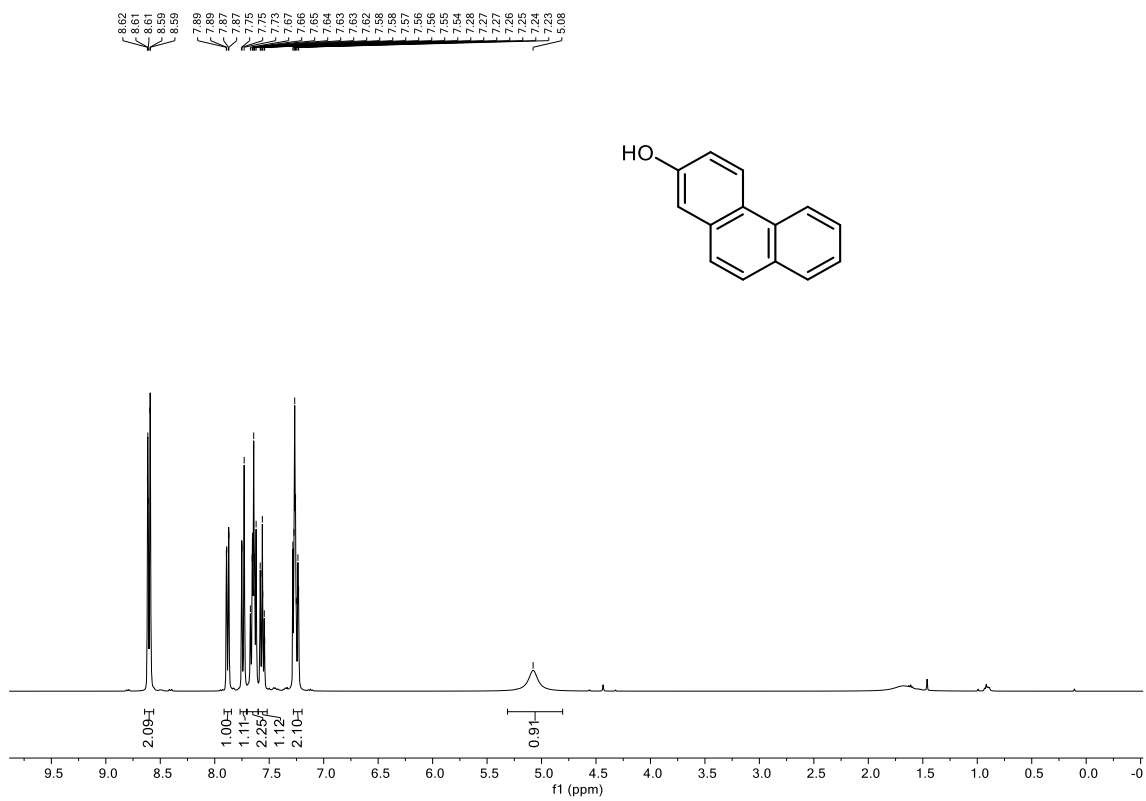
^1H NMR: (400 MHz, CDCl_3) **208**



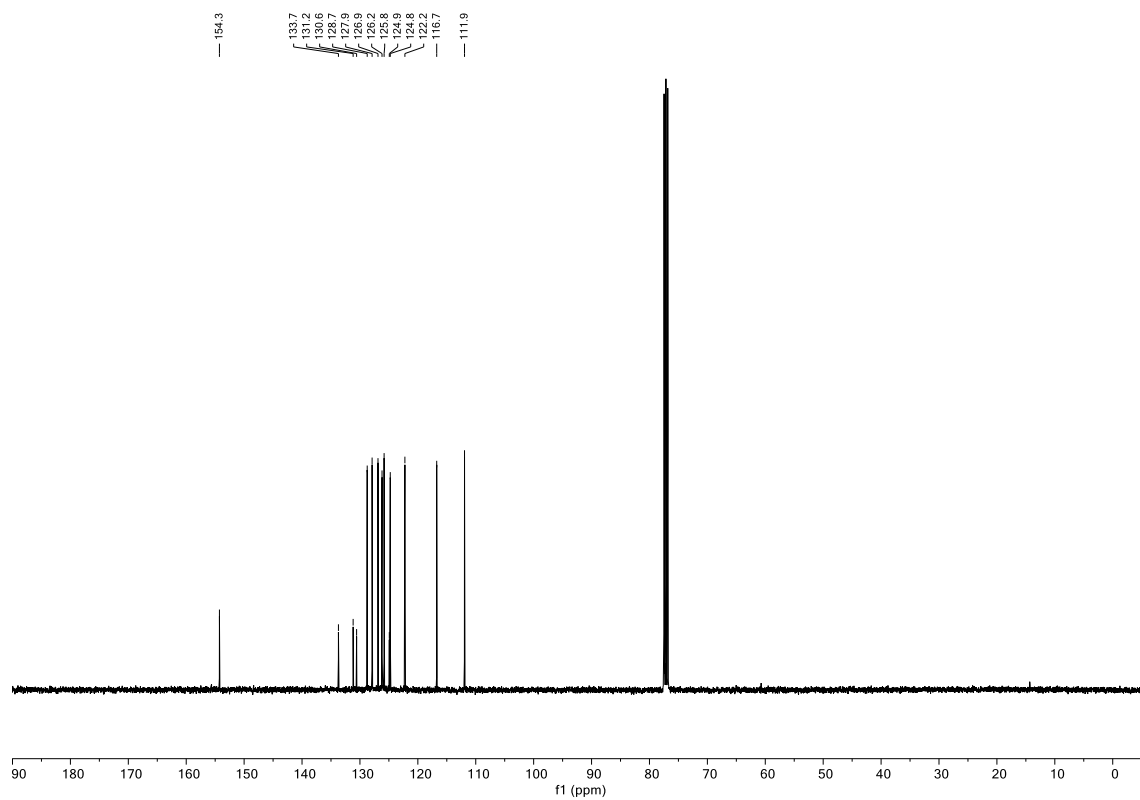
$^{13}\text{C}\{\text{H}\}$ NMR: (100 MHz, CDCl_3) **208**



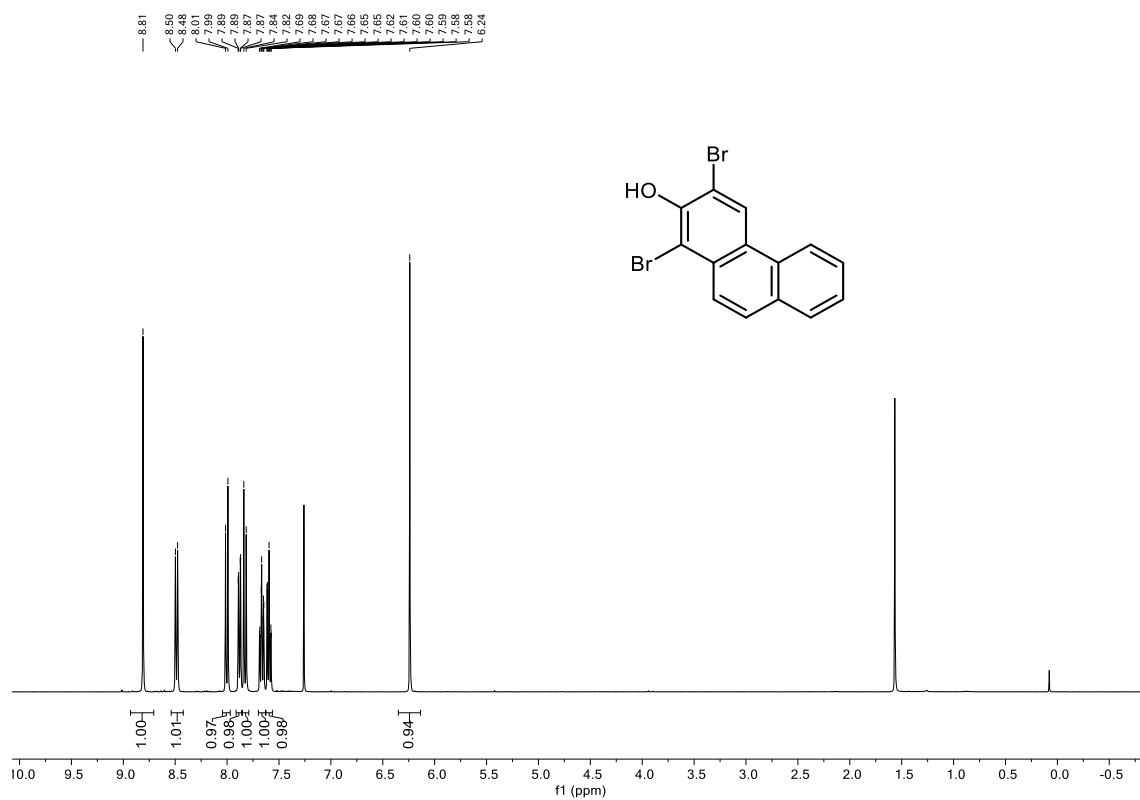
^1H NMR: (400 MHz, CDCl_3) **209**



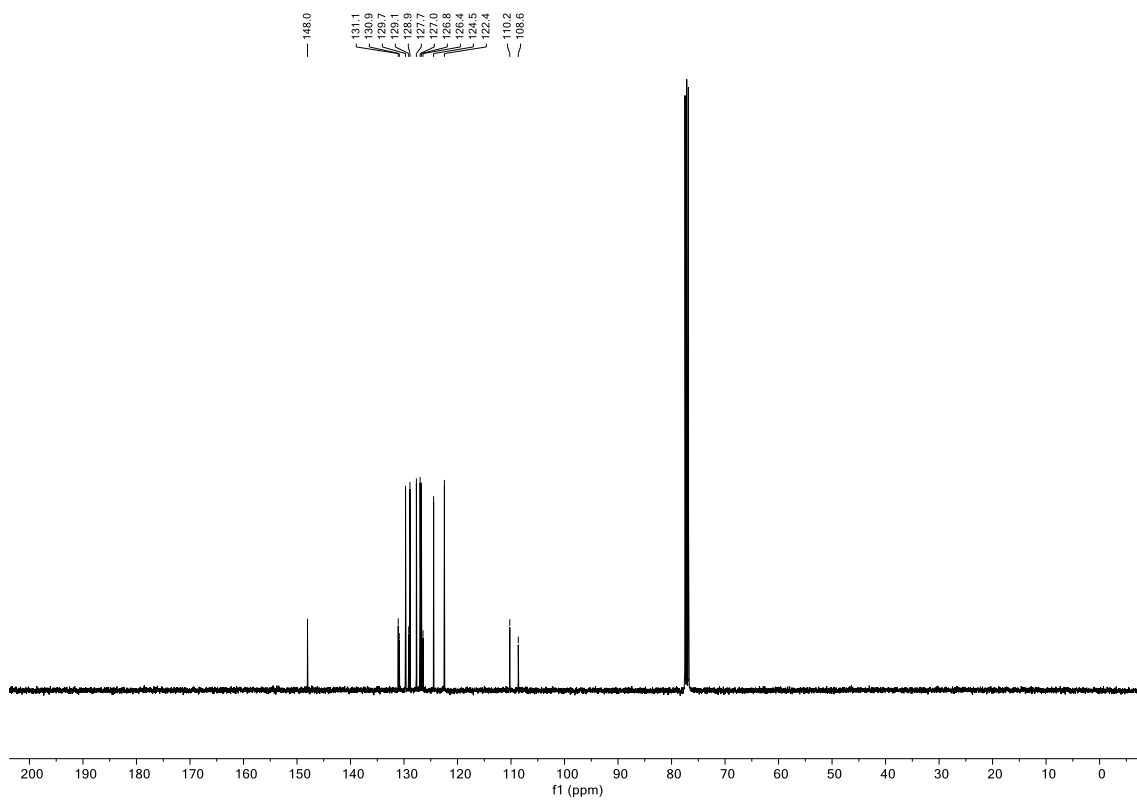
$^{13}\text{C}\{\text{H}\}$ NMR: (100 MHz, CDCl_3) **209**



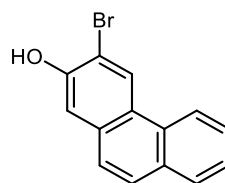
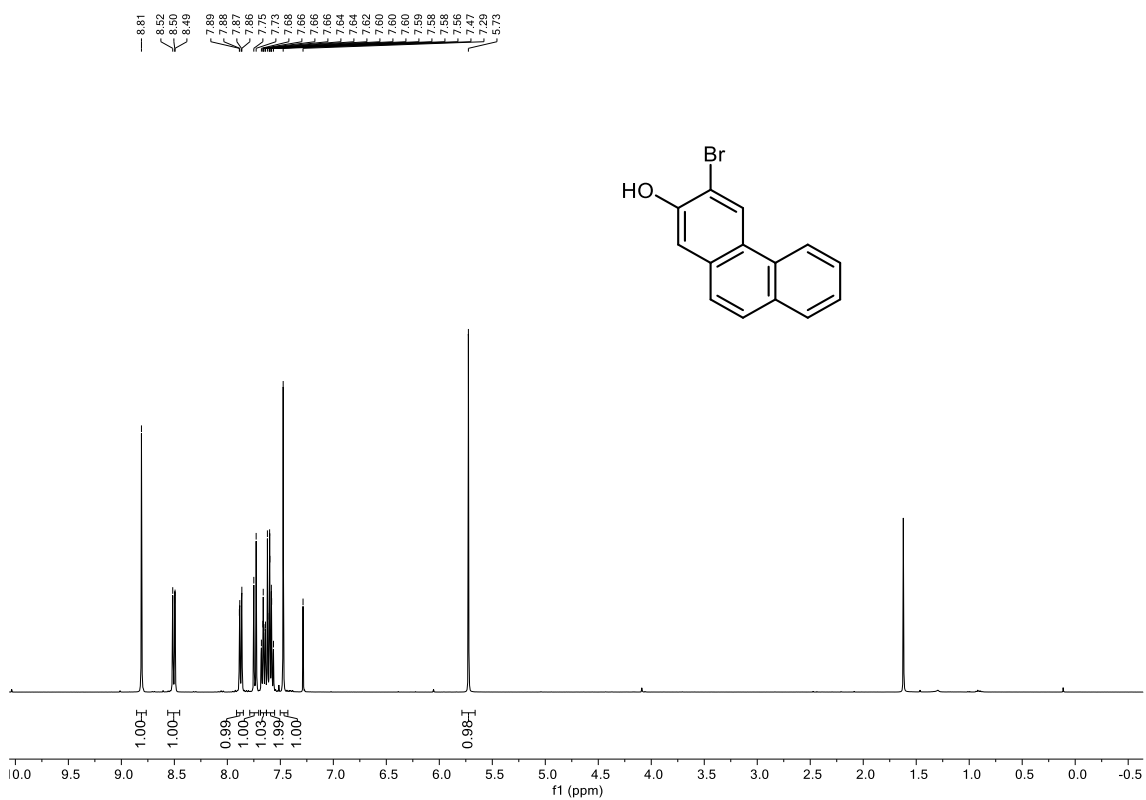
^1H NMR: (400 MHz, CDCl_3) **210**



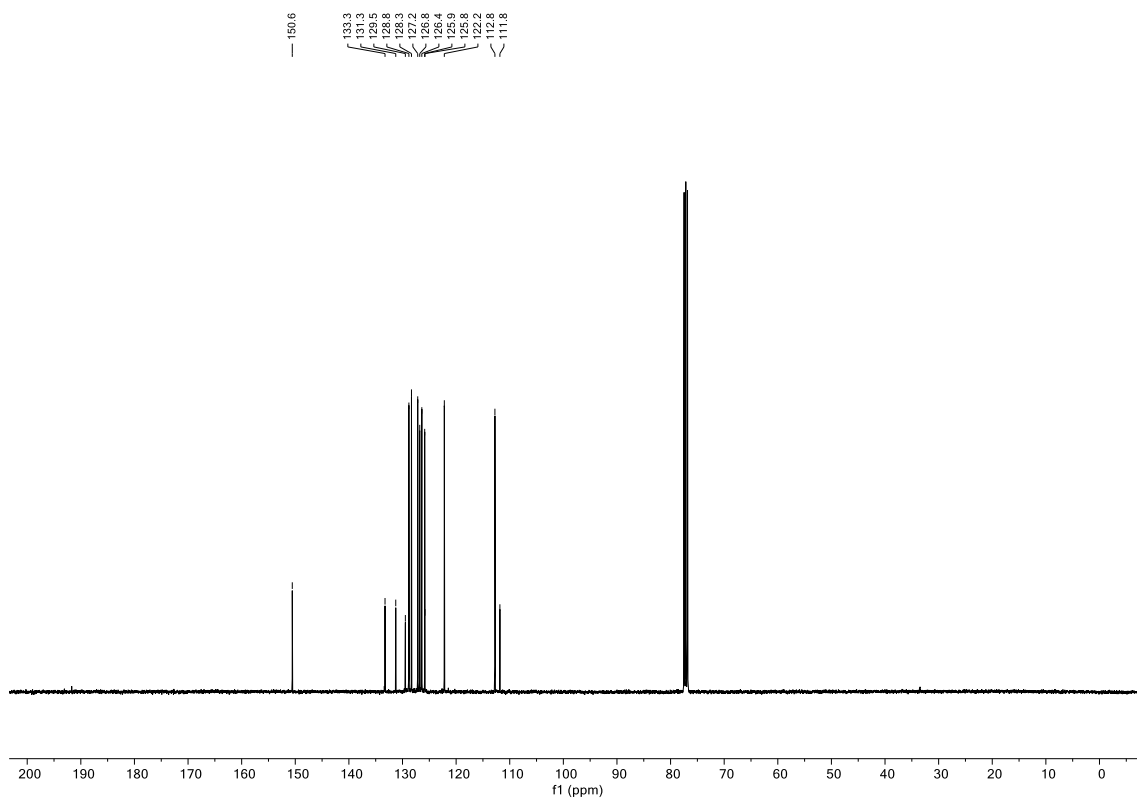
$^{13}\text{C}\{\text{H}\}$ NMR: (100 MHz, CDCl_3) **210**



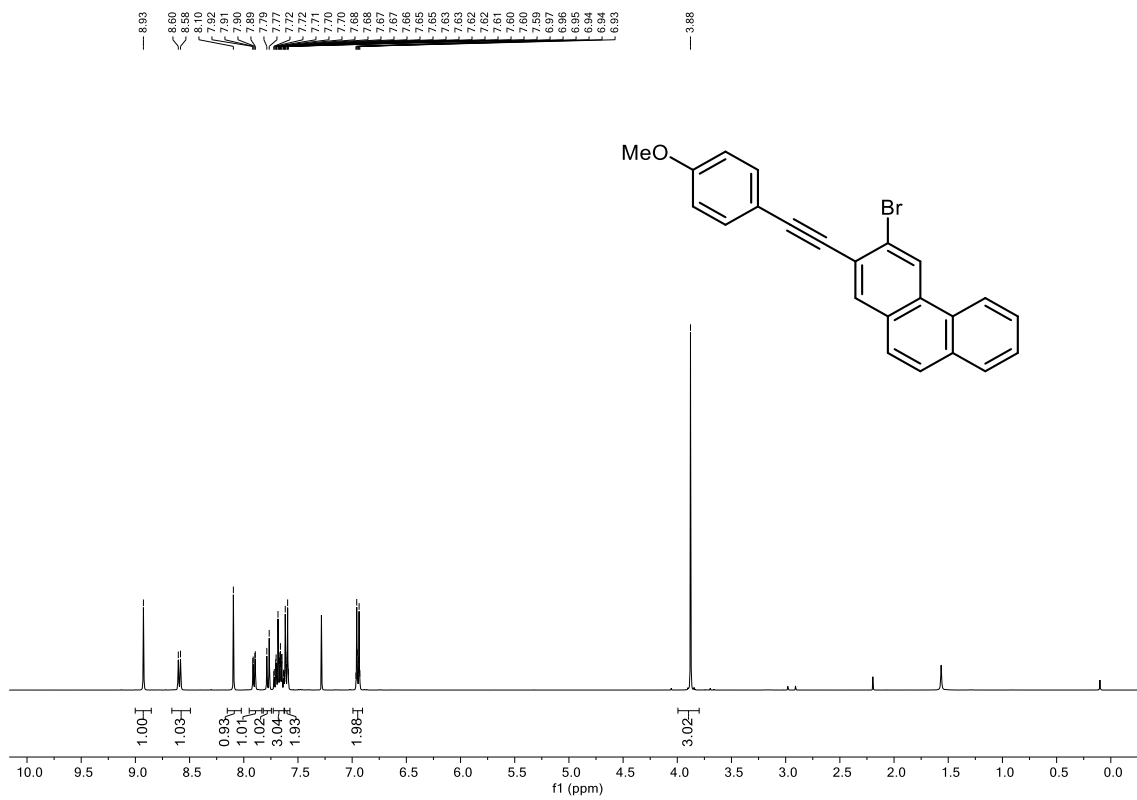
^1H NMR: (400 MHz, CDCl_3) **211**



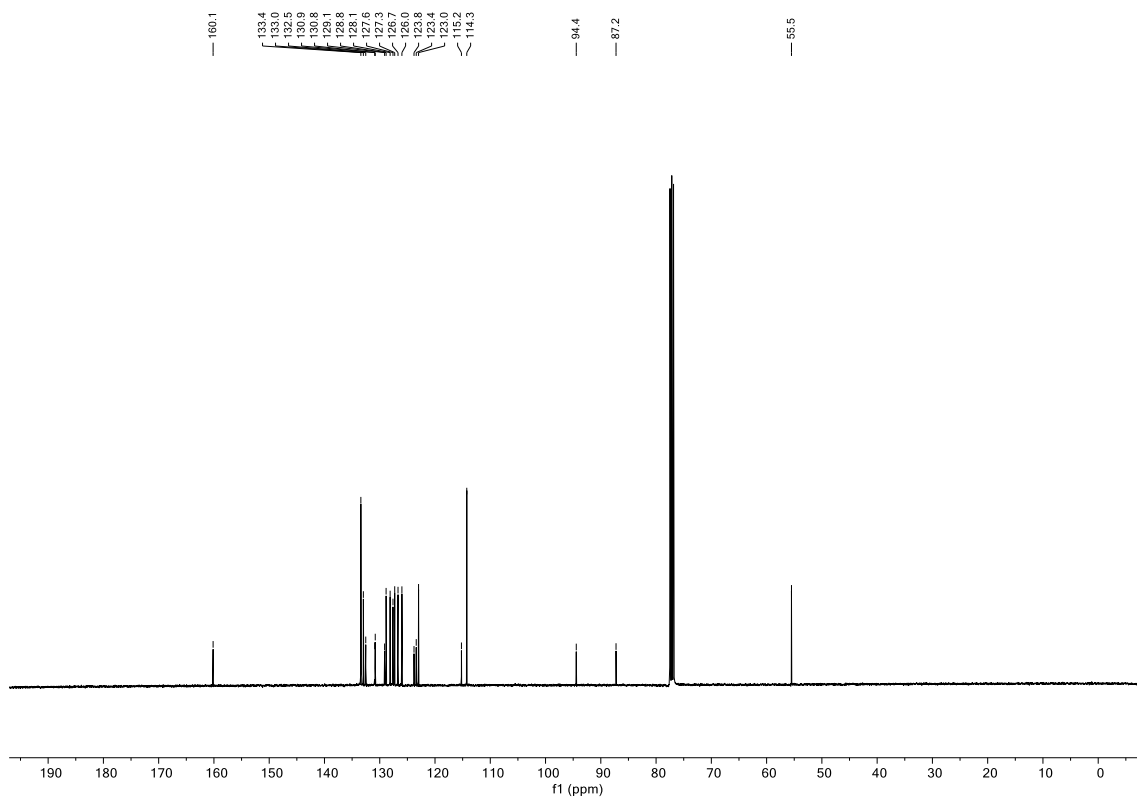
$^{13}\text{C}\{\text{H}\}$ NMR: (100 MHz, CDCl_3) **211**



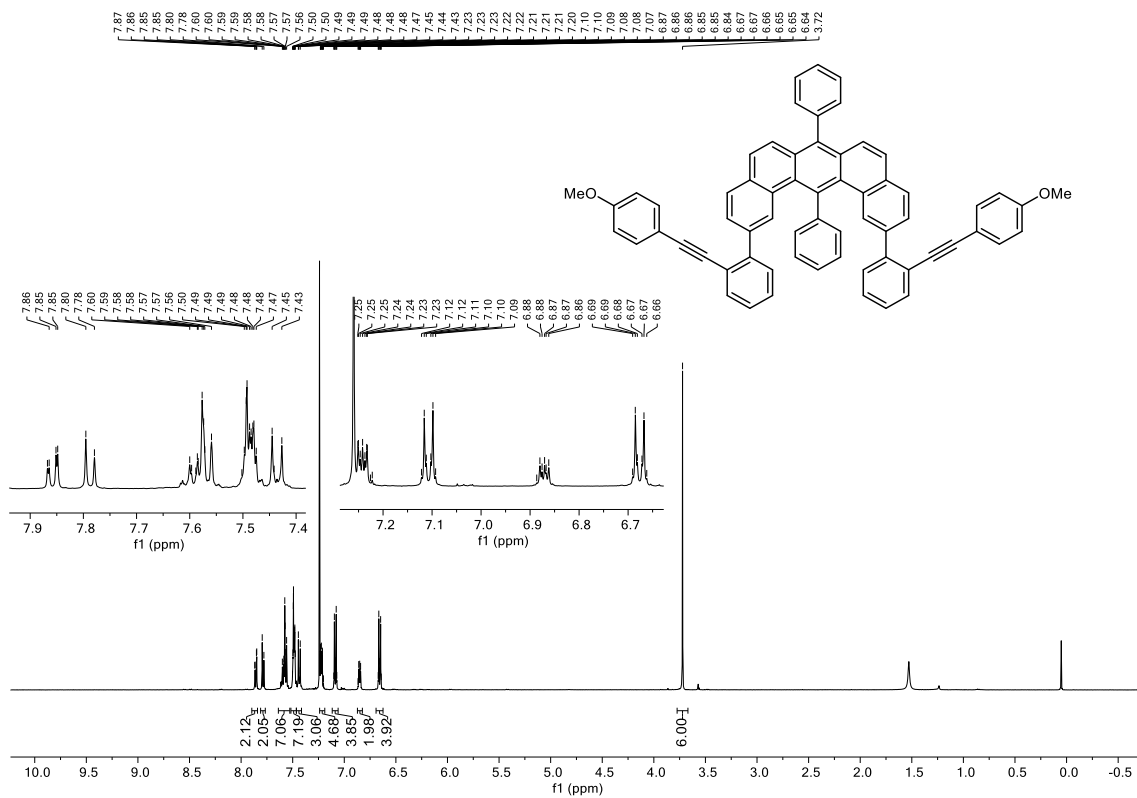
^1H NMR: (400 MHz, CDCl_3) **212**



$^{13}\text{C}\{\text{H}\}$ NMR: (100 MHz, CDCl_3) **212**

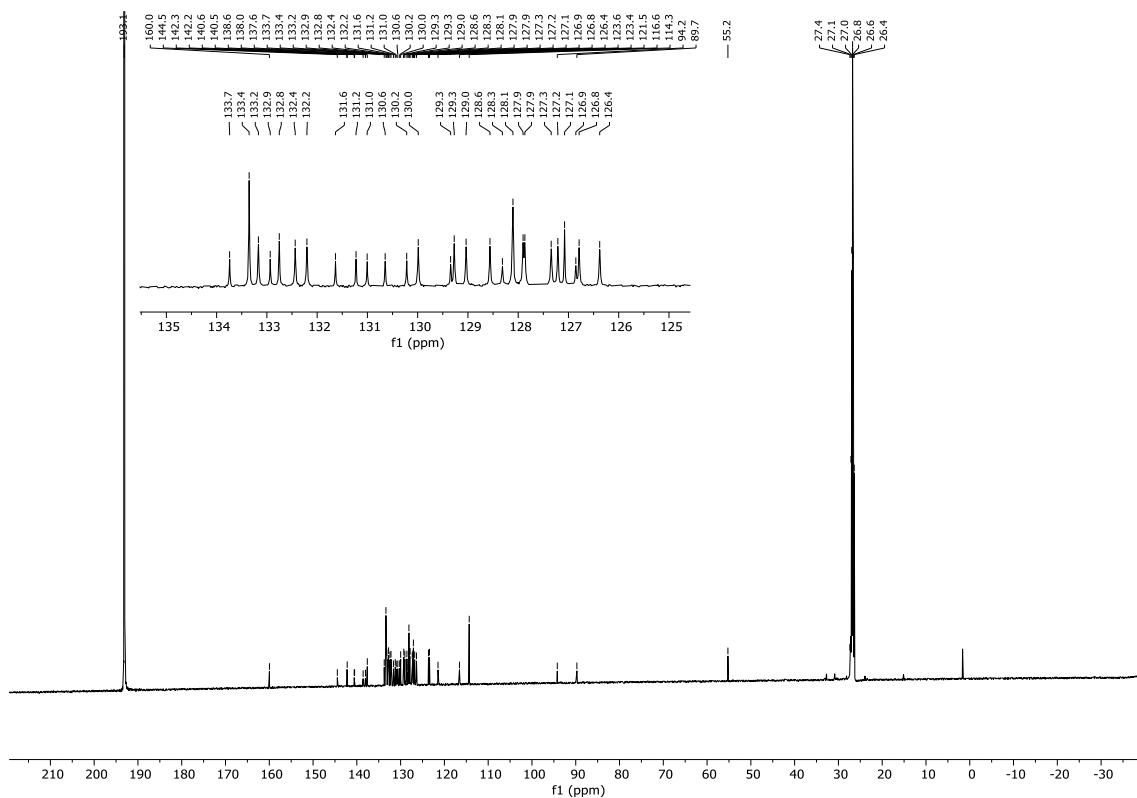


^1H NMR: (500 MHz, CDCl_3) **213**

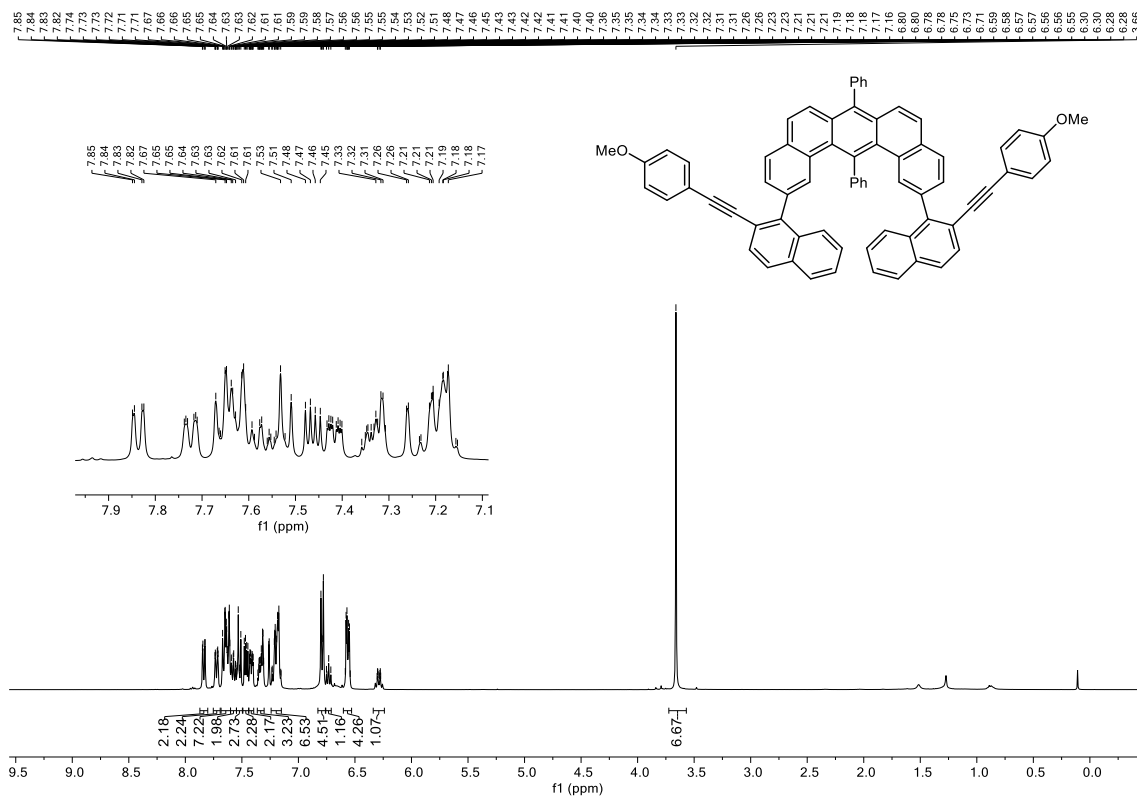


$^{13}\text{C}\{\text{H}\}$ NMR: (125 MHz, CDCl_3) **213**

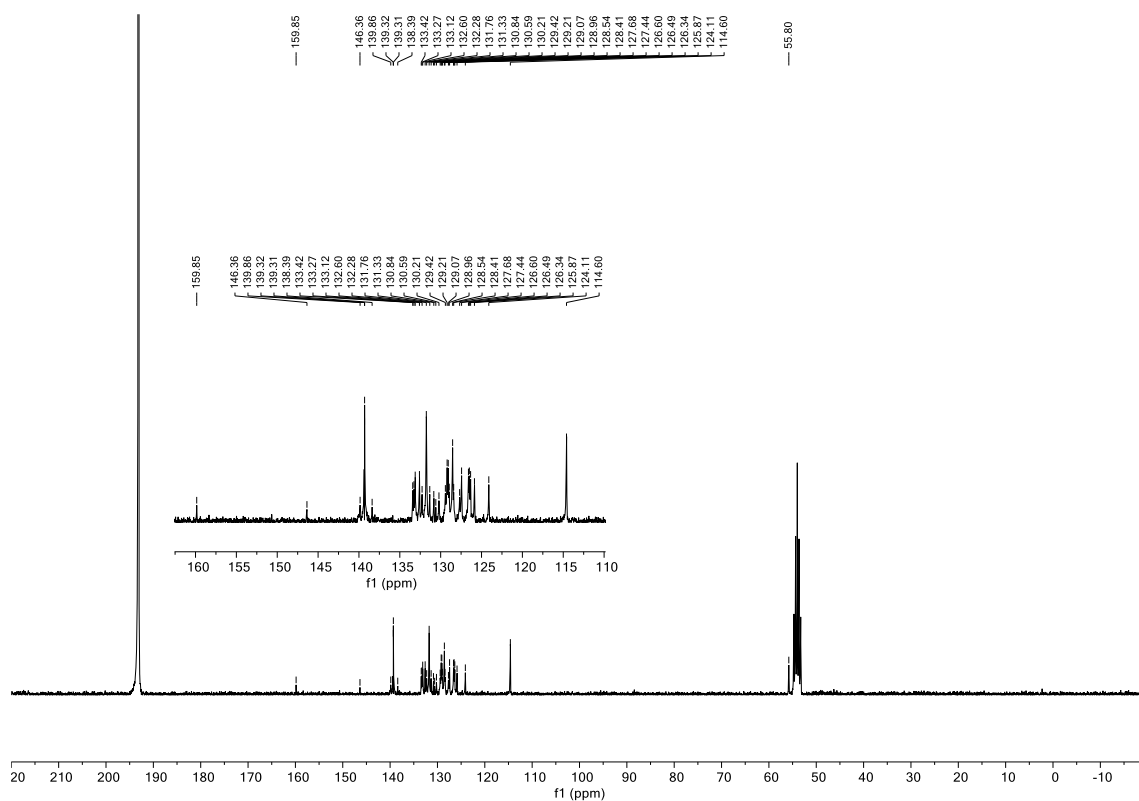
$^{13}\text{C}\{^1\text{H}\}$ NMR: (101 MHz, $\text{CS}_2:\text{C}_6\text{D}_{12}$ 5:1) **215**



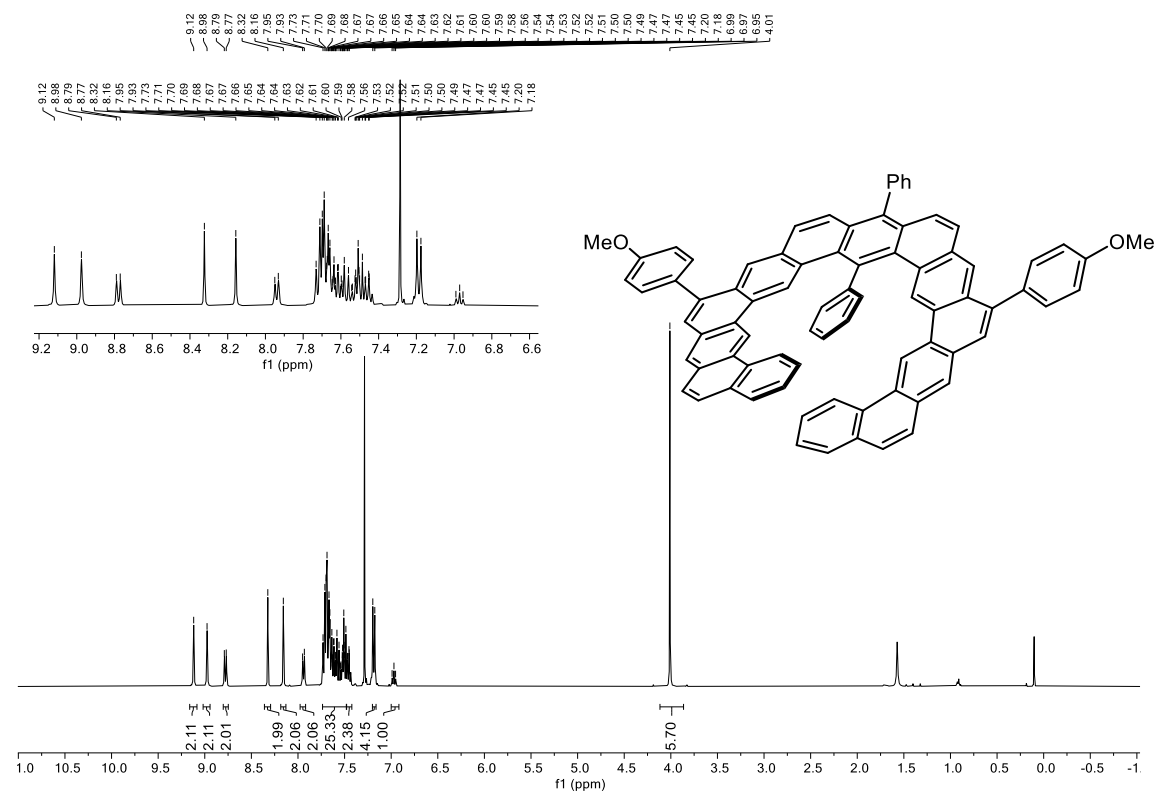
^1H NMR: (400 MHz, CDCl_3) **216**



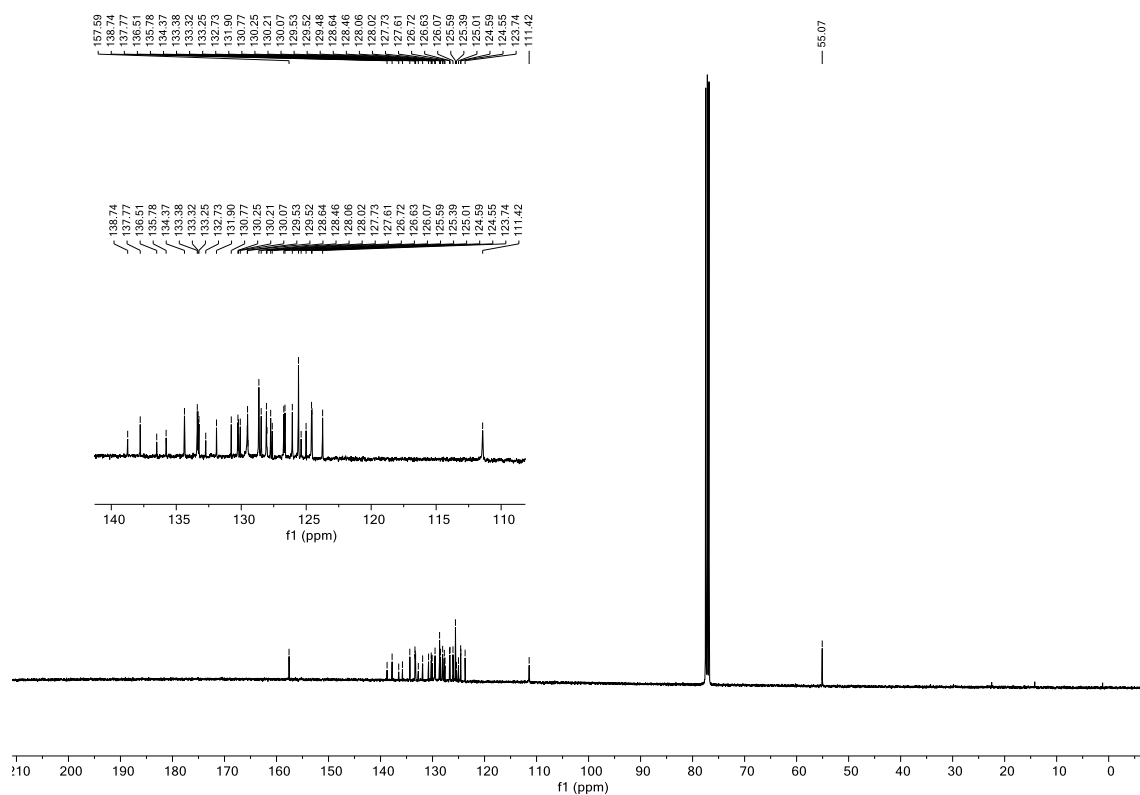
$^{13}\text{C}\{\text{H}\}$ NMR: (75 MHz, $\text{CS}_2:\text{CD}_2\text{Cl}_2$ 7:1) **166**



^1H NMR: (400 MHz, $\text{CS}_2:\text{CDCl}_3$ 5:1) **167**



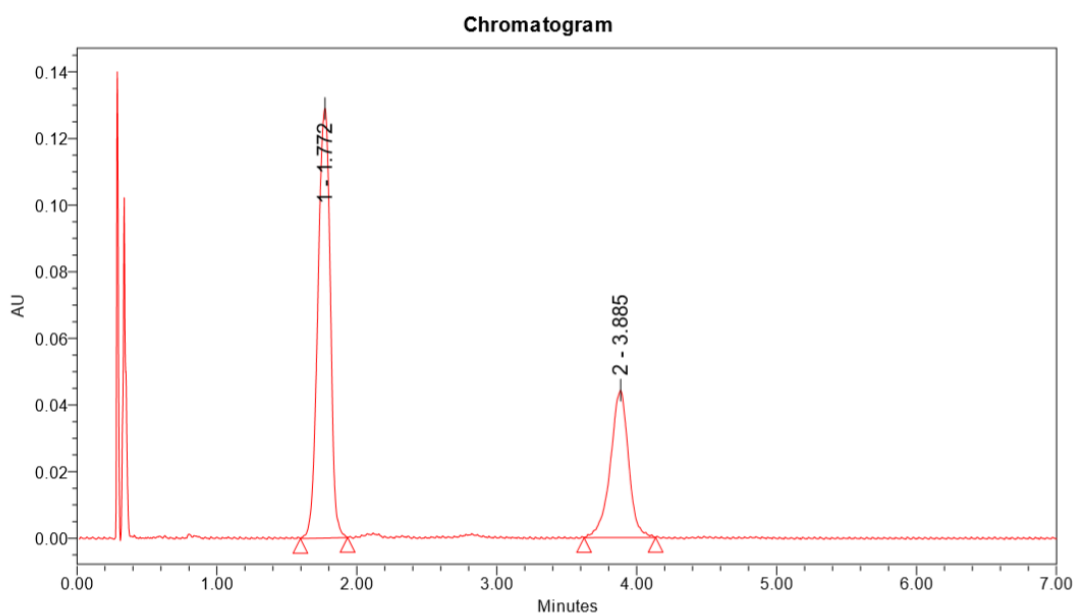
$^{13}\text{C}\{\text{H}\}$ NMR: (100 MHz, CDCl_3) **217b**



8.2. HPLC Chromatograms

163a with catalyst 147h, chiral separation, SFC

Sample: PA-RED-65endo



Component Results

	Name	RT	Area	Height	% Area
1	Enantiomer A	1.772	791904	128976	66.46
2	Enantiomer B	3.885	399610	44265	33.54

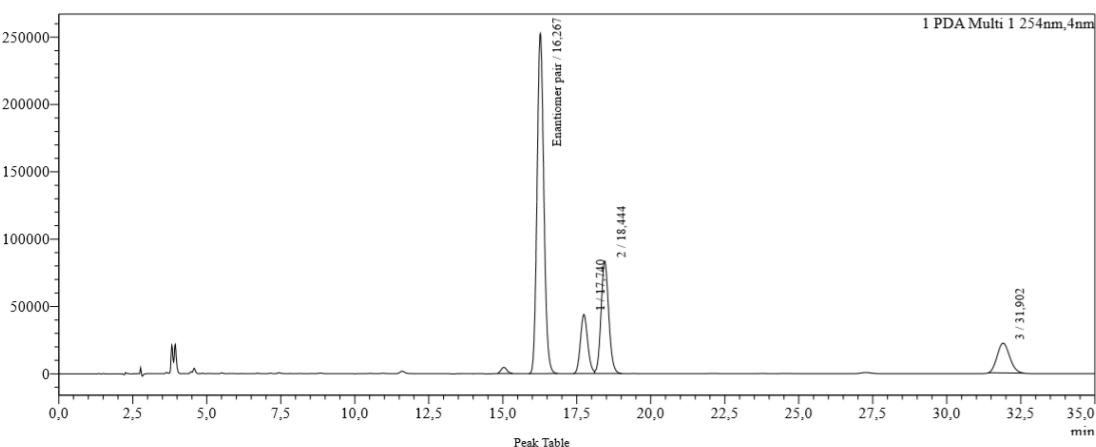
163a with catalyst 147h, achiral separation, HPLC

Injection Volume : 10
 Data File : PA-RED-65_MeCN-H2O_90-10_iso_1.0.lcd
 Method File : MeCN-H2O_90-10_iso_30m.lcm
 Comment : PA-RED-65 in MeCN-DCM 90-10
 MeCN-H2O 90-10, 30 min isocratic
 1.0 mL/min, 11.4 MPa, 295 K
 Zorbax SB-C18, 4.6x250mm, 3.5µm

Level# : 0

uAU

Chromatogram

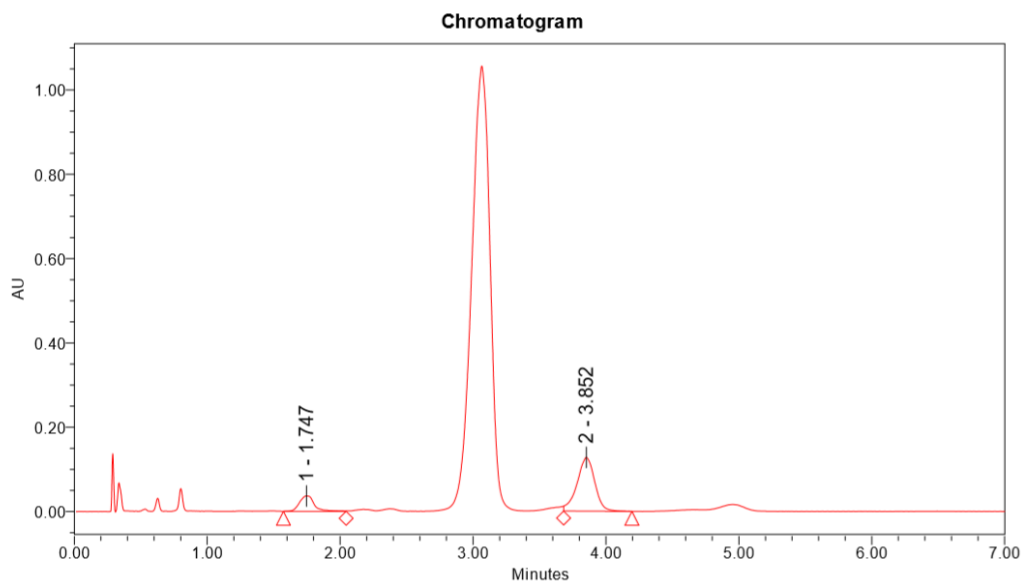


PDA Ch1 254nm

Peak#	Ret. Time	Area	Height	Area%
1	15.035	63771	4552	0.911
2	16.267	4027893	252783	57.526
3	17.740	752464	43928	10.747
4	18.444	1507236	83649	21.526
5	31.902	650531	22171	9.291
Total		7001894	407084	100.000

163a with catalyst 192a, chiral separation, SFC

Sample: PA-RED-135



Component Results

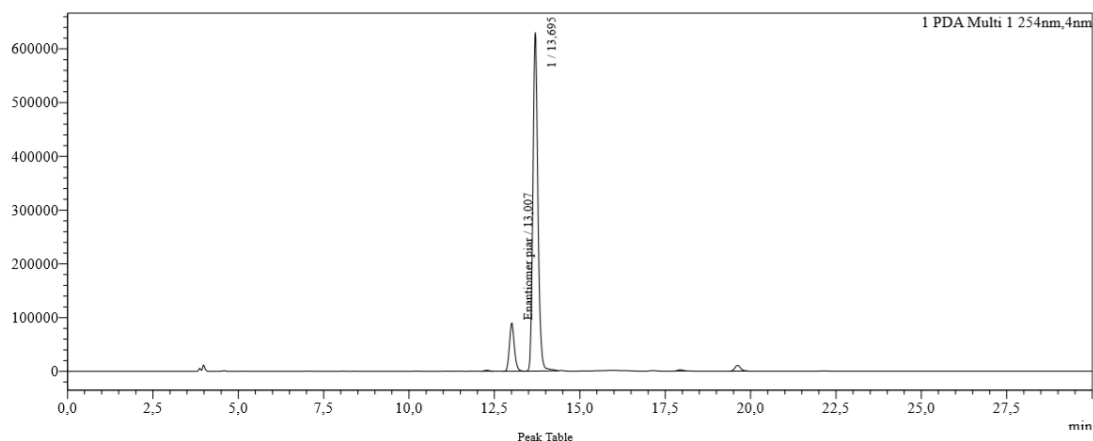
	Name	RT	Area	Height	% Area
1	Enantiomer A	1.747	283405	36396	19.34
2	Enantiomer B	3.852	1181923	127562	80.66

163a with catalyst 192a, achiral separation, HPLC

Injection Volume : 3
 Data File : PA-RED-135_MeCN-H2O_90-10_grad0-20m.lcd
 Method File : MeCN-H2O_90-10_grad0-20m.lcm
 Comment : PA-RED-135 in MeCN-DCM 90-10
 MeCN-H2O 90-10, gradient to 100-0 over 20 min
 1.0 mL/min, 295 K
 Zorbax SB-C18, 4.6x250mm, 3.5µm
 Level# : 0

uAU

Chromatogram

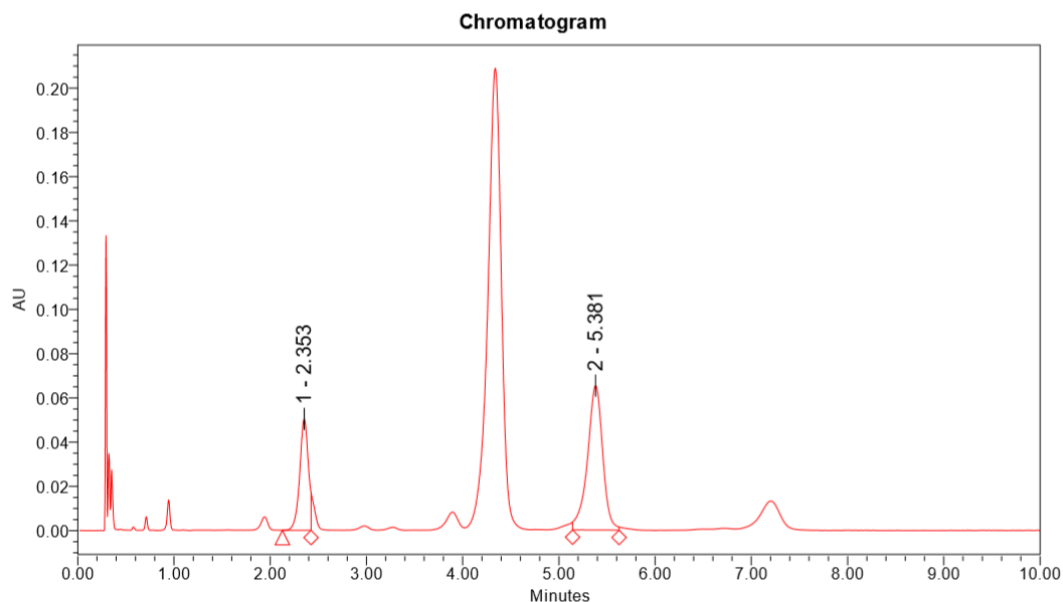


Peak Table

Peak#	Ret. Time	Area	Height	Area%
1	12.275	15962	1826	0.213
2	13.007	895252	89597	11.924
3	13.695	6450347	630587	85.910
4	17.940	22352	2212	0.298
5	19.618	124365	10541	1.656
Total		7508277	734764	100.000

163a with catalyst 192b, chiral separation, SFC

Sample: PA-RED-133



Component Results

	Name	RT	Area	Height	% Area
1	Enantiomer A	2.353	310292	50377	30.16
2	Enantiomer B	5.381	718442	65300	69.84

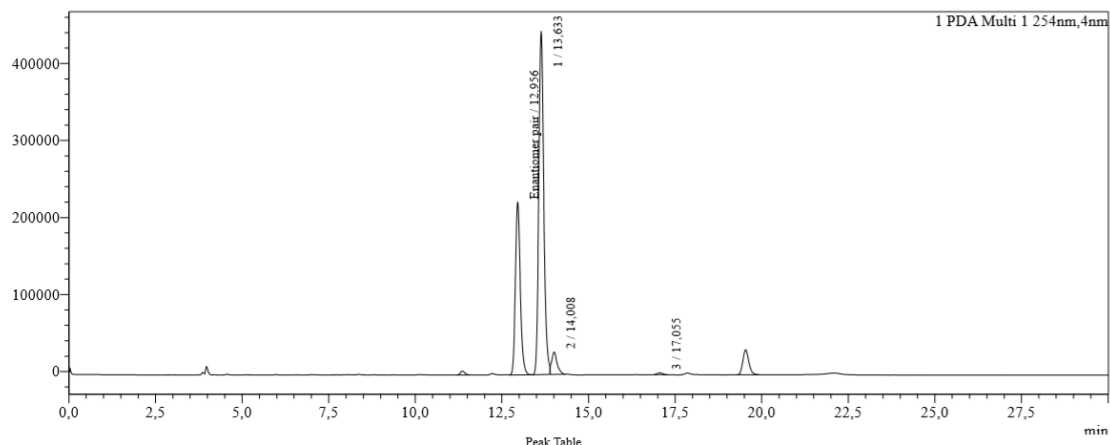
163a with catalyst 192b, achiral separation, HPLC

Injection Volume : 3
 Data File : PA-RED-133_MeCN-H2O_90-10_grad0-20m.lcd
 Method File : MeCN-H2O_90-10_grad0-20m.lcm
 Comment : PA-RED-133 in MeCN-DCM 90-10
 MeCN-H2O 90-10, gradient to 100-0 over 20 min
 1.0 mL/min, 295 K
 Zorbax SB-C18, 4.6x250mm, 3.5µm

Level# : 0

uAU

Chromatogram

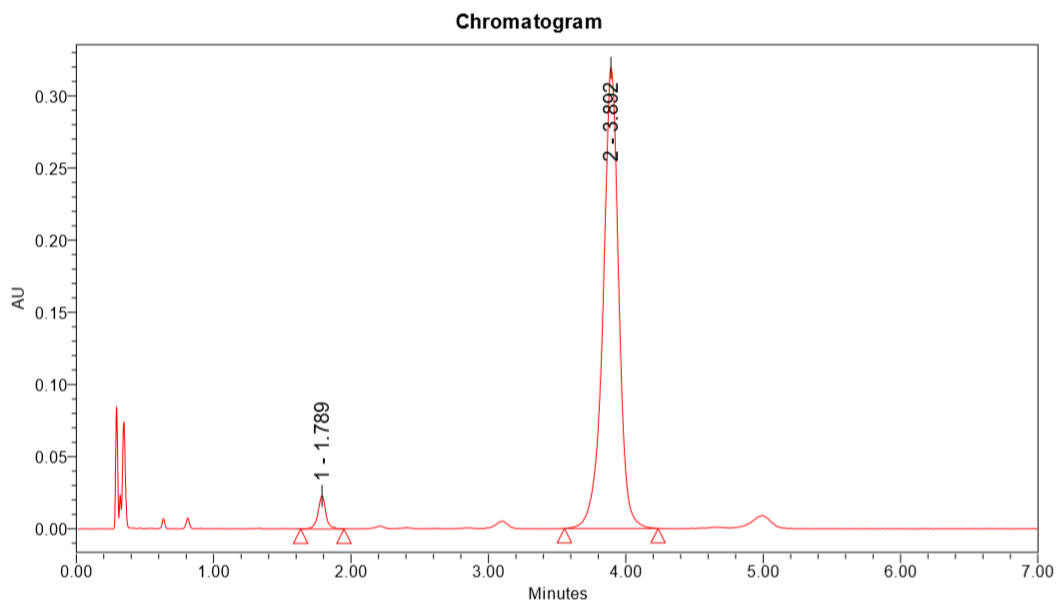


PDA Ch1 254nm

Peak#	Ret. Time	Area	Height	Area%
1	13.661	43890	4971	0.591
2	12.956	2202571	224076	29.655
3	13.633	4449282	446150	59.904
4	14.008	317014	28946	4.268
5	17.055	25558	2410	0.344
6	19.536	388987	32579	5.237
Total		7427301	739131	100.000

163a with catalyst 193a, chiral separation, SFC

Sample: PA-RED-141

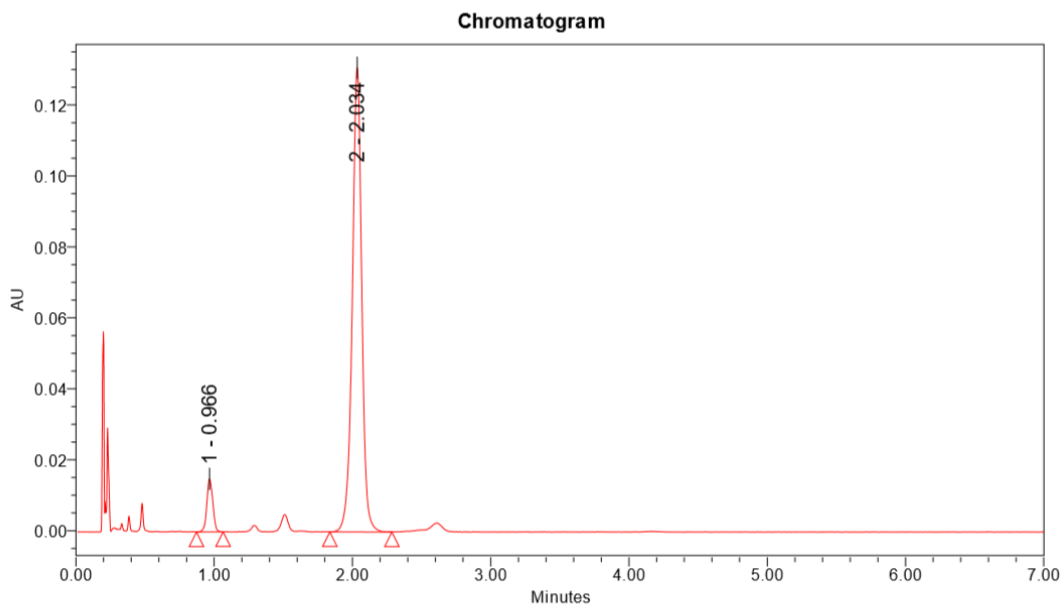


Component Results

	Name	RT	Area	Height	% Area
1	Enantiomer A	1.789	93133	23045	3.53
2	Enantiomer B	3.892	2545054	319217	96.47

163a with catalyst 193b, chiral separation, SFC

Sample: PA-RED-232_IA3-IPA35



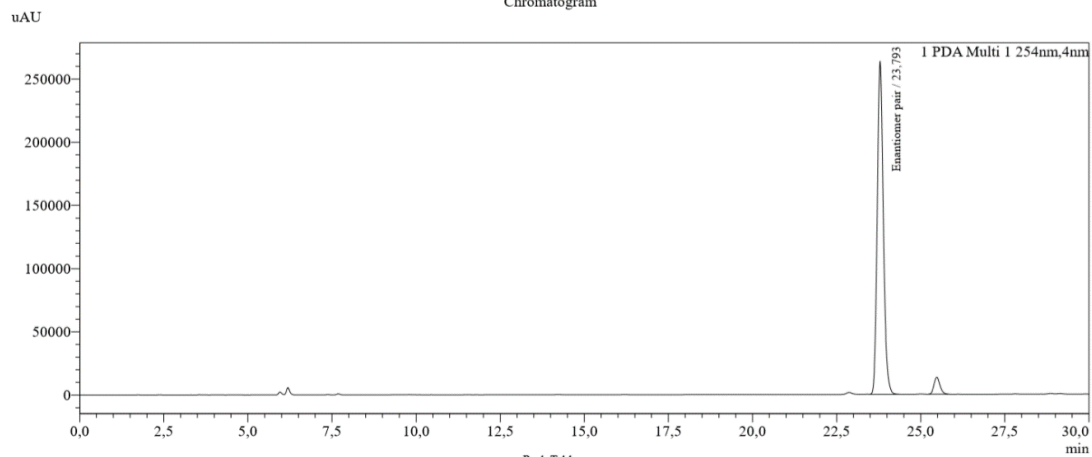
Component Results

	Name	RT	Area	Height	% Area
1	Enantiomer A	0.966	45331	14964	6.79
2	Enantiomer B	2.034	621992	130874	93.21

163a with catalyst 193b, achiral separation, HPLC

Injection Volume : 10
 Data File : PA-RED-232_MeCN-H2O_80-20_grad0-30m.lcd
 Method File : MeCN-H2O_80-20_grad0-30m.lcm
 Comment : PA-RED-232 in MeCN-DCM 90-10
 MeCN-H2O 80-20, gradient to 100-0 over 30 min
 1.0 mL/min, 295 K
 Zorbax SB-C18, 4.6x250mm, 3.5µm

Level# : 0
 Chromatogram

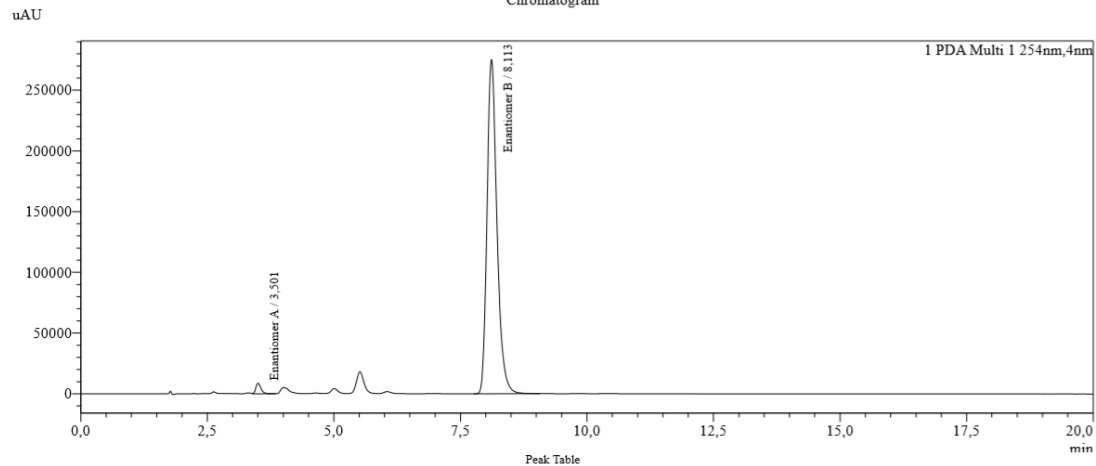


Peak#	Ret. Time	Area	Height	Area%
1	23.793	3311241	263350	93.464
2	25.477	166457	13409	4.698
3	32.174	65085	5281	1.837
Total		3542783	282040	100.000

163a with catalyst 193c, chiral separation, HPLC

Injection Volume : 5
 Data File : GU-ZIC-175_Hex-IPA_95-5_IA-3.lcd
 Method File : IA-3_Hex-IPA_95-5_25C_20m.lcm
 Comment : GU-ZIC-175 in Hex-DCM 90-10
 Hex-IPA 97-3, 20 min isocratic
 1.0 mL/min, 298 K
 IA-3, 4.6x150mm, 3µm

Level# : 0
 Chromatogram



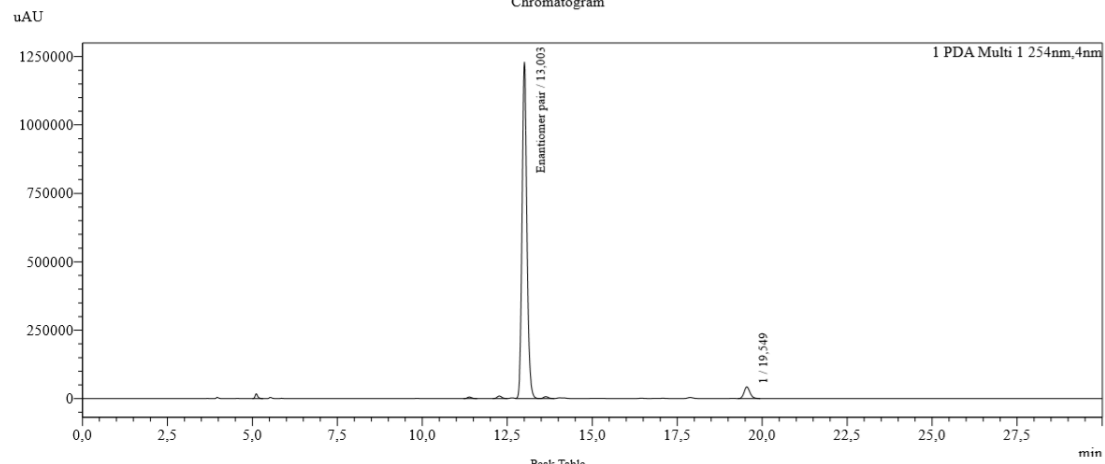
Peak#	Ret. Time	Area	Height	Area%
1	3.501	61694	8679	1.615
2	8.113	375821	275162	98.385
Total		3820314	283841	100.000

163a with catalyst 193c, achiral separation, HPLC

Injection Volume : 5
 Data File : GU-ZIC-175_MeCN-H2O_90-10_grad0-20m.lcd
 Method File : MeCN-H2O_90-10_grad0-20m.lcm
 Comment : GU-ZIC-175 in MeCN-DCM 90-10
 MeCN-H2O 90-10, gradient to 100-0 over 20 min
 1.0 mL/min, 295 K
 Zorbax SB-C18, 4.6x250mm, 3.5µm

Level# : 0

Chromatogram



PDA Ch1 254nm

Peak#	Ret. Time	Area	Height	Area%
1	5.113	97461	17503	0.750
2	11.387	49257	5541	0.379
3	12.266	85854	9197	0.660
4	13.003	12190138	1230197	93.753
5	13.632	63431	6721	0.503
6	19.549	514192	42973	3.955
Total		13002334	1312134	100.000

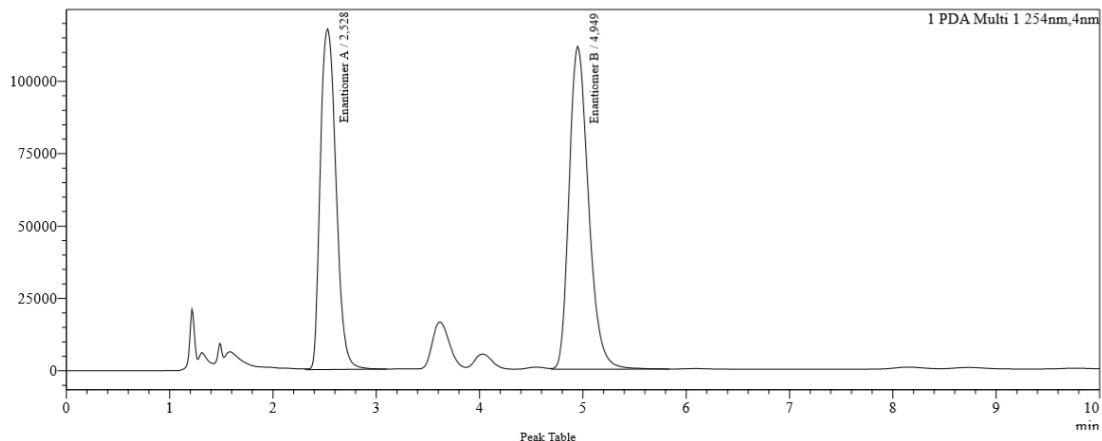
163a with catalyst 193d, chiral separation, HPLC

Injection Volume : 10
 Data File : PA-RED-241-clean_Hex-IPA_90-10_IG-U.lcd
 Method File : IG-U_Hex-IPA_90-10_25C_15m.lcm
 Comment : PA-RED-241-clean in Hex-DCM 90-10
 Hex-IPA 90-10, 15 min isocratic
 0.425 mL/min, 298 K
 IG-U, 3.0x100mm, 1.6µm

Level# : 0

uAU

Chromatogram



Peak#	Ret. Time	Area	Height	Area%
1	2.528	1243517	117739	46.052
2	4.949	1456747	111555	53.948
Total		2700264	229294	100.000

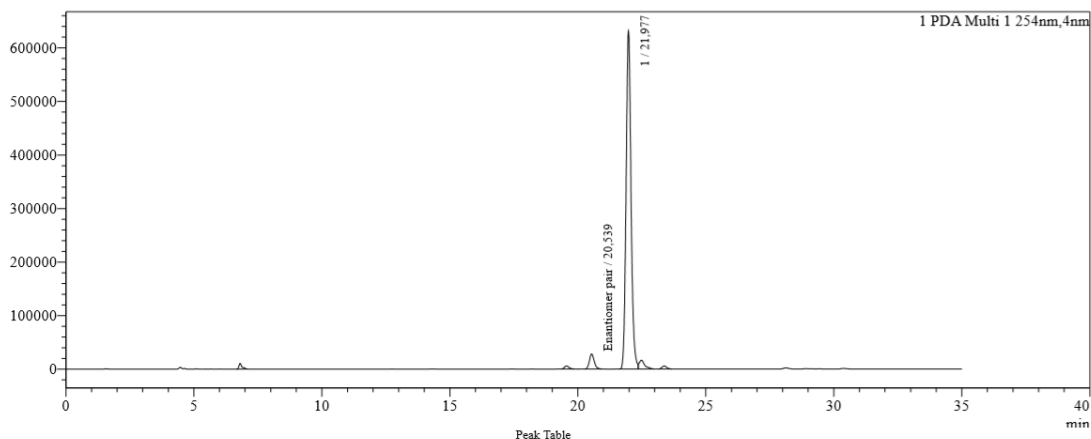
163a with catalyst 193d, achiral separation, HPLC

Injection Volume : 5
 Data File : PA-RED-241_MeCN-H2O_85-15_h5grad0-30m.lcd
 Method File : PA-RED-241.lcm
 Comment : PA-RED-241 in MeCN-DCM 90-10
 MeCN-H2O 85-15 5 min, gradient to 100-0 over 30 min
 1.0 mL/min, 295 K
 Zorbax SB-C18, 4.6x250mm, 3.5µm

Level# : 0

uAU

Chromatogram

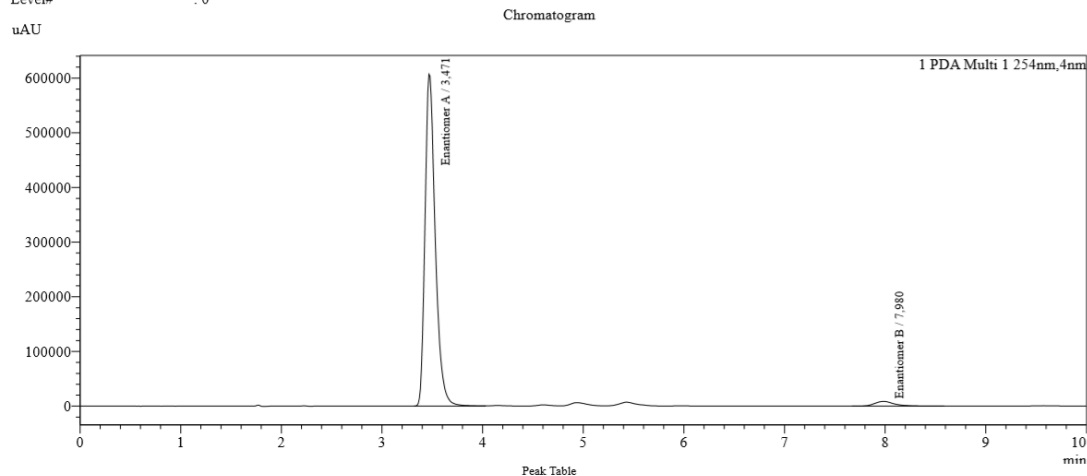


Peak#	Ret. Time	Area	Height	Area%
1	6.805	90142	10841	0.969
2	19.561	69237	5651	0.745
3	20.539	369082	27987	3.966
4	21.977	8463178	631757	90.938
5	22.484	243855	16390	2.620
6	23.373	70918	5651	0.762
Total		9306503	698278	100.000

163a with catalyst 193e, chiral separation, HPLC

Injection Volume : 5
 Data File : PA-RED-93_Hex-IPA_95-5_IA-3.lcd
 Method File : IA-3_Hex-IPA_95-5_25C_20m.lcm
 Comment : PA-RED-93 in Hex-DCM 90-10
 Hex-IPA 95-5, 20 min isocratic
 1.0 mL/min, 298 K
 IA-3, 4.6x150mm, 3µm

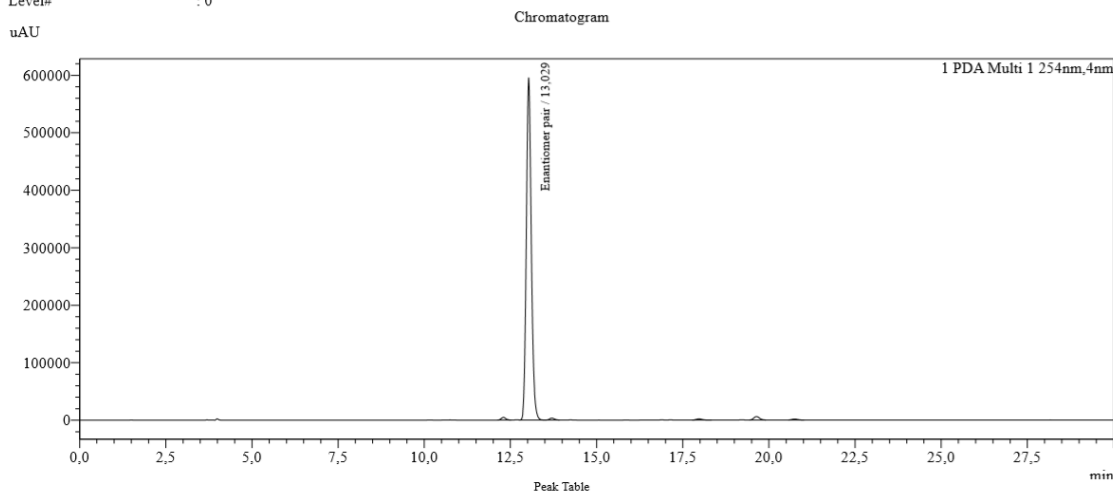
Level# : 0



163a with catalyst 193e, achiral separation, HPLC

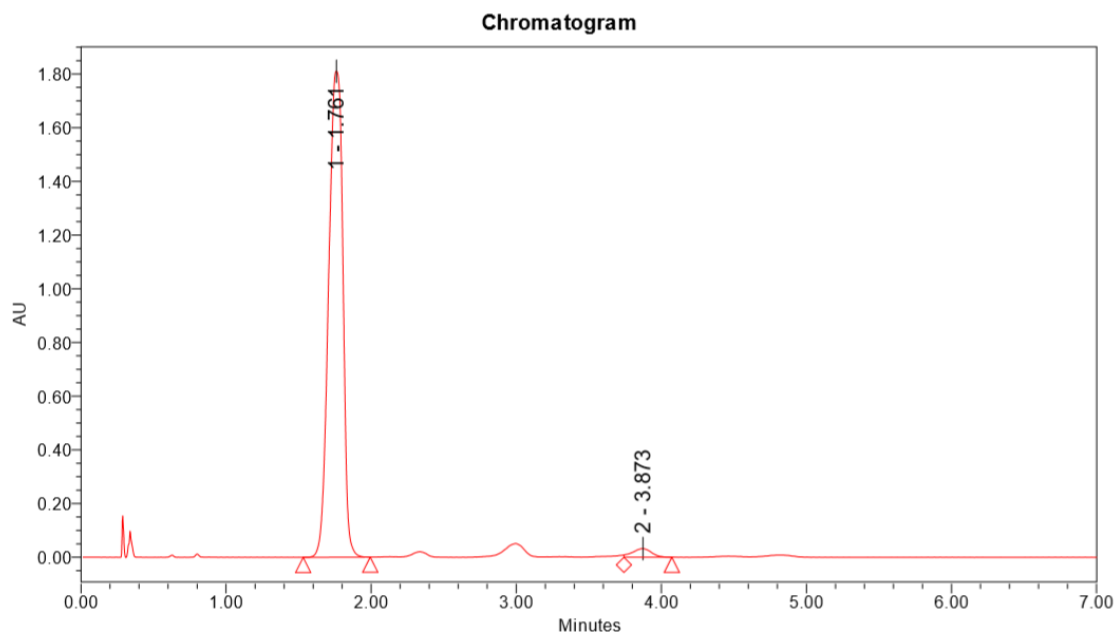
Injection Volume : 5
 Data File : PA-RED-93_MeCN-H2O_90-10_grad0-20m.lcd
 Method File : MeCN-H2O_90-10_grad0-20m.lcm
 Comment : PA-RED-93 in MeCN-DCM 90-10
 MeCN-H2O 90-10, gradient to 100-0 over 20 min
 1.0 mL/min, 295 K
 Zorbax SB-C18, 4.6x250mm, 3.5µm

Level# : 0



163a with catalyst **193f**, chiral separation, SFC

Sample: PA-RED-92crude

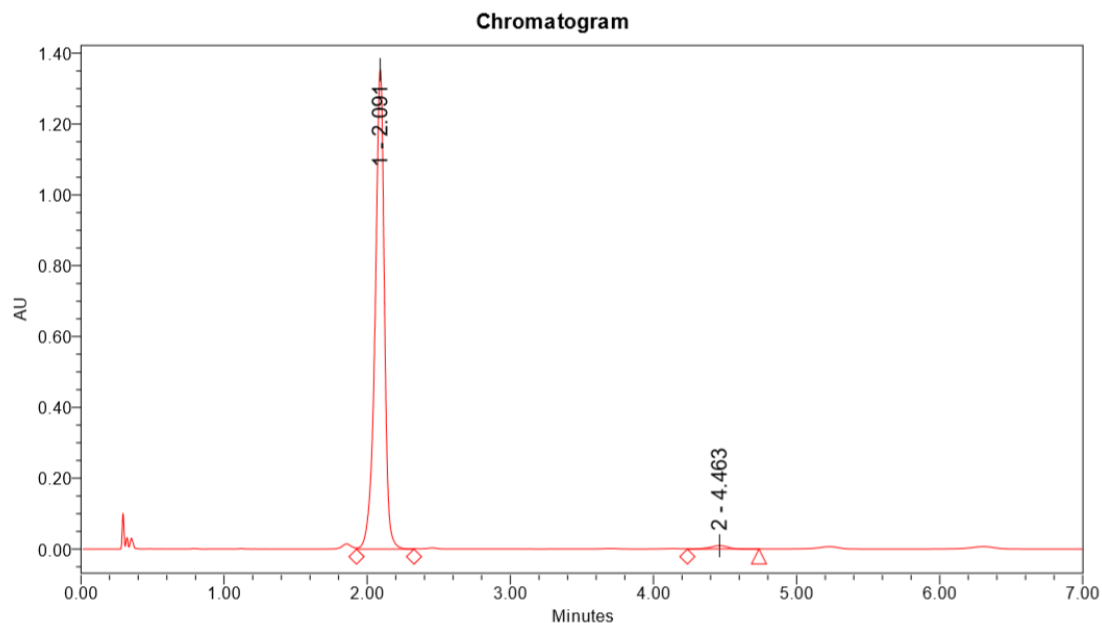


Component Results

	Name	RT	Area	Height	% Area
1	Enantiomer A	1.761	12289077	1810449	97.69
2	Enantiomer B	3.873	290641	32142	2.31

163b, chiral separation, SFC

Sample: PA-RED-113crude



Component Results

	Name	RT	Area	Height	% Area
1	Enantiomer A	2.091	6074414	1353799	98.57
2	Enantiomer B	4.463	88074	9695	1.43

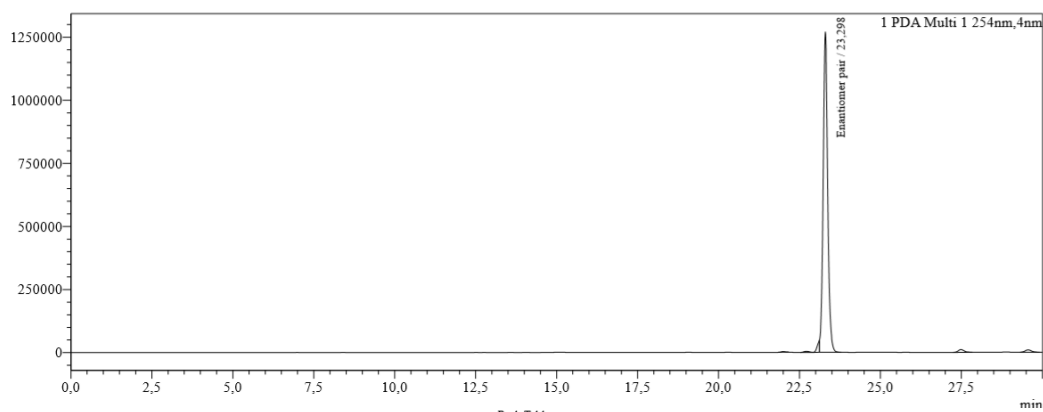
163b, achiral separation, HPLC

Injection Volume : 7
 Data File : PA-RED-113_MeCN-H2O_80-20_grad0-20m.lcd
 Method File : MeCN-H2O_80-20_grad0-20m.lcm
 Comment : PA-RED-113 in MeCN-DCM 90-10
 MeCN-H2O 80-20, gradient to 100-0 over 20 min
 1.0 mL/min, 295 K
 Zorbax SB-C18, 4.6x250mm, 3.5µm

Level# : 0

uAU

Chromatogram

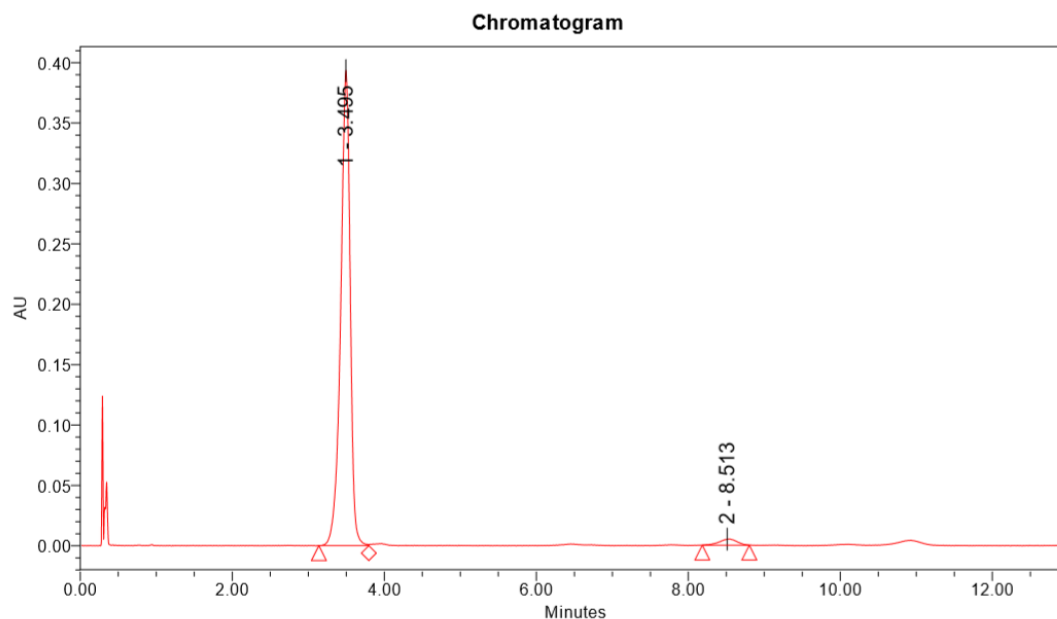


PDA Ch1 254nm

Peak#	Ret. Time	Area	Height	Area%
1	21.999	21252	2558	0.169
2	22.714	46066	4156	0.338
3	23.109	218243	44584	1.698
4	23.298	12293895	1270696	95.675
5	27.488	138358	10983	1.077
6	29.560	131366	9389	1.022
Total		12821680	1342166	100.000

163c, chiral separation, SFC

Sample: PA-RED-131



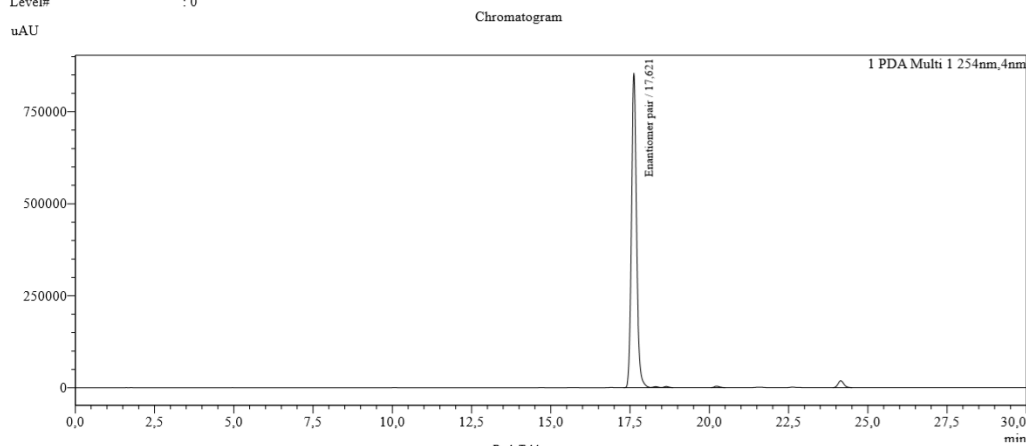
Component Results

	Name	RT	Area	Height	% Area
1	Enantiomer A	3.495	3416228	393358	97.63
2	Enantiomer B	8.513	82777	5104	2.37

163c, achiral separation, HPLC

Injection Volume : 5
 Data File : PA-RED-131crude_MeCN-H2O_90-10_grad0-20m.lcd
 Method File : PA-RED-131.lcm
 Comment : PA-RED-131crude in MeCN-DCM
 MeCN-H2O 90-10, gradient to 100-0 over 20 min
 1.0 mL/min, 295 K
 Zorbax SB-C18, 4.6x250mm, 3.5µm

Level# : 0

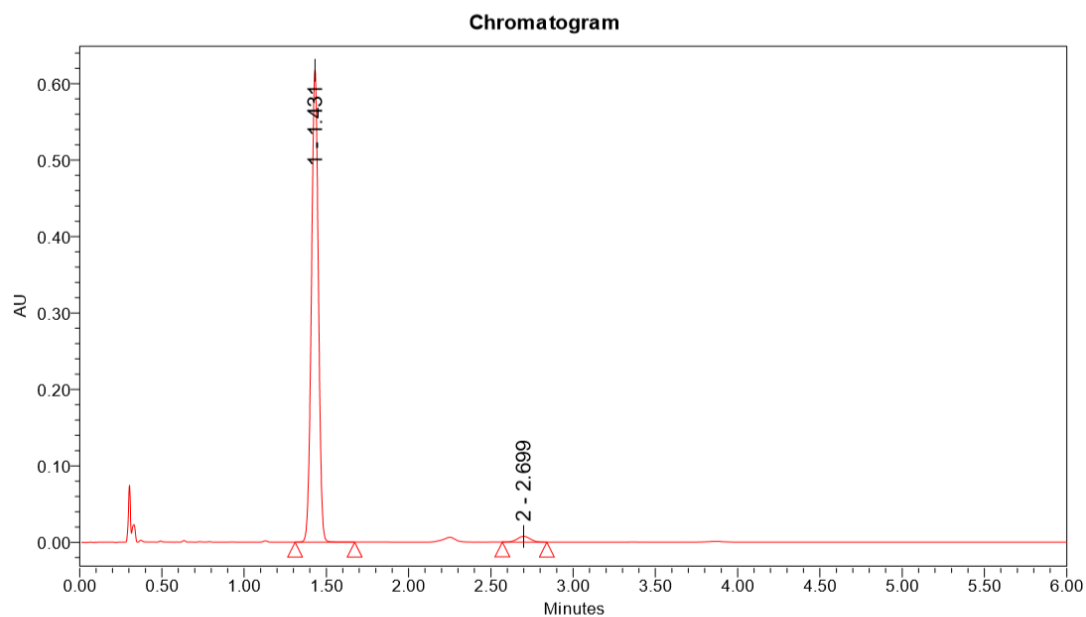


Peak Table

Peak#	Ret. Time	Area	Height	Area%
1	17.621	9551002	854990	96.481
2	18.208	30709	2738	0.310
3	18.644	32121	3163	0.324
4	20.731	45153	4003	0.456
5	24.146	240349	19938	2.428
Total		9899333	883881	100.000

163d, chiral separation, SFC

Sample: PA-RED-171



Component Results

	Name	RT	Area	Height	% Area
1	Enantiomer A	1.431	1809636	617956	97.74
2	Enantiomer B	2.699	41891	7543	2.26

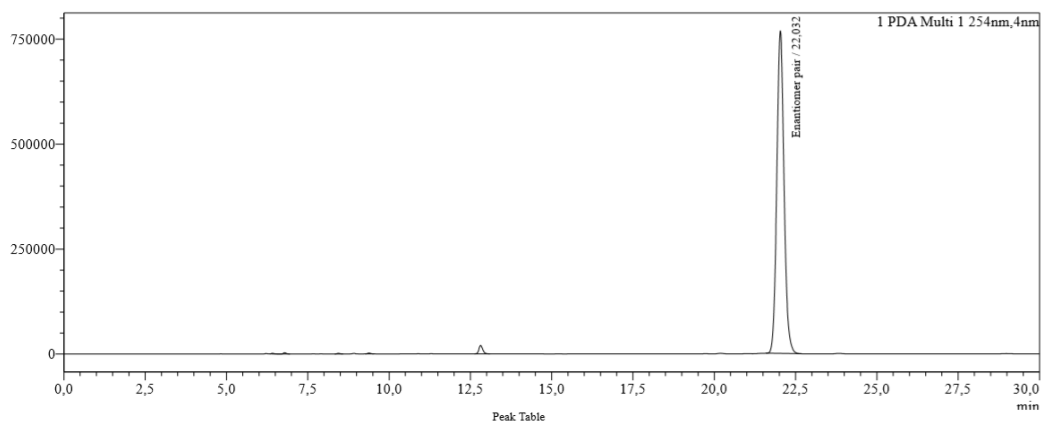
163d, achiral separation, HPLC

Injection Volume : 5
 Data File : PA-RED-171crude_MeCN-H2O_90-10_grad0-10m.lcd
 Method File : PA-RED-171.lcm
 Comment : PA-RED-171crude in MeCN-DCM
 MeCN-H2O 90-10, gradient to 100-0 over 10 min
 1.0 mL/min, 295 K
 Zorbax SB-C18, 4.6x250mm, 3.5µm

Level# : 0

uAU

Chromatogram

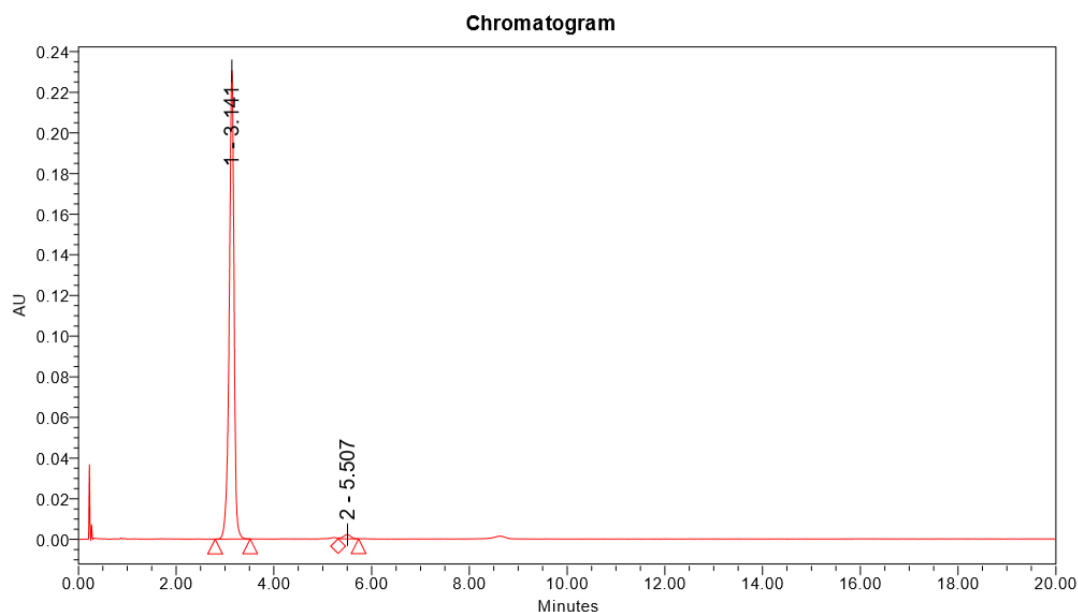


PDA Ch1 254nm

Peak#	Ret. Time	Area	Height	Area%
1	6.412	8562	1517	0.071
2	6.788	17794	3013	0.147
3	8.443	10149	1601	0.084
4	9.379	14047	2039	0.116
5	12.816	165157	20030	1.363
6	22.032	11898124	767750	98.219
Total		12113833	795951	100.000

163e, chiral separation, SFC

Sample: PA-RED-207_IA3-IPA25



Component Results

	Name	RT	Area	Height	% Area
1	Enantiomer A	3.141	1576452	230579	98.56
2	Enantiomer B	5.507	23046	2076	1.44

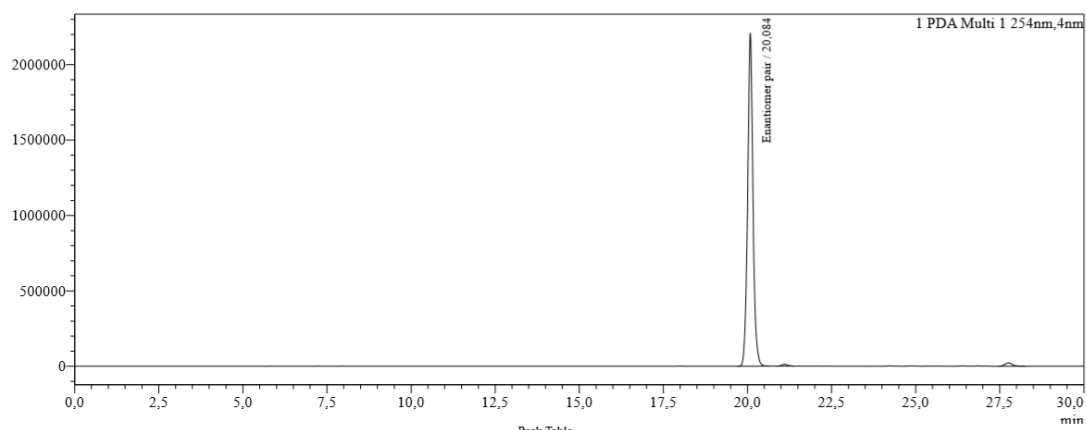
163e, achiral separation, HPLC

Injection Volume : 10
 Data File : PA-RED-207_MeCN-H2O_90-10_grad0-20m.lcd
 Method File : MeCN-H2O_90-10_grad0-20m.lcm
 Comment : PA-RED-207 in MeCN-DCM 90-10
 MeCN-H2O 90-10, gradient to 100-0 over 20 min
 1.0 mL/min, 295 K
 Zorbax SB-C18, 4.6x250mm, 3.5µm

Level# : 0

uAU

Chromatogram

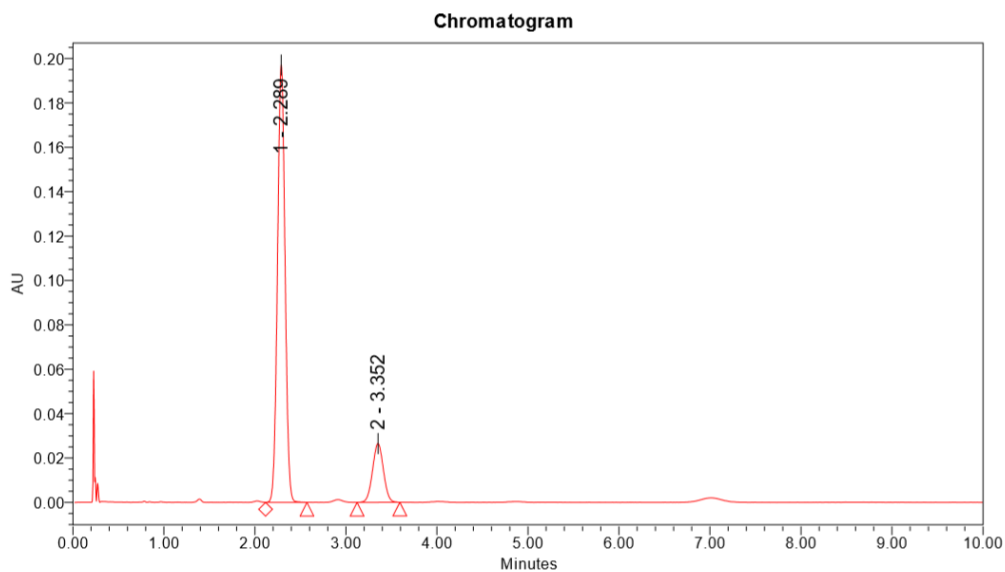


PDA Ch1 254nm

Peak	Ret. Time	Area	Height	Area%
1	20.084	24231951	2210017	98.063
2	21.102	140328	11985	0.568
3	27.756	338214	21587	1.369
Total		24710493	2243589	100.000

163f, chiral separation, SFC

Sample: PA-RED-183



Component Results

	Name	RT	Area	Height	% Area
1	Enantiomer A	2.289	1136619	197106	83.82
2	Enantiomer B	3.352	219380	26478	16.18

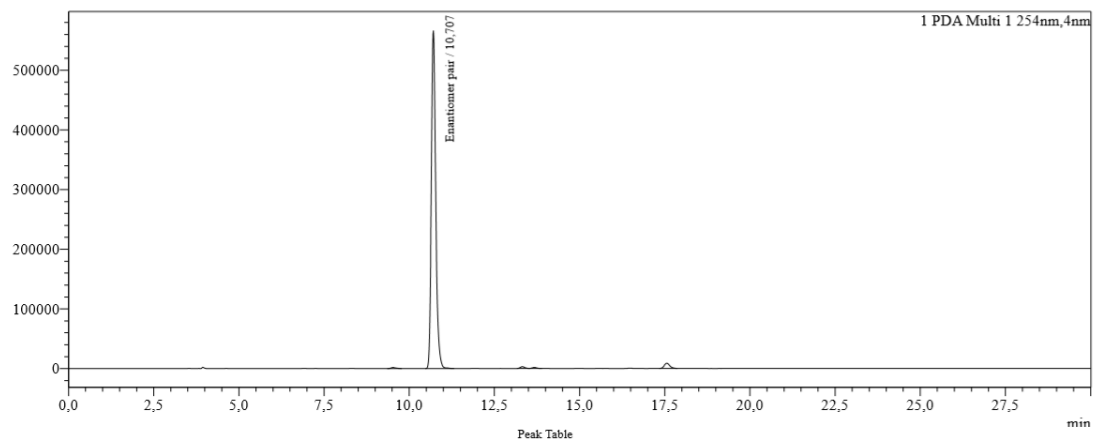
163f, achiral separation, HPLC

Injection Volume : 5
 Data File : PA-RED-183_MeCN-H2O_90-10_grad0-20m.lcd
 Method File : MeCN-H2O_90-10_grad0-20m.lcm
 Comment : PA-RED-183 in MeCN-DCM 90-10
 MeCN-H2O 90-10, gradient to 100-0 over 20 min
 1.0 mL/min, 295 K
 Zorbax SB-C18, 4.6x250mm, 3.5µm

Level# : 0

Chromatogram

uAU



PDA Ch1 254nm

Peak#	Ret. Time	Area	Height	Area%
1	9.322	17236	1768	0.329
2	10.707	5075729	566522	96.967
3	13.319	27843	3023	0.532
4	13.670	15119	1673	0.289
5	17.559	98541	8675	1.883
Total		5234468	581660	100.000

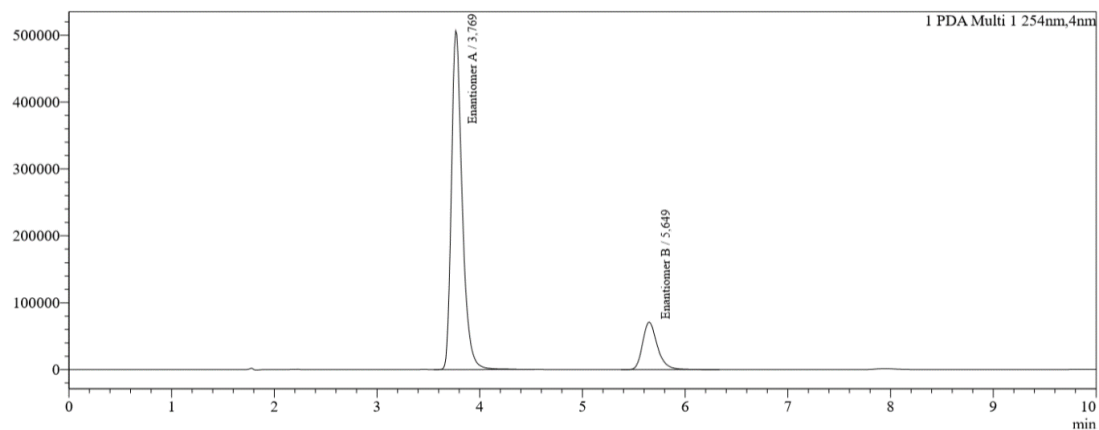
163g, chiral separation, HPLC

Injection Volume : 5
 Data File : PA-RED-238-clean_original_Hex-IPA_95-5_IA-3.lcd
 Method File : IA-3_Hex-IPA_95-5_25C_20m.lcm
 Comment : PA-RED-238-clean in Hex-DCM 90-10
 Hex-IPA 95-5, 20 min isocratic
 1.0 mL/min, 298 K
 IA-3, 4.6x150mm, 3µm

Level# : 0

uAU

Chromatogram



Peak Table

Peak#	Ret. Time	Area	Height	Area%
1	3.769	3699187	506655	83.926
2	5.649	708502	79915	16.074
Total		4407689	577570	100.000

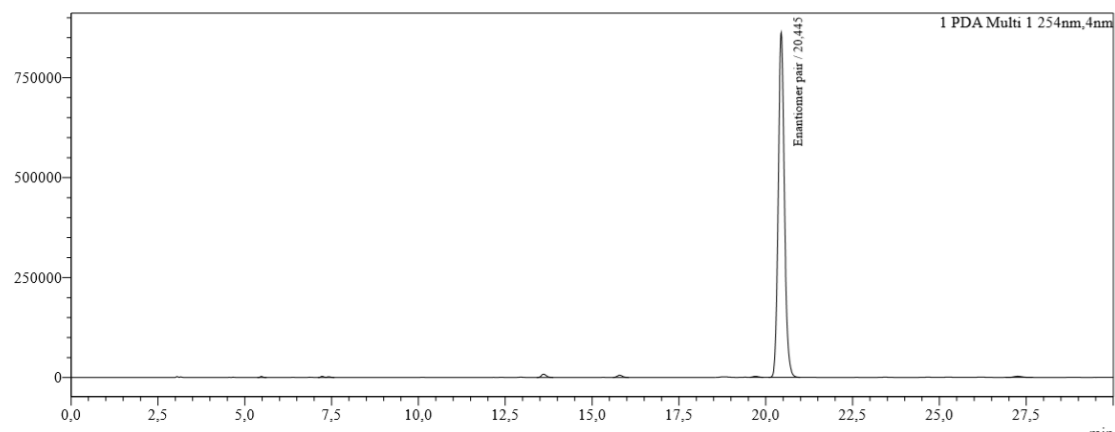
163g, achiral separation, HPLC

Injection Volume : 5
 Data File : PA-RED-238_MeCN-H2O_90-10_grad0-20m.lcd
 Method File : MeCN-H2O_90-10_grad0-20m.lcm
 Comment : PA-RED-238 in MeCN-DCM 90-10
 MeCN-H2O 90-10, gradient to 100-0 over 20 min
 1.0 mL/min, 295 K
 Zorbax SB-C18, 4.6x250mm, 3.5µm

Level# : 0

uAU

Chromatogram

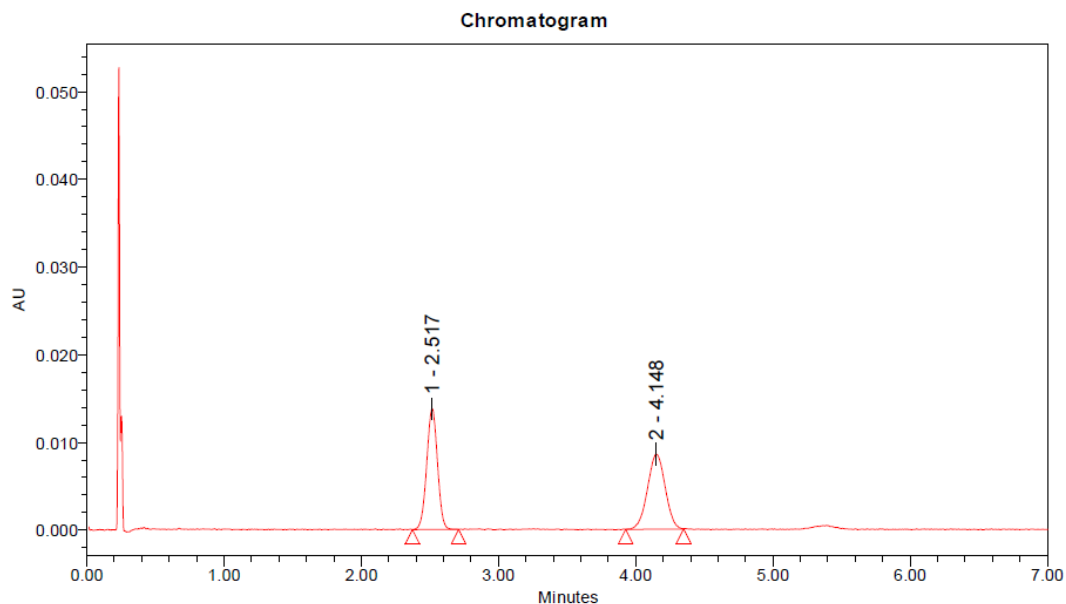


Peak Table

Peak#	Ret. Time	Area	Height	Area%
1	5.478	15563	2790	0.143
2	7.220	19490	3075	0.179
3	7.418	11982	1886	0.110
4	13.606	81895	8206	0.750
5	15.791	59085	5629	0.541
6	19.702	27952	2648	0.256
7	20.445	10651298	862645	97.595

163h, chiral separation, SFC

Sample: PA-RED-177-2_IG3-EtOH20

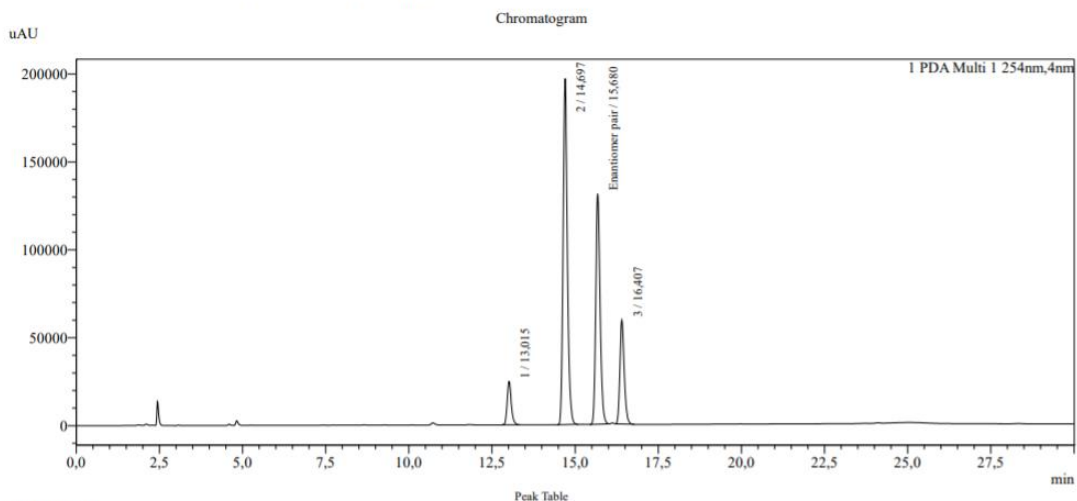


Component Results

	Name	RT	Area	Height	% Area
1	Enantiomer A	2.517	75381	13788	49.62
2	Enantiomer B	4.148	76537	8549	50.38

163h, achiral separation, HPLC

Sample Information
 Sample Name : PA-RED-177crude
 Injection Volume : 1
 Data File : PA-RED-177crude_MeCN-H2O_80-20_grad0-20m.lcd
 Comment : PA-RED-177crude in THF
 MeCN-H2O 80-20, gradient to 100-0 over 20 min
 1.0 mL/min, 295 K
 Zorbax SB-C18, 4.6x250mm, 3.5µm

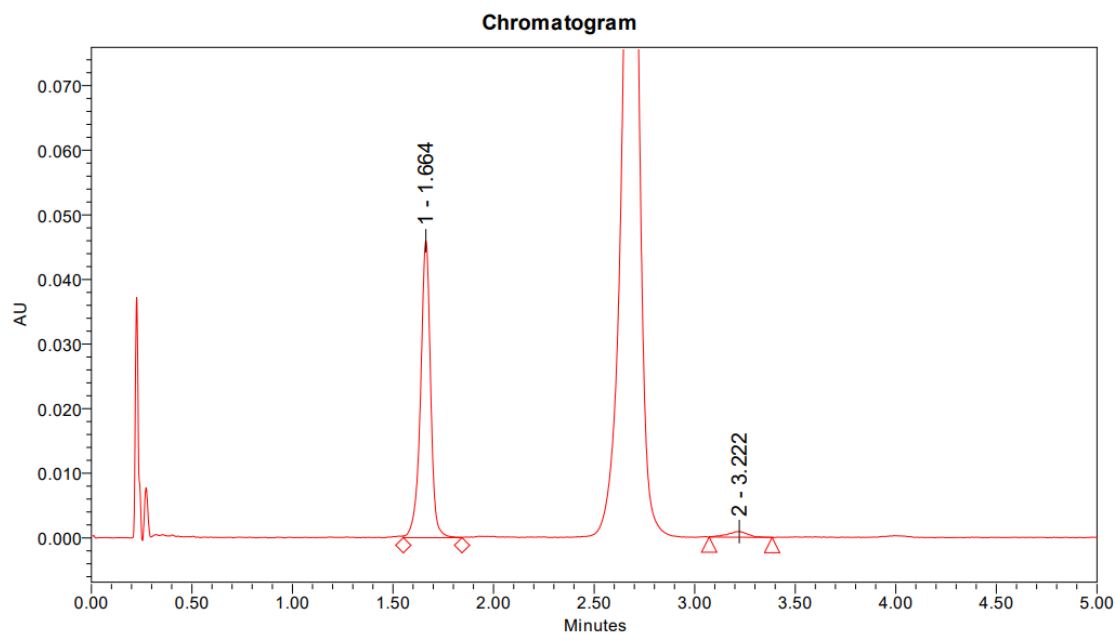


Peak Table

Peak#	Ret. Time	Area	Height	Area%
1	13.015	309552	24568	3.680
2	14.697	1743257	196787	47.379
3	15.680	1192389	131189	33.370
4	16.407	536388	59150	14.562
Total		3683586	411093	100.000

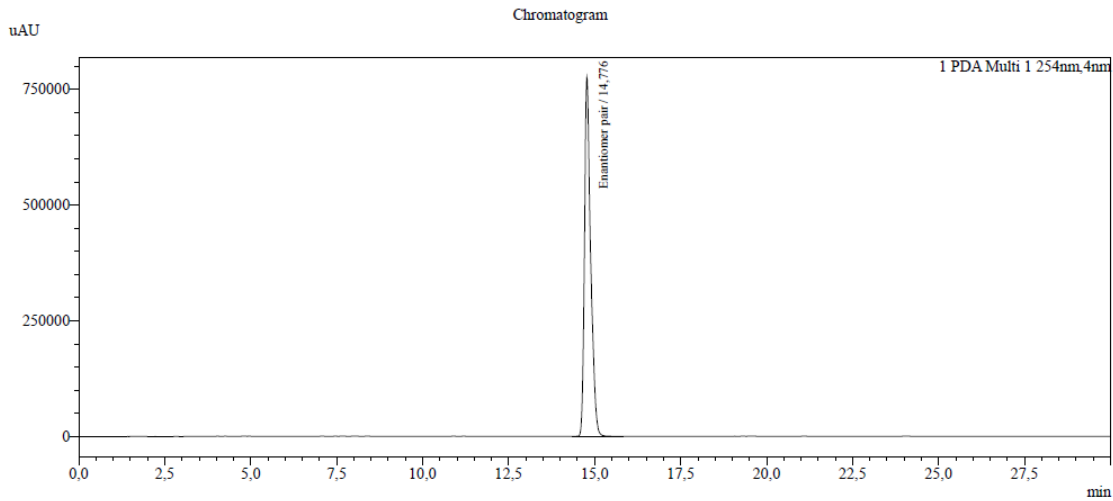
163j, chiral separation, SFC

Sample: PA-RED-179_IA3-IPA25



163j, achiral separation, HPLC

Sample Name : PA-RED-179
 Injection Volume : 5
 Data File : PA-RED-179_MeCN-H2O_90-10_grad0-20m.lcd
 Comment : PA-RED-179 in MeCN-DCM 90-10
 MeCN-H2O 90-10, gradient to 100-0 over 20 min
 1.0 mL/min, 295 K
 Zorbax SB-C18, 4.6x250mm, 3.5µm

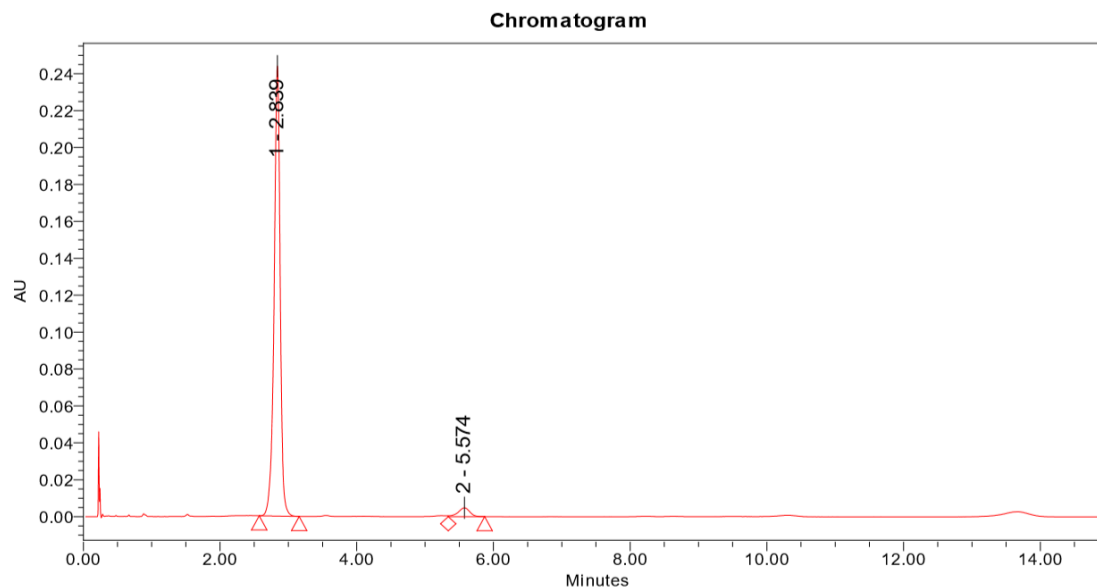


Peak Table

Peak#	Ret. time	Area	Height	Area%
1	14.776	9733087	773824	100.000
Total		9733087	773824	100.000

163k, chiral separation, SFC

Sample: PA-RED-Z6-2_IA3-IPA20

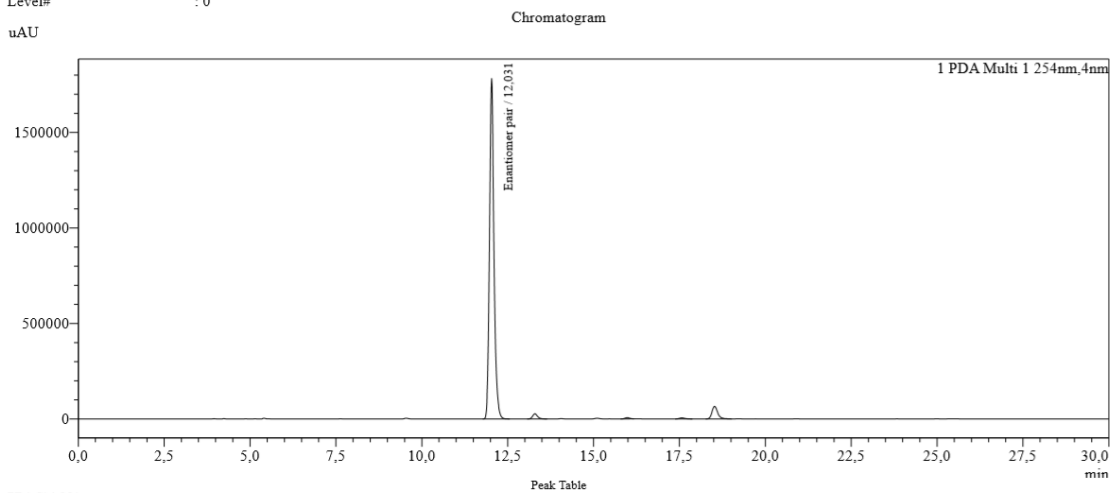


Component Results

	Name	RT	Area	Height	% Area
1	Enantiomer A	2.839	1509387	243898	96.40
2	Enantiomer B	5.574	56353	4787	3.60

163k, achiral separation, HPLC

Injection Volume : 5
 Data File : PA-RED-GuZic-6-1_MeCN-H2O_90-10_grad0-20m.lcd
 Method File : MeCN-H2O_90-10_grad0-20m.lcm
 Comment : PA-RED-GuZic-6-1 in MeCN-DCM 90-10
 MeCN-H2O 90-10, gradient to 100-0 over 20 min
 1.0 mL/min, 295 K
 Zorbax SB-C18, 4.6x250mm, 3.5µm
 Level# : 0

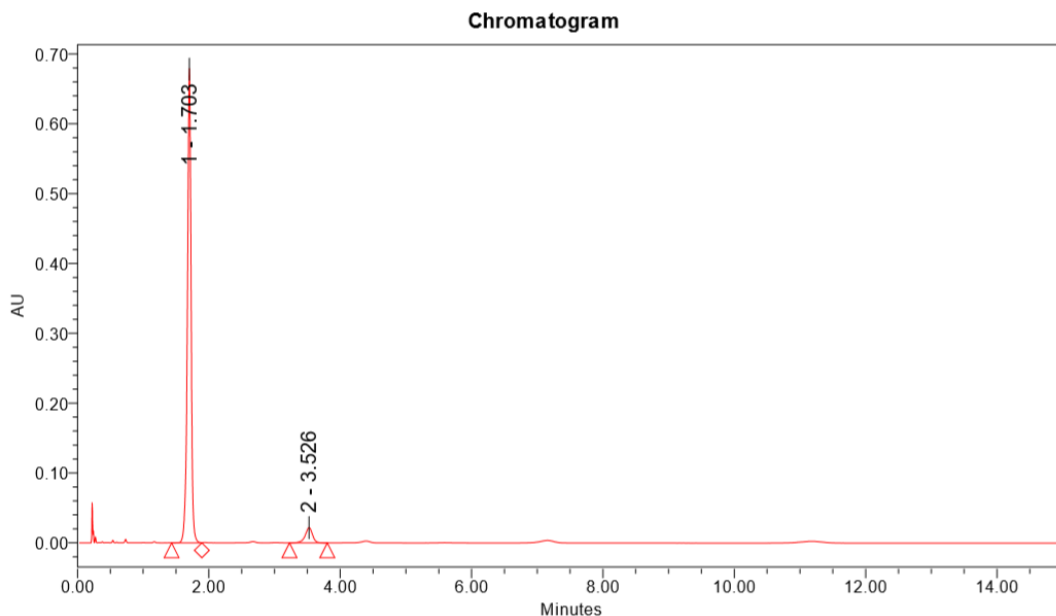


PDA Ch1 254nm

Peak#	Ret. Time	Area	Height	Area%
1	12.031	16167051	1783815	93.196
2	13.292	281477	27599	1.623
3	15.979	62620	6648	0.361
4	17.571	63172	2616	0.364
5	18.323	77323	6919	4.457
Total		17347443	1889596	100.000

163I, chiral separation, SFC

Sample: PA-RED-200_IA3-IPA25



Component Results

	Name	RT	Area	Height	% Area
1	Enantiomer A	1.703	2658762	679281	93.92
2	Enantiomer B	3.526	172060	21866	6.08

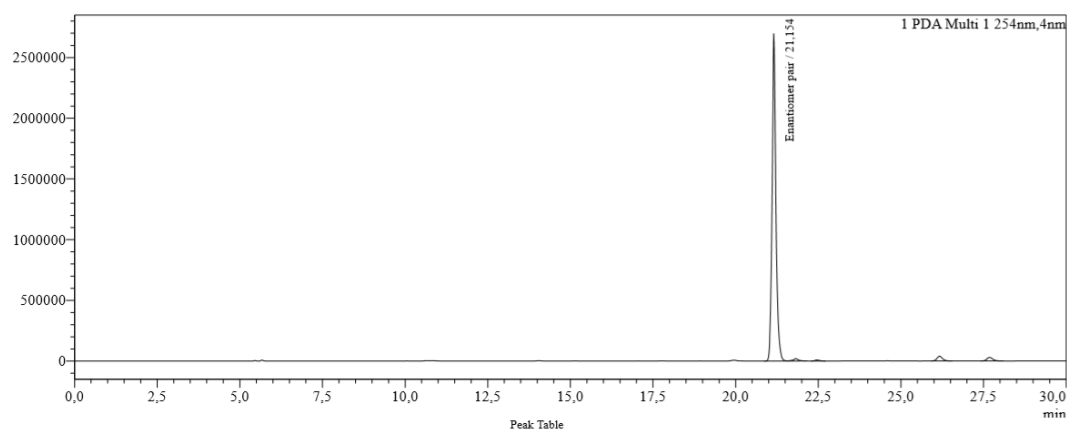
163I, achiral separation, HPLC

Injection Volume : 5
 Data File : PA-RED-200_MeCN-H2O_80-20_grad0-20m.lcd
 Method File : MeCN-H2O_80-20_grad0-20m.lcm
 Comment : PA-RED-200 in MeCN-DCM 90-10
 MeCN-H2O 80-20, gradient to 100-0 over 20 min
 1.0 mL/min, 295 K
 Zorbax SB-C18, 4.6x250mm, 3.5µm

Level# : 0

uAU

Chromatogram

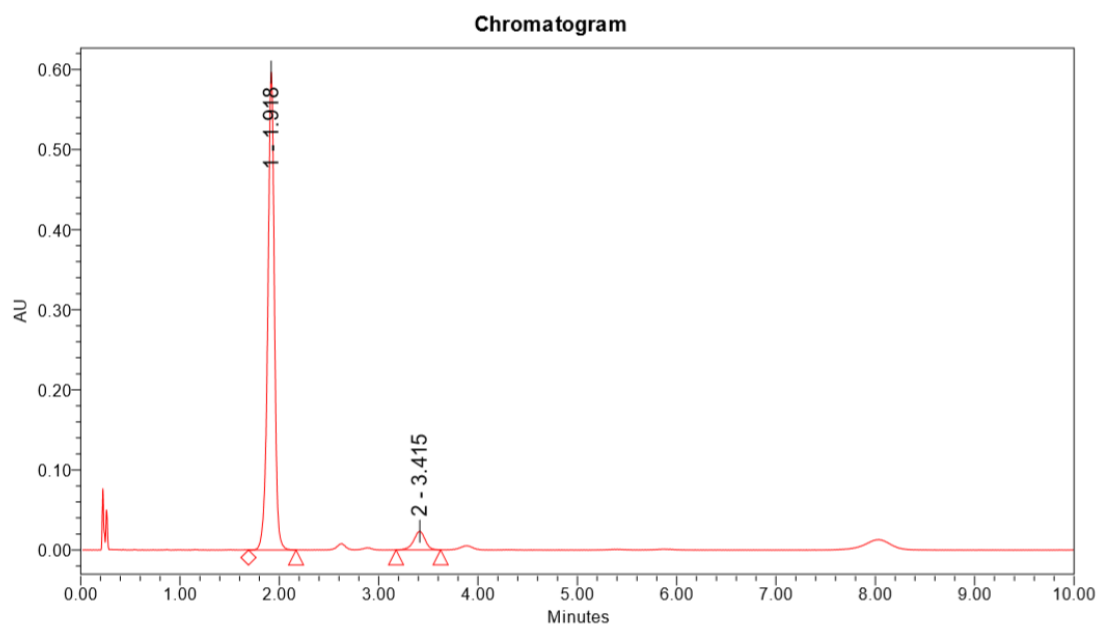


PDA Ch1 254nm

Peak#	Ret. Time	Area	Height	Area%
1	21.154	21355472	2697988	95.014
2	21.820	212749	18933	0.947
3	22.458	80033	8866	0.336
4	26.171	454683	39253	2.023
5	27.684	373313	29181	1.661
Total		22476249	2794221	100.000

163m, chiral separation, SFC

Sample: PA-RED-209_IA3-IPA35

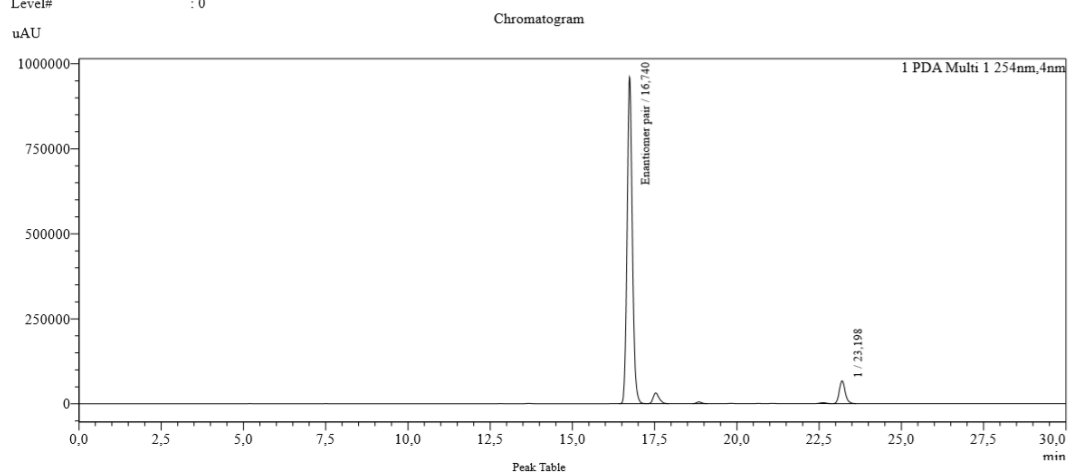


Component Results

	Name	RT	Area	Height	% Area
1	Enantiomer A	1.918	2774273	596782	93.62
2	Enantiomer B	3.415	189041	23419	6.38

163m, achiral separation, HPLC

Injection Volume : 10
 Data File : PA-RED-209_MeCN-H2O_90-10_grad0-20m.lcd
 Method File : MeCN-H2O_90-10_grad0-20m.lcm
 Comment : PA-RED-209 in MeCN-DCM 90-10
 MeCN-H2O 90-10, gradient to 100-0 over 20 min
 1.0 mL/min, 295 K
 Zorbax SB-C18, 4.6x250mm, 3.5µm
 Level# : 0



PDA Ch1 254nm

Peak#	Ret. Time	Area	Height	Area%
1	16.740	10523693	960883	88.847
2	17.534	403663	31534	3.385
3	18.844	55870	5211	0.469
4	22.619	30159	2623	0.253
5	23.198	84006	66950	7.046
Total		11923480	1067200	100.000

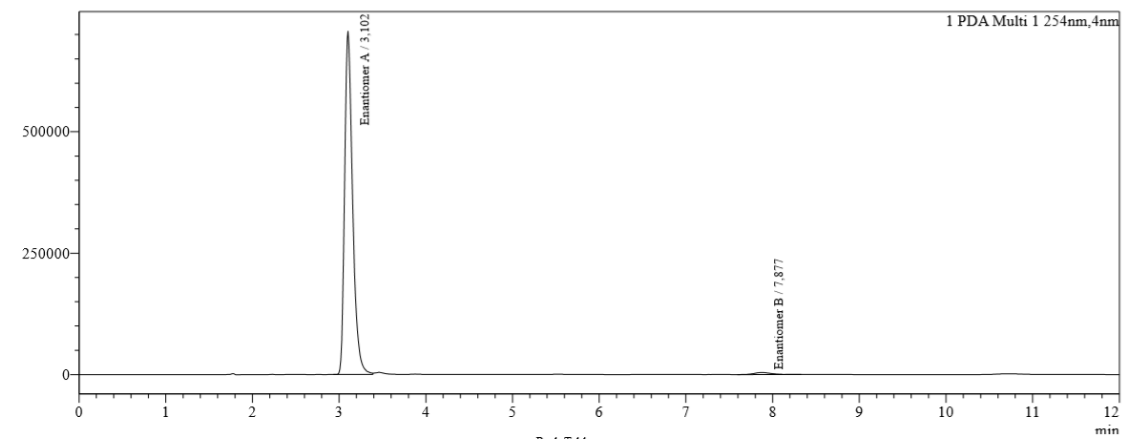
163n, chiral separation, HPLC

Injection Volume : 5
 Data File : PA-RED-240-clean_Hex-IPA_95-5_IA-3.lcd
 Method File : IA-3_Hex-IPA_95-5_25C_20m.lcm
 Comment : PA-RED-240-clean in Hex-DCM 90-10
 Hex-IPA 95-5, 20 min isocratic
 1.0 mL/min, 298 K
 IA-3, 4.6x150mm, 3µm

Level# : 0

uAU

Chromatogram



Peak#	Ret. Time	Area	Height	Area%
1	3.102	4563831	707653	98.771
2	7.877	56787	4192	1.229
Total		4620618	711845	100.000

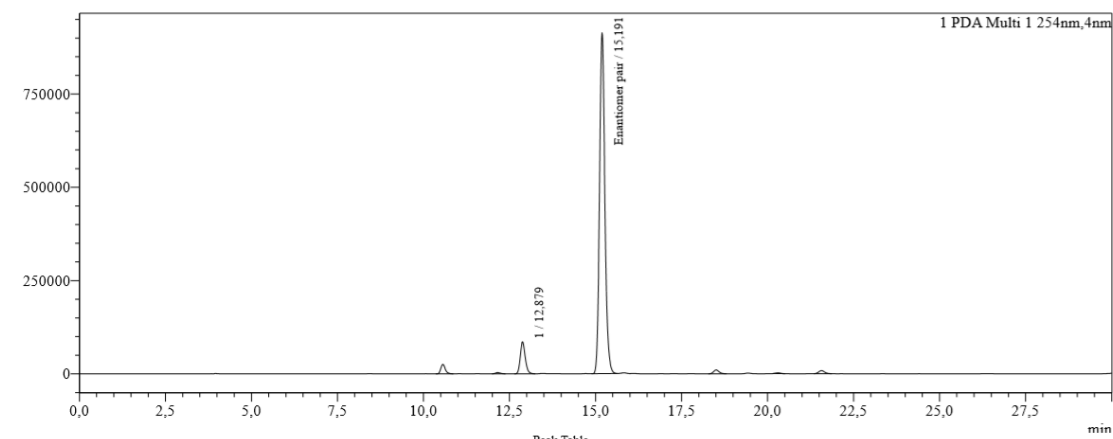
163n, achiral separation, HPLC

Injection Volume : 5
 Data File : PA-RED-240_MeCN-H2O_90-10_grad0-20m.lcd
 Method File : MeCN-H2O_90-10_grad0-20m.lcm
 Comment : PA-RED-240 in MeCN-DCM 90-10
 MeCN-H2O 90-10, gradient to 100-0 over 20 min
 1.0 mL/min, 295 K
 Zorbax SB-C18, 4.6x250mm, 3.5µm

Level# : 0

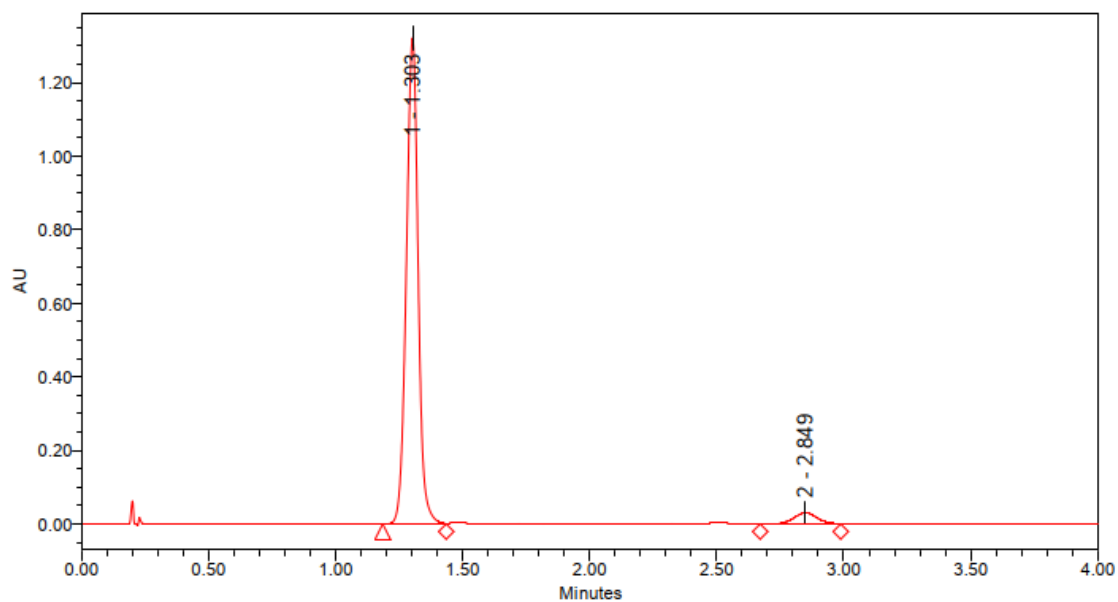
uAU

Chromatogram



Peak#	Ret. Time	Area	Height	Area%
1	10.562	229338	25492	2.045
2	12.155	32390	3345	0.289
3	12.879	835610	83896	7.611
4	15.191	9864413	914507	87.956
5	18.505	117065	10412	1.044
6	20.302	19221	1894	0.171
7	21.568	99127	8251	0.884

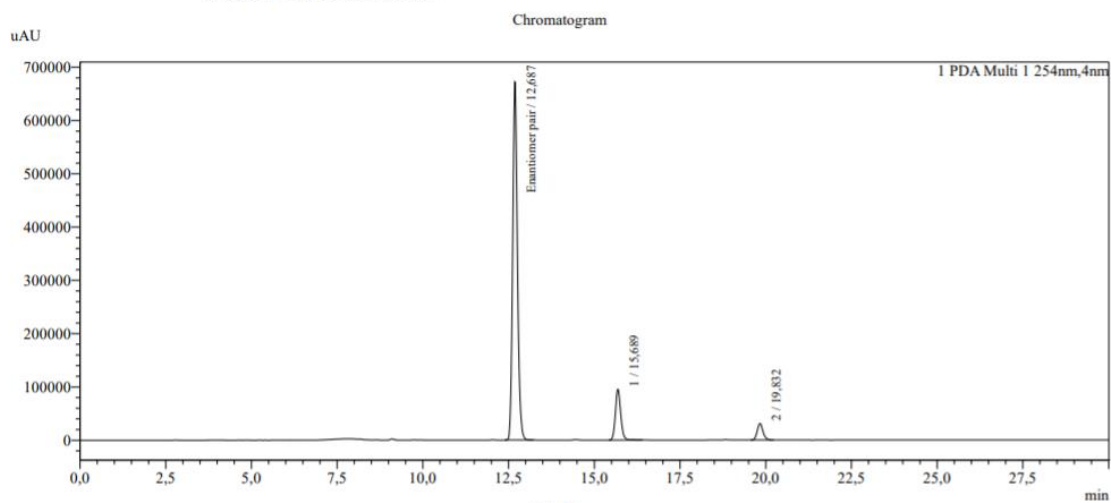
165a, chiral separation, SFC



165a, achiral separation, HPLC

Sample Information

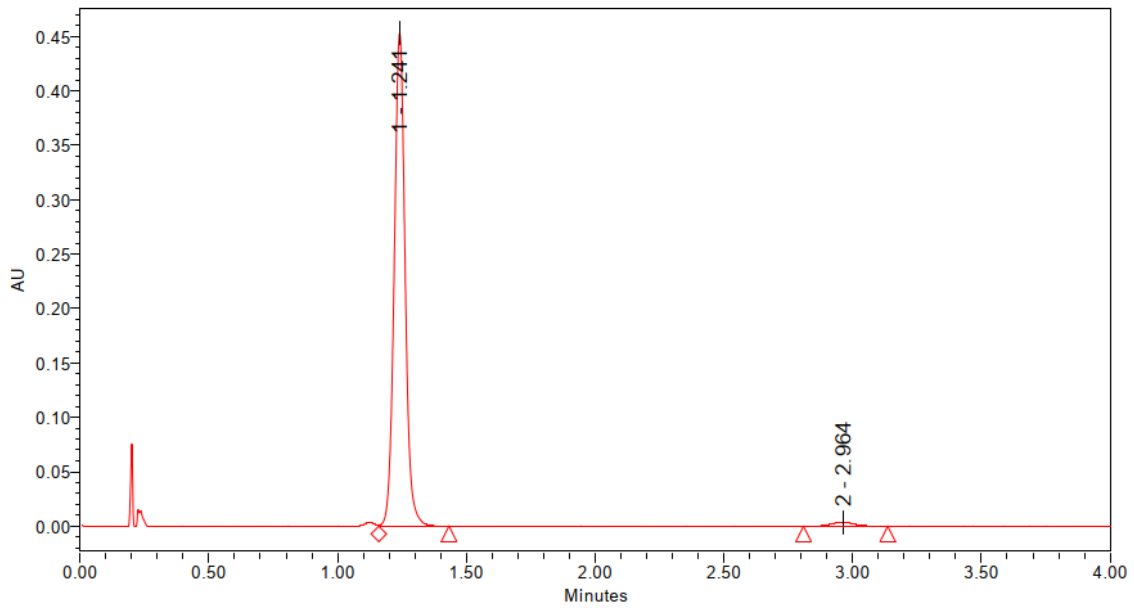
Sample Name : PaRed-TM7
 Injection Volume : 5
 Data File : PaRed-TM7_MeCN-H2O_90-10_grad0-20m.lcd
 Comment : PaRed-TM7 in MeCN-DCM 90-10
 MeCN-H2O 90-10, gradient to 100-0 in 20 min
 1,0 mL/min, 295 K
 Zorbax SB-C18, 4.6x250mm, 3.5µm



PDA Ch1 254nm

Peak#	Ret. Time	Area	Height	Area%
1	12.687	6471221	671564	82.278
2	15.689	1031793	95149	13.119
3	19.832	362024	30893	4.603
Total		7865038	797606	100.000

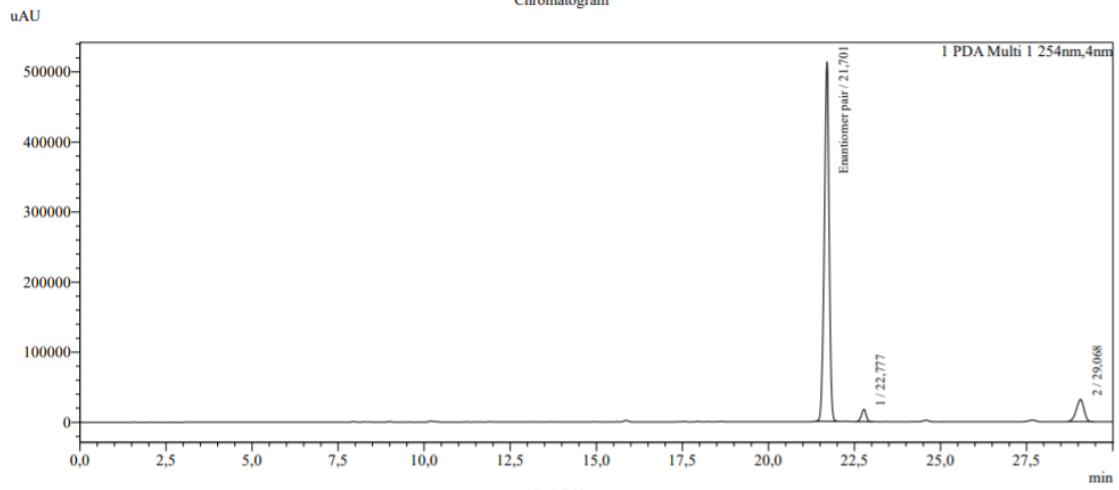
165b, chiral separation, SFC



165b, achiral separation, HPLC

Sample Name : PaRed-357
 Injection Volume : 3
 Data File : PaRed-357_MeCN-H2O_80-20_grad0-20m.lcd
 Comment : PaRed-357 in MeCN-DCM 90-10
 MeCN-H2O 80-20, gradient to 100-0 over 20 min
 1.0 mL/min, 295 K
 Zorbax SB-C18, 4.6x250mm, 3.5µm

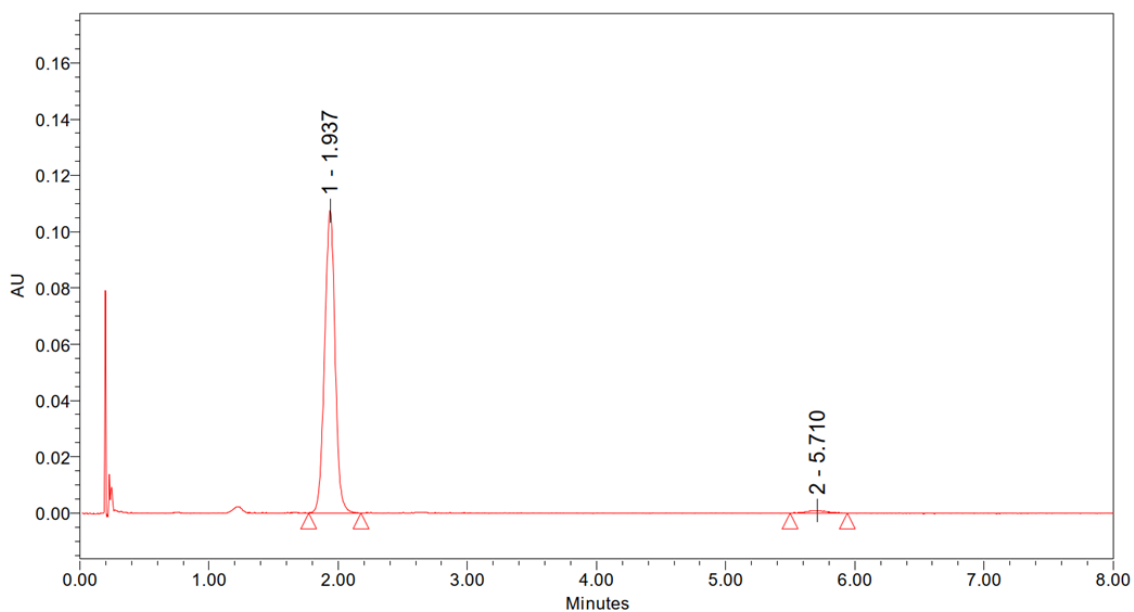
Chromatogram



Peak Table

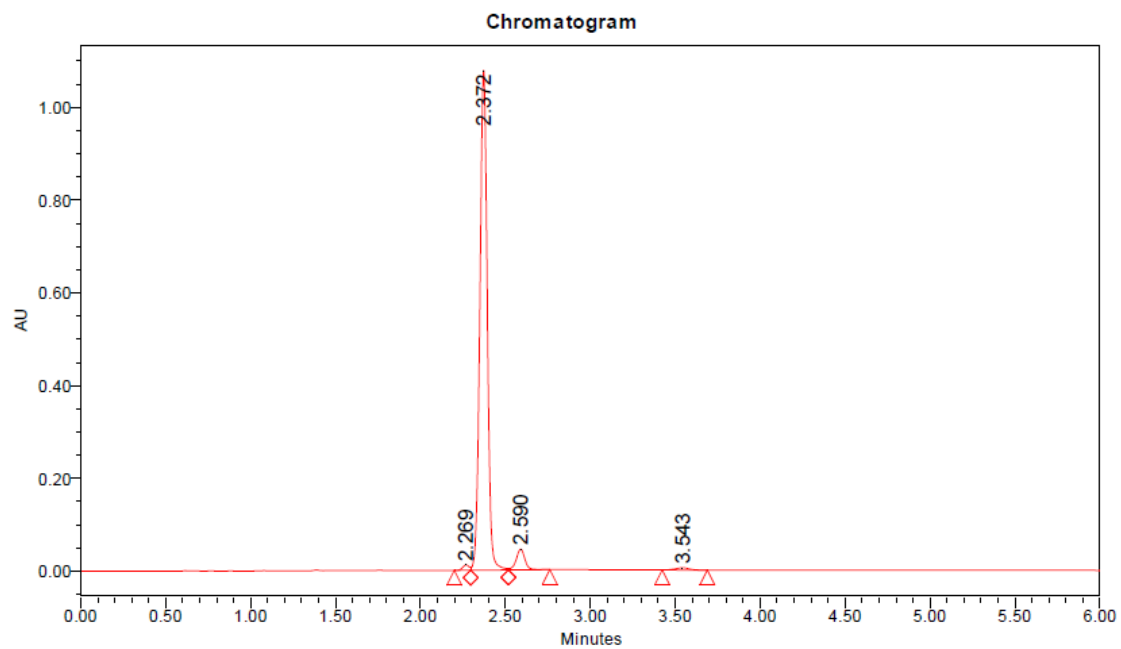
Peak#	Ret. Time	Area	Height	Area%
1	21.701	4982197	512190	88.387
2	22.777	166539	17453	3.054
3	29.068	488055	31691	8.658
Total		5636790	561333	100.000

165c, chiral separation, SFC



165c, achiral separation, HPLC

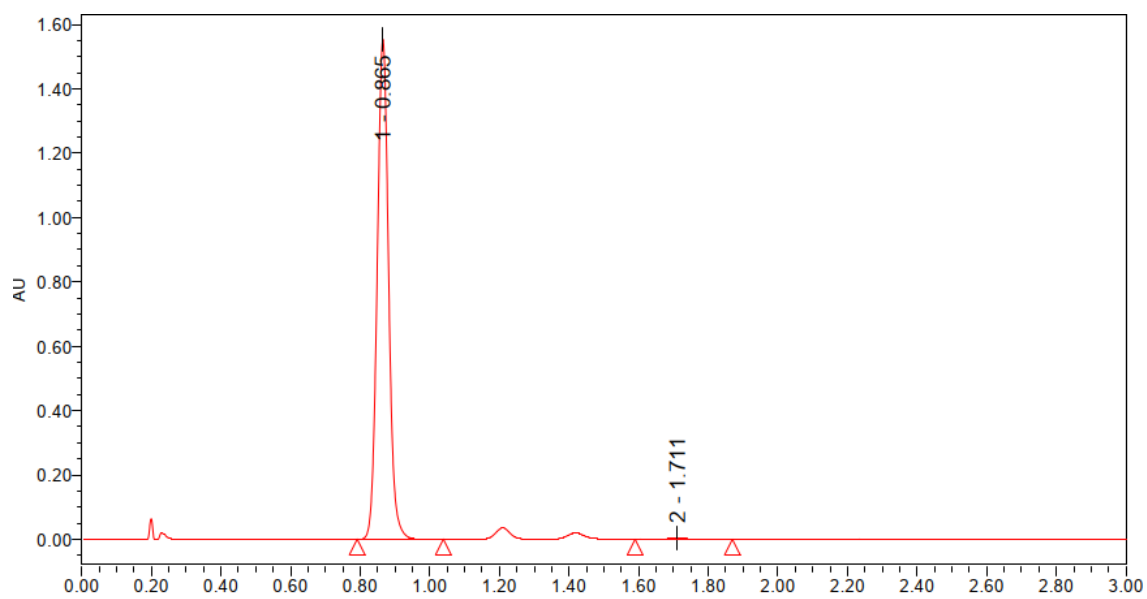
Sample: PaRed-335_ZorbaxC18-95eq10



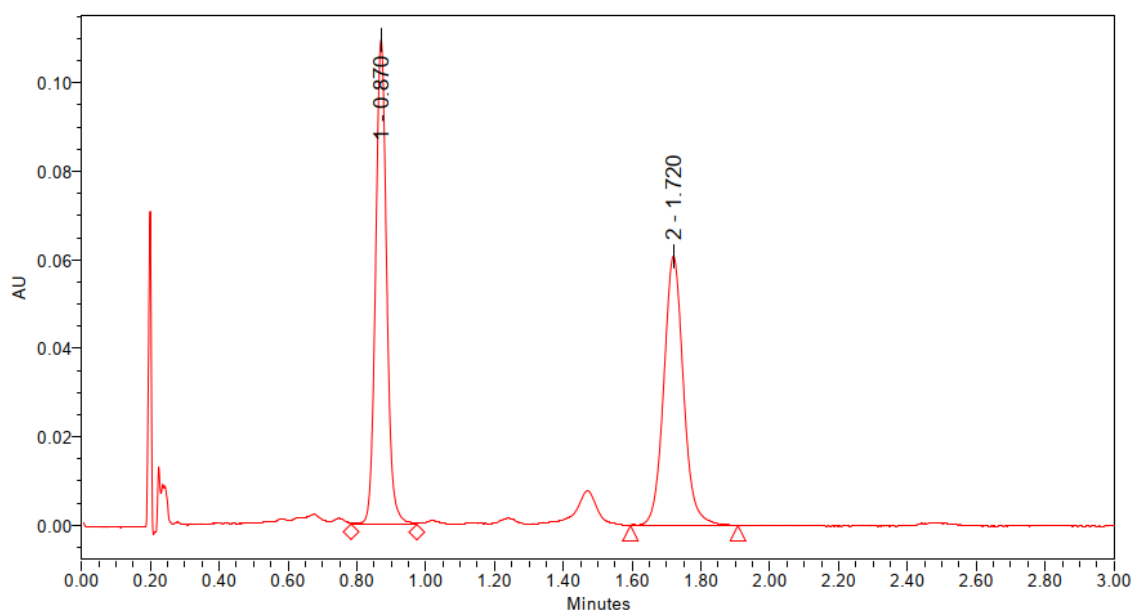
Component Results

	Name	RT	Area	Height	% Area
1	1	2.269	29237	11568	0.84
2	enantiomer pair	2.372	3264925	1077870	93.90
3	2	2.590	157121	44721	4.52
4	3	3.543	25619	4678	0.74

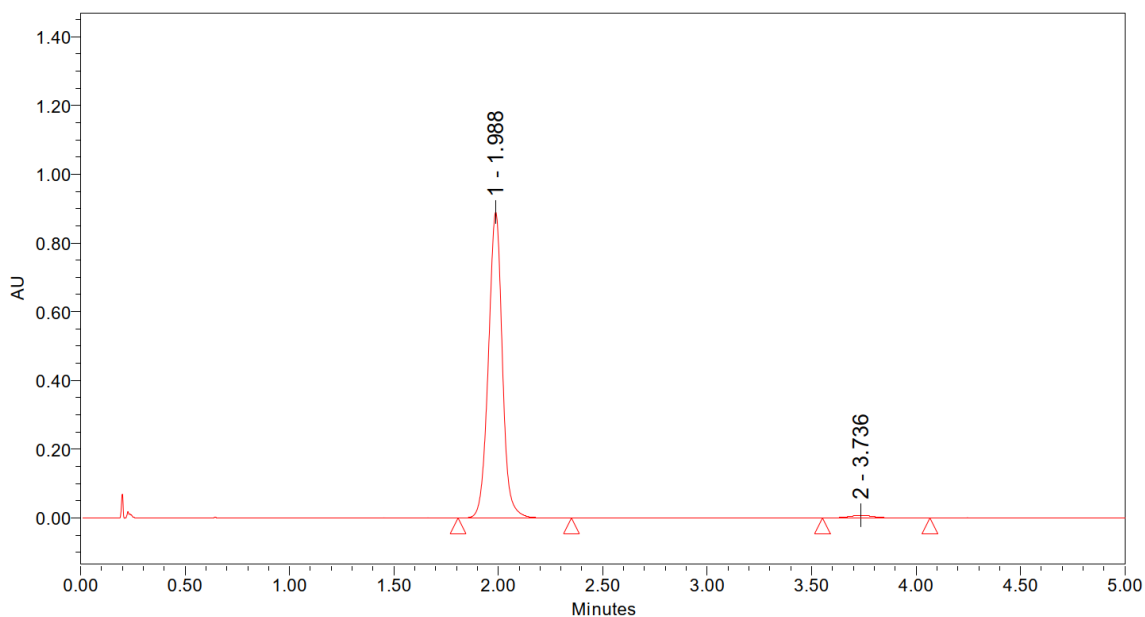
165d, chiral separation, SFC



165d, achiral separation, HPLC



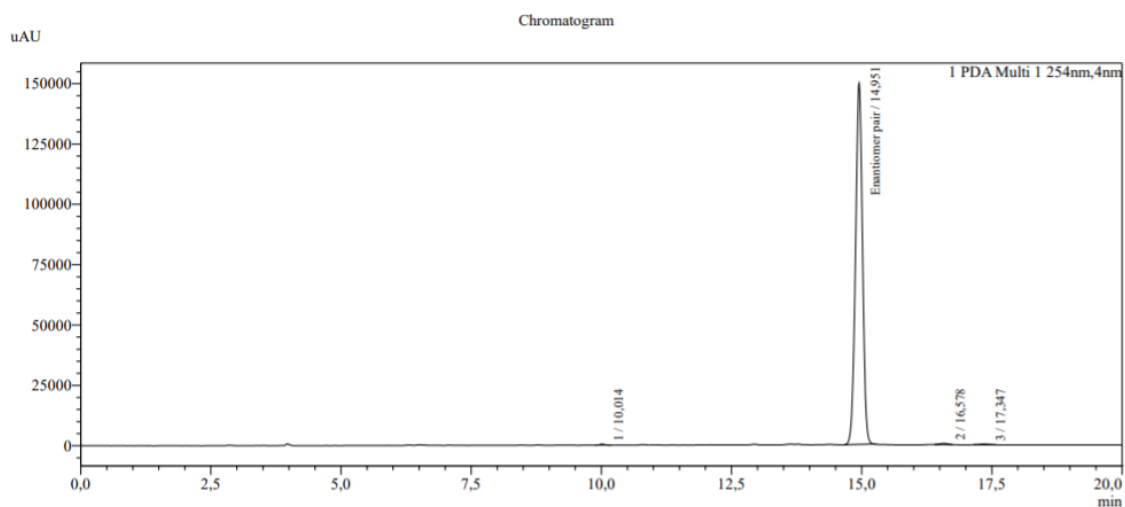
165e, chiral separation, SFC



165e, achiral separation, HPLC

Sample Information

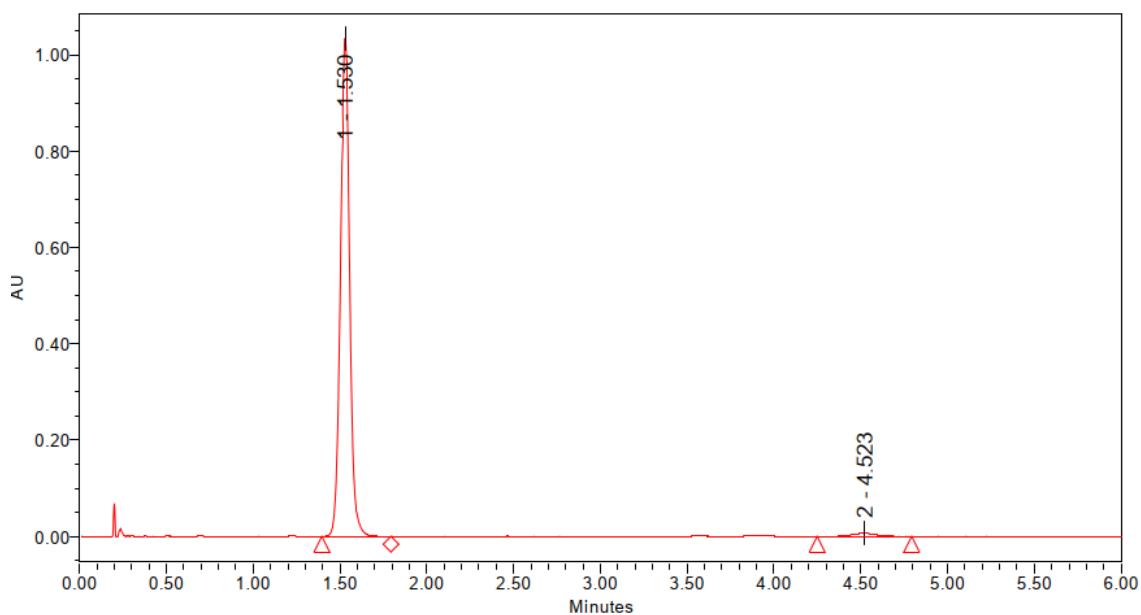
Sample Name : PaRed-359
 Injection Volume : 3
 Data File : PaRed-359_MeCN-H2O_90-10_grad0-10m.lcd
 Comment : PaRed-359 in MeCN-DCM 90-10
 MeCN-H2O 80-20, gradient to 100-0 over 20 min
 1.0 mL/min, 295 K
 Zorbax SB-C18, 4.6x250mm, 3.5µm



Peak Table

Peak#	Ret. Time	Area	Height	Area%
1	10.014	2825	411	0.201
2	14.951	1392961	149610	99.254
3	16.578	4114	461	0.307
4	17.347	3329	262	0.237
Total		1403428	150744	100.000

165f, chiral separation, SFC

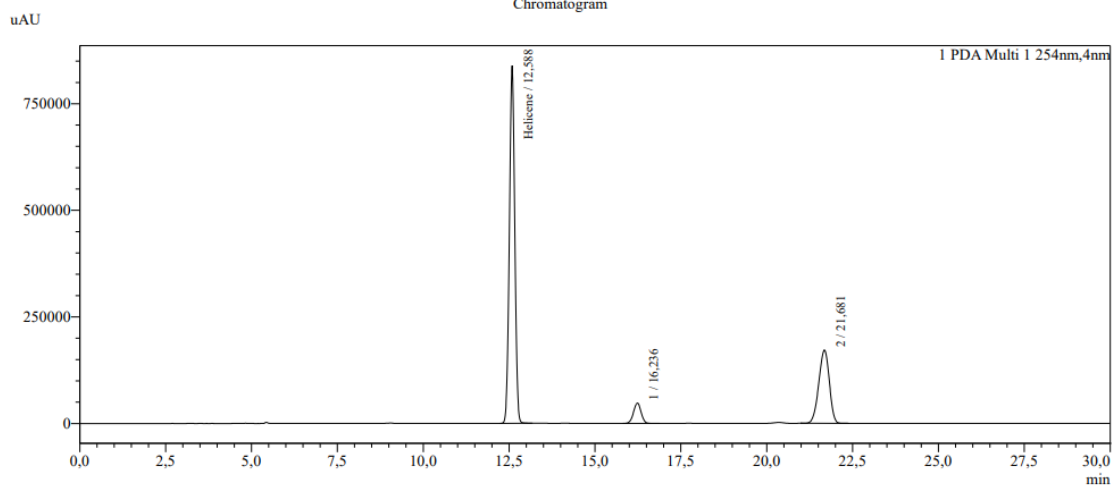


165f, achiral separation, HPLC

Sample Name : Pelva-178
 Injection Volume : 5
 Data File : PelVa-178_MeCN-H2O_95-5_grad0-5m.lcd
 Comment : Pelva-178 in MeCN-DCM 90-10
 MeCN-H2O 95-5, gradient to 100-0 over 5 min
 1.0 mL/min, 295 K
 Zorbax SB-C18, 4.6x250mm, 3.5µm

Sample Information

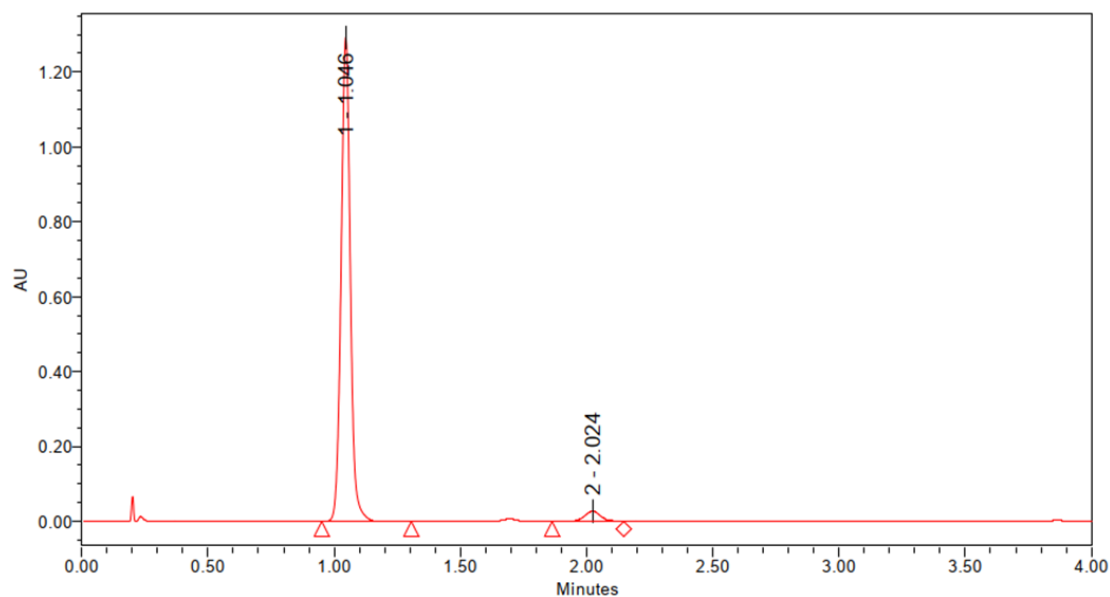
Chromatogram



Peak Table

Peak#	Ret. Time	Area	Height	Area%
1	12.588	9133026	838969	67.565
2	16.236	730838	47487	3.395
3	21.681	3663203	172020	27.041
Total		13547087	1058476	100.000

165g, chiral separation, SFC



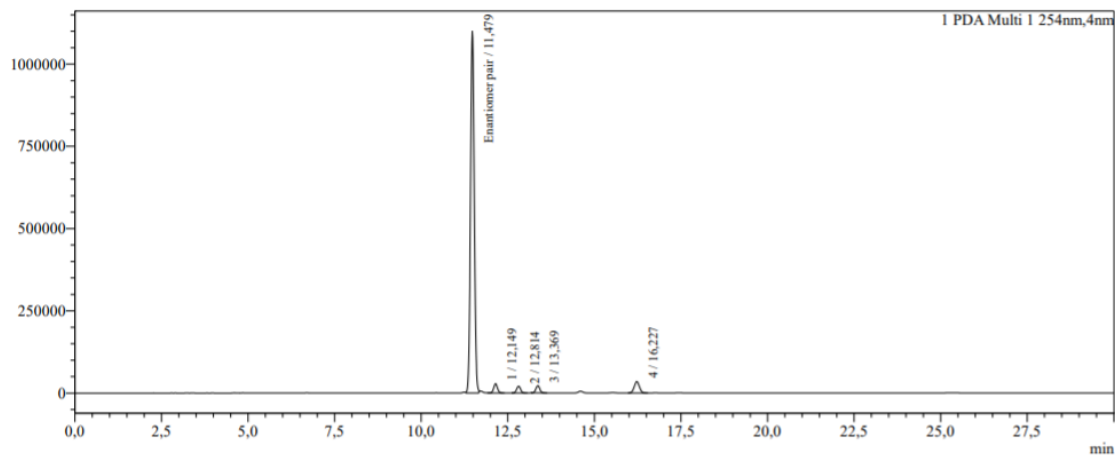
165g, achiral separation, HPLC

Sample Name : PaRed-391
 Injection Volume : 5
 Data File : PaRed-391_MeCN-H2O_90-10_grad0-10m.lcd
 Comment : PaRed-391 in MeCN-DCM 90-10
 MeCN-H2O 90-10, gradient to 100-0 over 10 min
 1.0 mL/min, 295 K
 Zorbax SB-C18, 4.6x250mm, 3.5µm

Sample Information

uAU

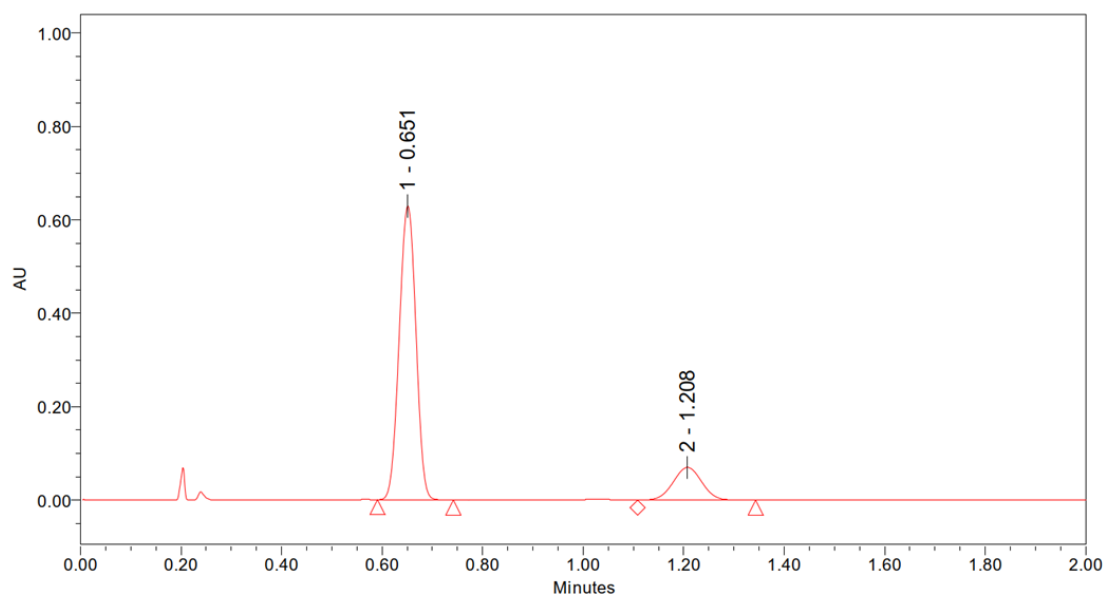
Chromatogram



Peak Table

Peak#	Ret. Time	Area	Height	Area%
1	11.479	8150713	1099523	90.039
2	12.149	217548	27995	2.348
3	12.814	159919	20413	1.767
4	13.369	172023	21549	1.900
5	16.227	357231	34456	3.946
Total		9052433	1203937	100.000

165h, chiral separation, SFC



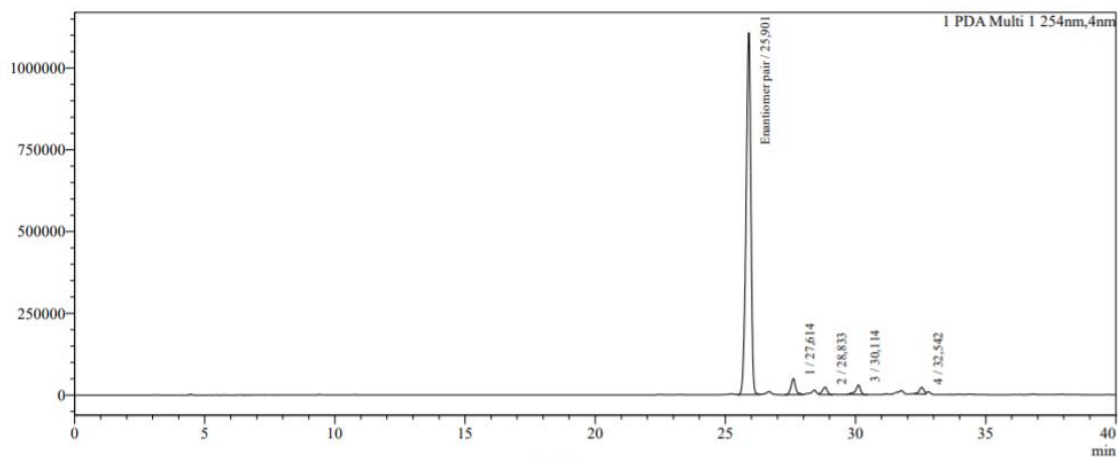
165h, achiral separation, HPLC

Sample Name : PaRed-395
 Injection Volume : 5
 Data File : PaRed-395_MeCN-H2O_80-20_grad0-30m.lcd
 Comment : PaRed-395 in MeCN-DCM 90-10
 MeCN-H2O 80-20, gradient to 100-0 over 30 min
 1.0 mL/min, 295 K
 Zorbax SB-C18, 4.6x250mm, 3.5µm

Sample Information

uAU

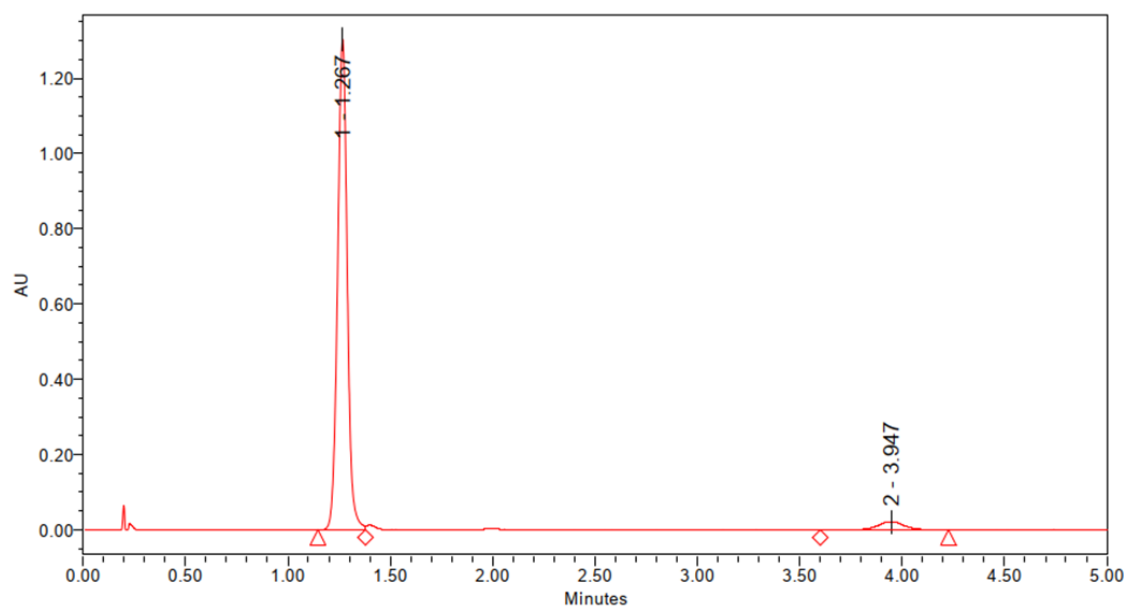
Chromatogram



Peak Table

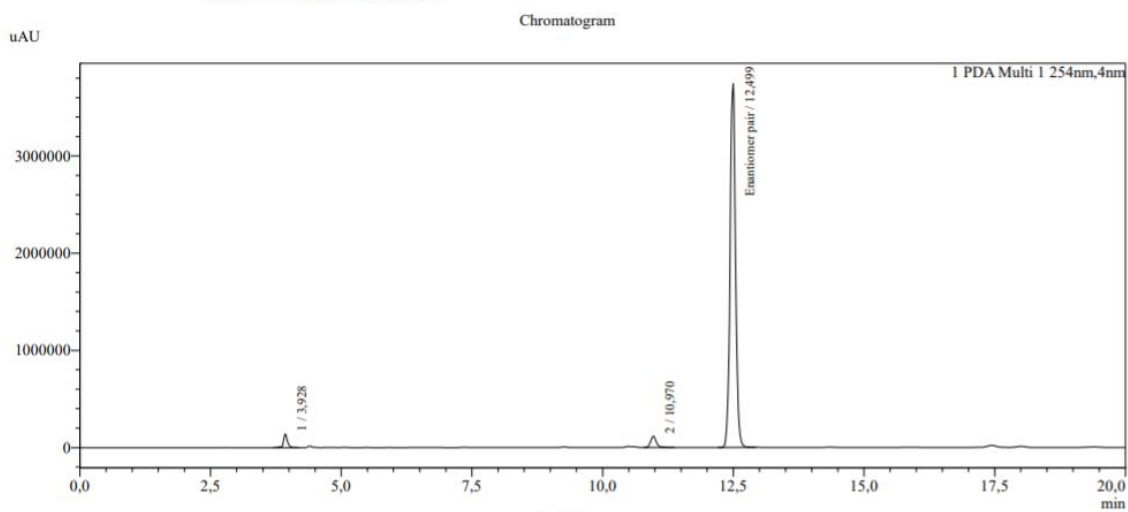
Peak#	Ret. Time	Area	Height	Area%
1	25.901	13837798	1106749	90.0099
2	27.614	600978	48907	3.9099
3	28.833	294133	23822	1.913
4	30.114	393442	29510	2.559
5	32.542	247488	20410	1.610
Total		15373837	1228098	100.0000

165i, chiral separation, SFC



165i, achiral separation, HPLC

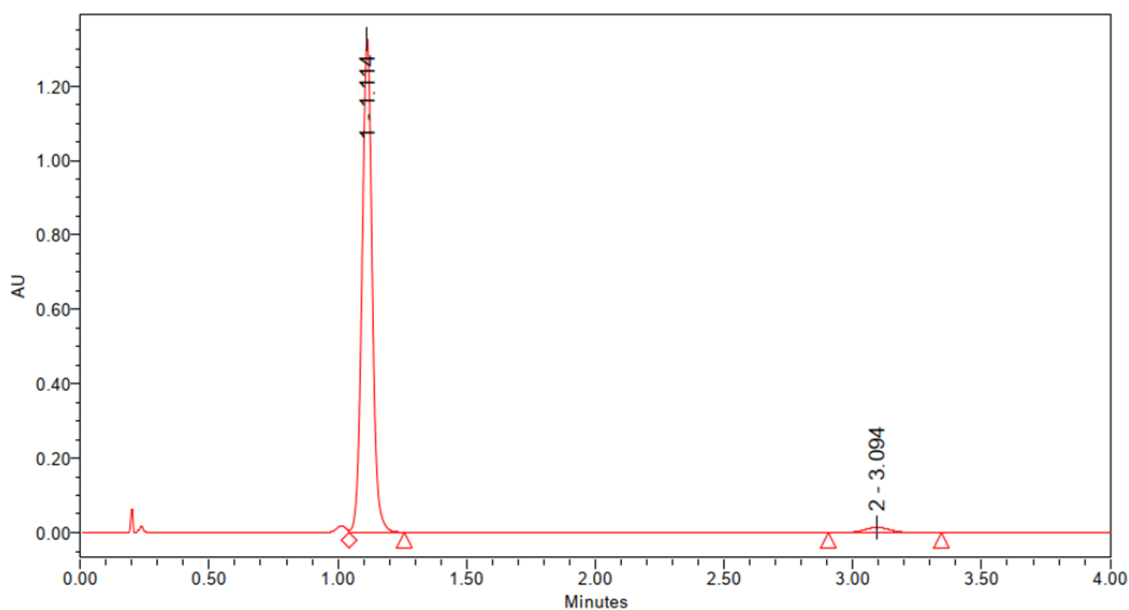
Sample Information
 Sample Name : PaRed-369
 Injection Volume : 10
 Data File : PaRed-369_MeCN-H2O_90-10_grad0-10m.lcd
 Comment : PaRed-369 in MeCN-DCM 90-10
 MeCN-H2O 90-10, gradient to 100-0 over 10 min
 1.0 mL/min, 295 K
 Zorbax SB-C18, 4.6x250mm, 3.5µm



Peak Table

Peak#	Ret. Time	Area	Height	Area%
1	3.928	726443	137811	2.518
2	10.970	888379	115424	3.079
3	12.499	27334870	3742097	94.403
Total		28849692	3995332	100.000

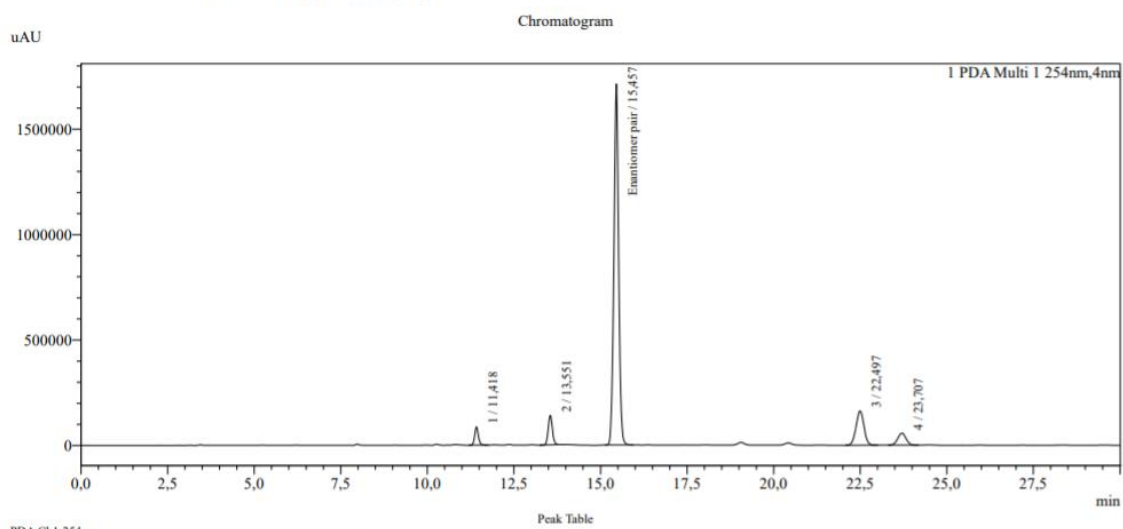
165j, chiral separation, SFC



165j, achiral separation, HPLC

Sample Information

Sample Name : PaRed-370
 Injection Volume : 7
 Data File : PaRed-370_MeCN-H2O_90-10_grad0-10m_long.lcd
 Comment : PaRed-370 in MeCN-DCM 90-10
 MeCN-H2O 90-10, gradient to 100-0 over 10 min
 1.0 mL/min, 295 K
 Zorbax SB-C18, 4.6x250mm, 3.5µm

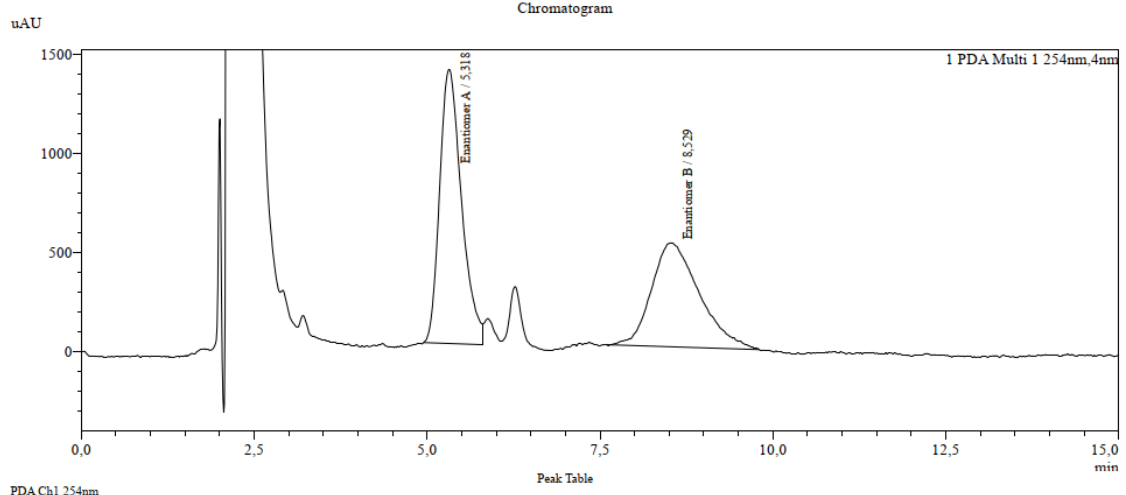


Peak Table

Peak#	Ret. Time	Area	Height	Area%
1	11.418	656660	86543	3.027
2	13.551	1182355	139847	5.451
3	15.457	16294028	1712821	75.122
4	22.497	2595481	162470	11.965
5	23.707	961961	57108	4.335
Total		21691486	2158789	100.000

217a with 222, chiral separation, SFC

Sample Information
 Sample Name : SA-SPA-174-CCC
 Injection Volume : 10
 Data File : SA-SPA-174-CCC_conc_Hex-IPA_90-10_IC-3.lcd
 Method File : IC-3_Hex-IPA_90-10_25C_20m.lcm
 Comment : SA-SPA-174-CCC in Hex-Tol-DCM 90-5-5
 Hex-IPA 90-10, 20 min isocratic
 1.0 mL/min, 298 K
 IC-3, 4.6x150mm, 3µm
 Level# : 0

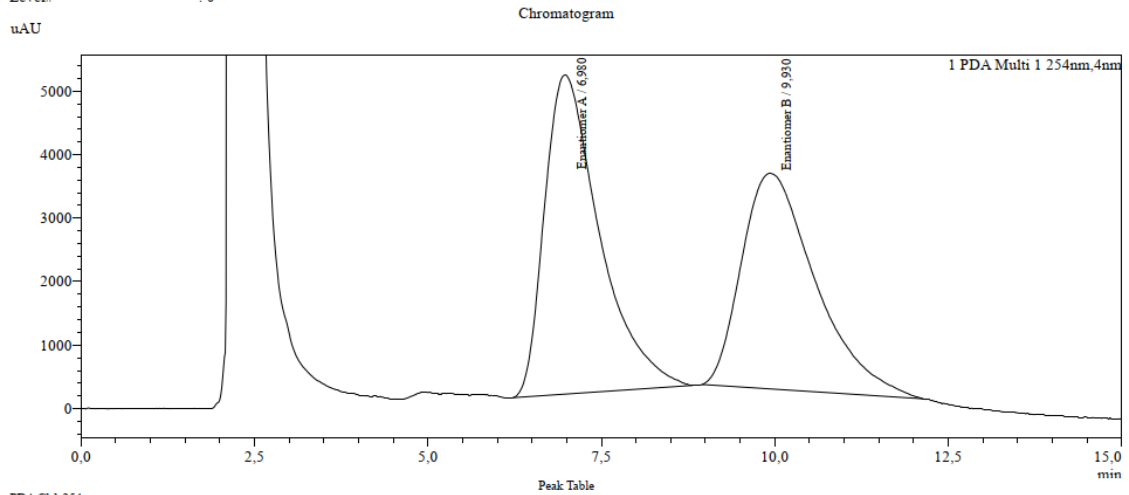


Peak Table

Peak#	Ret. Time	Area	Height	Area%
1	5.318	30407	1331	54.701
2	8.529	25180	523	45.299
Total		55587	1906	100.000

217b with 222, chiral separation, SFC

Sample Information
 Sample Name : SA-SPA-174-CCA
 Injection Volume : 10
 Data File : SA-SPA-174-CCA_Hept-IPA_95-5_IC-3.lcd
 Method File : IC-3_Hex-IPA_95-5_25C_30m.lcm
 Comment : SA-SPA-174-CCA in Hept-Tol 90-10
 Hex-IPA 95-5, 30 min isocratic
 1.0 mL/min, 298 K
 IC-3, 4.6x150mm, 3µm
 Level# : 0



Peak Table

Peak#	Ret. Time	Area	Height	Area%
1	6.980	277436	5026	52.450
2	9.930	251519	3398	47.550
Total		528955	8424	100.000

8.3. X-ray structures

Compound **163a**

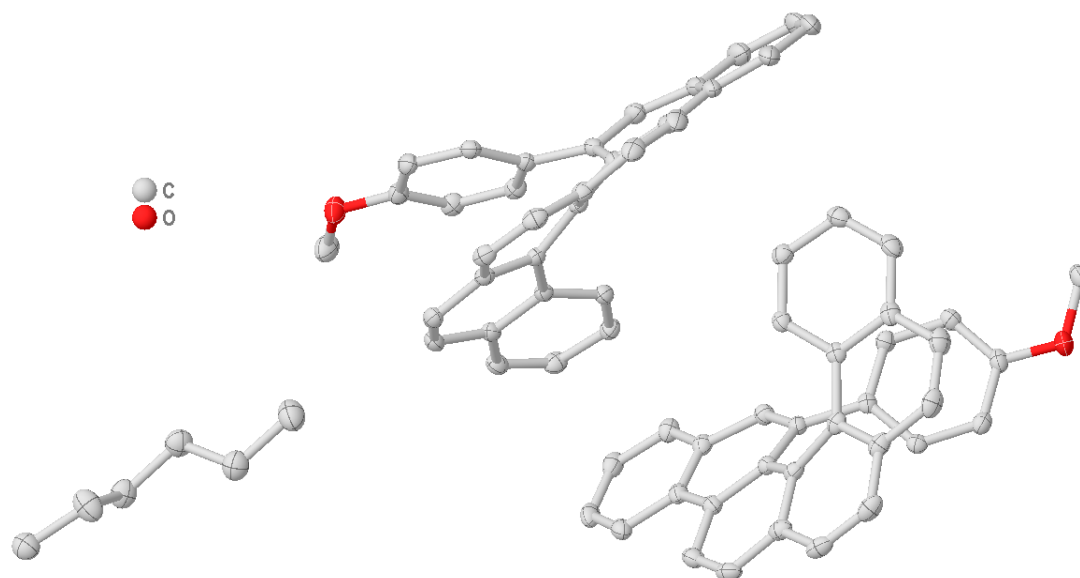


Figure 54. Full asymmetric unit of compound **163a**. Hydrogen atoms omitted for clarity. Displacement ellipsoids are drawn at 50% probability level.

Empirical formula	$C_{72}H_{58}O_2$
Formula weight	955.18
Temperature/K	100
Crystal system	monoclinic
Space group	$P2_1$
$a/\text{\AA}$	15.6559(3)
$b/\text{\AA}$	9.4564(2)
$c/\text{\AA}$	16.9184(3)
$\alpha/^\circ$	90
$\beta/^\circ$	91.50
$\gamma/^\circ$	90
Volume/ \AA^3	2503.88(8)
Z	2
$\rho_{\text{calc}}/\text{cm}^3$	1.267
μ/mm^{-1}	0.569

F(000)	1012.0
Crystal size/mm ³	0.256 × 0.214 × 0.156
Radiation	CuKα (λ = 1.54178)
2θ range for data collection/°	5.224 to 159.218
Index ranges	-19 ≤ h ≤ 19, -12 ≤ k ≤ 11, -21 ≤ l ≤ 21
Reflections collected	90298
Independent reflections	10589 [R _{int} = 0.0237, R _{sigma} = 0.0115]
Data/restraints/parameters	10589/1/735
Goodness-of-fit on F ²	1.015
Final R indexes [I ≥ 2σ (I)]	R ₁ = 0.0294, wR ₂ = 0.0793
Final R indexes [all data]	R ₁ = 0.0295, wR ₂ = 0.0794
Largest diff. peak/hole / e Å ⁻³	0.25/-0.20
Flack parameter	0.05(5)

Compound **163f**

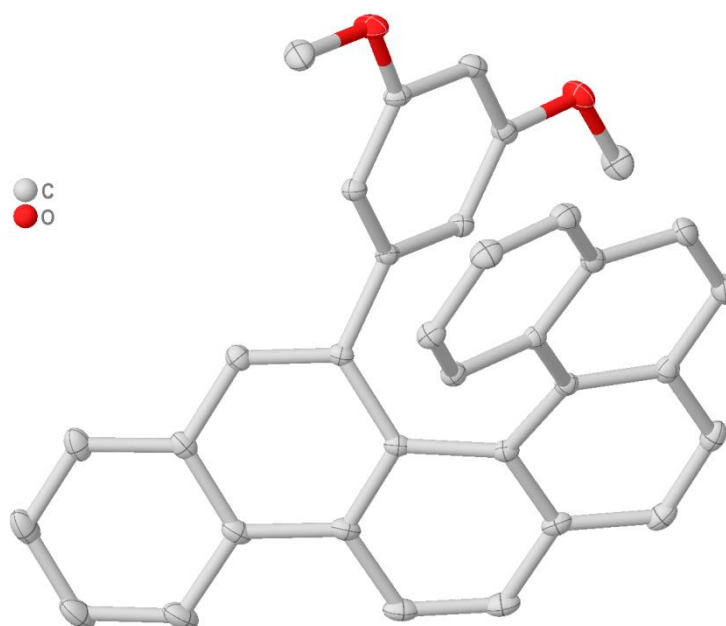


Figure S5. Full asymmetric unit of compound **163f**. Hydrogen atoms omitted for clarity. Displacement ellipsoids are drawn at 50% probability level.

Empirical formula	C ₃₄ H ₂₄ O ₂
Formula weight	464.53
Temperature/K	100
Crystal system	triclinic
Space group	P-1
a/Å	8.5181(6)
b/Å	11.8834(12)
c/Å	12.6170(12)
α/°	73.129(3)
β/°	78.555(4)
γ/°	69.985(3)
Volume/Å ³	1141.37(18)
Z	2
ρ _{calc} /cm ³	1.352
μ/mm ⁻¹	0.083
F(000)	488.0
Crystal size/mm ³	0.327 × 0.231 × 0.209

Radiation	MoK α ($\lambda = 0.71073$)
2 θ range for data collection/ $^\circ$	4.414 to 61.054
Index ranges	$-12 \leq h \leq 12$, $-16 \leq k \leq 16$, $-18 \leq l \leq 18$
Reflections collected	117731
Independent reflections	6952 [$R_{\text{int}} = 0.0180$, $R_{\text{sigma}} = 0.0082$]
Data/restraints/parameters	6952/0/397
Goodness-of-fit on F^2	1.045
Final R indexes [$I \geq 2\sigma(I)$]	$R_1 = 0.0374$, $wR_2 = 0.1086$
Final R indexes [all data]	$R_1 = 0.0387$, $wR_2 = 0.1106$
Largest diff. peak/hole / $e \text{ \AA}^{-3}$	0.48/-0.20

Compound **191k**

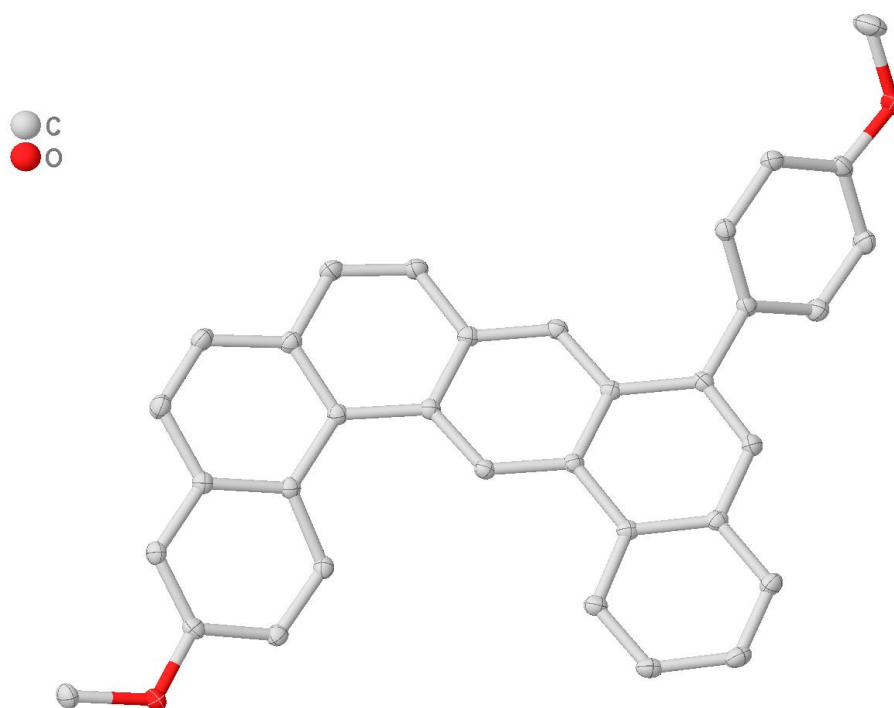


Figure S6. Full asymmetric unit of compound **191k**. Hydrogen atoms omitted for clarity. Displacement ellipsoids are drawn at 50% probability level.

Empirical formula	$C_{34}H_{24}O_2$
Formula weight	464.53
Temperature/K	100

Crystal system	monoclinic
Space group	P2 ₁ /c
a/Å	15.3812(18)
b/Å	7.1015(8)
c/Å	20.927(2)
α/°	90
β/°	91.725(4)
γ/°	90
Volume/Å ³	2284.8(4)
Z	4
ρ _{calc} /cm ³	1.350
μ/mm ⁻¹	0.082
F(000)	976.0
Crystal size/mm ³	0.38 × 0.127 × 0.058
Radiation	MoKα (λ = 0.71073)
2θ range for data collection/°	4.644 to 59.194
Index ranges	-21 ≤ h ≤ 21, -9 ≤ k ≤ 9, -29 ≤ l ≤ 29
Reflections collected	107134
Independent reflections	6403 [R _{int} = 0.0340, R _{sigma} = 0.0135]
Data/restraints/parameters	6403/3/336
Goodness-of-fit on F ²	1.042
Final R indexes [I >= 2σ (I)]	R ₁ = 0.0397, wR ₂ = 0.1148
Final R indexes [all data]	R ₁ = 0.0471, wR ₂ = 0.1231
Largest diff. peak/hole / e Å ⁻³	0.44/-0.22

Compound **161i**

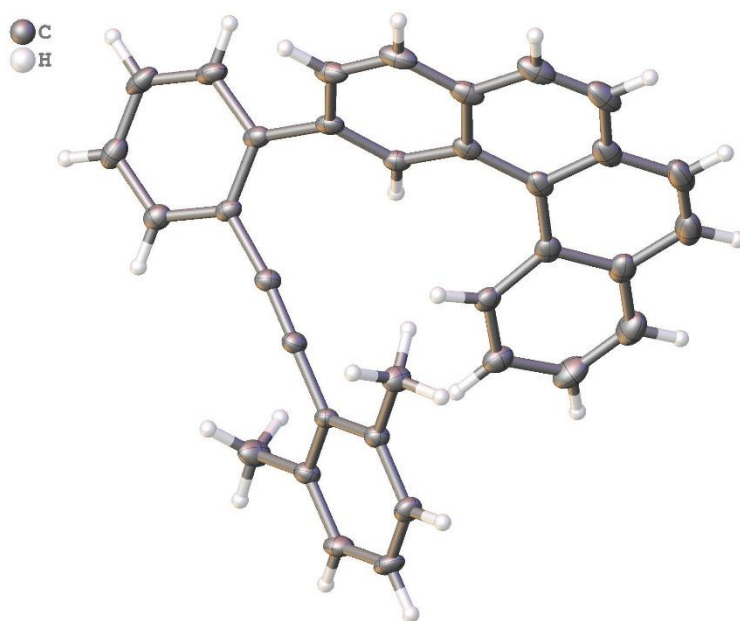


Figure 57. Full asymmetric unit of compound **161i**.

Identification code	0925_C2c
Empirical formula	C ₃₄ H ₂₄
Formula weight	432.53
Temperature/K	100.0
Crystal system	monoclinic
Space group	C2/c
a/Å	19.001(2)
b/Å	8.5285(9)
c/Å	29.885(4)
α/°	90
β/°	108.316(4)
γ/°	90
Volume/Å ³	4597.4(9)
Z	8
ρ _{calc} /cm ³	1.250
μ/mm ⁻¹	0.071
F(000)	1824.0

Crystal size/mm ³	0.203 × 0.194 × 0.166
Radiation	MoK α (λ = 0.71073)
2 θ range for data collection/°	4.516 to 57.464
Index ranges	-25 ≤ h ≤ 25, -11 ≤ k ≤ 11, -40 ≤ l ≤ 40
Reflections collected	108965
Independent reflections	5948 [R _{int} = 0.0421, R _{sigma} = 0.0158]
Data/restraints/parameters	5948/0/317
Goodness-of-fit on F ²	1.158
Final R indexes [I ≥ 2 σ (I)]	R ₁ = 0.0615, wR ₂ = 0.1291
Final R indexes [all data]	R ₁ = 0.0654, wR ₂ = 0.1312
Largest diff. peak/hole / e Å ⁻³	0.28/-0.20

Compound **185c**

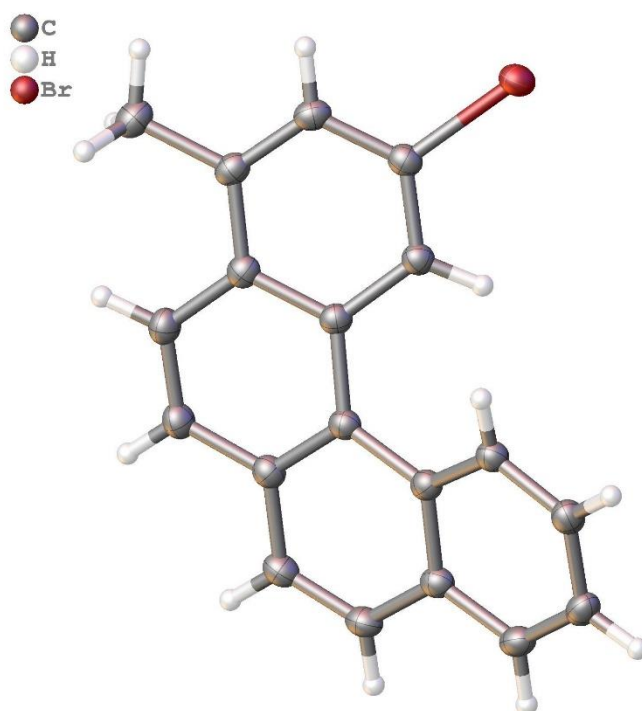


Figure 58. Full asymmetric unit of compound **185c**.

Identification code	mo_1024_CG_0m
Empirical formula	C ₁₉ H ₁₃ Br
Formula weight	321.20

Temperature/K	100.0
Crystal system	monoclinic
Space group	C2/c
a/Å	31.7662(14)
b/Å	3.92090(10)
c/Å	21.3149(8)
α /°	90
β /°	99.414(2)
γ /°	90
Volume/Å ³	2619.06(17)
Z	8
$\rho_{\text{calc}}/\text{g}/\text{cm}^3$	1.629
μ/mm^{-1}	3.124
F(000)	1296.0
Crystal size/mm ³	0.52 × 0.052 × 0.051
Radiation	MoK α (λ = 0.71073)
2 θ range for data collection/°	4.298 to 61.012
Index ranges	-44 ≤ h ≤ 43, -5 ≤ k ≤ 5, -29 ≤ l ≤ 30
Reflections collected	52711
Independent reflections	3987 [R _{int} = 0.0239, R _{sigma} = 0.0110]
Data/restraints/parameters	3987/0/188
Goodness-of-fit on F ²	1.030
Final R indexes [I >= 2 σ (I)]	R ₁ = 0.0252, wR ₂ = 0.0720
Final R indexes [all data]	R ₁ = 0.0314, wR ₂ = 0.0775
Largest diff. peak/hole / e Å ⁻³	0.46/-0.45

Compound **165a**

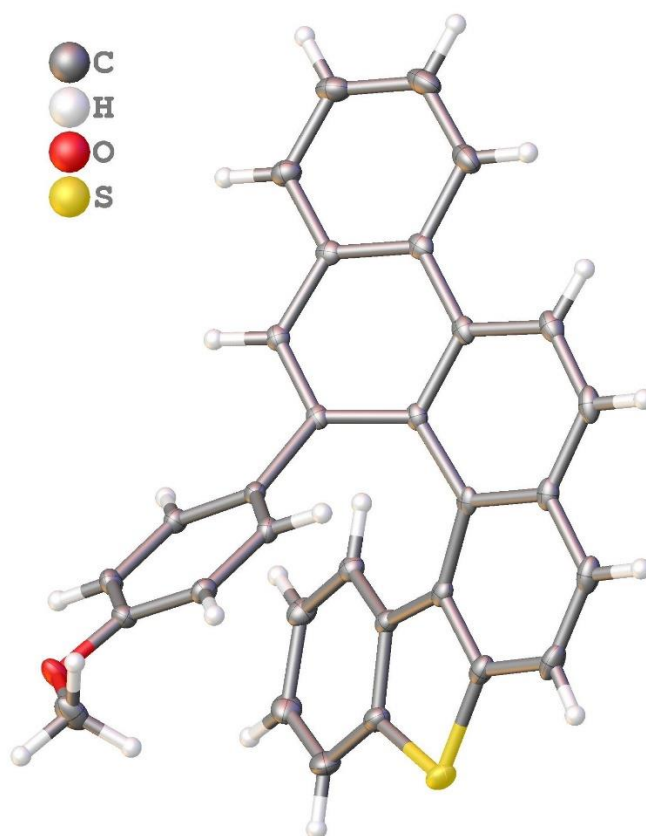


Figure 59. Molecular structure of full asymmetric unit of compound **165a**. Single crystals of **165a** were grown from a mixture of dichloromethane and hexane.

Identification code	mo_1317_CG_0m_4
Empirical formula	C ₃₁ H ₂₀ OS
Formula weight	440.53
Temperature/K	100.0
Crystal system	monoclinic
Space group	P2 ₁ /c
a/Å	11.787(3)
b/Å	23.039(5)
c/Å	16.407(3)
α/°	90
β/°	102.575(5)
γ/°	90
Volume/Å ³	4348.5(16)

Z	8
$\rho_{\text{calc}}/\text{cm}^3$	1.346
μ/mm^{-1}	0.172
F(000)	1840.0
Crystal size/ mm^3	0.235 × 0.209 × 0.039
Radiation	MoK α ($\lambda = 0.71073$)
2 θ range for data collection/ $^\circ$	3.958 to 61.038
Index ranges	-16 ≤ h ≤ 16, 0 ≤ k ≤ 32, 0 ≤ l ≤ 23
Reflections collected	12926
Independent reflections	12926 [$R_{\text{int}} = ?$, $R_{\text{sigma}} = 0.0344$]
Data/restraints/parameters	12926/0/598
Goodness-of-fit on F^2	1.063
Final R indexes [$I \geq 2\sigma(I)$]	$R_1 = 0.0421$, $wR_2 = 0.1097$
Final R indexes [all data]	$R_1 = 0.0541$, $wR_2 = 0.1171$
Largest diff. peak/hole / $e \text{ \AA}^{-3}$	0.39/-0.33

Compound **164d**

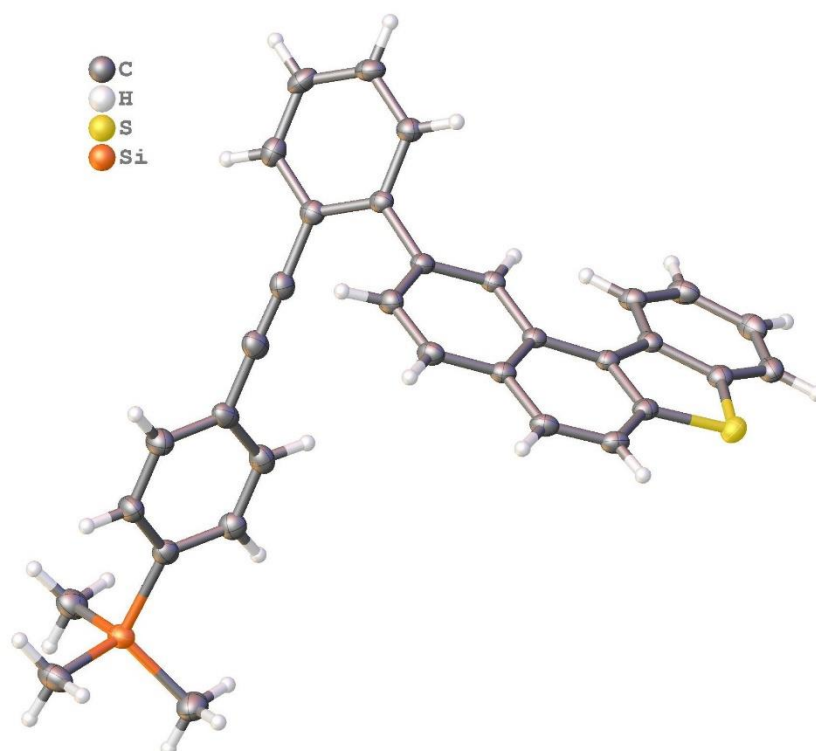


Figure 60. Molecular structure of full asymmetric unit of compound **164d**. Single crystals of **164d** were grown from a mixture of ethyl acetate and hexane.

Empirical formula	C ₃₃ H ₂₆ SSi
Formula weight	482.69
Temperature [K]	100
Crystal system	monoclinic
Space group (number)	<i>P</i> 2 ₁ / <i>c</i> (14)
<i>a</i> [Å]	17.251(8)
<i>b</i> [Å]	9.748(5)
<i>c</i> [Å]	17.305(10)
α [°]	90
β [°]	116.049(11)
γ [°]	90
Volume [Å ³]	2614(2)
<i>Z</i>	4
ρ_{calc} [gcm ⁻³]	1.226
μ [mm ⁻¹]	0.189

$F(000)$	1016
Crystal size [mm ³]	0.46×0.405×0.022
Crystal colour	colourless
Crystal shape	plate
Radiation	MoK α ($\lambda=0.71073$ Å)
2 θ range [°]	4.72 to 54.03 (0.78 Å)
Index ranges	-22≤h≤21, -12≤k≤12, -21 ≤ l ≤ 21
Reflections collected	91789
Independent reflections	5674 $R_{\text{int}} = 0.0443$ $R_{\text{sigma}} = 0.0177$
Completeness to $\theta = 25.242^\circ$	100.0 %
Data / Restraints / Parameters	5674/0/319
Goodness-of-fit on F^2	1.028
Final R indexes [$I \geq 2\sigma(I)$]	$R_1 = 0.0410$ $wR_2 = 0.0986$
Final R indexes [all data]	$R_1 = 0.0520$ $wR_2 = 0.1051$
Largest peak/hole [eÅ ⁻³]	0.41/-0.35

Compound **165f**

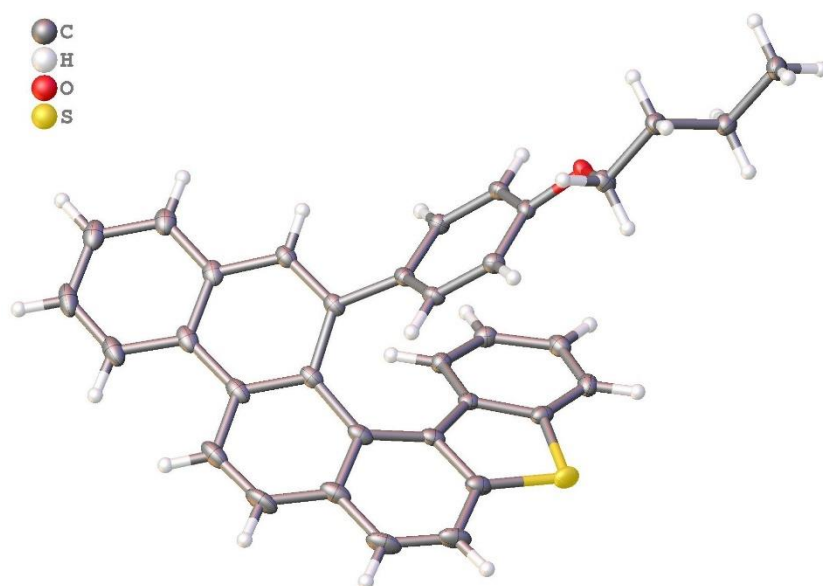


Figure 61. Molecular structure of full asymmetric unit of compound **165f**.

Empirical formula	C ₃₄ H ₂₆ OS
Formula weight	482.61
Temperature [K]	100.00
Crystal system	monoclinic
Space group (number)	<i>P</i> 2 ₁ / <i>c</i> (14)
<i>a</i> [Å]	16.291(4)
<i>b</i> [Å]	12.601(3)
<i>c</i> [Å]	11.913(2)
α [°]	90
β [°]	99.423(5)
γ [°]	90
Volume [Å ³]	2412.4(9)
<i>Z</i>	4
ρ_{calc} [gcm ⁻³]	1.329
μ [mm ⁻¹]	0.161
<i>F</i> (000)	1016
Crystal size [mm ³]	0.28×0.163×0.034
Crystal colour	colourless

Crystal shape	plate
Radiation	MoK α ($\lambda=0.71073$ Å)
2 θ range [°]	4.11 to 54.25 (0.78 Å)
Index ranges	-20 $\leq h \leq$ 20, -16 $\leq k \leq$ 16, -15 $\leq l \leq$ 15
Reflections collected	82076
Independent reflections	5331 $R_{\text{int}}=0.0400$ $R_{\text{sigma}}=0.0153$
Completeness to $\theta = 25.242^\circ$	100.0 %
Data / Restraints / Parameters	5331/0/327
Goodness-of-fit on F^2	1.058
Final R indexes [$I \geq 2\sigma(I)$]	$R_1=0.0352$ $wR_2 = 0.0891$
Final R indexes [all data]	$R_1=0.0413$ $wR_2 = 0.0942$
Largest peak/hole [eÅ $^{-3}$]	0.36/-0.44
Extinction coefficient	0.0035(6)

Compound **165b**

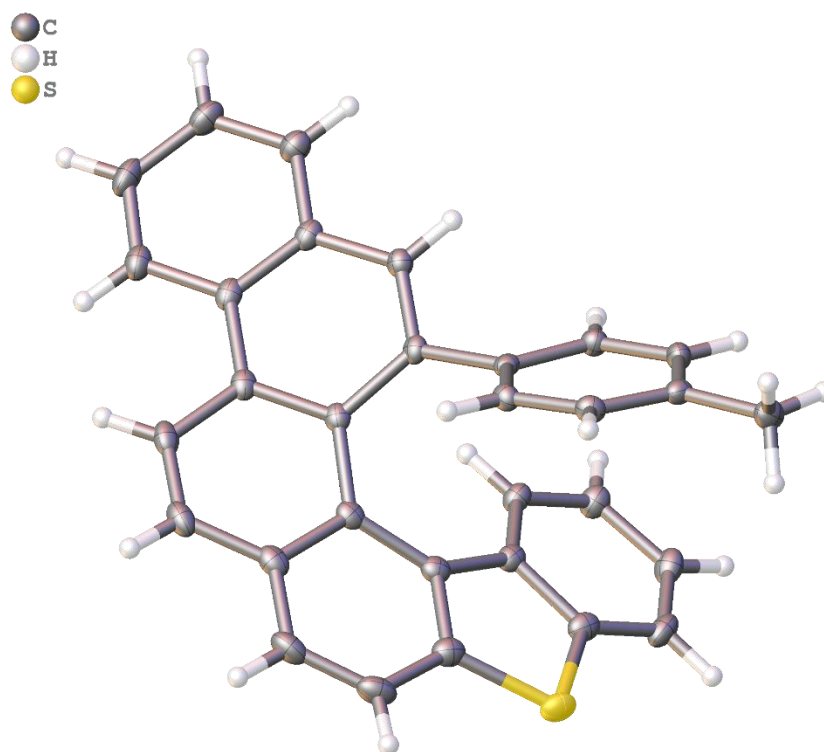


Figure 62. Molecular structure of full asymmetric unit of compound **165b**. Solvent molecules omitted for clarity.

Empirical formula	C ₃₁ H ₂₀ S
Formula weight	424.53
Temperature [K]	100.00
Crystal system	monoclinic
Space group (number)	<i>P</i> 2 ₁ / <i>c</i> (14)
<i>a</i> [Å]	8.715(4)
<i>b</i> [Å]	27.511(15)
<i>c</i> [Å]	8.826(3)
α [°]	90
β [°]	95.87(2)
γ [°]	90
Volume [Å ³]	2104.9(16)
<i>Z</i>	4
ρ_{calc} [gcm ⁻³]	1.340
μ [mm ⁻¹]	0.171
<i>F</i> (000)	888
Crystal size [mm ³]	0.281×0.067×0.025
Crystal colour	colourless
Crystal shape	needle
Radiation	MoK α (λ =0.71073 Å)
2 θ range [°]	4.70 to 55.76 (0.76 Å)
Index ranges	-10≤ <i>h</i> ≤11 -36≤ <i>k</i> ≤36

	-11 ≤ l ≤ 11
Reflections collected	34163
Independent reflections	5024 $R_{\text{int}}=0.0442$ $R_{\text{sigma}} = 0.0294$
Completeness to $\Theta = 25.242^\circ$	100.0 %
Data / Restraints / Parameters	5024/0/290
Goodness-of-fit on F^2	1.032
Final R indexes [$I \geq 2\sigma(I)$]	$R_1=0.0399$ $wR_2 = 0.0872$
Final R indexes [all data]	$R_1=0.0568$ $wR_2 = 0.0965$
Largest peak/hole [$\text{e}\text{\AA}^{-3}$]	0.30/-0.36

Compound **165g**

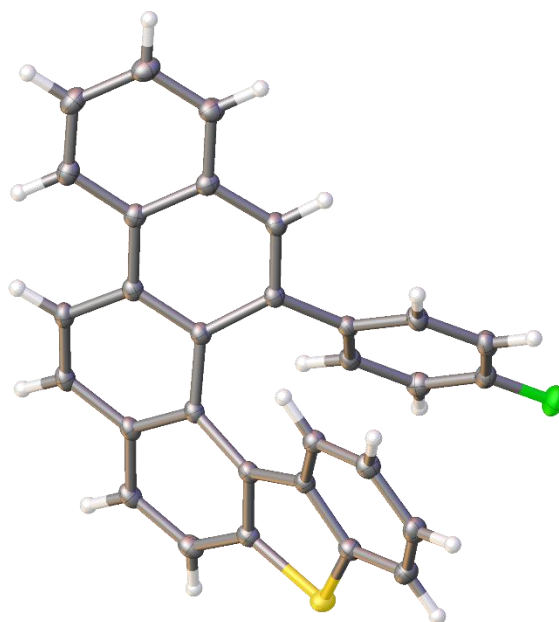


Figure 63. Molecular structure of full asymmetric unit of compound **165g**. Solvent molecules omitted for clarity.

Empirical formula	$\text{C}_{30}\text{H}_{17}\text{FS}$
Formula weight	428.49
Temperature [K]	100.00
Crystal system	monoclinic
Space group (number)	$P2_1/c$ (14)
a [\AA]	12.5573(9)
b [\AA]	12.1583(12)
c [\AA]	13.9137(13)
α [$^\circ$]	90
β [$^\circ$]	107.372(2)
γ [$^\circ$]	90
Volume [\AA^3]	2027.4(3)
Z	4

ρ_{calc} [gcm ⁻³]	1.404
μ [mm ⁻¹]	0.185
$F(000)$	888
Crystal size [mm ³]	0.308×0.217×0.128
Crystal colour	colourless
Crystal shape	block
Radiation	MoK α ($\lambda=0.71073$ Å)
2 θ range [°]	4.54 to 59.19 (0.72 Å)
Index ranges	-14≤h≤17 -16≤k≤16 -19 ≤ l ≤ 19
Reflections collected	37772
Independent reflections	5675 $R_{\text{int}}=0.0437$ $R_{\text{sigma}} = 0.0287$
Completeness to $\Theta = 25.242^\circ$	100.0 %
Data / Restraints / Parameters	5675/0/289
Goodness-of-fit on F^2	1.038
Final R indexes [$I \geq 2\sigma(I)$]	$R_1=0.0405$ $wR_2 = 0.0999$
Final R indexes [all data]	$R_1=0.0488$ $wR_2 = 0.1067$
Largest peak/hole [eÅ ⁻³]	0.37/-0.42

Compound **165j**

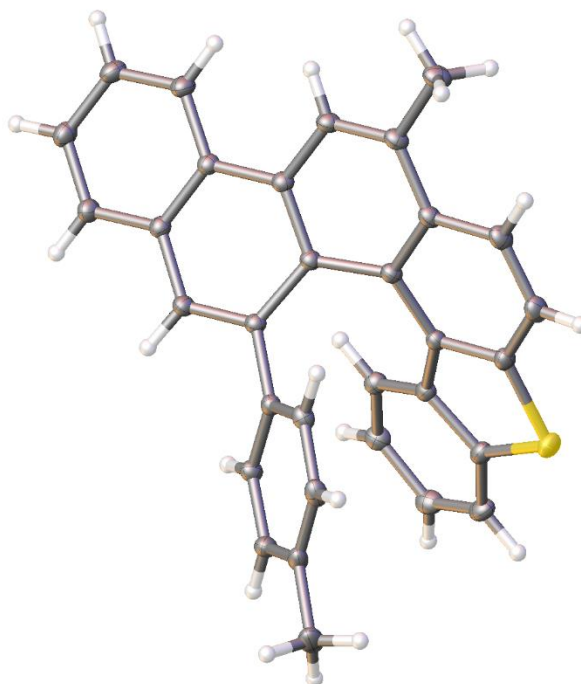


Figure 64. Molecular structure of full asymmetric unit of compound **165j**. Solvent molecules omitted for clarity.

Identification number	mo_1572_cg_0m
Empirical formula	C ₃₂ H ₂₂ S
Formula weight	438.55
Temperature [K]	100.00
Crystal system	monoclinic
Space group (number)	<i>P</i> 2 ₁ / <i>c</i> (14)
<i>a</i> [Å]	9.8315(6)
<i>b</i> [Å]	13.3998(14)
<i>c</i> [Å]	33.025(3)
α [°]	90
β [°]	93.372(2)
γ [°]	90
Volume [Å ³]	4343.2(7)
<i>Z</i>	8
ρ_{calc} [gcm ⁻³]	1.341
μ [mm ⁻¹]	0.168
<i>F</i> (000)	1840
Crystal size [mm ³]	0.352×0.26×0.076
Crystal colour	yellow
Crystal shape	plate
Radiation	MoK α (λ =0.71073 Å)
2 θ range [°]	3.92 to 66.97 (0.64 Å)
Index ranges	-15≤ <i>h</i> ≤14 -20≤ <i>k</i> ≤20

	-51 ≤ l ≤ 50
Reflections collected	171495
Independent reflections	15875 $R_{\text{int}} = 0.0361$ $R_{\text{sigma}} = 0.0236$
Completeness to $\Theta = 25.242^\circ$	100.0 %
Data / Restraints / Parameters	15875/0/599
Goodness-of-fit on F^2	1.038
Final R indexes [$I \geq 2\sigma(I)$]	$R_1 = 0.0420$ $wR_2 = 0.1035$
Final R indexes [all data]	$R_1 = 0.0586$ $wR_2 = 0.1142$
Largest peak/hole [$\text{e}\text{\AA}^{-3}$]	0.48/-0.30

Compound **166**

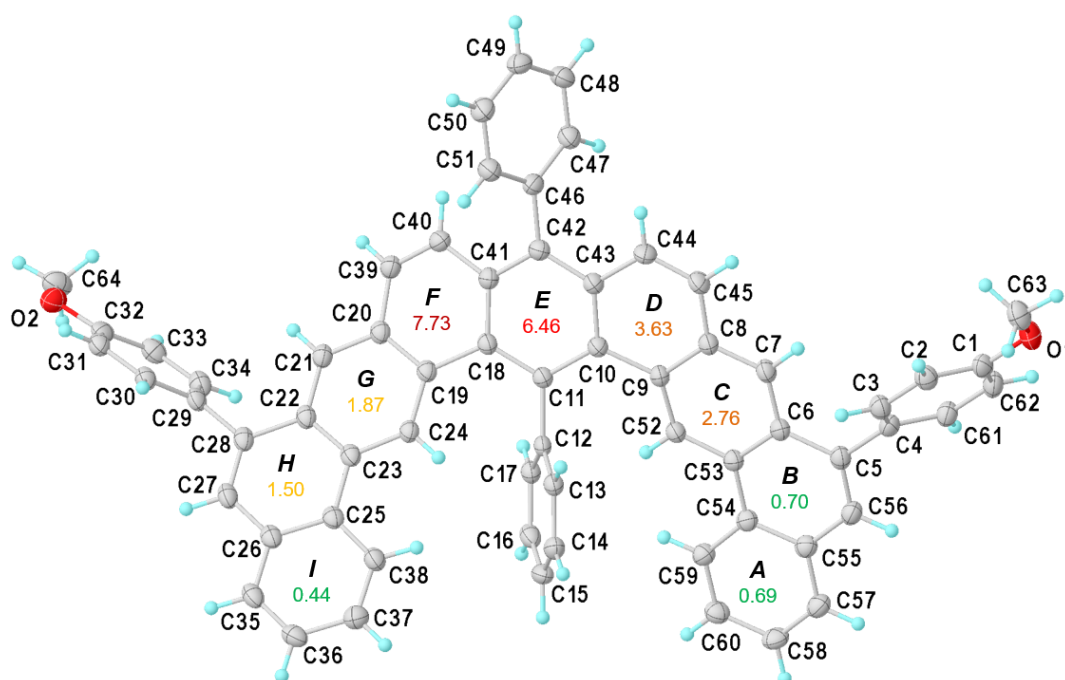


Figure 65. Molecular structure of full asymmetric unit and numbering scheme of compound **166**. Ellipsoids drawn at 50% probability level. Root mean square (RMS) deviations of fitted atoms of each benzene unit in the helical structure multiplied by 100 for a more convenient scale [\AA]. Single crystals of **166** were obtained by vapor diffusion method from chloroform and hexane. Non-merohedral twinning was found; final refinement against hkl data with batch scale factor of 0.407(1); Twin domain transformation matrix is $(-0.997 \ 0.005 \ 0.003 / 0.786 \ 0.114 \ 0.884 / 0.785 \ 1.112 \ -0.117)$ which corresponds to rotation of 179.973° .

CCDC	2062473
Empirical formula	$\text{C}_{64}\text{H}_{42}\text{O}_2$
Formula weight	842.97
Temperature/K	100

Crystal system	Triclinic
Space group	<i>P</i> -1
<i>a</i> /Å	10.6181(3)
<i>b</i> /Å	14.0858(4)
<i>c</i> /Å	15.7180(5)
α /°	93.3340(10)
β /°	103.9570(10)
γ /°	108.3030(10)
Volume/Å ³	2143.03(11)
<i>Z</i>	2
ρ_{calc} g/cm ³	1.306
μ /mm ⁻¹	0.596
<i>F</i> (000)	884.0
Crystal size/mm ³	0.164 × 0.137 × 0.133
Radiation	CuK α (λ = 1.54178)
2 θ range for data collection/°	5.856 to 149.076
Index ranges	-13 ≤ <i>h</i> ≤ 12, -17 ≤ <i>k</i> ≤ 17, 0 ≤ <i>l</i> ≤ 19
Reflections collected	8555
Independent reflections	8555 [<i>R</i> _{int} = ?, <i>R</i> _{sigma} = 0.0190]
Data/restraints/parameters	8555/0/598
Goodness-of-fit on <i>F</i> ²	1.039
Final <i>R</i> indexes [<i>I</i> >= 2 σ (<i>I</i>)]	<i>R</i> ₁ = 0.0387, <i>wR</i> ₂ = 0.1070
Final <i>R</i> indexes [all data]	<i>R</i> ₁ = 0.0416, <i>wR</i> ₂ = 0.1114
Largest diff. peak/hole / e Å ⁻³	0.27/-0.19

Table 11. Least-squares planes (x,y,z in crystal coordinates) for each benzene unit in the helical structure calculated by shelXL-2018/3 and deviation for each atom [Å] used to define plane.

A	$- 7.9115(43) x + 12.1239(44) y - 0.0763(96) z = 0.4523(37)$				
C54	C55	C57	C58	C59	C60
-0.0101(10)	0.0098(10)	-0.0017(11)	-0.0063(11)	0.0060(11)	0.0022(10)
B	$- 7.7995(40) x + 12.2927(38) y + 0.4397 (90) z = 0.5728(45)$				
C5	C6	C53	C54	C55	C56
-0.0030(10)	-0.0044(10)	0.0039(9)	0.0037(10)	-0.0109(10)	0.0108(10)
C	$- 7.9614(40) x + 12.1348(41) y + 0.5519(88) z = 0.4026(49)$				
C6	C7	C8	C9	C52	C53
-0.0328	0.0190(10)	0.0186(10)	-0.0429(10)	0.0300(10)	0.0080(10)
D	$8.4551(38) x - 11.4721(48) y - 0.0102(92) z = 0.5012(57)$				
C8	C9	C10	C43	C44	C45
0.0031(10)	-0.0454(10)	0.0614(10)	-0.0358(10)	-0.0096(11)	0.0264(11)
E	$8.8173(34) x - 10.3864(55) y + 1.6131(89) z = 1.9674(51)$				
C10	C11	C18	C41	C42	C43
-0.0844(10)	0.0288(10)	0.0608(10)	-0.0957(10)	0.0385(10)	0.0521(10)
F	$8.1881(38) x - 8.8057(64) y + 5.4046(82) z = 4.0623(47)$				
C18	C19	C20	C39	C40	C41
-0.1233	0.0770(10)	0.0250(10)	-0.0878(10)	0.0404(10)	0.0687(10)
G	$8.3003(37) x - 5.8359(71) y + 6.4519(79) z = 5.5378(32)$				
C19	C20	C21	C22	C23	C24
-0.0270(9)	0.0295(10)	-0.0099(10)	-0.0126(10)	0.0146(10)	0.0054(10)
H	$8.3648(36) x - 4.4219(75) y + 6.4043(80) z = 5.6687(29)$				
C22	C23	C25	C26	C27	C28
0.0018(10)	0.0172(9)	-0.0204(9)	0.0044	0.0160(10)	- 0.0190(10)
I	$8.5791(39) x - 4.3729(79) y + 5.9160(90) z = 5.5150(24)$				
C25	C26	C35	C36	C37	C38
0.0047(10)	-0.0076(10)	0.0053(10)	0.0001(11)	-0.0030(11)	0.0006(10)

Compound 168

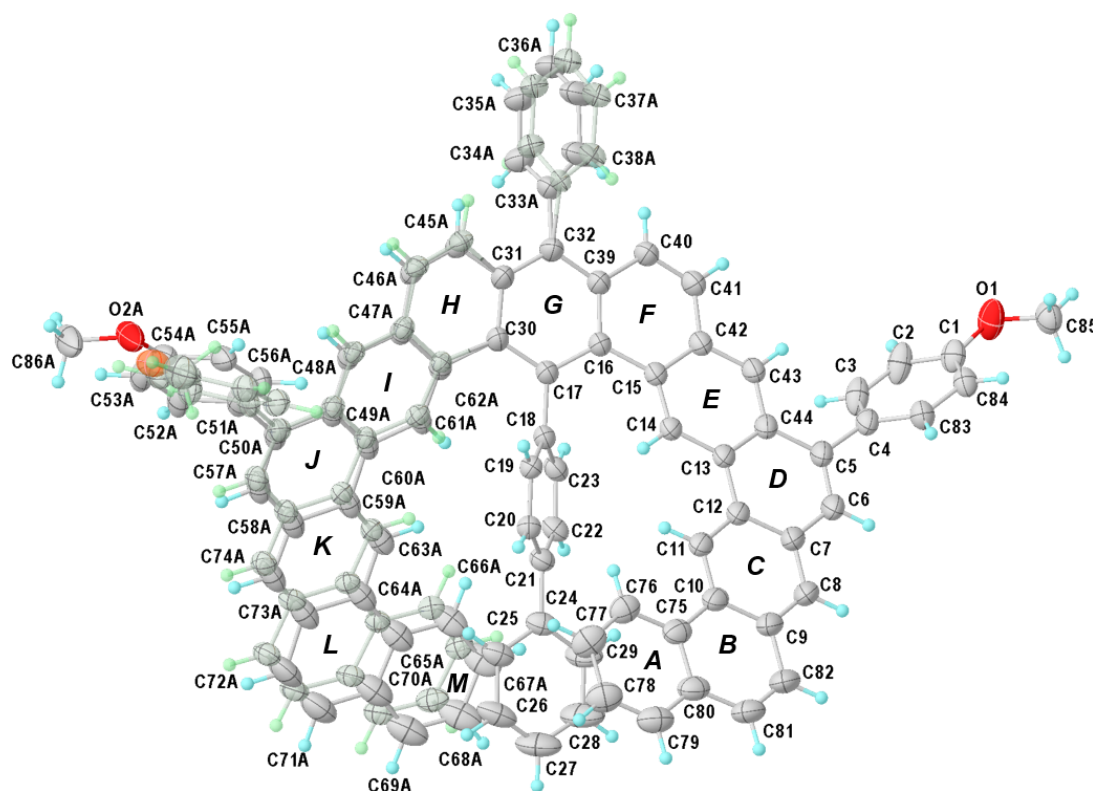


Figure 66. Single crystals of **168** were obtained after approximately 3 months from a solvent mixture consisting mainly of cyclohexane. There were several failed attempts with other solvents that possibly remain in the solvent mixture, which is of relevance in regards of the solvent mask applied in the structure model.

A solvent mask was calculated in Olex² and 2778 electrons were found in a volume of 11225 Å³ in one void per unit cell. This is consistent with the presence of 3 cyclohexane molecules per asymmetric unit which account for 2592 electrons per unit cell. There are still small remaining residual densities that were not reached by the mask due to the disorder oscillating into the masked regions. The packing diagram (Figure 67) shows the honeycomb super-structure, where continuous channels are formed along the c-axis.

CCDC	2010181
Empirical formula	C ₈₆ H ₅₄ O ₂
Formula weight	1119.29
Temperature/K	100
Crystal system	Trigonal
Space group	<i>R</i> -3
a/Å	41.6459(6)
b/Å	41.6459(6)

c/Å	23.5385(6)
α /°	90
β /°	90
γ /°	120
Volume/Å ³	35355.2(14)
Z	18
ρ_{calc} /cm ³	0.946
μ /mm ⁻¹	0.426
<i>F</i> (000)	10548.0
Crystal size/mm ³	0.294 × 0.188 × 0.076
Radiation	CuK α (λ = 1.54178)
2 θ range for data collection/°	4.482 to 149.182
Index ranges	-52 ≤ <i>h</i> ≤ 51, -52 ≤ <i>k</i> ≤ 51, -29 ≤ <i>l</i> ≤ 29
Reflections collected	437017
Independent reflections	16068 [<i>R</i> _{int} = 0.0436, <i>R</i> _{sigma} = 0.0094]
Data/restraints/parameters	16068/336/1113
Goodness-of-fit on <i>F</i> ²	1.082
Final <i>R</i> indexes [<i>I</i> >= 2 σ (<i>I</i>)]	<i>R</i> ₁ = 0.0787, <i>wR</i> ₂ = 0.2681
Final <i>R</i> indexes [all data]	<i>R</i> ₁ = 0.0901, <i>wR</i> ₂ = 0.2887
Largest diff. peak/hole / e Å ⁻³	0.70/-0.31

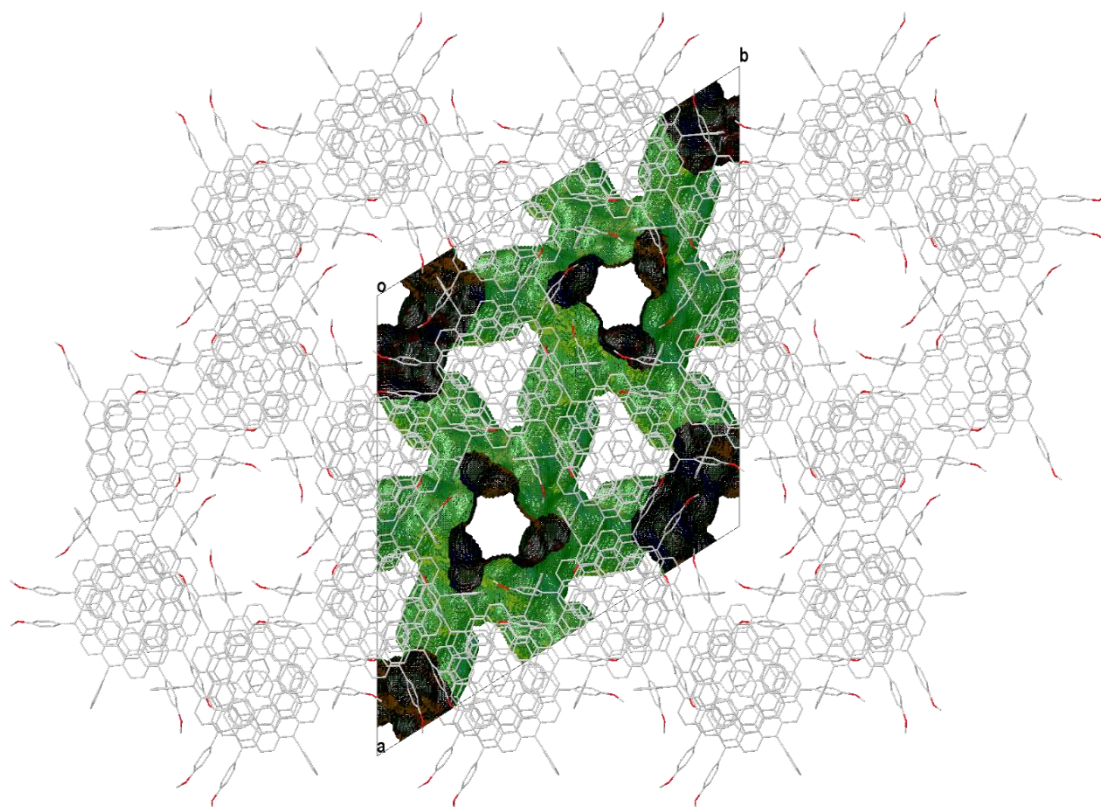


Figure 67. Packing diagram of **168** along c-axis (Only major part depicted). The centers of the honeycomb superstructures contain continuous solvent channels. Solvent mask volume inside green mesh.

Table 12. Least-squares planes (x,y,z in crystal coordinates) for each benzene unit in the helical structure calculated by shelXL-2018/3 and deviation for each atom [Å] used to define plane (Only major part of disorder).

A	$10.1280(417) x - 15.1817(427) y + 21.8561(96) z = 3.7593(302)$				
C75	C76	C77	C78	C79	C80
0.0142(15)	-0.0076(17)	-0.0053(20)	0.0115(21)	-0.0045(21)	- 0.0083(18)
B	$11.0060(435) x - 17.1181(455) y + 21.3986(116) z = 3.0931(307)$				
C9	C10	C75	C80	C81	C82
0.0064(21)	0.0153(17)	-0.0256(16)	0.0140(19)	0.0094(24)	- 0.0195(25)
C	$11.8192(395) x - 18.0402(407) y + 21.1366(110) z = 3.0213(0273)$				
C7	C8	C9	C10	C11	C12
-0.0076(20)	0.0035(22)	0.0049(20)	-0.0093(16)	0.0053(15)	0.0032(16)
D	$10.8672(387) x - 18.3070(398) y + 21.1127(110) z = 2.3260 (244)$				
C5	C6	C7	C12	C13	C44
-0.0079(19)	0.0078(21)	0.0040(19)	-0.0148(16)	0.0145(15)	-

					0.0037(16)
E	9.0465(331) x - 18.2880(309) y + 21.1474(85) z = 1.3666(210)				
C13	C14	C15	C42	C43	C44
-0.0174(14)	-0.0225(13)	0.0437(13)	-0.0258(15)	-0.0141(16)	0.0361(15)
F	2.4493(375) x - 12.5449(371) y + 22.3061(70) z = 1.9897(246)				
C15	C16	C39	C40	C41	C42
-0.0676(14)	0.0914(14)	-0.0472(16)	-0.0264(18)	0.0508(17)	- 0.0010(15)
G	- 5.8748(425) x - 6.8031(432) y + 22.4192(73) z = 1.3784(298)				
C16	C17	C30	C31	C32	C39
-0.0783(15)	0.0121(16)	0.0659(18)	-0.0787(19)	0.0112(19)	0.0679(17)
H	- 11.9429(1082) x + 1.2581(1140) y + 22.3391(173) z = 3.7331 (632)				
C30	C31	C45A	C46A	C47A	C62A
-0.1271(25)	0.0025(38)	0.1095(57)	-0.0804(51)	-0.0506(38)	0.1461(35)
I	- 17.2558(843) x + 10.2263(904) y + 21.3974(219) z = 6.7913(706)				
C47A	C48A	C49A	C60A	C61A	C62A
0.0303(34)	0.0051(33)	-0.0287(33)	0.0157(37)	0.0207(41)	- 0.0432(37)
J	- 19.1200(850) x + 12.4638(861) y + 20.8251(252) z = 6.8935(745)				
C49A	C50A	C57A	C58A	C59A	C60A
0.0125(33)	-0.0129(33)	0.0029(37)	0.0077(40)	-0.0077(40)	- 0.0025(36)
K	- 18.9487(1134) x + 10.9880(1160) y + 20.9376(326) z = 5.9553(1066)				
C58A	C59A	C63A	C64A	C73A	C74A
-0.0080(44)	0.0059(49)	-0.0001(57)	-0.0038(55)	0.0018(58)	0.0042(55)
L	- 17.9638(1362) x + 9.0384(1439) y + 21.2361(368) z = 5.4943(1236)				
C64A	C65A	C70A	C71A	C72A	C73A
-0.0024(53)	0.0059(56)	0.0000(64)	-0.0106(76)	0.0140(79)	- 0.0069(62)
M	- 16.8684(1566) x + 8.0536(1396) y + 21.5198(393) z = 5.8402(1243)				
C65A	C66A	C67A	C68A	C69A	C70A

-0.0220(61)	0.0076(69)	0.0134(60)	-0.0201(62)	0.0058(61)	0.0153(59)
-------------	------------	------------	-------------	------------	------------

Compound **169**

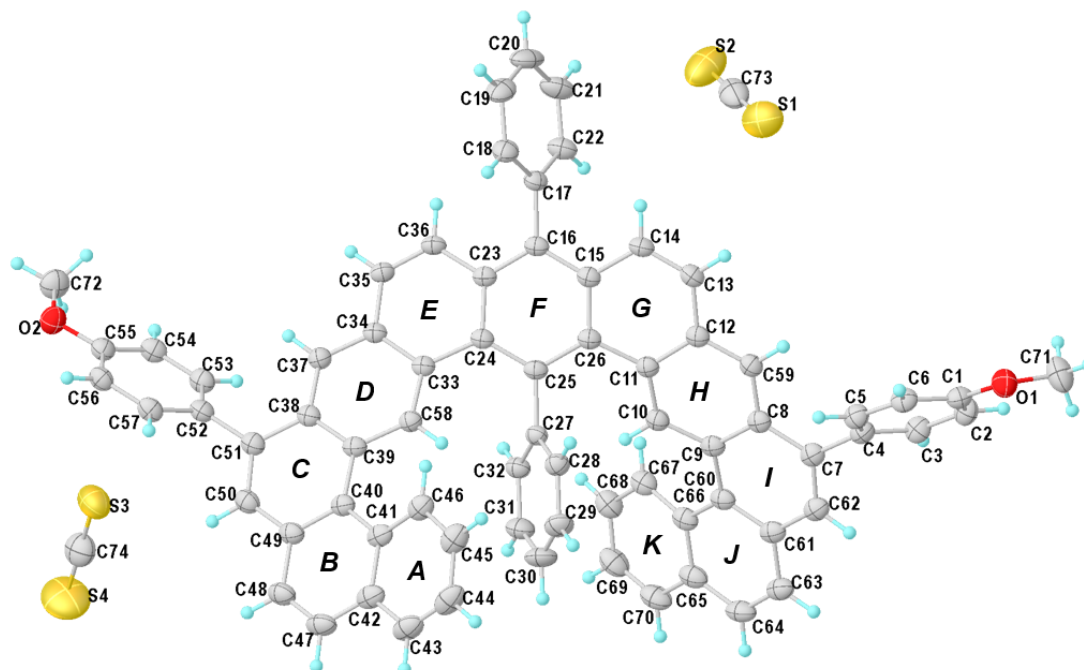


Figure 68. Molecular structure of full asymmetric unit and numbering scheme of compound **169**. Ellipsoids drawn at 50% probability level. Single crystals of **169** were obtained from a solution of carbon disulfide and dichloromethane.

CCDC	2062474
Empirical formula	C ₇₄ H ₄₆ O ₂ S ₄
Formula weight	1095.35
Temperature/K	150
Crystal system	Monoclinic
Space group	<i>P</i> 2 ₁ / <i>n</i>
<i>a</i> /Å	15.5775(19)
<i>b</i> /Å	16.354(2)
<i>c</i> /Å	21.465(3)
α /°	90
β /°	99.803(4)
γ /°	90
Volume/Å ³	5388.6(12)

Z	4
$\rho_{\text{calc}}/\text{cm}^3$	1.350
μ/mm^{-1}	0.228
$F(000)$	2280.0
Crystal size/ mm^3	$0.503 \times 0.247 \times 0.112$
Radiation	MoK α ($\lambda = 0.71073$)
2 θ range for data collection/ $^\circ$	4.324 to 54.384
Index ranges	$-20 \leq h \leq 20, -20 \leq k \leq 21, -27 \leq l \leq 27$
Reflections collected	112736
Independent reflections	11963 [$R_{\text{int}} = 0.0264, R_{\text{sigma}} = 0.0142$]
Data/restraints/parameters	11963/0/723
Goodness-of-fit on F^2	1.029
Final R indexes [$I \geq 2\sigma(I)$]	$R_1 = 0.0500, wR_2 = 0.1383$
Final R indexes [all data]	$R_1 = 0.0571, wR_2 = 0.1451$
Largest diff. peak/hole / $e \text{ \AA}^{-3}$	0.61/-0.93

Table 13. Least-squares planes (x,y,z in crystal coordinates) for each benzene unit in the helical structure calculated by shelXL-2018/3 and deviation for each atom [\AA] used to define plane (Only major part of disorder).

A	$12.5134(73) x - 5.6210(117) y + 7.3523(151) z = 10.9055(151)$				
C41	C42	C43	C44	C45	C46
-0.0479(12)	0.0489(12)	-0.0096(14)	-0.0313(14)	0.0316(13)	0.0083(13)
B	$10.5073(83) x - 7.9703(102) y + 9.2644(139) z = 8.9596(146)$				
C40	C41	C42	C47	C48	C49
-0.0795(11)	0.0676(12)	-0.0063(12)	-0.0470(13)	0.0355(13)	0.0297(12)
C	$8.3617(89) x - 9.4399(90) y + 11.0546(122) z = 7.2744(129)$				
C38	C39	C40	C49	C50	C51
-0.0155(11)	-0.0577(11)	0.0895(11)	-0.0466(12)	-0.0319(12)	0.0622(12)
D*	$6.0092 (9.9990) x - 10.6712 (9.9990) y + 12.3865 (9.9990) z = 5.4540 (9.9990)$				
C33	C34	C37	C38	C39	C58

-0.0492(1011)	0.0411(828)	0.0118(229)	-0.0557(1141)	0.0465(960)	0.0056(124)
-0.386*X + 0.653*Y - 0.652*Z - 5.454 = 0					
0.049	-0.041	-0.012	0.056	-0.046	-0.006
E	6.1213(90) x - 8.6814(88) y + 14.4461(102) z = 7.7727(91)				
C23	C24	C33	C34	C35	C36
0.0561	-0.1010(11)	0.0663(11)	0.0142(11)	-0.0655(11)	0.0299(11)
F	5.0653(92) x - 5.5549(96) y + 17.4793(81) z = 10.4854(77)				
C15	C16	C23	C24	C25	C26
0.0755(11)	0.0148(11)	-0.0897(11)	0.0739(11)	0.0151(11)	-0.0894(11)
G	5.8532(91) x - 1.7763(105) y + 18.0937(77) z = 12.9065(63)				
C11	C12	C13	C14	C15	C26
-0.0918(11)	0.0029(11)	0.0681(12)	-0.0436(12)	-0.0511(11)	0.1154(11)
H	6.2022(92) x + 2.3174(104) y + 17.7151(83) z = 14.8194(59)				
C8	C9	C10	C11	C12	C59
0.0816(11)	-0.0876(11)	0.0096(11)	0.0749(11)	-0.0816(11)	0.0030(11)
I	8.9800(84) x + 2.8819(103) y + 14.7701(103) z = 13.6862(84)				
C7	C8	C9	C60	C61	C62
-0.0435(11)	-0.0194(11)	0.0787(11)	-0.0791(11)	0.0193(11)	0.0440(12)
J	10.7954(79) x + 2.4801(113) y + 12.3751(122) z = 12.0311(106)				
C60	C61	C63	C64	C65	C66
0.0722(11)	-0.0354(12)	-0.0249(12)	0.0450(13)	-0.0053(12)	-0.0516(12)
K	12.4142(73) x + 1.4538(125) y + 9.7256(144) z = 9.8867(119)				
C65	C66	C67	C68	C69	C70
-0.0311(13)	0.0404(12)	-0.0176(12)	-0.0158(13)	0.0260(14)	-0.0019(14)

*Mean plane of D (red highlighted): Obviously the s. u. produced by shelXL 2016/6 are absurd in value. We suspect a numerical bug in shelXL 2016/6 in the calculation of estimated uncertainties from the covariance matrix. This was only encountered for that specific composition of atoms, mean planes defined by only five atoms of that range give reasonable values. The atom-plane distances appear plausible when compared to the same mean plane calculated by Olex² (blue highlighted), giving the same results as shelXL 2016/6. However, there are no s. u. available as Olex² is not using the covariance matrix.

Compound **215**

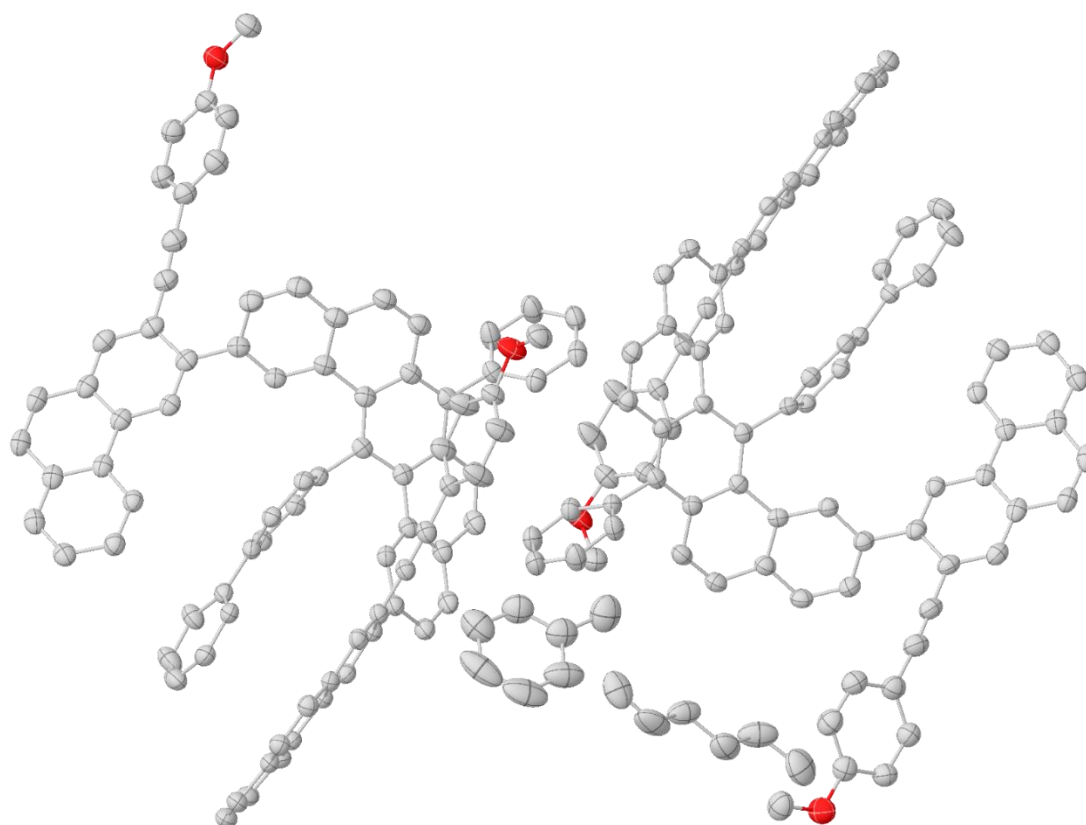


Figure 69. Molecular structure of full asymmetric unit of compound **165**. Hydrogen atoms and labels omitted for clarity. Ellipsoids drawn at 50% probability level. Single crystals of **165** were grown from a mixture of toluene and hexane. The crystals were rather small in size and did show signs of deterioration during the lengthy data collection of 104 hours, possibly due to loss of co-crystallized solvent. Although the R-indices leave something to be desired and the residual density map hints at some disorder, the gross molecular structure determination was accomplished unambiguously.

CCDC	2062475
Empirical formula	$C_{182}H_{123}O_4$
Formula weight	2373.80
Temperature/K	100
Crystal system	Triclinic
Space group	<i>P</i> -1
a/Å	16.856(6)
b/Å	19.263(9)
c/Å	21.424(8)
α /°	100.963(11)
β /°	112.032(15)

$\gamma/^\circ$	94.622(10)
Volume/ \AA^3	6242(4)
Z	2
$\rho_{\text{calc}} \text{ g/cm}^3$	1.263
μ/mm^{-1}	0.074
$F(000)$	2494.0
Crystal size/ mm^3	$0.192 \times 0.088 \times 0.04$
Radiation	MoK α ($\lambda = 0.71073$)
2θ range for data collection/ $^\circ$	3.988 to 54.228
Index ranges	$-21 \leq h \leq 21, -24 \leq k \leq 24, -27 \leq l \leq 27$
Reflections collected	337891
Independent reflections	27454 [$R_{\text{int}} = 0.0493, R_{\text{sigma}} = 0.0253$]
Data/restraints/parameters	27454/73/1709
Goodness-of-fit on F^2	1.200
Final R indexes [$I \geq 2\sigma(I)$]	$R_1 = 0.0973, wR_2 = 0.2640$
Final R indexes [all data]	$R_1 = 0.1162, wR_2 = 0.2930$
Largest diff. peak/hole / $e \text{\AA}^{-3}$	1.08/-0.59

Compound **217a**

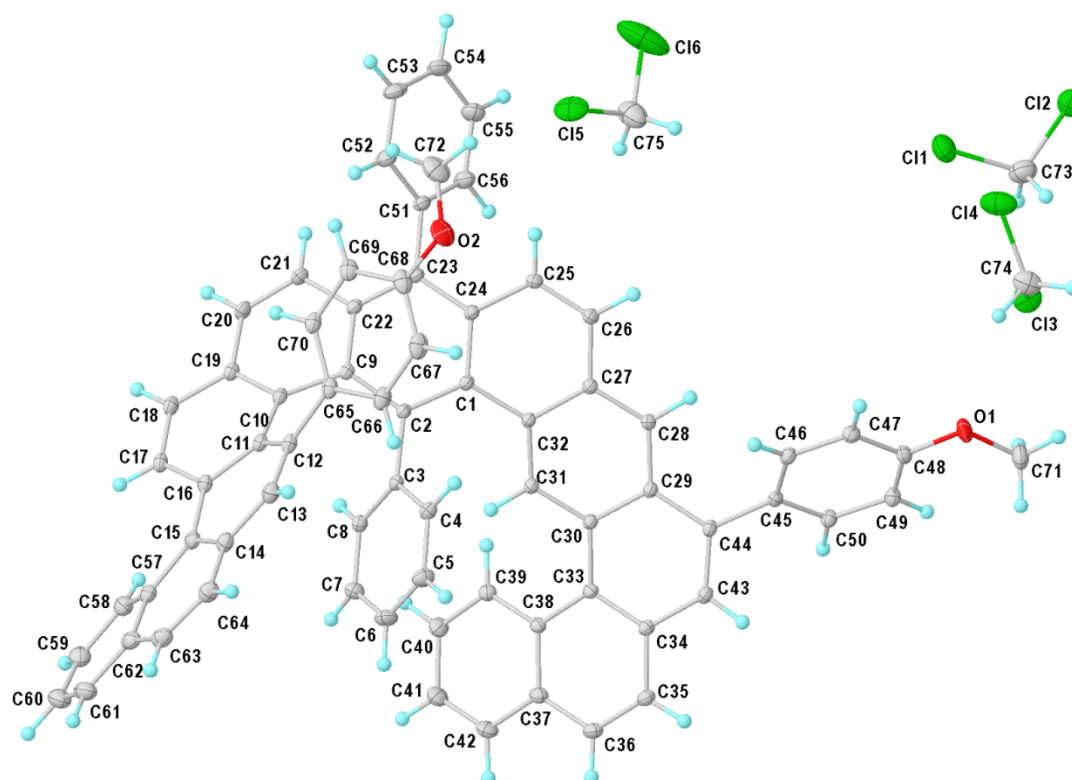


Figure 70. Molecular structure of full asymmetric unit and numbering scheme of compound **217a**. Ellipsoids drawn at 50% probability level. Single crystals of **217a** were obtained by diffusion method from a mixture of chloroform and dichloromethane as solvent and hexane as antisolvent.

CCDC	2062476
Empirical formula	C _{74.5} H ₅₁ Cl ₅ O ₂
Formula weight	1155.40
Temperature/K	100
Crystal system	Triclinic
Space group	<i>P</i> -1
<i>a</i> /Å	11.7422(8)
<i>b</i> /Å	14.2405(11)
<i>c</i> /Å	17.6414(15)
α /°	98.551(3)
β /°	103.588(3)
γ /°	102.474(3)
Volume/Å ³	2737.1(4)

Z	2
$\rho_{\text{calc}}/\text{cm}^3$	1.402
μ/mm^{-1}	0.317
$F(000)$	1198.0
Crystal size/ mm^3	$0.281 \times 0.137 \times 0.082$
Radiation	MoK α ($\lambda = 0.71073$)
2θ range for data collection/ $^\circ$	4.566 to 61.098
Index ranges	$-16 \leq h \leq 16, -20 \leq k \leq 20, -25 \leq l \leq 25$
Reflections collected	209338
Independent reflections	16738 [$R_{\text{int}} = 0.0229, R_{\text{sigma}} = 0.0109$]
Data/restraints/parameters	16738/22/883
Goodness-of-fit on F^2	1.025
Final R indexes [$I \geq 2\sigma(I)$]	$R_1 = 0.0394, wR_2 = 0.1084$
Final R indexes [all data]	$R_1 = 0.0418, wR_2 = 0.1106$
Largest diff. peak/hole / $e \text{ \AA}^{-3}$	1.30/-0.83

Compound **217b**

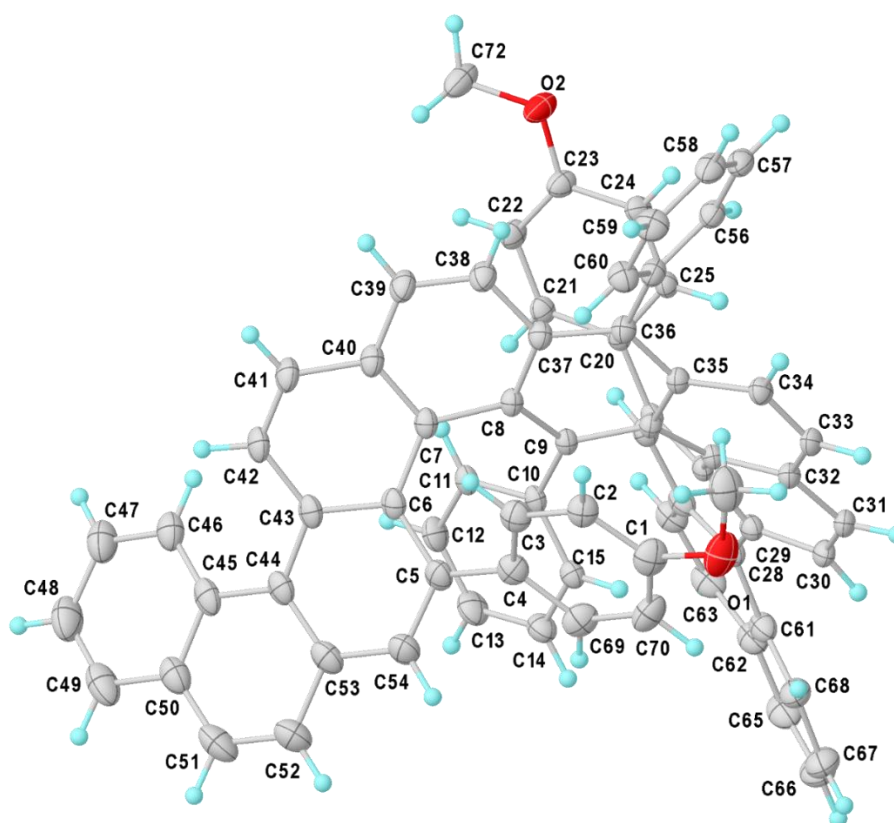


Figure 71. Molecular structure of full asymmetric unit and numbering scheme of compound **217b**. Ellipsoids drawn at 25% probability level.

Single crystals of **217b** were obtained from a mixture of tetrahydrofuran and pentane.

A solvent mask was calculated and 260 electrons were found in a volume of \AA^3 in one void per unit cell. This can be accounted to the presence of 3 molecules of either tetrahydrofuran or pentane per asymmetric unit which account for 240-252 electrons per unit cell. Some of the electron density shape resembles five-membered rings, however most is smeared out along a continuous cavity along the a-axis (Figure 72).

CCDC	2062477
Empirical formula	$\text{C}_{84}\text{H}_{70}\text{O}_5$
Formula weight	1159.40
Temperature/K	100
Crystal system	Triclinic
Space group	<i>P</i> -1
a/ \AA	10.3815(7)
b/ \AA	15.4555(11)

c/Å	20.4534(14)
α /°	108.938(3)
β /°	99.480(3)
γ /°	94.671(3)
Volume/Å ³	3029.6(4)
Z	2
ρ_{calc} g/cm ³	1.271
μ /mm ⁻¹	0.602
<i>F</i> (000)	1228.0
Crystal size/mm ³	0.198 × 0.195 × 0.049
Radiation	CuK α (λ = 1.54178)
2 θ range for data collection/°	6.284 to 149.426
Index ranges	-12 ≤ <i>h</i> ≤ 11, -19 ≤ <i>k</i> ≤ 19, -25 ≤ <i>l</i> ≤ 25
Reflections collected	38061
Independent reflections	12212 [<i>R</i> _{int} = 0.0304, <i>R</i> _{sigma} = 0.0346]
Data/restraints/parameters	12212/0/669
Goodness-of-fit on <i>F</i> ²	1.036
Final <i>R</i> indexes [<i>I</i> ≥ 2 σ (<i>I</i>)]	<i>R</i> ₁ = 0.0629, <i>wR</i> ₂ = 0.1841
Final <i>R</i> indexes [all data]	<i>R</i> ₁ = 0.0699, <i>wR</i> ₂ = 0.1914
Largest diff. peak/hole / e Å ⁻³	0.63/-0.30

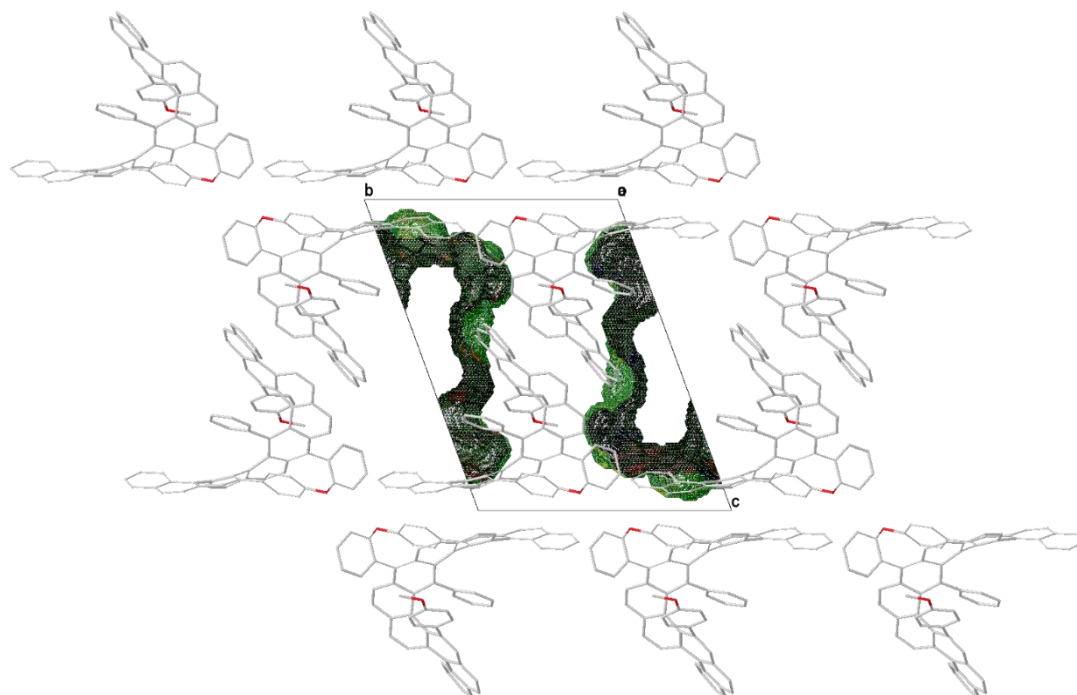


Figure 72. Packing diagram of **217b** along a-axis. Solvent mask volume inside green mesh.

8.4. Photophysical properties of helicenes

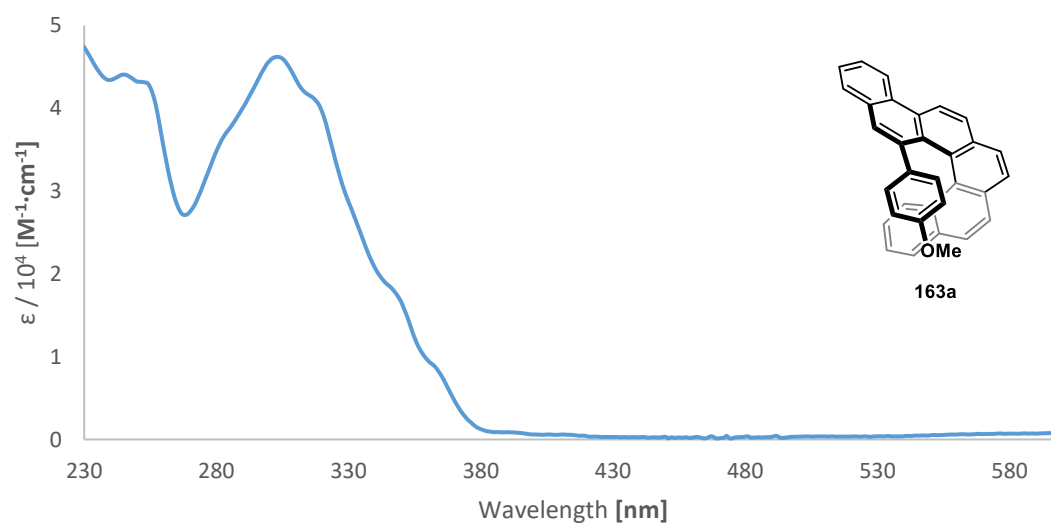


Figure 73. Absorption spectrum of **163a**.

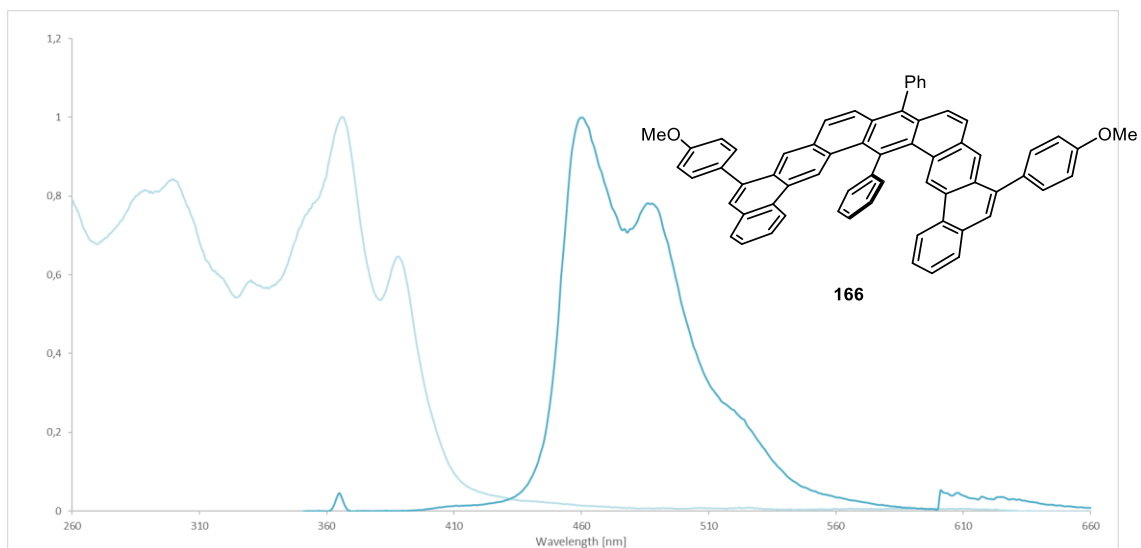


Figure 74. Normalized UV-Vis and fluorescence spectra of expanded helicene **166**.

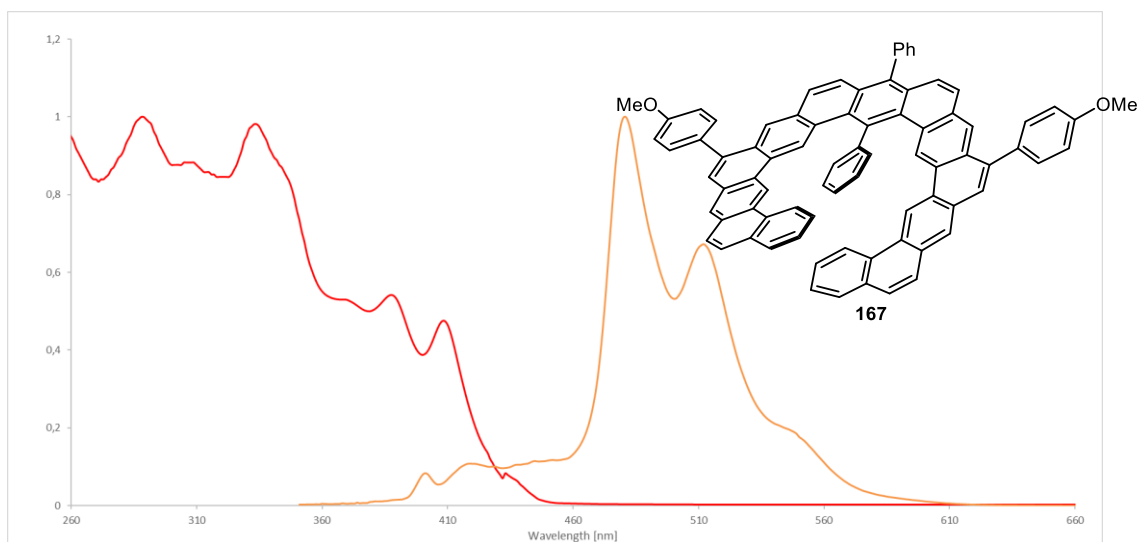


Figure 75. Normalized UV-Vis and fluorescence spectra of expanded helicene **167**.

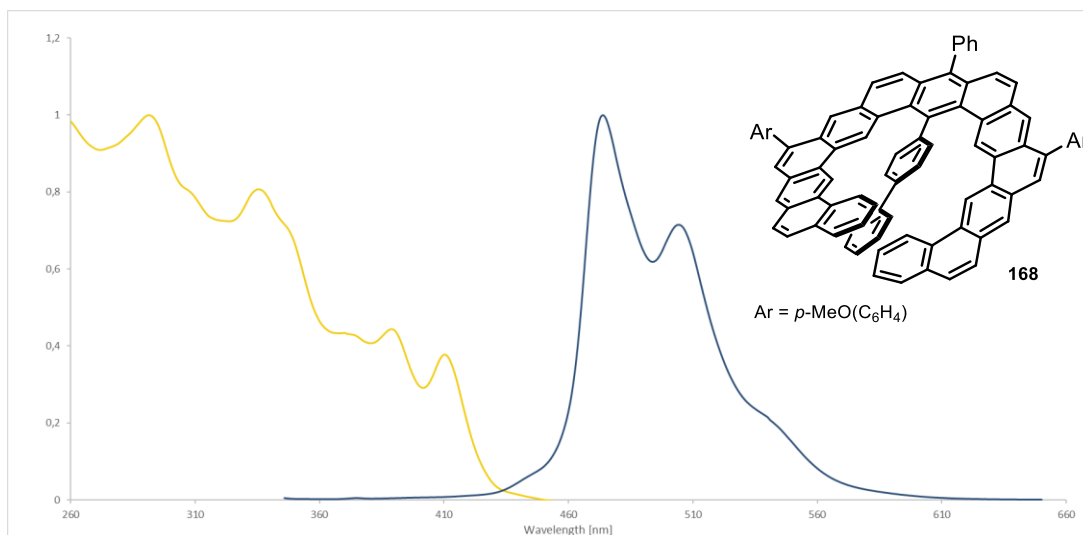


Figure 76. Normalized UV-Vis and fluorescence spectra of expanded helicene **168**.

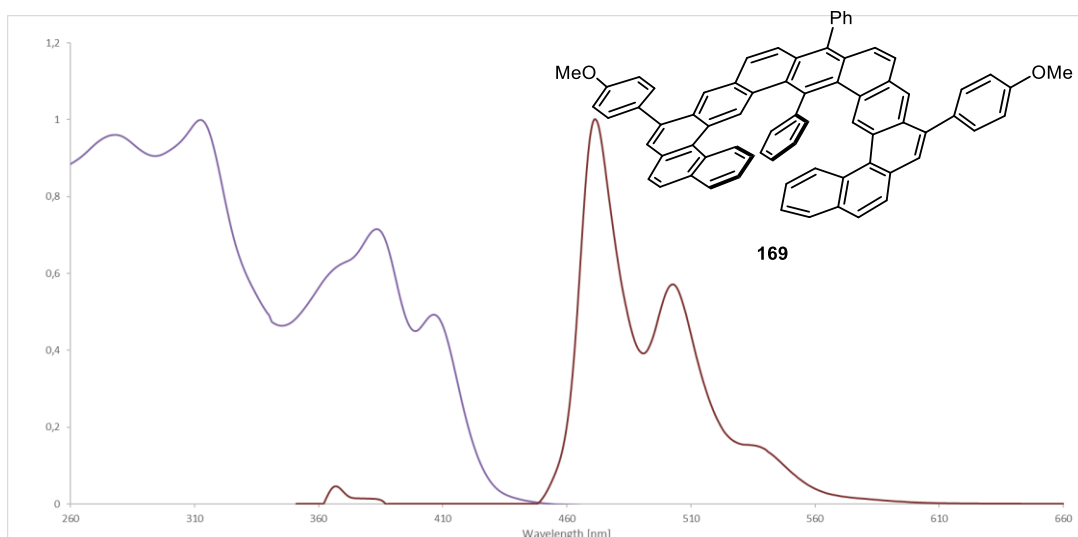


Figure 77. Normalized UV-Vis and fluorescence spectra of expanded helicene **169**.

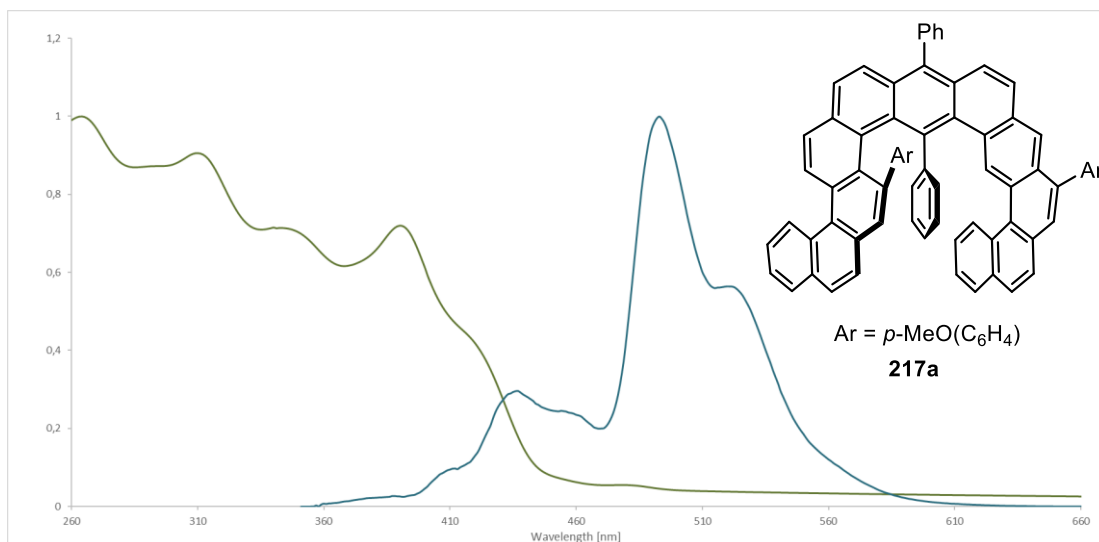


Figure 78. Normalized UV-Vis and fluorescence spectra of expanded helicene **217a**.

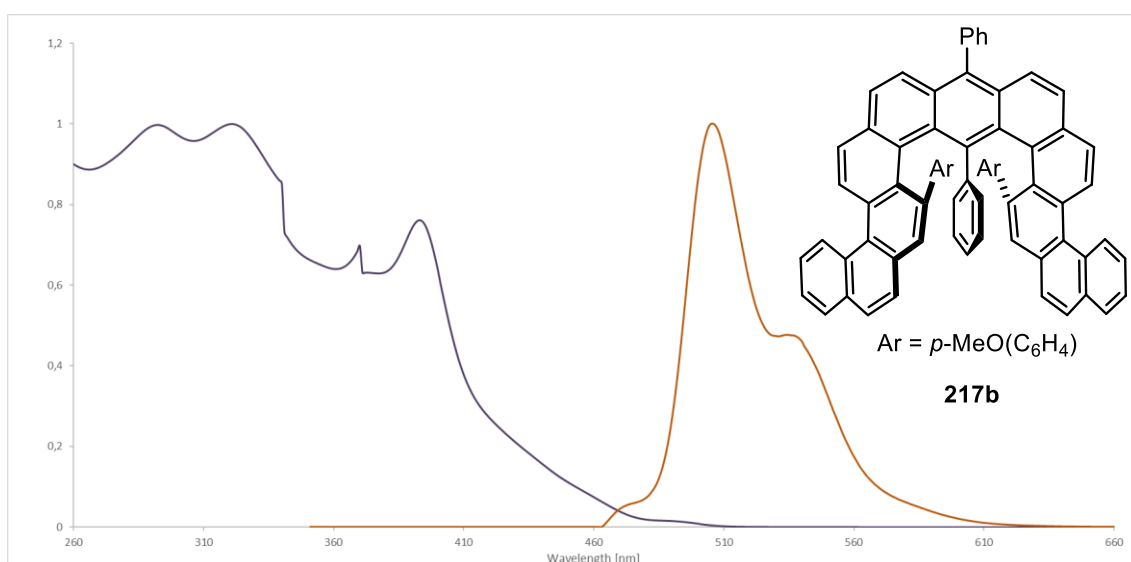


Figure 79. Normalized UV-Vis and fluorescence spectra of expanded helicene **217b**.

Curriculum Vitae. Pablo Redero

Nationality: Spanish

Address: Wiesenstraße 21, Göttingen, 37073, DE

Telephone: (+34) 686501015

E-mail: pablo.redero-garcia@chemie.uni-goettingen.de

Languages: Spanish (native), English (advanced), German (upper intermediate), French (intermediate)

Research Experience

PhD in chemistry

Georg-August-Universität Göttingen, Göttingen, DE: Prof. Dr. Manuel Alcarazo 2018-2022

Medicinal Chemistry Internship

Eli Lilly and Company, Madrid, ES 2018

Master's thesis

Universidad Complutense, Madrid, ES: Prof. Dr. Ángeles Canales 2017-2018

Bachelor's thesis

Universidad de Salamanca, Salamanca, ES: Prof. Dr. David Díez 2016-2017

Research internship

Organic Chemistry department, Universidad de Salamanca, Salamanca, 2016

ES: Prof. Dr. David Díez

Education

PhD in Chemistry (Dr. rer. nat.), Georg-August-Universität Göttingen, Göttingen, DE. 2018-2022

Master's in chemistry, Universidad Complutense, Madrid, ES

Publications

- Espada, R. Haro, J. Castañon, C. Sayago, F. Perez-Cozar, L. Cano, **P. Redero**, M. Molina-Martín, H. Broughton, R. E. Stites, B. D. Pascal, P. R. Griffin, J. A. Dodge, M. J. Chalmers, *J. Am. Soc. Mass Spectrom.* **2019**, 30, 2580-2583.
- **P. Redero**, T. Hartung, J. Zhang, L. D. M. Nicholls, G. Zichen, M. Simon, C. Golz, M. Alcarazo, *Angew. Chem. Int. Ed.* **2020**, 59, 23527-23531.
- S. Suárez-Pantiga, **P. Redero**, X. Aniban, M. Simon, C. Golz, R.A. Mata, M. Alcarazo, *Chem. – Eur. J.* **2021**, 27, 13358-13366.

Conferences and Public Presentations

- Poster co-author, International Symposium on Synthesis and Catalysis – IsySyCat17, Évora, PT, September 2017
- Poster presenter, 13. GöttingerChemieForum, Göttingen, DE, July 2021.
- Oral presentation, GöttingerChemieForum, Göttingen, DE, July 2021
- Poster presenter, 14. Jungchemikerforum, Göttingen, DE, June 2022.